Radioactive Waste Management ISBN 978-92-64-99095-1

Self-sealing of Fractures in Argillaceous Formations in the Context of Geological Disposal of Radioactive Waste

Review and Synthesis

Report prepared by

Helmut Bock
Q+S Consult, Bad Bentheim, Germany

Boris Dehandschutter
Federal Agency for Nuclear Control, Brussels, Belgium

C. Derek Martin
Department of Civil & Environmental Engineering, University of Alberta, Edmonton, Canada

Martin Mazurek and Antoine de Haller
Rock-Water Interaction (RWI), Institute of Geological Sciences, University of Bern, Switzerland

Frédéric Skoczylas and Catherine Davy
Ecole Centrale de Lille Laboratoire de Mécanique, Villeneuve d'Ascq, France

NEA No. 6184

NUCLEAR ENERGY AGENCY
ORGANISATION FOR ECONOMIC CO-OPERATION AND DEVELOPMENT

ORGANISATION FOR ECONOMIC CO-OPERATION AND DEVELOPMENT

The OECD is a unique forum where the governments of 31 democracies work together to address the economic, social and environmental challenges of globalisation. The OECD is also at the forefront of efforts to understand and to help governments respond to new developments and concerns, such as corporate governance, the information economy and the challenges of an ageing population. The Organisation provides a setting where governments can compare policy experiences, seek answers to common problems, identify good practice and work to co-ordinate domestic and international policies.

The OECD member countries are: Australia, Austria, Belgium, Canada, Chile, the Czech Republic, Denmark, Finland, France, Germany, Greece, Hungary, Iceland, Ireland, Italy, Japan, Korea, Luxembourg, Mexico, the Netherlands, New Zealand, Norway, Poland, Portugal, the Slovak Republic, Spain, Sweden, Switzerland, Turkey, the United Kingdom and the United States. The Commission of the European Communities takes part in the work of the OECD.

OECD Publishing disseminates widely the results of the Organisation's statistics gathering and research on economic, social and environmental issues, as well as the conventions, guidelines and standards agreed by its members.

* * *

This work is published on the responsibility of the Secretary-General of the OECD. The opinions expressed and arguments employed herein do not necessarily reflect the official views of the Organisation or of the governments of its member countries.

NUCLEAR ENERGY AGENCY

The OECD Nuclear Energy Agency (NEA) was established on 1 February 1958 under the name of the OEEC European Nuclear Energy Agency. It received its present designation on 20 April 1972, when Japan became its first non-European full member. NEA membership today consists of 28 OECD member countries: Australia, Austria, Belgium, Canada, the Czech Republic, Denmark, Finland, France, Germany, Greece, Hungary, Iceland, Ireland, Italy, Japan, Luxembourg, Mexico, the Netherlands, Norway, Portugal, Republic of Korea, the Slovak Republic, Spain, Sweden, Switzerland, Turkey, the United Kingdom and the United States. The Commission of the European Communities also takes part in the work of the Agency.

The mission of the NEA is:

- to assist its member countries in maintaining and further developing, through international co-operation, the scientific, technological and legal bases required for a safe, environmentally friendly and economical use of nuclear energy for peaceful purposes, as well as
- to provide authoritative assessments and to forge common understandings on key issues, as input to government decisions on nuclear energy policy and to broader OECD policy analyses in areas such as energy and sustainable development.

Specific areas of competence of the NEA include safety and regulation of nuclear activities, radioactive waste management, radiological protection, nuclear science, economic and technical analyses of the nuclear fuel cycle, nuclear law and liability, and public information. The NEA Data Bank provides nuclear data and computer program services for participating countries.

In these and related tasks, the NEA works in close collaboration with the International Atomic Energy Agency in Vienna, with which it has a Co-operation Agreement, as well as with other international organisations in the nuclear field.

FOREWORD

An important aspect of assessing the long-term safety of deep geological disposal of radioactive waste is developing a comprehensive understanding of the geological environment and processes in order to define the initial conditions for the disposal system, as well as to provide a sound scientific basis for constraining its future evolution. The NEA Working Group on the Characterisation, the Understanding and the Performance of Argillaceous Rocks as Repository Host Formations (the NEA Clay Club) is devoted to improving the scientific basis for clay host rocks in the context of geological disposal. The Self-sealing Project is part of this mission.

The suitability of an argillaceous formation as host rock for the disposal of radioactive waste is based, amongst others, on the lack of hydraulically active fractures within the repository system. Undisputedly, various types of fractures will be found in argillaceous formations at repository depth. They are site-specific natural fractures (e.g. geologic faults or bedding plane breaks) and induced fractures (e.g. features within the excavation-disturbed zone (EDZ) in the rock around the underground openings). Observations in underground research laboratories (URLs) suggest that, in connection with underground excavations, hydraulically inactive natural fractures might become reactivated, and that a network of induced fractures will be formed which may become transport pathways within the multi-barrier repository system. The hydraulic conductivity of such a network may be orders of magnitude higher than that of the intact host rock. On the other hand, observations also suggest that fractures in argillaceous geological deposits do have the capacity to become, with the passage of time, less conductive and hydraulically insignificant. That capacity is commonly termed “self-sealing”.

Self-sealing is of importance in the understanding of long-term radionuclide mobility and the safety of deep geological repositories for radioactive waste. It is often cited as one of the decisive factors favouring the choice of argillaceous formations as host rocks for deep disposals. Self-sealing directly addresses the long-term functionality of the host rock as a migration barrier. When self-sealing proceeds in reasonable time, fractures will not persist as preferential pathways for radionuclide migration, and thus the system becomes diffusion-dominated.

It is scientific consensus that self-sealing is attributable to a number of processes and mechanisms, such as the closing of fracture apertures by increased pressure, swelling and slaking of fracture walls and precipitation of minerals within the fracture. The time required for self-sealing to occur in argillaceous media depends, in part, on its mineralogy and geologic history. In plastic clays, self-sealing occurs relatively quickly, typically within a time span of a few months, whereas in more indurated argillaceous rocks self-sealing is significantly slower, typically of the order of years.

This report provides an overview and synthesis of the current understanding of and conceptual approaches to the processes that lead to the sealing of natural and induced fractures in argillaceous media at typical repository depths. The topic is considered in the context of host rock for deep geological disposal of radioactive waste. Argillaceous media that could be used in an engineered barrier system (EBS) in different host rock are not considered. The undertaking is based on a thorough review of the fundamental pre-requisites for the problem specification, such as repository conditions and evolution, composition and structure of argillaceous formations, mechanical properties of

argillaceous materials at various scales, fractures in argillaceous formations, concepts of the transport of fluids and gases in argillaceous formations and precipitation of minerals in fractures and associated geochemical aspects. Systematic evidence of self-sealing has been collected with reference to four laboratory tests, URL field tests and geologic and geotechnical analogues, whereby the bulk of the information stems from the URLs at Bure (Callovo-Oxfordian formation), Mol (Boom Clay) and Mont Terri (Opalinus Clay). The physical, mechanical, geochemical and hydro-mechanical processes and mechanisms have been reviewed and their respective contribution to the sealing of fractures assessed.

The report concludes that scientific knowledge of self-sealing has progressed to a level which, for soft and slightly to moderately indurated argillaceous formations, could justify the inclusion of sealing processes in the performance assessment of deep geological repositories.

ACKNOWLEDGEMENTS

The Self-sealing Project would not have been achieved without the important support, in many forms, of various people and organisations. Foremost among these are the members of the NEA Clay Club, whose commitment to the project and dedication to scientific excellence underlie all aspects of this report. The Secretariat recognises Philippe Lalieux and Patrick Landais, under whose tenures as Clay Club chairpersons this project was conceived and executed.

Initial work under the auspices of the Clay Club on the topic of self-sealing was conducted under contract by the British Geological Survey (BGS). Notable contributions were made by Dr. Steve Horseman, to whom this report is dedicated. His passing was a loss to the project and, more importantly, to many friends and colleagues. The efforts by BGS, and especially by Dr. Robert Cuss, to fulfil the project's commitments are recognised. *G2R/Nancy-Université* and the *Centre national de la recherche scientifique* (both in France) also made initial contributions.

The continuation, re-evaluation and expansion of work on the topic of self-sealing, along with the preparation of this report, was accomplished under contract by Dr. Helmut Bock (Q+S Consult, Germany). Dr. Bock provided much-needed leadership and direction to the scientific analysis and report writing. He proved adept at synthesising diverse data and at integrating input from numerous co-authors and experts.

The project was supported in the NEA Secretariat by Sylvie Voinis and, later, by Betsy Forinash. Particular thanks go to Ellie Bock (Mena Creek, Australia) for proofreading the manuscript.

The Self-sealing Project was financially supported by:

- Andra *(Agence nationale pour la gestion des déchets radioactifs)*, France;
- ENSI *(Eidgenössisches Nuklearsicherheitsinspektorat*, formerly HSK), Switzerland;
- GRS *(Gesellschaft für Anlagen- und Reaktorsicherheit mbH)*, Germany;
- Mecsekerc *(Környezetvédelmi Zártkörően Működı Részvénytársaság)*, Hungary;
- Nagra *(Nationale Genossenschaft für die Lagerung radioaktiver Abfälle)*, Switzerland;
- NDA (Nuclear Decommissioning Authority; formerly NIREX), United Kingdom;
- NUMO (Nuclear Waste Management Organisation), Japan;
- NWMO (Nuclear Waste Management Organisation), Canada;
- ONDRAF/NIRAS (Agency for Radioactive Waste and Enriched Fissile Materials), Belgium;
- OPG (Ontario Power Generation), Canada; and
- SCK•CEN (Nuclear Research Centre), Belgium.

In addition to providing financial resources, some organisations, notably Andra, Nagra and SCK•CEN, contributed by providing access to published and unpublished data, concepts and interpretations, and by detailed reviews of draft versions of this report. An additional review by Dr. C. Derek Martin (University of Alberta, Canada) was supported by NWMO. The report bears testament to the collective effort and expertise of all those who contributed.

Table of contents **Page**

List of figures

List of tables

Appendices

List of figures in appendices

List of tables in appendices

List of symbols

Symbol	Description	Unit
Latin symbols		
A	area	m^2
a	tunnel radius	m
a_g	geometric aperture of fracture	m
a_{g0}	geometric aperture of fracture at seating pressure σ_{ns}	m
a_h	hydraulic aperture of fracture	m
C	compression index	-
C	rugosity coefficient	-
C_f	fracture compression index	-
C_s	shape factor	-
c	cohesion	Pa
c_u	unconfined undrained shear strength	Pa
cc	crack closure	m
cc_0	initial crack aperture	m
D	degree of induration	-
d	distance	m
E	Young's modulus	Pa
e	void ratio	-
e	fluid flow thickness	m
e_0	reference (or initial) void ratio	-
G	shear modulus	Pa
g	gravity acceleration	m/s^2
H	height	m
i	dilatation angle	°
K	hydraulic conductivity	m/s
K	bulk modulus	Pa
K_0	coefficient of earth pressure at rest	-
K_2	curvature parameter	-
k	permeability	m^2
k	Boltzmann constant	-
L	length; length interval	m
m	material constant (Hoek and Brown)	-
N	normal force	N
n	porosity	-
n	number	-
n	concentration of ions in intermatrix pores	-
p	mean normal stress	Pa
p_c	confining pressure	Pa
p_s	swelling pressure	Pa
Q	flow rate	m^3/s
q	mean shear stress	Pa
q_u	unconfined compressive strength	Pa
R_H	hydraulic radius (of capillary)	m
r	radius	m
S	specific surface	m^2/g
S	shear force	N
S_ε	swelling strain index	-
s	material constant (Hoek and Brown)	-

T	Transmissivity	m^2/s
T	temperature	°
T_0	tensile strength	Pa
t	time	s
u	porewater pressure	Pa
V	volume	m^3
v	velocity	m/s
w	water content	-
w_l	liquid limit	-
w_p	plastic limit	-
x	macroscopic path length	m
z	depth	m

Greek symbols

α	thermal volumetric expansion	-
β	inertial coefficient (Forchheimer)	1/m
δ	volumetric dilation	-
δ_n	normal displacement	m
$\delta_{n\,max}$	maximum possible closure of fracture	m
δ_s	shear displacement	m
ε	strain	-
ϕ	friction angle	°
ϕ_R	residual friction angle	°
Λ	pore reference length	m
η	viscosity creep parameter	-
λ	negative slope of virgin compaction curve in semi-ln-plot	-
μ_w	dynamic viscosity	Pa s
ν	Poisson ratio	-
ρ	bulk density (saturated)	kg/m^3
ρ_d	bulk density (dry)	kg/m^3
ρ_s	grain density	kg/m^3
ρ_w	density of water	kg/m^3
σ	stress	Pa
$\sigma_1\ \sigma_2\ \sigma_3$	principal stresses	Pa
σ_{dam}	damage threshold	Pa
σ_H (σ_h)	maximum (minimum) horizontal normal stress component	Pa
σ_m	interatomic cohesive strength	Pa
σ_n	normal stress	Pa
σ_{ns}	seating pressure	Pa
σ_v	vertical normal stress component	Pa
τ	shear stress	Pa
τ	turtuosity	-

Note: Symbols with more than one meaning (e.g. “C”, “e”, “K” and “n”, “S”, “T” and “τ”) are distinguishable on the basis of their use.

List of abbreviations

Abbreviation	Description
AC/DC	adaptive continuum / discontinuum code
ASR	anelastic strain recovery
B	borehole (general)
BCF	Boda Clay formation
BGS	British Geological Survey
CDT	Cañon Diablo meteorite Troilite
COX	Callovo-Oxfordian argillites
CSL	critical state line
CSP	clay smear potential
DFN	discrete fracture network
EBS	engineered barrier system
EDZ	excavation-damaged zone
EdZ	excavation-disturbed zone
EN	European Standard
EPM	equivalent porous medium
ESEM	environmental scanning electron microscope
EU	European Union
FEPCAT	features, events and processes catalogue for argillaceous media
GSI	geological strength index
HLW	high level waste
ISO	International Organisation for Standardisation
ISRM	International Society for Rock Mechanics
JEWG	Joint European working group
LVDT	linear variable displacement transducer
MIP	mercury injection porosity
OCR	overconsolidation ratio
OoM	order of magnitude
OPA	Opalinus Clay
PA	performance assessment
PDB	Peedee formation belemnite
PFFR	phyllosilicate framework fault rock
PI	pulse injection hydraulic test
PLT	plate loading test
ppm / ppt	parts per million / parts per thousand
PW	pulse withdrawal hydraulic test
REE	rare earth elements
REV	representative elementary volume
RI	rate injection hydraulic test
RMR	rock mass rating
SEM	scanning electron microscope
SGR	shale gouge ratio
SMOW	standard mean ocean water
SSF	shale smear factor
UCS	unconfined compressive strength
URF	underground research facility
URL	underground research laboratory
XRD	X-ray diffraction

1. INTRODUCTION

1.1 Motivation

Various national programmes in the assessment of deep geological repositories for radioactive waste have shown that argillaceous formations, considered in these programmes, have a very low hydraulic conductivity and that transport is dominated by diffusion. Theoretically, fractures within these formations have the potential to act as preferential flow paths however there are indications that natural fractures in argillaceous formations exhibit similar hydraulic properties as intact rock (results from hydro testing, sealing faults in hydrocarbon production etc.). Assuming that fracturing is a dilational process calls for an explanation of why initially hydraulic active features become tight over time. The phenomenon of fractures becoming, with the passage of time, less conductive and finally hydraulically insignificant is commonly termed *"self-sealing"*[1].

Self-sealing is of importance in the understanding of long-term radionuclide mobility and safety of deep geological repositories for radioactive waste. It is often cited as one of the decisive factors favouring the choice of argillaceous formations as host rocks for deep disposals. Self-sealing directly addresses the functionality of the host rock as a migration barrier. When the self-sealing process proceeds in reasonable time, natural or man-induced fractures, which may have been re-activated or created by the repository construction or by the emplacement of the waste, will not persist as preferential pathways for radionuclide migration, and thus the system becomes diffusion-dominated.

There are a number of known processes which may lead to a sealing of fractures. In a review of those features, events and processes which are relevant for the safe disposal of radioactive waste in argillaceous media ("FEPCAT"; Mazurek *et al.* 2003)[2] the current state of knowledge on self-sealing in argillaceous geological formations is described as follows:

> "Self-sealing mechanisms have been widely observed in a variety of argillaceous rocks, and the basic physico-chemical and hydro-mechanical processes leading to self-sealing are well understood. In plastic clays, self-sealing is expected to be a rather quick process. In more indurated argillaceous rocks, self-sealing is expected to be slower. However, the currently available knowledge is not yet sufficient to permit detailed predictions concerning the kinetics of the self-sealing process in various types of argillaceous media" (p. 28).

And:

> "... studies should be continued to allow more quantitative assessments." (p. 240).

---

[1] "Sealing" (or "self-sealing") should be distinguished from "healing" (or "self-healing"); for definition of key terms, see Section 2.1.

[2] For list of references, see Appendix A.7

Within the Clay Club of the OECD/NEA, interest in specific information on the self-sealing behaviour of argillaceous formations was expressed as early as 1999. That interest prevailed throughout the years to follow. For details on the initiation and development of the Clay Club Self-Sealing Project, refer to Appendix A.1.

1.2 Project team

One of the main challenges of the project is coping with the high degree of scientific and technical complexity surrounding the self-sealing topic. The project involves a wide spectrum of subjects such as geology, hydrogeology, geochemistry, geomechanics (both soil and rock mechanics) and geo-engineering, and of technical approaches and methods such as laboratory and field testing, observations in underground research laboratories, natural analogues and conceptual and numerical modelling. As a consequence, a team with expertise in the relevant scientific and technical fields was established as shown in Table 1-1.

Table 1-1. Project team

Name	In-kind support from	Affiliation	Key Expertise
Helmut Bock	OECD / NEA	Q+S Consult Bad Bentheim, Germany	Project co-ordination Geomechanics and geo-engineering
Boris Dehandschutter	ONDRAF / NIRAS	Federal Agency for Nuclear Control, Brussels, Belgium (formerly Geology section of the KUniv. Leuven, Belgium)	Natural and induced fracture systems
C. Derek Martin	NWMO	Department of Civil & Environmental Engineering, University of Alberta, Edmonton, Canada	Geomechanics and geo-engineering
Martin Mazurek Antoine de Haller	NAGRA	Rock-Water Interaction (RWI), Institute of Geological Sciences University of Bern, Switzerland	Geochemistry
Frédéric Skoczylas Catherine Davy	ANDRA	Ecole Centrale de Lille Laboratoire de Mécanique Villeneuve d' Ascp, France	Gas and liquid permeability, mechanical behaviour of porous material and material

1.3 Objectives and expected benefits

In line with the Terms of Reference (Appendix A.1) the principal objectives of this report are as follows:

Overview and synthesis of the current understanding of, and conceptual approaches to, the processes that lead to self-sealing of natural and man-induced fractures in argillaceous media at typical repository depths.

Benefits for the Clay Club members are expected to be:

- Availability of a document on existing data sets and current knowledge on the PA-important topic of self-sealing,
- identification of commonalties and differences between sites and stimulation of the exchange of information across members,
- identification of gaps in current knowledge, and
- avoidance of duplication efforts.

The self-sealing topic is in certain ways linked with other key Clay Club issues and activities, such as episodic flow, palaeo-circulations, long-term significance of the excavation damaged zone (EDZ), rock-water interactions and the CLAYTRAC project (Mazurek *et al.* 2009).

Links also exist with some EU initiatives (*e.g.* SELFRAC[3] and NFPRO[4] projects), company-sponsored R&D projects (*e.g.* FORPRO[5], France) and ongoing studies in underground laboratories (*e.g.* Mont Terri Underground Research Laboratory, Switzerland).

1.4 Report structure

To achieve the objectives of this study, a dedicated step-wise approach to the issue of self-sealing was carried out as indicated in Figure 1-1.

In the study the following major steps were undertaken:

- Review of fundamental pre-requisites for problem specification (Chapter 2), including reviews of the key terms used in this report (Section 2.1), of the conditions and evolution of proposed deep geologic repositories in argillaceous formations (Section 2.2) and of the characteristics of argillaceous formations, which are associated with self-sealing (Section 2.3). The latter section encompasses a wide range of aspects of argillaceous formations: Their composition, structure and state conditions (Section 2.3.1 and Appendix A.2), their mechanical properties at various scales (Section 2.3.2 and Appendix A.3), far-field fractures such as joints, bedding plane breaks and faults, and excavation-related fractures such as shears, extension fractures and cracks (Section 2.3.3 and Appendix A.4), concepts of fluid and gas transport (Section 2.3.4 and Appendix A.5) and geochemical aspects (Section 2.3.5 and Appendix A.6).

[3] SELFRAC is an EU project in relation to its 5th Framework R&D activities. The project focused on fracturing processes in Boom Clay and Opalinus Clay and included experimental work (in the laboratory and in underground research laboratories) together with predictive modelling studies (Bernier *et al.* 2004).

[4] NFPRO: "Near-field performance ...": is an EU project within the 6th Framework Euratom Programme with some 40 partners. Of interest are the Work Packages 3 (co-ordinator: H.-J. Alheid, BGR) and 4 (co-ordinator: J. F. Aranyossy, ANDRA) with a Sub- Work Package 4.4 on long-term development of the EDZ, amongst them self-sealing and gas transport aspects (co-ordinator: P. Marschall, NAGRA).

[5] FORPRO (FORmations géologiques PROfondes) is an ANDRA-CNRS research initiative with a number of French University inputs aimed at improving knowledge of the behaviour of deep geological formations. Some laboratory work is presently underway on the problem of fracture sealing.

Figure 1-1. Flow chart and guide to the report

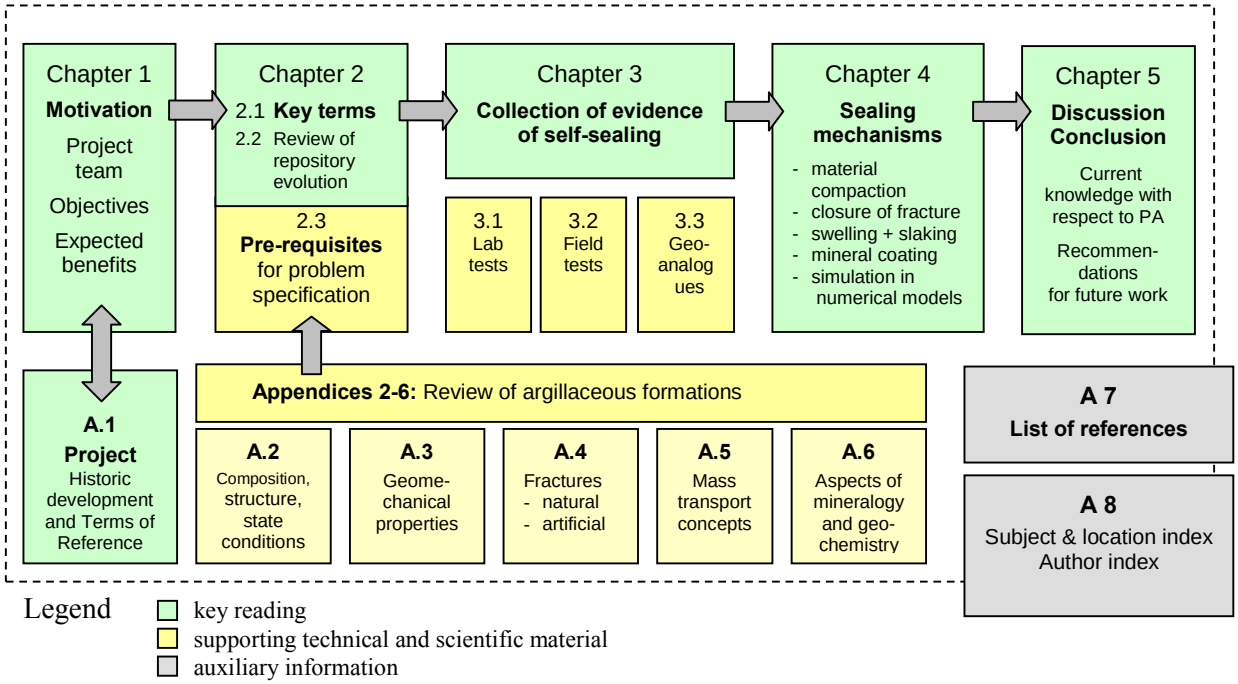

- Collection of evidence of self-sealing in argillaceous formations (Chapter 3), with particular reference to laboratory tests (Section 3.1), URL field tests (Section 3.2) and existing studies of geologic and geotechnical analogues (Section 3.3).

- Identification of processes and mechanisms which contribute to sealing (Chapter 4), with particular consideration of material compaction (Section 4.1), mechanical closure of fractures (Section 4.2), physico-chemical processes within the microscopic space, leading to swelling and slaking (Sections 4.3 and 4.4) and precipitation of minerals in fractures (Section 4.5).

- Finally, an evaluation of the current state of knowledge (Chapter 5) with identification of existing uncertainties and recommendations for future work.

1.5 Cut-off date

The issue of self-sealing is of on-going concern to many industries, institutions and scientists, not only in the field of nuclear waste isolation but also in drilling and shaft sinking and in the petroleum and gas-producing industries. There is a constant stream of new and emerging information. To ensure the overall feasibility of this report, a cut-off date was determined past which new publications or documents were not further identified or considered in a systematic manner. For the purposes of this report, the cut-off date was determined to be 18 March 2008.

2. PREREQUISITES AND FUNDAMENTALS FOR PROBLEM SPECIFICATION

2.1 Key terms and sign convention

To assist in a clear understanding of report content, and to avoid any ambiguities, certain key terms are presented at the onset of this report. The common definition of the relevant terms is quoted, and comments are made on how to understand these terms in the context of this report.

"Sealing" / "self-sealing"

Definition by Tsang and Bernier (2005; p. 8):

> Sealing = "Reduction of fracture permeability [transmissivity] by any hydromechanical, hydrochemical, or hydrobiochemical processes"
>
> Comments:
>
> The term "sealing" implies that the process is considered in the context of specified actions, e.g. physical, geomechanical, hydromechanical, chemical, biological.
>
> The prefix "self-" implies that the sealing process is occurring spontaneously, i. e. without any consideration of or knowledge on the kinetics of the sealing process.
>
> In this report, the term "sealing", with and without prefix[6], is used in the above sense.

"Healing" / "self-healing"

Definition by Tsang and Bernier (2005; p. 8):

> Healing = "Sealing with loss of memory of the pre-healing state. Thus, for example, a healed fracture will not be a specially preferred site for new fracturing just because of its history"
>
> Comments:
>
> Healed fractures imply that the deformational and strength properties of the healed material have become identical to those of the intrinsic (i.e. non-fractured) material. A "healed" fracture is also "sealed", whereas a "sealed" fracture is not necessarily "healed".

[6] Bernier *et al.* (2004) used the generic terms "sealing" and "healing" strictly without any prefixes. Against the background, however, that the terms "self-sealing" and "self-healing" are well established within the geo-scientific community and literature, the continuous use of the prefix "self-" within this report is considered meaningful, if practised in the specified sense.

The term “healing” implies that the process is considered in the context of specified actions, e.g. physical, geomechanical, hydromechanical, chemical, biological.

The prefix “self-“ implies that the healing process is occurring spontaneously, i. e. without any consideration of or knowledge on the kinetics of the healing process.

In this report, the term “healing”, with and without prefix, is used in the above sense.

EDZ and EdZ

Definition by Tsang and Bernier (2005; p. 8):

EDZ:“The Excavation Damaged Zone (EDZ) is a zone with hydromechanical and geochemical modifications including significant changes in flow and transport properties“.

EdZ:“The Excavation Disturbed Zone (EdZ) is a zone with hydromechanical and geochemical modifications, without major changes in flow and transport properties“.

Comments:

In the above definitions the only differences between EDZ and EdZ are the descriptive terms *“significant”* and *“major”*. With regard to flow and transport properties it is implied that the term *“significant”* is associated with porosity and permeability enhancements through plastic deformation (e.g. fracturing) whilst the term *“without major changes …”* is associated with porosity and permeability changes in the (quasi-) elastic range (e.g. by change of the effective stress state).

The EDZ is that zone which, at its inner surface, is bound by the underground excavation (e.g. gallery; tunnel; shaft) and, at its outer surface, by the EdZ. The outer surface of the EdZ is further away from the excavation at which the EdZ conditions converge towards those of the host rock in its undisturbed state The boundary between EDZ and EdZ can be quite irregularly shaped, particularly in well-bedded strata as is the case in most argillaceous formations (refer to Section A.4.2.4).

The terms EDZ and EdZ relate to specific states of the host rock surrounding underground openings. Those states are characterised by the occurrence of structural changes (i.e. fractures) and, more generally, by changes of the hydro-mechanical properties (deformational; strength; hydraulic conductivity etc.) from the intrinsic host rock values. For considerations around “self-sealing”, hydraulic property changes are of particular interest.

For further details on EDZ and EdZ, refer to Appendix 4, Section A.4.2.

Sign convention of stress and strain

If not explicitly specified otherwise, the following sign convention holds for this report:

Stress σ:	compressive:	positive
	tensile:	negative

Principal stresses $\sigma_1 \geq \sigma_2 \geq \sigma_3$ where:

σ_1 = major principal stress
σ_2 = intermediate principal stress
σ_3 = minor principal stress

Very common is the consideration of the normal stress components acting in vertical (σ_v) and in distinct horizontal directions (σ_H and σ_h where σ_H being the major and σ_h the minor horizontal normal stress component).

Strain ε: shortening: positive
extensional: negative

2.2 Repository conditions and evolution

Self-sealing of fractures in argillaceous formations must be considered in the context of the applicable repository conditions. Typically, such conditions change over time (Figure 2-1). Within the evolution of the repository, two distinct phases may be distinguished, the operating phase and the post-closure phase. The operating phase may be further divided into pre- and post-emplacement sub-phases.

Operating phase

In the French programme, the operating phase is initiated with the excavation of the access tunnels and shafts and will last until the closure of the repository, which could be a period of time in the order of 100 years. This phase is characterised by the installation of various engineered components, such as excavation and ground support of the emplacement tunnels, the emplacement of waste canisters and subsequent backfilling with adequate materials. The emplacement tunnels themselves must be kept open only for a relatively short period of time after construction (of the order of a few weeks up to a few years, depending on the disposal concept) until such time as waste containers and buffer material are emplaced.

In connection with the tunnel excavation and prior to waste emplacement and back-filling, the host rock surrounding the excavated underground openings will become, to certain degrees, fractured (development of an EDZ) and desaturated (e.g. by tunnel ventilation). After the emplacement of waste and adjacent buffers, the system is characterised by complex thermo-hydro-mechanical-chemical processes and interactions between the surrounding rock and backfill, leading to distinctively transient conditions. Examples of such conditions are the onset of a gradual resaturation of the EDZ rock after backfilling of the emplacement tunnel and the subsequent saturation of the backfill material which, in turn, will trigger swelling pressures from the backfill onto the EDZ rock. Further examples are the decaying heat emanated from the emplaced waste, the associated heat dissipation processes into the adjacent buffer and EDZ rock (which may result in an increase of rock stresses and porewater pressure due to the thermal expansion of solids and porewater and a thermally-related reduction in strength), thermally-accelerated rock deformations (creep) compacting the EDZ, and thermally-induced water transport arising from a reduction of water viscosity. All such transient processes will last well beyond the operating phase and closure of the repository. The various processes will proceed over differing time spans, and as such these will be relevant for PA (Figure 2-2).

Figure 2-1. Schematic graph of key aspects of the repository development (Andra 2005a)

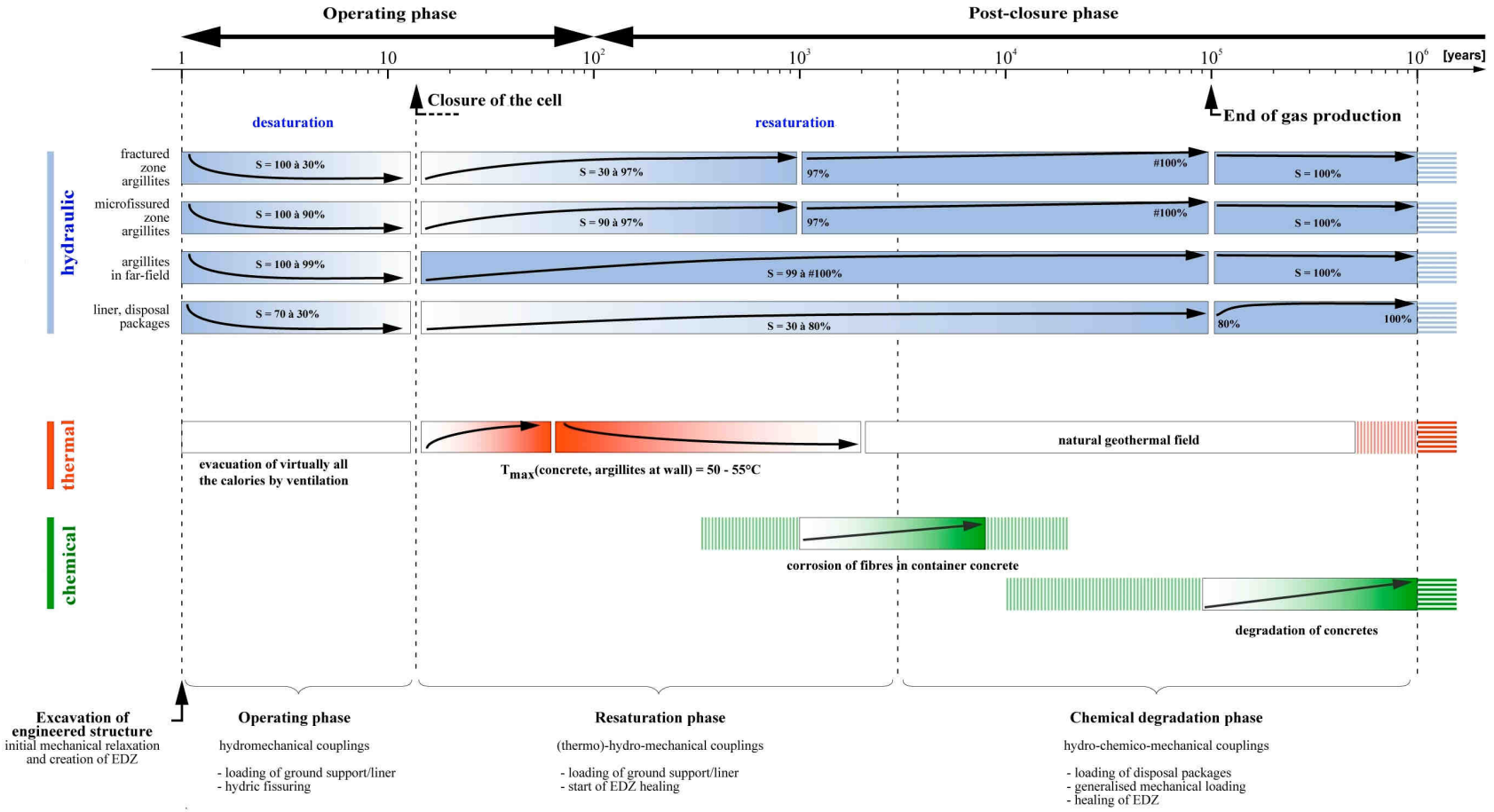

Figure 2-2. Schematic representation of relevant phenomena associated with the evolution of deep geological repositories for radioactive waste
Top: Early closure phase; Bottom: Long-term evolution
(after Marschall *et al.* 2003)

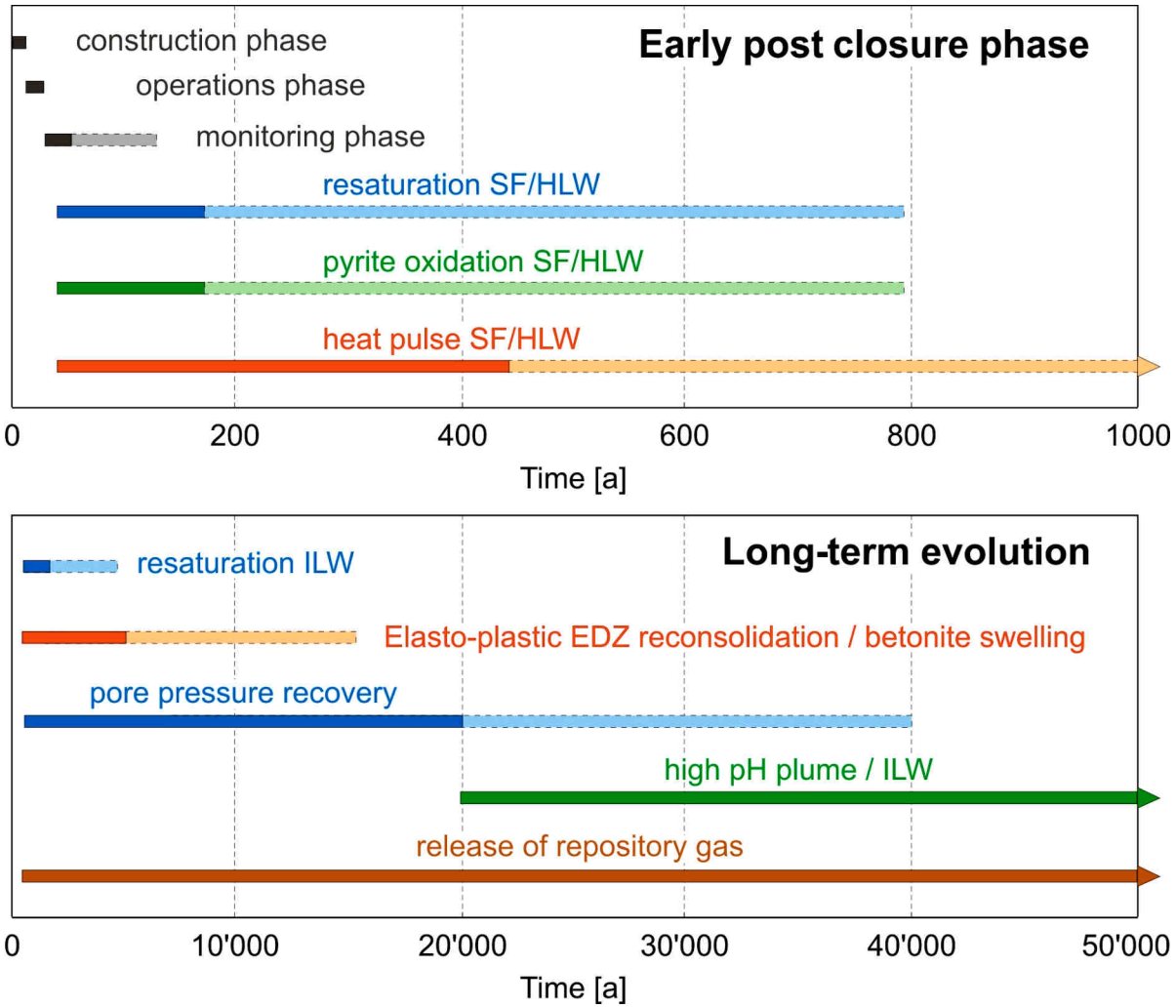

Post-closure phase

After closure of the repository the support system of the emplacement tunnels will degrade gradually and the host rock will adjust to the new situation, eventually reaching a new equilibrium. In this context, the hydraulic and transport properties in the EDZ are of particular interest, especially the development of the effective hydraulic conductivity in axial tunnel direction (= along the axis of the emplacement tunnels for spent fuel and high level wastes) over time.

For examples of details of the repository design, development and performance assessment (PA) refer to Andra (2005a), Nagra (2002a and b) and Ondraf/Niras (2002).

2.3 Fundamentals implied in the self-sealing of argillaceous formations

Self-sealing of fractures in argillaceous formations requires background knowledge on certain fundamentals which are implied in the topic. These include:

- composition, structure and *in situ* state conditions;
- geomechanical properties (deformational, strength, swelling, etc.);
- fractures (natural and artificially-induced);
- hydro-mechanical properties with particular reference to fluid flow along fractures, and
- geochemical aspects in connection with mineral precipitation in fractures.

The above aspects are briefly discussed below. Specific details are presented in the respective Appendices A.2 to A.6.

2.3.1 Composition, structure and state conditions (ref. also to Appendix A.2)

Argillaceous formations encompass a very wide range of soil and rock types, ranging from fine-grained clastic sediments (unlithified mud and clay), through diagenetically lithified sediments (= sedimentary rocks such as moderately indurated mudstones and claystones, fissile and often highly indurated shales), to metamorphic rocks (e.g. slates). Across such a wide spectrum, the characteristics and the physical and geotechnical properties of argillaceous media vary enormously.

Various geological as well as geotechnical classification schemes have been proposed for argillaceous formations. Within the geological scheme there is not yet a consistent and generally accepted terminology (Appendix A.2; Tables A.2-1 and A.2.3; Horseman *et al.* 2005; Mazurek *et al.* 2003). This is in contrast to the geomechancial scheme which is standardised, for soils in ISO 14688-1 and –2 and for rocks in ISO 14689-1. It is for this reason that, within this report, the geomechanical terminology and classification is generally preferred [7].

ISO defines soil as an assemblage of particles which can be separated "by gentle mechanical means" and which includes variable amounts of water and air. Rock is defined as a naturally occurring assemblage of minerals, consolidated, cemented, or otherwise bonded together, so as to form material of "generally greater strength and stiffness than soils". Argillaceous soils and rocks are characterised by a high portion of "fine-grained" (silt) to "very fine-grained" (clay) mineral particles. The transition between soil and rock can be specified by the unconfined undrained shear strength c_u and the unconfined compressive strength q_u, respectively (Table 2-1). The geomechanical classification of argillaceous media for engineering purposes is shown in Table 2-2. It is based on the predominant particle size, the plasticity and the genesis of the soil or rock. The terms 'mudstone' and 'shale' in the fine-grained sedimentary rock class of Table 2-2 are used to distinguish between the rocks with bedding planes of ≥ 6 mm spacing (mudstone) and < 6 mm spacing (shale).

Argillaceous formations are characterised by a high portion of clay minerals. That portion, the type of clay minerals and their structure have a decisive influence on the formations' mechanical, hydromechanical and geochemical behaviour at micro- and macro-scales. The current state of any argillaceous formation under consideration as host rock for deep geological disposal is predominately

[7] A consistent use of the geomechanical terminology throughout this report, however, was not possible as, for historic reasons, established formation names are not necessarily compatible with currently applied terminology and classification. Examples are the "Opalinus Clay" which, geomechanically, is a claystone rather than a clay, and the "Callovo-Oxfordian argillite" which also is a claystone and not a metamorphic rock as suggested by the term "argillite" (Tables A.2-1 to A.2-3 of Appendix A.2).

a result of its specific geological history. Amongst the most important parameters which characterise such state conditions are the porosity of the soil or rock, the natural water content and the *in situ* stress state.

Table 2-1. Soil-rock transition as specified by the shear strength in ISO Standards

Soil (ISO 14688-2)							**Rock** (ISO 14689-1)						
Unconfined undrained shear strength c_u [kPa]							Unconfined compressive strength q_u [MPa]						
< 10	10-20	20-40	40-75	75-150	150-300	> 300	< 1	1-5	5-25	25-50	50-100	100-250	> 250
extremely low	very low	low	medium	high	very high	extremely high (*)	extremely weak (**)	very weak	weak	medium strong	strong	very strong	extremely strong

Legend: (*) Materials with shear strength greater than 300 kPa may behave as weak rocks and should be described as rocks according to ISO 14689-1.

(**) Some extremely weak rocks will behave as soils and should be described as soils according to ISO 14688-1.

Table 2-2. Geomechanical classification of argillaceous soils and rocks
(modified from ISO 14688-2 and 14689-1)

<table>
<tr><td colspan="3">Genetic Group</td><td colspan="2">Soil
(clastic sediment)</td><td colspan="3">Rock
(clastic sedimentary rock)</td><td>Rock
(metamorphic)</td></tr>
<tr><td colspan="3">Geologic Process</td><td colspan="2">Sedimentation</td><td colspan="3">Diagenesis</td><td>Metamorphosis</td></tr>
<tr><td colspan="3">Usual Structure</td><td colspan="2">bedded</td><td colspan="3">bedded</td><td>foliated</td></tr>
<tr><td colspan="3">Composition</td><td colspan="5">Grains of rock, quartz, feldspars, clay minerals</td><td>(**)</td></tr>
<tr><td rowspan="4">Predominant grain size [mm]</td><td rowspan="4">0,063

0,002</td><td>Medium-gr.</td><td colspan="2">Sand</td><td>(*)</td><td colspan="2">Sandstone</td><td rowspan="4">Schist
Phyllite
Slate

Mylonite (***)</td></tr>
<tr><td rowspan="2">Fine-grained</td><td>coarse</td><td rowspan="3">Silt</td><td rowspan="3">argillaceous</td><td rowspan="3">Mudstone
Shale:
fissile mudstone</td><td>Siltstone
(> 50% fine-grained particles)</td></tr>
<tr><td>medium</td></tr>
<tr><td>Very fine-grained</td><td>fine</td><td>Clay
← normally over-→ consolidated</td><td>Claystone
(≥ 50% very fine-grained particles)</td></tr>
</table>

Legend: (*) arenaceous

(**) quartz, feldspars, micas, dark minerals

(***) generic term for fine-grained, completely recrystallised shear zone material, independently of the host rock type

Typically, the geological history of an argillaceous formation can be characterised by a sequence of events as follows:

1. Flocculation and aggregation of clay particles in seawater.
2. Sedimentation of the clay aggregates at the seafloor, eventually in combination with other fine-grained clastic particles (silt), and subsequent burial by deposition of other aggregates on top of it.
3. Compaction due to increased effective overburden pressure.
   This mechanical process is associated with a number of major physical and structural changes (in particular: drainage of free porewater, development of excess porewater pressures, rotation of the clay particles into a sub-horizontal flaky structure). The effects are most pronounced for overburden depths of up to about 500 m ("burial stage"; Müller 1967). At greater overburden depths (>500m; "deep-burial stage") the significance of the mechanical compaction is less well developed and chemical processes such as cementation, re-crystallisation and growth of new minerals become dominant (Wolf and Chilingarian 1992). After reaching maximal overburden, eventually combined with tectonic stressing, finally:
4. Uplift (not necessarily back to the topographic surface) and reduction of the overburden by vertical erosion.

The above burial – compaction – uplift – erosion sequence is generally well recognisable at specific repository sites (see Figures A.2-10 to A.2-12 in Appendix A.2). Some important geomechanical effects of such sequence are indicated in the example of Figure 2-3 which shows the geologic evolution of the Meuse/Haute-Marne site in terms of burial pressure versus porosity of the Callovo-Oxfordian formation as deduced from porosity logging and geochemical data.

Figure 2-3. Geologic evolution of the Meuse/Haute-Marne site in terms of burial pressure versus porosity

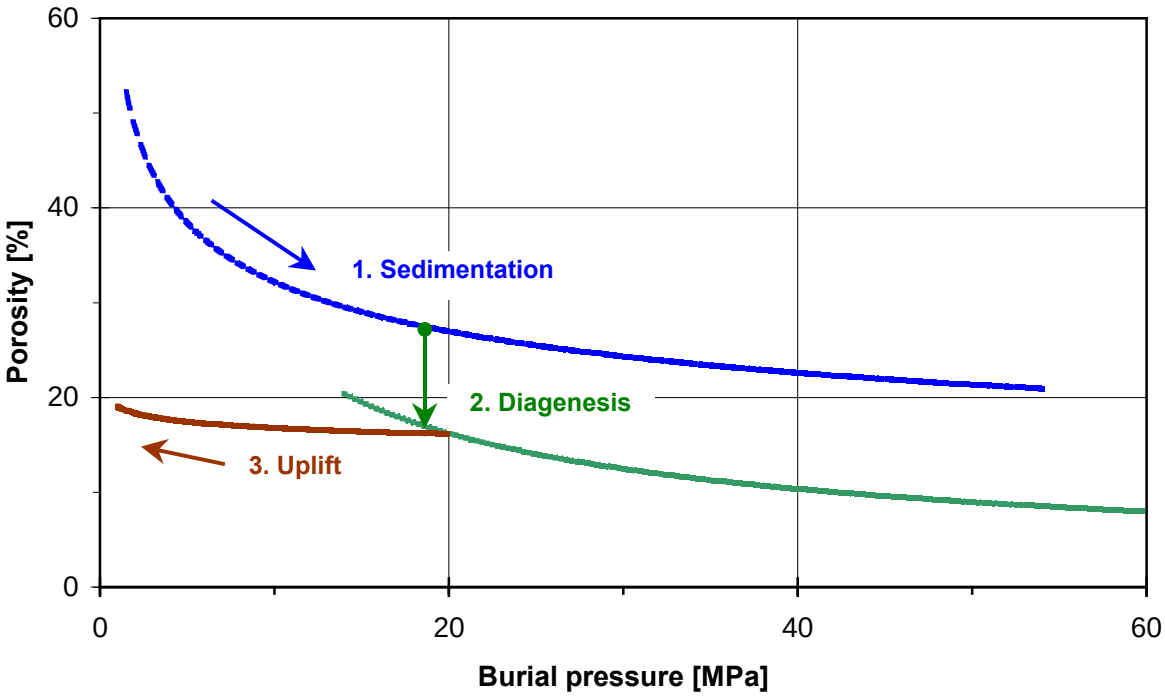

2.3.2 Geomechanical properties (ref. also to Appendix A.3)

Stemming from the large variety of argillaceous soils and rocks (see Section 2.3.1 and Appendix A.2.1), the values of the pertinent geomechanical parameters vary within a very wide range. It therefore makes limited sense to develop a set of 'typical' parameter values for argillaceous media in general. Instead, site- and project-specific data sets are required (Table 2-3).

Table 2-3. Basic geological characteristics and some geotechnical parameter values of major argillaceous formations (actualised after Boisson 2005)

Parameter		**Boom Clay (Mol URF)**	**Callovo-Oxfordian (Bure URL at –490m Level)**	**Opalinus Clay (Benken / Mont Terri URL(1))**	**Toarcian-Domerian Shales (Tournemire URL)**	**Boda Clay (Pécs)**
Geologic age	stratigraphic	Oligocene	Callovo-Oxfordian	Lower Dogger	Lias	Permian
	absolute [Ma]	32 - 29	163 - 158	176 - 172	*ca.* 180	250 – 260
Burial depth at present [m]		186	490	539 / 230	250 - 500	0/800 (2)
Maximum burial depth [m]		186	820	1650 / 1350	1000	3500 - 4500
Degree of induration D		low	slight	moderate	high	very high
Sum of all clay minerals [%wt]		60	25 to 60	54 / 66	25 - 50	35 - 50
Sum of swelling clay minerals [%wt]		40	10 to 40	32 / 45	9 – 15	0-2
Grain density ρ_s [kg/m³]		2 650	2 700	2 720 / 2 700	2 650	2 730
Bulk density (saturated) ρ [kg/m³]		2 000	2 430	2 520 / 2 430	2 600	2 720
Water loss porosity n [%]		36.3	19.5	10.8 / 13.7	10.5	0.5 – 1.5 (3)
Water content w [%wt]		21.5	8	4 / 6.4	4.0	< 1
Hydraulic conductivity $K_\perp$ [m/s]		$7 * 10^{-12}$	10^{-13}	$0.2 * 10^{-13}$ / $0.7 * 10^{-13}$	*ca.* $1.5 * 10^{-14}$	$3 * 10^{-9}$ to $1 * 10^{-12}$
K-Anisotropy [$K_{//} / K_\perp$]		2 - 3	2 to 3	1 – 10	2	-
Unconfined compressive strength q_u [MPa]		2.0	15-80	6-28 / 11-15 anisotropic	32	90 – 120
Young's modulus E [GPa]		3	$E_\perp$: 5 – 40 $E_{//}$: 6 - 50 (anisotropic)	6-11 / 4-10 (anisotropic)	$E_\perp$: 15 – 32 $E_{//}$: 8 - 14	30 – 40 (anisotropic)
Poisson's ratio ν [-]		0.43	0.3	0.27 / 0.29	0.2	0.20 – 0.25
Swelling pressure p [MPa]		0.9	1.0 (3)	0.8 (4) / 0.6-1.2	$p_\perp$: 0.1 – 0.6 $p_{//}$: 0.3 – 0.5	0

Remarks: (1) Actualised compilation for Mont Terri URL in Bock (2009)

(2) Within the investigated site

(3) Value for Hg-injection porosity; no water-loss porosity data available.

(4) Recent tests (Zhang *et al.* 2009), designed along the clay-colloid concept, provided significantly higher swelling pressures, 10 to 12 MPa for the Callovo-Oxfordian argillites and 5 to 6 MPa for the Opalinus Clay. The magnitudes of these swelling pressures are close to those of the overburden pressures acting at the respective sampling depths.

Each parameter set constitutes the input parameters of a site-specific 'Ground Model' for the design of the repository in question and the prediction of its future behaviour. The specification of constitutive laws appropriate for the soils and rocks in the model is required as well as the derivation

of their mechanical parameter values in laboratory and/or field testing ('derived values' in the sense of Eurocode 7; EN 1997-2, 2007) and their interpretation in terms of 'characteristic' and 'design values' in the sense of Eurocode 7; EN 1997-1 (2004). The transfer from 'derived' to 'characteristic' and 'design' values is hereby based on the evaluation of the sampling and testing procedures, possible scale effects, regional experience and experience with the specific geo-material under consideration (Figure A.3-3 in Appendix A.3).

For consideration of self-sealing in argillaceous formations, it is the strength properties which are of particular concern as these are closely linked to fracturing and failure and, thus, to fluid flow and self-sealing. Sections A.3.3 to A.3.4 of Appendix A.3 provide a comprehensive review of the strength properties and current understanding around fracturing processes in argillaceous media. These considerations include terminology, the brittle/ductile behaviour, different modes of fracturing and failure (tension; extension; shear; multi-shear) and alternative strength criteria (e.g. Mohr-Coulomb; Hoek-Brown; Critical State concept and Cam-Clay model).

2.3.3 Natural and artificial fractures (ref. also to Appendix A.4)

Natural and artificially-induced fractures are commonly observed in argillaceous formations both in surface outcrops and in URLs. Knowledge on their types and formation processes is one of the prerequisites for understanding self-sealing.

Terminology

Natural fractures are macroscopically visible geologic features such as bedding plane breaks, fissures, cracks, joints, faults and veins (Table 2-4).

Table 2-4. Terminology of natural fractures in argillaceous formations
(after Mandl 2005 and Ulusay and Hudson 2007)

Geologic term	Definition / characteristics	Usual extent
Crack	Partial fracture, with some parts still cohering	small
Fissure	Open crack, arranged in an irregular, non-systematic manner	
Bedding plane	Latent break, susceptible to opening in unloading regimes (e.g. tunnel excavation); mechanically of particular importance when activated in shear	
Joint	Break in the continuity of a geologic body along which there has been *no visible* displacement. Most frequently arranged in a systematic manner (set of joints; conjugate and/or orthogonal joint system).	
Fault	Shear fracture or fracture zone along which there has been *a visible* displacement, from a few centimetres to a few kilometres in scale.	large
Vein	Fracture, related to tectonic (most frequently) or diagenetic (rarely) activity, partially or totally filled with minerals precipitated from aqueous fluids	all dimensions

In repositories, artificially-induced fractures are caused predominately by the excavation of the emplacement tunnels and also by thermal effects from the emplaced waste. Some common types of induced fractures are listed in Table 2-5.

Table 2-5. Terminology of induced fractures in argillaceous repositories

Technical term	Definition / characteristics	Comment
Fracture	Planes of separations in a solid material	Generic term
Discontinuity	Generic term for all types of mechanically relevant fracture and failure planes	The term includes also natural fractures
Crack	Partial fracture, with some parts still cohering	as in Table 2-4
Tension fracture	Brittle fracture in a tensile stress field with minor principal effective stress $\sigma_3' < 0$	Occurrence limited; whether or not a tensile fracture progresses into a tensile failure depends on energy considerations
Extension fracture	Brittle fracture in a compressive stress field with major principal effective stress $\sigma_1' >> 0$	Occurrence wide-spread; only occurring at relatively small effective σ_3' values ≥ 0
Shear fracture	Brittle or ductile fracture, characterised either by the formation of a discrete shear plane or of abundant shear planes in the material	A discrete shear plane is often developing after the formation of numerous extension fractures
Desiccation fracture	Fractures developing due to moisture extraction and associate material shrinkage	In argillaceous materials commonly restricted to shallow depth
Spalling	Breaking-off of plate-like pieces from a free underground rock surface (e.g. from an unsupported tunnel wall)	Violent spalling => rock burst (not observed in underground laboratories in argillaceous formations)
Buckling (or 'kinking')	Instability in the form of sudden deflection of a series of slender rock columns	Well-bedded rock is particularly amenable to this type of instability

Natural fractures

Genetically, natural fractures can be classified into two categories. The first category is related to near-surface environments and includes structures generated by stress release, e.g. induced by erosion or deglaciation. The second category includes fractures generated by tectonic activity and occurring at all crustal levels. Because such structures may focus fluid flow, they are frequently mineralised and therefore present as veins. Vein minerals document the existence of past fluid flow, and may completely seal the structures (see Appendix A.6).

Because of its comparatively simple geologic evolution within its deposition – burial – erosion sequence (Section 2.3.1 and Appendix A.2.4; Figure A.2-8), the Boom Clay is of principal importance in identifying that particular inventory of natural fractures which may be considered as the most elementary one in argillaceous formations. Relevant studies have been carried out by Dehandschutter *et al.* (2005a; 2005b) both at the surface in large clay open pits and underground in the HADES URF.

In surface outcrops there are three types of systematic natural fractures as follows:

1. “Meso-planes” (m-scale): Discrete shear planes as part of a normal fault system

2. “Micro-planes” (cm-scale): Multiple shear joints

3. “Sub-vertical joints” (dm- to m-scale): Mixed-mode extensional fractures, forming an orthogonal joint system.

The above natural fractures of the Boom Clay could only be observed in surface outcrops. They have not been observed underground in the HADES URF at depths below 223m of the surface (Dehandschutter 2004) where solely excavation-induced fractures have been observed (Appendix 4, Section A.4.2).

Extension fractures are prone to become water-conducting features. In this respect, the sub-vertical joints of the orthogonal joint system are of particular interest. Geologically, the absence of an orthogonal joint system in the HADES URF is noteworthy as, in other geological settings, such system commonly prevails at greater depths. Dehandschutter *et al.* (2005a) inferred that the orthogonal joint system of the Boom Clay was formed close to the surface down to a depth of about 70m, where confining pressure and local stress field conditions favoured the development of such a system. The joint formation process was seen as being associated with an episodic uplift of the Boom Clay and an anisotropy of the horizontally acting principal stresses (see also Section A.4.1.4.2). The latter findings are in agreement with the generally accepted joint formation theories (Mandl 2005). Although unlikely, the uncertainty of its burial history (and also the mechanical properties of the Boom Clay during its geological history) cannot fully exclude that the joints were actually formed at the level of the URF. If so, they must have been fully sealed after their formation as is evidenced by the detailed observations in the HADES URF. The topic of the formation of the orthogonal joint system in argillaceous formations thus remains of some general interest as it might constitute a geologic self-sealing analogue.

Natural fractures have been observed in slightly and moderately indurated formations such as the Callovo-Oxfordian argillite and the Opalinus Clay (for both see Section A.4.1.3 in Appendix 4), and in strongly indurated formations such as the Toarcian-Domerian shales at Tournemire. With regard to the Opalinus Clay, studies were carried out by Mazurek *et al.* (1996) in clay pits of northern Switzerland. Characteristic are sub-vertical extension joints. Surface water infiltrate along these joints into the rock as is evidenced by oxidation seams. Identical to Dehandschutter’s (2004) observations in the Boom Clay, the occurrence of these joints is limited to the uppermost strata of the Opalinus Clay (order of some 10 metres). They could not be observed at greater depths neither in boreholes nor in the Mont Terri URL. Other natural fractures, however, could be observed underground in the URLs. An example is the ‘Main Fault’ at Mont Terri (Figure 2-4; see also Figures A.4-7 and A.4-8 in Appendix 4).

Faults were, besides bedding, identified as the generally most frequent structural feature encountered in Mont Terri (Table 2-6). They have extents in the order of metres to tens of metres, and their walls were often slickensided and polished. A few celestite-calcite veins were also recognised at Mont Terri, and their origin is still being investigated (see Figure A.6-4 in Appendix A.6). Calcite-celestite veins occurring in the Jurassic sequence (including the Effingen Beds marls and argillaceous limestones) at Oftringen, near Olten, Switzerland, are interpreted to have precipitated from descending Miocene seawater (open system behaviour; see Appendix A.6).

Despite obvious deformation having taken place during the course of their geologic history, there is, at the URL level, actually not much evidence of enhanced water transmissivity along these faults. Slightly different observations have been made in the relatively massive Toarcian-Domerian

formation of the Tournemire URL where certain natural fractures are weakly water conducting (Figure 2-5).

Figure 2-4. Illustration of the Main Fault in Gallery 98 at Mont Terri
Top: Photo view, © Comet, Zurich - Bottom: Structural geological interpretation
(from Nussbaum and Bossart 2008)

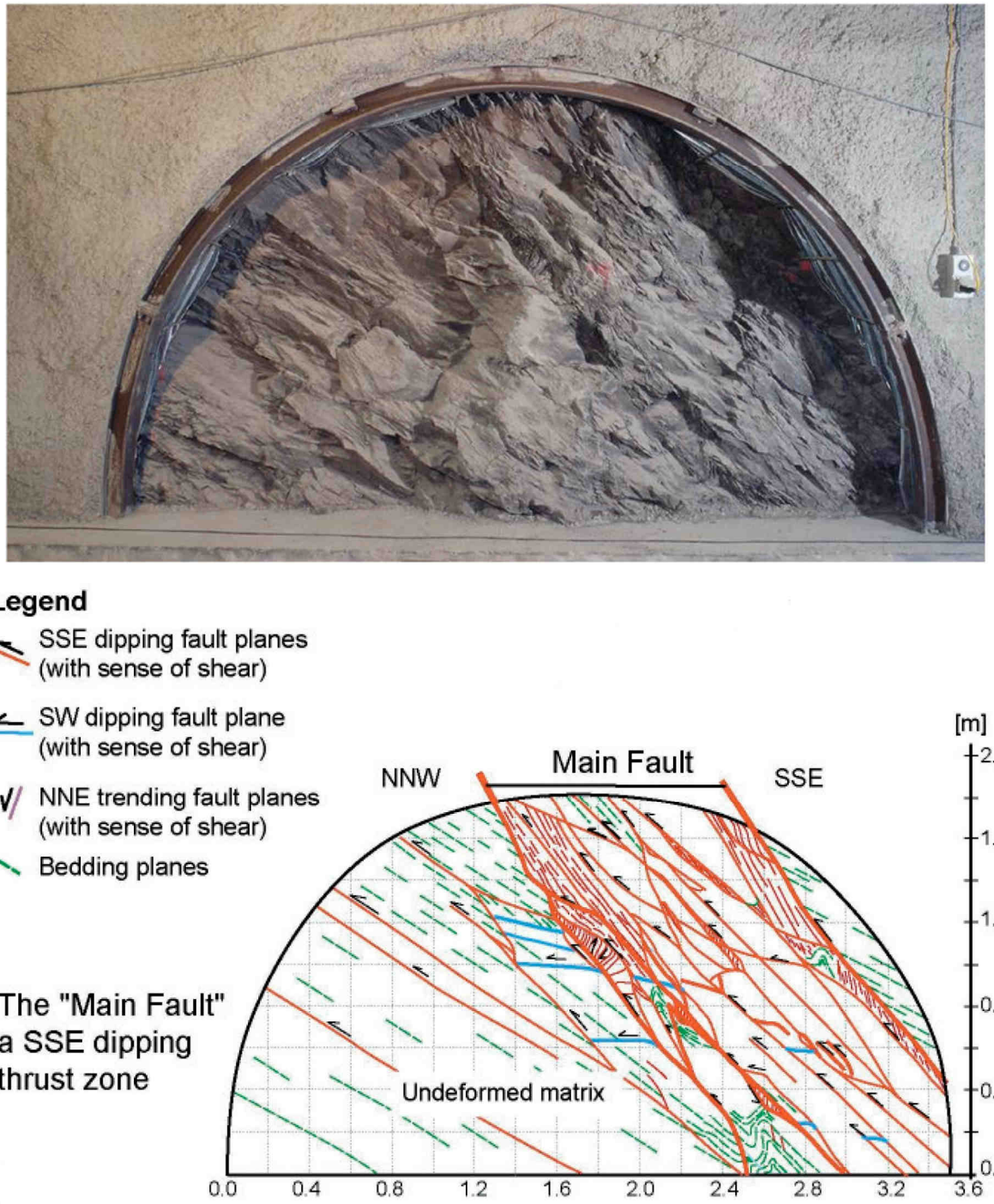

Table 2-6. Types of discontinuity features derived from tunnel mapping in the Mont Terri URL
(after Lanyon 2008)

Feature type	Logged in core	Extent	Open/closed	Hydraulic significance
SSE dipping fault planes	Yes	Extensive >10m	May be reactivated in EDZ, closed in rock mass	Potentially significant within EDZ
S-SW dipping fault planes	Yes	<5m Seem to be bounded by SSE dipping faults	May be reactivated in EDZ, closed in rock mass	Potentially significant within EDZ
Bedding planes	?	Extensive	May fail in slip in EDZ, closed in rock mass	Potentially significant within EDZ
Stress induced extension fractures	Yes	0.5-1m	Open	Open but may be limited in connectivity
Desaturation cracks	No (logged in BHGA18, A26)	0.5-1.5m	Open at tunnel wall	Probably only open very local to tunnel wall and likely to close on resaturation
Siderite layers	Not recorded	0.2-1m	Weakly cemented but not open	May be more locally permeable than host rock but not significant compared to fractures.

Figure 2-5. Wet spots along a bedding plane break in a drift of the Tournemire URL
(IRSN Brochure)

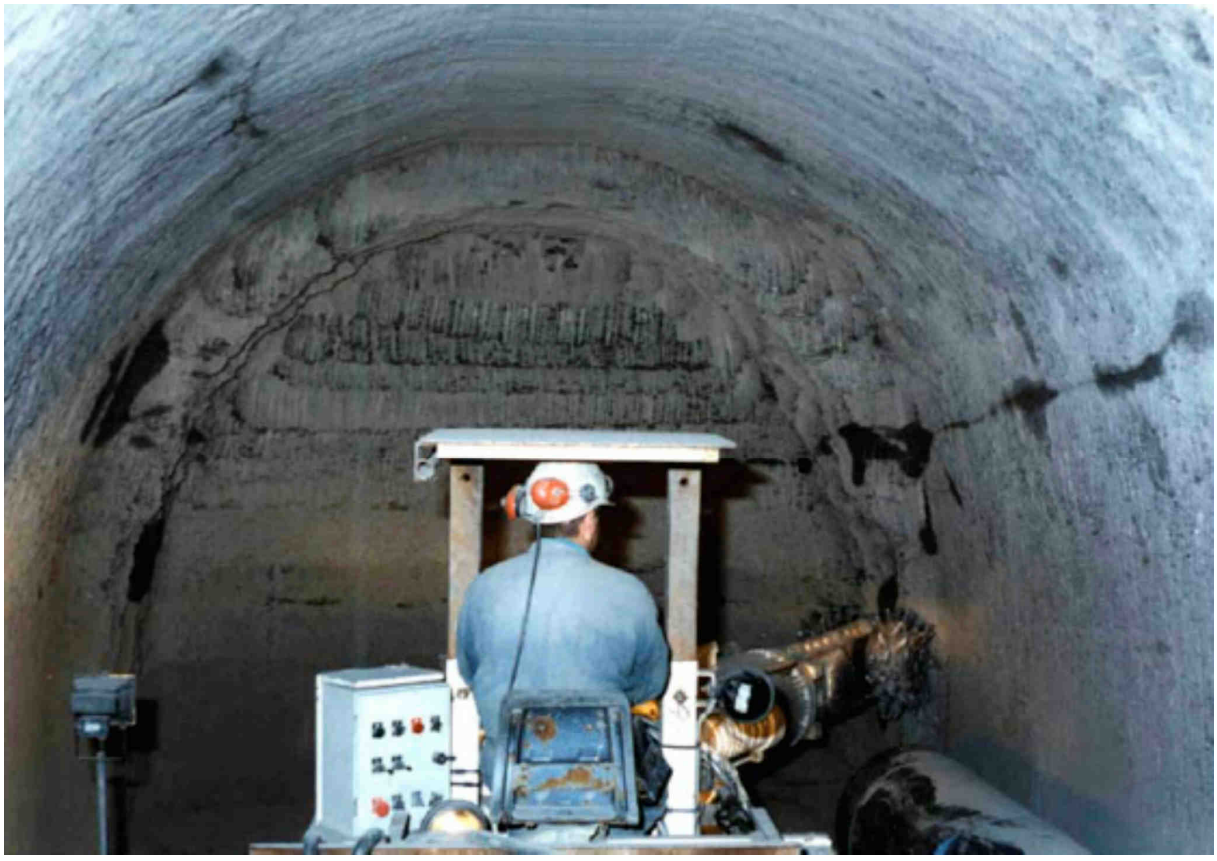

Artificially-induced fractures

Underground excavations in argillaceous formations are regularly connected with the formation of micro- and macro-scale fractures in the region of the rock immediately surrounding the excavation. This region forms the EDZ. In practice, the formation of such EDZ fractures cannot be completely avoided by any technical means.

The identification and mapping of the EDZ fractures is a common objective of past and on-going URL investigations. Particularly detailed work has been carried out in the URLs at Mol, Meuse/Haute-Marne and Mont Terri (Appendix A.4.2). An example of the conceptualised EDZ fracture system is shown in Figure 2-6 b. It depicts an early conceptualisation of the EDZ in the Gallery 1998 of the Mont Terri URL showing extensile EDZ fractures and bedding-parallel unloading features. More recent EDZ conceptualisations account for additional features and phenomena (refer to Section A.4.2.4).

Figure 2-6. EDZ fractures in the Mont Terri URL
(from Armand *et al.* 2008)
(a): EDZ fractures of a tunnel sidewall (excavation 1989) as seen from a side niche (excavation 1996)
(b): Early conceptual model of the EDZ around a tunnel after Bossart *et al.* (2002)

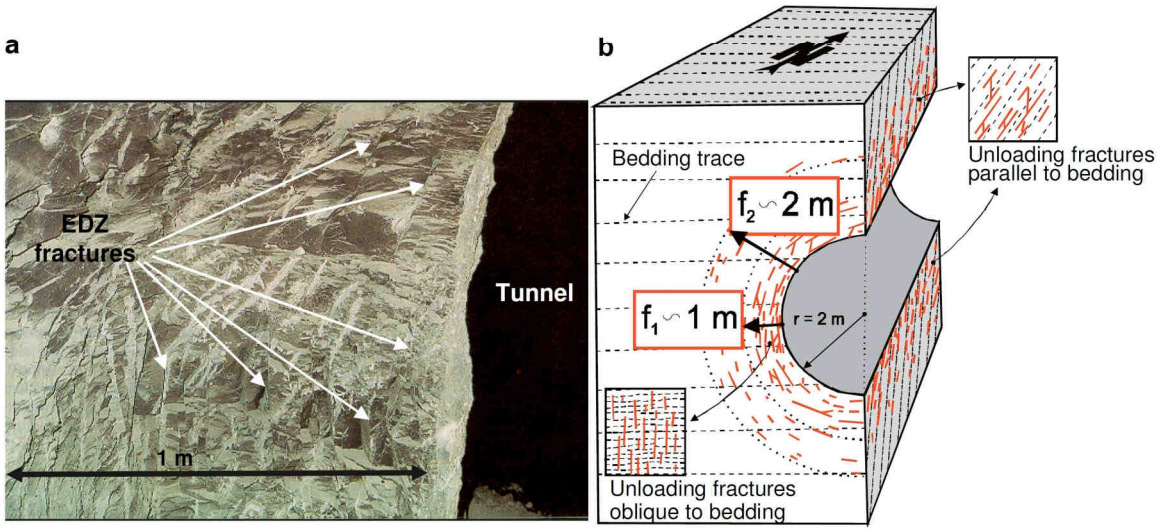

Useful reference can also be made to other geo-engineering fields such as traffic tunnel construction, reservoir (petroleum) engineering and mining engineering. Figure 2-7 shows physical models (scale 1:20) of the EDZ around a gallery in horizontally-bedded coal-bearing strata. Although the modelled overburden height of about 1200 m is well in excess of the overburden generally considered in deep geological repositories (in the order of ~ 500 m), the models presented at Figure 2-7 are quite useful as they tend to exaggerate features which may be disguised and otherwise overlooked. The physical model delineates excessive buckling of the strata in the unsupported tunnel invert whilst buckling in the roof strata is widely suppressed by anchor support (left) and steel arch support (right). Note the very substantial dilatation of the sidewall rock by a combination of tension joints, graben structures and slip along bedding planes which is particularly pronounced in the steel arch ground support system (right in Figure 2-7). Note also the formation of a void at the base of the wedge-shaped buckled zones, both in the roof (marginal) and in the invert (substantial), which potentially may become a preferred channel-type conduit for mass transport along the gallery axis.

Figure 2-7. Physical model (scale 1:20) of the EDZ around a gallery in horizontally-bedded coal-bearing strata (from Jacobi 1981)
Ground support by systematic rock bolting (left) and steel sets (right)

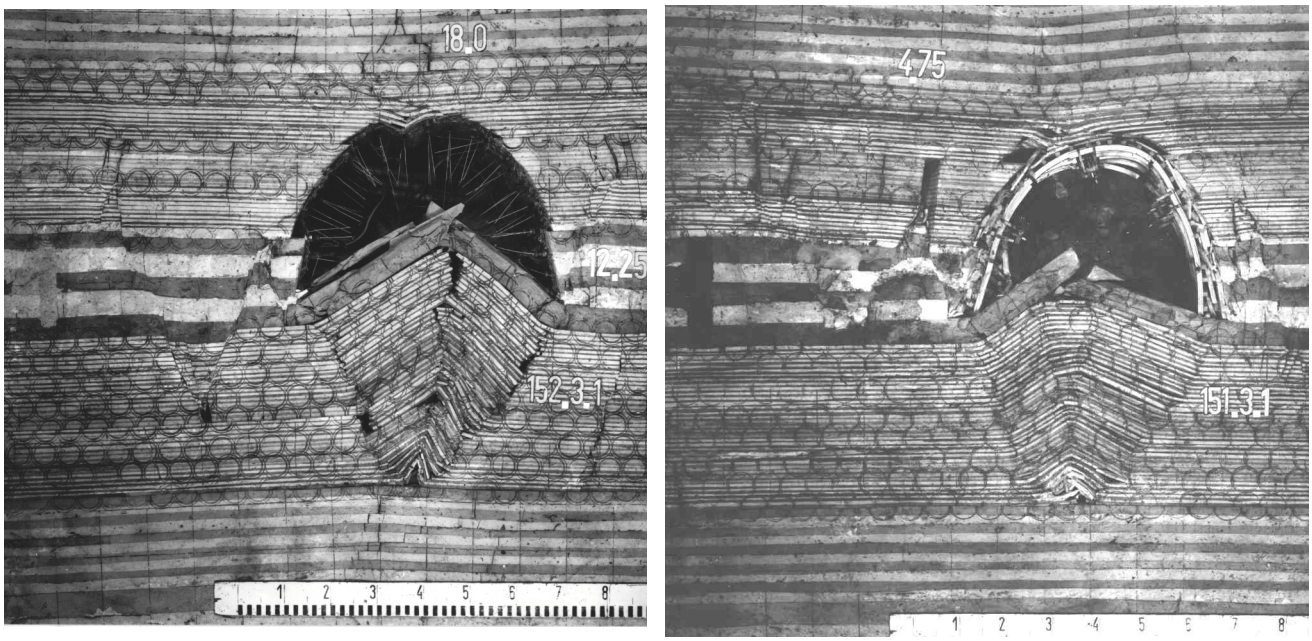

Clearly, there is very broad knowledge available on the EDZ fractures in argillaceous formations in general and on their type, formation mechanism and extent towards the undisturbed far field rock in particular. The example of Figure 2-8 shows the conceptual EDZ structure of a repository tunnel in horizontally bedded Opalinus Clay, currently considered as a repository option in the Zürcher Weinland region of northern Switzerland. It encompasses the following EDZ features:

- Extension fractures in a narrow zone within the tunnel sidewalls;
- disturbed bedding planes (or bedding parallel features) within the buckling planes;
- bounding shear structures around the buckling zones;
- inner shear structures formed within the buckling zone;
- highly disturbed bedding features tangential to the tunnel roof and floor and in the apex of the buckling zone.

Figure 2-8. Schematised EDZ fracture pattern around a conceptual repository tunnel in horizontally bedded Opalinus Clay (Lanyon *et al.* 2005)

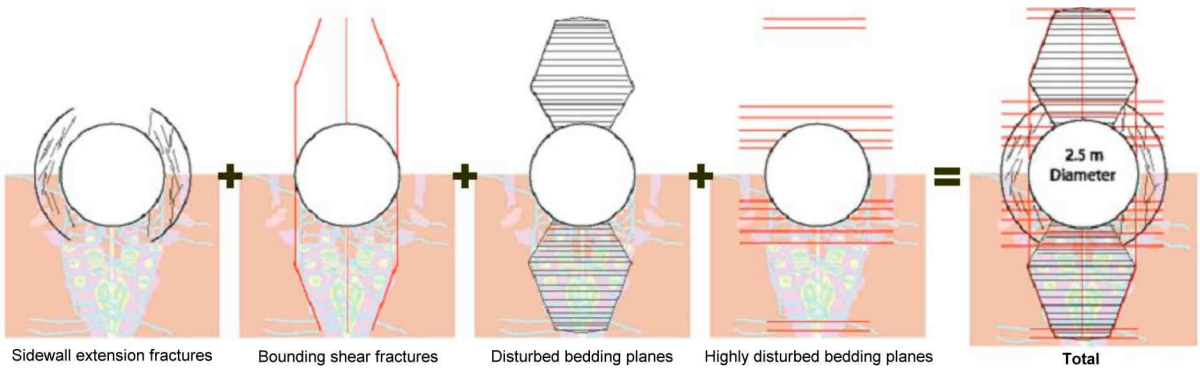

Overall and in the context of the self-sealing topic, the contemporary level of understanding of EDZ structures and processes in argillaceous formations can be considered to be generally sufficient. This also applies to the connectivity of the EDZ fractures along the tunnel axis which is of prime importance for the assessment of fluid transports in repositories.

2.3.4 Mass transport (ref. also to Appendix A.5)

Self-sealing of damaged rock implies that the mass transport property of the rock mass is reduced, eventually approaching that of the undisturbed rock matrix. Essentially, there are two conceptual approaches for the description of mass transport in fractured rock as follows:

1. Porous medium concepts, describing the flow and transport processes in the framework of classical continuum mechanics. The range of applicability of continuum approaches is given by the condition, that a representative elementary volume (REV) must exist, where flow and transport behaviour of the medium is described by homogeneous properties (e.g. effective permeability and porosity of the REV).

2. Discrete approaches, describing the medium as a large system of discrete fractures or channels with homogeneous or heterogeneous flow and transport parameters. The characterisation of a discrete fracture network comprises the fracture geometry (fracture inventory, orientations, fracture frequencies) and the flow and transport properties of the individual fractures (e.g. fracture transmissivity, fracture aperture)

Continuum approaches are commonly used to characterise the flow and transport parameters of undisturbed argillaceous rock. The porosity and intrinsic permeability values of some argillaceous formations in their natural state are summarised in Table 2-7. In this context, it is worth mentioning that much of the water present in argillaceous rock will be adsorbed on the internal and external surfaces of clay minerals, to the degree that it may not be able to participate in advective transport under normally encountered pressure gradients.

Table 2-7. Porosity and intrinsic permeability values of some argillaceous URL sites

Formation (location)	Porosity n [%]	Permeability k [m^2]	Reference
Boom Clay (HADES URF)	36.3	200 to 400 $*$ 10^{-21}	Bernier *et al.* (2004)
Opalinus Clay (Mont Terri URL)	13.7 ± 2.5	$k_{\perp \text{ ss water}}$ $7 * 10^{-21}$ $k_{// \text{ ss water}}$ $20 * 10^{-21}$	Bock (2009)
Callovo-Oxfordian (Bure URL)	12 ± 1	k_{water} 5 to 20 $*$ 10^{-21}	Fouché *et al.* (2004) Boisson (2005)
	14 (carbonate facies) to 19.5 (argillaceous facies)	k_{water} 10^{-19} to 10^{-21}	Zhang and Rothfuchs (2004) Delay *et al.* (2006)

For fractured geo-materials, as is typically the case in the EDZ, the notions of the above continuum concept may be used, however in many applications the discrete fracture network approach is more appropriate. The underlying assumption is that, based on the understanding of the coupled

hydro-mechanical processes of a single fracture, the hydromechanical behaviour of the complex fracture network can be determined (ref. to Section 4.5). In Appendix A.5 it is shown that the hydraulic transmissivity T of a single fracture is proportional to the cube of the hydraulic fracture aperture a_h, if the fracture aperture is greater than its roughness and the flow is laminar:

$$T \sim a_h^{\,3} \qquad \text{(Eq. 2-1)}$$

where: T = hydraulic transmissivity of fracture [m²/s]
a_h = hydraulic fracture aperture [m]

Packer tests were conducted at the Mont Terri URL in boreholes, extending radially from the tunnel wall. Profiles of interval transmissivity were measured along the boreholes. Table 2-8 shows local transmissivity values in various zones of the Opalinus Clay wall of the *Galerie de Secours* at Mont Terri.

Table 2-8. Local transmissivity T in the wall rock of the *Galerie de Secours* at Mont Terri
(after Nagra 2002b)

Distance from gallery wall [m]	Structures observed	Local transmissivity T [m²/s]
0 – 0.70 (max. 1.25)	Network of EDZ fractures (at least partially interconnected); often de-saturated; some with gypsum on fracture surface	10^{-10} to $5 * 10^{-7}$
0.70 – 2.00	in the majority discrete fractures, not interconnected	10^{-12} to 10^{-9}
2.00 – 4.00	no macroscopic fractures	$5 * 10^{-13}$ to 10^{-12}

Within the SELFRAC project (Bernier *et al.* 2004), the influence of the porosity and the discontinuities on the global permeability has been investigated in much detail. Induced fractures along tunnels were characterised in various *in situ* experiments of the HADES and Mont Terri URLs and in laboratory tests (Sections 3.1 and 3.2). It was concluded that fractures and porosity changes due to excavation are now well characterised and quantified as well as their influence on the permeability.

2.3.5 Mineral precipitation and geochemical aspects (ref. also to Appendix A.6)

Precipitation of newly formed minerals in open EDZ fractures is a process which may contribute to a reduction of the fractures' transmissivity thus possibly contributing towards sealing of the formation. Although mineral precipitation can seal tectonically induced fractures (see Appendix A.6), it is not considered to be a process that could substantially contribute to self-sealing over the future time period of interest (1 Ma). This is because repository sites are generally located in tectonically and hydrothermally quiet areas, meaning that the driving forces needed for vein mineralisations are expected not to be present.

The precipitation process of minerals in EDZ fractures depends on the geochemical conditions of the host formation and the physico-chemical evolution of the repository system. The first aspect is discussed in Appendix A.6. With regard to the development of the (geo-) chemical regime of the repository system there exists a considerable number of processes, both short- and long-term, as

indicated in Figure 2-9 for the "French Case" of the Bure URL. The short-term situation is characterised by the repository construction, emplacement operations and monitoring until the closure of the repository and lasts for about 100 years in total.

Figure 2-9. Examples of short- and long-term geochemical evolution of deep geological repositories
("French Case" of the Bure URL after Aranyossy 2005)

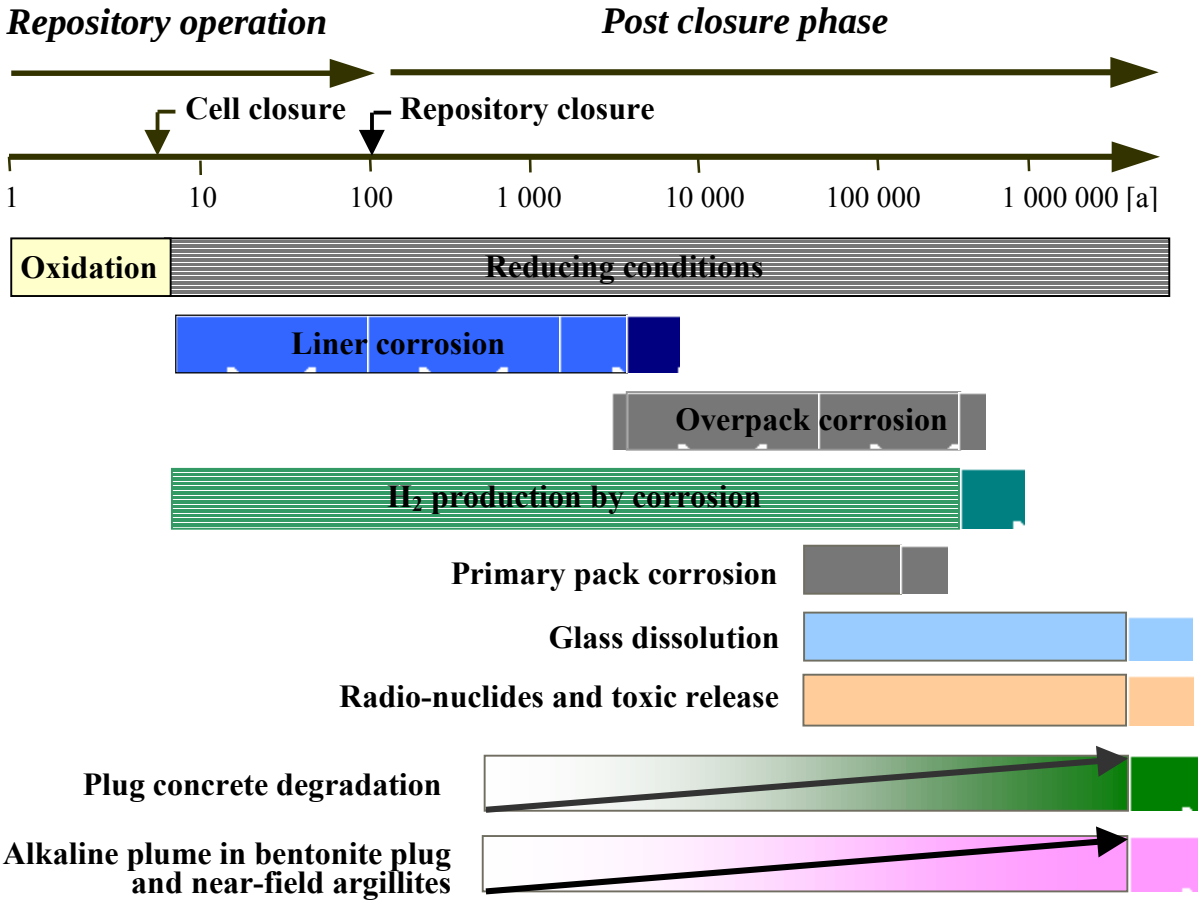

Immediately after the excavation of the emplacement tunnels, there are two principal mechanisms which may lead to changes in the physico-chemical boundary conditions of the excavated rock, as long as the rock is not perfectly sealed by the tunnel lining (Figure 2-10):

(1) oxidation and

(2) desaturation.

The mineralogical changes which are associated with these processes will be considered in Section 4.5.

In long terms beyond the repository closure (e.g. > 100 years), research has, so far, focussed on the problem of interaction between the changing geochemical repository conditions and the matrix of argillaceous materials (e.g. precipitation due to interactions between cementitious fluids and rock; effects from glass corrosion; Nagra 2002b). Investigations on long-term mineral precipitation onto EDZ fracture surfaces are still pending.

Figure 2-10. Mechanisms of chemical weathering in the tunnel wall rock of argillaceous formations (after Oyama and Chigira 1999; from Horseman *et al.* 2004)

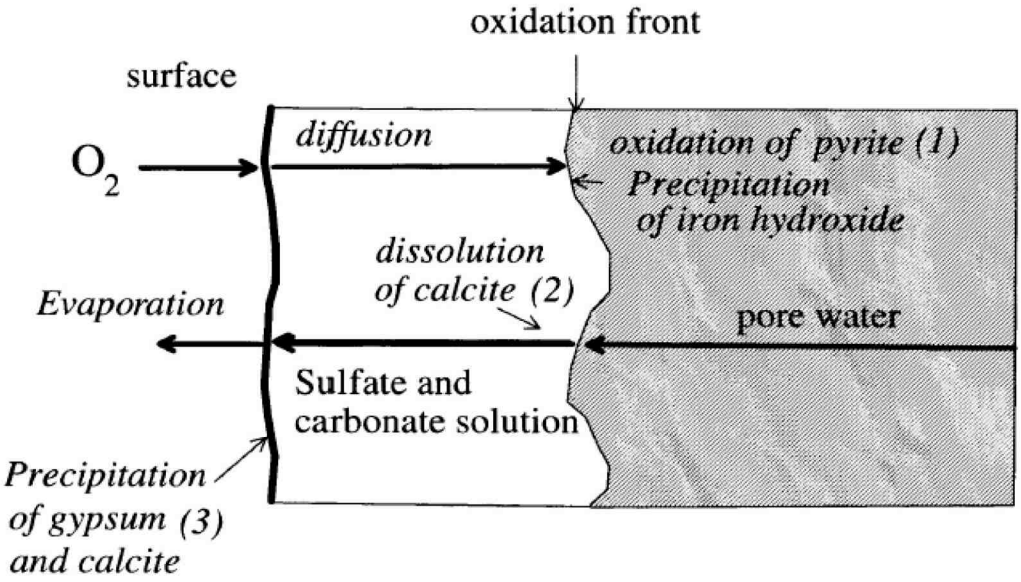

3. EVIDENCE OF SELF-SEALING

The suitability of argillaceous formations as host rock for the disposal of radioactive waste is based principally on its low material permeability and lack of hydraulically-active fractures. Low permeability is intrinsically connected with argillaceous materials as such (Section 4.1). With regard to fractures, it is documented in Appendix A.4 that various types of fractures exist in argillaceous formations. Natural fractures are common in outcrops at the topographic surface and also, but to a lesser degree, at depths usually considered suitable for deep geological repositories. Artificially-induced fractures are generated in connection with the excavation of the repository underground structures. They constitute essential structural elements of the EDZ. The formation of such EDZ fractures cannot completely be avoided by any practical means.

There is considerable direct and indirect evidence that fluid-conductive fractures will, with the passage of time, seal and that such processes of self-sealing are quite common in argillaceous media. As will be outlined in the following sections relevant evidence has been collected in laboratory tests (Section 3.1), URL field tests (Section 3.2) and in studies of geological and geotechnical analogues (Section 3.3).

3.1 Evidence in laboratory tests

3.1.1 Introduction

Table 3-1 compiles laboratory tests and testing conditions under which self-sealing effects have been observed. For the sake of conciseness only some of the most recent tests are presented.

The compilation is structured according to the type of loading and coupled load-permeability test conditions implemented in the test. When including direct evidence from an inspection of tested samples, six such types are distinguished as follows:

1. direct evidence by inspection of tested samples (Section 3.1.2);

2. combined isotropic loading ($\sigma_1 = \sigma_2 = \sigma_3$) and permeability tests (Section 3.1.3);

3. combined triaxial loading ($\sigma_1 > \sigma_2 = \sigma_3$) and permeability tests on hollow cylinders (Section 3.1.4);

4. combined direct shear and permeability tests (Section 3.1.5);

5. recompaction and resaturation in combined triaxial and permeability tests (Section 3.1.6); and

6. experimental discrimination between mechanical closure of fractures by increased normal stress and swelling of the fracture wall material (Section 3.1.7).

Table 3-1. Overview of laboratory tests presented in Section 3.1

Report Section	Reference	Argillaceous formation	Type of fracture	Test condition / test equipment				Permeability test medium			Direction of k	
				isotropic test	triaxial test	direct shear σ_n	direct shear τ	chemical fluid	water	gas	axial	radial
3.1.2	Bernier *et al.* (2004) (SELFRAC); NAGRA (2002b)	Boom OPA	circular hole	direct evidence by inspection of tested sample								
					+			+	+		+	
3.1.3	Bernier *et al.* (2004) (SELFRAC)	OPA Boom	artif. axial	+				+			+	
3.1.4			artif. radial		+				+			+
3.1.5	Gutierreza *et al.* (2000)	K.S.*	natural			+	+		+			+
	Buzzi *et al.* (2007)	Toa**	artificial			+	(+)		+			+
3.1.6	Zhang and Rothfuchs (2008)	COX OPA	artificial natural	+	+			+	+	+	+	+
3.1.7	Davy *et al.* (2007)	COX	artificial	+				+		+	+	

Legend:
* Kimmeridge Shale
** Toarcian argillite and mortar
COX Callovo-Oxfordian argillite
OPA Opalinus Clay
\+ fully applicable
(+) partially applicable

3.1.2 Direct evidence by inspection of test samples

Direct evidence by visualisation of the self-sealing process of fractures and its evolution over time may be gained by repeated microfocus X-ray computer tomography scanning of test samples. Such evidence was collected e.g. by Bernier *et al.* (2004) in connection with the SELFRAC Project on core samples of the Boom Clay and Opalinus Clay. For all Boom Clay samples, the hydraulic conductivity K measured at the end of the tests was comparable to that of the undisturbed clay ($K \sim 10^{-12}$ m/s), and the initial planar fracture was no longer discernible (Figure 3-1).

Figure 3-1. Visualisation of the sealing process of a Boom Clay sample by µCT technique
(a) before and (b) after saturation of the axial fracture. Sample Ø = 38 mm
(from Bernier *et al.* 2004)

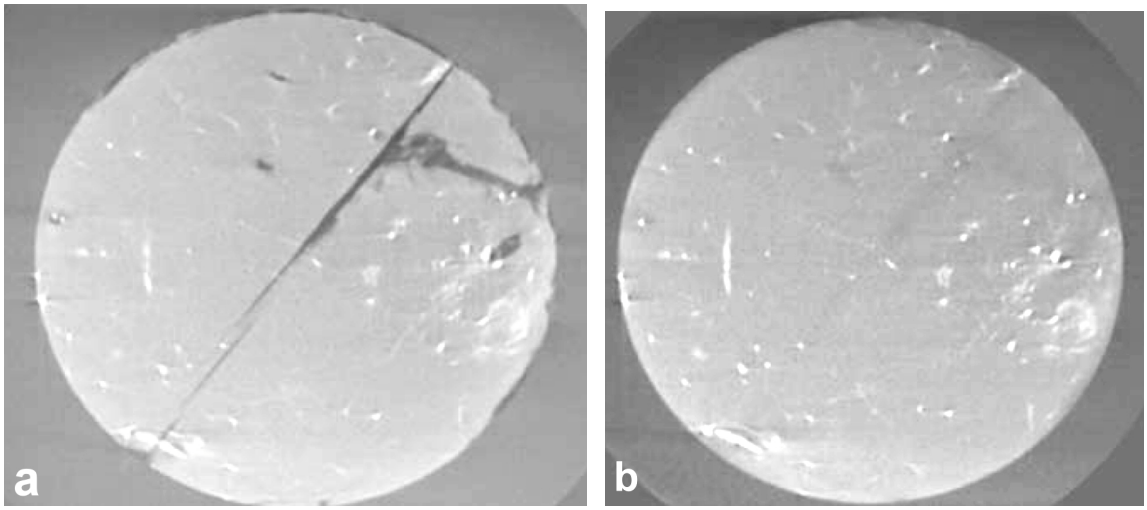

It was found that the chemical composition of the interstitial water has a marked influence on the speed of the sealing process. For Boom Clay the sealing process occurs very quickly following saturation of the system.

Direct evidence might also be gained by inspection of a (dismantled) test specimen after completion of the test. In connection with the SELFRAC Project, for instance, an initial central hole, which was drilled along the axis of a Boom Clay sample, turned out to be completely closed (see Figure 3-3 in Section 3.1.3 below). Similar observations were made in Opalinus Clay, although the sealing process in the indurated Opalinus Clay turned out to be significantly slower than in the plastic Boom Clay. Figure 3-2 (top) shows cross sections of two Opalinus Clay cylindrical core samples, each with a small axial hole in its centre. The samples were subjected to triaxial testing as shown in the bottom sketch of Figure 3-2. Test a (left in Figure 3-2) was carried out with water circulation and Test b (right) without water circulation in the centre bore. Whilst the inner bore of Sample a) collapsed at a confining pressure of 13 MPa, no such collapse was recorded for Sample b), even when subjected to a substantially higher confining pressure of 30 MPa. The test series thus indicates the particular influence of saturation (water uptake) on the closure of a cylindrical void which, from its geometry, might be considered an extreme form of an open fracture (see also Table 5-1 on p. 159).

More quantitative evidence is gained in laboratory tests in which the *change* of the permeability of a fractured argillaceous sample is systematically monitored in dependency of certain control parameters. A decrease in the permeability of the sample is then taken as evidence of some self-sealing effects. Control parameters which are commonly employed are the pressure level applied to the external surface of the fractured sample (usually in the form of a confining pressure p_c), the type of fluid used in the permeability test (gas or water), the chemical composition of the fluid (e.g. nitrogen; argon; artificial formation water) and environmental factors such as temperature, relative humidity and atmospheric pressure level.

Figure 3-2. Cross sections of two Opalinus Clay core samples with a small inner borehole
Closure of the inner borehole was observed were the axis was about parallel to bedding
(from Nagra 2002b)

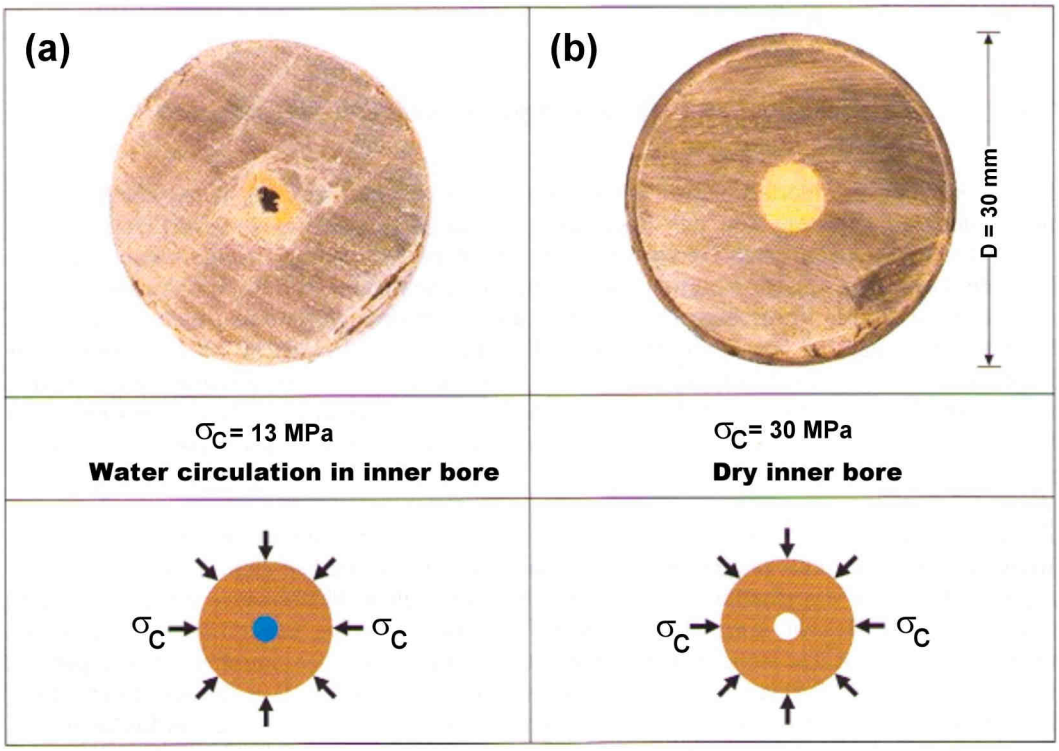

3.1.3 Combined isotropic loading ($\sigma_1 = \sigma_2 = \sigma_3$) and permeability tests

Combined isotropic load and permeameter tests were performed by SCK.CEN in context with the SELFRAC Project (Bernier *et al.* 2004). The main objectives of the isotropic laboratory tests were as follows:

- assessing the permeability change of single-fractured samples of Boom Clay and Opalinus Clay in dependency of the geometry and dimension of the fracture and of the isotropic stress level;
- establishing the influence of the chemical composition of the permeability test fluid onto the sealing behaviour of the clay sample; and
- employing the micro-focus X-ray computer tomography technique for direct observation of the sealing process.

Prior to the installation of the cylindrical samples in a permeameter cell, a small central hole was drilled along the axis of each sample. The sample was then split creating a discrete extensional fracture along its entire axis. The isotropic tests consisted in testing combined mechanical and chemical sealing effects. The sample was subjected to an increasing isotropic pressure whilst the

evolution of the hydraulic conductivity was monitored by applying a hydraulic gradient in axial direction. Throughout the test the mean porewater pressure and mean effective stress were kept in balance. The influence of the injected fluid chemistry on the self-sealing capacity of the clay was especially tested. Micro-focus X-ray computer tomography (μCT) was used as an imaging technique to visualise the sealing process of the fracture (see previous Figure 3-1). As a result, self-sealing phenomena have been clearly observed both in the Boom Clay and Opalinus Clay.

It was generally found that the chemical composition of the interstitial water had a marked influence on the speed of the sealing process. The tested fluids led to different sealing rates and to different cohesion levels. The use of an alkaline fluid was favourable for both parameters. For the Opalinus Clay the difference between the various fluids tested was rather small. The hydraulic conductivity measured at the end of the tests varied between $2 * 10^{-12}$ m/s for the low-salinity artificial formation water and around $6 * 10^{-12}$ m/s for the same solution saturated with Calcium hydroxide. A slower evolution towards the final value was observed for the high-salinity artificial formation water.

After releasing the isotropic pressure and dismantling the Boom Clay samples, the central hole was found to be completely closed. However, a fissured central zone with a lowered density could still be observed. The extent of that zone was clearly dependent on the original hole diameter (6 and 12 mm, respectively). Figure 3-3 shows two images of a slice at mid-height of a Boom Clay sample after dismantling from the isotropic cell. The left image averages the clay matrix without highlighting the fractures. The initial central hole of 12 mm diameter is indicated by a white dashed circle. It can be depicted that a low-density, eye-shaped zone (black spots) has developed around the original hole with a preferred orientation parallel to bedding. The right image shows the same slice but with superimposed fractures (in white) occurring in the sample. It is apparent that the fractures are confined to the low-density, eye-shaped central zone.

Figure 3-3. Cut of a Boom Clay sample at mid height after isotropic pressurisation
(from Bernier *et al.* 2004)
Left: Density image (dashed circle: Contour of the initial central axial hole).
Right: With fractures (white) superimposed.
Note the alignment of the density and fracture image zones along bedding (~ horizontal in the picture).

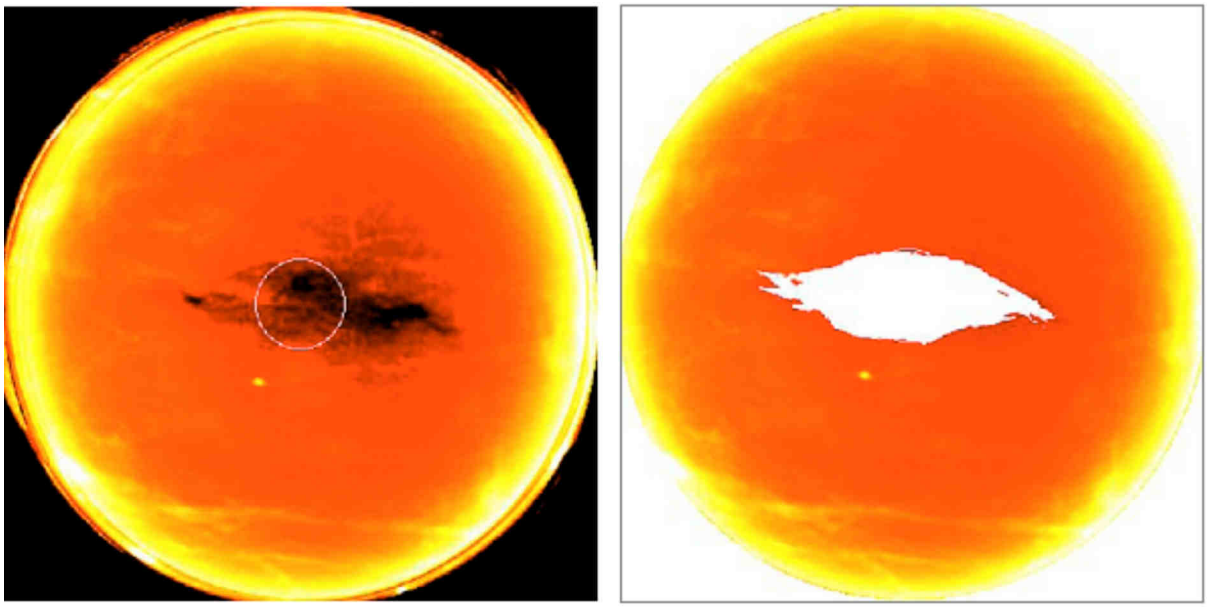

For the Opalinus Clay, the sample with the smallest internal hole diameter (2 mm) showed evidence of self-sealing. However, as for the permeameter tests, the intrinsic hydraulic conductivity value of the undisturbed rock was not reached within the testing time of about 6 months. Obviously, the self-sealing process in the indurated Opalinus Clay is significantly slower than in the plastic Boom Clay.

In total, the combined isotropic load and permeability tests revealed that, for the plastic Boom Clay as well as for the indurated Opalinus Clay, there is a clear tendency toward fracture sealing. The composition of the interstitial water chemistry has a marked influence on the speed of the sealing process. The micro-focus X-ray computer tomography (μCT) is a useful imaging technique for visualisation of the sealing process.

3.1.4 Combined triaxial loading ($\sigma_1 > \sigma_2 = \sigma_3$) and permeability tests on hollow cylinders [8]

Tests were performed by LMR-EPFL (Laboratoire Mécanique des Roches - Ecole Polytechnique Fédérale de Lausanne) in a specially designed triaxial cells (Type LEGEP; acronym for Laboratoire de Géotechnique) on hollow cylindrical Boom Clay and Opalinus Clay samples (Figure 3-4). A radial flow was generated in the sample by imposing a constant pressure difference between the outer cylinder mantle and the inner bore.

Figure 3-4. Modified LEGEP testing device
(from Bernier *et al.* 2004)

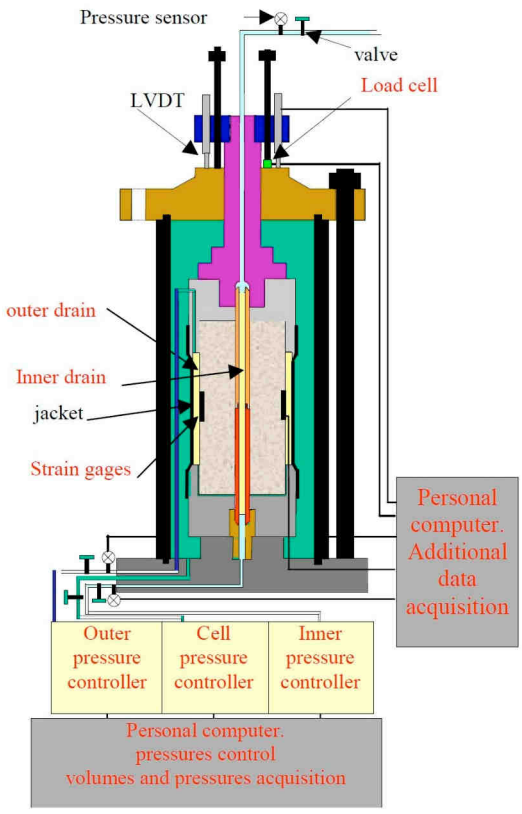

The experimental challenge of the tests was to generate, in a well controlled manner, fractures in the sample and to quantify the associated permeability changes without removing the sample from the LEGEP cell. The testing procedure consisted of three steps as follows:

1. undisturbed sample: permeability measurement by means of a radial fluid flow in the sample, both convergent (from outside towards the inner bore) and divergent (*vice versa*);
2. creation of a discrete extension fracture across the axis of the sample by lowering the effective axial stress ($\sigma_{axial}' = \sigma_3' \rightarrow 0$ at a mantle pressure $p_c = \sigma_1 = \sigma_2 > \sigma_3'$) and radial permeability measurement just after fracturing of the sample; and
3. from time to time, further permeability measurements under constant confining pressure.

[8] There are also laboratory tests on unfractured intact cylinder samples on both Boom Clay and Opalinus Clay, indicating the permeability evolution during consolidation and shearing and thus the relationship between permeability and effective stress (porosity) (SELFRAC Project; Bernier *et al.* 2004).

Step 2 permits measuring the increase of permeability which is related to localised crack generation, whilst Step 3 enables the checking of the potential sealing capability of the tested clays.

For the Boom Clay six such tests were carried out as part of the SELFRAC Project (Bernier *et al.* 2004). The first test was not completely successful as no tensile fracture occurred in the sample. Nevertheless, the hydraulic conductivity measurements (4.3 to 4.4 $*$ 10^{-12} m/s) of this test were quite interesting because no change in the hydraulic conductivity was observed, even under an axial extensional deformation of up to 10% and a very clear development of shear bands in the sample. This result is in line with earlier observations made by the Laboratoire 3S (Sols, Solides, Structures), Grenoble, France, on Boom Clay samples in triaxial compression tests. After adaptation of the testing procedure, the further five Boom Clay tests were entirely successful with the creation of discrete tensile fractures across the sample axis.

The following conclusions can be drawn from the tests:

- The laboratory measurements of the hydraulic conductivity on intact samples range from about 2.3 $*$ 10^{-12} to 4.1 $*$ 10^{-12} m/s and are in excellent agreement with values usually reported in literature (2 to 4 $*$ 10^{-12} m/s);

- as soon as the tensile fracture arises in the sample (after 0.5 to 1% of deformation), a huge increase in flow (several orders of magnitude) is observed;

- once the induced fracture is closed and subjected to a certain normal stress level, the hydraulic conductivity measured a few days after fracturing is found to be similar to that measured in unfractured samples.

The test indicate that fractures in Boom Clay can become very quickly sealed when subjected to an almost hydrostatic stress state close to that prevailing *in situ* (~4.5 MPa total stress). After the removal of the samples from the triaxial permeameter cell, the fractures were hardly discernible. A small amount of pull was required to reopen the fractures. This points to some (unfortunately not yet quantified) healing effects.

For the Opalinus Clay three samples (Sample A, B and D) of the sandy facies from the Mont Terri URL were investigated as part of the SELFRAC Project, commencing in early 2004. Owing to the extremely low hydraulic conductivity of the undisturbed Opalinus Clay (in the order of 10^{-13} m/s; see Table 4-1), very long testing times were experienced. A small sealing effect was noted some two months after sample fracturing and the tests were carried on till the end of the SELFRAC project and lasted for more than ten months. The following conclusions can be drawn (refer to Figure 3-5):

- the hydraulic conductivity values for virgin samples measured in the laboratory tests are within the same order of magnitude as those derived from *in situ* experiments (water inflows in boreholes, hydraulic testing) carried out in the Mont Terri URL. They amount to about 3 $*$ 10^{-13} m/s for flows parallel to the bedding planes within undisturbed Opalinus Clay of the sandy facies;

- after extension fracturing of the sample, flow increased by about 4 to 5 orders of magnitude. The hydraulic conductivity, derived from the flow measurements just after fracturing, amounted to between 2 $*$ 10^{-9} and 1 $*$ 10^{-8} m/s. This range is rather consistent with hydraulic conductivity values in the EDZ of the Mont Terri URL which have been derived from a number of experiments with differing concepts and instrumentation. Martin and Lanyon (2002), for instance, reported conductivity values of the order of

10^{-8} to 10^{-7} m/s for the sidewall rocks and of about 10^{-10} m/s for the rocks in the invert and roof; and

- the development of the hydraulic conductivity with time under constant confining pressure is marked by a decrease of about one order of magnitude some eight months after fracturing (Figure 3-5). This rate is similar (a bit slower) to that measured in the EH-1 *in situ* test at Mont Terri (ref. to Section 3.2.2).

Figure 3-5. Evolution of the hydraulic conductivity of fractured Opalinus Clay samples with time (from Bernier *et al.* 2004)

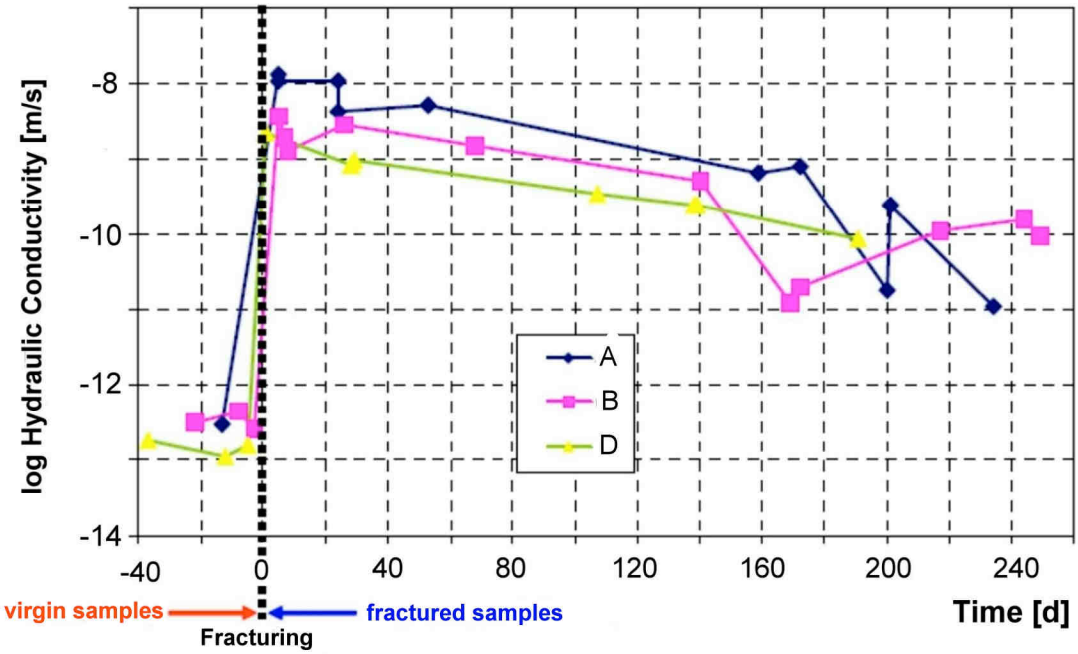

In total, the permeability tests of triaxially loaded fractured hollow cylindrical samples revealed that, for the plastic Boom Clay as well as for the indurated Opalinus Clay, there is a clear tendency towards fracture sealing, whereas healing is quite limited. For Boom Clay the sealing process occurs very quickly after saturation of the system.

3.1.5 Combined direct shear and permeability tests

The displacement of a discrete fracture in a direct shear test can be sub-divided into two components:

(a) component normal to the fracture plane δ_n, in response to a change of the effective normal stress $\Delta\sigma_n$' (= normal displacement in the sense of an opening or closure of the fracture; equivalent with a change in the fracture aperture), and

(b) component along the fracture plane δ_s, in response to a change of the effective shear stress $\Delta\tau_n$' acting along the plane (= shear displacement; with or without any δ_n, the latter termed dilation / contraction in this context).

Figure 3-6. Direct shear testing device modified for coupled stress-permeability measurements (after Gutierreza *et al.* 2000)
Top: Side view - Bottom: Top view with indication of flow paths from central hole

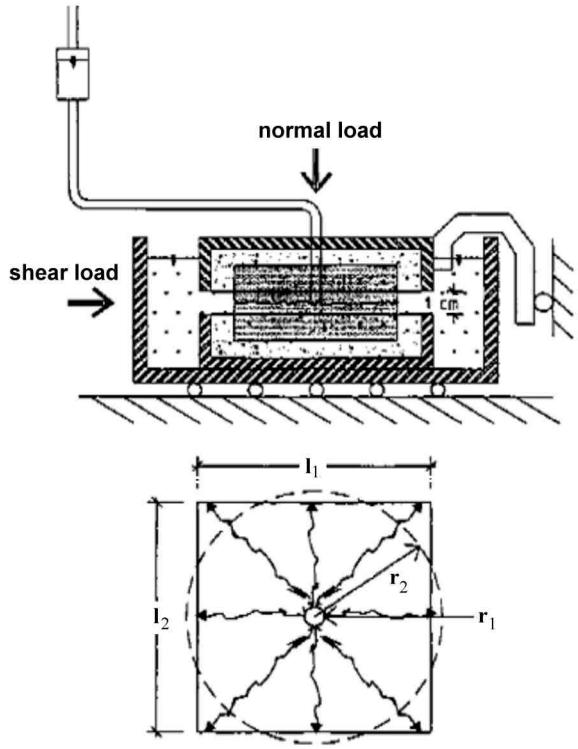

A common testing device which (in contrast to triaxial testing) allows the control of the normal stress σ_n independent of the shear stress τ_n (and *vice versa*) is the direct shear apparatus (top of Figure 3-6). Such a device was used by Gutierreza *et al.* (2000) and Buzzi *et al.* (2007) in coupled stress-permeability tests of argillaceous samples. For permeability measurements, that part of the specimen above the fracture plane was equipped with a small centre hole (∅ of about 2.5 to 3.2 mm). Water was injected into that hole, e.g. at a constant flow rate or at a constant pressure head. The fracture transmissivity was then calculated assuming radial flow from the injection hole (bottom of Figure 3-6).

Table 3-2 provides an overview on the test specifications and presents some of the main results. In the tests of Gutierreza *et al.* (2000) the initial fracture permeability of the four samples tested were in the range 2.7 to 7.2 $* 10^{-10}$ m², showing that the fractures are much more conductive than the intact rock samples which had a permeability of 1.1 $* 10^{-19}$ m².

Table 3-2. Key specifications of coupled stress-permeability direct shear tests carried out by Gutierreza *et al.* (2000) and Buzzi *et al.* (2007)

Reference	Tested rock	Type of fracture	Test sample area [cm²]	Water intake hole ∅ [mm]	Permeability k [m²]		Permeability reduction [order of magnitude]	
					Matrix	Initial fracture	normal load	in shear
Gutierreza *et al.* (2000)	Kimmeridge Shale (Upper Jurassic) of North Sea	natural (re-conditioned if sealed or mineralised)	72.3	3.2	~1.1 x 10^{-19}	2.7 to 7.2 x 10^{-10}	1	~ 6
Buzzi *et al.* (2007)	Toarcian argillite of IRSN Tournemire	mortar / argillite interface with artificial roughness	31.2	2.5	~10^{-20} to 10^{-22}	appr. 10^{-12}	~ 2	not specified

3.1.5.1 Normal displacement behaviour of Kimmeridge Shale fractures

Figure 3-7 shows the variation in fracture permeability measured from the radial flow tests at different levels of constant effective normal stress σ_n' during normal loading and unloading. The shape of the permeability vs. normal stress curve follows closely that of the normal displacement vs. normal stress curve. Even after loading to about σ_n' = 10 MPa, which is about twice the unconfined compressive strength of the intact shale, the normal loading has not fully closed the fracture. The measured fracture permeability of $3 * 10^{-11}$ m² is about one order of magnitude lower than the initial permeability. Even an additional cycle of normal stress loading cannot completely close the fractures.

Figure 3-7. Reduction of the fracture transmissivity (normalised) with increasing normal effective stress σ_n' acting onto the fracture (data from Gutierreza *et al.* 2000)

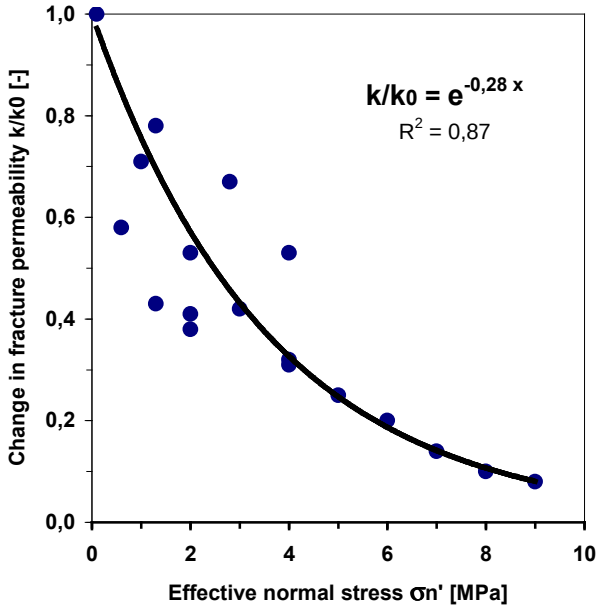

3.1.5.2 Shear displacement behaviour of Kimmeridge Shale fractures

Figure 3-8 (left) shows the results of the shear loading under four different levels of constant effective normal stress σ_n'. Each test shows an almost linear initial portion, followed by a non-linear portion leading to a well-defined peak. All curves exhibit post-peak strain softening. The peak shear stresses for the four samples occurred after the sample had been sheared by about 1 mm of shear displacement. Residual shear stress is clearly obtained in tests under constant normal stresses of σ_n' = 1 and 2 MPa, as indicated by the almost constant shear stress with increasing shear deformation.

Figure 3-8 (right) shows the measured shear-induced normal displacements δ_n (dilation / contraction; displacement component normal to the fracture plane) for the same tests. Dilation (= negative values; see sign convention in Section 2.1) is obtained for the tests at σ_n'= 1 and 2 MPa, while positive values (= contraction) is obtained for the other two tests, except for the initial portion of the test at σ_n' = 4 MPa. Dilation can be attributed to the opening of the fracture, as the fracture surfaces ride on top of the fracture asperities, whilst contraction can be attributed to grinding of the asperities and local gouging.

Figure 3-8. Shear stress (left) and dilation (right) against shear displacement for Kimmeridge Shale at various levels of normal effective stress σ_n' (from Gutierreza *et al.* 2000)[9]

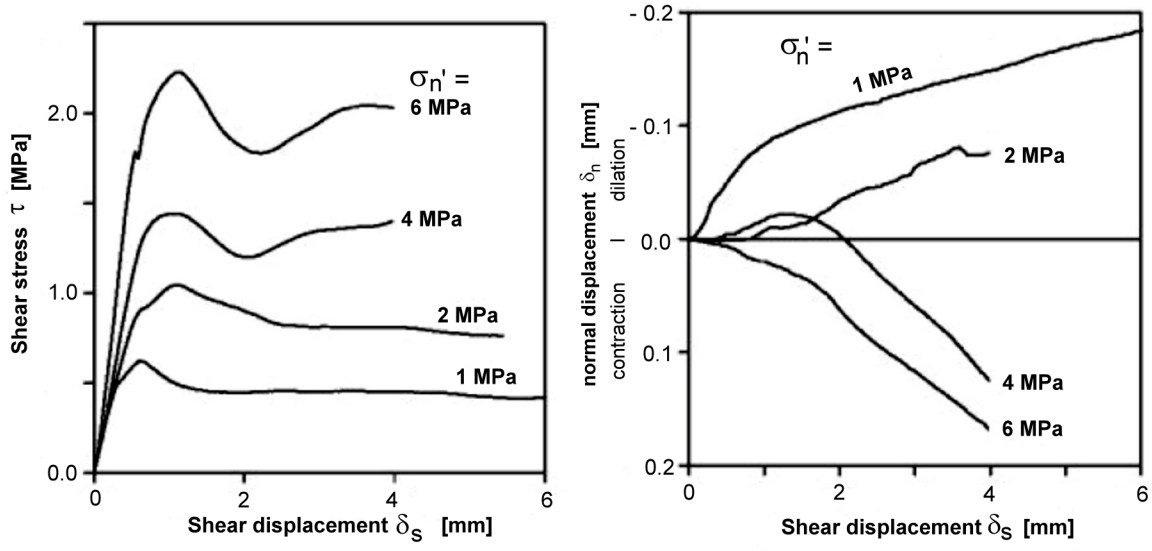

Figure 3-9. Permeability change due to shearing of Kimmeridge Shale, plotted against normal effective stress σ_n' (data from Gutierreza *et al.* 2000)

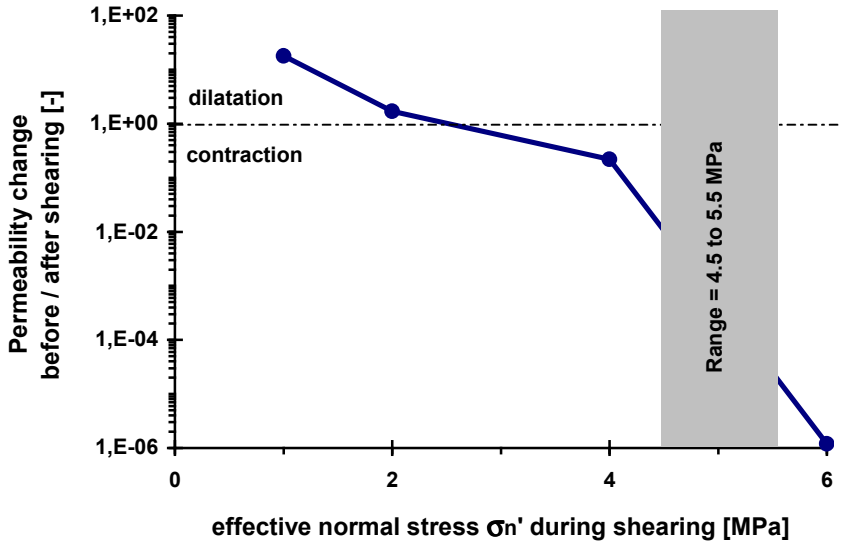

The change in fracture permeability, expressed as a ratio of the permeabilities measured after and before shearing, is shown in Figure 3-9 against the effective normal stress σ_n' applied in the shear test. A permeability increase was observed for the tests at σ_n'= 1 and 2 MPa, with a factor of 10 increase in permeability for the test at σ_n' = 1 MPa. For the other two tests, which had normal stresses

[9] Similar tests were also carried out by Popp and Salzer (2007) for the Opalinus Clay yielding comparable results.

close to or higher than the unconfined compressive strength of the intact rock, reductions in fracture permeability were obtained due to fracture contraction. For the test at σ_n' = 6 MPa, the fracture permeability after shearing was about six orders of magnitude lower than before shearing. This reduction in permeability could be attributed not only to the mechanical closure of the fracture, but also to gouge formation and re-worked particles blocking the fracture apertures. It is worth noting that, despite this significant permeability reduction, the fracture permeability of $9.7 * 10^{-17}$ m² of the Kimmeridge Shale fracture still is about three orders of magnitude higher than the matrix permeability of $1.1 * 10^{-19}$ m². This indicates that, for the tested material, shearing a fracture to its residual shear strength will not completely close the fracture (Gutierreza *et al.* 2000).

3.1.5.3 Displacement behaviour of mortar/Toarcian argillite interface

Buzzi *et al.* (2007) reported on hydro-mechanical direct shear tests on interfaces between Toarcian argillites and mortar. The prime purpose of the tests were the study of the behaviour of the contact zone between an argillaceous host rock and a concrete bulkhead within an underground repository. However, the tests also shed some light onto the fracture self-sealing problem.

To enhance the reproducibility of the tests an artificial roughness pattern of the contact plane was established in each test (Figure 3-10). The upper and lower parts of the samples were assembled either well aligned (i.e. without an initial lateral displacement) or de-aligned (with a certain amount of initial lateral off-set).

Figure 3-10. Top view onto artificial roughness pattern of the Toarcian argillite surface
Depth and width of the grooves:1 mm – ∅ of the sample: 63 mm
(from Buzzi *et al.* 2007; reprinted with permission from Elsevier)

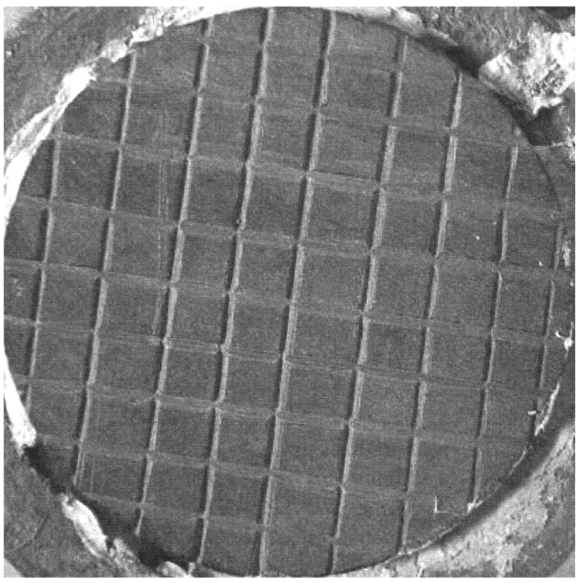

Figure 3-11 (left) shows the response of the (aligned or de-aligned) samples when applying an effective normal stress σ_n' to the contact plane. Generally, there is a decrease in the fracture transmissivity of about one to maximally three orders of magnitude for σ_n' ≤ 21 MPa. It can be further depicted that the samples, which were subjected to an initial lateral (= shear) displacement, show a

higher normal stiffness, which means that a greater normal stress σ_n' is required to obtain the same decrease of the transmissivity than with the well-aligned samples.

The increase of σ_n' and the associated decrease of the relative normal displacement is connected with a decrease of the fracture aperture a_h (Figure 3-11, right). For well-matched samples, this decrease is large at the beginning of the compression but the aperture tends to converge towards a finite (non-zero) value as compression is increased. The change in the hydraulic aperture seems to be more regular for the mismatched samples (hatched curves in Figure 3-11) than for the matched samples (continuous curves).

Figure 3-11. Dependency between hydraulic transmissivity and effective normal stress (left) and hydraulic aperture and relative normal displacement (right)
(from Buzzi *et al.* 2007)

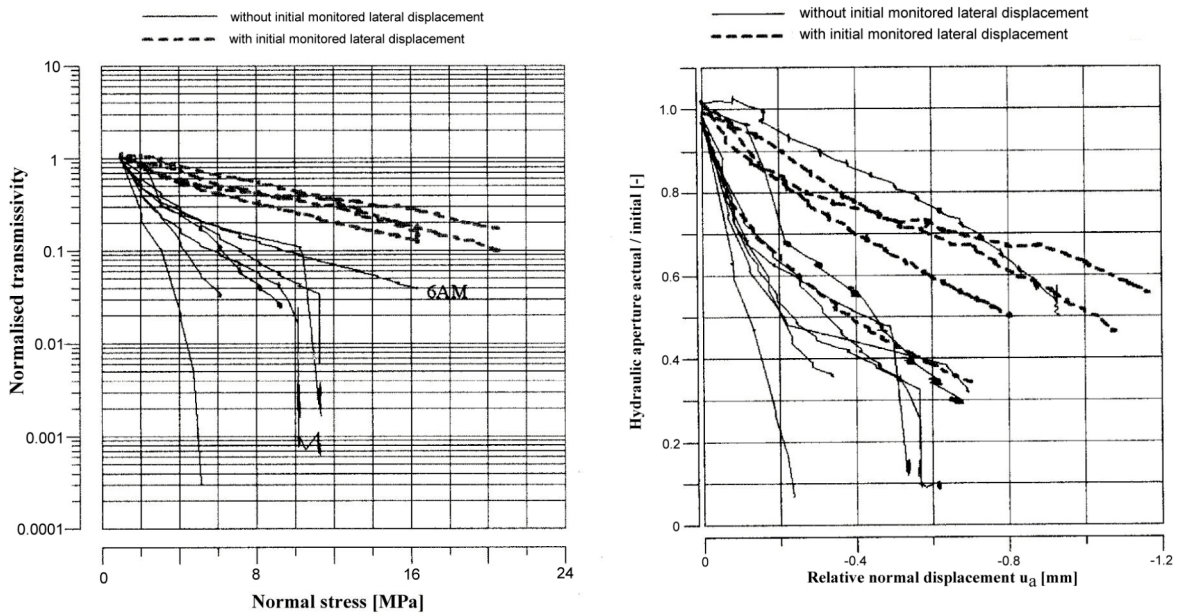

Note: Ordinate of figure left: Transmissivity normalised to its initial value before fracture compaction

3.1.6 Recompaction and resaturation in combined triaxial and permeability tests

Zhang and Rothfuchs (2008) carried out various damage and sealing experiments on core samples from the Callovo-Oxfordian argillite (COX) of the Bure URL and on core samples from the Opalinus Clay (OPA) of the Mont Terri URL. The damage and sealing behaviour was characterised by measuring changes in gas permeability due to recompaction and resaturation under relevant repository conditions.

3.1.6.1 Recompaction tests

The sealing of fractures due to recompaction was examined on strongly damaged COX and OPA samples by permeability measurements under compressive stress. Triaxially tested and shear-fractured COX samples were recompacted in different loading paths, e.g. isotropic loading by

simultaneously increasing axial and radial stress $\sigma_1 = \sigma_2 = \sigma_3$, or deviatoric loading by increasing σ_1 at $\sigma_2 = \sigma_3$ = constant or at σ_1/σ_3-ratios = constant. During reloading, gas permeability k along the sample axis was measured. Figure 3-12 shows the measured permeability values as a function of the applied axial stress and the reloading paths. It is obvious that not only isotropic recompaction, but also deviatoric reloading reduced the permeability significantly.

Generally, the increase of the applied stress of 10 MPa is connected with a permeability decrease of about one to two orders of magnitude.

Figure 3-12. Permeability change of fractured COX samples along various recompaction paths in isotropic and triaxial compression
(from Zhang and Rothfuchs 2008)

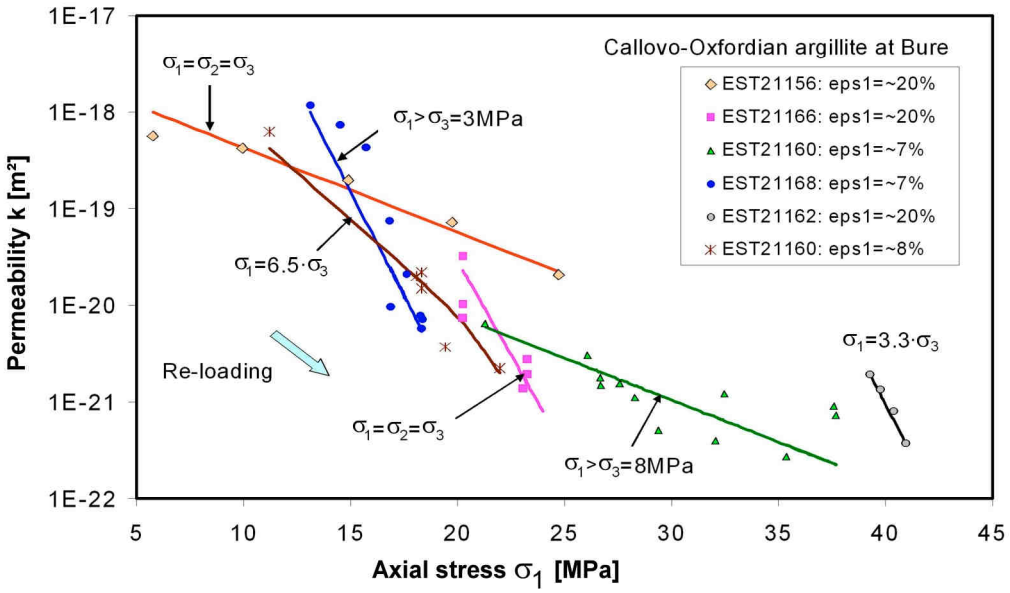

In another test, a large OPA sample (L = 600mm; ∅ = 260mm) from the Mont Terri URL was used (Figure 3-13). As a result of coring and the long time storage without sufficient confinement, the sample was already highly damaged before the test. Along the bedding planes, multiple macro-fractures have developed, some of them prevailing throughout the sample along its axis.

The large-scale sealing test focused on examining the effect of normal stress on gas permeability along the fractures. The fractured sample had an initial permeability of $k = 5 * 10^{-14}$ m^2, which was measured at a radial stress of 3 MPa and an axial stress of 19 MPa. Whilst keeping the axial stress constant, the radial stress was, in a stepwise manner, increased to 18 MPa and the gas permeability along the sample axis measured at an injection pressure of 0.3 to 0.7 MPa. Figure 3-14 shows that the increase in radial stress led to a drastic decrease in the permeability down to about 10^{-19} m^2, which is some five orders of magnitude lower than the initial value. As the radial stress was reduced again to its initial seating level of 3 MPa, the permeability increased to 10^{-16} m^2 which still is two orders of magnitude lower than the initial value.

Figure 3-13. Large fractured sample of the Opalinus Clay from the Mont Terri URL
(Zhang *et al.* 2008)

Figure 3-14. Permeability change of large fractured Opalinus Clay sample as a function of the confining pressure $p_c = \sigma_2 = \sigma_3$ along loading and unloading paths
(Zhang *et al.* 2008)

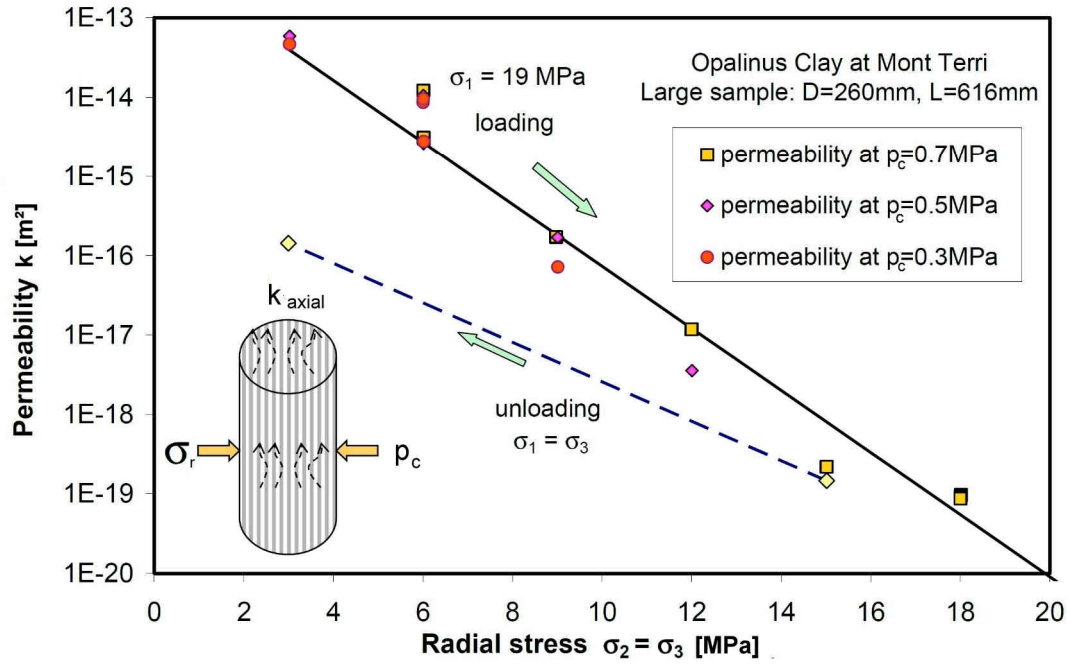

In order to simulate the EDZ conditions around boreholes, an additional sealing test was conducted on a damaged hollow COX sample (L = 103mm; $\varnothing_o$ = 80mm) with a central borehole of $\varnothing_i$ = 20 mm. The gas permeability both in radial and axial direction was examined in dependency of the external confining pressure. The measured data are shown in Figure 3-15 from which the following details can be depicted:

Radial permeability (Figure 3-15 top): Under confining stresses ranging from 2 to 28 MPa, nitrogen gas was injected into the central hole at a pressure of 0.2 MPa. The gas outflow at the outer cylindrical surface was measured thus yielding information on the radial permeability. The initial permeability of the damaged sample at a confining pressure of 2 MPa was $3 * 10^{-16}$ m^2. Increasing the confining pressure to 28 MPa caused an exponential reduction in permeability down to 10^{-21} m^2, which is five orders of magnitude lower than the initial value. The comparatively very high confining pressure of 28 MPa resulted in a pronounced plastic closure of the fractures which is indicated by the much lower permeability values measured along the unloading path. The difference in permeability along the loading and unloading paths is two orders of magnitude and comparable to the large OPA sample (Figure 3-14).

Axial permeability (Figure 3-15 bottom): After measurement of the radial permeability, the central hole and the annular gap between sample and jacket were manually sealed with silicon. Subsequently, the sample was subjected to external confining pressures of up to 26 MPa. The gas permeability test in axial direction was implemented by injecting nitrogen at the top of the sample and measuring its outflow at the bottom. Because of the incompressibility of the silicon material in the hole, the confining pressure lead to a back-pressure at the borehole wall and hence to a recompaction

of the hollow sample. The observed relationship between axial permeability and confining pressure is very similar to that of the radial permeability (comparing top and bottom of Figure 3-15).

Figure 3-15. Permeability reduction of a damaged hollow COX sample in radial (top) and axial (bottom) direction due to isotropic compression $\sigma_1 = \sigma_2 = \sigma_3$
(Zhang *et al.* 2008)

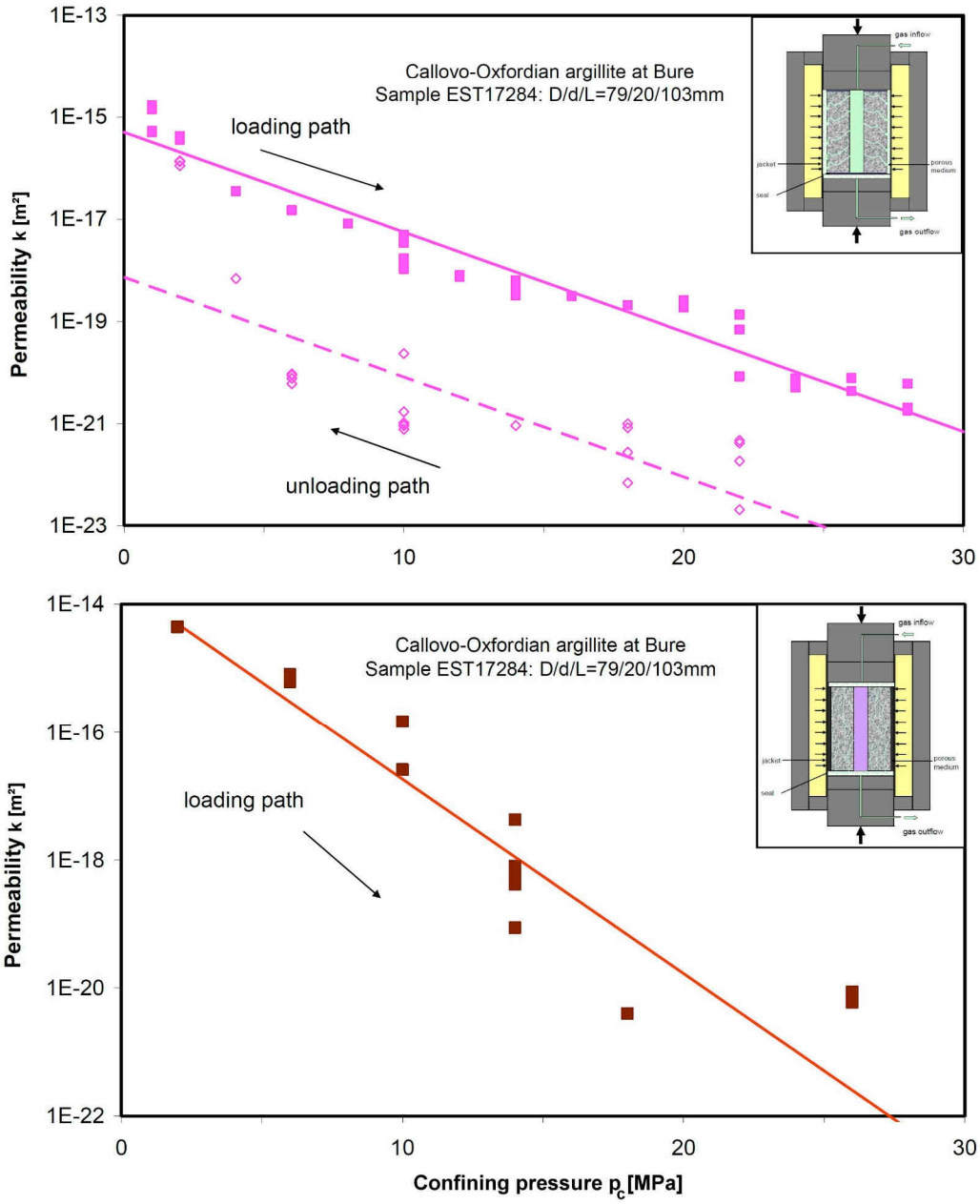

3.1.6.2 Resaturation tests

One of the key factors controlling the sealing behaviour of damaged clay rocks is their swelling potential. Zhang and Rothfuchs (2008) investigated the swelling capacity of the Callovo-Oxfordian argillite (COX) at Bure and of the Opalinus Clay (OPA) at Mont Terri in two free-swelling

tests as shown in Figure 3-16. Initially, the samples were dried over a period of two months at a relative humidity of 23 %. This caused a water loss of about 4.0 to 4.5 % and was associated with a volume reduction of 0.3 % of the COX and 1.5 % of the OPA sample, respectively. In the subsequent resaturation phase, which lasted more than six months at a relative humidity of 100 %, the water content increased to a value of up to 12 % which is about 80 % higher than the natural water content. The water uptake resulted in a progressive volume expansion of up to 8 % of the COX and 11.2 % of the OPA sample. Further expansion could have been expected if wetting would have been continued. The high swelling capacity of the clay rocks was also confirmed in triaxial testing. For instance, in a stress state of σ_1 = 15 MPa and $\sigma_2 = \sigma_3$ = 12 MPa and a water pressure of 4.5 MPa, a COX sample expanded gradually at a rate of ~10^{-10} s^{-1} over the test duration of one month.

Figure 3-16. Shrinking and swelling behaviour of samples from Bure (COX) and Mont Terri (OPA) by exposing the samples to different relative humidity (RH) environment
(Zhang and Rothfuchs 2008)

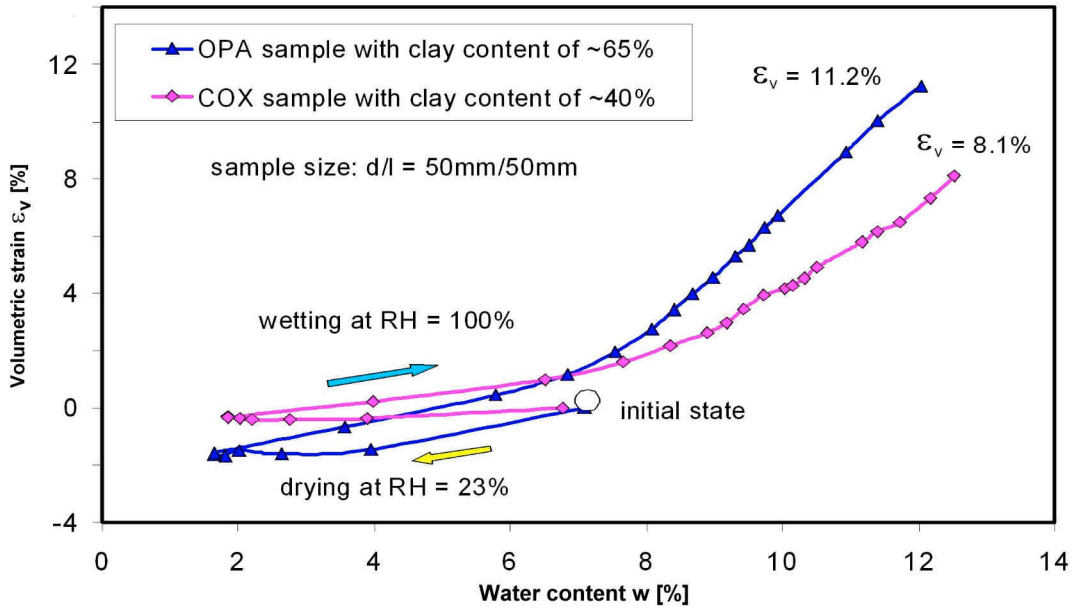

Resaturation-induced sealing was also investigated by gas permeability tests on triaxially loaded damaged COX samples (L = 80 mm; ∅ = 86 mm). Figure 3-17 shows the results of two sealing tests. In a first stage lasting over more than two months, gas permeability was measured in axial direction by injecting nitrogen into the fractured samples at a pressure of 0.75 MPa. The confining pressure of the samples was held constant at $\sigma_2 = \sigma_3$ = 1.5 MPa. A gradual reduction in permeability was observed from a range of $4 * 10^{-16}$ to $9 * 10^{-17}$ m^2 to a range of $1 * 10^{-16}$ to $1 * 10^{-17}$ m^2. This indicates a gradual re-consolidation of the pre-existing fractures (top of Figure 3-17). In a second phase, which lasted over five months, synthetic formation water was injected into the samples at pressures of 1.0 to 1.5 MPa. No water outflow was observed indicating that the injected water was fully consumed by the samples in the resaturation process. Finally, nitrogen was again injected over another period of two months. Throughout this period, very low permeability values in the range of $5 * 10^{-22}$ to $2 * 10^{-21}$ m^2 were recorded (bottom of Figure 3-17). These permeability values are about five orders of magnitude lower than the values before resaturation and are typical for the intact state of the tested samples.

Figure 3-17. Long-term gas permeability tests on damaged samples from Bure (COX) before and after resaturation (Zhang *et al.* 2008)

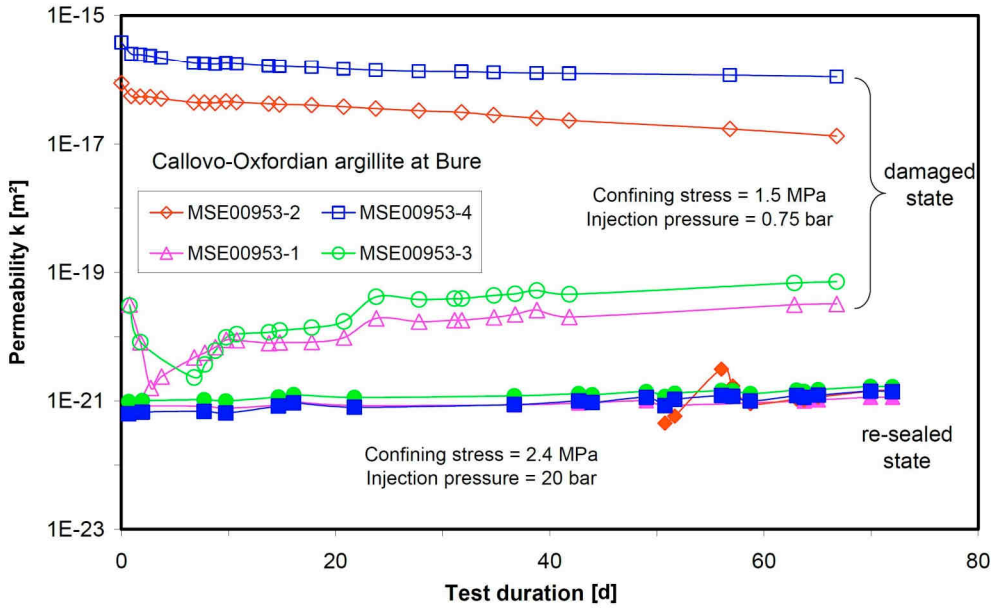

A similar result as for the COX samples was obtained on the large OPA sample shown in Figure 3-13. After a water injection phase of over one month (not shown in Figure 3-18) and at a confining pressure of $\sigma_2 = \sigma_3 = 3$ MPa, nitrogen was injected with an injection pressure, first of 0.5 MPa then of 0.7 MPa, yielding a permeability value of about $1 * 10^{-18}$ m^2 (Figure 3-18). That value is about two orders of magnitude lower than for the state before water injection. An increase of the confining pressure from 3 to 6 MPa reduced the permeability significantly below 10^{-20} m^2, which is equivalent with the permeability of the intact rock.

Figure 3-18. Gas permeability tests of a re-sealed large Opalinus Clay sample after resaturation (after Zhang *et al.* 2008)

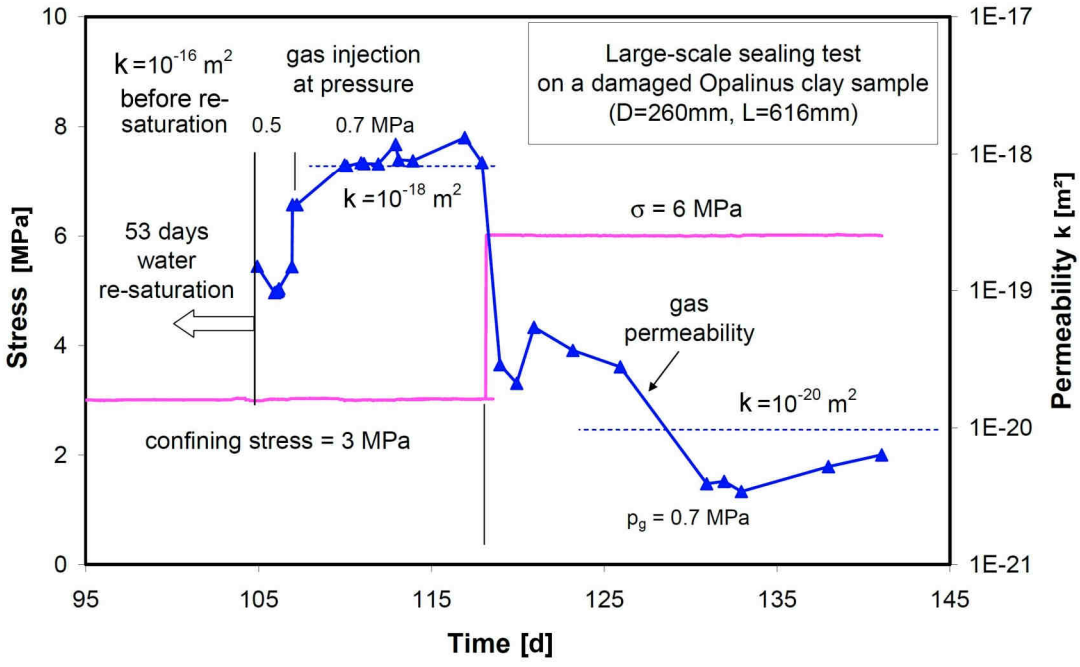

A water injection sealing test was also carried out on the damaged hollow COX sample which was tested earlier on its radial and axial permeability (see Figure 3-15). Under a confining pressure of 2 MPa, synthetic formation water was injected at the sample bottom at a pressure of 1 MPa. Over two months, a volume of about 20 cm^3 water was injected, and no water outflow was observed. From these data, the permeability to water was roughly estimated to be ~10^{-20} m^2 which is in the same order of magnitude as for intact rock. Additionally, that water permeability value is three orders of magnitude lower than the gas permeability of 10^{-17} m^2 which was measured before at the same confining stress. After water injection, nitrogen gas was injected at the opposite side of the sample. Under confining stresses of 2 to 3 MPa, a gas breakthrough pressure of ~1 MPa was recorded, accompanied by a sudden outflow of gas at a permeability of 10^{-15} m^2, similarly to that shown in Figure 3-18. After breaking, however, the gas permeability dropped to 10^{-18} m^2 and remained at that value. This observation suggests that some of the sealed fractures were reopened by the gas pressure and then closed again by swelling and creep deformation of the clay matrix.

As usually observed in argillaceous materials, the permeability to water is still several orders of magnitude lower than the permeability to gas (Figure 3-19). The tests carried out by Davy *et al.* (2007) on other COX samples with artificial macro-cracks (ref. to Section 3.1.7 below) also resulted in water permeability values of 10^{-18} to 10^{-21} m^2 which are two to seven orders of magnitude smaller than the gas permeability.

Figure 3-19. Comparison of transmissivity T to air and water (left) **and hydraulic apertures** (right)
Tests from EZ-A Experiment at Mont Terri (Lanyon 2008)

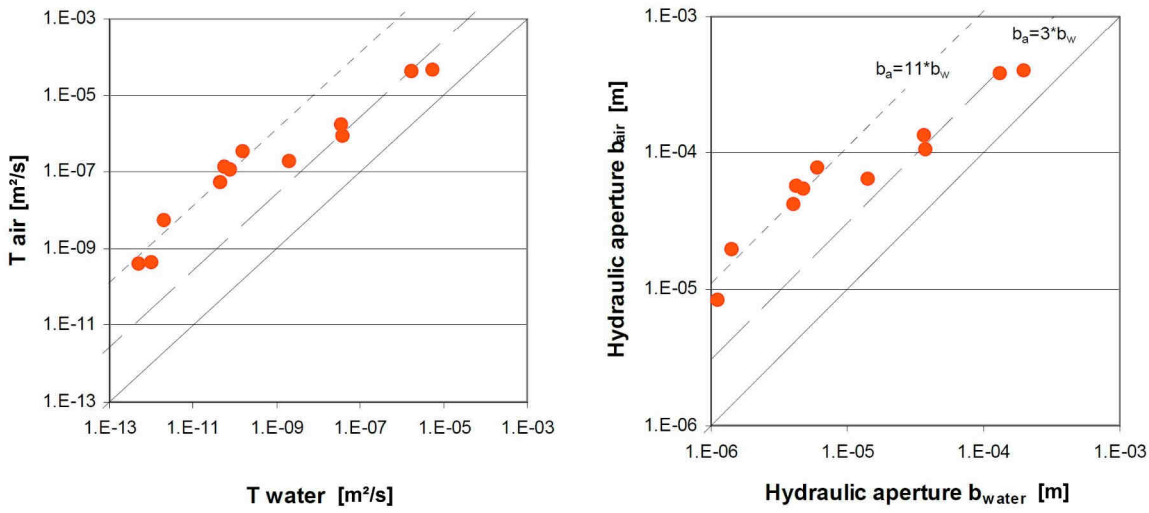

3.1.7 Discrimination between mechanical closure of fractures and swelling of fracture wall material (ref. also to Section A.5.3.2)

Closing of open fractures is highly effective in lowering the overall permeability. From earlier investigations it is known that there are two main factors which contribute for such a closure: (a) increase of the normal stress acting onto the fracture and (b) swelling of the fracture wall material by water uptake.

A new approach to separate the two influencing factors was undertaken by Davy *et al.* (2007). Callovo-Oxfordian argillite core samples of the Bure URL were investigated in the laboratory with the following main characteristics:

- creation of a discrete failure plane by means of a Brazilian test (indirect tensile test → axial splitting of the core sample and formation of an extensional fracture);
- placement of the fractured sample inside a triaxial cell and monitoring of the opening / closing of the fracture aperture by a set of four external LVDT displacement transducers (Figure 3-20); and
- simultaneously to fracture aperture monitoring, carrying out permeability tests in axial sample direction (i. e. along the fracture) whilst systematically varying the following two factors:
  - Variable 1: Confining pressure p_c ranging from 0 to 17 MPa
  - Variable 2: Type of test fluid
    (a) Gas: inert 99% pure Argon (viscosity of $2.2 * 10^{-5}$ Pa s)
    (b) Water: de-mineralised, or added with 1.75 g/l NaCl and 0.014 g/l $CaCO_3$ to simulate formation porewater conditions (viscosity of $1.005 * 10^{-3}$ Pa s)

Figure 3-20. Schematic experimental set-up for measuring the closure/opening of a macro crack in a triaxially confined sample
(from Davy *et al.* 2007)

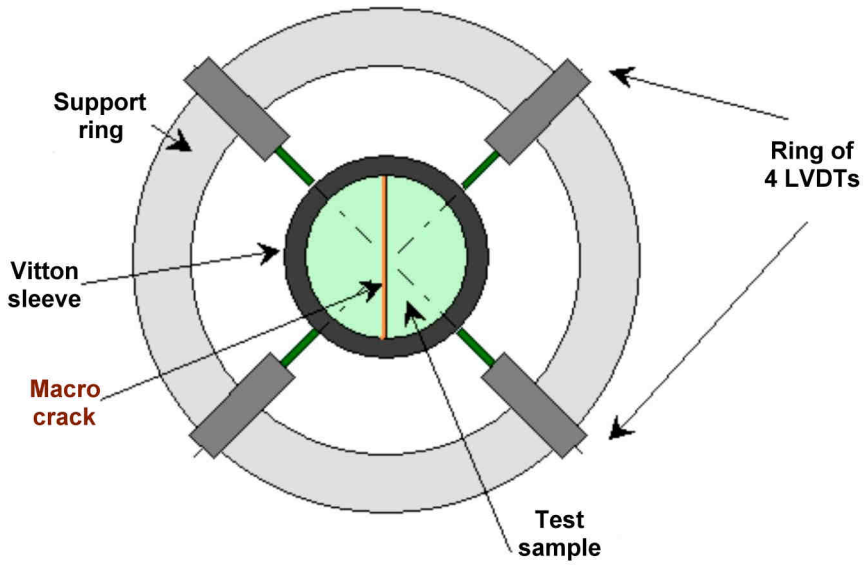

3.1.7.1 Pre-loading and gas injection tests

Figure 3-21 shows the evolution of the confining pressure $p_c \leq 17$ MPa versus the crack closure cc in cyclic loading of three samples. Three successive phases were identified as follows:

(1) first loading phase, lower range (in Sample 1 of up to ~ 3 MPa): p_c grows slowly with cc. This is interpreted as the progressive closing of the macro crack with hardly any squeezing of the asperities;

(2) first loading phase, upper range (in Sample 1 from ~ 3 up to 17 MPa): Stiffening of the crack closure response. This is interpreted as related to the progressive squeezing of the fracture asperities; and

(3) unloading and subsequent loading-unloading cycles: The evolution of p_c versus cc is linear and almost identical in the various cycles. This is interpreted as an elastic response of the crack.

Figure 3-21. Dependency between confining pressure p_c and macro crack closure cc in gas injection tests of three samples
Numbers (1) to (3): Test loading phases (from Davy *et al.* 2007)

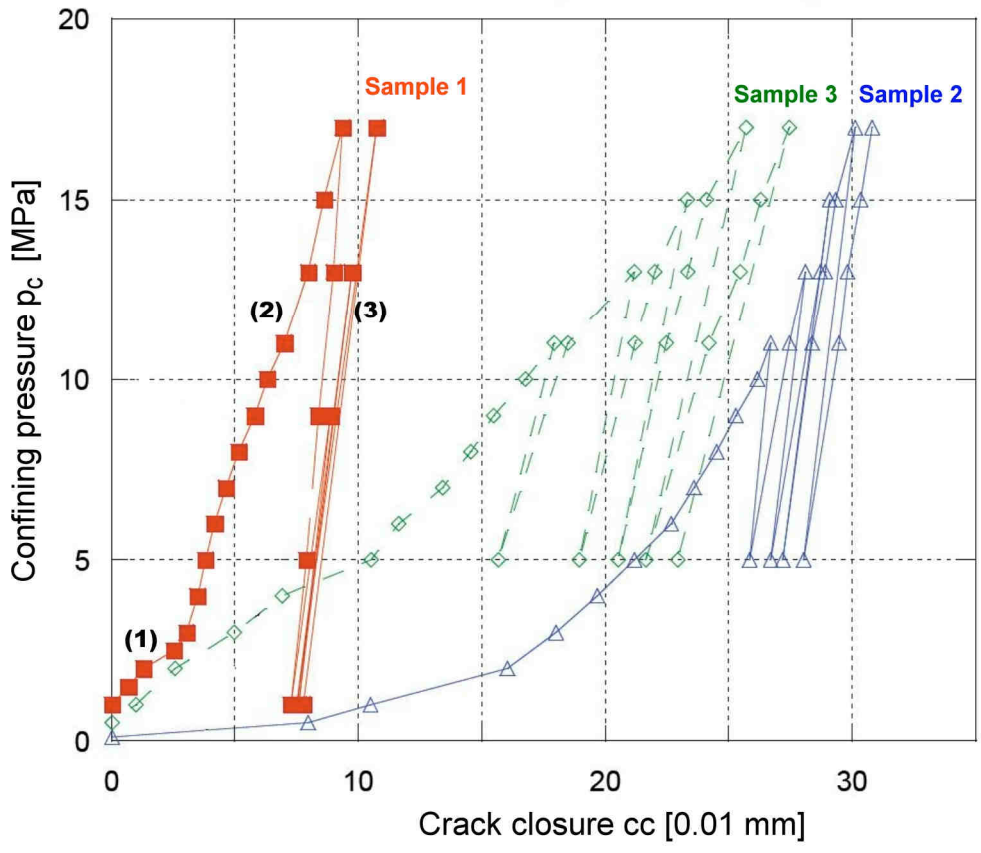

A plot of the measured gas permeability k versus the confining pressure p_c is shown in Figure A.5.2 and repeated here as Figure 3-22. In this diagram, k is normalised to the initial sample

permeability k_0 and the crack closure cc is subtracted from the initial aperture of the crack (cc_0). It can be depicted that, in gas injection tests, there is a common (k/k_0) versus ($cc\text{-}cc_0$) – relationship of the three tested samples, irrespectively of the substantially different initial crack closure amounts as shown in Figure 3-21.

Figure 3-22. Dependency between normalised permeability k/k_0 and macro crack closure variation ($cc\text{-}cc_0$) in gas injection tests of three samples
(from Davy *et al.* 2007)

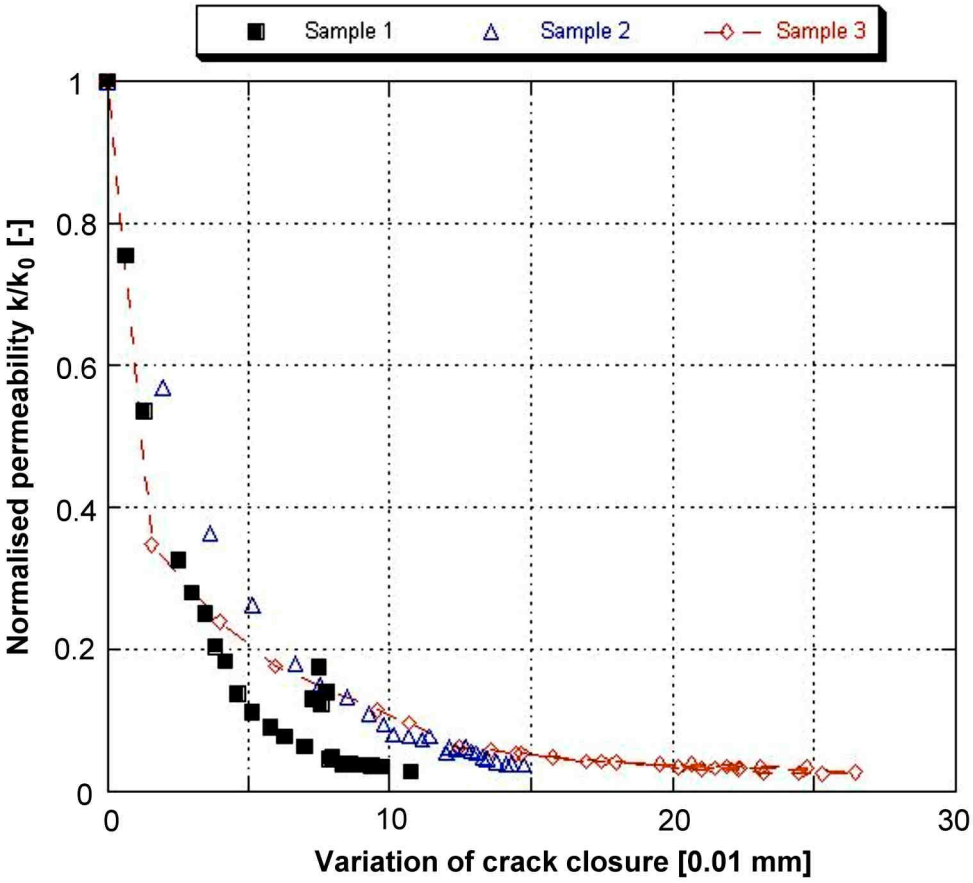

3.1.7.2 Water injection tests

Water permeability tests led to results which are substantially different from those of the gas permeability tests. In comparison with the gas permeability tests, the evolution of the relationship between confining pressure p_c (again of up to 17 MPa) versus the crack closure cc is quite irregular and characteristic of additionally occurring phenomena. As indicated in Figure 3-23 crack closure may become negative (= apparent opening as measured by the LVDTs) when p_c is held constant. Clearly, this phenomenon is due to sample swelling. Swelling may be of two origins: (1) local swelling of the fracture wall material, and/or (2) global swelling of the bulk material. For all tests, visual *a posteriori* inspection of the water permeability samples revealed very limited water penetration into the sample. It therefore could reasonably be assumed that swelling is limited to the macro-cracked fracture zone.

Figure 3-23. Example of a water injection test: Dependency between confining pressure p_c and macro crack closure cc
(from Davy *et al.* 2007)

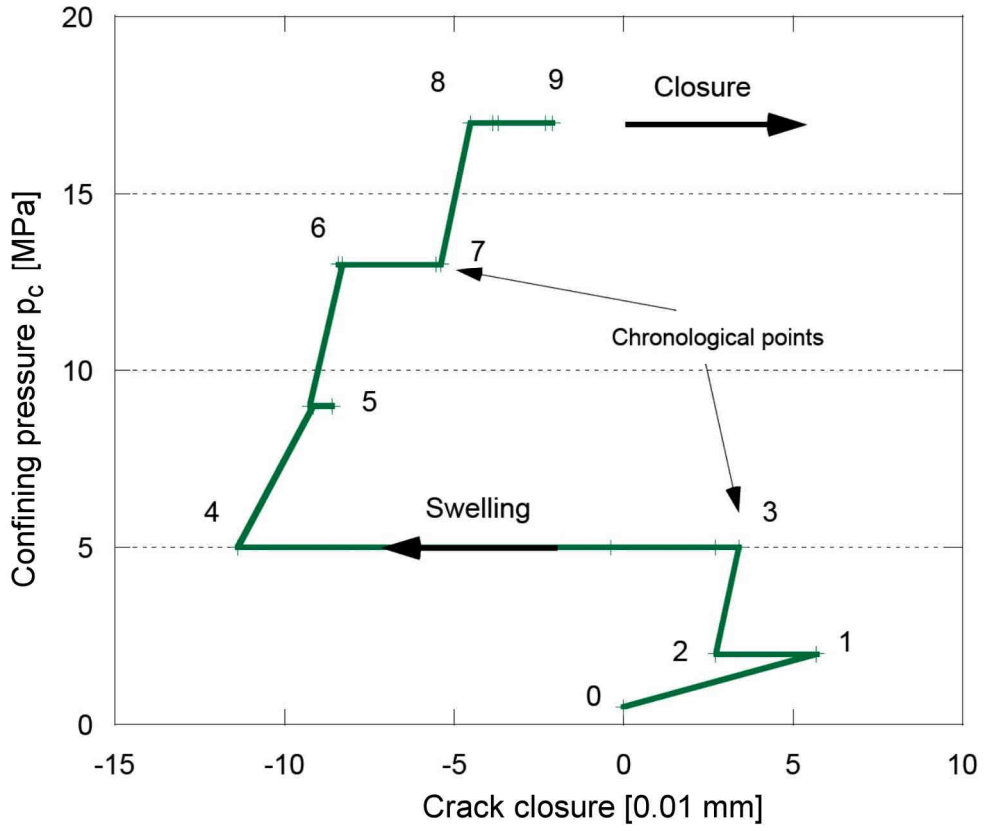

The permeability measured in the water injection tests varies from 10^{-18} to 10^{-21} m². The values are about two to eight orders of magnitude smaller than the values of the gas permeability tests. Comparatively low k-values are obtained after only a few hours of water injection. After an injection period of some two to ten days the water permeability of all four tested samples dropped to values close to the intrinsic bulk permeability of about 10^{-21} m² becoming insensitive to confining pressure variation Δp_c. This means a complete sealing of the macro crack.

3.1.8 Summary of self-sealing evidence in laboratory tests

Table 3-3 summarises the above laboratory tests in which self-sealing has been observed and specifies the order of magnitude of the monitored sealing effects.

Table 3-3. Self-sealing effects in laboratory tests
(summary of quantitative results; for details refer to text)

Report Section	Reference / Institution	Material	Permeability test medium			Monitored change in permeability (self-sealing effect)
			chemical fluid	water	gas	Legend: ↓ = decrease K = hydraulic conductivity [m/s] k = permeability [m²] OoM = Order of magnitude
3.1.3	Bernier *et al.* (2004) (SELFRAC)	OPA Boom	+			K ↓ to ~ intrinsic values: 2 to 6 x 10^{-12} [m/s]
3.1.4	EPF Lausanne			+		K ~ unchanged when sample subject to shear banding (sample extension of up to 10%) Boom: k very quickly ↓ to ~ intrinsic values when subjected to pressure of ~4.5 MPa OPA: saturation: K ↓ 1 OoM over 8 months
3.1.5	Gutierreza *et al.* (2000)	K.S.*		+		K ↓ 1 OoM in normal loading; ~6 OoM in shear
	Buzzi *et al.* (2007)	Toa **		+		K ↓ 2 OoM in normal loading; shear not specified
3.1.6	Zhang and Rothfuchs (2008)	COX OPA	+	+	+	*Recompaction:* COX: k ↓ 1-2 OoM for 10 MPa Large fractured OPA: k ↓ 5 OoM for 18 MPa *Resaturation:* COX: k ↓ 5 OoM in 5 months OPA: k ↓ 2 OoM in 1 month *Gas breakthrough experiment:* OPA: k ↓ 3 OoM in ~1month by Δp=3MPa
3.1.7	Davy *et al.* (2007)	COX	+		+	COX: k ↓ 1-3 OoM Influence of saturation swelling > static loading

Legend: * Kimmeridge Shale
** Toarcian argillite and mortar
COX Callovo-Oxfordian argillite
OPA Opalinus Clay

In summary: When referring to laboratory tests with samples in the millimetre to metre range, self-sealing is a very common process in a wide variety of argillaceous soils and rocks which are currently considered in context with deep geological repositories, from plastic clays (Boom Clay in the HADES URF) to indurated clays (Opalinus Clay from Mont Terri and Callovo-Oxfordian argillites from the Meuse-Haute Marne URL).

3.2 Evidence in URL field tests

3.2.1 Introduction

URL field tests can be considered as a key to confidence building in the performance of argillaceous formations to host long-lived radioactive waste and spent fuel. Scientifically, many URL programmes constitute research right at the forefront of geomechanics and geo-engineering.

The structure, applied for this Section 3.2, reflects the particular importance of the Mont Terri URL in Switzerland, the HADES URF in Belgium and the Bure URL in France in considering the topic of self-sealing in argillaceous formations (Table 3-4). For the sake of conciseness, URLs in non-argillaceous geologic materials, such as granite or rock salt, will not be considered within this report. This is despite the fact that *in situ* experiments in such formations may provide valuable supplementary information (e.g. Martino *et al.* 2007; Wallner at al. 2007).

Table 3-4. Overview of URL field tests presented in Section 3.2

Report Section	URL/URF	Target Formation	Overburden height [m]	*In situ* tests of relevance to self-sealing
3.2.2	Mont Terri, Switzerland	Opalinus Clay (OPA)	~240	EB Engineered barrier experiment EH EDZ self-sealing experiment EZ-A EDZ cut-off experiment SE SELFRAC-I and –II experiments HG-A Gas path through host rock and along seal SE-H Self-sealing with heat (Timodaz) = ongoing
3.2.3	HADES, Mol, Belgium	Boom Clay	230	Oxidation front in mine-by test (Connecting Gallery) Time-dependent hydromechanical response (SELFRAC-III) Collapsing borehole and instrumented core experiments (SELFRAC-IV)
3.2.4	Bure URL, France	Callovo-Oxfordian (COX)	490	KEY EDZ sealing barrier experiment

3.2.2 Mont Terri URL

The Mont Terri URL can be accessed underground from the Reconnaissance Gallery of an existing motorway tunnel. The URL has been sequentially excavated since 1996 (Figure 3-24; refer also to Section A.2.6.4). Most of the tests, of relevance to self-sealing, have been carried out in Gallery 98 (see also Figure 3-30).

Figure 3-24. Excavation stages of the Mont Terri URL (Bossart and Thury 2008)

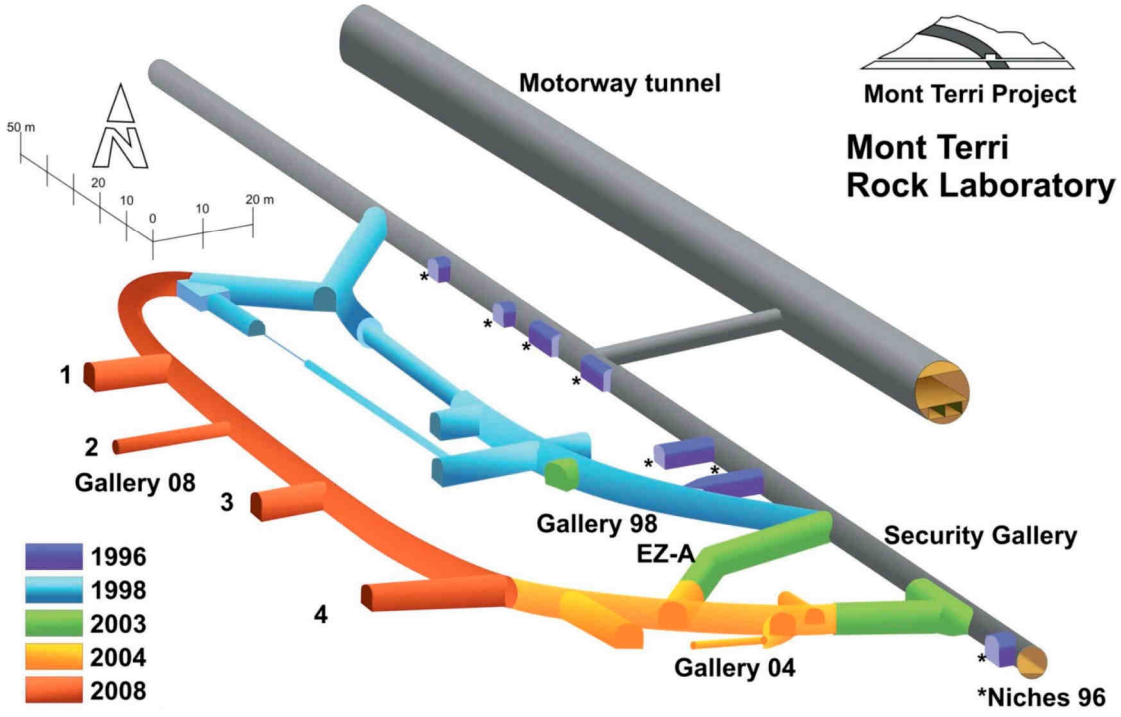

3.2.2.1 Influence of resaturation on the transmissivity of fractures

Early evidence on the influence of resaturation to sealing of fractures was gathered in 1999-2001 in connection with the Gas Frac Self-sealing (GS) Experiment (Enachescu *et al.* 2002). Extensive hydraulic and gas tests were conducted on an artificially created hydrofrac (Daneshy *et al.* 2004). There were strong indications that long-term resaturation of the formation could cause a decrease of the transmissivity to values of approximately $8 * 10^{-13}$ m²/s which is just short of the undisturbed formation transmissivity of $4 * 10^{-13}$ m²/s. While the GS experiment concentrated on a single fracture where effective stress and fracture aperture could be controlled, other experiments focussed on the EDZ and the associated fracture network. The influence of resaturation on fracture transmissivity was investigated in the EH Experiment (Meier *et al.* 2002; review by Armand *et al.* 2008) and also within the EB (Engineered Barrier) Experiment (Alheid *et al.* 2004).

The EH Experiment explicitly focused on EDZ self-sealing. Initial pneumatic testing of approximately 80 short radial boreholes, distributed over six test sites, was used to identify suitable URL sites for extended testing. Additional boreholes were drilled in areas where high permeability zones were identified. All sites revealed a heterogeneous EDZ system. The depth of the highly permeable non-saturated or partially saturated EDZ regions varied between 20 and 90 cm. Two sites in the Gallery 98 were selected for further testing: (1) A single extensional fracture in the SW wall and (2) a fracture network in the NE wall of the Gallery 98. The single fracture was oriented parallel to the gallery wall and was intersected by two boreholes at about 70 cm depth. Initial testing revealed a relatively high transmissivity of $2 * 10^{-8}$ m²/s. After commencing resaturation and within the time frame considered, the fracture transmissivity decreased by a rate of almost one order of magnitude per annum.

In the second test (EH-1 Experiment), the fracture network was intersected by a series of 16 closely spaced boreholes (Figure 3-25) which were drilled into the sidewall rock of the Gallery 98. Each borehole was about 1.0 m deep and intersected narrowly spaced extensional EDZ fractures. The EDZ of the test location is a rather heterogeneous fracture network: In the upper zone (boreholes above a line which runs along BEH-68 – BEH-30 – BEH-32 – BEH-64 in Figure 3-25) that network is located more close to the tunnel wall at depths to about 0.40 m maximally, whereas in the lower zone it is located more at depths of between 0.40 and 0.80 m.

Figure 3-25. EH-1 Experiment: Configuration of the boreholes (with borehole number) for permeability testing in the EDZ of the Gallery 98 at Mont Terri (Heitz *et al.* 2003).
Numbers between the boreholes: Distances in centimetres.

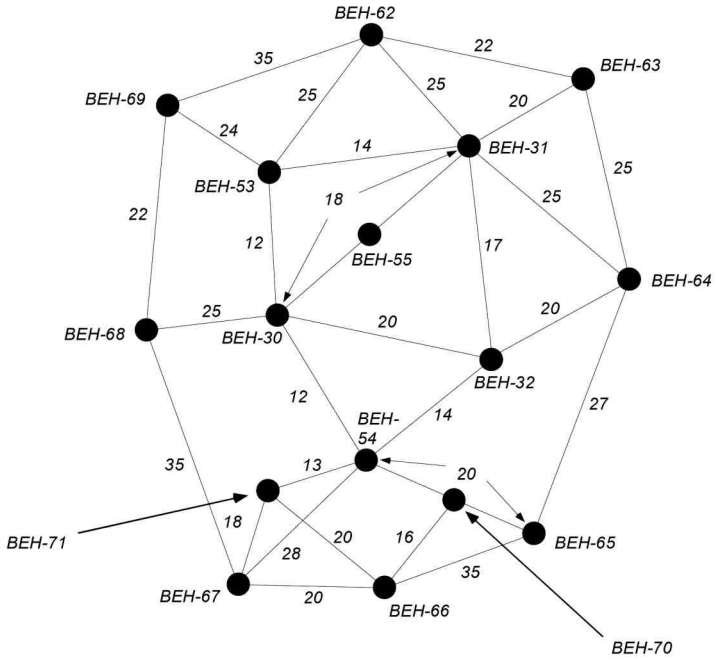

Fourteen (14) of the boreholes were equipped with a single packer system to seal the holes for pressure testing as shown in Figure 3-26. The remaining two boreholes (BEH 54 and 55) accommodated extensometers for the control of the opening / closure of the fractures. The tested area was artificially resaturated by injecting water into the interval flow lines. Synthetic porewater ("Pearson water") was used in order to limit swelling effects and osmotic phenomena. A series of ten hydraulic injection tests was performed (Meier *et al.* 2002; Bossart *et al.* 2002) distributed over a time span of more than three years from 1999 to April 2002. The hydraulic pressure was applied in Borehole BEH-31, whilst observing the pore pressure response of the saturated rock in the adjacent boreholes. The testing set-up of the constant rate injection tests (RI-Tests) consisted of a nitrogen bottle with a pressure reduction valve pressurising the water stored in a pressure vessel. The pressure vessel itself was connected through a flow controller to the test interval (Figure 3-26, top). The actual weight of the water-filled pressure vessel was measured by a scale to verify the recorded flow rates.

Figure 3-27 shows the development of the measured hydraulic transmissivity over the three-year testing period. It can be seen that there is a constant decrease of the transmissivity, from about $5 * 10^{-7}$ m²/s initially (Test 1) to about $2 * 10^{-9}$ m²/s at the end of the EH-1 Experiment (Test 10). This gives evidence of the significant influence of resaturation onto the sealing of fractures.

Figure 3-26. EH-1 Experiment: Schematic set-up of the hydraulic constant rate injection (RI) tests and instrumentation of boreholes (from Heitz *et al.* 2003)

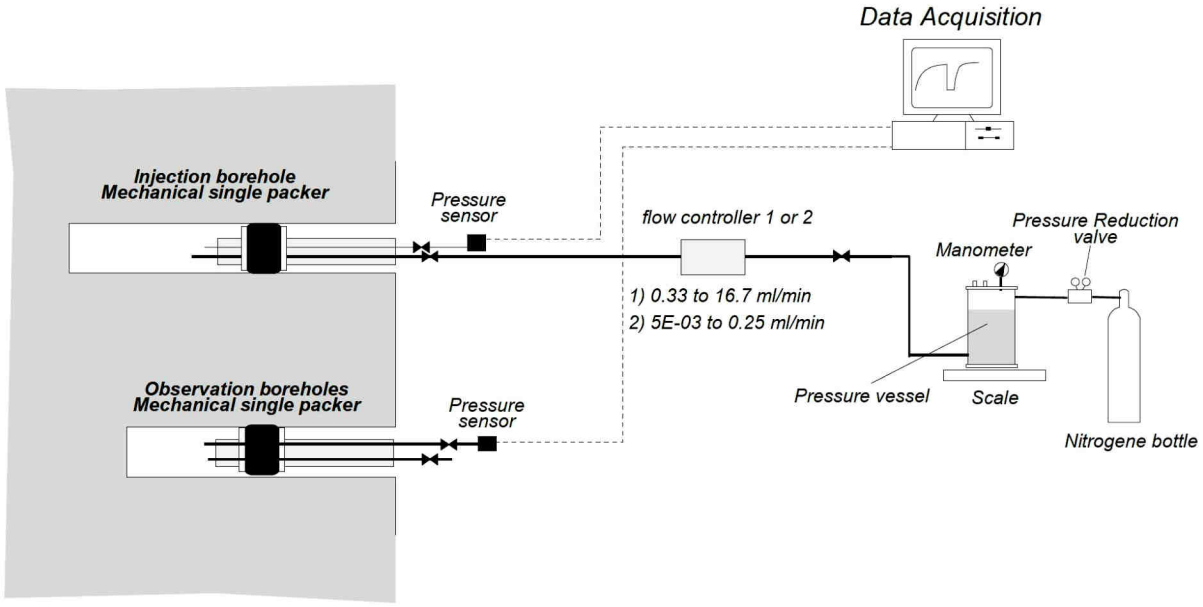

Figure 3-27. Result of the EH-1 Experiment: Continuous decrease of fracture transmissivity between Tests 1 and 10 (from Heitz *et al.* 2003)
Note: Tests 11 to 18 are part of the SELFRAC-I Plate Load Test which was carried out immediately after the EH-1 Experiment (see Section 3.2.2.2 and Figure 3-32 below).

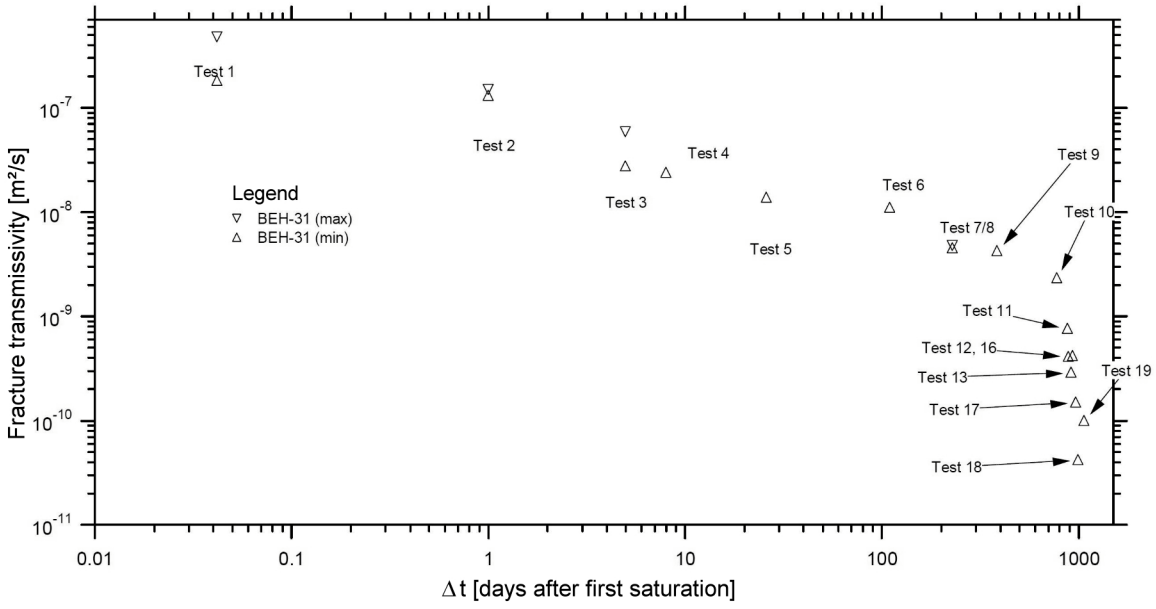

The resaturation tests which were carried out from 2001 to 2003 as part of the EB Experiment (Alheid *et al.* 2004) reconfirmed the EH-1 test results. During the time of observation the hydraulic conductivity generally decreased by some two orders of magnitude (Figure 3-28), i.e. at a rate of about 10^{-1} m/s/a. All tests revealed a maximum of the hydraulic conductivity at a depth of about 0.60 m from the tunnel sidewall (Figure 3-29), indicating a discontinuous structure of the EDZ fracture network.

Figure 3-28. Development of the hydraulic conductivity as calculated from constant head tests over a period of two years (data from Alheid *et al.* 2004)

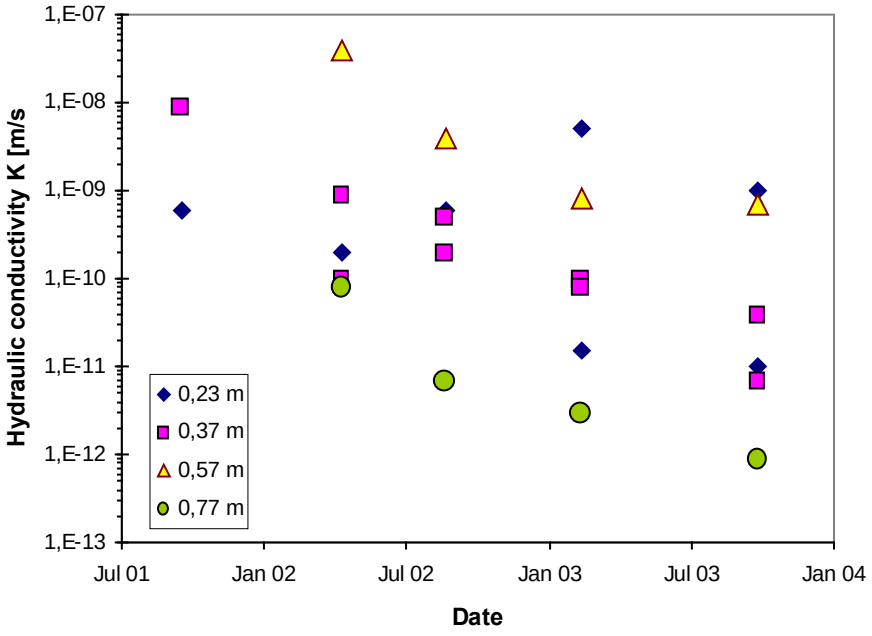

Figure 3-29. Hydraulic conductivity as deduced from constant head tests as a function of depth of the tunnel sidewall rock (data from Alheid *et al.* 2004)

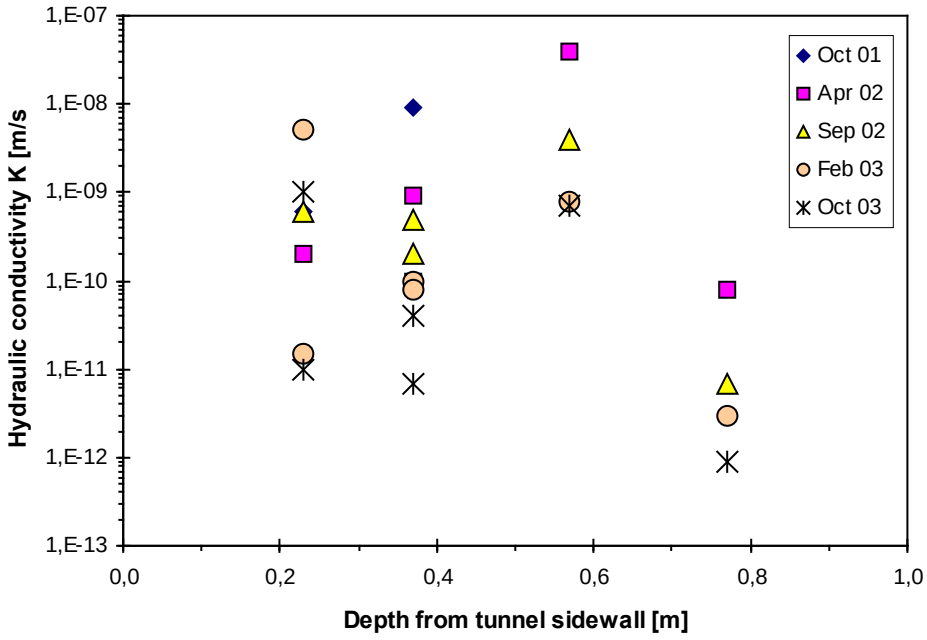

3.2.2.2 Mechanically stimulated closure of fractures – SELFRAC-I and –II Experiments

As part of the SELFRAC project, two *in situ* tests of importance to self-sealing were carried out in the Mont Terri URL to simulate the influence of the bentonite backfill swelling pressure onto the transmissivity of the EDZ. They are:

- SELFRAC-I: Plate Loading Test (PLT) of the tunnel wall and determination of the changes of the transmissivity of the EDZ fractures in dependency of the PLT pressure; and

- SELFRAC-II: Combined borehole dilatometer and water pressure tests in a borehole for the determination of the axial transmissivity of the borehole EDZ in dependency of the dilatometer pressure.

The test site locations within the Gallery 98 are indicated in Figure 3-30.

Figure 3-30. Locations of the SELFRAC-I and –II Tests in the Gallery 98 of the Mont Terri URL

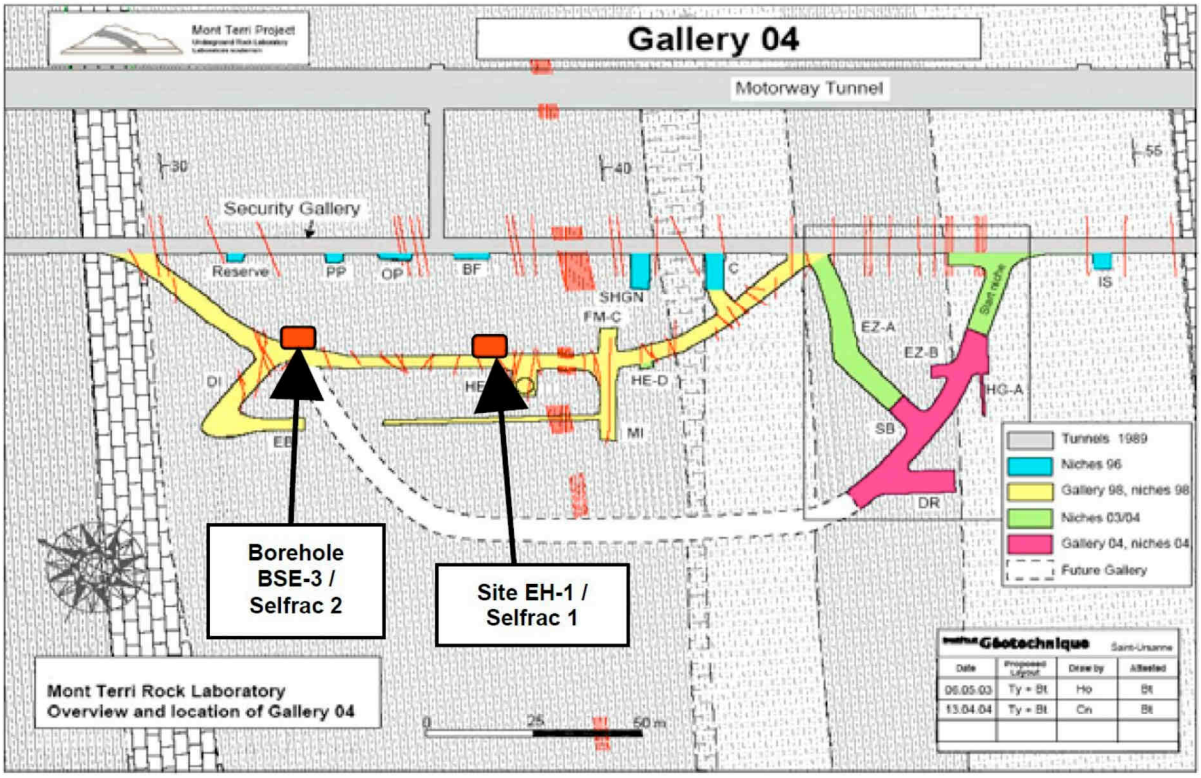

SELFRAC-I Experiment: Plate loading test (PLT)

This experiment was carried out at the same site as the EH-1 Experiment (see Section 3.2.2.1). The existing hydraulic stimulation and observation boreholes (Figure 3-25) could be readily used. In fact, Test No. 10 of April 2002 (Figure 3-27) can be equally understood as the termination test of the EH-1 Experiment as well as the initiation test of the SELFRAC-I Experiment.

Figure 3-31 shows a schematic view of the experimental set-up of the SELFRAC plate loading test.

Figure 3-31. SELFRAC-I plate load testing set-up in the Gallery 98 of the Mont Terri URL
(from Heitz *et al.* 2003)

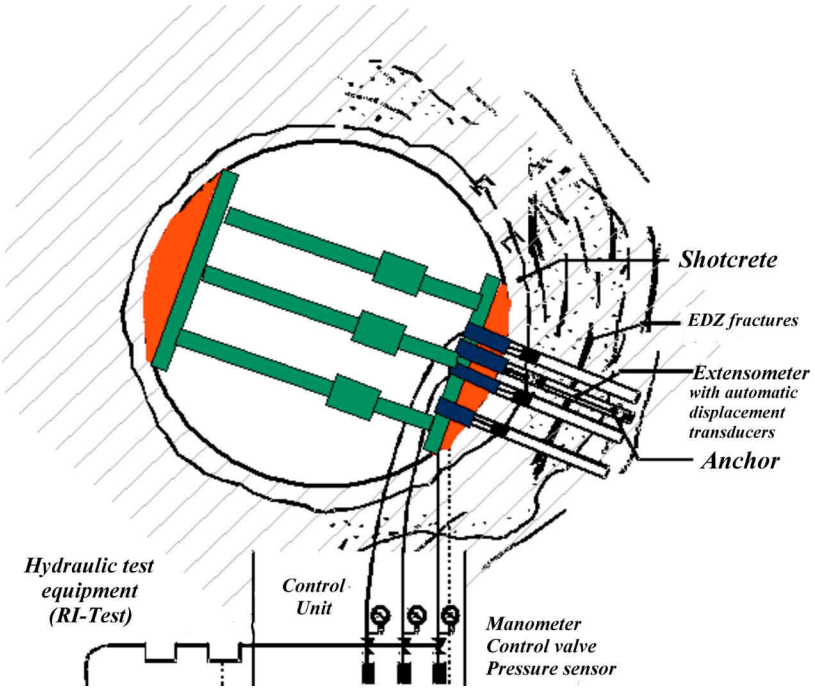

The PLTest was carried of over a time span of about one year (from January 2002 to January 2003). The PLT equipment was oriented in such a way as to apply the load in about normal direction to the extensional EDZ fractures in the sidewall rock. The rock, subjected to the PLT pressure, was kept saturated over the entire testing period as already practised in the EH-1 Experiment.

The load of the PLT was applied in four steps with PLT bearing pressures amounting to 1, 2, 3 and 4.8 MPa, respectively (Figure 3-32; right-side scale). During each of the four test stages the applied pressure was held constant over a period of about one month. In each of the plate load testing stages periodic hydraulic constant rate injection tests were performed (Test Nos. 11 ... 18). A final test was conducted once the load was released (Test No. 19).

As a result there is a clear dependency between the applied PLT bearing pressure and the fracture transmissivity T in the sense that an increase of the PLT pressure is associated with a decrease of T (Figure 3-32). The tests showed a reduction of the transmissivity of about 1½ orders of magnitude for a PLT pressure of 4.8 MPa (Figure 3-33).

Figure 3-32. Result of the SELFRAC-I Experiment: Continuous decrease of the fracture transmissivity between Tests 10 and 18 due to PLT pressure (from Heitz *et al.* 2003).
Note: Test 10 = part of the EH-1 Experiment (see Figure 3-27); Test 19 = after full release of the PLT bearing pressure.

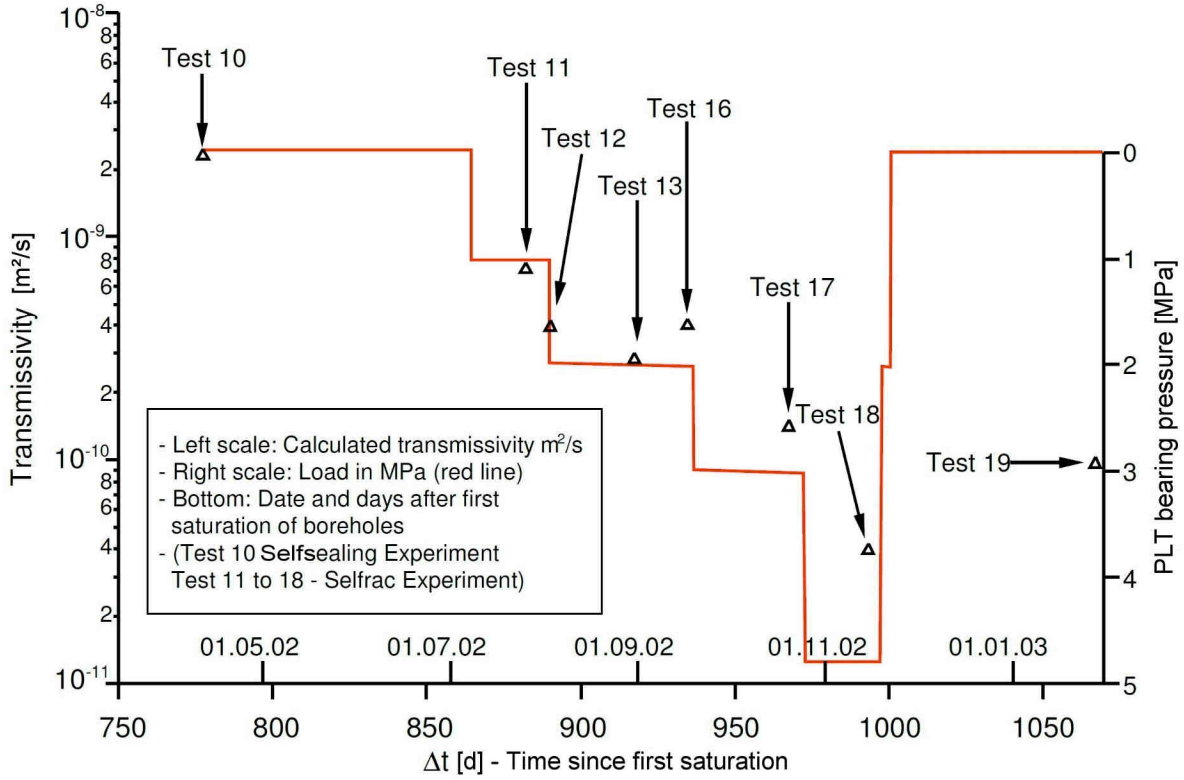

Bock and Konietzky (1997) reviewed the theory and praxis of PLTests in tunnels, i.e. exactly the configuration of the Mont Terri SELFRAC-I testing set-up. They found that, in underground openings, the pressure distribution in the rock abutment beneath the load platens tends to differ substantially from what is commonly assumed with reference to the classical Boussinesq theory. In

particular, they found that, with increased abutment depth, the actual PLT pressure tends to become smaller than theoretically anticipated. The consequence for the SELFRAC-I test is that the above finding (1½ orders of magnitude decrease of T for 4.8 MPa PLT pressure; see Figure 3-33) can be considered a conservative estimate.

Figure 3-33. Result of the SELFRAC-I Experiment: Transmissivity versus PLT bearing pressure

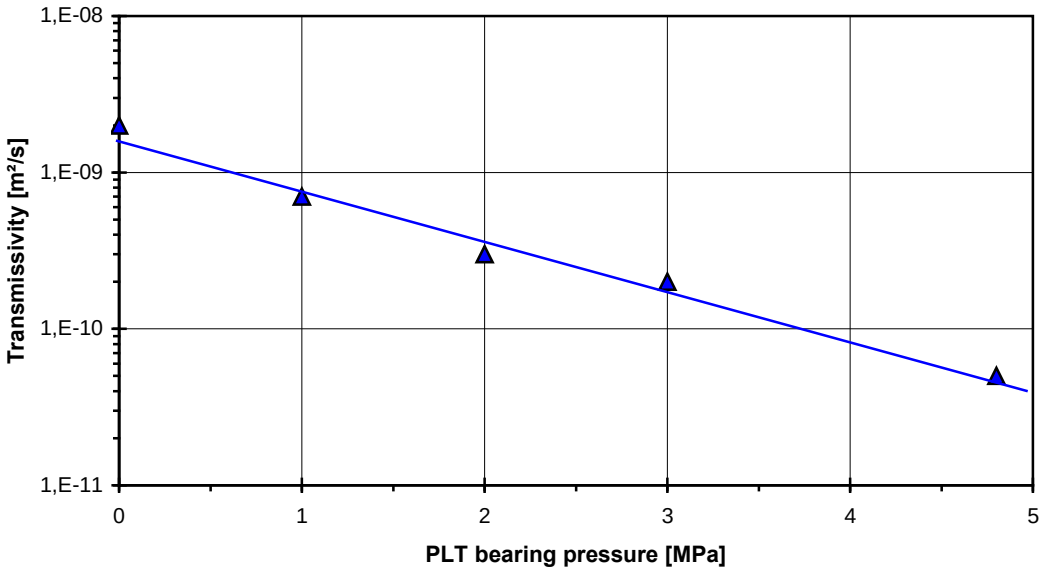

SELFRAC-II Experiment: Packer and dilatometer test

Whilst the set-up of the SELFRAC-I Experiment was focussed on the closure of the EDZ fractures by applying a PLT pressure in radial direction and thus on the determination of local changes of the fracture transmissivity, the SELFRAC-II Experiment was aimed at investigating the transmissivity changes in axial tunnel (or in this case borehole) direction. The basic idea was to investigate the axial transmissivity of the borehole EDZ as a small-scale replica of an emplacement tunnel EDZ. The SELFRAC-I and –II experiments thus complement each other.

For the SELFRAC-II experiment a new borehole (BSE-3) was drilled in radial tunnel direction (12.1 m total depth of which 11.9 m were in Opalinus Clay and the first 0.2 m in concrete tunnel lining). A test string was installed, consisting of a 1 m long dilatometer probe near the deep end of the borehole and two inflatable packers further up (Figure 3-34).

Three types of hydraulic tests were carried out in the 2.88 m long Interval 1 (I 1) between the dilatometer and the deep end of the borehole as follows:

- Constant rate injection (RI)
- Pulse injection (PI) and
- Pulse withdrawal (PW).

Figure 3-34. SELFRAC-II testing set-up consisting of a string of two inflatable packers and one dilatometer probe separating three test intervals I1, I2 and I3
(after Bühler 2005)

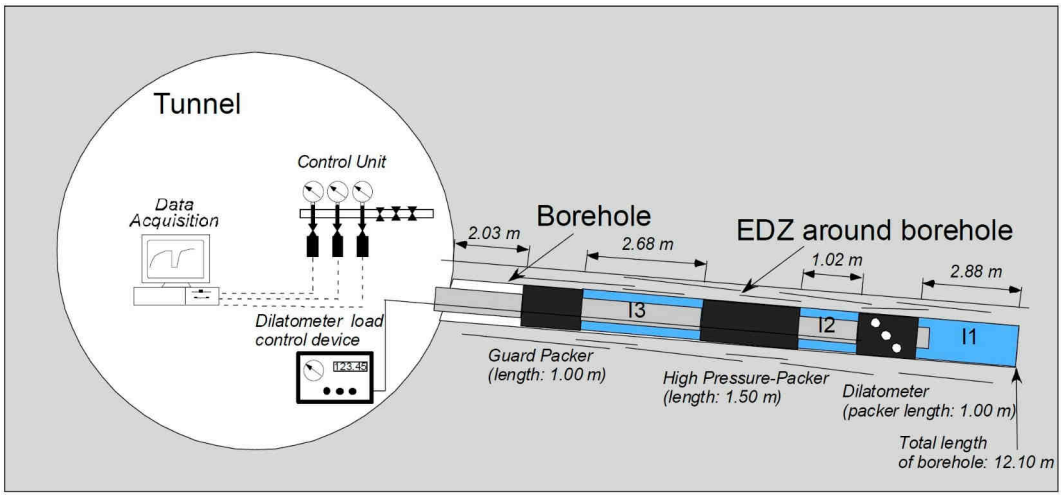

It was found that the borehole developed an EDZ with a distinctively higher transmissivity along the borehole wall than in the rock mass. The key result of the experiment was that the transmissivity in *axial borehole* direction can be significantly reduced by mechanical means, i.e. by the application of the inflating pressure of the packer dilatometer. In the SELFRAC-II test that reduction was of about two orders of magnitude when applying an effective dilatometer pressure of about 35 bar (= 3.5 MPa) (Figure 3-35 and Table 3-5).

Figure 3-35. SELFRAC-II Experiment: Transmissivity values derived from hydraulic testing and effective dilatometer pressure vs. time
(Bühler 2005)

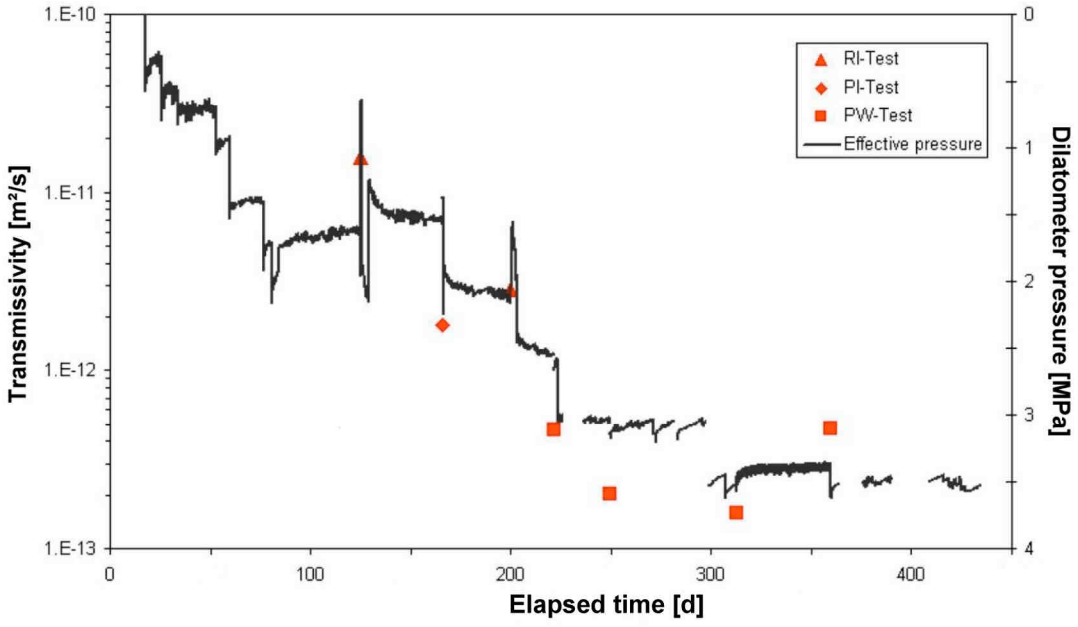

Table 3-5. Results of SELFRAC-II hydraulic tests performed in borehole Interval 1

Test	Type of test	Transmissivity [m²/s]	Hydraulic Conductivity [m/s]	Nominal Dilatometer Pressure [MPa]
RI/HI-Test-week09-04	Rate Injection/Head Injection Test	1.57E-11	5.46E-12	3.0
PI-Test-week15-04	Pulse Injection Test	1.80E-12	6.23E-13	3.0
RI-Test-week20-04	Rate Injection Test	2.86E-12	9.92E-13	3.5
PW-Test-week23-04	Pulse Withdrawal Test	4.62E-13	1.60E-13	4.0
PW-Test-week27-04	Pulse Withdrawal Test	2.02E-13	7.03E-14	4.0
PW-Test-week36-04	Pulse Withdrawal Test	1.59E-13	5.52E-14	5.0
PW-Test-week43-04	Pulse Withdrawal Test	4.70E-13	1.63E-13	5.0

At the end of the SELFRAC-II project period the following static pressures were measured: 1.75 MPa in Interval 1, 1.33 MPa in Interval 2 and 0.6 MPa in Interval 3.

3.2.2.3 HG-A Experiment

The HG-A experiment was conceived as a long-term *in situ* test at the Mont Terri URL, aimed at investigating, under realistic conditions, gas transport capacity of the host rock and the EDZ as well as the hydro-mechanical evolution of a back-filled and sealed tunnel section. Amongst its specific objectives is the discrimination between different self-sealing mechanisms, such as mechanically stimulated fracture closure, long-term consolidation and swelling (Marschall *et al.* 2008c).

The experiment, which commenced in 2005 and is still ongoing, is designed to be carried out in the following six phases:

(1) excavation of a 13 m long microtunnel and monitoring of key geotechnical parameters during the open tunnel phase;

(2) backfilling and sealing of the tunnel with a large-size hydraulic packer system (∅ 940 mm; sealing length 3000 mm; ref. to Figure 3-36). The sealed section was equipped with 12 piezometers which were embedded within the packer sleeve in three sections S1 to S3;

(3) artificial resaturation of the sealed tunnel section;

(4) carrying out of a series of long-term water injection tests for determining the hydraulic conductivity of the rock on the tunnel scale;

(5) carrying out of gas injection tests; and

(6) dismantling of the test site.

Figure 3-36. HG-A Experiment: Emplacement of the megapacker
(from Marschall *et al.* 2008c)

Phases 3 and 4 are of particular interest for the self-sealing topic. Saturation of the test section commenced in November 2006 when the megapacker was inflated to 1700 kPa and the test section saturated by injection into a line in the floor of the microtunnel. Following saturation a series of injection tests were performed throughout 2007 and into 2008. The effect of ongoing water injection on the conductance of the flow paths from the test section is shown in Figure 3-37 in terms of a "Sealing Index", which has been defined as the ratio between the injection rate [ml/min] and the test section pressure [kPa relative to atmospheric]. The index is considered as a simple diagnostic measure for the change in flow capacity of the damaged zone around the seal section. Beyond such index graphs, the injection tests were also subjected to more systematic interpretations, comprising

diagnostic hydrotest analyses and numerical simulations of the test sequences. Analyses of more recent tests suggest an equivalent hydraulic conductivity of the test zone in the order of 2 to 5 x 10^{-11} m/s. The recent estimates are about one to two orders of magnitude lower than the early test results from January 2007, still about two orders of magnitude higher than the conductivity of the intact Opalinus Clay. Variation of the packer pressure of up to 3 MPa revealed some effects on the hydraulic conductivity, however not as much as from resaturation and consolidation, processes which are still ongoing.

Figure 3-37. Decline of "Sealing Index" in course of the saturation phase of the HG-A Experiment (from Marschall *et al.* 2008c)

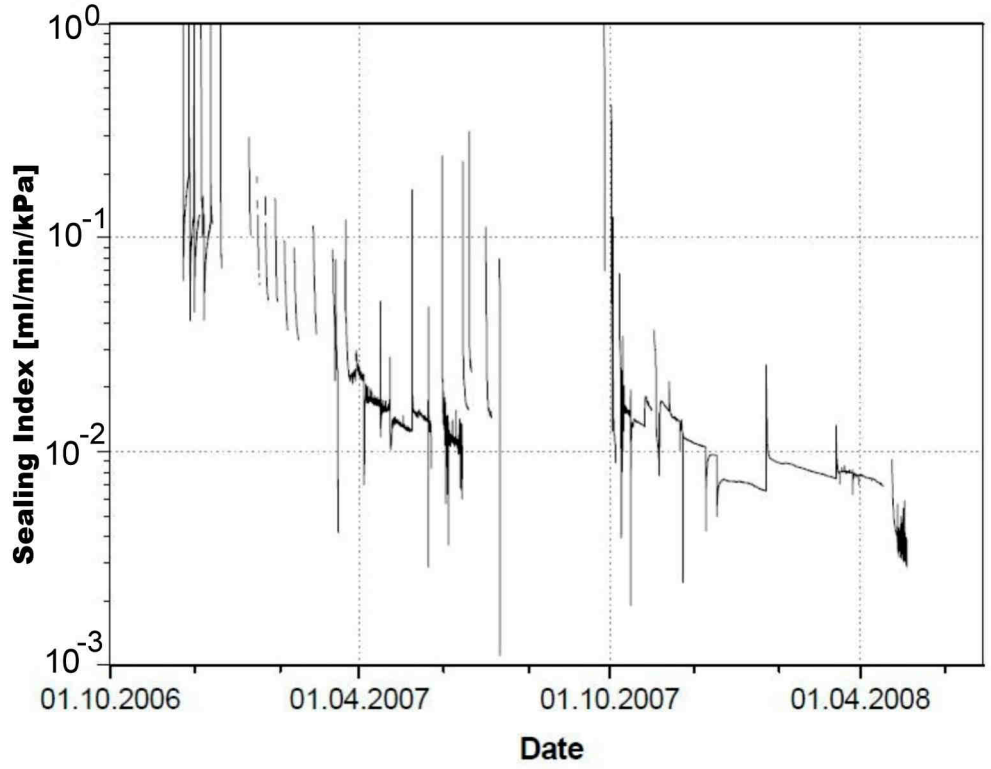

3.2.2.4 EDZ sealing barrier test: The EZ-A Cut-Off Experiment

The objective of this experiment was the evaluation of the effectiveness of bentonite filled cross-cut slots as barriers of EDZ flow pathways along a drift (Nussbaum *et al.* 2005). Although not explicitly dedicated to self-sealing, the EZ-A Experiment yielded some information which is of interest to the self-sealing topic. The experiment was carried out at two locations in the Mont Terri URL, namely in the northern entrance of Gallery 98 and in the EZ-A niche (Armand *et al.* 2007). In December 2005 different cross-cut slots perpendicular to the drift axis were opened in the roof, sidewalls and invert for the experiment (Figure 3-38). The slots were about 0.2 to 0.06 m wide and about 1.3 to 1.5 m deep. They were either (a) filled with bricks of highly compacted swelling clay (mixture of sand and bentonite), (b) equipped with mechanical flat jacks for pressurising the slot sidewalls or (c) filled with resin.

Prior to the cutting of two 1.5 m spaced slots in the invert of the gallery, cross-hole permeability tests were carried out in nine boreholes (Boreholes BEZ-A-1 to -9). To minimise the

likelihood of swelling or other alteration of the EDZ fractures, pre-slot tests were performed by air injection only. In turn, air and water injection was carried out in the post-slot permeability testing phase. Hereby, Borehole BEZ-A-5, located between the slots, served as main injection borehole (Figure 3-39). The injected water was tracer-marked for subsequent identification of any water-conducting features by means of an UV lamp. Ten boreholes (BEZ-A-31 to BEZ-A-40) were drilled towards the end of the EZ-A cut-off experiment (from 5 to 7 April 2005) to provide drillcores for that identification. It turned out that this procedure enabled a secure identification of water-conducting features within a EDZ fracture network.

Figure 3-38. Construction and filling of slots as part of the EZ-A Experiment in Mont Terri
Top: Cutting of slots in the roof; Bottom left: Slot filled with bentonite bricks; Bottom right: Cutting a slot in the invert (Armand *et al.* 2008)

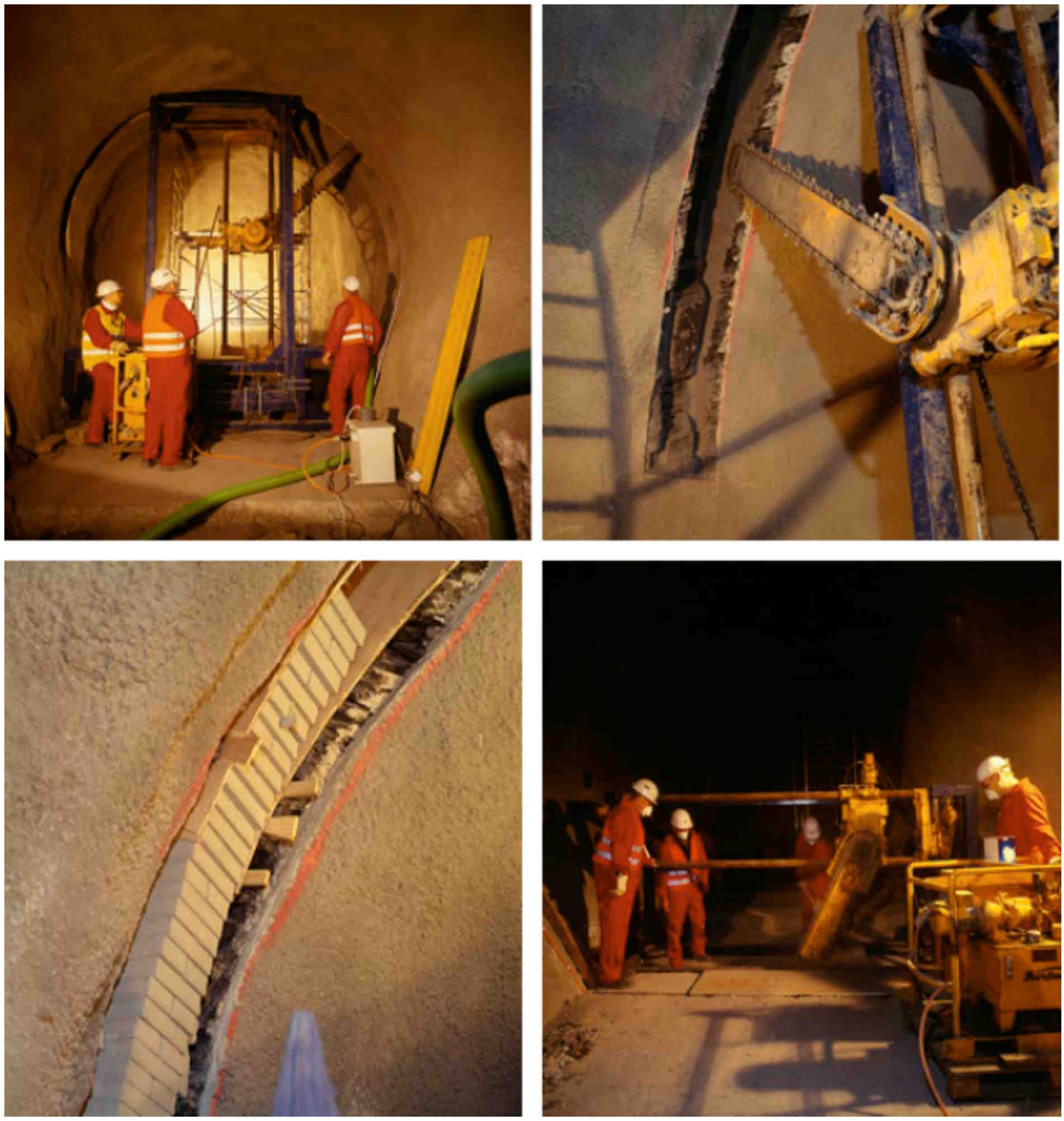

Figure 3-39. Plan view of the test section in the invert of the gallery with the location of pre-slot Boreholes BEZ-A-1 to –A-9 and post-slot Boreholes BEZ-A-31 to –A-40
(after Nussbaum *et al.* 2005)

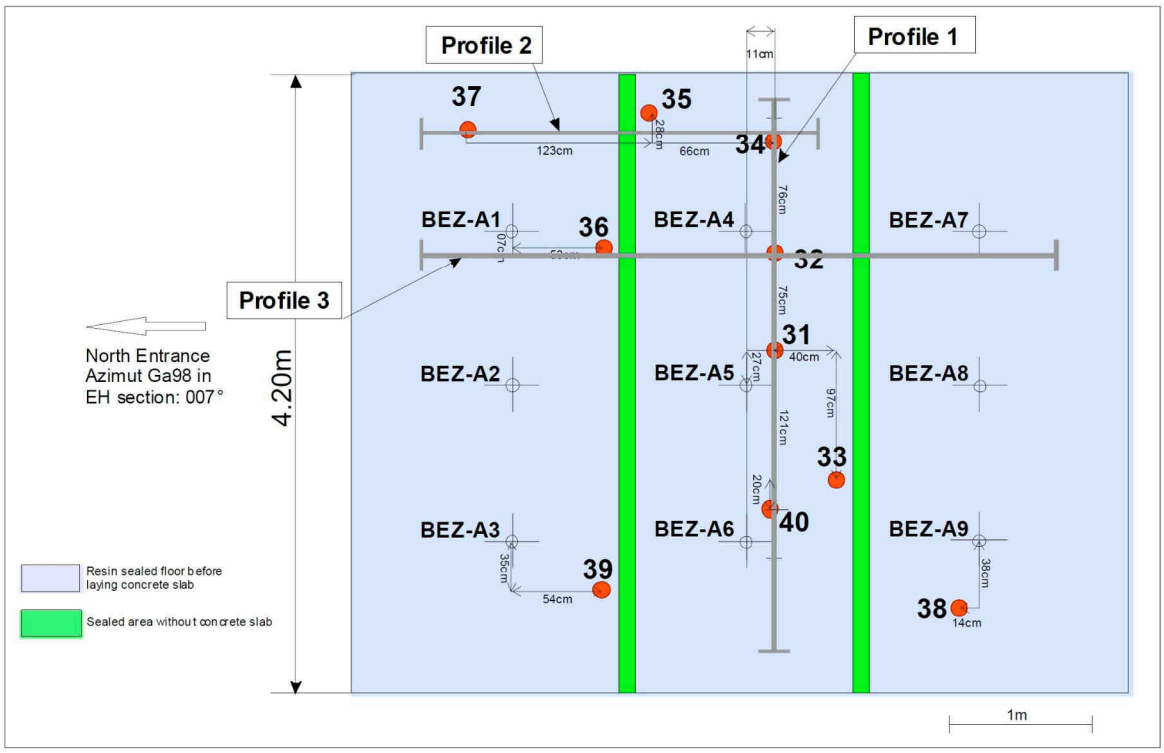

Figure 3-40. Self-sealing features in core fragments of Borehole BEZ-A-32 (Armand *et al.* 2008)
(a): In normal light: Wet and muddy fracture surface with traces of gypsum (white spots)
(b): In UV light: Green colours indicate the entry of fluorescence-doped water into fine EDZ fracture network (Photos: Ch. Nussbaum)

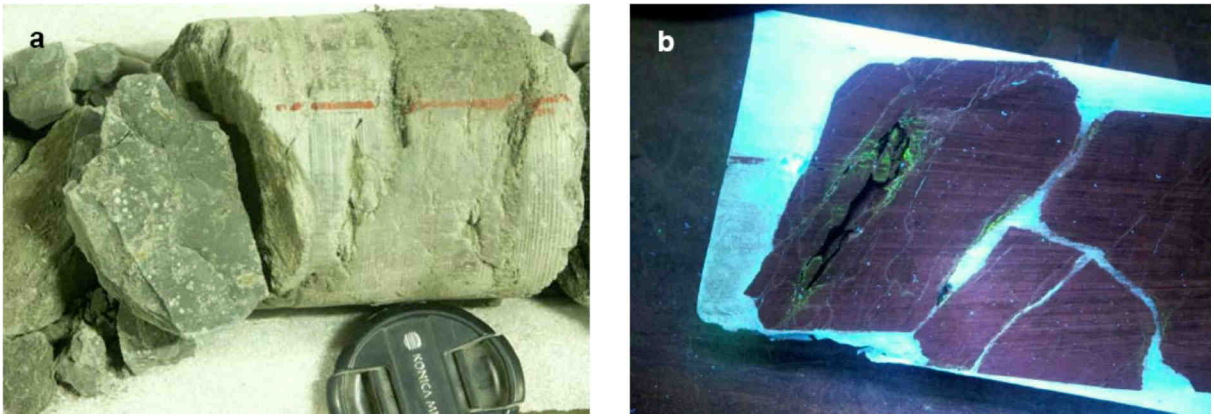

Preferential water pathways along reactivated faults and EDZ fractures could be clearly identified. The particular fault pattern, consisting of two differently oriented fault sets (SSE-dipping

and W- to WNW-dipping faults; ref. to Section A.4.1.3), enabled a flow of the injected water from one side of a slot to the other side along the side walls of the gallery and below the slots, thus indicating that the tectonic fracture network can be of major importance in Mont Terri. On the other hand, self-sealing phenomena were also observed (Nussbaum *et al.* 2005), especially in the two reactivated fault plane sets (identification in drillcores of BEZ-A-31, BEZ-A-32, BEZ-A-33, BEZ-A-34, BEZ-A-38 and BEZ-A-40) and in sub-horizontal unloading joints (EDZ fractures) (in drillcores BEZ-A-34 and BEZ-A-35).

3.2.2.5 Texture and structure of self-sealed fracture zones

The texture and structure of the "self-sealed features", as observed in the EZ-A Experiment and shown in Figure 3-40, was more closely studied by Badertscher *et al.* (2008). The "self-sealed features" were understood as old tectonic faults. Three specific sealing zones from BEZ-A-33/34 and BEZ-A-38 drillcores (see Figure 3-39) were chosen for analyses by means of laser grain size measurements, thin section observations, X-ray diffraction (XRD) and scanning electron microscope (SEM).

As previously anticipated it was found that, within the "self-sealing" zones and compared to the matrix, there exist

- a significant higher portion of relatively small grains (Figure 3-41);
- a higher portion of phyllo-silicates and a lower portion of quartz and calcite;
- a preferred alignment of the platy minerals in the direction of the fault and
- virtually no voids.

Most importantly, however, is the finding that a rather small amount of swelling minerals (< 5%) seemed to be sufficient to have lead to a sealing of the fault plane. Swelling minerals were only identified within the grain size fraction <2 µm.

Figure 3-41. Contrast in grain size distribution between self-sealed zones and matrix
(samples from BEZ-A34/38 drillcore samples; data from Badertscher *et al.* 2008)

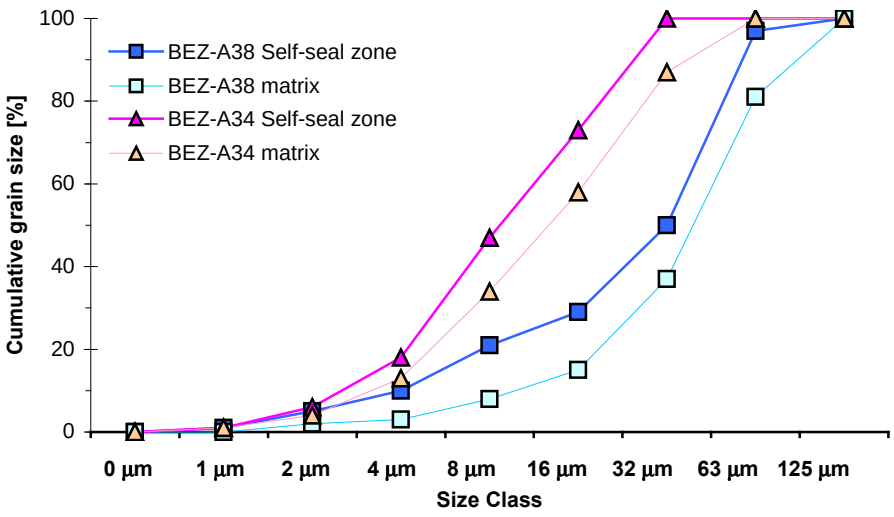

3.2.3 HADES URF at Mol

Evidence of self-sealing was observed during the construction of the Connecting Gallery in the HADES URF in the year 2001-02 (Bernier *et al.* 2004) (Figure 3-42; refer also to Section A.2.6.6).

Figure 3-42. Locations of the SELFRAC-III and –IV Experiments in the HADES URF (after Bernier *et al.* 2004)

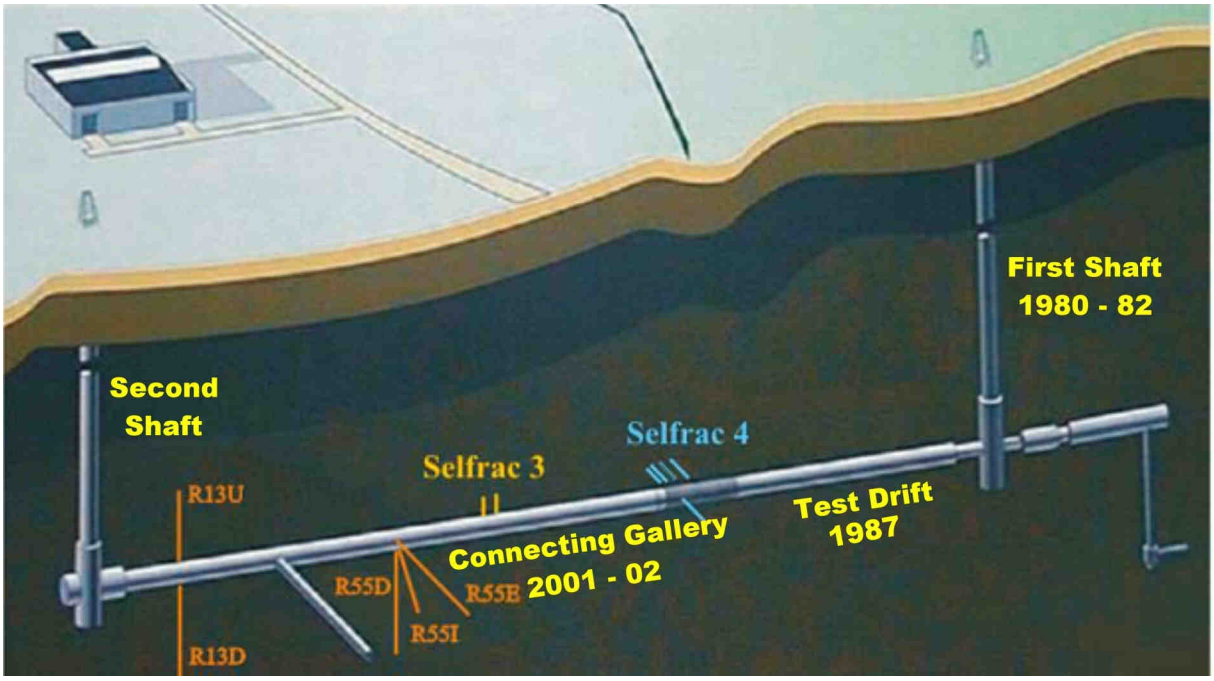

3.2.3.1 Oxidation front of 15 year old fractures

About 6 m before the excavation face of the Connecting Gallery reached the end of the existing Test Drift, fractures were observed which could be clearly related to the Test Drift excavation of the year 1987 some 15 years earlier (Figures 3-42 and 3-43). Some of the fracture surfaces showed traces of oxidation but only within the last metre from the Test Drift face. The bulk of the old excavation-induced fractures showed no signs of oxidation whatsoever. Obviously, these had been effectively sealed from the air of the Test Drift. This observation also shows that fractures can be reactivated, indicating that, in the plastic Boom Clay, healing has not yet (or only partially) occurred within the given time span of 15 years (Bastiaens *et al.* 2007).

Figure 3-43. Superposition of excavation-induced fractures at the approach of the Connecting Gallery to the Test Drift constructed some 15 years earlier (from Bastiaens *et al.* 2007)

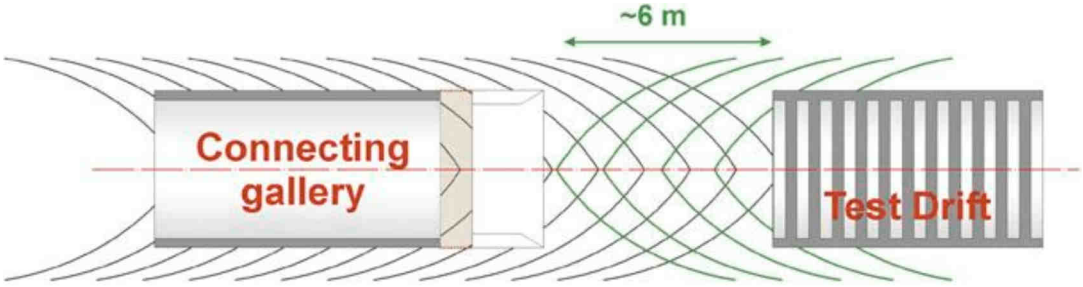

Partial healing was also observed when taking core samples. Some excavation-induced fractures became apparent only after core manipulation and drying. Before this, the cores did not show any signs of discontinuities.

3.2.3.2 Hydromechanical evolution around a repository-scale drift (SELFRAC-III Experiment)

Hydraulic conductivity around the Connecting Gallery was derived from constant head tests in steady-state flow regime applying Darcy's law. Most measurements were performed in the piezometers R55E and R55D (Figure 3-42). Results are shown in Figure 3-44. An increase of the hydraulic conductivity was observed up to about 6-8 m into the host rock. The values outside this influenced zone were ~6 * 10^{-12} m/s for the vertical piezometer R55D and ~4 * 10^{-12} m/s for the horizontal piezometer R55E. These values are consistent with hydraulic conductivity values for undisturbed clay obtained from previous *in situ* experiments (de Cannière *et al.* 1994), although slightly higher. About one year after the first measuring campaign on R55D, the first five filters were tested again. The new values were systematically lower, although not much (by about a factor of 2). The first four filters of R55E were tested again as well; the obtained values were almost identical to those obtained one year earlier (slightly lower in the first two filters).

Based upon these results and other results reported in the literature, Bernier *et al.* (2004) concluded that only the effective secondary stresses, acting within the clay adjacent to the excavation, could account for the variations of the hydraulic conductivity measured in the Connecting Gallery. Obviously, fractures do not play an important role in this case. The SELFRAC-III Experiment indicates that, for the Boom Clay of the HADES URF, the increase in hydraulic conductivity in the disturbed zone does not seem to jeopardise the safety of a disposal site for nuclear waste as the increase in hydraulic conductivity is limited to one order of magnitude, as the extent of that zone is limited to several metres around the excavation and as the hydraulic conductivity is restored to its initial value within a few years.

Figure 3-44. Distribution of the hydraulic conductivity K around the Connecting Gallery of the HADES URF and its development from 2004 to 2005 (after Bernier *et al.* 2004)

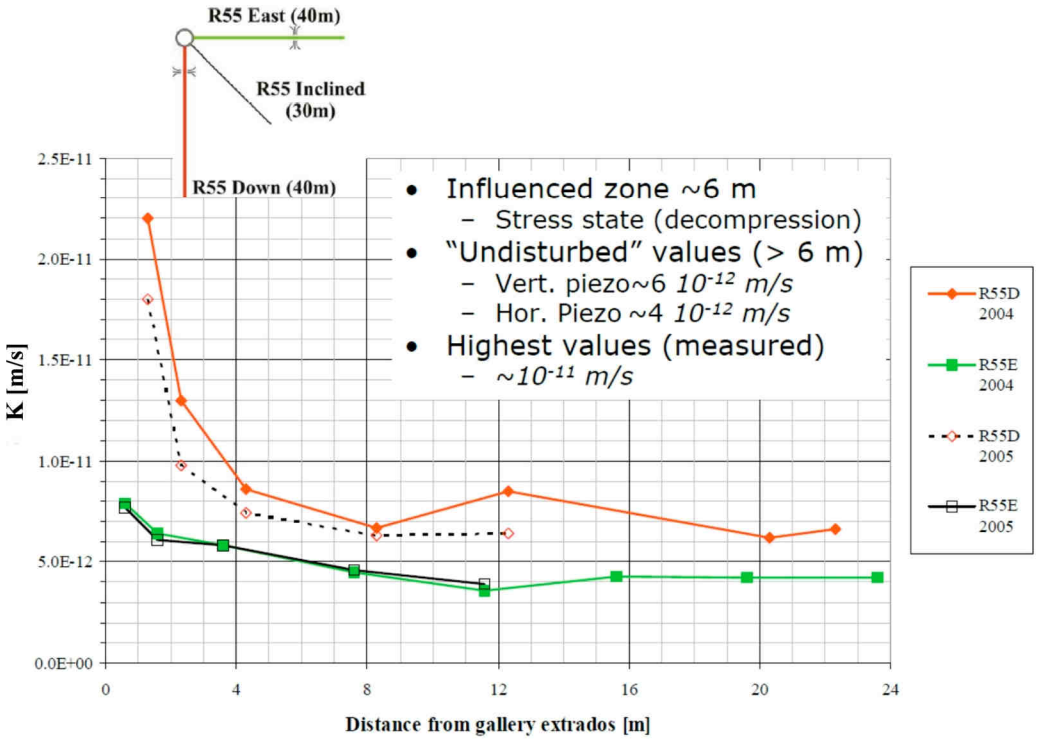

3.2.3.3 Collapsing borehole and re-installed instrumented core tests (SELFRAC-IV Experiment)

(a) Collapsing borehole experiment (long-term seismic measurement; Bastiaens *et al.* 2007)

The set-up consisted of four parallel observation boreholes (Nos. 2003-03 through to 2003-06) which were located around a central collapsing borehole (No. 2004-03) as is shown in Figure 3-45. Each observation hole was equipped with three seismic transmitters and two receivers at depths between 5.4 m and 7.6 m (Figure 3-46). All sensors were oriented in the direction of the central borehole. In the central borehole four transmitters and four receivers were placed at borehole depths of between 5.1 m and 7.9 m (not represented in Figure 3-46). That part of the central borehole, which was allowed to collapse, was located between 5 m and 8 m depth. Displacement sensors monitored the vertical and horizontal closure of the closing part of the central borehole.

Figure 3-45. SELFRAC-IV collapsing borehole experiment
Location map (left) and photograph (right)
of the four observation boreholes and the central collapsing borehole

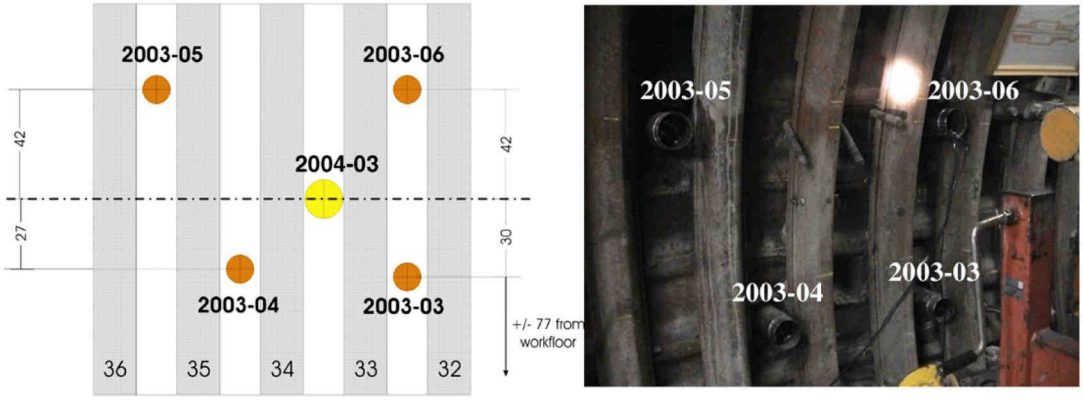

In a first phase, the four observation boreholes were installed (December 2003). After installation, the transmitters and receivers were pressed (by means of springs) against the borehole wall. In most cases seismic coupling was immediately achieved. The automated seismic measurements were repeated daily at midnight. To improve the signal-to-noise ratio the signals were stacked 256 times.

Following a stabilisation period, the central hole was drilled in July 2004. The measurements were evaluated with regard to seismic velocity and seismic amplitude of the P-waves for various travel paths in different directions.

Bastiaens *et al.* (2007) concluded that long-term seismic measurements are able to reveal disturbances and detect the evolution of sealing processes in the Boom Clay. It has been shown that, over a period of some two months, breakouts and convergence of the wall of the uncased central hole led to a quasi complete closure of that hole. Throughout that closing period the rock surrounding the central hole was damaged which was reflected in a decrease of P-wave velocities between observation boreholes and a loss of the higher frequencies. After closure of the hole, reconsolidation of the surrounding rock occurred leading to a partial recovery of the seismic properties.

Figure 3-46. SELFRAC-IV collapsing borehole experiment
Top: Borehole lay-out showing transmitters (white marks) and receivers (dark marks) in observation boreholes. Collapsing borehole in the centre.
Bottom: Measuring example of the development of the P-wave peak amplitude between two observation boreholes within the period from 6 December 2003 to 23 May 2005 (left) and direction of the travel path in the lower hemisphere projection (right).

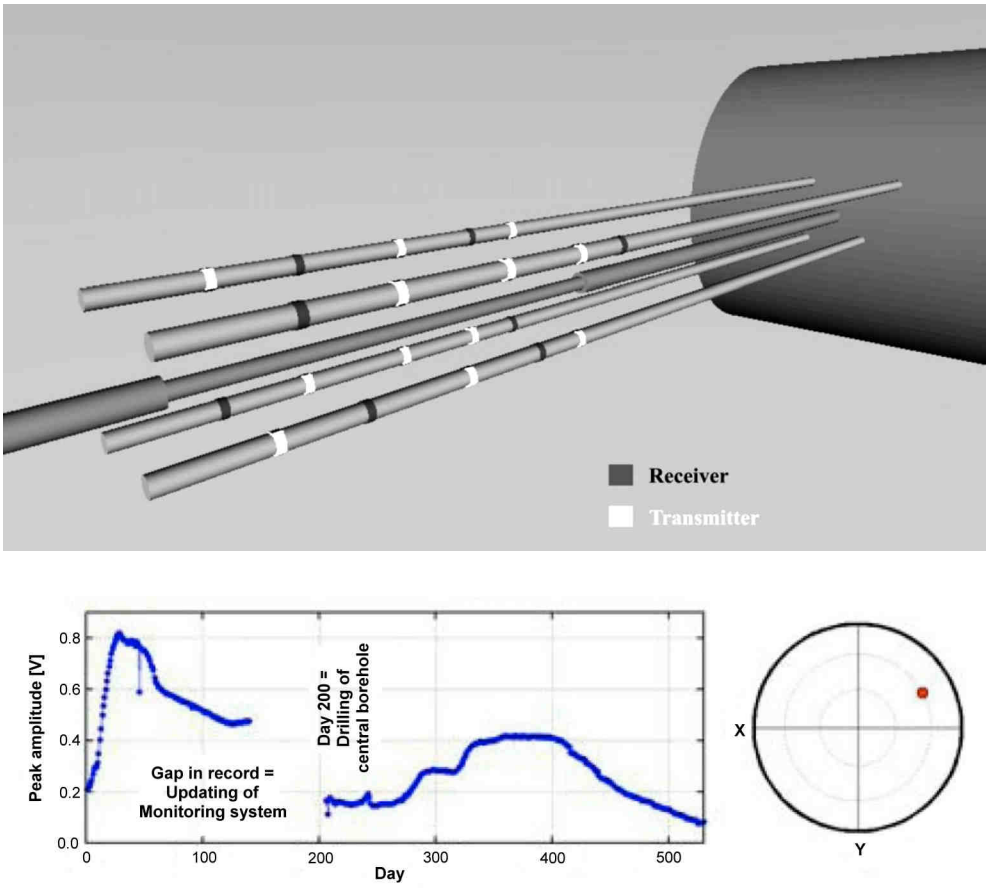

(b) Instrumented core experiment

During drilling of the central borehole, a 0.567 m long clay core was recovered, instantaneously instrumented and, about 6 hours after the core was taken, re-installed in a freshly drilled 6.5 m deep borehole. One end of the core was equipped with a seismic receiver, the other end with a transmitter. Two clearly visible fracture planes of the core were instrumented with pore pressure sensors (piezometers), whereby each fracture was equipped with two sensors on opposing sites of the core (Figure 3-47).

After re-installation of the core, the piezometers measured values which are consistent with the water pressure prevailing at the installation depth. To test the sealing of the fractures in the core, the pressure at Piezometer 2 (see Figure 3-47) was set to atmospheric level for several weeks. The neighbouring sensors also showed a pressure decrease, but from Figure 3-48 it is apparent that the fractures and the interface between the core and the borehole wall must have been partially sealed. Although the distance between piezometer Sensors 1 and 2 amounted to merely 50 mm and a fracture plane created a direct connection between them, the response of Sensor 1 was rather gradual and the

equilibrium value high. The reaction at Sensors 3 and 4 was similar but less pronounced due to the larger distance from Sensor 2.

Figure 3-47. Instrumented core experiment in the HADES URF
Left: Position of porewater pressure sensors (1 ... 4) and fractures in the instrumented core
Right: Detail of the instrumented core with fracture and groove for the installation of a pore pressure sensor (Note: the other sensor is installed on the opposite side of the core)
(from Bastiaens *et al.* 2007)

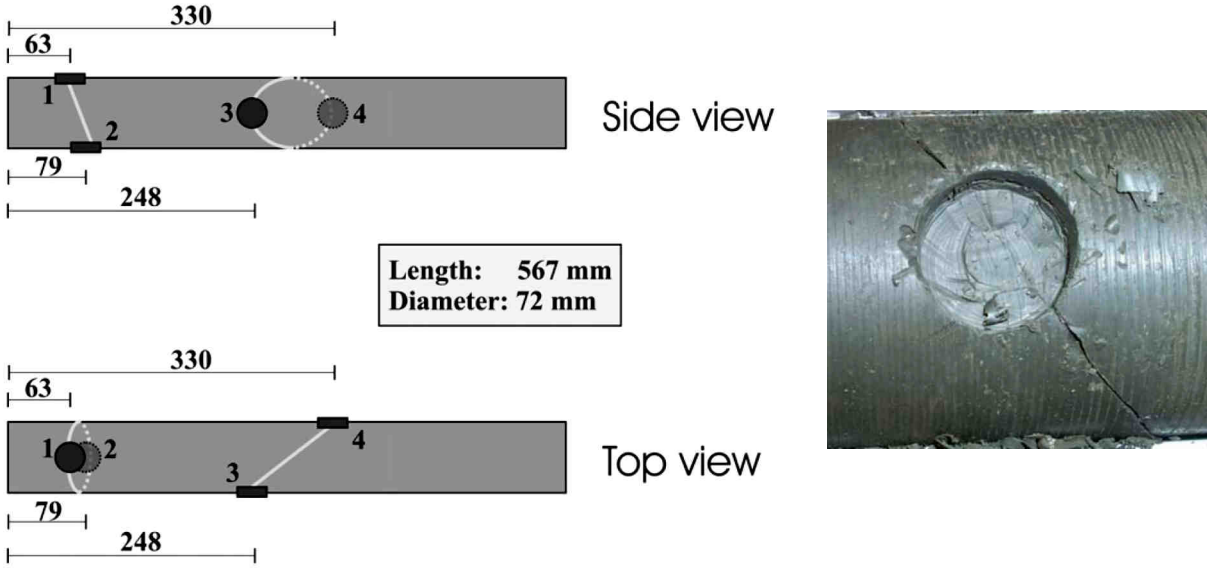

Figure 3-48. Result of the instrumented core experiment
Forced pressure drop of Piezometer Sensor 2 to atmospheric level (~ 100 kPa; out of scale in figure) whilst monitoring the pore pressure response at the other 3 piezometers. Despite a distance of merely 50 mm along the fracture, the associated drop in Piezometer 1 (bolt line) remains quite marginal, even more so for Piezometers 3 and 4 further away (after Bastiaens *et al.* 2007).

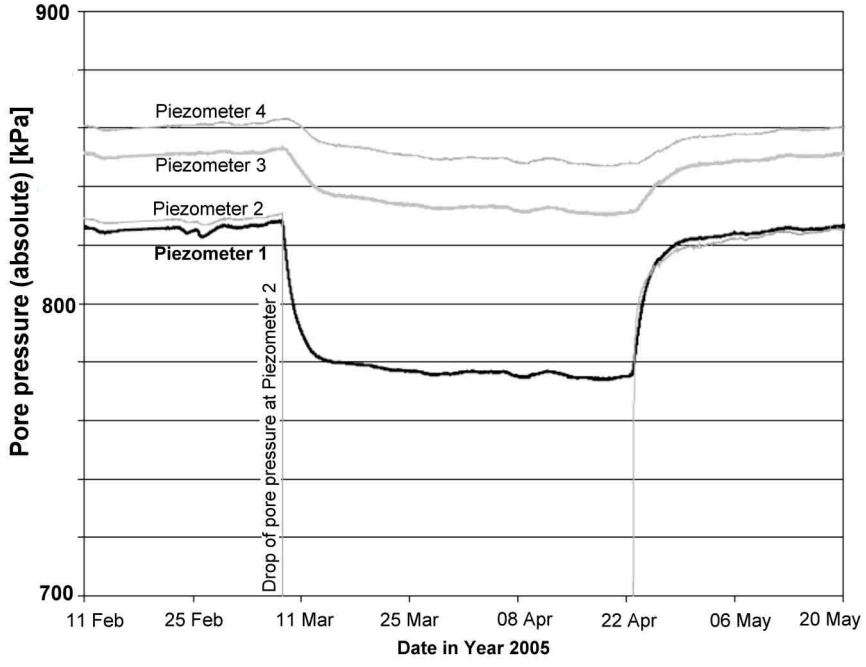

3.2.4 Bure URL

3.2.4.1 EDZ sealing barrier test: The KEY Experiment

The KEY experiment, carried out in the GKE Drift of the Bure URL (Figure 3-49; refer also to A.2.6.1), is much in line with the earlier EZ-A cut-off experiment of Mont Terri (see Section 3.2.2.4). Its prime objectives are the EDZ/EdZ characterisation of the permeability and pore pressure field in the near vicinity of the drifts at the -490 m Level (Zone 1 in Figure 3-50) and the testing of the effectiveness of slots in cutting hydraulic advective transport in axial direction of the drift (Zone 2 in Figure 3-50) and of subsequent pressurisation of the slots by swelling materials and mechanical jacking (Zone 3 in Figure 3-50) (Andra 2005b and 2006; Delay *et al.* 2007; Lavanchy *et al.* 2007). A specific focus of the KEY experiment was the transfer of the large-scale slot cutting technology from the EZ-A Experiment and its adjustment and further development to the site-specific needs of the Callovo-Oxfordian formation in the Bure URL. Similar to the EZ-A Experiment of Mont Terri, the KEY Experiment yielded some indirect information on the self-sealing topic.

Figure 3-49. General layout of the Bure URL
Experimental drifts at -445 and -490 m Levels were excavated between end of 2004 and mid-2006 (after Delay *et al.* 2007)

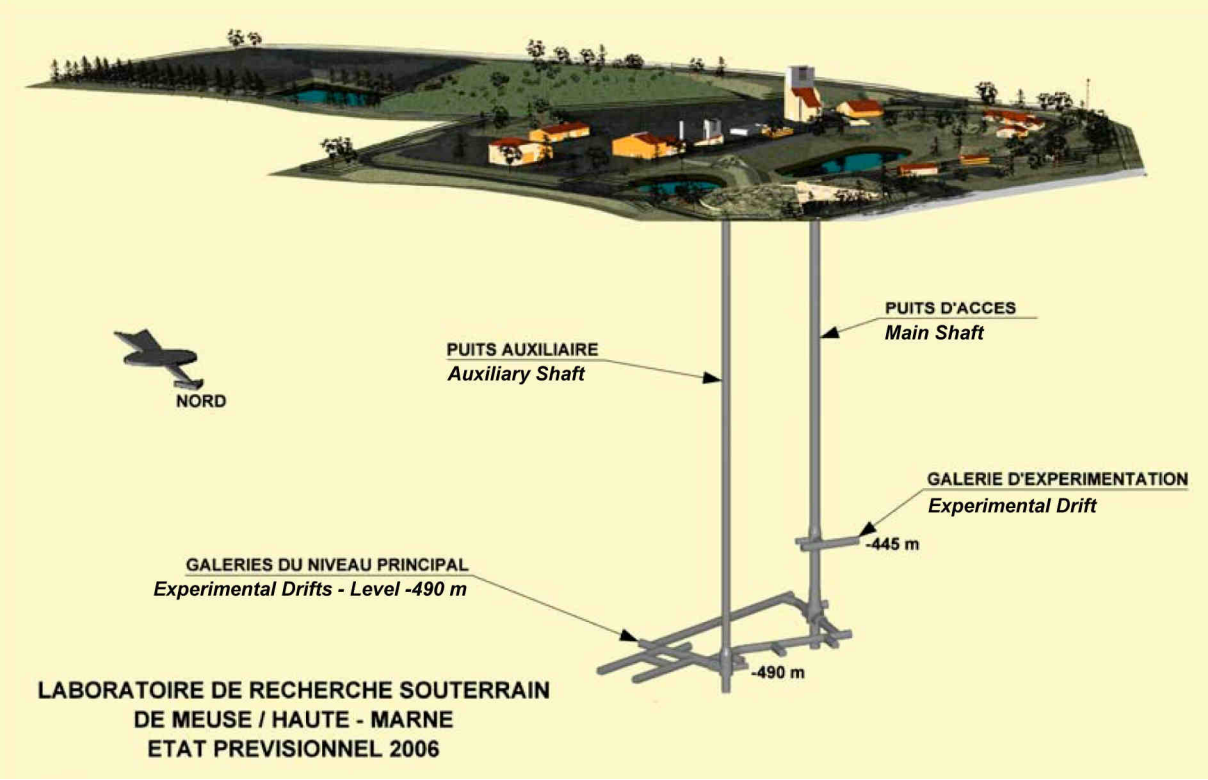

The tests, dedicated to the transport characterisation of the EDZ/EdZ, were performed with gas or water in 12 short boreholes drilled from the drift floor some 2 to 3.5 metres downward. The procedure included several types of tests including single-hole tests (pulse; constant rate injection; etc.), multi-hole interference tests and dipole tracer tests. In addition, some of the tests were repeated after days, weeks and months to investigate any changes of the EDZ flow properties.

Slot cutting itself was carried out in the floor strata of the GKE Drift by means of a specially designed saw equipment which functioned without any problems. Two slots, each 7 cm wide and about 2.0 to 2.1 m deep, were cut and subsequently filled with resin (Figures 3-51 and 3-52). A third slot, 33 cm wide and 2.0 m deep, was also cut. It should be noted that the vertical and unsupported saw-cut remained stable and open for about one month after which it was back-filled with bentonite bricks for a swelling pressure test.

Figure 3-50. Set up of the KEY experiment (after Lavanchy *et al.* 2007)

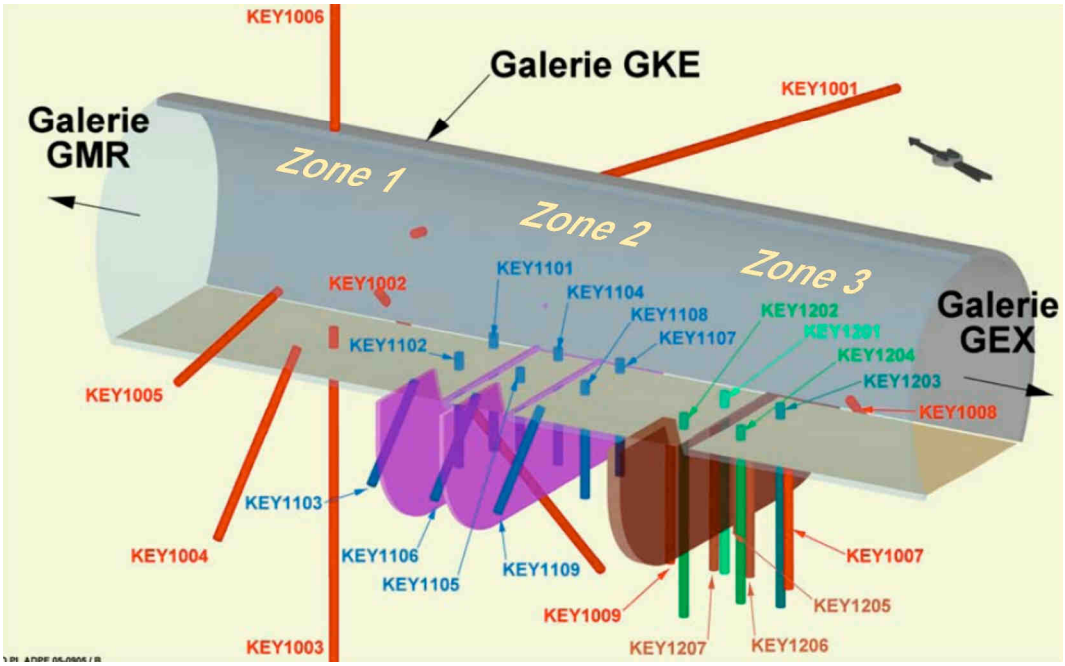

Figure 3-51. Geometry of the 7 cm wide saw cut slot KEY No. 1 (Andra 2005b)

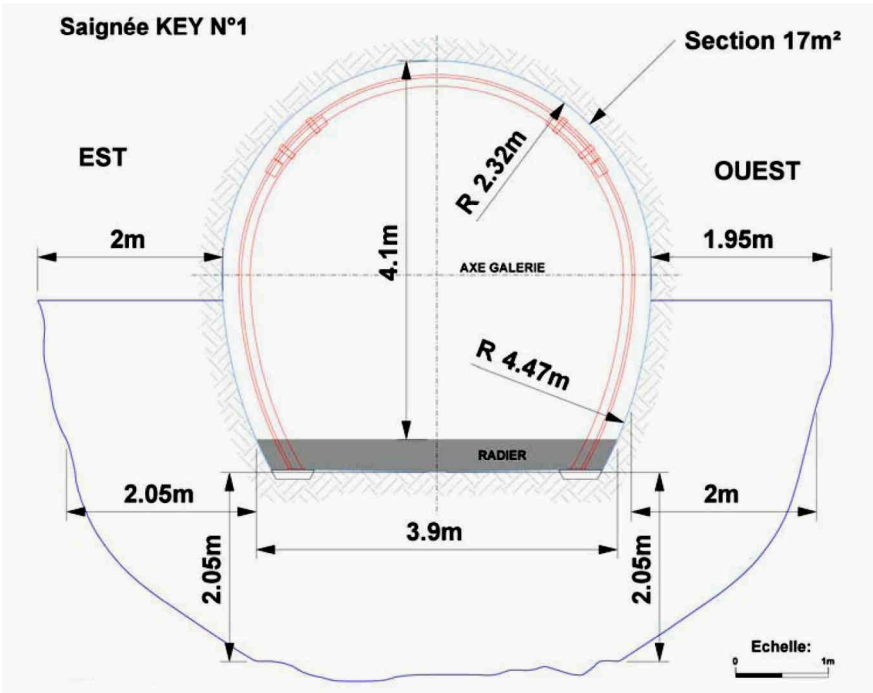

Figure 3-52. Saw cutting of a 7 cm wide slot in the Bure URL
(out of Andra 2005b)

The following main results were achieved within the 3 m x 3.2 m drift floor strata test zone shown in Figure 3-53:

- The pre-slot permeability distribution around the drift was quite heterogeneous. Various permeability domains could be identified depending on the position and orientation of the borehole as well as distance from the drift floor as follows (Delay *et al.* 2007):

  - In the first metre beneath the floor there were values in the range of between $1*10^{-9}$ m² and $5*10^{-14}$ m², except for some parts (three out of nine domains) where the permeability was measured to be equivalent with that of the saturated undisturbed rock ($<1*10^{-20}$ m²); and

  - at depths of between 1 and 2 metres beneath the floor there were constantly values close to that of the undisturbed rock.

- After cutting and filling of the slots with resins, all flow paths oriented along the drift, which were identified prior to slot cutting, appeared to be interrupted by the resin infill (Figure 3-53).

- However, new vertical connections to the drift floor appeared locally in many boreholes, thus showing an increase of the EDZ with depth (Lavanchy *et al.* 2007).

Figure 3-53. Sequence of permeability tests in nine boreholes (KEY Nos. 1101 ... 09) adjacent to and in between KEY Slots Nos. 1 and 2 with indication of old and new flow pathways and interruptions by resin-filled slots (from Andra 2005b)

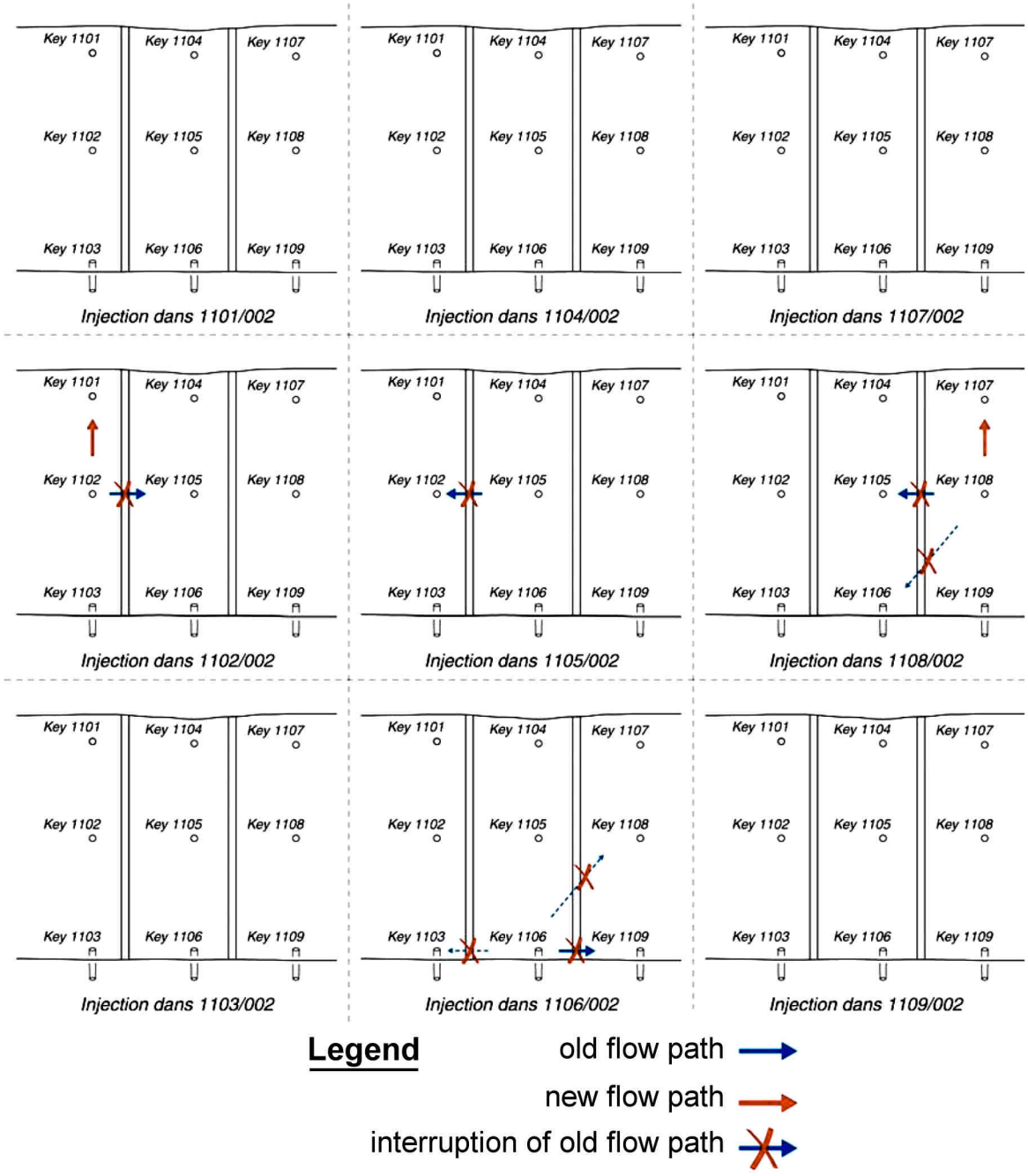

In general, the results of the KEY experiment has proven that the slot cutting concept can stop any water flow along drifts, as long as the slots are deeper than the extent of the fractured zone in the EDZ. Locally, the EDZ can be extended by the existence of the slots and adjacent boreholes, however, there seems to be no hydraulic short-circuit generated by the slot cutting procedure itself.

3.2.5 Summary of self-sealing evidence in URL field tests

Table 3-6 summarises the URL field tests, presented above, in which self-sealing has been observed. It also specifies the order of magnitude of the monitored sealing effects.

Table 3-6. Examples of URL tests in which sealing effects have been observed (summary)

Report Section	Location	Test Objective	Experiment Technique employed	Main result Legend: as in Table 3-3
3.2.2	Mont Terri URL	Influence of resaturation on fracture transmissivity T	EB (engineered barrier) Experiment	In the EDZ-fractured zone: K ↓ at a rate of $\sim 10^{-1}$ [m/s] per annum
			GS (gas frac self-sealing) Experiment	T ↓ to ~ intrinsic levels of $\sim 8*10^{-13}$ [m²/s] in ~2 years (1999 – 2001)
			EH-Experim. Part a): Single EDZ fracture	T ↓ at a rate of $\sim 10^{-1}$ [m²/s] per annum
			EH-Experim. Part b): EDZ fracture network	T ↓ from $\sim 5*10^{-7} \rightarrow 2 * 10^{-9}$ [m²/s] in ~3 years (1999 – April 2002)
		Influence of mechanical stimulation of fracture closure on T	SELFRAC I: Directional loading of EDZ extension fractures by Plate Load Test (PLT)	T ↓ from $\sim 2 * 10^{-9} \rightarrow 5 * 10^{-11}$ [m²/s] at PLT pressure of 4.8 MPa
			SELFRAC II: Isotropic loading of radial EDZ borehole combined with hydraulic testing in adjacent test intervals	T ↓ from $\sim 5*10^{-11} \rightarrow 2 * 10^{-13}$ [m²/s] at an effective dilatometer pressure of ~3.5 MPa
		Cutting off EDZ flow paths along the tunnel axis	EZ-A Experiment: EDZ cut-off by axial slots	k ↓ during water injection.
3.2.3	HADES URF	Depth of EDZ at which flow along fractures	Connecting Gallery: Oxidation of ~15 year old EDZ fractures	Evidence of sealing of EDZ fractures from air circulation of old test drift beyond 1 m depth
		Influence of resaturation on permeability k	SELFRAC III:	In the EDZ-fractured zone: k ↓ by ~ ½ 10^{-1} [m²] per annum Porewater pressure build-up in some nearest piezometers around the gallery measuring initially suction, then atmospheric pressure (opening of fracture).
			SELFRAC IV a: Collapsing borehole test	Qualitative evidence: Complete collapse of borehole after two months, followed by a recovery of stresses and porewater pressure
			SELFRAC IV b: Instrumented core	Qualitative evidence of sealing of the Boom Clay
3.2.4	Bure URL	Cutting off EDZ flow paths along the tunnel axis	KEY Experiment by cutting axial slots	Down to 1m depth: EDZ flow paths effectively cut-off: k ↓ from $\sim 1* 10^{-9}$ - $5* 10^{-14}$ [m²] ↓↓ to $1* 10^{-20}$ [m²] (≈ intrinsic value).

In summary: When referring to *in situ* URL tests with samples in the 1 m to 10 m range, self-sealing is a very common phenomenon in a wide variety of argillaceous soils and rocks which are currently considered in context with deep geological repositories, from plastic clays (Boom Clay in the HADES URF) to indurated clays (Opalinus Clay at Mont Terri and Callovo-Oxfordian argillites at the Meuse-Haute Marne URL).

3.3 Evidence in geological and geotechnical analogues

3.3.1 Introduction

The object of the following compilation are argillaceous formations with a different degree of induration. It includes moderately indurated Opalinus Clay (Section 3.3.2) and tectonically strongly affected Boda Clay (Section 3.3.3). It furthermore includes hard fissile claystones as a rock variety with a very high degree of induration (Section 3.3.4). The 'Clay Smear' concept of the hydrocarbons industry is briefly reviewed on its applicability to repositories in argillaceous formations (Section 3.3.5). Furthermore, some indirect field evidence is put forward in the form of tracer concentration profiles in porewater (Section 3.3.6) and the specific occurrence of the orthogonal joint system in argillaceous formations (Section 3.3.7).

Field observations on self-sealing in argillaceous formations have been made in surface outcrops, shallow and deep boreholes and in geotechnical structures such as traffic tunnels. The investigations can be classified either as direct evidence (e.g. mapping of water-bearing structures in tunnels) or indirect evidence (e.g. structural analysis of geological fault zones; logging of boreholes; establishing tracer profiles). Accordingly, there is a large pool of technical and scientific methods which may be employed (Table 3-7).

Table 3-7. Overview of field observations on self-sealing effects in argillaceous formations presented in Section 3.3

Report Section	Method applied	Target Formation	Over-burden [m]	Study object
3.3.2	Mapping; core & borehole logging	Opalinus Clay (OPA)	≤ 40 m	Surface outcrops; shallow boreholes
	Tunnel mapping		≤ 800 m	Traffic tunnels in Northern Switzerland
3.3.3	Core logging and permeability testing	Boda Clay (BCF)	~1050	Structure of fault zones
3.3.4	Mapping and lab micro-porosity studies	Variscan claystone	n.a.	Reconstruction of the permeability evolution of fault zone lithotypes
3.3.5	Mapping, core logging; modelling	Sandstone-claystone sequence	n.a.	Specification of Clay Smear Potential (CSP), Shale Gouge Ratio (SGR), etc.
3.3.6	Borehole logging; chemical analysis	argillaceous formations in general	100-500m range	Tracer concentration profiles
3.3.7	Mapping and joint formation theory		0 – ~300m	Surface outcrops and URLs

3.3.2 Field observations in Opalinus Clay

3.3.2.1 Surface outcrops and shallow boreholes

Phenomena observed in clay pits of northern Switzerland (Mazurek *et al.* 1996) give evidence of a well-developed groundwater circulation system in the near-surface Opalinus Clay. In the uppermost 10 to 15 m, joint and fault systems have several cm-thick oxidation rims (Figure 3-54), and gypsum occurs on fracture surfaces.

Figure 3-54. Oxidation rims of fractures in Opalinus Clay
(Clay pit Siblingen; Photo: A. Gautschi).

As part of a research project focussing on various aspects of hazardous waste disposal in the Opalinus Clay of the adjacent SW-Germany under the auspices of the Geological Survey of the State of Baden-Württemberg, a wide variety of hydraulic tests and drill core analyses was performed in 47 shallow boreholes (Hekel 1994). Examples are shown in Figures 3-55 and 3-56.

The results consistently show that, in an upper section (10 - 30 m depth beneath the topographic surface), there is a relatively high hydraulic conductivity which ranges from about 10^{-7} to 10^{-4} m/s. That upper section contains numerous sub-vertical and horizontal fractures caused or reactivated by stress release due to erosion of the overlying strata. Further below, the hydraulic conductivity decreases by several orders of magnitude (Figure 3-56) and, in one borehole, saline waters occur at a depth of about 50 m, suggesting little or no advective flow over geologic times. There is an inverse correlation between hydraulic conductivity and chloride content (Figure 3-56, left).

It was found that the thickness of the highly permeable upper domain is closely related to the geomorphologic evolution and the current topographic relief. Thicker zones of chemical and mechanical alteration (up to 30 m thick) are developed beneath old valleys and topographic ridges, whereas thinner zones generally occur below geologically young valley systems (Hekel 1994).

Figure 3-55. Borehole camera logs in Opalinus Clay showing discrete inflow locations during pumping visualised by limonite traces
(from Hekel 1994).

At greater depths the permeability of the Opalinus Clay decreases by several orders of magnitude (Figure 3-56 right). Hydraulic tests in deeper boreholes (test intervals below 300 m; Nagra 2002b, p. 321) yielded hydraulic conductivities of $<10^{-12}$ m/s, even though joints and faults were included in some of the test intervals.

Figure 3-56. Typical hydraulic conductivity borehole profiles
Left: Opalinus Clay at near-surface levels (Southern Germany; after Hekel 1994)
Right: Over greater depth range (Palfris Formation, Wellenberg, Switzerland; after Nagra 1997)

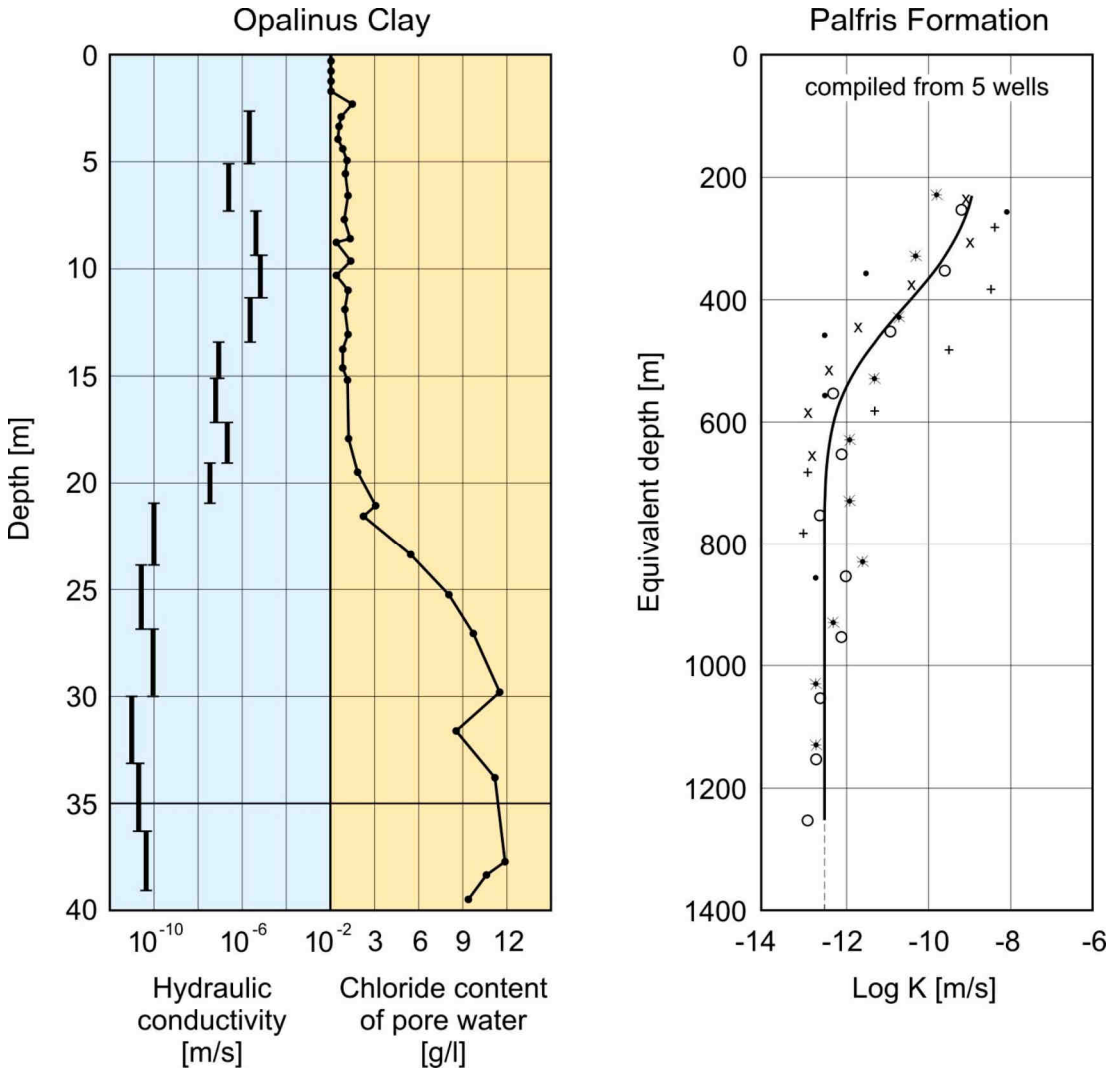

3.3.2.2 Observations in geotechnical systems: Traffic tunnels of northern Switzerland

The above-mentioned observations are consistent with hydrogeological observations and data from Opalinus Clay sections in traffic tunnels in the Folded Jura Mountains of northern Switzerland, some of the tunnels were more than 100 years old (Figure 3-57 and Table 3-8; Gautschi 2001). Over a total length of 6600 m and despite extensive faulting, no water inflows could be detected in tunnel sections passing through the Opalinus Clay where the overburden exceeds 200 m. Slight water inflows have been observed in a few cases with less than 200m overburden. In most cases, however, and even in locations of relatively high deformations of the strata and faults, there is no observable water inflows to the tunnels.

The absence of water-conducting features, even in deformed and faulted zones, provides indirect evidence for an effective self-sealing capability of the Opalinus Clay.

Table 3-8. Hydrogeological information from Opalinus Clay sections of tunnels in the folded Jura Mountains, Switzerland (from Gautschi 2001; for location of tunnels, refer to Figure 3-57)

Tunnel and year of construction	Observed section in the Opalinus Clay		Over-burden [m]	Characterisation of water flow, degree of rock deformation
Bözberg A3 road tunnel (1991)	200 m (west tunnel), 120 m (east tunnel)		120	No indication of water during construction; one damp patch at gap between liner elements in tunnel after one year. Opalinus Clay partly strongly tectonised
Bözberg railway tunnel (~ 1874)	130 m		200	No water inflows. Opalinus Clay less strongly tectonised than in road tunnel
Hauenstein Base railway tunnel (1914)	120 m		300–400	No water inflows. Opalinus Clay less disturbed, dipping with an angle of ~ 45°
Upper Hauenstein Railway tunnel (~ 1860)	150 m (tunnel), 100 m (shaft)		180	No water inflows. Opalinus Clay less disturbed, dipping with an angle of ~ 30°
Belchen A2 road tunnel (1965)	4 x 500 m (4 parallel pilot tunnels, 2 each in E- and W-tunnel; no data for main tunnel)		100–300	One damp patch in fracture zone with calcite. Opalinus Clay generally strongly tectonised and imbricated. Overburden < 150 m
Weissenstein Railway tunnel (1907)	375 m		400–500	No water inflows. Opalinus Clay strongly disturbed, generally steeply dipping (core of two anticlines)
Grenchenberg Railway tunnel (1914)	350 m		700–800	No water inflows. Opalinus Clay strongly disturbed, generally steeply dipping (core of anticline)
Mont Terri A16 road tunnel (1991)	South: 2x240 m	Reconnaissance / security tunnel, road tunnel parallel to security tunnel)	300	No indication of water inflows. Opalinus Clay slightly disturbed, dipping with an angle of approx. 30° (southern limb of anticline)
	North: 2x140 m		150–200	Two drip points in limy-sandy intercalation. Opalinus Clay strongly tectonised, imbricated (overthrust northern limb of anticline)
Mont Russelin A16 road tunnel (1991)	2 x 1100 m (pilot tunnel and main tunnel, around 40 m beside pilot tunnel)		300–400	No indication of water inflows. Opalinus Clay generally strongly tectonised and imbricated (core of anticline)
Raimeux A16 road tunnel (1996)	240 m (reconnaissance tunnel)		120–140	One drip point in clayey facies; one water inflow in calcareous facies (NaCl-rich water). Opalinus Clay subvertical, strongly tectonised.

The above observations are supplemented by evidence from various sites in northern Switzerland (Table 3-9) and by clay porewater hydrochemical and isotopic data (refer to Section 3.3.6 below).

Figure 3-57. Location map of the traffic tunnel study sites in Opalinus Clay of northern Switzerland with major geotectonic units (from Gautschi 2001)

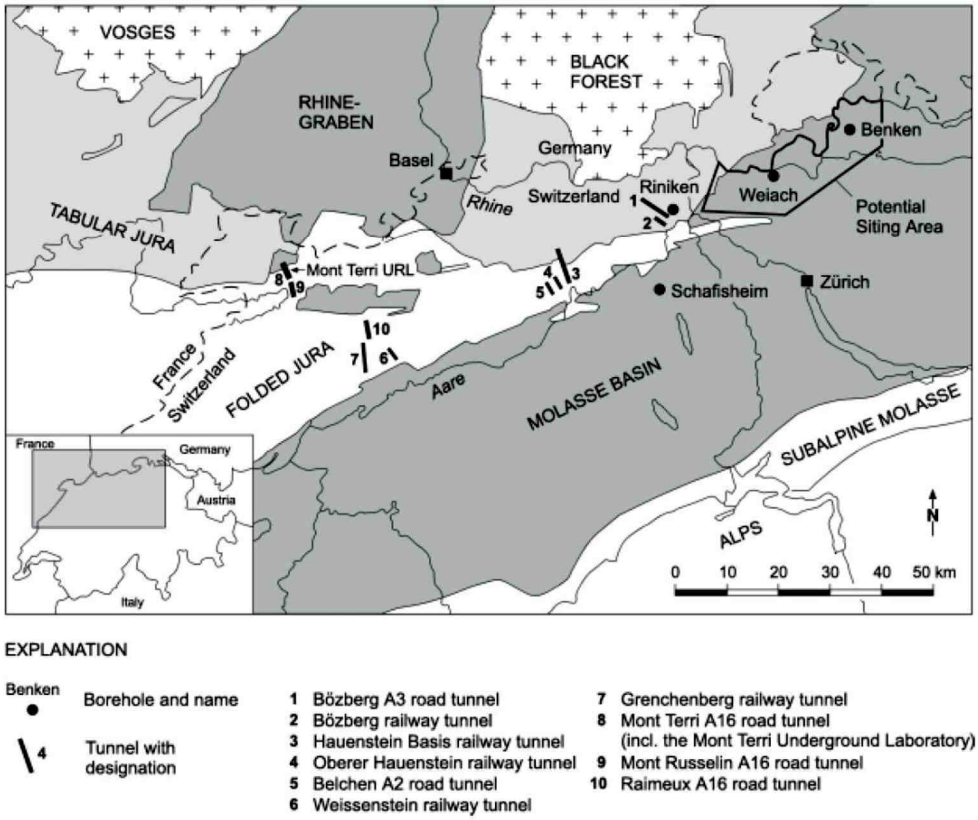

Table 3-9. Field evidence for self-sealing of fractures in the Opalinus Clay of northern Switzerland (after Nagra 2002b: 332)

Locality	Evidence	Consequences on current state
Folded Jura Mountains	Geological mapping in old railways and road tunnels: No wet spots at greater overburden	At high overburden, the hydraulic conductivity of brittle structures (faults; joints) is very small
Central Molasse basin	Distinct deformation structures disclosed in the drillholes Schafisheim and Riniken: No increased hydraulic conductivity in packer tests	Today, even large brittle structures (faults, joints etc.) are hydraulically not distinguishable from the rock matrix
Eastern Molasse basin	Small brittle structures disclosed in drillholes Weiach and Benken: No increased hydraulic conductivity in packer tests	
Entire area of northern Switzerland (Molasse basin and folded Jura Mountains)	In the Opalinus Clay vein infillings are extremely rare and insignificant in volume. No mineralogical differences between fault gouges and host rock matrix; no mineralogical alteration or cementation in the rock matrix along brittle fault structures	Over its geological evolution history, the Opalinus Clay was not subject to any major rock matrix – water interactions which are associated with significant advective transport

3.3.3 Field observations in Boda Clay Formation (BCF)

The Permian Boda Clay Formation (BCF) in Hungary had been strongly affected by tectonic events. A comprehensive characterisation programme was carried out between 1993 and 1999 (ref. to Section A.2.6.8). Most of the explored discontinuities are of tectonic (and lithological) origin and are entirely closed and hydraulically irrelevant. The joints and fractures are generally completely filled with various (clayey, carbonate or sulphatic) infilling materials (Szücs *et al.* 2005; Figure 3-58). No time frame is specified which might be needed to achieve such type and degree of self-sealing.

Figure 3-58. Sample of a Cretaceous tectonic zone of the Permian Boda Claystone Formation (from Szücs *et al.* 2005)

3.3.4 Field observations on faults in hard fissile claystone

Based on field outcrop and laboratory analysis studies, Holland *et al.* (2006) reconstructed the evolution of microstructure and corresponding transport properties in normal fault zones of hard fissile claystones (Figure 3-59). The study area was in the Variscan foreland thrust belt in the Ardennes, Belgium, and Eifel, Germany. Holland *et al.* (2006) showed that upper crustal fault zones in strong, brittle lithologies were subject to early sectional re-sealing, consisting of claystone, which led to local barriers to along-fault fluid flow.

Detailed mapping showed that the processes of fault gouge evolution in hard claystones started with cataclasis that produced a soft clay gouge which filled the space between the initial fragments. This re-sealed the initially highly porous and permeable damage zone. It was shown that there are four different lithotypes from (1) intact shale in the wall rock, (2 and 3) broken wall rock fragments with various amounts of clay to (4) a fully reworked gouge. These lithotypes reflect different evolutionary stages. The similar mineralogy of the different lithotypes suggests that the main process involved is mechanical fragmentation with minor contribution by diagenetic changes or weathering, accompanied by large changes in microstructure, porosity and transport properties. While the wall rock has a very low porosity and permeability, initial deformation resulted in a much higher porosity with large pores. The reworked clay gouge also has a high porosity, but its pore size corresponds to a lower permeability and higher capillary seal capacity.

Figure 3-59. Details of a fault zone in hard fissile Variscan claystone shown as a photo collage (right) and as field interpretation (left). The fault zone is sub-parallel to the bedding of a claystone/sandstone sequence. Its width is variable and shows a heterogeneous assemblage of strands of fault gouge and differently deformed claystone material. Localisation towards a single slip-plane is not evident (from Holland *et al.* 2006; reprinted with permission from Elsevier).

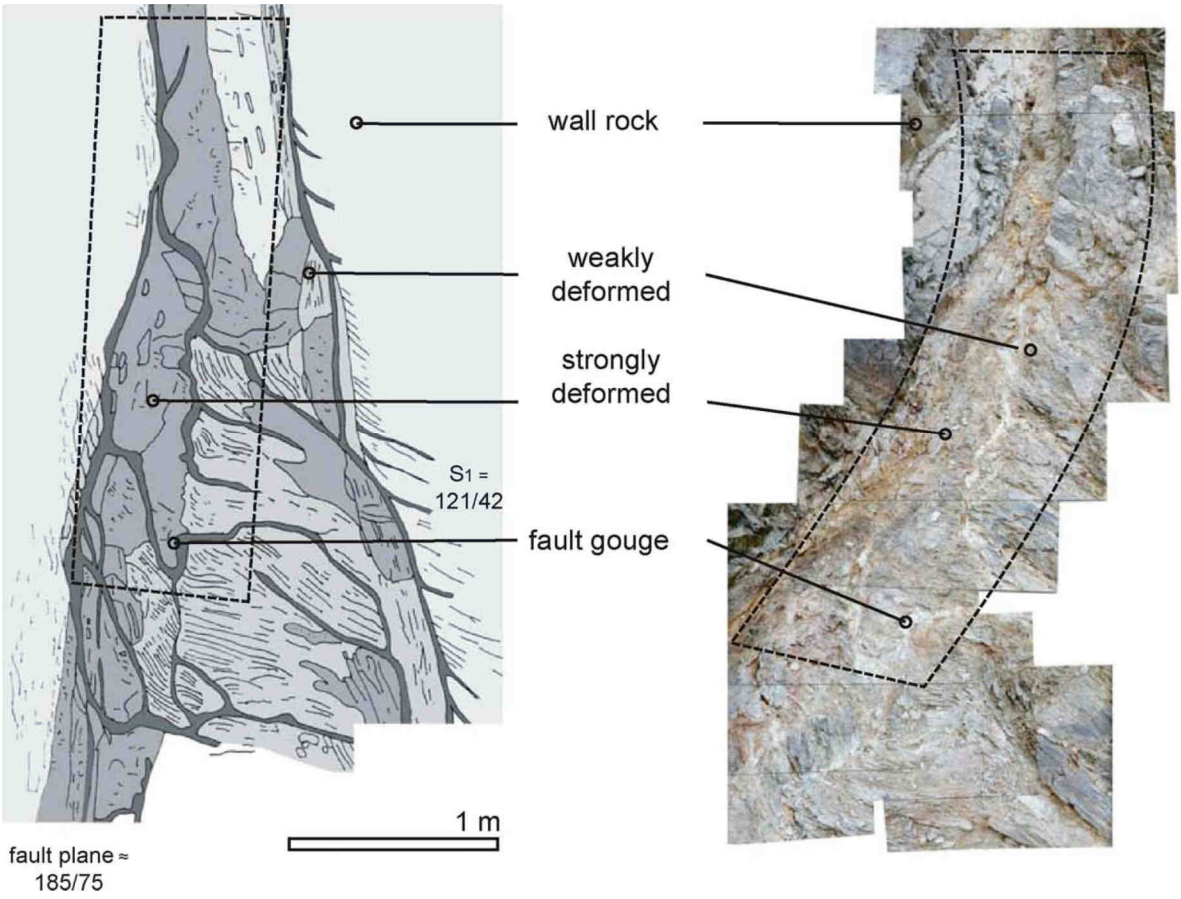

The evolution of fault gouge with progressive throw is interpreted by Holland *et al.* (2006) as follows (Figure 3-60): A cohesive and undeformed shale with a low permeability ('wall rock' type) reacts on initial faulting by a loss of cohesion due to kinking, folding and microfracturing of the fabric into the 'distorted rock' lithotype. The 'distorted rock' is easily recognisable by the deformed foliation and poor coherence. The increase in porosity (up to ~28%) is an effect of the distortion of the fabric resulting in relatively large pores and corresponding low entry pressures in Hg injection experiments. This rock type may reflect what is commonly termed 'deformation zone'. Due to the dense crack network, the highest permeability among the four lithotypes can be expected at this stage. Reddish discolouring of the deformed lithotypes might document alteration of pyrite into Fe-oxides. Progressive deformation / fault throw breaks down the fabric further to a 'transition material'. The total porosity hardly changes at this stage while the distribution of pore size promotes smaller diameters due to the overall reduction in grain size. The final 'clay gouge' type is the end member of the fault development and is dominated by an almost pure clay. The mechanical breakdown at shallow depth ends with a large volume of small pores. Despite the high porosity, the initial entry pressure is almost recovered.

Figure 3-60. Evolution model of fault zone lithotypes
The axes show the logarithm of the Hg injection pressure (at 20% saturation) versus the bulk porosity (vol. %) (from Holland *et al.* 2006; reprinted with permission from Elsevier)

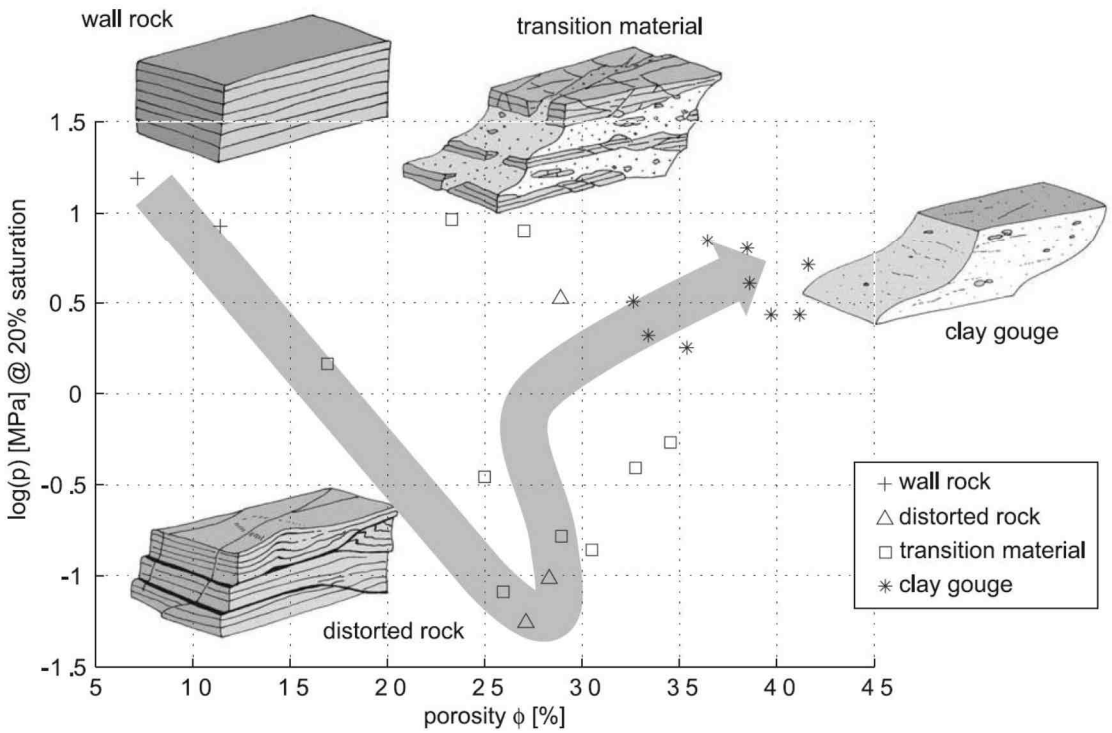

3.3.5 Empirical factors of the hydrocarbons industry

In an attempt to predict the likely sealing capacity of a fault plane, a number of fault-seal algorithms have been developed within the hydrocarbons industry. These include the 'Shale Gouge Ratio' (SGR), 'Clay Smear Potential'(CSP) and the 'Shale Smear Factor' (SSF). For a review of these empirical factors, ref. to Horseman *et al.* (2005) and Jolley *et al.* (2007). The algorithms give estimates of pore pressure differences across faults, and thus of the sealing capacity. Some further considerations on this topic are made in Section 4.2.2 in relation with sealing mechanisms of fractures when subjected to shear.

'Clay Smear' is a loosely defined term. In its most general meaning, the term includes all processes that somehow transform clay in the wall rock into clay in the fault. Zee and Urai (2005) carried out detailed field observations of normal faults formed at shallow depth in a deltaic sand–clay sequence. The study identified the main structural elements during the early stages of fault development. More than 450 segmented faults were investigated, many of which contain clay smear. The finding was that all faults had a continuous clay smear, except for the places where a sand bed had an offset smaller than its thickness, and therefore had not moved past clay. Several processes of clay incorporation into the fault gouge were identified (e.g. lateral clay injection and "preferred smear"; Zee and Urai 2005, p. 2298). Although on average the clay content observed correlates well with the average clay content of the faulted section, there are large variations in clay content controlled by local complexity in deformation in line with observations mentioned in the previous Section 3.3.4.

3.3.6 Tracer concentration profiles in porewater

In the framework of the CLAYTRAC project, the spatial distributions of conservative porewater tracers (halogens, stable water isotopes, noble gases) in argillaceous units were studied (Mazurek *et al.* 2009). The main objectives included the identification of the relevant solute transport process(es), the time scales related to the build-up of the currently observed tracer distributions, and aspects related to scale issues (e.g. applicability of laboratory-derived diffusion coefficients on the formation scale). One of the advantages of the chosen approach is the fact that the tracer distributions integrate processes that occurred in the formation over long time scales (thousands to millions of years), thus extending the narrow time window of observations made in boreholes or underground facilities.

With regard to the hydraulic relevance of faults (or, conversely, their self-sealing capacity), the following conclusions were drawn:

- With the exception of Opalinus Clay at Mont Terri and Mont Russelin, all sites considered within CLAYTRAC are located in near-horizontally bedded basins. Boom Clay at Mol and Essen, London Clay at Bradwell, the Callovo-Oxfordian at Bure and Opalinus Clay at Benken are essentially devoid of brittle discontinuities and so not suited to explore their possible hydraulic significance.

- The Couche Silteuse (Gard, southern France) contains fractures and faults in Boreholes MAR402 and MAR501, but there is no evident correlation in variations of tracer contents. Admittedly, the tracer-data base in these boreholes is limited.

- The Toarcian-Domerian at Tournemire is highly indurated and fractured. On a large scale, there is no clear link between tracer concentrations and brittle structures. On a scale of up to 1 m, local disturbances were identified, although it is not evident to what extent these anomalies can be related to the disturbance created by the construction of the tunnel. It was shown that enhanced hydraulic conductivities measured in borehole tests are not applicable on the scale of the formation, probably due to limited connectivity on a large scale.

- The tracer profiles for Cl^-, $\delta^{18}O$, δ^2H and He across the Opalinus Clay at Mont Terri intersects the Main Fault, an about 1 m thick thrust containing abundantly crushed fault rock (ref. to Figures 2-4 and Figures A.4.7 and .8 in Appendix A.4). Figure 3-61 gives evidence that there are no anomalies in tracer contents that could be related to this fault. Together with the known hydraulic insignificance of this fault at present time, it is concluded that the transport properties of this fault are not markedly different from those of the rock matrix, and that this has been so for extended periods of time in the past.

In total: Five study sites are essentially unfractured, whereas four contain various types of brittle structures. In the latter, contents of porewater tracers are not disturbed by the discontinuities.

Figure 3-61. Model calculation (lines) rationalising the observed Cl^- profile (symbols) across Opalinus Clay at Mont Terri (Mazurek *et al.* 2009).
Note that the Main Fault (shown in pink) does nor affect the Cl^- –distribution in the profile. Grey areas represent aquifers embedding Opalinus Clay. The initial Cl^- concentration is assumed to be equivalent to that in present sea water, and numbers indicate the time in Ma elapsed since flushing of the upper aquifer with meteoric water

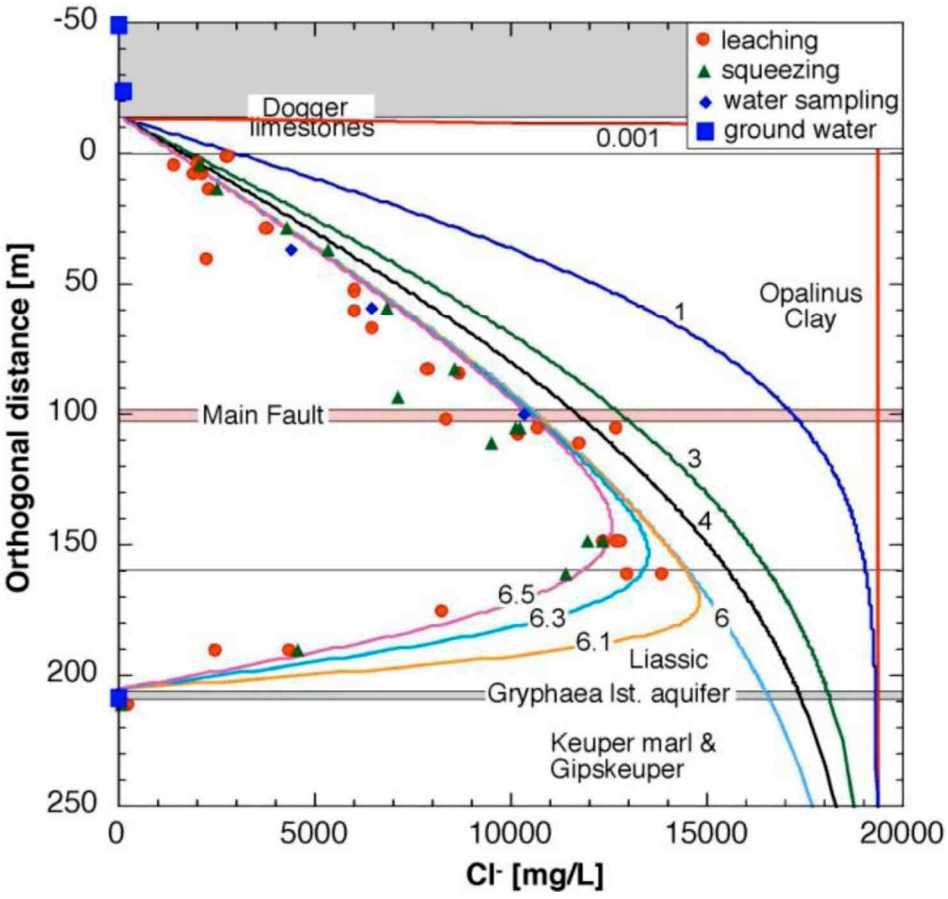

3.3.7 Characteristics of the orthogonal joint system in argillaceous formations

A geologic self-sealing analogue might be constituted by the specific characteristics of the orthogonal joint system in argillaceous formations (Section A.4.1.4). According to most theories (Mandl 2005) the orthogonal joint system should have been generated in an early uplift phase of a basin evolution and should be present not only at the topographic surface but also at depth in the existing URLs. The latter, however, is not necessarily the case as evidenced by the apparent non-existence of the orthogonal joint system in the URLs of Mol (Dehandschutter 2005) and Mont Terri (Nussbaum *et al.* 2005).

The lack of the orthogonal joint system at URL levels can only be reasonably explained either by an alternative theory of the formation of the joint system (Dehandschutter 2004) or by the assumption that, in course of its geological history, the joint system has been perfectly sealed (and healed).

3.3.8 Summary of self-sealing observations in geological and geotechnical analogues

There are numerous observations in natural and geotechnical systems which strongly indicate the occurrence and, in fact, prevalence of self-sealing in argillaceous formations, at least where their consistency is soft or slightly indurated.

- In the Opalinus Clay of S.-W. Germany hydraulic tests in shallow boreholes (< ~50 m) revealed that the hydraulic conductivity is comparatively high near the surface but quickly decreases with depth by several orders of magnitude, approaching the intrinsic value of the undisturbed Opalinus Clay ($<10^{-12}$ m/s) (Hekel 1994).

- The above finding of a rapid permeability decrease with depth is supported by observations in traffic tunnels in the folded Swiss Jura Mountains and by hydraulic tests in deeper boreholes (test intervals below 300 m) of northern Switzerland (Tables 3-8 and 3-9), even though joints and faults were included in some of the test intervals.

- The Permian Boda Clay Formation (BCF) in Hungary, which had been strongly affected by tectonic events and is intersected by numerous discontinuities of tectonic and diagenetic origins, carries clear signs of self-sealing (Figure 3-58). Precipitation of newly formed minerals in open fractures, e.g. in the form of veins, contribute to a reduction of the fractures' transmissivity and to sealing of the formation.

- The evolution of the microstructure and corresponding transport properties in normal fault zones of hard fissile claystones was studied by Holland *et al.* (2006) in the Variscan foreland thrust belt of the Ardennes, Belgium, and Eifel, Germany. It has been shown that the upper crustal fault zones in strong, brittle lithologies were subject to early sectional re-sealing, consisting of claystone, which led to local barriers to along-fault fluid flow.

- In argillaceous units, the contents of the conservative porewater tracers (halogens, stable water isotopes, noble gases) are essentially unaffected by the discontinuities. This points to an effective sealing of these discontinuities (CLAYTRAC project; Mazurek *et al.* 2009).

- The specific characteristics of the orthogonal joint system in argillaceous formations can only be reasonably explained either by an alternative to the standard joint formation theory or by the assumption that, in course of its geological history, the joint system has been perfectly sealed.

In summary: When referring to geological and geotechnical analogues with sample dimensions of up to ~1 km range, self-sealing is a very common process in a wide variety of argillaceous soils and rocks such as those currently considered in context with deep geological repositories (Boom Clay; Boda Clay; Callovo-Oxfordian argillites; Opalinus Clay) and in shales and slates of interest to the hydrocarbons industry.

3.4 Conclusion of Chapter 3

Overwhelming evidence has been compiled that self-sealing is a very common phenomenon in a wide variety of argillaceous soils and rocks currently being considered in the context of deep geological repositories.

Self-sealing can be observed over a large spread of scales: At the millimetre to metre scale in laboratory test samples (Section 3.1), at about repository scales (10 to 100 m range) in URL field tests (Section 3.2) and at the kilometre scale in geologic and geotechnical analogues such as old traffic tunnels and hydrocarbon reservoirs (Section 3.3).

Self-sealing occurs at various rates which depend on the site-specific circumstances such as the type of clay minerals, degree of induration and chemistry of the porewater. In referring to Tables 3-3 and 3-6, which summarise the results of the laboratory and URL field self-sealing tests considered within this report, it becomes apparent that there is a consistent permeability reduction trend, irrespectively of the type and dimension of the test. Typically, the reduction rate is in the order of about 10^{-1} to 10^{-2} per annum, meaning that, over a time span of one year, the permeability is reduced to 10^{-2} of its initial value.

4. SEALING MECHANISMS AND MODELLING

Self-sealing of fractures in argillaceous repositories is a phenomenon which is associated with various mechanisms controlled by numerous factors. For safety assessment and PA it is important to understand the sealing mechanisms and their possible interactions with each other.

In laboratory and field tests and in geologic and geotechnical analogues described in the previous Section 3, ample evidence has been collected not only on the existence of self-sealing as such but on the large variety of processes which obviously are involved in self-sealing in argillaceous media. In line with that evidence and following Marschall *et al.* (2008b), it is suggested that the following mechanisms contribute to sealing in argillaceous formations:

1. Compaction of the intact rock body (compression of solid framework; pore space reduction).

2. Mechanical closure of fractures (increased normal stress acting normal to the fracture; contractant behaviour in shear; creep of the fracture wall material).

3. Physico-chemical interaction between the weakly/strongly bound porewater in the micro-, meso- and macropores and the clay platelet skeleton. Macroscopically, that interaction is evidenced as swelling and disaggregation of clay aggregates.

4. Sedimentation combined with clogging of fractures by colloidal phases.

5. Precipitation of solutes in the form of mineral coatings of fracture walls.

These mechanisms are considered in Sections 4.1 to 4.5 below. Aspects of numerical modelling under the inclusion of sealing mechanisms will be considered in Section 4.6.

4.1 Sealing by material compaction [10]

Compaction of argillaceous materials may principally be achieved by a reduction of the volume of the solid particles and/or the reduction of the pore space between the particles. In argillaceous media a high portion of solid particles consists of clay platelets which tend to assemble in complex frameworks as schematically shown in Figure A.2-9. In contrast to the individual platelets, the framework as a whole is reasonably deformable when subjected to external and/or internal loads. This might lead to significant changes in the shape and volume of the framework's voids ('pore space') and thus to changes of the fluid flow characteristics of the material.

The theoretical formulation of fluid flow and the movements of solutes in porous media is the domain of the porous media theory (Coussy 2004). The underlying assumptions of that theory and

[10] In this context, the term "sealing" is used in a wider sense than in the definition of Tsang and Bernier (2005) (see Section 2.1) who assign that term exclusively to fractures.

some of its key terms and concepts (e.g. 'porosity', 'Darcy's law', 'permeability', 'hydraulic conductivity') are reviewed in Appendix A.5.

4.1.1 Applicability of porous media theory to argillaceous formations

The impact of compaction on the transport properties of clayey formations can be deduced from the diagram of Figure 4-1 (Mazurek *et al.* 2009). It depicts the experimentally determined relationship between the water-accessible porosity *n* and the hydraulic conductivity *K* of various argillaceous formations, from soft unconsolidated sea-floor sediments to strongly indurated shales. From the diagram it is evident that, for a porosity larger than ca. 0.1, there is an approximate linear correlation between porosity and the logarithm of hydraulic conductivity. Boom Clay, Callovo-Oxfordian argillites and Opalinus Clay compare well with this general trend (ref. also to values presented in Table A.5-2). The good correlation and the relatively narrow uncertainty ranges suggest that fluid flow through normally and over-consolidated clays as well as through moderately indurated shale can be described adequately by means of classical continuum concepts, representing the material as a porous medium (matrix porosity).

Figure 4-1. Hydraulic conductivity of various argillaceous formations
(after Mazurek *et al.* 2009)

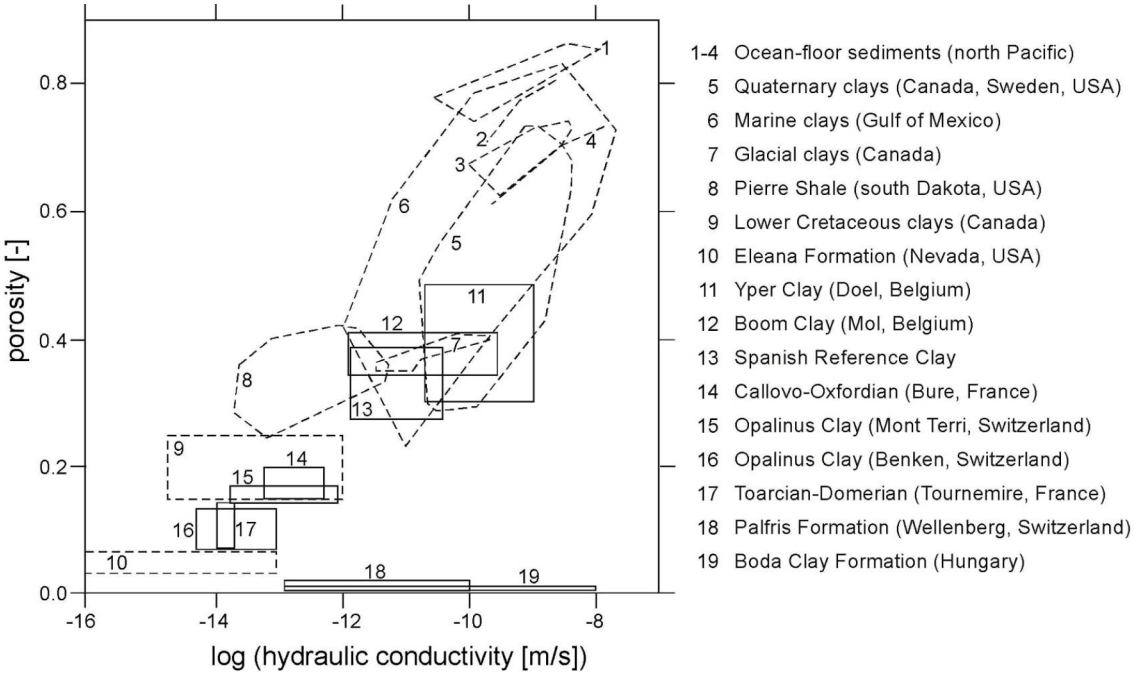

The trend of a linear *n*-versus-log*(K)* relationship, as shown in Figure 4-1, does not include highly compacted formations with a very small porosity, such as the Palfris formation in Switzerland or the Boda Clay formations in Hungary (Nos. 20 and 21 in Figure 4-1). In these formations comparatively high effective hydraulic conductivity with relatively large uncertainty ranges have been recorded. Physically, that effect can be interpreted by an increased hydraulic significance of fractures in the form of cracks and joints within the medium and an associated switch from matrix to fracture permeability. Discrete fracture network approaches may then represent more appropriate conceptual models of fluid flow transport within such formations (see Section 4.2).

4.1.2 The Kozeny-Carman relationship

Formal expressions of fluid flow in porous media exist in the form of porosity-stress and porosity-permeability coupling equations.

Porosity-stress coupling (consolidation):

$$n \approx n_0 - \kappa \log (p'/p_0') \qquad \text{(Eq. 4-1)}$$

where: n = porosity [-]
n_0 = porosity at a reference point in time [-]
p' = effective stress [Pa]
p_0' = effective stress at a reference point in time [Pa]
κ = negative slope of the unloading/reloading curve [-]

Porosity-permeability coupling (*Kozeny-Carman relationship)*:

$$K = [n^3 / (1-n)^2] \; [\rho_w * g / (\tau^2 * C_s * \rho_s^2 * S^2 * \mu_w)] \qquad \text{(Eq. 4-2)}$$

where: K = hydraulic conductivity [m/s]
n = porosity [-]
ρ_w = density of water [g/m³]
g = gravity acceleration [m/s²]
τ = turtuosity [-]
C_s = shape factor [-]
ρ_s = grain density of solids [g/m³]
S = specific surface [m²/g]
μ_w = dynamic viscosity of porewater [g/(m * s)]

Equation 4-2 provides an insight into the sensitivity of the hydraulic conductivity *K* on some important material properties. For small porosity values ($n << 1$), *K* is predicted to vary with the cube of porosity, explaining the dramatic decrease in flow rates as sediments become more compacted. The equation also predicts that *K* will vary with the reciprocal of the square of the specific surface, providing a possible explanation of the very low hydraulic conductivity of a smectite-rich clay (e.g. bentonite) with high specific surface when contrasted with, for example, a kaolinite-rich clay having a similar total porosity. The Kozeny-Carman equation works well for coarse-grained materials such as sand and some silts, and a graph of *K* against $n^3/(1-n)^2$ gives a linear relationship for these materials (Horseman *et al.* 2005).

Olsen (1962) and Dewhurst *et al.* (1999) tested the applicability of the Kozeny-Carman equation to flow in saturated clays and claystones. They noted fairly large discrepancies between predicted and measured hydraulic flows, concluding that Eq. 4-2 is accompanied with significant conceptual problems and should only be used for order of magnitude estimates of the hydraulic properties. This finding is in line with observations in the Opalinus Clay at Benken and Mont Terri. As summarised in Table 4-1, the estimate of the hydraulic conductivity via the Kozeny-Carman relationship yields values which are about a full order of magnitude higher than those determined in direct permeameter tests.

Table 4-1. K-values of the Opalinus Clay at Benken and Mont Terri: Comparison of the results from permeameter tests and estimates after Kozeny-Carman
(after Nagra 2002b)

Location	Mean Effective Stress [MPa]	Hydraulic conductivity K [m/s]	
		Permeameter test	after Kozeny-Carman ($C_s = 2.5$; $\tau = 1.41$)
Benken	12 – 16	$K_{//} = 0.3 – 0.6 \times 10^{-13}$ $K_{\perp} = 0.06 – 0.3 \times 10^{-13}$	$K \approx 5 \times 10^{-13}$
Mont Terri URL[11]	4 – 5	$K_{\perp, 50°, 35°} = 1 – 2 \times 10^{-13}$ $K_{\perp} = 0.6 – 1.2 \times 10^{-13}$	$K \approx 10 \times 10^{-13}$

4.1.3 Other porosity-permeability relationships

Valfouskaya *et al.* (2005) propose the following theoretical relation between the pore network and the intrinsic permeability of argillaceous rocks:

$$k = [1 / (8 * F)] [2 \varepsilon / (S * \rho)]^2 \qquad \text{(Eq. 4-3)}$$

where: k = intrinsic permeability [m²]
ε = porosity [-]
F = formation factor (generally equal to ε^{-2})
S = specific surface [m²/g]
ρ = bulk density [g/m³]

For the Callovo-Oxfordian argillites it is (ref. to Tables 2-3 and 2-7): $\varepsilon = 0{,}15$ thus → $F = 44$; $S = 40$ m²/g and $\rho = 2{,}43 * 10^3$ kg/m³. These parameters yield $k = 2.7 * 10^{-20}$ [m²] or, due to Eq. A.5-9, $K = 2.7 * 10^{-13}$ [m/s], values which are in agreement with on-site measurements.

Equation 4-3 is similar to the Wong and Pengra (1995) relationship:

$$k = \sigma_0 \Lambda^2 / 8 \qquad \text{(Eq. 4-4)}$$

where: k = intrinsic permeability [m²]
σ_0 = conductivity [-] (which can be obtained by 1/F)
Λ = pore reference length [m].

In Johnson *et al.* (1986) Λ is defined as the ratio volume/surface weighted by the field parameter E:

$$\Lambda = 2 \left| \frac{\int_{\tau} \mathbf{E}^2(\mathbf{r})\, dv}{\int_{s} \mathbf{E}^2(\mathbf{r})\, ds} \right| \qquad \text{(Eq. 4-5)}$$

[11] The actual K-values for Mont Terri are: $K_{\perp} = 0.7 \times 10^{-13}$ [m/s] and $K_{//} = 2 \times 10^{-13}$ [m/s] (Bock 2009)

Λ is equal to $2\varepsilon/s$ when E is uniform. In the Callovo-Oxfordian argillites $\Lambda \approx 2 * 10^{-8}$ m, which is the mean pore diameter measured by mercury intrusion.

4.1.4 Capillary-bundle model and transition to discrete fracture model

Many of the concepts of fluid flow in soils and rocks stem from the theory of laminar flow in capillaries. It is generally agreed that most of the pore space in clays is actually interconnected, but that significant groundwater flow only occurs in a fraction of this total space. Groundwater flow in clay will occur along the paths of least resistance and, given the magnitude of the forces of clay-water interaction (Section A.2.3 in Appendix A.2), these paths probably comprise networks of larger pores (macro-pores). For an actual porous medium, the interconnected void spaces can be regarded as a number of tortuous pore channels. The tortuosity (τ) is defined as the average ratio of the microscopic path length (L) to the macroscopic path length (x) in the medium:

$$\tau = L / x \geq 1 \qquad \text{(Eq.4-6)}$$

Calculations are fairly insensitive to τ and, in the absence of experimental data, this parameter is usually taken as $\sqrt{2} = 1.41$.

Consideration of a single capillary is the basic building block of so-called capillary-bundle models of single and two-phase flow in porous media (Dullien 1992). The flow rate in a single circular capillary is given by the Hagen-Poiseuille equation:

$$Q = - [\pi r^4 / (8 * \mu_w)] (dp / dL) \qquad \text{(Eq.4-7)}$$

where: Q = flow rate [$m^3 s^{-1}$]
r = radius of circular capillary [m]
μ_w = dynamic viscosity of percolating liquid [Pa * s]
dp/dL = pressure gradient along the length of the tube.

The hydraulic radius R_H of the capillary is defined by:

$$R_H = \text{wetted capillary area / wetted perimeter} = r^2 \pi / (2 r \pi) = r/2 \qquad \text{(Eq.4-8)}$$

Flow in a capillary of any arbitrary cross-sectional shape can then be written as:

$$Q = - [A * R_H^2 / (C_s * \mu_w)] (dp / dL) \qquad \text{(Eq.4-9)}$$

where: A = cross-sectional area [m^2]
R_H = hydraulic radius [m]
C_s = shape factor

For flow in capillaries with circular cross-section the shape factor C_s is equal to 2, whilst for flow between flat parallel plates it is equal to 3. Olsen (1962) assumed $C_s = 2.5$ for the pore channels of a saturated clay rich medium.

The 'cubic law' (Eq. 4-10; see also Eq. A.5-15 in Appendix A.5) for flow in a fracture of aperture a_h is derived from Eq. 4-9 by setting $C_s = 3$ and $R_H = a_h/2$:

$$T = \rho_w * g * a_h^3 / (12\,\mu_w) \qquad \text{(Eq. 4-10)}$$

where: T = fracture transmissivity [m^2/s]
ρ_w = density of percolating liquid [g/m^3]
g = gravity acceleration [$m * s^{-2}$]
a_h = hydraulic aperture of fracture [m]
μ_w = dynamic viscosity of percolating liquid [$Pa * s$]

Flow through fractures is of prime concern in PA. Sealing mechanisms of fractures will be considered in detail in the following Sections 4.2 to 4.4.

4.1.5 Interim conclusion on sealing by material compaction

For deep geological repositories in moderately indurated argillaceous formations, sealing by additional compaction (i.e. porosity reduction) of the rock matrix is of limited importance. The argillaceous material, considered in this context, has already been geologically precompacted to the degree that its intrinsic permeability is hardly of any concern in PA. In fact, the matrix permeability of these formations is so low that diffusion, and not advection, has become the dominating mass transport mechanism.

4.2 Sealing by mechanical closure of fractures

For modelling fluid flow in fractured argillaceous media, in particular in media within the EDZ, the use of fracture network models is an obvious alternative to the porous media approach of Section 4.1. For more information on the alternative modelling approaches refer to Section 4.6. One of the keys in the successful application of fracture network models is a comprehensive understanding of the coupled hydro-mechanical processes of a single fracture. Consequently, the considerations of the following Sections 4.2 to 4.3 will specifically relate to discrete water-filled fractures. The focus will be on the interaction between the fracture characteristics and its hydraulic transmissivity, whereby the fracture characteristics depends, amongst others, on the type of fracture discussed in Section A.3.3.3. It is of particular interest as to how far environmentally and/or technically induced changes of the fracture characteristics reduce the fracture's transmissivity, potentially towards zero (i.e. full sealing).

From the 'cubic law' of Eq. 4-10 it is evident that the fracture transmissivity T sensitively depends on the hydraulic fracture aperture a_h. That aperture is an idealised parallel plate configuration as shown in Figure 4-2. Real fractures are characterised by a certain degree of roughness, i.e. a spatial variability of the real geometric fracture aperture $a_g = a_g(x)$. The equivalent hydraulic fracture aperture a_h, used in the cubic law is a parameter determined by dedicated experiments (hydraulic tests) or by using empirical relationships between geometric and hydraulic apertures (Bear 1988).

Figure 4-2. Discrete fracture with hydraulic aperture a_h
Indicated are normal forces N and shear forces S acting onto fracture plane

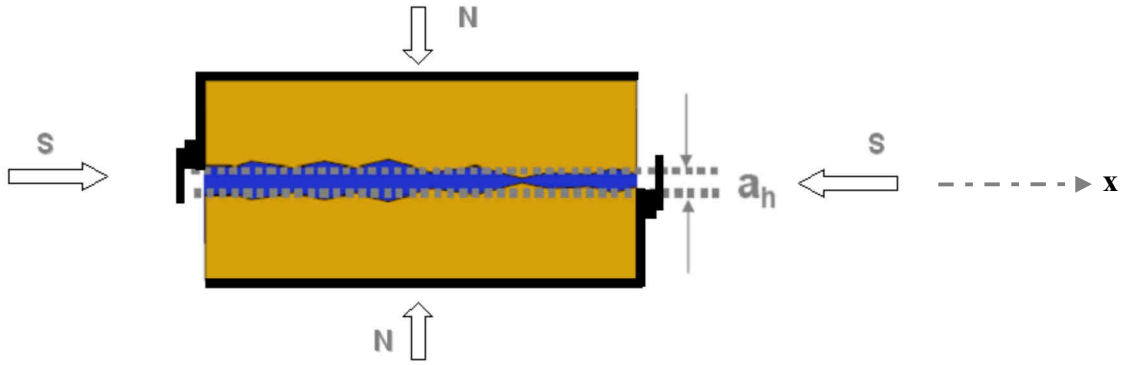

Evidently, the closure of apertures is associated with a lowering of the fracture transmissivity. Mechanically, such closure can be caused by the following three processes:

1. closure of the fracture due to the increase of the effective normal stress σ_n' acting across the fracture plane, either by an increase of the normal load N and/or decrease of the fluid (water and/or gas) pressure in the fracture;

2. contraction of fractures when subjected to shear (shear forces S); and

3. creep of the fracture wall material towards the open fracture space.

These three processes will be discussed in the following Sections 4.2.1 to 4.2.3.

4.2.1 Closing of fractures by increased effective normal stress

In a thought experiment and following Goodman (1974), by placing a rock block lightly onto a rough surface, the proportion of the surface area in actual contact with the block is almost zero. The entire contact force is sustained at a few (minimally three) points. Under increasing normal load, the contacts enlarge by elastic deformation, crushing and indirect tensile cracking of the contact asperities, whilst the deformation also brings further regions into contact. The enlargement of the contact asperities is stimulated by water uptake in the fracture, as the strength of argillaceous materials, and thus of the fracture wall asperities, is significantly reduced with increased water content.

It is possible to pursue the fracture closing mechanisms mathematically and develop a theory of normal displacement δ_n of the contact zone under increasing effective normal stress σ_n', as done for metals by Bowden and Tabor (1964). Unlike metals however, the geometry and state of natural fracture planes is so poorly defined that Goodman (1974) considered a semi-empirical approach more appropriate.

There are two physical constraints to the amount of the normal displacement δ_n of fracture planes. The first constraint is the maximum $\delta_{n\,max}$ to which a fracture can be closed. It is:

$$\delta_{n\,max} < a_g \qquad \text{(Eq. 4-11)}$$

where: a_g= geometric fracture aperture

The second constraint comes from the negligible tensile strength of fractures, although fractures with some tensile strength can be a useful concept for the analysis of rock masses with incipient parting planes. Combining these two constraints implies that the normal stress σ_n versus normal displacement δ_n relationship has to be fitted into a quarter σ_n - δ_n space as shown in Figure 4-3a. A satisfactory relationship is the hyperbola:

$$\sigma_n = [\delta_n / (\delta_{n\,max} - \delta_n)]\, \sigma_{n\,s} + \sigma_{n\,s} \qquad (\text{for } \delta_n < \delta_{n\,max}) \qquad \text{(Eq. 4-12 a)}$$

where:

$\delta_{n\,max}$ = maximum possible closure of fracture [m]

$\sigma_{n\,s}$ = seating pressure defining the initial condition for measuring δ_n [Pa]

Indeed, for $\delta_n \rightarrow \delta_{n\,max}$ it is $\sigma_n \rightarrow \infty$ (and the material strength will become relevant) and for $\delta_n \rightarrow -\infty$ (= complete opening of the fracture) it is $\sigma_n \rightarrow 0$. The slope of the σ_n - δ_n curve at any given point is termed normal stiffness k_n.

Solving (Eq. 4-12a) for δ_n yields:

$$\delta_n = \delta_{n\,max} - (\delta_{n\,max} * \sigma_{n\,s}) / \sigma_n \qquad (\text{for } \sigma_n > \sigma_{n\,s}) \qquad \text{(Eq. 4-12 b)}$$

Equation 4-12 b describes a line in a $(1/\sigma_n)$ - δ_n diagram (Figure 4-3b).
The factor $[1/(\sigma_{n\,s} * \delta_{n\,max})]$ is the slope of the line and $\delta_{n\,max}$ the intercept with the δ_n–axis.

Figure 4-3. Fracture compression model
(after Goodman 1974)

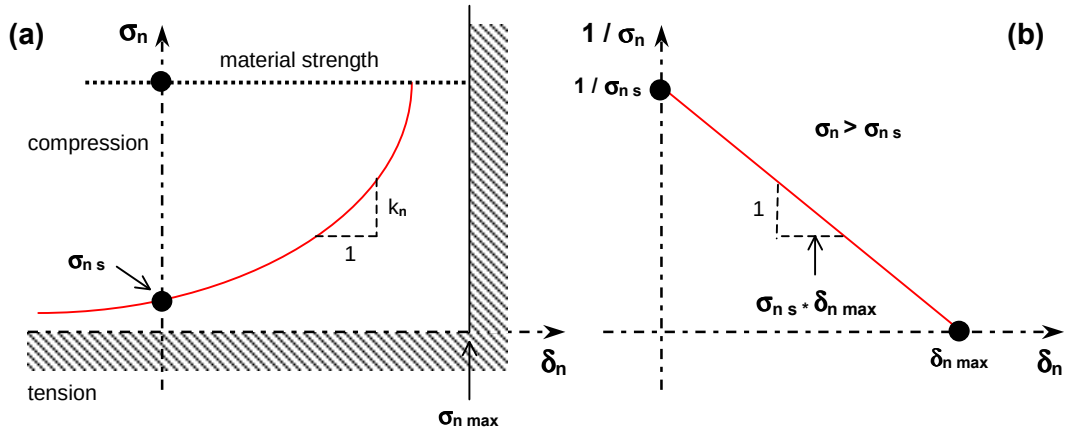

A hyperbolic σ_n - δ_n function, similar to that of Eq. 4-12a, was also proposed by Bandis *et al.* (1983).

Experimental evidence suggests that Goodman's formulation on fracture closure is a reasonable first approximation. Experiments on rough model fractures performed by Bock (1976) resulted in similar σ_n -δ_n curves (Figure 4-4a). However, converting the data into a $(1/\sigma_n)$ - δ_n diagram yielded major deviations from linear trends (Figure 4-4b).

Figure 4-4. Fracture closure experiments
(a) σ_n - δ_n diagram - (b) $(1/\sigma_n)$ - δ_n diagram - (c) Regression analysis for Test 160 - (d) semi-log σ_n - δ_n plot (after Bock 1976)

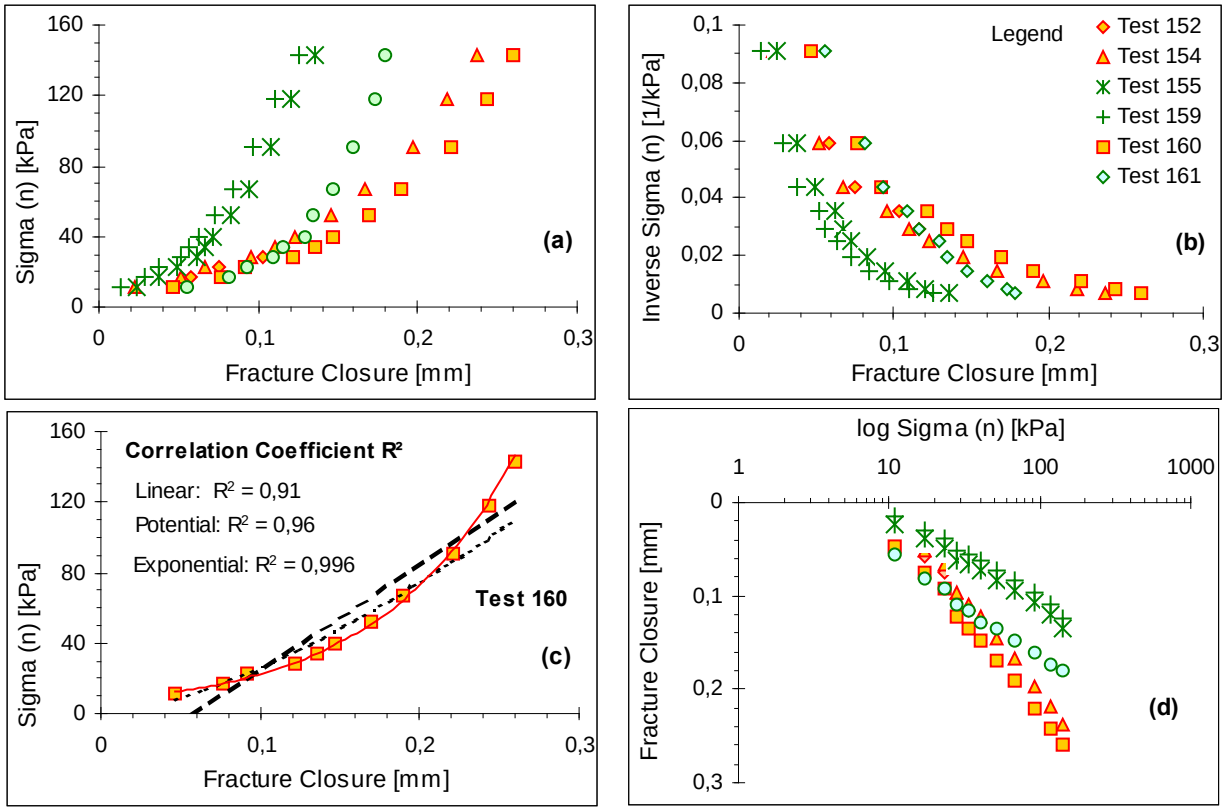

Detailed trend analyses revealed that a potential approximation and, in particular, an exponential approximation provided a better fit, as demonstrated for a test example in Figure 4-4c.

The best fit, however, is achieved when the data are plotted in a semi-logarithmic σ_n - δ_n diagram, in which the test data align to almost perfect linear trends (Figure 4-4d). This observation suggests that the closure of fractures is formally identical to that of uniaxial compression of soil under confined conditions (compaction). In soil mechanics, the stress-strain relationship under laterally confined conditions is experimentally determined in the oedometer test and commonly expressed in terms of a compression index C (Figure 4-5):

$$e - e_0 = - C * \log (\sigma_n' / \sigma_{n0}') = - \lambda * 2.3026 * \ln (\sigma_n' / \sigma_{n0}') \qquad \text{(Eq. 4-13 a)}$$

where:
e = void ratio [-]
e_0 = reference (or initial) void ratio
σ_n' = effective compaction pressure [Pa]
σ_{n0}' = effective compaction pressure at reference (or initial) void ratio e_0
C = negative slope of the compaction curve in the e- ($\log \sigma_n$) plot
λ = negative slope of the virgin compaction curve in the e- ($\ln \sigma_n$) plot

The index C is sensitive on the degree of consolidation. It is termed "Compression Index" and denoted C_c for normally consolidated soils and C_s for over-consolidated soils.

Figure 4-5. Example of a soil compaction test

In the example: C_c = 0.2001 (λ= 0.0870) and C_s = 0.0406 (κ= 0.0171) (after Kempfert and Raithel 2007)

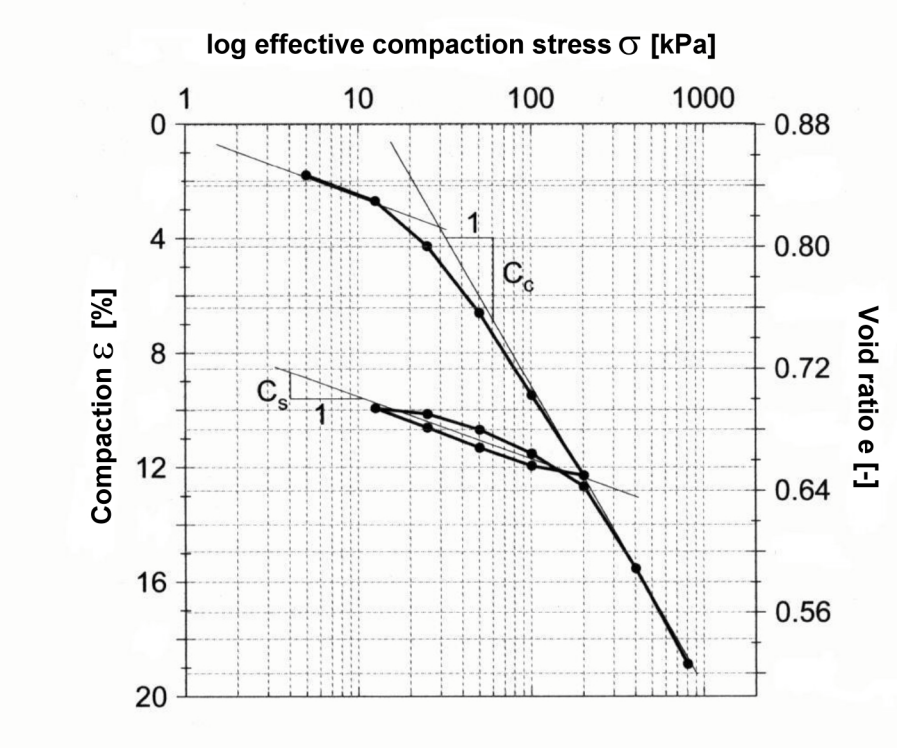

Analogously and as depicted in Figure 4-4d, the closure of fractures may then be expressed by:

$$\delta_n - a_{g0} = - C_f * \log (\sigma_n' / \sigma_{ns}') \qquad \text{(Eq. 4-13b)}$$

where: C_f = fracture compression index [-]
a_{g0} = reference fracture aperture at seating pressure σ_{ns} [m]

The six tests graphed in Figure 4-4d clearly show two distinct δ_n - log σ_n trends. Three tests (Test Nos. 155, 159 and 161, indicated in green) have a comparatively low, relatively identical value C_{f1} and three tests (Test Nos. 152, 154 and 160, indicated in red) have a comparatively high, relatively identical value C_{f2} (with $C_{f1} < C_{f2}$). The physical reason for this feature is that in the first series of tests (Test Nos. 155, 159 and 161) and prior to the start of the fracture closure experiment, the asperities of the two opposing fracture walls were matched to each other, whereas in the second series (Test Nos. 155, 159 and 161) this was not the case. This observation points to the sensitivity of C_f as a material parameter for describing the mechanical behaviour of the closure of fractures under changing effective normal stress.

4.2.2 Contraction of fractures in shear

The deformation of fractures in shear under the action of shear forces S (Figure 4-2) is commonly expressed in terms of the displacement component δ_s which acts along the fracture plane. Shearing of fractures is accompanied with an over-riding of the fracture wall asperities, grinding off the asperities and a re-structuring of the fracture wall material. These mechanisms are the reasons that there is also a significant displacement component δ_n acting across (i.e. normal to) the fracture plane. Note that the sign convention adopted in this report is that a negative δ_n characterises an opening of the fracture (termed "dilation") and a positive δ_n a closure of the fracture ("contraction"). The contraction mechanism is of particular interest to sealing.

Over-riding of asperities without rock breakage is unlikely except at zero normal stress $\sigma_n = 0$ when the asperities are inclined to the shear direction at an angle less than $(90° - \phi_f)$ (where ϕ_f is the friction angle of the flat fracture surface). In the presence of normal stress $\sigma_n > 0$, the work required to dilate against the normal force N will exceed the work sufficient to shear through some asperities. Thus dilatancy decreases as σ_n increases. The latter finding is experimentally confirmed by shear displacement tests of the Opalinus Clay shown in Figure 4-6.

Figure 4-6. Shear displacement tests of Opalinus Clay under various normal stress levels
Top: shear stress τ_s – shear displacement δ_s curves; bottom: δ_n vs. δ_s curves (after Popp and Salzer 2007)

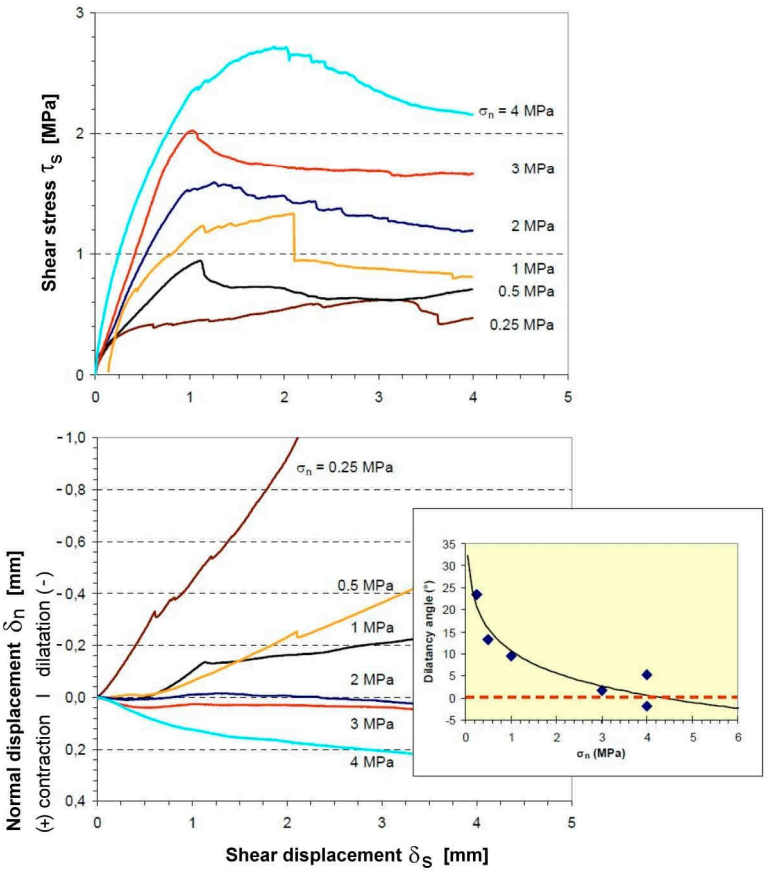

The insert at the bottom right of Figure 4-6 shows the dilatation angle *i* as a function of the normal stress σ_n where *i* is defined as:

$$i = -\delta_n / \delta_s \qquad \text{(Eq. 4-14)}$$

Popp and Salzer (2007) gave an analytical formula for the effective dilation angle *i* in the form of the Minkley Shear Model:

$$i = \arctan(\tau/\sigma_n) - \arctan \mu_k \qquad \text{(Eq. 4-15a)}$$

$$\text{where} \quad \mu_k = \tan[\phi_R + i_0 * e \exp(-K_2 * \sigma_n / q_u)] \qquad \text{(Eq. 4-15b)}$$

where: ϕ_R = angle of residual friction
i_0 = upsliding angle
e = natural logarithm
q_u = uniaxial compressive strength of the material in the contact area
K_2 = curvature parameter.

As shown in Figure 4-6, for the tested Opalinus Clay samples *i* becomes negative, i.e. contractant, once σ_n exceeds about 3 MPa. This is well below the unconfined compressive strength level of 15 MPa for $q_{u \perp ss}$ and 11 MPa (for $q_{u//ss}$) (Bock 2009). Conventionally it is thought (Makurat and Gutierreza 1997; Gutierreza *et al.* 2000) that a reduction of fracture permeability in shear can only be achieved if $\sigma_n \geq$ UCS. Accordingly, the ratio σ'_n / q_u has been proposed as a key parameter for determining the permeability reduction in fractures and the sealing potential of fractures that have undergone large shear deformation.

Figure 4-7. Micro-structural processes within fault rocks of the North Sea Brent Field
Schematised, considering clay content (vertical) and degree of burial (horizontal) (after Jolley *et al.* 2007)

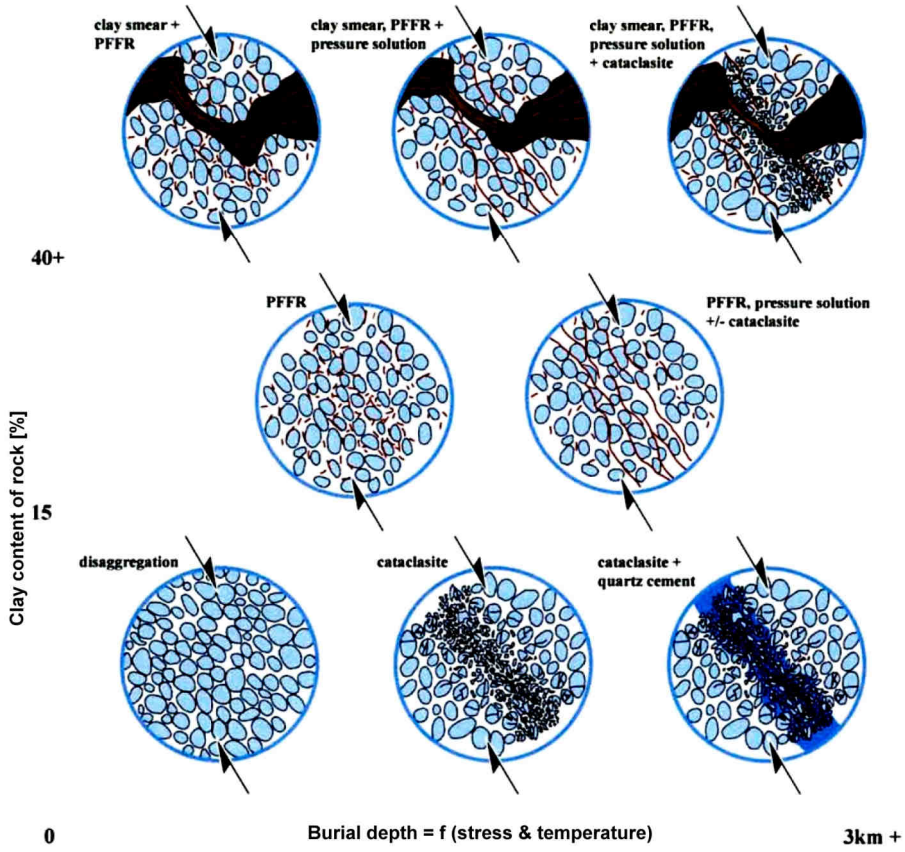

The above discrepancy implies that, in argillaceous media, not only is the mechanical contraction of fractures of significance to permeability reduction in shear but also some other factors such as re-orientation of the platelet structure in the fracture wall and gouge formation. Of particular importance in this regard are the textural and structural studies of fault shear zones in the hydrocarbons industry. Figure 4-7 is a schematic sketch of the micro-structural processes within fault zones observed in the strata of the Brent Group reservoir of the North Sea.

The exact suite of fault rocks that form within the fault zone varies systematically with the prevailing physical-chemical micro-scale deformation mechanisms. In turn, these are controlled by factors such as the clay content and grain size of the host rocks as well as the pre-, syn- and post-deformation stress and temperature history (Jolley *et al.* 2007). It was found that impure sand (15 to 40% clay content) deforms and produces 'phyllosilicate-framework' fault rocks ('PFFR', Figure 4-7, top and centre). Deformation-induced influx of clay particles from the surrounding matrix and mixing of these particles with the framework grains in the fault result in a rapid decrease in porosity and permeability. Faulting of discrete shale beds often results in the formation of clay smears in the faults, which often have permeabilities of $k < 10^{-19}$ m² being well below that of the source shale beds. Figure 4-8 shows that a clay content of the host rock of > 15% always leads to a fault permeability $k < 10^{-16}$ m² and that of > 40% clay content to $k < 10^{-19}$ m².

Figure 4-8. Fault permeability as a function of host rock clay content
Brent Field, North Sea
(data from Jolley *et al.* 2007)

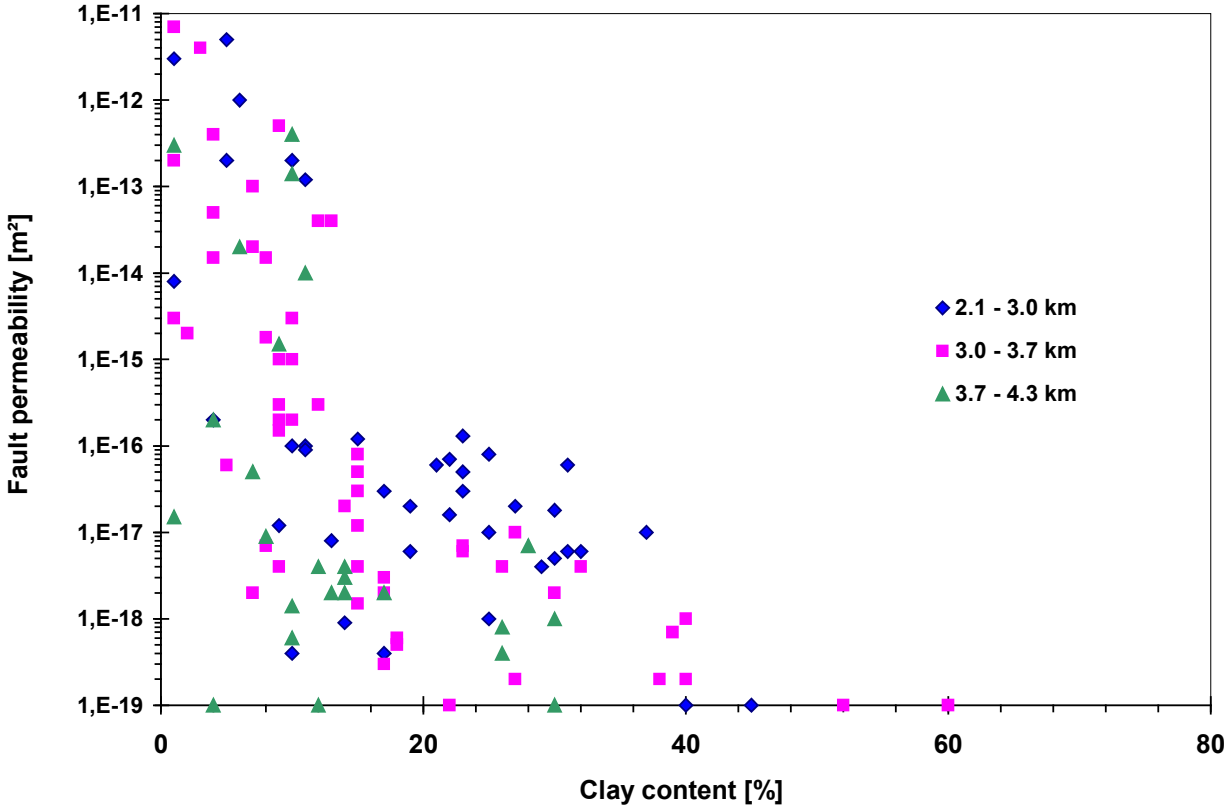

Evidence exists that the above threshold values between clay content and permeability apply not only to clay smears in faults but also to argillaceous material in general. That evidence is based on geo-engineering laboratory tests of sand-clay mixtures and on borehole permeability tests in argillaceous formations as briefly outlined in the following.

The content level at which clay minerals are becoming the controlling constituents in the mechanical behaviour of composite bodies has been a long-standing concern in geo-engineering, for instance in the construction of soil embankments or earth dams. Figure 4-9 shows the results of some laboratory permeability tests on sand-clay mixtures. Two types of natural clay (Clay I and II) were homogenised with well-graded sand, either fine sand ($0.06 < \varnothing \leq 0.2$ mm) or coarse sand ($0.6 < \varnothing \leq 2$ mm). Clay I has an intrinsic hydraulic conductivity of $K_I = 1.1 * 10^{-10}$ m/s and a Plasticity Index $P.I._I$ of 51%. The respective values for Clay II are $K_{II} = 1.7 * 10^{-10}$ m/s and $P.I._{II} = 20\%$. From Figure 4-9 it can be depicted that from a clay mineral content of about 20 to 30% onward the permeability of a sand-clay mixture is essentially identical to that of the intrinsic clay.

Figure 4-9. Hydraulic conductivity K of sand-clay mixtures as determined in laboratory tests
Note that as from a clay mineral content of about 20 to 30% the permeability is equivalent to that of pure clay (after Leussink *et al.* 1964)

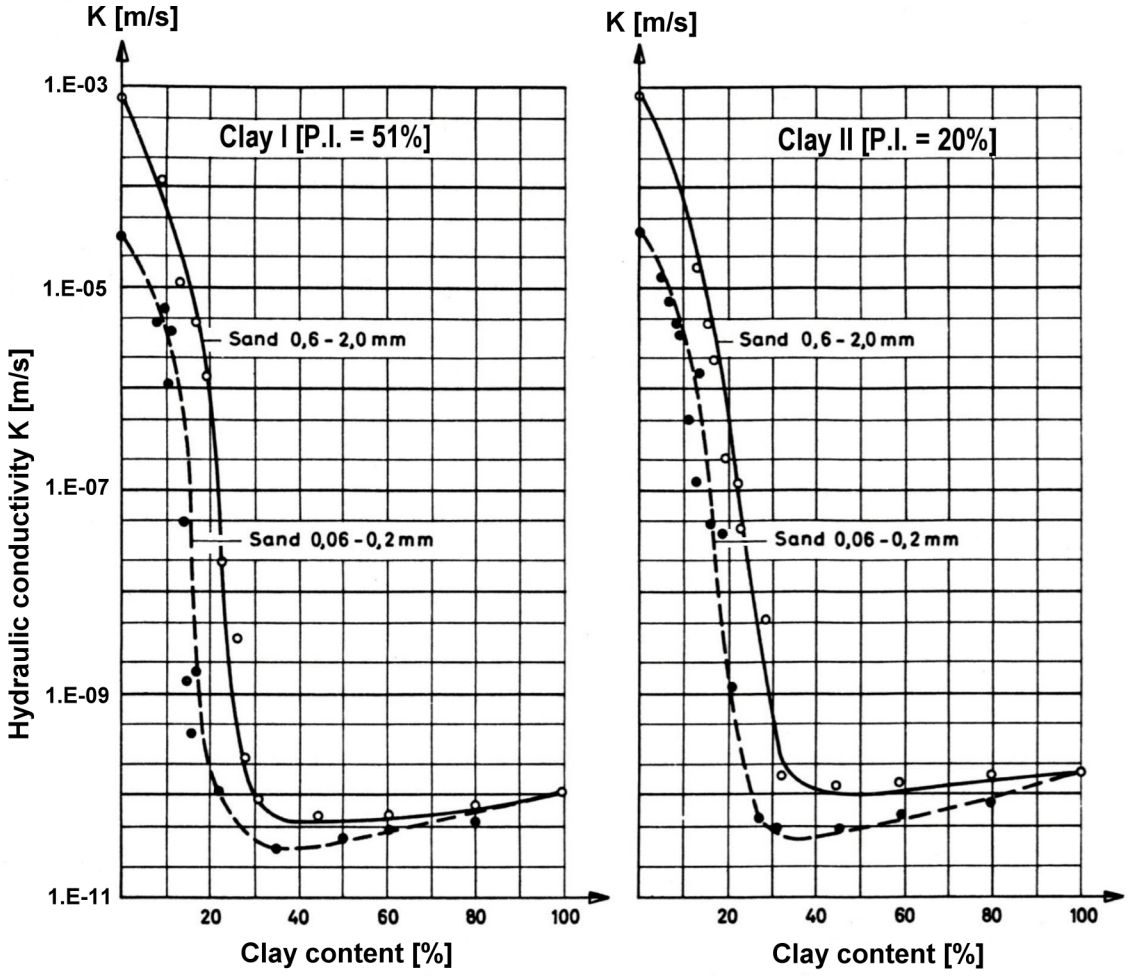

As part of a recent study, Nagra (2009) revisited borehole permeability tests against the background of an improved specification of the interdependency between the clay content of the tested formation and the measured permeability. Only such borehole sections were considered in which near-surface decompaction could be excluded, i.e. >200 m deep sections of boreholes in northern Switzerland and >600 m deep sections in the Wellenberg boreholes in the Swiss Alps.

Figure 4-10 compiles the results showing a total of 127 data points and confirming the trend of a generally decreasing hydraulic conductivity K with increasing clay content. Specifically, it can be depicted that for clay mineral contents of >25 % K reduces to values of < 10^{-9} m/s, and for clay mineral contents of >40 % to values of <10^{-11} m/s.

Figure 4-10. Hydraulic conductivity K versus clay mineral content of some sedimentary formations in Switzerland (modified after Nagra 2009)

NOTE: - Hydraulic conductivity determined from packer tests in deep boreholes
- Clay mineral content averaged over the respective test interval
- Ancillary lines: K-values at 25% and 40% clay mineral content, respectively

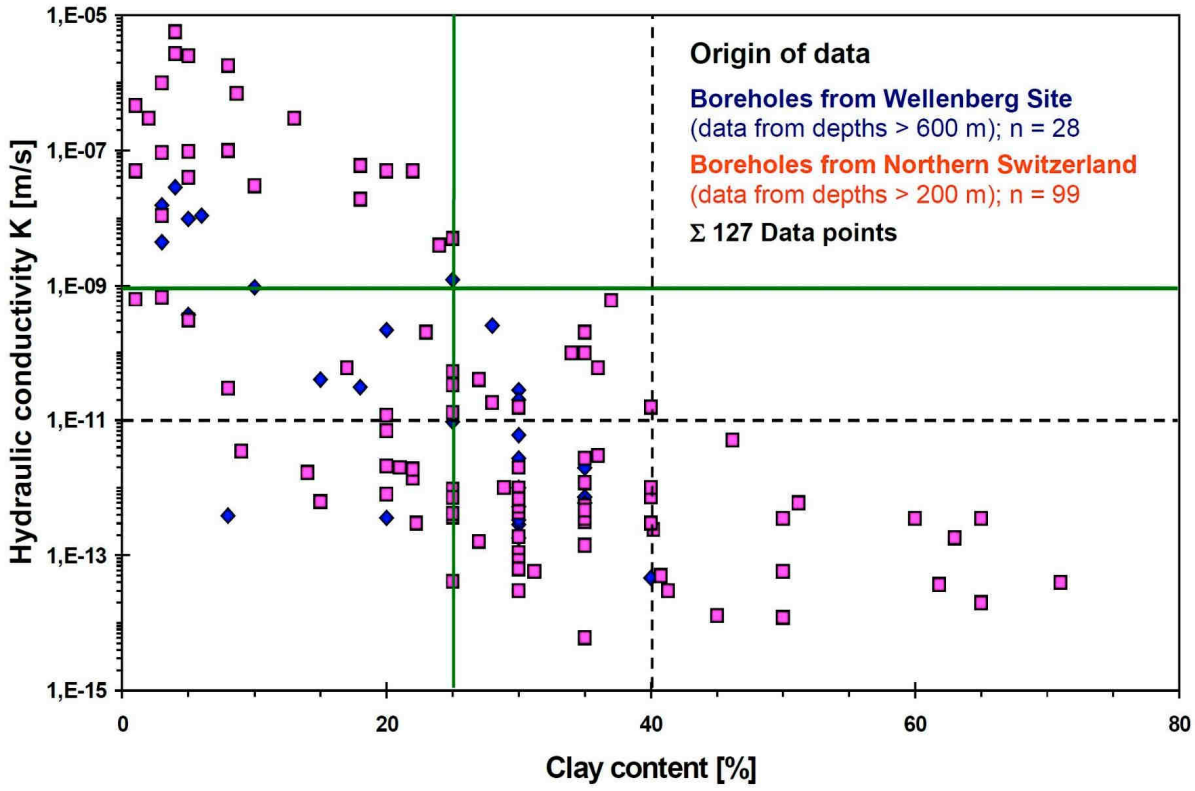

For reference purposes, Table 4-2 summarises the pertinent permeability parameters of the argillaceous materials of the URLs at Mol, Mont Terri and Bure.

Table 4-2. Permeability and clay content of argillaceous formations at major URL sites
(combination of Tables 2-3, 2-7 and A.5-2)

Formation (Location)	Permeability k_{water} [m^2]	Hydraulic Conductivity K_{water} [m/s]	Clay content [% wt]	
	see Equation A.5-9		all clay minerals	swelling clay minerals
Boom Clay (Mol, HADES URF)	200 to 400 $*$ 10^{-21}	200 to 400 $*$ 10^{-14}	60	40
Opalinus Clay (Mont Terri URL)	$\perp$ ss $7*10^{-21}$ // ss $20*10^{-21}$	$\perp$ ss $7*10^{-14}$ // ss $20*10^{-14}$	66	45
Callovo-Oxfordian (Bure URL)	$1*10^{-19}$ to $1*10^{-21}$	$1*10^{-12}$ to $1*10^{-14}$	25-60	10-40

4.2.3 'Creep' of fracture wall material

It is obvious that 'creep' of fracture wall material may contribute, in course of time, to the closure of fractures. There is a bundle of micro-mechanisms commonly made responsible for macro-scale 'creep', many of them quite vague and often difficult to specify in a specific application. The postulated creep mechanisms are based on processes such as diffusion, pressure dissolution, dislocation glide of minerals and sub-critical crack growth through pore fluid chemistry effects.

Various generic creep laws have been proposed for argillaceous materials, amongst them the visco-plastic Lemaitre creep model for transient creep (Horseman *et al.* 2006) and a simple Norton power law, considering steady-state creep only (Zhang *et al.* 2007b). Bock (2009) noted the following creep law for uniaxially loaded samples:

$$\varepsilon_1(t) = 2\,\sigma_1' / (9\,K) + \sigma_1 / (3\,G_2) + \sigma_1 / (3\,G_1) * [1 - e^{-(G1\,t/\eta 1)}] + \sigma_1 / (3\,\eta_2)\,t \qquad \text{(Eq. 4-16a)}$$

where: $\varepsilon_1(t)$ = axial strain of uniaxial test
σ_1' = deviatoric effective stress
K = bulk modulus with $K = E / [3\,(1-2\nu)]$
G_1, G_2 = shear moduli
η_1, η_2 = viscosity parameters

An alternative formulation of Equation (4.16a) is:

$$\varepsilon_1(t) = \varepsilon_e + \varepsilon_f\,[1 - \exp(-t / T_1)] + [\Delta\varepsilon_1 / \Delta t] * t \qquad \text{(Eq. 4-16b)}$$

where: 1st term = instantaneous (or elastic) strain ε_e
2nd term = primary consolidation
3rd term = secondary consolidation (creep proper)

The above law represents a material which shows an instantaneous (elastic) response together with a transient (primary) creep and steady-state (secondary) creep. The accelerated (tertiary) creep is not considered within this model. Table 4-3 compiles some of the results on the steady-state (secondary) creep of the Opalinus Clay.

Table 4-3. Steady-state (secondary) creep parameters of Opalinus Clay material
(after Bock 2009)

Steady-state creep $\Delta\varepsilon_1 / \Delta t$ [s^{-1}]	Test conditions		Number of tests
	Range of (σ_1 - σ_3) [MPa]	Temperature [℃]	
$(3.2 \pm 1.4) * 10^{-12}$	13	30	3
$(620 \pm 250) * 10^{-12}$	2.3 - 5.6	58	3

For the Opalinus Clay in the Zürcher Weinland (Benken), Nagra (2002b) has adopted a modified Salzer creep law (Salzer *et al.* 1998). The modification relates to the introduction of a stress deviator threshold value of some 7.5 MPa, before any creep can occur. That value was deduced from the local *in situ* stress situation at Benken assuming that the observed deviatoric stress can only be maintained over geological times if creep starts at least at that level. The situation at Mont Terri is different (different consolidation, stress path and *in situ* stress field). The threshold value of a formation therefore is not necessarily a constant but depends on various factors and thus needs to be evaluated for every site independently.

The existence of a creep threshold and, where positive its exact level, are subject to ongoing debate. This becomes apparent when considering recent investigations on steady-state creep parameters of the Opalinus Clay material at Mont Terri carried out by Lux *et al.* (2007). In general it was found that a "wide scattering" of the steady-state creep parameter values obviously is "a typical feature" of claystone and that there is a relatively low dependency on the level of confining stresses. The investigations concluded in the diagram of Figure 4-11 in which the strain rate $\varepsilon_1/\Delta t$ is graphed as function of the deviatoric effective stress $\Delta\sigma$' down to a level of 1 MPa, i.e. well below Nagra's threshold level of 7.5 MPa at Benken.

Figure 4-11. Range of steady-state creep parameter values of the Opalinus Clay at Mont Terri as extrapolated from eight creep tests MT-7 ... MT-16
(modified after Lux *et al.* 2007)

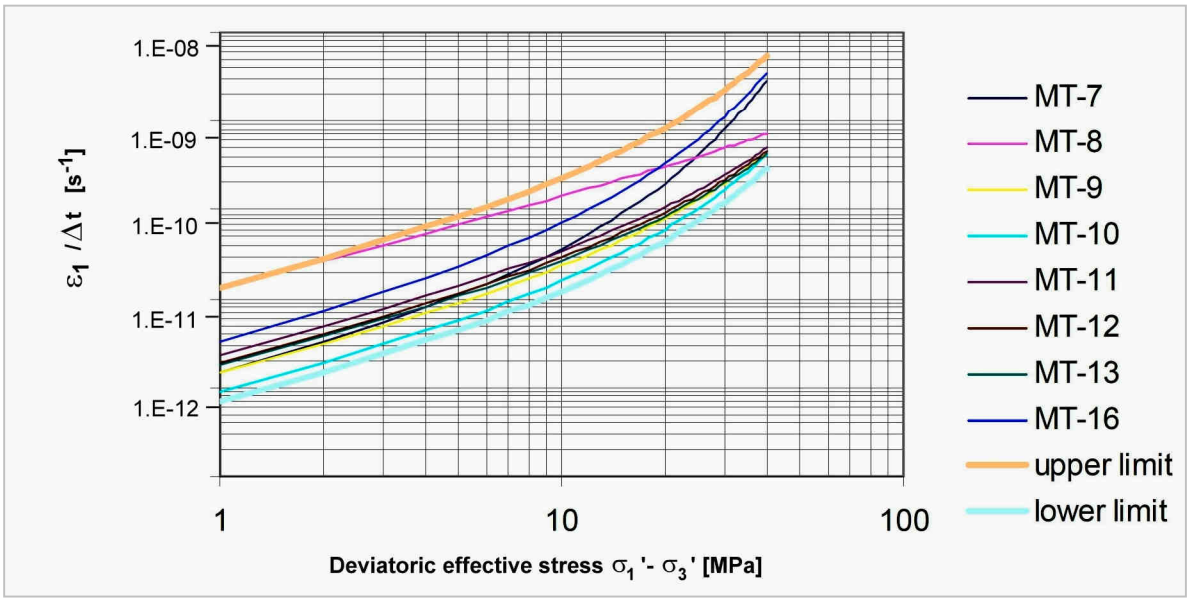

For the Callovo-Oxfordian argillite creep was observed by Zhang *et al.* (2004; 2007b) in laboratory samples under very low stresses of < 1 MPa. Their results suggested that there is no creep onset and no significant scale and anisotropy effects on the creep behaviour. Following a transient creep phase over several months, quasi-steady state creep was observed (Figure 4-12 upper). The creep rate seemed to be less dependent on the stress level (Figure 4-12 lower).

Figure 4-12. Creep observed in Callovo-Oxfordian argillites in laboratory tests
(from Zhang *et al.* 2004)

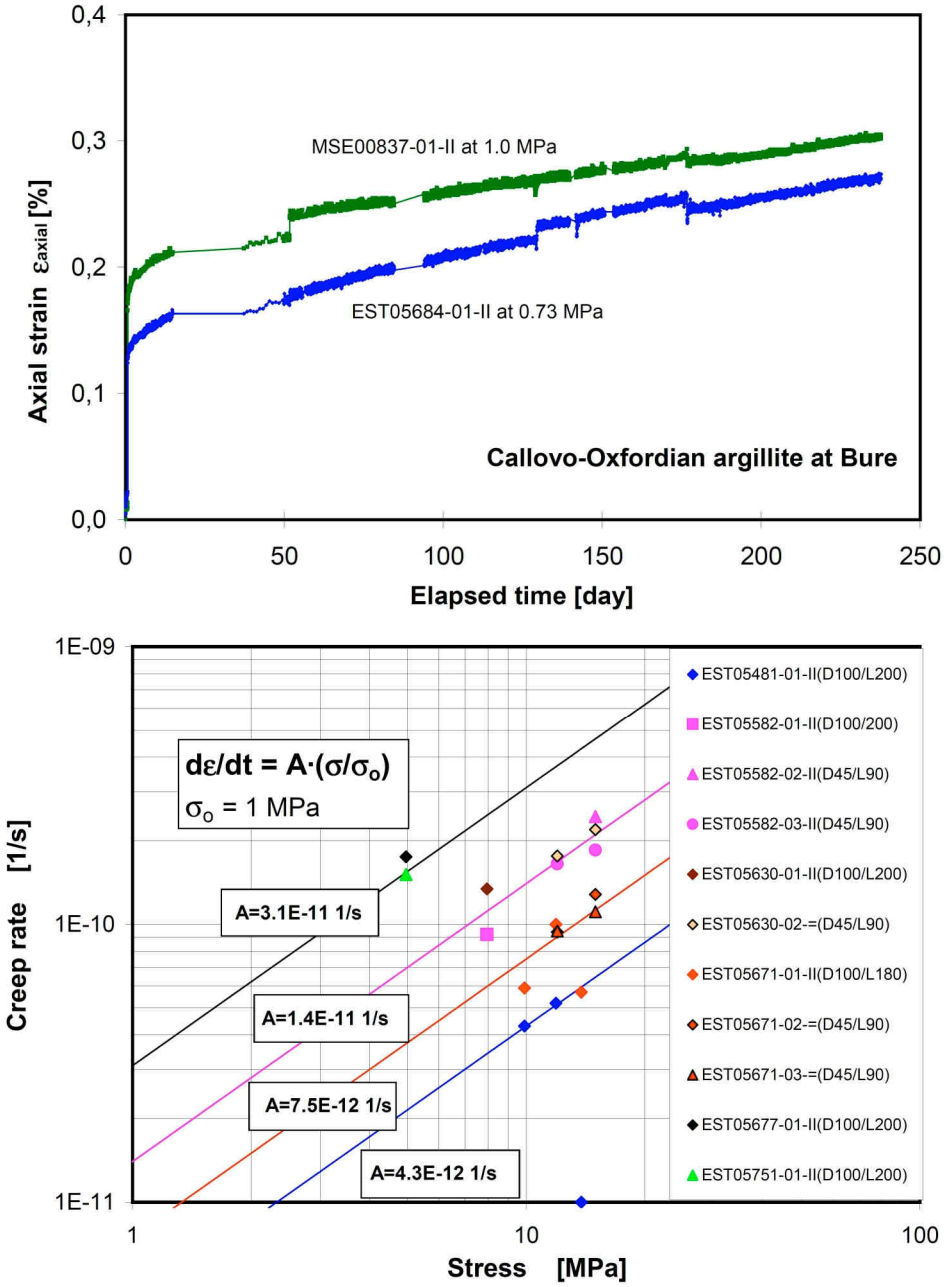

Whether the level of secondary creep is significant or not is still subject to debate (Lebon 2009) because, by common standards, the creep rate is very low and approaches the resolution of the

measuring equipment. Long tests might furthermore be influenced by ambient conditions (variation of temperature and/or hygrometry).

4.2.4 Comparison of influencing factors

In the following section, the above three mechanisms are compared by order of magnitude estimates of their respective potential in closing a fracture and, implicitly, in their sealing capacity. For that purpose a synthetic case is considered under assumptions and input parameters relevant for the Opalinus Clay (Table 4-4).

The results of the estimate are presented in the last column of Table 4-4.

Table 4-4. Order of magnitude estimate of the potential of mechanisms in closing of Opalinus Clay fractures

Report Section	Mechanism	Assumptions and input parameters	Result: Fracture closing potential
4.2.1	Closure of fracture by increased normal stress	Increase of effective normal stress $\Delta\sigma_n$‘ =2 MPa Normal stiffness: k_n = 8 GPa/m (Popp and Salzer 2007), at stress level of ~2 MPa. Initial seating pressure δ_{ns}: not relevant	$\delta_{n\ normal\ stress}$ = 0.25 [mm]
4.2.2	Contraction in shear	Level of effective normal stress σ_n‘ = 4 MPa → i = - δ_n/δ_s = -1° (Popp and Salzer 2007) Assumed shear displacement δ_s = 20 mm	$\delta_{n\ shear}$ = 0,34 [mm]
4.2.3	Creep of fracture wall material	Effective tangential stress σ_t‘ acting along open fracture wall: σ_t‘ = 10 MPa → Strain rate (Figure 4-11; Lux *et al.* 2007): $d\varepsilon_t/dt = 2 * 10^{-11}$ [s^{-1}] Volume constancy (→ $d\varepsilon_t/dt = 0{,}5 * d\varepsilon_n/dt$) Assumed length of open fracture: l_{frac} = 100mm	$\delta_{n\ creep}$ = 0.03 [mm/a]

Instantaneous mechanical closure of fractures can equally be achieved by an increase of the normal load or by shearing along the fracture, provided that, in shearing, the normal stress is maintained at a level of at least some 4 MPa. Increase in normal load and shearing can contribute in about equal portions to the closure of fractures. Note that in the above estimate the assumed increase of the effective normal stress $\Delta\sigma_n$‘ of 2 MPa is quite conservative. In the Swiss repository concept the loading pressure corresponds to the expected swelling pressure of the backfill material of some 5 MPa (Armand *et al.* 2008).

In longer terms (of the order of 10 years and beyond) creep of the fracture wall material might also become a contributing factor. The level of tangential stress σ_t‘ of 10 MPa, which was assumed to prevail along an open fracture, coincides with the order of magnitude of the mean effective stresses at locations which are prime targets within the Swiss repository concept. At an effective deviatoric stress level of 2 MPa the creep fracture closure rate would be about a full order magnitude

lower, i.e. 0.003 [mm/a], provided that there is no creep threshold or, if existing, is lower than the assumed deviatoric stress level of 2 MPa.

Considering that a reduction of a hydraulic aperture of a mere 0.1 mm can lead to a decrease of the effective transmissivity T of about 1 x 10^{-6} m²/s and thus to a decrease of the intrinsic transmissivity of the Opalinus Clay by 6 to 8 orders of magnitude (Nagra 2002b), it is evident that the above mechanisms will play an important role in the fracture sealing.

4.3 Sealing triggered by physico-chemical processes within the microscopic pore space

The description of the sealing mechanisms of EDZ fractures draws on the concept of an initially intact rock, fractured by mechanical unloading (stress redistribution by the excavation of underground structures, see Appendix A.4). Accordingly, the fracturing and sealing processes can be decomposed in three major stages as shown on a nanometre scale in the schematic sketch of Figure 4-13 (Marschall *et al.* 2008b):

Figure 4-13. Conceptualisation of physico-chemical sealing factors at the microscopic scale
(after Marschall *et al.* 2008b)

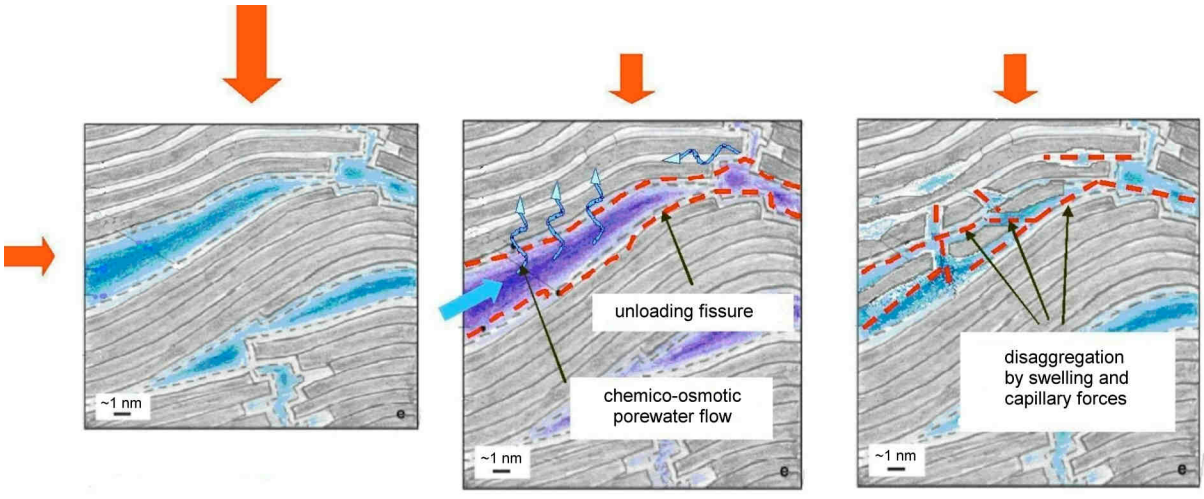

Stage 1 (Figure 4-13, left): Initial thermodynamic equilibrium of intact rock, in particular quasi-static distribution of bound and free water at primary stress state.

Stage 2 (Figure 4-13, centre): Thermodynamic disequilibrium, both in the solid and liquid phases, due to mechanical unloading (e.g. rock excavation) and establishment of a secondary stress state. Fissures and fractures may be created in the rock matrix, which will be preferably aligned along the clay platelets. Extended fracturing promotes a permeability increase, which may initiate advective inflow of porewater with a different chemistry or even may result in the invasion of a gas phase (e.g. tunnel ventilation). The increase in porosity and, in particular, the creation of new mineral surfaces give rise to chemico-osmotic gradients as driving forces for the mobilisation and redistribution of bound and free water. The uptake of water by clay minerals, enforced by capillary

forces and chemical potentials, leads to progressive swelling and disaggregation of clay particles along the walls of the fissures and fractures.

Stage 3 (Figure 4-13, right): New thermodynamic equilibrium after redistribution of porewater due to chemico-osmotic and capillary forces and back-filling of the emplacement galleries and its associated swelling pressures (tertiary stress state). When a new equilibrium is finally reached it is anticipated that the fractures are largely sealed and the permeability is close to the intrinsic permeability of the intact rock matrix.

In the above Stages 2 and 3, there are two principal physico-chemical processes involved which are of particular importance to sealing of fractures: Swelling and slaking. These processes will be reviewed in the following Sections 4.3.1 and 4.3.2.

4.3.1 Swelling

4.3.1.1 General

Swelling of argillaceous rocks is a time-dependent process by which free water is drawn into the material resulting in a volume increase. Under unconfined conditions the volume increase is always substantially larger than that in any confined state and can be explained by invoking conventional poroelastic concepts. If the material is constrained, then a swelling pressure is developed which acts against the constraint. The reverse process of swelling is shrinkage, caused by an expulsion of water from the material. Swelling and shrinking are processes which are not necessarily fully reversible as structural changes might be provoked, in particular during shrinking (e.g. desiccation cracking; Figure A.4-1b). Structural disintegration of the material due to repeated (cyclic) swelling/shrinking is usually considered a "slaking" phenomenon (see Section 4.3.2).

According to the ISRM definition (Ulusay and Hudson 2007), the swelling mechanism in rock is a combination of physico-chemical reaction involving water and stress relief. The physico-chemical reaction with water is usually the major contribution but it can only take place simultaneously with, or following, stress relief. Such stress relief is caused by either the removal of overburden or raised pore fluid pressures. Mechanical swelling in argillaceous media thus is the inverse to consolidation, and is associated with the dissipation of negative excess pore pressures.

Physico-chemical swelling involves the reduction of internal forces acting within the intact material. The swelling behaviour of argillaceous material is essentially related to the composition (type of clay minerals), the fabric of the intact rock and changes in water chemistry. The presence of an inter-particle cement can inhibit swelling of the clay fabric. However, cementing agents such as calcite and silica tend to behave in a brittle manner and are easily damaged (e.g. in the formation process of the EDZ). In fact, it appears likely that fabric damage is a necessary prerequisite for swelling in some argillaceous rocks. This form of fabric damage is sometimes referred to as 'bond'.

4.3.1.2 Micro-structural processes

According to Nüesch (1991), three types of internal non-equilibrium swelling mechanisms can be distinguished (ref. also to Section A.2.3.2): (1) intra-crystalline swelling due to the insertion of hydration water, (2) water absorption at free lamella surfaces, and (3) osmotic swelling due to the adsorption of water in between clay lamellae.

1. Intra-crystalline swelling in argillaceous material is based on the hydration of the exchangeable cations (e.g. Ca^{2+}, Mg^{2+}, Na^{+}, K^{+}) positioned at the inner surfaces of clay minerals, i.e. in between T- and O-Layers (see Section A.2.3.1). The mechanism is particularly pronounced in 3-Layer [T-O-T] minerals. For smectites, as an example, the spacing between the adjacent clay platelets amounts, in oven-dried conditions, to about 10 Å (= 1 nm) and can be increased to a multiple of that amount when wetted. The resulting swelling pressures can be calculated in line with the hydration theory (Nüesch 1991).

2. Water absorption swelling in argillaceous material is caused by hydration at the outer surface of clay mineral particles (Low 1987). Those surfaces carry residual negative charges, mainly as a result of the isomorphous substitution of aluminium or silicon atoms of lower valence, but also due to dissociation of hydroxyl ions (see Section A.2.3). Water interacts with the negatively charged surfaces of the clay minerals and forms hydrogen bonds with the silicate oxygen. Hydration with the cations on the silicate surfaces reduces the free energy of water and thus provides a driving force to cause spontaneous water absorption and swelling until the activity or chemical potential of associated water becomes equal to that of free water. This causes the cations to form a disperse layer adjacent to the particle, the cation concentration decreasing with increasing distance from the outer surface until the concentration becomes equal to that in the 'normal water' in the void space (Wong and Wang 1997).

3. Movement of water by osmosis is another possible mechanism which causes internal non-equilibrium swelling (Mitchell 1993). The association of negatively charged clay particle surfaces with positively charged layers of dispersed cations produces what is termed a 'double diffusive layer'. Interaction of two such differently charged layers generates an osmotic pressure. Any physico-chemical change within the double diffusive layer is accompanied with a change in the osmotic pressure and swelling. Physico-chemical changes can be provoked e.g. by inward migration of water into the intramatrix pores and/or by outward diffusion of chemical ions causing a dilution of the intramatrix pore fluid.

According to Nüesch (1991) the osmotic swelling pressure is as follows:

$$p = 2\,n * k\,T\,(\cosh u - 1) \qquad \text{(Eq. 4-17a)}$$

where: p = osmotic swelling pressure
n = concentration of ions in intramatrix pores
k = Boltzmann constant
T = temperature [°K]
u = electric potential in the centre between adjacent clay particles

or approximately:

$$p = K / (d^2 * v^2) \qquad \text{(Eq. 4-17b)}$$

where: K = clay-specific constant
d = half distance between adjacent clay particles
v = valence of ions

Despite the considerable volume of research on the subject, the precise mechanisms of swelling in clays and shales remain somewhat controversial (Low 1987). *Intra*-particle swelling by the introduction of interlayer water into specific clay minerals such as smectite, must be distinguished from *inter*-particle swelling, which occurs in most natural clays regardless of their precise clay

mineralogy. Current concepts of inter-particle swelling postulate the existence of forces of attraction and repulsion between the clay platelets. As mentioned above, the forces of repulsion, which are of particular concern to swelling, have two main components: Hydration forces which are either associated with adsorbed cations at the inner (crystalline) surface (Mechanism 1, above) or with those at the outer clay mineral surface (Mechanism 2), and osmotic forces associated with the differences in ion concentration between the inter-particle solution and the bulk porewater (Mechanism 3). The forces of hydration operate over distances of only a molecular order of magnitude, whereas the osmotic forces are thought to be effective over much greater distances, of a maximum order of about 1000 Å (Horseman *et al.* 2005).

4.3.1.3 Macro-scale swelling

The approach to deduce macro-scale swelling parameters of argillaceous materials from micro-scale observation and characterisation has not succeeded in geo-engineering practice, evidently due to the high number and complexity of the physico-chemical processes involved. Instead generic approaches are common. The major factors which control the macro-scale swell potential and the amount of swell of argillaceous media may be divided into two main groups: (1) compositional factors and (2) geometric, geotechnical and environmental factors. Table 4-5 summarises these factors in some detail.

Table 4-5. Factors controlling macro-scale swelling
(adapted from Horseman *et al.* 2005)

Compositional factors	Geometric, geotechnical and environmental factors
• Type of clay particles • Amount of clay particles • Diagenetic bonds between particles • Particle shape and size distribution • Porewater composition	• Structure and fabric of material and strata • Thickness of strata • Density and water content • Availability of water (moisture): Permeability and water paths • Confining pressure: Stress conditions and stress history • Temperature

Quantitative information on swelling is gained from dedicated tests which may be broadly divided into those tests attempting to measure the deformation resulting from swelling without confinement, and those attempting to measure the swelling pressure developing in confinement (Hobbs and Jones 1995). A large number of experimental methods have been designed to determine swelling characteristics. Offer *et al.* (cited by Horseman *et al.* 2005) list at least 25 different techniques. Of particular practical importance are the following three test types:

1. Axial and radial free swelling strain (completely unconstrained conditions)
2. Axial swelling strain test (constrained radial conditions; insignificant axial surcharge)
3. Axial swelling pressure as function of axial swelling strain (constrained radial conditions).

A test of the first kind (completely unconstrained conditions) are the saturation and desaturation experiments on Opalinus Clay samples which were carried out by Wolter (2003) by means of an ASR (Anelastic Strain Recovery) testing rig. In these tests, a free standing core sample

was placed in a climate chamber and subjected to various controlled moisture conditions whilst the change of its geometric dimensions was continuously monitored. Figure 4-14 gives an example of the test results. The results highlight the particular sensitivity of saturation (and desaturation) for swelling (and shrinkage) as is evidenced in the very significant magnitude of the monitored strain rate (order of some ± 2 x 10^{-3} per day). The tests also provide evidence about the particular influence of the bedding planes, resulting in a distinct anisotropic hydro-mechanical behaviour of argillaceous materials with regard to saturation / resaturation (compare the different responses of the axial strain ε_{axial} in P- and S-Samples).

Figure 4-14. Sensitivity of saturation (top) and desaturation (bottom) processes resulting in swelling and shrinkage strain of argillaceous samples in ASR testing
[Opalinus Clay; after Wolter 2003; note the distinctly different behaviour of P-Samples (left) and S-Samples (right)]

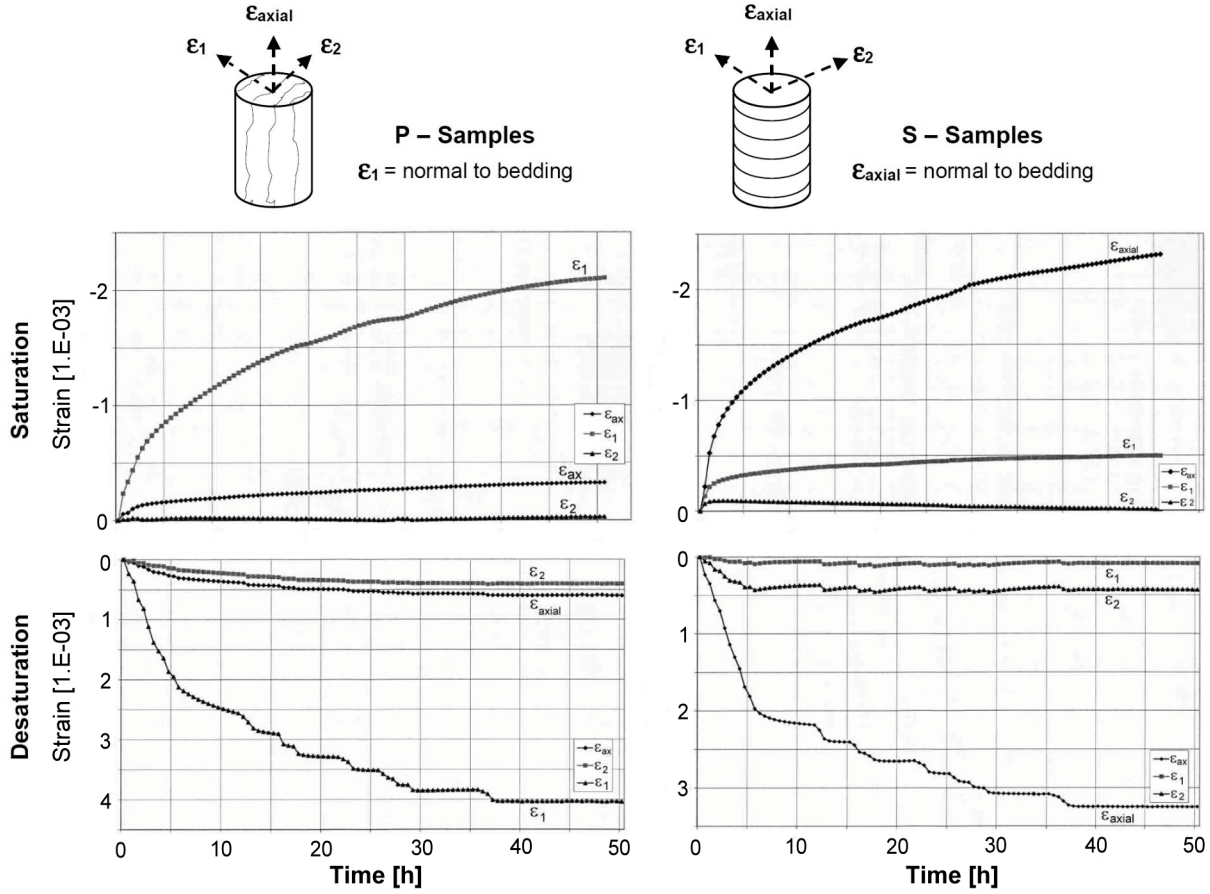

The results of the second test type (axial swelling strain test under constrained radial conditions; oedometer testing set-up) is commonly characterised by the swelling strain index S_ε:

$$S_{\varepsilon\,axial} = (\delta_{axial} / H_0) * 100 \ [\ \% \ ] \qquad \text{(Eq. 4-15)}$$

where: δ_{axial} = maximum swelling displacement
H_0 = initial height of the specimen before swelling

The swelling strain index S_ε is of particular interest when considering sealing of fractures through swelling of the fracture wall material. Results of laboratory swelling tests on Opalinus Clay are presented in Table 4-6.

Table 4-6. Swelling strain index S_ε of the silty-shaly facies of the Opalinus Clay at various seating pressures p_0 as deduced from laboratory tests

p_0 [kPa]	Sample direction	Swelling strain index S_ε [%]	Reference
50	$\perp$ ss	$S_{\varepsilon \perp ss} = 7\ (\pm\ 2)$	Bock (2001)
	// ss	$S_{\varepsilon // ss} = \sim 1$	
15 - 20	$\perp$ ss	$S_{\varepsilon \perp ss} = 1.4 - 7.5$	Nagra (2002b)
	// ss	$S_{\varepsilon // ss} = 1 - 4.5$	

Zhang *et al.* (2007b) and Wileveau and Rothfuchs (2007) document some swelling and shrinking tests under triaxial stress conditions. Given different boundary conditions ($\varepsilon_{lateral} \neq 0$) their tests results are not directly comparable to those listed in Table 4-6. For an effective confining pressure of $p_c' = \sigma_3 = 1$ MPa, they found a volumetric decrease of 1.6% (time span of four months) for the shrinking phase, and a volumetric increase of 2.4% (time span of six months) for the swelling phase.

Results also exist for the third test type (axial swelling pressure as a function of axial swelling strain in radially constrained radial conditions) of the Opalinus Clay. Like with the swelling strain, there is a high degree of anisotropy in the swelling pressures with values ranging from 0.1 to 0.6 MPa parallel to bedding, and from 0.8 to 1.4 MPa normal to bedding (Bock 2001; Nagra 2002b).

Recently, Zhang *et al.* (2004; 2007b; 2009) have performed various swelling experiments on the Callovo-Oxfordian argillite and the Opalinus Clay under suction- and load-controlled conditions. The results suggest that:

a) the claystones in fully unconstraint conditions ($p_c = p_0 = 0$) can take up great amounts of water from the humid environment (RH = relative humidity), much more than the water content in the natural and saturated state w_o (Figure 4-15);

b) the large amount of the water uptake causes a significant expansion up to 8-12% over ten months (Figure 4-15); and

c) the swelling pressure Π, which was measured by wetting samples with water vapour under axially-fixed and laterally-unconstraint conditions, increases with water uptake to high levels of 10.5 MPa on COX and 5.5 MPa on OPA (Figure 4-16).

The high swelling pressures are very close to the overburden stresses at the sampling depths of 240 m in the Mont Terri and 490 m in the Bure URL, suggesting that the adsorbed water-films are capable of carrying the lithostatic stress (Horseman *et al.* 1996; Rodwell *et al.* 1999).

Figure 4-15. Free swelling strain of the Callovo-Oxfordian argillite (left) and the Opalinus Clay (right) as a function of water uptake from humid environment
(from Zhang *et al.* 2009)

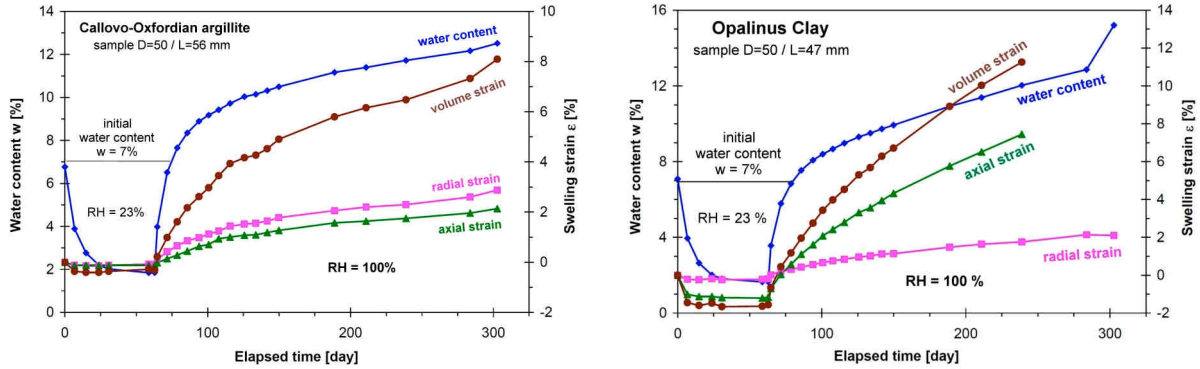

Figure 4-16. Swelling pressures of the Callovo-Oxfordian-argillite (left) and the Opalinus Clay (right) measured in axially-fixed and laterally-unconstraint conditions
(from Zhang *et al.* 2009)

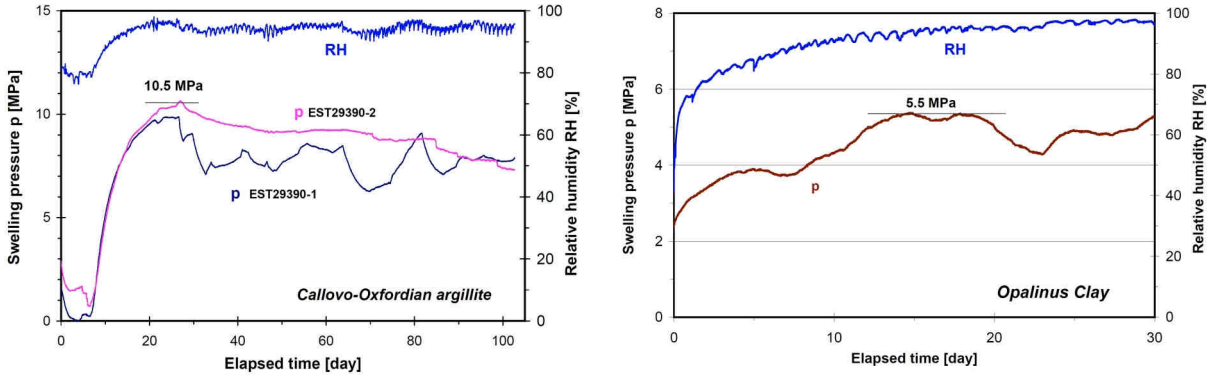

4.3.2 Slaking

The definition of "slaking", its distinction from "swelling" and the underlying mechanisms are still subject to debate. According to the ISRM Suggested Methods (Ulusay and Hudson 2007), slaking "of swell susceptible rocks can occur if they are subject to swelling-drying cycles or intensive air-drying". Common to slaking is that it is connected with a significant degree of structural disintegration of the material in the form of progressive fracturing (Figure 4-17) and that the argillaceous material is decaying into smaller slabs, pieces and particles.

Micro-mechanically, slaking of argillaceous material is often associated with the impact of capillary forces on the microstructure of the rock. When suction pressure is applied to a fully saturated rock sample (e.g. desaturation by ventilation) the effective stress acting on the sample increases and the sample shrinks. In reverse, resaturation of a partially saturated sample is connected with a reduction of suction pressure and, consequently, of the effective stress leading to an expansion of the sample. Both actions, desaturation and resaturation, may lead to microscopic failures and, if the

suction changes are of significant magnitude and repeatedly applied, also to macroscopic fracturing of solid materials.

In line with Moriwaki (1974; cited in Horseman *et al.* 2005) slaking might be based on at least one of the following two mechanisms:

- Body slaking: Rapidly occurring traverses of comparatively large portions of material with no apparent deterioration between cracks, apparently originating from some internal processes within the material (Figure 4-18).

- Surface slaking in line with dispersion: Loss of mass due to "sloughing" of tiny flakes of grains from the material of the fracture surface, with no apparent cracks in the underlying material. The flakes are dispersed into the water-filled pore or fracture space (spontaneous suspension).

Body slaking will be considered in the following whilst surface slaking and dispersion will be briefly discussed in Section 4.4.

Figure 4-17. Progressive cracking of Callovo-Oxfordian argillite during hydration/dehydration cycles (ESEM - Environmental Scanning Electron Microscope pictures)
(Montes *et al.* 2004)

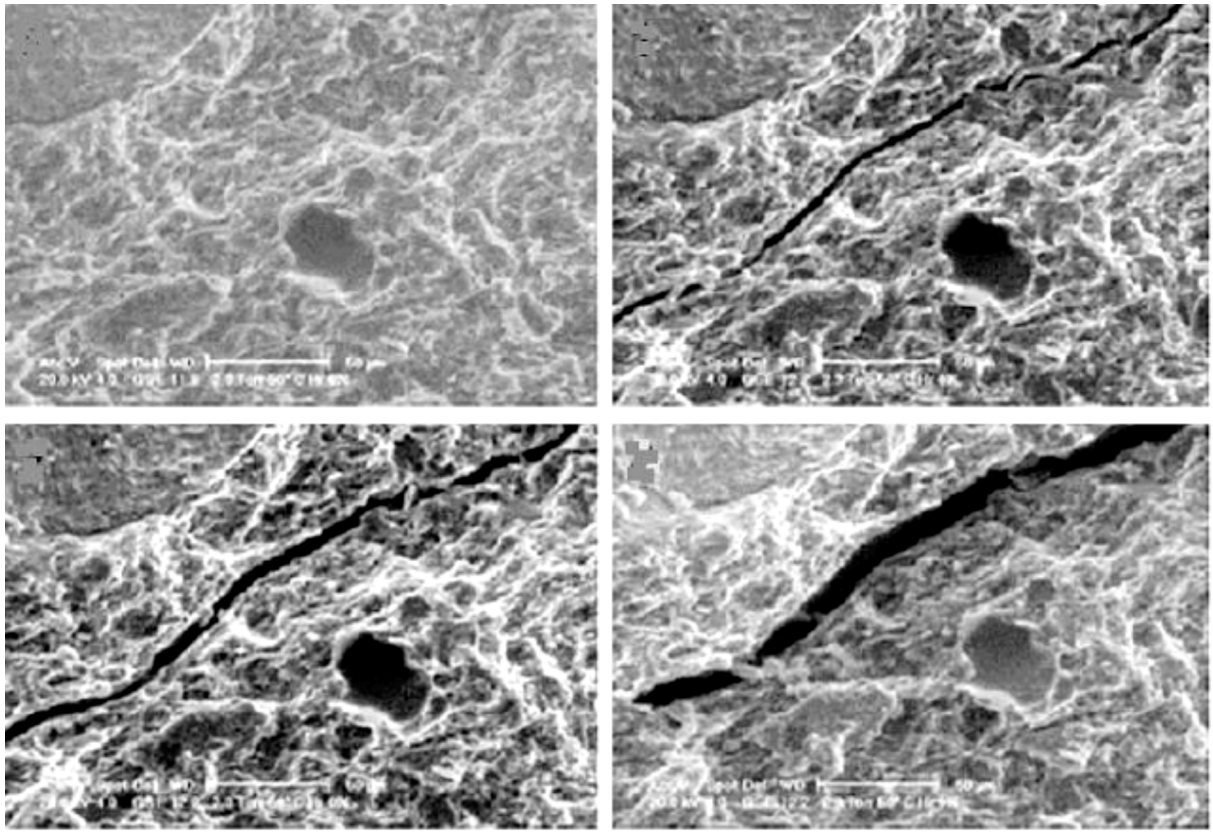

Figure 4-18. Body slaking in an EDZ test specimen before and after combined water/gas permeameter experiment (Fröhlich 2004)

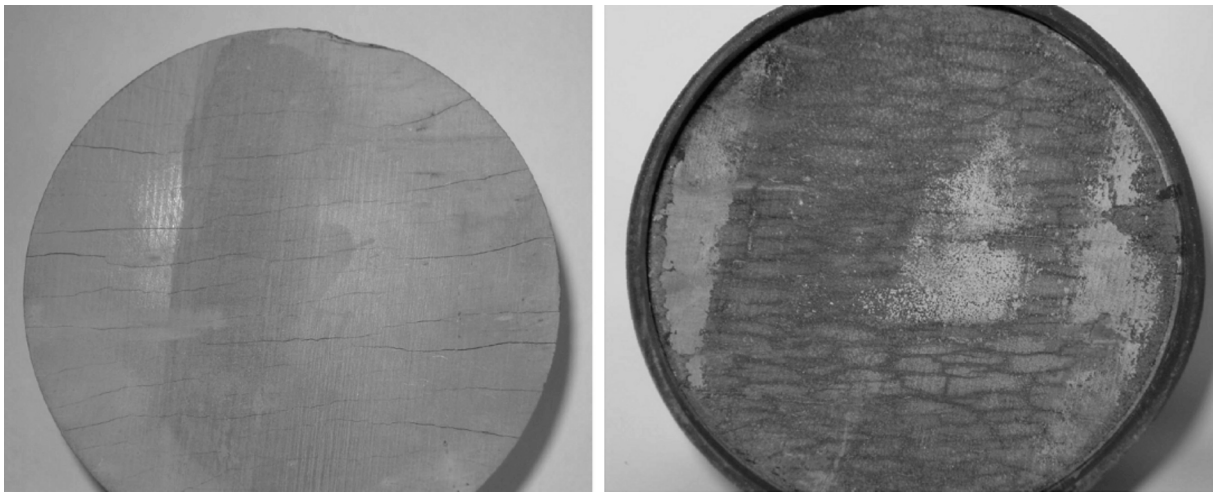

The effect of body slaking onto the fracture transmissivity and thus onto the sealing potential of fractured argillaceous media can be comprehended as follows: Consider a body with a given fracture (Figure 4-19, left). Its initial transmissivity T_0, as measured over the height H of the body, is proportional of the cube of the fracture aperture $a_{h\,0}$:

$$T_0 \sim a_{h\,0}^3 \qquad \text{(Eq. 4-10a)}$$

The formation of a slaking fracture 1 (Figure 4-19, right) will somehow change the hydraulic transmissivity of the area under consideration. From inspection of Figure 4-18 it is reasonable to assume that both the total volume of the body and the total fracture volume remain constant and that, after slaking, the apertures of initial and slaking fractures will tend to become equal to each other $a_{h1} = a_{h\,S\,1}$.

Figure 4-19. Consideration of the influence of body slaking onto transmissivity

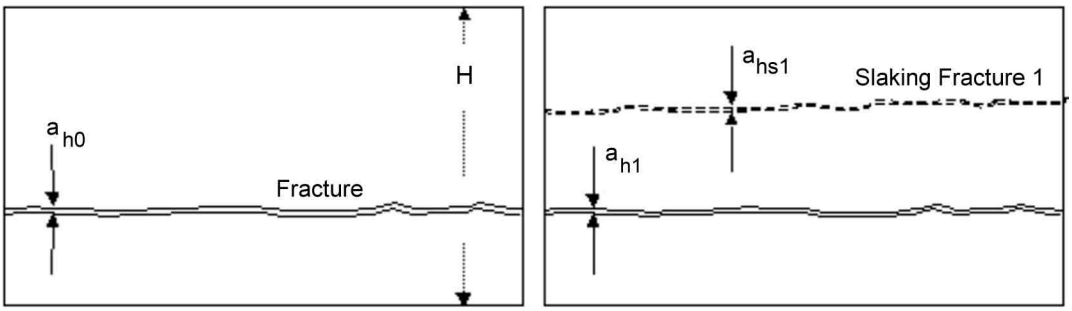

It then is:

$$a_{h\,1} = a_{hs1} = (1/2) * a_{h\,0} \qquad \text{(Eq. 4-19a)}$$

and:

$$T_1 \sim 2 * [a_{h0}/2]^3 \quad \text{(Eq. 4-19b)}$$

or, generally, with n slaking fractures:

$$T_n \sim [a_{h0}/(n+1)]^2 \quad \text{(Eq. 4-19c)}$$

Body slaking thus tends to reduce the transmissivity of a fractured body by the square of the additional number of slaking fractures. The more intense the body slaking, the lower the overall transmissivity. Note that, within these considerations, the body height H remains constant, as solely slaking is considered without any swelling of the material.

Micro-mechanically, body slaking of argillaceous material might be explained by the compression of trapped air and subsequent tension cracking around the air pocket. When a not fully saturated argillaceous material is immersed in water, some air in the material will be trapped within the material at a finite depth beneath its surface. The same applies when an unsaturated argillaceous rock is wetted or flooded via its fractures. As the pore size of argillaceous materials is very small, strong capillary forces will be generated (van Genuchten model; Figure 4-20) pulling the water towards the trapped air. The trapped air will then be compressed by this capillary-driven water infiltration. Wetting stops when the pressure in the air pocket equals the capillary pressure of the water. However, the argillaceous material surrounding the air-compressed pocket may fail in tension well before such equilibrium is reached. The energy stored in the compressed air pocket might then drive the initial micro-crack to macro-scale lengths (similar to the Griffith crack extension mechanism, see Section A.3.3.3), resulting in body slaking. The importance of this mechanism can be demonstrated by the absence of slaking when slake testing is performed under a vacuum (Horseman *et al.* 2005).

Figure 4-20. Capillary pressure curves of the Opalinus Clay
(Zhang *et al.* 2008)

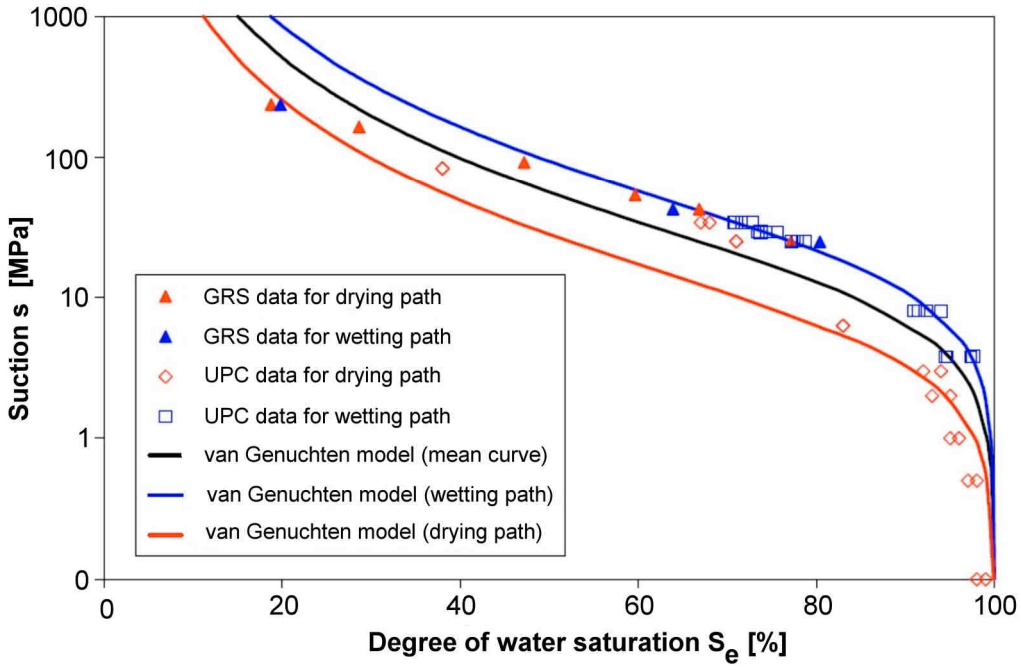

Experimental evidence on body slaking has been gained in the context of various research programmes (e.g. Bossart *et al.* 2002, Bernier *et al.* 2004). Clear indications were found which demonstrate that the process of disaggregation of the fractured EDZ can be expected to start already during the operational phase of the repository (open tunnel phase; subject to type and dimension of tunnel lining) as a consequence of seasonal variations in tunnel ventilation. In the context of the ventilation experiment in the Mont Terri URL (Mayor and Velasco 2008), significant fluctuations of capillary pressure were monitored in the EDZ during drying and wetting periods, respectively.

4.3.3 Comparison of influencing factors swelling and body slaking

In the following the processes of swelling and slaking are compared by undertaking an order of magnitude estimate of their respective potential in fracture closing and, implicitly, in their sealing capacity. For that purpose a synthetic case is considered under assumptions and input parameters relevant for the Opalinus Clay (Table 4-7).

Table 4-7. Order of magnitude estimate of swelling and body slaking potentials in closing of Opalinus Clay fractures

Report Section	Influencing factor	Assumptions and input parameters	Result: Fracture closing potential
4.3.1	Swelling	Depth of de-saturation in fracture wall matrix = 50mm (Mayor and Velasco 2008;), linear saturation profile Saturation increase from 80 to 100% Swelling strain indices: $S_{\varepsilon \perp ss}$ = 5%; $S_{\varepsilon //ss}$ = 1% Swelling pressure constraint: 50 kPa	$\delta_{n\ swelling\ \perp ss}$ = 1.25 [mm] $\delta_{n\ swelling\ //ss}$ = 0.25 [mm]
4.3.2	Body slaking	No. of slaking fractures / initial fracture = 3 Aperture of initial fracture = 0.1 [mm]	$\delta_{n\ slaking}$ = 0.025 [mm]

From the above table and when compared with Table 4-4, it becomes apparent that swelling tends to be the biggest potential contributor in the closure of Opalinus Clay fractures. This result is fully in line with laboratory and field experience with various argillaceous materials, as outlined in Sections 3.1 and 3.2. Compared with swelling, body slaking appears to be of lesser importance, however it still exerts an influence, particularly in clays with low smectite content and/or with a high degree of cementation.

4.4 Surface slaking, sedimentation and clogging of fractures

In comparison with body slaking, surface slaking and the dispersion of the flaked material are far less amenable when considering fracture sealing. Where an argillaceous material has access to free water, repulsion between clay particles occurs due to the expansion of double layers (Section A.2.3.2). If the repulsion is so large that the diagenetic bonds between particles are broken then those particles, located at the fracture wall, will be pushed apart and dispersed into the water-filled fracture

space. The slaked particles are very small and might be dispersed as colloids[12]. Surface slaking thus may be considered as "homogenisation" of the fracture system whereby clay material is dispersed into the fracture space at the cost of the fracture wall material, effectively "smearing out" (and possibly sealing) the fracture space over a larger volume.

To become effective in the sense of fracture sealing, the assembly of dispersed and subsequently flocculated particles and colloids is to be considered in terms of its structural stability against a hydraulic gradient acting along the fracture. If that stability does not exist the particles will start moving with the fracture fluid, however it is conceivable that the moving particles will become trapped within the fracture space. Trapping could be by sedimentation (thus narrowing of the effective fracture aperture) or by clogging at fracture wall asperities (thus increasing the turtuosity of the fracture channel). The associated physico-chemical conditions and their changes, which are necessary for switching between the various stages of disaggregation / reaggregation on one hand and dispersion / coagulation on the other, are complex and, to date, no dedicated test results appear to be available on these mechanisms in fractures.

To the best knowledge of the authors, only very few studies have been performed concerning the behaviour of colloids in clays and shales, all of them related to intact (unfractured) media. In the Opalinus Clay at Mont Terri colloids were studied in several water samples collected *in situ* (Degueldre *et al.* 1998). Investigations were focussed to the size range 0.001 to 0.010 $*$ 10^{-3} mm because only such small colloids are potentially mobile in the pore space, with a concentration of 10-20 ppt being derived. In the Opalinus Clay at Benken colloids include clay minerals, quartz, calcite, Fe hydroxides and organics, even though their stability under *in situ* conditions is limited. The mobility of colloids is very low due to the very low permeability and nanometre-scale pore structure of the Opalinus Clay. Model calculations indicate that colloid-related transport is negligible (Voegelin and Kretzschmar 2001). In the Boom Clay, which was found to act as an ultrafilter, mobile colloids should only be present in very low concentrations (Ondraf/Niras 2002). Generally, colloid transport in the studied argillaceous media is considered irrelevant, at least in cases where fracture flow is not relevant (Mazurek *et al.* 2003).

4.5 Sealing by precipitation of minerals (mineral coating)

It is conceivable that precipitation of minerals in open fractures might contribute to a reduction of the fractures' transmissivity, thus possibly leading to a sealing of fractured argillaceous formations. That mechanism is quite common in geologic analogues. Sealing processes in sedimentary rocks can be linked to specific stages of fluid migration and may be related to major geodynamic events (see Appendix A.6.1 and A.6.2). Most of the observed geologic fracture infills, such as the celestite veins in the Callovo-Oxfordian argillites (Section A.4.1.3.2), have been interpreted as local early diagenetic features and are not necessarily related to tectonics. However, the Effingen Beds (marl and argillaceous limestone) at Oftringen (near Olten, Switzerland) host calcite-celestite veins which apparently precipitated from descending Miocene seawater (see Appendix A.6). Today, these geologic features are hydraulically inert mineralised fracture zones and veins. As mentioned in Section 2.3.3, Opalinus Clay has been affected by some substantial faulting at Mont Terri as well as in the Molasse Basin and contains major faults, sometimes with m–tick breccia. Mineralisation of these structures is completely absent or, in some rare cases, very minor. This means that since the time the faults were created, there is no or very little geochemical evidence of fluid flow along these structures.

[12] With regard to size distribution, colloids are defined as particles with sizes ranging from 0,001 to 1 $*$ 10^{-3} mm. For comparison, in soil mechanics the particle size of clay is defined as < 2 $*$ 10^{-3} mm).

As consistently observed in URL experiments there are essentially two physico-chemical processes leading to the precipitation of minerals in EDZ fractures (Figure 4-21; see also Figure 2-10): (1) evaporation and (2) oxidation. Both processes are triggered by the excavation of the underground galleries and the associated changes in the environmental and geochemical boundary conditions of the EDZ rock (tunnel ventilation and oxygen access).

Figure 4-21. Sealing by mineral precipitation of fractures in argillaceous rocks due to evaporation (top) and oxidation (bottom) (schematic; after Mayor and Velasco 2008)

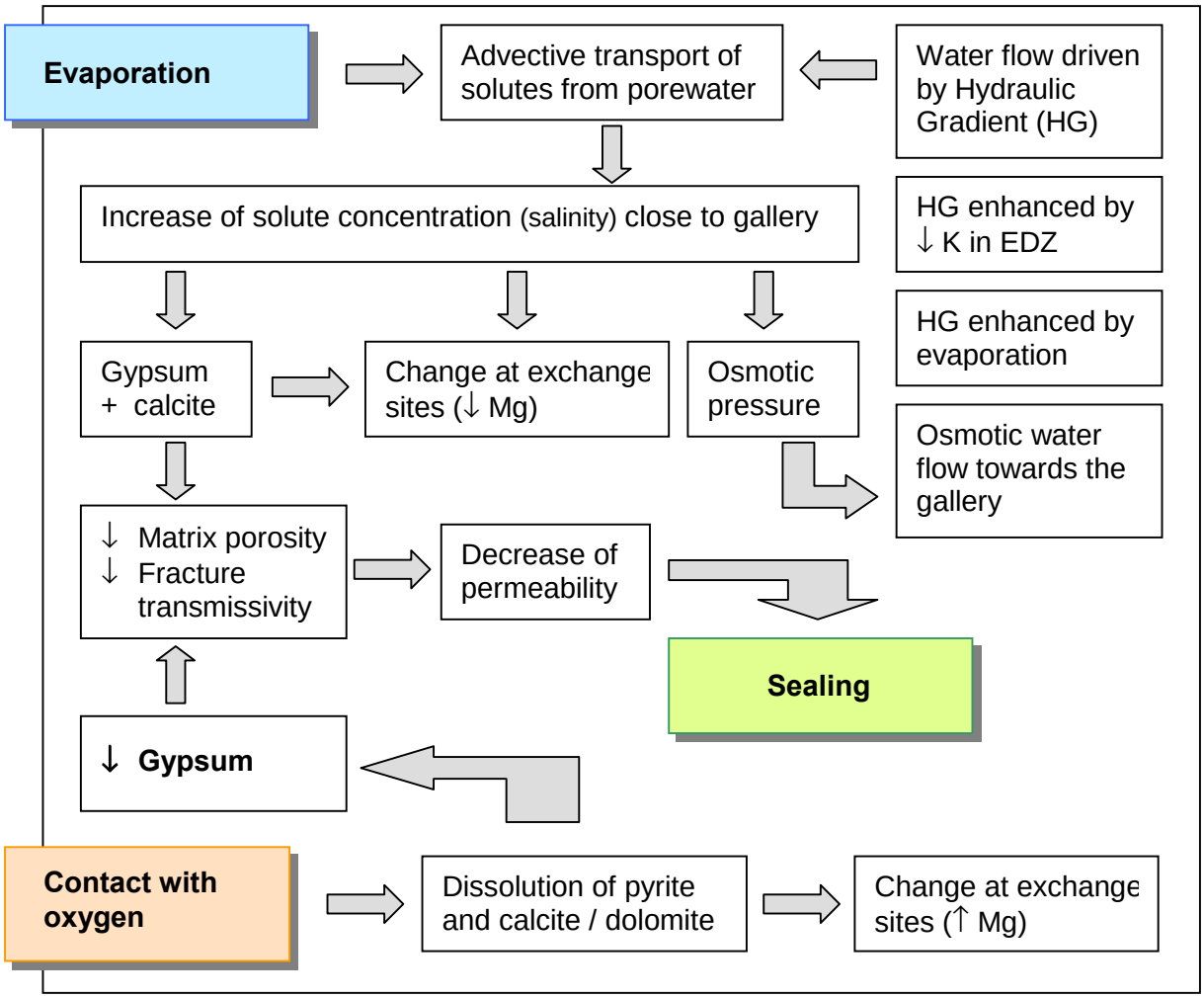

4.5.1 Concentration of minerals by evaporation at the tunnel wall

Ventilation of underground openings, particularly if low-humidity air has direct access onto the tunnel wall rock, can cause a desaturation of the EDZ rock and transportation of the porewater towards the excavated surface, where it evaporates. In the VE-Experiment at Mont Terri (Mayor *et al.* 2008) the analysis of the porewater chemistry showed that solutes are transported by capillary-driven advection towards the tunnel wall, leading to increased chloride and sulphate concentrations in the EDZ rock over a depth of about 40 cm from the wall. With regard to exchangeable cations, sodium and potassium at exchange positions of the clayey rock are practically constant with depth. For

calcium and magnesium there is an inverse concentration profile in the first 40 to 60 cm of the tunnel wall rock (Figure 4-22).

The salinity gradients imply that the water flow towards the excavated tunnel wall may also be osmotically-driven, but this process appears to be of no practical relevance, because of the comparatively low osmotic efficiency of the Opalinus Clay (about 10%; Nagra 2002b). Overall, it can be concluded that, after more than eight years of tunnel ventilation incorporating two extreme desaturation / resaturation cycles, the geochemical changes in the clayey rock around the excavated VE-microtunnel have a negligible effect upon the hydromechanical behaviour of the clayey rock, with regard to both matrix and fracture permeability.

Figure 4-22. Variation of the calcium and magnesium cation concentration in the sidewall rock of the micro-tunnel at Mont Terri (from Mayor and Velasco 2008)

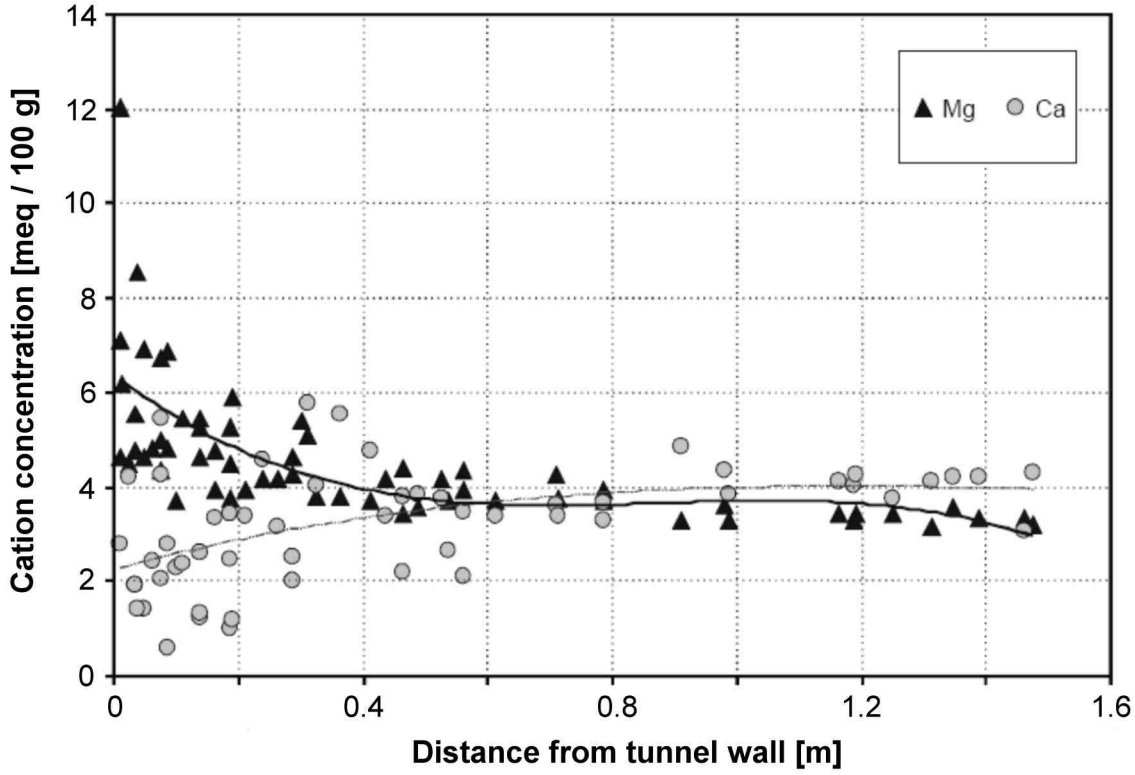

4.5.2 Mineral precipitation due to oxidation

The only oxidation process of relevance is that of pyrite (FeS_2) which can lead to acidification of the porewater. Argillaceous rocks contain some portions of pyrite, commonly in the order of about 1 weight-%. Sulphuric acid, formed by pyrite oxidation, can react with calcite to form gypsum (Figure 4-23). Traces of calcite are also common within argillaceous rocks. This process is not necessarily exclusively chemical. Autotropic bacteria obtain their energy from the oxidation of inorganic compounds and when atmospheric oxygen is consumed. Proteinaceous body materials are produced from atmospheric CO_2 and nutrients such as nitrogen are usually available in pyritic shales to support bacterial growth and reproduction (Horseman *et al.* 2004).

Pristine pyrite commonly occurs as intact framboidal or rhomboidal mineral structures (Figure 4-24 top) which are dispersed within the argillaceous rock matrix. Oxidation transforms these structures into anhydrite and/or gypsum (Figure 4-24 bottom).

Figure 4-23. Pyrite oxidation and formation of gypsum (from Mayor and Velasco 2008)

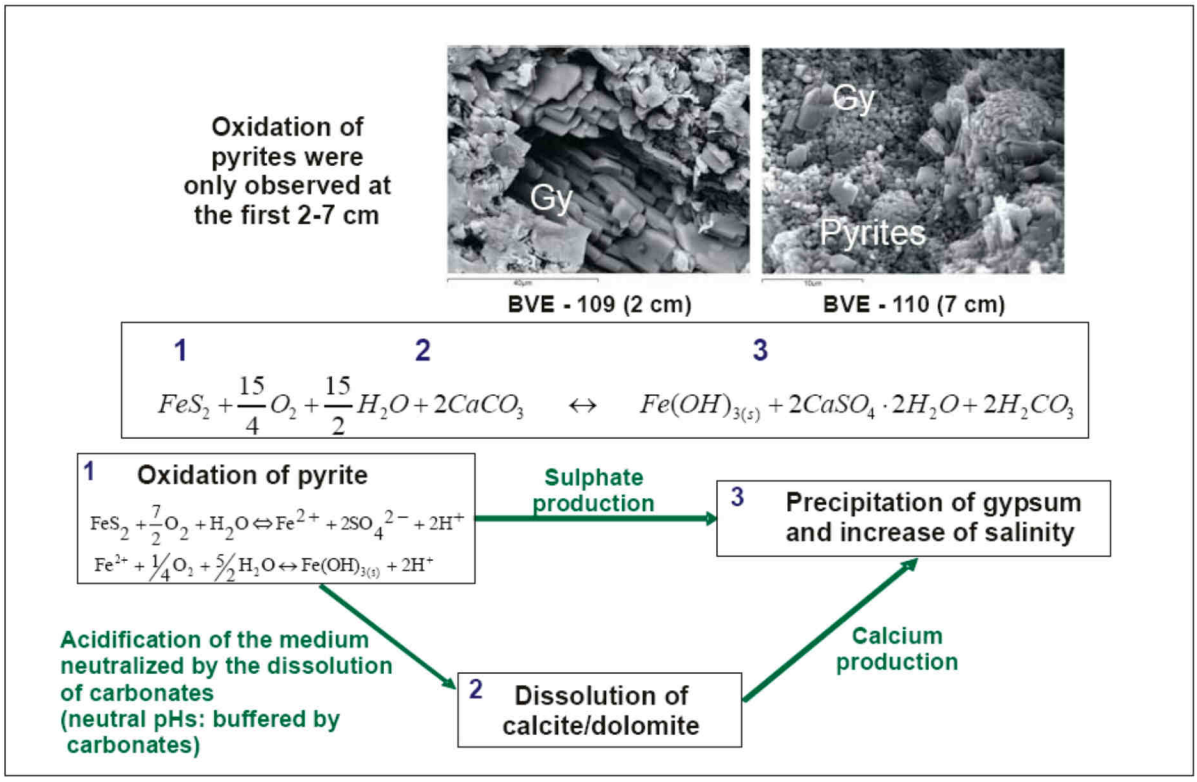

There are several observations and investigations on the advance rate of pyrite oxidation into the argillaceous rock. In the Hades URF, traces of oxidation were observed on 15 years old EDZ fractures which have progressed from the Test Drift in the Boom Clay (Section 3.2.3.1, Figure 3-43). In the Toarcian - Domerian shales of the Tournemire URL, the EDZ in the about 100 years old railway tunnel extends about 150 cm from the tunnel surface in the rock as indicated by some gypsum-covered fractures (Charpentier *et al.* 2001). Oxygen isotopes are disturbed more than 10 m indicating air diffusion around this old tunnel at a significant distance from the tunnel (Charpentier *et al.* 2003).

In the Opalinus Clay of northern Switzerland pyrite oxidation rates were studied by Mäder and Mazurek (1998) in the Mont Terri URL (time frame of up to ten years), in the Upper Hauenstein railway tunnel (time frame of up to 150 years) and also in surface outcrop of the Siblingen clay pit (time frame of several 10,000 years). The progression of the pyrite oxidation can be summarised as follows:

- *After 0-10 years:* Partial desaturation of the EDZ rock and formation of fractures with up to several mm high apertures. Over a depth of about 0.70 m from the excavation surface, localised formation of gypsum on fracture surfaces, however without any visible oxidation seams.

- *After about 10 – 200 years:* Formation of 3 to 15 mm thick oxidation rims along fractures or joints with partial (<20%) oxidation of pyrite. The penetration depth of oxidation within the EDZ amounts to at least 1.6 m.

- *Order of 10 000 years:* At the topographical surface, which is subject to geological weathering, the penetration depth of oxidation may reach the order of some tens of metres (see Figures 3-54 to 3-56). That amount, however, cannot be extrapolated to the confined conditions of a deep underground geological repository.

Figure 4-24. SEM pictures of pyrite oxidation process (after Clauer 2005)
Top: Pristine state with (1) framboesian, (2) big rhomboidal and (3) small rhomboidal structures
Bottom: (4) Complete alteration of framboesian pyrite into anhydrite / gypsum

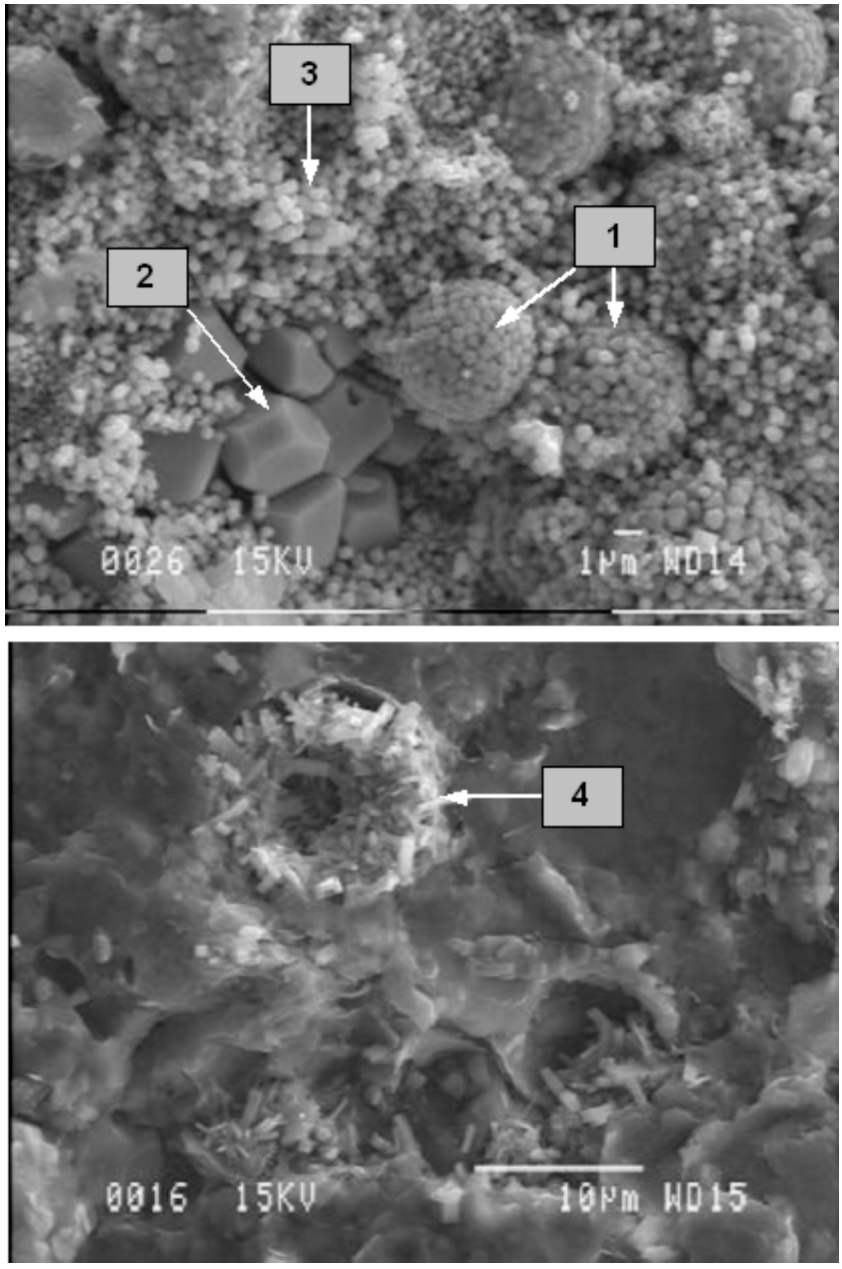

A short- and long-term estimate of the amount of the pyrite oxidation in underground repositories is presented in Nagra (2002b). In the emplacement operations phase until cell closure, less than 0.1‰ of pyrite will become oxidised. Until repository closure (~ 100 years) 5 to 10 mm thick oxidation rims will be formed along the conductive EDZ fractures and about 0.4‰ of pyrite will become oxidised. Overall, the geochemical alterations of the Opalinus Clay in the repository operation phase are negligible. In the post-closure repository phase, any remaining residual air will eventually be consumed by chemical reactions and biological activity. The EDZ will then return to an anoxic state. Any mineral coatings on fractures which, despite of the above, might have been precipitated during the oxidation phase would then be subject to changed chemical conditions and may be re-dissolved. The long-term geochemical evolution of the damaged rock and its effects on the transport properties of the EDZ remains to be elucidated.

In conclusion, seals arising from mineral precipitation on fractures are unlikely to be formed within the repository operation phase and, if formed, may not be stable after repository closure. Fracture closure by mineral precipitation should therefore not be accounted for in PA considerations on sealing.

4.6 Simulation of sealing mechanisms in numerical models

4.6.1 Modelling approaches

From the evidence compiled in Chapter 3 and qualitative assessment of the repository concepts for argillaceous formations, it can principally be expected that partial or even full sealing of EDZ fractures around the backfilled underground structures will occur. Ignoring sealing effects would surely result in an inadequately designed repository concept. A quantitative assessment and prediction of the sealing behaviour in PA requires the implementation of the pertinent sealing mechanisms, as discussed before, in suitable coupled hydro-mechanical simulation tools. In principle, both continuum and discontinuum (fracture network) approaches might be adopted for modelling the evolution of the EDZ in the various repository phases, requiring different formulations and parameterisations in the respective hydro-mechanical process models.

Following Marschall *et al.* (2008b), a distinction can be made between classical continuum and discontinuous Discrete Fracture Network (DFN) formulations. In the classical continuum formulation the hydro-mechanical coupling approach comprises:

1. a general relationship between mechanical stress and porewater pressure ("effective stress" concept);

2. an appropriate representation of the stress-deformation behaviour of the rock (material law); and

3. a parametric relationship between deformation and effective hydraulic properties for all possible stress paths (porosity-permeability relationship).

The determination of the site-specific porosity-permeability relationship in these models might be quite difficult, as the permeability of a deformed rock can be subject to drastic changes, particularly in stress paths associated with high strain localisation. Further complications are faced where experimental data is required to be up-scaled from laboratory to field scales.

In the discontinuous Discrete Fracture Network (DFN) formulation the hydro-mechanical coupling approach comprises:

1. a general relationship between mechanical stress and porewater pressure along the fractures of the fracture network ("effective stress" acting on the fracture planes);

2. a comprehensive geometric characterisation of the fracture network (e.g. size, spatial frequency, orientation of the different fracture classes);

3. a functional relationship between effective stress and fracture aperture (fracture closure law); and

4. a relationship between fracture aperture and fracture transmissivity.

The simulation of fluid flow in non-deformable fracture networks is a well-established scientific area in hydrogeology. Mature numerical codes are available to simulate flow and transport processes even for huge fracture networks with millions of fractures (e.g. www.fracman.com; www.connectflow.com). These codes allow for systematic conversion of hydraulic fracture network properties into effective hydraulic conductivity of the corresponding equivalent porous medium (Figure 4-25), if the fracture connections of the network fulfils certain conditions (cf. Bear *et al.* 1993). Homogenisation approaches for stress-dependent permeability in DFN models are described in Kim *et al.* (2004) and Min *et al.* (2004).

Figure 4-25. Postulated equivalence between DFN and EPM models
(after Marschall 2005)

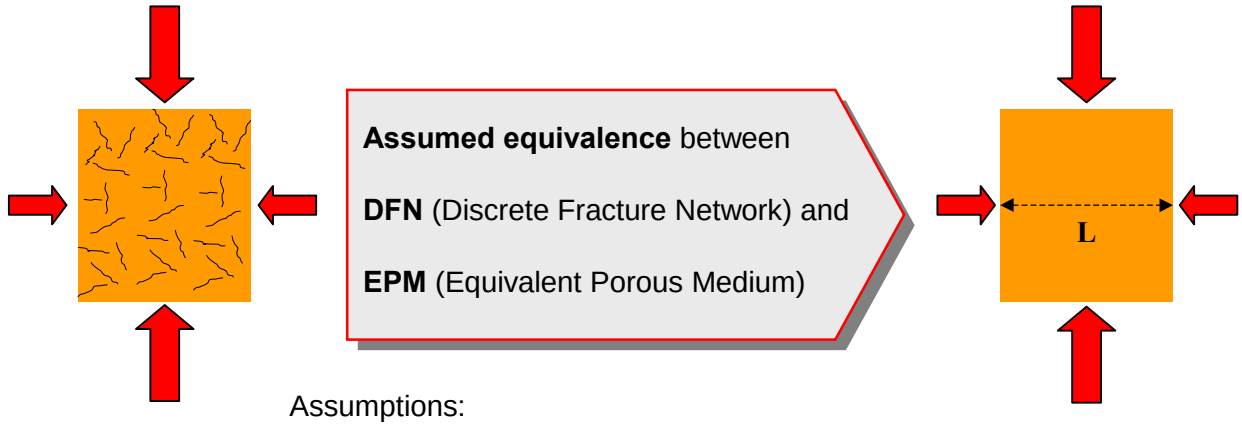

Assumptions:

- Isotropic fracture orientation
- Fracture size << scale of observation L

4.6.2 Modelling Example 1: Bure URL and 3-D Adaptive Continuum / Discontinuum code

In this model the ground water flow through the fracture network was simulated to evaluate the damage-induced permeability around the disposal drifts of the Bure URL.

Itasca has developed a new code, termed the Adaptive Continuum/Discontinuum Code (AC/DC, Billaux 2004), using periodic discontinuum elements as mesh and dynamically selecting the element-appropriate properties to be used in various parts of the model, depending on the level of deformation in each part (i.e. switch locally from a continuum to a discontinuum description based on specified selection criteria). The code was tested in the framework of the SAFETI project (Dedecker *et al.* 2007), using the data of the Meuse/Haute-Marne site. From the mechanical parameters of argillite, modelling infers plausible micro-crack networks, comparable with those observed during the last years within the EDZ in the Bure URL along the shaft and the experimental drifts (Figure 4-26).

Figure 4-26. Connected micro-crack network, obtained by 3D modelling (®AC/DC)
Meuse/Haute-Marne URL, circular drift, two years after excavation (Itasca 2004)
Only micro-cracks are figured

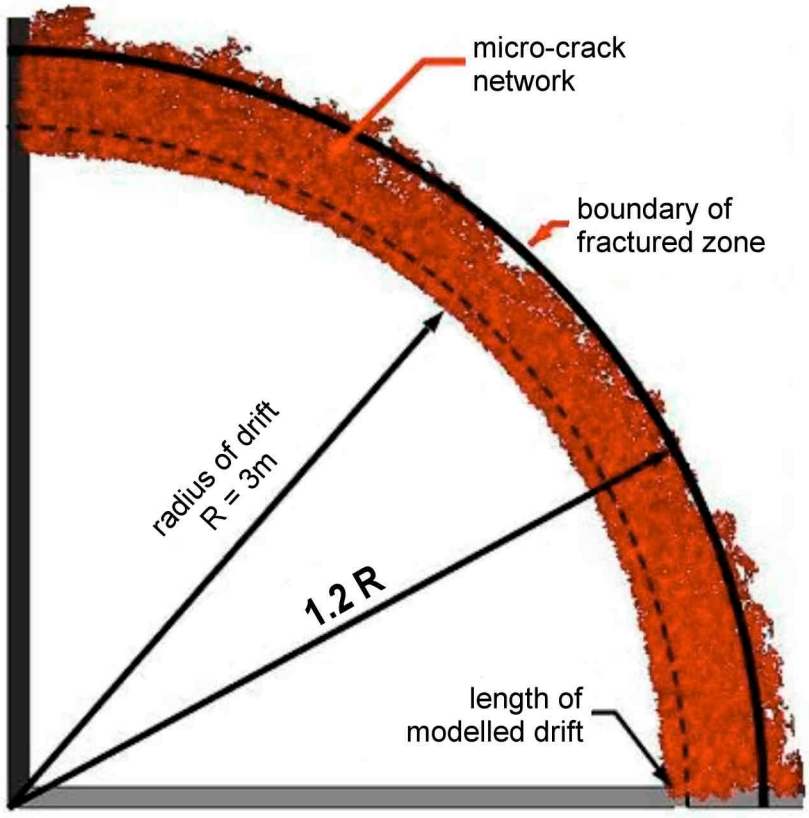

Hydraulic properties of the fractures in the model

As shown in Sections 4.1.3 and A.5.4.1, the transmissivity of a single fracture can be deduced from the general equation:

$$T = \alpha e^{n} \qquad (\text{for } 1 \leq n \leq 3) \qquad \text{(Eq. 4-10a)}$$

where: α = $[\tau / (12\ C)]$
τ = part of the fracture accessible to the fluid
C = rugosity coefficient.

For n=1 Eq. 4-10a is equivalent to the Darcy law for a homogenous porous medium when considering α as the hydraulic conductivity. For n=3, it corresponds to the Poiseuille equation for a flow between two plates.

In a first step, the geometric characteristics of each fracture was deduced from the micro-crack network obtained in the AC/DC model as follows (for details, see Dedecker *et al.* 2007):

- the fracture extension is obtained by identifying all those micro-cracks which are located in about identical planes and are positioned close enough to become interconnected;

- the fracture aperture is deduced from the mean relative displacement of separated particles creating the micro-crack; and

- the exponent 'n' was selected to be equal to 2, in reference to a previous application with the Opalinus Clay in the Mont Terri URL (Billaux *et al.* 2004). The coefficient 'α' was fitted to the permeability test results of the Callovo-Oxfordian argillite carried out by Davy *et al.* (2007).

The next step was the determination of an equivalent permeability of the EDZ, which can be used for the total performance assessment of the repository. The approach is based on simulations of a uniform-gradient flow parallel to the drift, in the reconstituted 3D-fracture network with the groundwater code 3FLO (Billaux 1990; Billaux *et al.* 1993). The equivalent permeability was evaluated from the computed flow rates. For this, the medium was considered to be fully saturated to be able to highlight variations of the equivalent permeability. Mechanical equilibrium leads to a stabilisation of the equivalent permeability.

Using the characteristics of the fractures, as detailed above, the results are as follows:

- the flow section varies between 2 and 4 m² whatever the hypotheses (this is the section of a 20 cm-thick annulus whereas the connected fracture envelop corresponds to a 60 cm thick annulus);

- the equivalent hydraulic conductivity amounts to values of either between $4*10^{-14}$ and $7*10^{-14}$ m/s (which is very close to the argillite matrix permeability), or between 10^{-12} and $9*10^{-12}$ m/s, depending on the experimental data used for calibration (in a drift oriented along the horizontal major stress the permeability measured *in situ* just after excavation is around 10^{-9} m/s); and

- in the case of the shaft, the influence of the liner clearly appears on the evolution of the permeability, even if this influence remains relatively small.

The analysis highlighted the sensitivity of α and of the aperture e on the result, with two difficulties:

- the calibration of α from sample tests requires the assumption of an initial aperture of the tested fracture; and

- the fracture apertures obtained in the simulation turned out to be smaller than the displacements measured *in situ* in the EDZ. This is perhaps due to a scale effect; the

aperture of a fracture could be greater than the aperture of each micro-crack which makes it up.

Overall, the numerical simulation was capable of correctly reproducing the trend and the order of magnitude in the reduction of the hydraulic conductivity with time, thus modelling the sealing behaviour of the EDZ (Figure 4-27).

Figure 4-27. Computed variation of the equivalent hydraulic conductivity in the EDZ rock of a drift in the Bure URL for three time steps with conductivity trend indicated (®3FLO code)

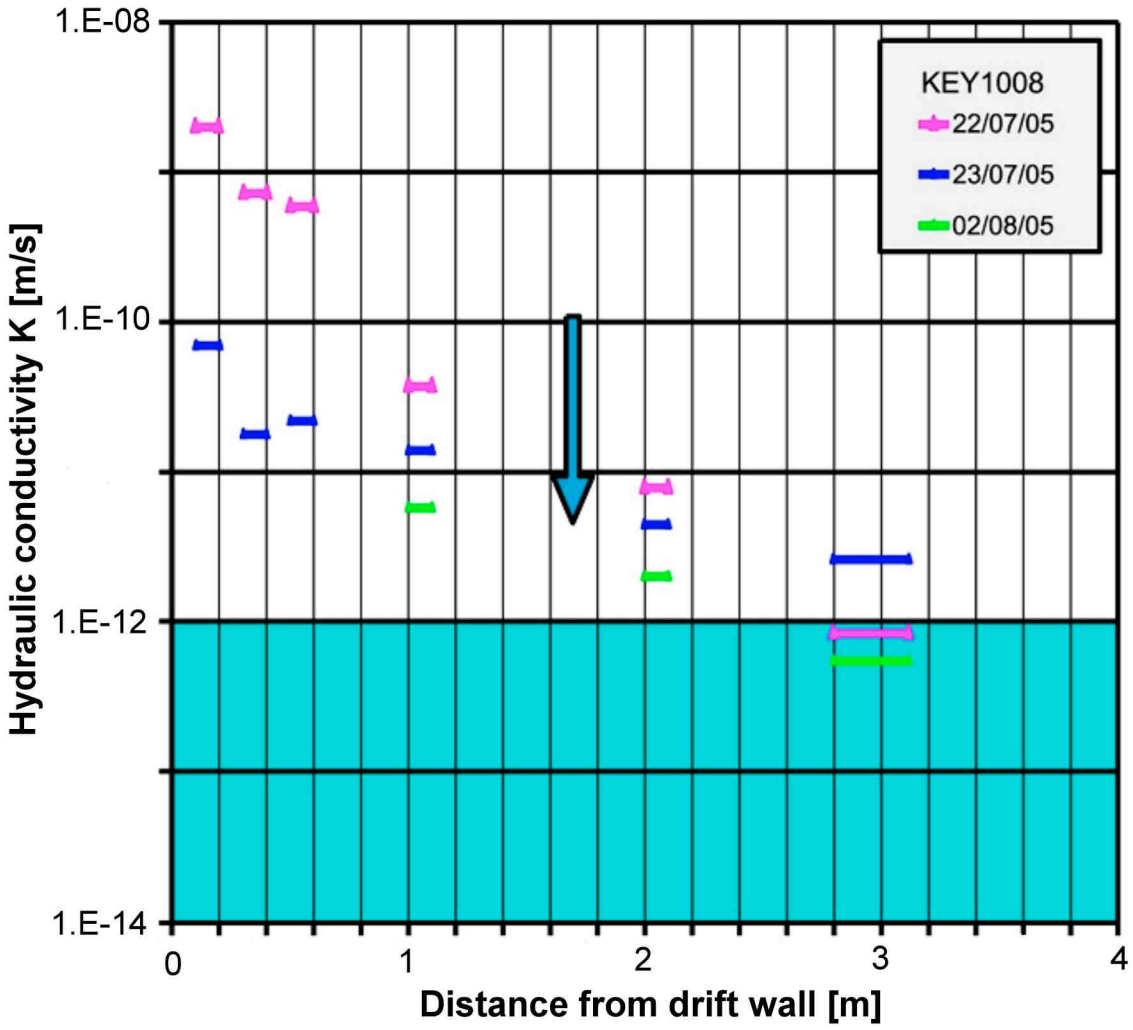

4.6.3 Modelling Example 2: Mont Terri URL and DFN Approach

The following example, taken from Marschall *et al.* (2008b), describes a generic study, aimed at simulating self-sealing processes in the EDZ of a backfilled tunnel section by sequential coupling of a DFN model with a geomechanical model (Lanyon 2005, 2006). Due to its generic nature, the model was not calibrated in a comprehensive manner. Nevertheless, the studies give valuable insight in the evolution of the hydraulic conductance of the EDZ after backfilling of the

tunnel. Of particular interest was the impact of a radial stress component due to the swelling pressure of the backfill onto the closure / opening behaviour of EDZ fractures.

The structural model of the EDZ fracture network around an emplacement tunnel was developed on the basis of field observations at the Mont Terri URL (Martin *et al.* 2002). Fracture transmissivities for hydraulic conditioning of the fracture network were derived from various EDZ characterisation studies (e.g. Meier *et al.* 2002). Figure 4-28a displays a realisation of the fracture network around the tunnel (colour coding represents the transmissivity distribution), which contained the following four classes of features (compare also with Figure 2-8):

- extension fractures in the tunnel sidewalls,
- disturbed bedding planes within the bedding slip zone,
- highly disturbed bedding planes, associated with deformation zones, and
- bounding and inner shear fractures associated with the bedding slip zone.

Figure 4-28. Modelling self-sealing processes with DFN models
(a) EDZ structure model based on observations from the Mont Terri URL (after Martin *et al.* 2002),
(b) hyperbolic fracture closure mechanism after Nagra (2002b) and
(c) change of effective stress in the EDZ due to a swelling pressure of the buffer material of 12 MPa (Marschall *et al.* 2008b)

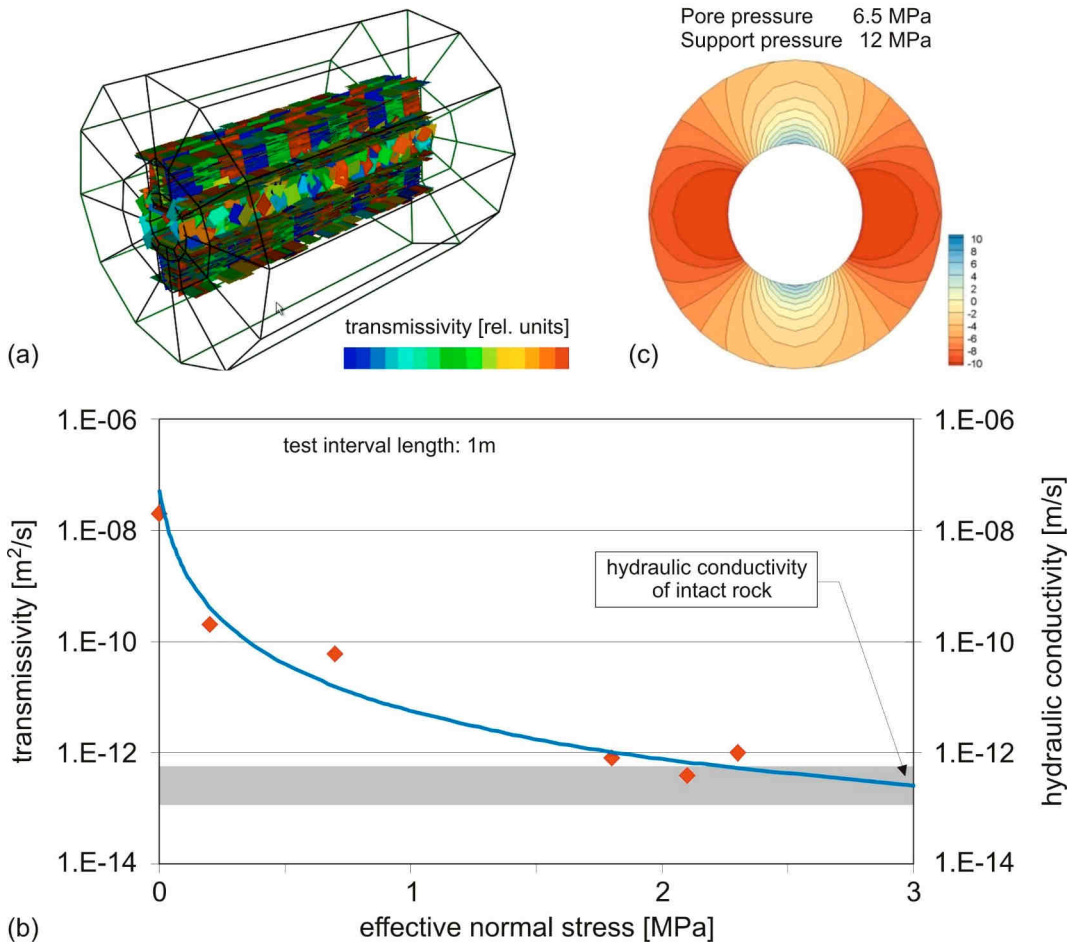

A normal closure mechanism with a hyperbolic stress-aperture relationship was assumed to apply for all classes of fractures. The closure law was taken from experimental investigations at the Mont Terri URL (Nagra 2002b; cf. Figure 4-28b; for alternative and extended normal closure laws of fractures, see Section 4.2.1).

Furthermore, it was assumed that pore pressure in the backfilled tunnel will increase due to the resaturation process and that a radial support pressure will act onto the tunnel walls due to the swelling of the backfill material. In the example, support pressures between 8 and 12 MPa and static formation pressures between 4 and 6.5 MPa were assumed (cf. Figure 4-28c). The calculated change of mean stress was then converted into a mean normal stress, acting on the individual fractures of the DFN.

Simulations of porewater flow under an axial pressure gradient were conducted for various closure scenarios, assuming an impermeable tunnel backfill. The total flux along the EDZ turned out to depend strongly on the generic assumptions for the DFN geometry (i.e. interconnectivity of the structural network). Of particular interest is the impact of the radial stress on the transmissivities of the individual fractures. Figure 4-29 depicts the EDZ network and the individual fracture elements that are predicted to undergo either an increase or a reduction in effective stress. Fractures that are close to the tunnel and approximately tangential to the tunnel wall (mainly the class of "extension fractures in the tunnel sidewalls") experience the greatest increase in normal stress, while fractures that are either oriented radially to the tunnel ("bounding shear fractures" or are distant from the tunnel dilate. Note however, that fracture closure would have been expected to be greater because of the low initial stresses near the tunnel wall. This is a result of the use of the hyperbolic law where the fracture stiffness increases with effective normal stress.

Figure 4-29. DFN simulations of porewater flow under axial hydraulic gradient, assuming a radial support pressure on the tunnel wall.
Note: Extension fractures in the tunnel sidewalls tend to close, while shear fractures open due to reduction of effective normal stress.

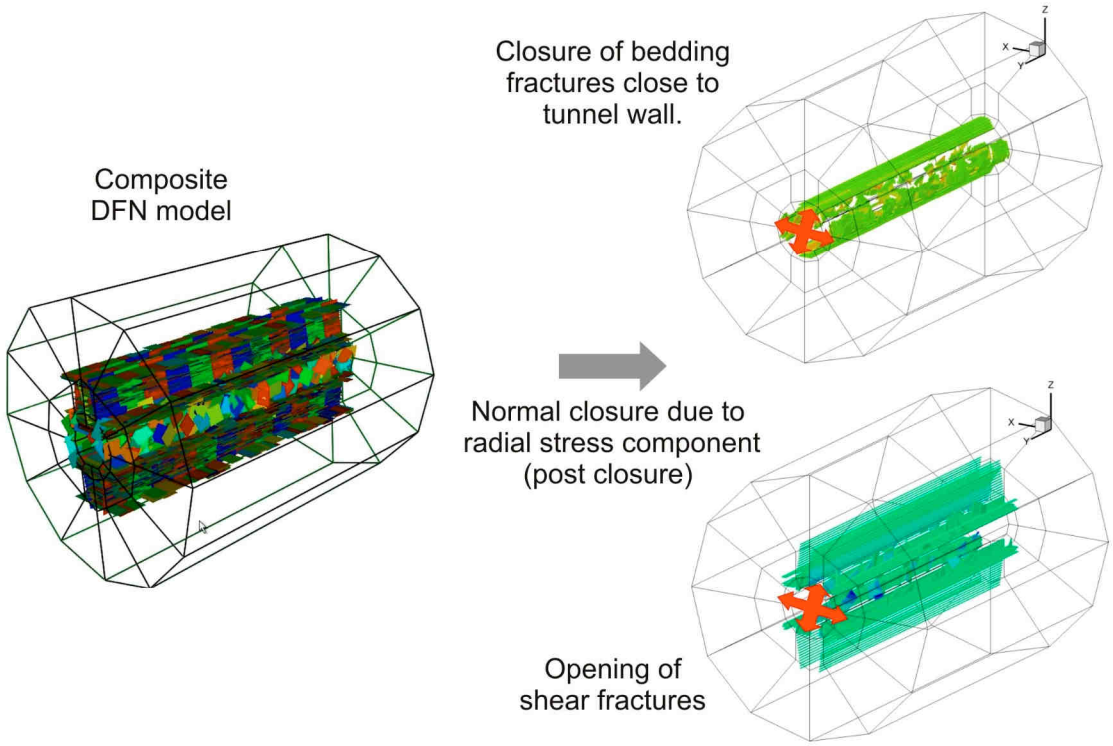

The results are of considerable interest in various aspects for the construction and the long-term performance of the disposal system. Thus it is obvious, that unexpectedly high swelling pressures in the bentonite buffer could open certain EDZ fracture systems such as the bounding shear features. Similarly, pre-existing tectonic features could be reactivated, resulting in a reduced barrier function of the intact host rock. Furthermore, sensitivity studies demonstrate that the effective conductivity along the EDZ is largely determined by the length and transmissivity of the bedding fractures and bounding shear fractures, while locally transmissive sidewall fractures have a relatively minor effect. It is believed that a minimisation of the effective EDZ conductivity could be achieved by optimisation of excavation procedures (e.g. excavation speed, excavation method).

4.6.4 Summary of considerations on sealing mechanisms in numerical models

Today, there is a multitude of hydro-mechanically coupled computer codes available capable of simulating sealing processes in geo-materials. As shown in the previous two examples, the modelling approaches and current data base allow for the validation of certain aspects of sealing, such as fracture closure under increasing normal stress.

So far, not all mechanisms of relevance to fracture sealing, as shown in Sections 4.2 to 4.5, have been implemented in numerical modelling. This, obviously, is due to lack in simulation capacity, inadequate or questionable constitutive formulations and low priority assessment of specific mechanisms. The mechanisms to be mentioned in this regard are permeability reduction in shear, slaking and, in particular, swelling of fracture wall material in resaturation. In principle, it can be assumed that all relevant fracture sealing processes can eventually be numerically modelled, provided that their relevant mechanisms are captured and the parameterisation is correct.

However, against the background of the numerous factors and mechanisms which exert a sizeable influence on fracture sealing, it is unlikely that the formulation of a universal sealing code for argillaceous rocks is a good idea and, in fact, may become feasible at all. Instead, a range of research models and related simplified PA-models appears to be a more appropriate way forward for considering this issue in a Safety Case. In these models partial aspects and corresponding input parameters shall be considered according to rock- and site-specific arguments and justifications.

4.7 Conclusion of Chapter 4

Within this report, seven sealing mechanisms (M) were identified which can contribute to permeability reduction in argillaceous formations, one of which relates to the matrix (M-1) and six to fractures (M-2 ... M-7). The respective mechanisms were considered on their underlying geomechanical, hydromechanical and/or geochemical characteristics and on their individual sealing potential of argillaceous formations in repository conditions. The following conclusions can be drawn:

M-1 Sealing of the rock matrix by additional compaction (Section 4.1):
Very good knowledge on underlying processes. Low sealing potential.

M-2 Sealing by increase of the effective normal stress σ_n‘ acting across the fracture plane (Section 4.2.1):
Good knowledge on underlying processes. Moderate to high sealing potential.

M-3 Sealing by contraction of fracture when subjected to shear (Section 4.2.2):
Good knowledge on underlying processes. Moderate to very high sealing potential.

M-4 Sealing by creep of fracture wall material (Section 4.2.3):
Limited knowledge on underlying processes and limited data base. High to very high sealing potential.

M-5 Sealing by swelling of the fracture wall material (Section 4.3.1):
Reasonable knowledge on underlying processes, however, often inadequate data base. Very high sealing potential.

M-6 Sealing by slaking:
a. Body slaking (Section 4.3.2): Limited knowledge on underlying processes. Poor data base. Limited to moderate sealing potential.
b. Surface slaking (Section 4.4): Virtually non-existing knowledge on underlying processes. Data base non-existent. Unknown (most likely limited) sealing potential.

M-7 Sealing by mineral precipitation onto fracture walls (Section 4.5):
Reasonable knowledge on underlying processes and data base. Limited sealing potential.

By means of three selected examples, it was demonstrated that (with the exception of Mechanism 6) the above sealing mechanisms can principally be incorporated into contemporary computer simulation codes. Problems however exist in the often poor data base.

5. DISCUSSION, CONCLUSIONS AND RECOMMENDATIONS

The systematic review of the self-sealing phenomenon in combination with the analysis of various sealing mechanisms, as described in this report, yielded advanced insights into self-sealing in argillaceous formations. The major insights gained are summarised and discussed in Section 5.1.

The review broadened the base for conclusions to be drawn in regard to the current state of knowledge on the various self-sealing issues and their relevance for PA (Section 5.2).

Based on the considerations of Section 5.2, a prioritised list of recommendations is finally provided on possible future work (Section 5.3).

5.1 Advanced insights into self-sealing

5.1.1 Consolidated evidence on self-sealing

This report has significantly consolidated the evidence on self-sealing in argillaceous formations. From that evidence it is reconfirmed that self-sealing is a common phenomenon in a wide variety of argillaceous formations which are currently considered in context with deep geological repositories; from plastic clays (Boom Clay in the HADES URF) to moderately indurated clays (Opalinus Clay at Mont Terri and Callovo-Oxfordian argillites at the Meuse-Haute Marne URL).

The most compelling evidence on self-sealing stems from the fact that it is observed over a large spread of scales in terms of length and time. At the millimetre to metre scale, self-sealing is observed in laboratory test samples (Section 3.1), at repository scales (10m to 100m range) in URL field tests (Section 3.2) and at the kilometre scale in geologic and geotechnical analogues such as traffic tunnels and hydrocarbon reservoirs (Section 3.3). Over geological time scales, it is, for example, evidenced in the existence of hydraulically and geochemically inactive geological faults (Sections 2.3.3; 3.3.5 and A.4.2.4; Section 3.3.6), in the existence of veins (Section A.6.1) and in the sealing of hard fissile claystones (Section 3.3.4). Relating to a time scale of the order of 100 years, convincing evidence for self-sealing of natural and induced fractures has been found in old traffic tunnels (Section 3.3.2.2). Numerous laboratory and URL experiments have shown that, in soft and moderately indurated formations, self-sealing commonly occurs within a time span of months up to a few years (Section 3.4).

5.1.2 Improved specification of conditions for the occurrence of self-sealing

The report has advanced the knowledge on the general geo-conditions (G) (geologic, hydrogeological, geochemical, geotechnical) which must prevail in deep geological repositories that argillaceous formations become amenable to self-sealing. Noticeable in this regard are the following general findings:

G-1 Degree of induration

The potential of self-sealing in argillaceous formations depends, amongst other factors, on the degree of induration of the host rock (Table 2-3).

The report has shown that, at typical repository depths[13], low and slightly to moderately indurated formations will be subject to self-sealing, provided the other general conditions (see below) will prevail. For high to very highly indurated formations this is not necessarily the case and each case must be investigated in more detail before any conclusions can be drawn. However, geologic studies indicate that even hard fissile claystones can become sealed (Section 3.3.4). The ultimate threshold for the occurrence of self-sealing seems to be the transition point from sedimentary to metamorphic rocks (Table 2-2). Swelling clay minerals are generally absent in metamorphic rocks and it is obvious that metamorphic argillaceous rocks such as schists, phyllites and slates have negligible self-sealing capabilities.

G-2 Type and content of clay minerals

The potential for self-sealing in argillaceous formations depends also on type and content of the clay minerals in the rock.

When considering argillaceous formations, there must be a certain threshold level in the clay mineral content of the rock below which self-sealing becomes ineffective. That level depends, amongst other factors, on the type of clay minerals and will be lowered by the presence of swelling clay minerals (e.g. smectites). The report has shown that the threshold is, very conservatively estimated, at a level of about 40% clay mineral content in weight. That percentage level was deduced from studies and tests in various engineering fields: From studies on fault smear in the hydrocarbons industry (Figure 4-8), from laboratory tests on sand-clay mixtures in geo-engineering (Figure 4-9) and from borehole permeability tests in various sedimentary formations (Figure 4-10). All these studies give testimony of the fact that the threshold level is definitely lower than the ≥ 50% level of "very fine-grained particles" which, in the geomechanical classification, marks the boundary between siltstone and claystone (Table 2-2).

Despite being a very conservative estimate and possibly as low as 25%, a threshold level of the clay mineral content of 40% is used for the further deliberations of this report.

Table 4-2 shows that, with the exception of the upper 25 m of the Callovo-Oxfordian formation, the clay mineral content of the three major argillaceous formations, considered within this report, is well above the 40%-level, which means that they are amenable to self-sealing. As mentioned above, the presence of swelling clay minerals reduces that level significantly. Figure 4-8 refers to a threshold value as low as 15% clay content. However, threshold values < 40% should only be used after dedicated investigations have been carried out as there are numerous geologic factors, such as tectonic fractures, grain fabric and diagenetic bonding of the clay minerals, which exert an influence on the self-sealing capability (Sections A.2.3 to A.2.5).

G-3 Fractures in general

Self-sealing is intrinsically connected with the reduction of the hydraulic transmissivity of natural and/or artificial fractures (Section 2.3.3 and Appendix A.4). In a repository project,

[13] Repository depths are proposed to be in the range of between 250 m to about 1000 m (see Section Appendix A.2.6).

sufficiently detailed knowledge on the actual fracture inventory is required for the assessment of the self-sealing behaviour

G-3.1 Natural fractures
The report has shown that for argillaceous formations there is a generally good knowledge on the inventory of natural fractures at typical repository depths. At Mont Terri, for example, faults were, besides bedding planes, identified as the generally most frequent natural structural feature (Table 2-6).

In spite of the obvious deformation having taken place in course of their geologic history, there is, at the URL level, actually not much evidence of enhanced water transmissivity along the faults (e.g. Figure 2-4). This is also confirmed by observations in more than 100 year old traffic tunnels of northern Switzerland where, in the moderately indurated Opalinus Clay over a total length of 6600 m and despite extensive faulting, no water inflows could be detected once the tunnel overburden exceeded 200 m (Section 3.3.2.2). Slightly different observations have been made in the highly indurated Toarcian-Domerian formation of the Tournemire URL where parts of the natural fractures are weakly water conducting.

G-3.2 Artificial fractures in the EDZ
The report has shown that, in context with self-sealing, the contemporary level of understanding of the EDZ structures and processes in argillaceous formations is generally sufficient (Sections 2.3.3 and A.4.2).

Important parts of the EDZ fractures can consist of reactivated natural fractures, in particular in the form of bedding plane breaks, which, in conjunction with artificial fractures, may form composite structures such as wedges (Figure 2-7), deep-seated buckled shear bodies (Figure A.4-21) and mushroom-shaped fracture zones (Figure A.4-23).

5.1.3 Sealing mechanisms

Within this report, seven sealing mechanisms (M) have been identified which can contribute to permeability reduction in argillaceous formations. One mechanism relates to the matrix (M-1)[14] and six mechanisms to fractures (M-2 to M-7). The mechanisms M-2 to M-7 imply that a permeability change is associated with a change (i.e. decrease) of the effective fracture aperture in response to mechanical, hydromechanical and/or geochemical processes.

Overall, the following mechanisms could be distinguished:

- Mechanically (matrix):

  M-1 Sealing of the rock matrix by additional compaction (porosity reduction)

- Mechanically (fracture):

  M-2 Increase of the effective normal stress σ_n‘ acting across the fracture plane (either increase of the normal load and/or decrease of the water pressure in the fracture), stimulated by water uptake in the fracture leading to weakening of the fracture asperities

[14] see Footnote 10 in Section 4.1

M-3 Contraction of fracture when subjected to shear

M-4 Creep of the fracture wall material towards the open fracture space

- Hydromechanically (and, in parts, also chemically)

M-5 Swelling of the fracture wall material

M-6 Slaking

- Geochemically

M-7 Mineral precipitation onto fracture walls.

The respective mechanisms were considered and discussed on their underlying geomechanical, hydromechanical and/or geochemical characteristics and on their individual sealing potential of argillaceous formations in repository conditions. The following conclusions can be drawn:

M-1 With regard to M-1 (matrix porosity reduction), it was shown that, over the time period of interest in PA (1 Ma), sealing of the rock matrix by additional compaction is of limited importance in soft argillaceous formations (Section 3.2.3.2) and of no practical importance in moderately to highly indurated argillaceous formations (Section 4.1).

M-2 With regard to M-2 (fracture closure by increased normal effective stress[15]), it was shown that the commonly adopted hyperbolic formulation of the stress/fracture closure relationship is a first approximation only. Experimental evidence is provided which suggests that the closure behaviour of fractures is more appropriately characterised in analogy with the oedometer test of soil mechanics. That test is a compaction test under laterally constrained conditions. The stress / fracture-closure relationship is described by a fracture compression index C_f which, formally, is in full agreement with the well established compression index C of the oedometer test (Section 4.2.1). In this regard the achievements of the report are twofold: Geomechanically, the new approach yields a unified model for compression in constrained conditions which is applicable to both soil mechanics (compaction of intact media) and rock mechanics (compaction of fractures). Furthermore and from a PA perspective, the new relationship yields a more realistic mathematical formulation of the fracture closure behaviour in repositories.

M-3 With regard to M-3 (fracture closure by contraction in shear[16]), it was shown that a minimum normal stress level is required to instigate contraction of fractures (otherwise dilatation = opening of fractures will occur). Dilatation / contraction can be physically explained by shearing off / squeezing of the fracture asperities. For predominately brittle materials such as Kimmeridge Shale (Section 3.1.5.2) it is commonly assumed that fracture contraction (and thus reduction of the fracture permeability) can only be achieved if the normal stress is higher than the unconfined compressive strength UCS of the fracture wall material. This, however, does not hold for soft and moderately indurated argillaceous media. For Opalinus Clay, for example, the UCS of between 11 and 15 MPa is well above that dilatation /

[15] In the post-closure phase of a repository (Section 2.2) such situation will apply e.g. to extensional EDZ fractures, as depicted in Figures 2-6 and A.4-19, when being subjected to pressures from the back-fill of the emplacement tunnels due to swelling and tunnel convergence.

[16] Such situation could possibly apply to buckled strata, as depicted in Figures 2-7 and A.4-21.

contraction threshold level (which is about 3 MPa; Section 4.2.2). This observation allows the conclusion that some other mechanisms, in addition to dilatation/contraction, must prevail within the shearing process of fractures. Guided by observations from the hydrocarbons industry the likely processes are re-orientation of the platelets in the fracture wall and gouge formation (Figures 4-7 and 4-8).

M-4 With regard to M-4 (creep of fracture wall material towards the open fracture space), it was noted that a bundle of micro-mechanisms is made responsible for macro-scale 'creep', many of them quite vague and often difficult to specify in a specific application. The postulated creep mechanisms are based on processes such as diffusion, pressure dissolution, dislocation glide of minerals and sub-critical crack growth through pore fluid chemistry effects. Based on generic creep data of the Opalinus Clay, an order of magnitude estimate indicates that, in longer terms of the order of 10 years and beyond, creep of the fracture wall material might become a contributing factor in the closure of fractures. However, it has to be pointed out that for such conclusion the experimental data base still is limited and that there are continuous questions on the existence of a creep threshold and, if existing, on its magnitude (Section 4.2.3).

M-5 With regard to M-5 (swelling of the fracture wall material), it was shown that swelling of argillaceous materials is reasonably well understood with regard to the underlying micro-scale mechanisms. However, the approach to deduce macro-scale swelling parameters from micro-scale observation and characterisation has not succeeded in geo-engineering practice, evidently due to the high number and the degree of complexity of the physico-chemical processes involved. Instead generic approaches are prevailing and a significant number of swelling pressure and swelling heave tests have been conducted on claystones. The information from these tests can be used to infer the fracture closure due to swelling processes. It was shown that swelling is one of the most dominant factors, if not the most dominant factor at all, in the sealing of fractures (Table 4-4).

M-6 With regard to M-6 (slaking), it was noted that slaking often becomes apparent in course of repeated swelling and shrinking of argillaceous materials. It is connected with structural disintegration in the form of progressive fracturing and material decaying into smaller slabs, pieces, particles and colloides. Within this report two mechanisms were distinguished: Body slaking, and surface slaking in line with dispersion.

- Body slaking is understood as a process which takes place in course of resaturation. It is characterised by rapidly occurring traverses of large portions of material with no apparent deterioration between the newly formed cracks (Section 4.3.2). This type of slaking can be linked with some capillary suction processes within the material. It was shown that, in constrained conditions, body slaking tends to reduce the transmissivity of a fractured body by the square of the additional number of slaking fractures (Figures 4-16 and 4-17). This means the more intense body slaking, the lower the overall transmissivity.

- Surface slaking is understood as a process which takes place in saturated conditions. It is characterised by a loss of mass due to "sloughing" of tiny flakes of grains from the material of the fracture surface, with no apparent cracks in the underlying material. The flakes are dispersed into the water-filled fracture space (spontaneous suspension). It was noted that, with regard to fractured argillaceous media, dedicated tests on these mechanisms obviously do not exist. The same applies for the mechanism of flocculation

of the dispersed particles and the subsequent sedimentation and clogging phases and mechanisms in the fracture space. However, it can be expected that, due to the very low water flow and velocity in the repositories, the latter two mechanisms are of minor, if any, importance.

M-7 With regard to M-7 (mineral precipitation), it was shown that there are numerous examples (e.g. veins) which substantiate that mineral precipitation can seal natural fractures in argillaceous formations. However, it is unlikely that mineral precipitation of this kind will contribute to self-sealing over the time period which is of interest in PA (1 Ma). This is because repository sites are generally located in tectonically and hydrothermally quiet areas, meaning that the driving forces needed for fracture mineralisations are expected not to be present. Moreover, if mineral coating of fractures would be formed as a result of chemical reactions within the repository system (Section 4.5), it would not be clear whether such coatings would remain chemically stable in the long term following repository closure. Mineral precipitation in fractures should therefore not be accounted for in PA considerations on fracture sealing.

5.1.4 Rate and order of magnitude of sealing mechanisms

The various sealing mechanisms identified within this report contribute at different rates and to different degrees towards fracture sealing. The respective rates and degrees depend on the site-specific circumstances such as degree of induration, type of clay minerals and chemistry of the porewater of the host formation.

In referring to Tables 3-3 and 3-6, which summarise the results of the laboratory and URL field self-sealing tests on EDZ fractures considered within this report, it became apparent that there is a consistent permeability reduction trend, irrespective of the type and dimension of the test. Referring to a testing time of the order of months to up to a few years (which is the common time span of the tests so far carried out), the reduction rate typically is in the order of about 10^{-1} to 10^{-2} per annum, meaning that, over a time span of one year, the permeability is reduced *to* 10^{-2} of its initial value (note: not *by* an amount of 10^{-2} of its initial value). In some cases there were even significantly higher rates of up to 10^{-6} per annum (shear testing, Section 3.1.5.2; testing of large de-stressed Opalinus Clay sample, Section 3.1.6).

Surely, the above permeability reduction rates cannot be extrapolated over much longer periods, otherwise the permeability of the fractured system would soon become lower than the intrinsic permeability of the intact material. What, however, can be stated is that, in the tests, the fracture permeability converges to the matrix permeability within a relatively short period of time, which, for soft clays, is in the order of months up to a year and, for slight to moderately indurated claystones, in the order of years to tens of years.

In the report and with reference to the Opalinus Clay, order of magnitude estimates have been made on the potential of the various mechanisms in contributing towards the closure of fractures (Tables 4-4 and 4-7). It became apparent that, at least over relatively short durations (order of months to some few years), swelling of the fracture wall material tends to be the biggest contributor to fracture sealing.

The particular contribution of swelling also became apparent when considering the influence of the fracture wall roughness on sealing. In Table 5-1 three classes of fracture wall roughness are distinguished, from a smooth wall to the extreme form of an open void. The table summarises and

interprets the findings of the report on the likely fracture sealing mechanisms in dependence of the fracture wall roughness. As can be seen, swelling is the only mechanism which exerts a high influence on the sealing of all three roughness types.

In Section 3.1 it was outlined that, given their geometry, cylindrical voids might be considered an extreme form of open fractures. In the report, various EDZ features which resemble open cylindrical voids have been identified (e.g. Figures 2-7; 2-8 and A.4-21; see also DFN model simulations in Section 4.6.3).

Table 5-1. Likely sealing mechanisms for various roughness pattern of fracture surfaces

Fracture wall roughness	Normal stress	Shear	Creep	Swelling	Slaking
smooth *)	+	o	o	+	-
rough *)	o	+	o	+	o
extreme 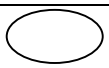	-	-	o	+	+

Legend: + Mechanism of relevance
o Mechanism of some influence
- Mechanism with insignificant influence

Note *): A higher differentiation of the roughness pattern, e.g. in line with fracture mechanics the consideration of the fracture types [Type I (extensional), Type II (in-plane shear), Type III (out-of-plane shear)], will hardly affect the principal findings of the table.

It should be realised that, beyond the roughness pattern, there is also the *dimension* (D) of the fracture aperture which must be of influence in fracture sealing. This, in particular, applies to open voids and gives justification for considering this case explicitly as follows:

D-1 Dimension of cylindrical voids or channels in the EDZ
Sealing of voids or channels will depend predominately on swelling and slaking mechanisms (Table 5-1). The mechanically-driven sealing processes M-1 to M-3 are, at best, of minor influence. There must be a certain size limit of voids beyond which even swelling and sealing might become exhausted in filling and sealing the void. For soft and indurated clay that upper size limit is essentially unknown. However, from Figures 3-2 and 3-3 and from observations in the Mont Terri URL[17] it can be stated that the size limit must be well above the centimetre, if not the decimetre domain.

[17] In areas of the Mont Terri URL where wet spots were observed 80 mm diameter boreholes were completely closed with plastified clay due to swelling and slaking of the borehole walls (Blümling 2009).

5.2 Classification of self-sealing issues according to state of knowledge and potential relevance for PA

In the following, a classification of the pertinent self-sealing issues is given with respect to their current state of knowledge and relevance for PA. The classification approach is similar to that pursued in the FEPCAT project (Mazurek *et al.* 2003).

5.2.1 State of knowledge

For all issues, the state of knowledge is considered strictly with reference to self-sealing. In this consideration several aspects are implied. They include the definition / understanding of an issue in a general sense, its applicability to specific repository cases, and the issue's impact on self-sealing. As an example, the classification of Issue G-1 (degree of induration of host rock) implies, amongst others, consideration of aspects as follows:

Aspect 1: Degree of induration in a general sense.
- Question: Is the degree of induration as such reasonably well defined?
- Answer: Yes.
- Reasoning: It is a descriptive term, predominately depending on the maximum burial depth of its geological history. For the purpose of this report, the definition given in Table 2-3 (Page 33) is fully sufficient.

Aspect 2: Degree of induration in a specific repository case.
- Question: Can the degree of induration be reasonably well determined?
- Answer: Yes.
- Reasoning: As shown in Table 2-3, the degree of induration is embedded in a suite of geological and geotechnical standard parameters. In a repository case, information on these parameters is commonly available through standard site investigation programmes.

Aspect 3: Relationship to self-sealing.
- Question: Is the formation amenable / effective to self-sealing?
- Answer: Yes (for soft and slight to moderately indurated formation)
  Likely (for high degree of induration)
  Possible (for very high degree of induration)
  No (for metamorphic argillaceous formations).
- Reasoning: see report, Section 3.

Inspection is employed to generalise the above three aspects in a unified qualification term. Hereby, the simple 3-grade classification scale "good"(+) – "fair"(o) – "poor / non-existing" (-) was applied.

The overall rating of Issue G-1 then is as follows:

+ for soft and slight to moderately indurated argillaceous formation

o for high to very high degree of induration

Table 5-2 gives the relevant classification for all self-sealing issues considered.

Table 5-2. Classification of the current state of knowledge on issues related to self-sealing

Case / Issue			State of knowledge on ...			
Code	Description		... general principle / definition	.... methods for determining site-specific parameters	.... interrelation / influence on self-sealing	Overall Rating
G-1	Degree of induration	soft, slight to moderate	+	+	+	+
		high to very high	+	+	o	o
G-2	Clay mineral Content (CC)	CC ≥ 40%	+	+	+	+
		? % < CC < 40%	+	+	o	o
G-3.1	Natural fractures		+	+	+	+
G-3.2	EDZ fractures		+	+	+	+
M-1	Matrix compaction	soft	+	+	o	+
		indurated and stiff	+	+	-	o
M-2	Fracture closure mechanisms	Normal stress increase	+	+	+	+
M-3		Shear stress (contraction)	+	o	+	+
M-4		Creep	+	o	+	o
M-5		Swelling	o	+	+	o
M-6		Slaking – body	o	o	+	o
		Slaking – surface	-	-	o	-
M-7		Mineral precipitation	o	o	o	o
D-1	Sealing of cylindrical voids	cm – dimension	+	+	+	+
		dm – dimension	+	o	+	o
		m – dimension	+	-	-	-

Legend: + good knowledge
o fair knowledge
- poor / non-existing knowledge

5.2.2 PA relevance

As a next step, each self-sealing issue was classified according to the simple scheme of Table 5-3. The scheme is very much in line with that of the FEPCAT project (Mazurek *et al.* 2003). The overall rating of the state of knowledge as deduced in Table 5-2, is an input parameter in Table 5-3 (see first column).

Table 5-3. Classification scheme of impact of self-sealing issues for PA
(after FEPCAT, Mazurek *et al.* 2003)

State of knowledge on self-sealing issue (Table 5-2, last column)	**PA relevance**	**Consequences from a PA perspective**	**Class**
good (+) General consensus that issue can be adequately characterised in terms of processes and parameters.	high	Methods and tools are available for a sufficient quantitative understanding	**1**
fair (o) Degree of knowledge on issue and/or its relevance for PA are heterogeneous for different programmes and disposal concepts.	high (at least potentially)	More work / thoughts needed at least in some cases	**2**
fair (o) to poor (-) No general consensus that issue can be adequately characterised and/or its relevance in specific programmes and disposal concepts.	high (at least potentially)	Substantially more work / thoughts needed at least in some cases	**3**
good (+) Issue is well characterised.	low	No urgent actions needed	**4**
fair (o) to poor (-) Degree to which issue is characterised may be quite limited.	low	No urgent actions needed	**5**

In the above table, Classes 1, 4 and 5 mean that data and understanding are either available or not necessary from a PA perspective. Classes 2 and 3 mean that knowledge may be limited, at least for some programmes and disposal concepts, despite a potential PA relevance. For some of these issues, there is a potential for future actions at a national or international level. However, it must be stressed that even issues classified as 2 or 3 may be non-issues for some programmes and disposal concepts, and the fact that they have been assigned these classes must not be mistaken as general prompts for new actions.

The results of the overall assessment of the self-sealing issues with regard to their relevance for PA is summarised in Table 5-4.

Even though the classification of Table 5-4 surely is a gross simplification of a highly complex situation, it may be used by each national organisation as a potential checklist to qualify its own state on the issue of self-sealing in a disposal project. However, the table must not be mistaken as a universal rating for the following main reasons:

- The relevance of an issue for the assessment of the self-sealing potential and parameters depends on system-specific requirements and boundary conditions (*e.g.* type of waste, disposal concept, type of engineered barriers). Some issue might be of importance in one concept but not at all in another.

- The degree of knowledge on a self-sealing issue varies among disposal projects at different stages of maturity (regional or generic feasibility study, site-specific work from the surface, site-specific underground research laboratory etc.).

Table 5-4. Classification of self-sealing issues according to the state of knowledge and PA relevance

Code	Self-sealing case / issue		State of knowledge in respect to self-sealing	Relevance for PA	Class (Tab. 5-3)
G-1	Degree of induration of host rock	soft, slight to moderate	good	high	**1**
		high to very high	fair	high (potentially)	**2**
G-2	Clay mineral content (CC) of host rock	CC ≥ 40%	good	high	**1**
		15% ≤ CC < 40%	fair	high (potentially)	**2**
G-3.1	Natural fractures		good	high	**1**
G-3.2	Size and structure of the EDZ		good	high	**1**
M-1	Compaction of EDZ rock matrix	soft clay	good	limited	**4**
		indurate and stiff clay	good	none	**5**
M-2	Fracture closure mechanism by ...	normal stress increase	good	high	**1**
M-3		shear stress (contraction)	good	high	**1**
M-4		creep	fair experimental data base limited; continuous questions on the existence of a creep threshold	high	**2**
M-5		swelling of fracture wall material	good to fair, (e.g. open questions at micro scale, clay-colloid model)	very high	**2**
M-6		slaking: body slaking	good	high to limited	**1**
		slaking: surface slaking	limited to non-existent	low	**5**
M-7		mineral precipitation	fair questions on long-term stability in repository conditions	limited	**4**
D-1	Sealing of open cylindrical voids	cm-dimension	good	high	**1**
		dm-dimension	fair	high	**2**
		≥ m-dimension	non-existent	low	**5**

It seems quite remarkable that, in Table 5-4, there is not a single self-sealing issue which has been assigned to Class 3 which, according to Table 5-3, requires "*substantially more work / thoughts, ... at least in some cases*". Obviously, the general knowledge on self-sealing has progressed to a level at which major deficiencies are absent.

5.3 Recommendations

General recommendation

This report has revealed that knowledge on self-sealing in argillaceous formations has progressed to a level where major influencing factors and mechanisms can be described in a scientifically consistent manner. It is recommended that, based on the ranking given in Table 5-4, independent checks and judgements must be made by each national organisation in so far the current level of knowledge is sufficient for a state's respective needs to progress towards linking the scientific insights on self-sealing with its particular PA and the safety case (e.g. NEA 2007).

Specific recommendations

Irrespective of the above, there are still certain outstanding questions on self-sealing and thus potential targets for further and advanced investigations. Generally, these questions are connected with the Class 2 issues of Table 5-4. It is recommended that the potential value of further dedicated scientific efforts on self-sealing be considered against the background of the specific circumstances of national programmes, in particular on the following issues (prioritised listing):

1. Investigation on all of those factors which impose limits to self-sealing, in particular high to very high degree of induration (G-1) and clay mineral content < 40% (G-2). There are indications that sealing might become effective at significantly lower clay mineral content levels (at about 25%; see Figures 4-8 to 4-10), however these findings have to be confirmed for argillaceous rocks. The general scope of such investigations would be to narrow the range of uncertainty of the respective limits and thus of the applicability of self-sealing.

2. Adoption of numerical modelling codes for implementation of the sealing mechanisms described in Sections 4.2 and 4.3 and back-analysis of EDZ case studies for further confidence building.

3. Advancement of the understanding on swelling (M-5) as the commonly most influential factor in self-sealing. Horseman *et al.* (1996) and Rodwell *et al.* (1999) suggested that, in clay rocks, the adsorbed interparticle water films are stress supporting and capable of carrying the lithostatic stress, and that the disjoining (or swelling) pressure acting in the water films is equivalent to the effective stress. This was recently confirmed by laboratory experiments on Callovo-Oxfordian argillite and Opalinus Clay samples (Zhang *et al.* 2009). Adequate conceptual models under consideration of this effect may be helpful for better understanding and interpreting strongly-coupled hydro-mechanical processes in claystone (such as water and gas transport, rheological deformation and self-sealing of fractures).

4. Investigation on creep (M-4): Broadening of the data base with particular reference to the existence / non-existence of a creep threshold.

5. Investigation on the closure of open voids in the dimension of decimetres (D-1).

All of the above specific recommendations touch on quite fundamental questions and problems. Surely, pure and applied research into relevant fundamental geomechanical and hydro-mechanical aspects will also be beneficial for the topic of self-sealing.

In this regard mention is made of the following issues:

- validity of Darcy's law in low-permeability rocks (ref. e.g. to Mazurek *et al.* 2009);
- clay mineralogy and coupled thermo-hydro-mechanical and chemical processes;
- investigation on thermal impact on the fracturing and sealing (TIMODAZ project);
- gas migration through the sealed EDZ fractures.

Appendices

APPENDIX 1

HISTORY OF THE SELF-SEALING PROJECT AND TERMS OF REFERENCE

Overview

This appendix provides, in addition to Section 1 of the main text, some detailed information on the development of the Clay Club Self-Sealing Project since its initiation in 1999. In particular it refers to the Terms of Reference of the year 2006 which constitute the base of this project report.

A.1.1 History of the Self-Sealing Project

Within the Clay Club of the OECD/NEA, interest in specific information on the self-sealing behaviour of clay-rich geological formations was expressed as early as 1999[18]. In 2002, a review project was initiated on that topic and the work commissioned to the British Geological Survey (BGS), Nottingham, UK. Unfortunately, the project was marred with difficulties, particularly caused by the untimely death of the chief investigator, Steven Horseman. Despite this tragic situation, BGS managed to submit a very substantial draft report (Horseman *et al.* 2005). The draft contains some useful information and the report at hand repeatedly makes reference to it. Overall however, the Clay Club found that the draft did not match its needs and terminated the contract with the BGS in 2006.

Irrespective of the above set-back, there was, within the Clay Club, agreement on the continuous importance of the project[19], and on the need to produce a document which satisfies OECD/NEA standards. In November 2006, a seed contract for the resumption of the project was placed by Nagra with Helmut Bock from Q+S Consult, Bad Bentheim, Germany[20]. The continuation of the work was secured by two follow-on contracts with the OECD/NEA Clay Club in 2007[21] and 2008[22]. In essence, the work commissioned was to assemble and co-ordinate a new Expert Group, to up-date the information base and to accept responsibility for finalising the report.

The tasks and activities of the respective three project phases since 2006 can be understood as Terms of Reference of this report. They are summarised in the following section.

---

[18] 9th meeting of the IGSC Working Group on Measurement and Physical Understanding of Groundwater Flow through Argillaceous Media ("Clay Club"), Madrid, Spain, 25 to 28 May 1999 (see NEA/ RWM/CLAYCLUB(99)1)

[19] 15th meeting of the "Clay Club", Issy-les-Moulineaux, France, 8 to 10 November 2005 (see NEA/RWM/CLAYCLUB (2005)6)

[20] NAGRA Contract No. 905.170.955.09 of 13 November 2006

[21] OECD/NEA Contract No. JA00042814 of 16 / 24 April 2007

[22] OECD/NEA Contract No.JA00047363 of 11 / 21 February 2008

A.1.2 Terms of Reference

Project Phase 1 (November – December 2006):

Review of the BGS draft report (Horseman *et al.* 2005) taking into consideration the comments received from Clay Club members on that report (Blümling 2005a; Lebon 2005; Li *et al.* 2005; Mazurek and Mäder 2005).

Development of a revised structure of the proposed new report (in the form of a detailed table of contents), thus implicitly/explicitly stating which of the content of the BGS draft report shall be maintained, suppressed/deleted and/or added. It turned out that a major overhaul was needed; in fact to a degree that the new report has to be generated practically "from scratch", i. e. has to be written independently from the BGS draft report.

Specification of a time frame and a team of supporting experts for preparation of the new report and submission of the project proposal to the Clay Club.[23]

Project Phase 2 (April - September 2007):

Assessment on what new information, relevant to the topic of self-sealing, is available since that addressed in the 2005 BGS draft report, with particular reference to laboratory experiments, *in situ* tests in URLs and field observations.

Assembly and co-ordination of a Team of Experts contributing through in-kind support of Clay Club Organisations (ref. to Section 1.2 of main text).

Submission of a preliminary technical report and conclusions to be presented at the 17th Clay Club Meeting in Lille, France[24].

Project Phase 3 (April 2008 – March 2009):

Drafting (by September 2008) and finalising of a comprehensive updated report (by March 2009) along the lines developed in Project Phases 1 and 2.[25]

---

[23] Proposal of H. Bock of 20th December, 2006 to OECD/NEA-CC for a revised self-sealing report, 9 p.

[24] Q+S Consult Progress Report of 11th September, 2007 on "Self-Sealing Properties of Clays - Update of Empirical Data and Results from Laboratory and Field Tests, 34 p. submitted to OECD/NEA-CC and Power-Point presentation, 18 slides.

[25] Q+S Consult Progress Report of 10th September, 2008 (main text 42 p. plus appendices 205 p.); Power-Point presentation, 17 slides, to 18th Clay Club Meeting in London, UK, 19th September 2008 (see NEA/RWM/CLAYCLUB(2008)1)

APPENDIX 2
COMPOSITION, STRUCTURE AND STATE CONDITIONS OF ARGILLACEOUS FORMATIONS

Overview

This appendix provides, in addition to Section 2.3.1 of the main text, some detailed information on argillaceous formations which are essential for the understanding of self-sealing features and processes. It includes generic aspects of argillaceous formations (e.g. terminology, classification, clay mineralogy; state conditions within the geological cycle) as well as site-specific aspects (type of argillaceous soils or rocks, geological history of the various sites currently considered in the context of the radioactive waste disposal problem).

A.2.1 Geological terminology and classification

From a geological perspective, argillaceous formations encompass a very wide range of soils and rocks, ranging from fine-grained clastic sediments (unlithified mud and clay), through to diagenetically lithified sediments (sedimentary rocks such as moderately indurated mudstones and claystones, fissile and often highly indurated shales), and metamorphic rocks (e.g. slates and schist). Across such a wide spectrum, the characteristics and the physical and geotechnical properties of argillaceous media vary enormously.

Given the large variety of argillaceous soils and rocks, it is not surprising that various geological classification systems have been proposed (for a review, refer to Horseman *et al.* 2005). The geological classification of argillaceous media has yet to be fully standardised and a comparison of the existing systems of classification reveals a number of disagreements.

The classification shown in Table A.2-1 from Potter *et al.* (1980) is based largely on grain size, the thickness of the partings (laminations), and the degree of induration or metamorphic alteration. Clay particles are defined as being less than 4 μm, and a mudrock is considered to be 'laminated' if the separation between layers is less than 10 mm. Terminology for the description of stratification and parting is summarised in Table A.2-2. The geological classification of argillaceous rocks of Lundgard and Samuels (1980) is given in Table A.2-3.

In the classification system proposed by Potter *et al.* (1980), the suffix 'stone' is used to denote layering greater than 10 mm (i. e. beds) and the suffix 'shale' is used to denote layering less than 10 mm (i.e. laminations). The term 'claystone' is therefore used to describe bedded clay-rich rocks and the term 'clayshale' is used for rocks of similar composition which exhibit laminations.

According to Potter *et al.* (1980) the term 'argillite' is applied to weakly metamorphosed argillaceous rock exhibiting neither fissility nor slaty cleavage, but with some alterations of clay minerals and micas to sericite, chlorite, epidote or green biotite.

Table A.2-1. Geological classification of argillaceous media
(after Potter *et al.* 1980, modified by Horseman *et al.* 2005)

Description		**Percentage clay-size fraction**		
		0 – 32 %	**33 – 65 %**	**66 – 100 %**
Field adjective		gritty	loamy	fat or slick
Non-indurated	Beds	Bedded Silt	Bedded Mud	Bedded Claymud
	Laminae	Laminated Silt	Laminated Mud	Laminated Claymud
Indurated	Beds	Siltstone	Mudstone	Claystone
	Laminae	Siltshale *	Mudshale	Clayshale
Metamorphosed	Low	Quartz Argillite	Argillite	
	Medium	Quartz Slate	Slate	
	High	Phyllite and/or Mica Schist		

*) The term "Siltshale" replaces the term "Laminated Siltstone" of the original classification

Table A.2-2. Description of stratification and partings (after Potter *et al.* 1980).

Stratification	**Laminations**				**Bedding**	
	very thin	thin	medium	thick	very thin	thin
Partings	papery	fissile	platy	flaggy	slabby	
Compositional trend	← Clay and organic contents increase Sand, silt and carbonate contents increase →					

Table A.2-3. Geological classification of argillaceous rocks (Lundgard and Samuels, 1980).

Sediment	**Indurated**	**Metamorphosed**	
Silt	**Siltite**		**Quartzite**
2/3 silt			
Mud	Non-laminated: Mudstone	Cleavage: Slate	Without cleavage: Argillite
	Laminated and fissile: Mudshale		With cleavage: Schist
1/3 silt			
Clay	Non-laminated: Claystone	Cleavage: Slate	Without cleavage: Argillite
	Laminated and fissile: Clayshale		With cleavage: Schist

A.2.2 Geomechanical terminology and classification

From a geomechanical perspective, argillaceous media are considered either as 'soil' or as 'rock'. As already described in the main part of the report in Section 2.3.1 and in Tables 2-1 and 2-2, the terminology and classification are standardised; for soils in ISO 14688-1 and –2 and for rocks in ISO 14689-1.

Given the particular importance of discontinuities in geo-engineering design and construction, geomechanical classification places substantial emphasis on the characteristics of the bedding planes, and on discontinuities in general. Table A.2-4 presents the geomechanical classification of the discontinuity spacing. The term 'spacing' refers to the mean or modal spacing of a set of discontinuities and is the perpendicular distance between adjacent discontinuities. For sediments and sedimentary rocks 'spacing' of bedding is equivalent with the bedding 'thickness'.

Table A.2-4. Geomechanical classification and terms for discontinuity spacing
(from ISO 14689-1)

Spacing [mm]	Term for bedding thickness	Term for other discontinuities (e.g. joint, fissure, cleavage, fault)
> 2 000	Very thick	Very wide
2 000 to 600	Thick	Wide
600 to 200	Medium	Medium
200 to 60	Thin	Close
60 to 20	Very thin	Very close
20 to 6	Thickly laminated	Extremely close
< 6	Thinly laminated	Extremely close

Note that the graduation of the discontinuity spacing (left column of Table A.2-4) is a consequent extrapolation of the soil particle size graduation scheme.

A.2.3 Brief review on clay minerals

Argillaceous formations are characterised by a high portion of clay minerals having a dominant influence on the formations' mechanical, geochemical and hydromechanical behaviour at micro- and macro-scales.

The example of Figure A.2-1 illustrates this for the Opalinus Clay of northern Switzerland (Nagra 2002b). On a medium scale (~1mm; top right in Figure A.2-1) the clay particles are horizontally bedded. This bedding, which is macroscopically evident in practically any hand specimen, is responsible for anisotropies in conductivity and diffusivity of the rock (ref. to Section A.3-2). On a nanometre (nm) scale (bottom left in Figure A.2-1), the specific properties of the clay minerals and their interaction with the porewater are most important. Approximately 75% of the pores have apertures in the range of 1 – 25 nm. This very fine pore structure is the reason for the low hydraulic conductivity despite the significant water content of the Opalinus Clay. Because of the interaction of the porewater with the surface of the clay minerals, only a fraction (approx. 50 %) is free water, the remainder being bound (ref. to below). On a larger field scale (~10 m scale; top left of

Figure A.2-1), natural fractures such as faults and joints are potential structural elements and have to be considered in due detail (refer to Section A.4).

Figure A.2-1. Texture and structure of the Opalinus Clay at various scales
(Nagra 2002 b)

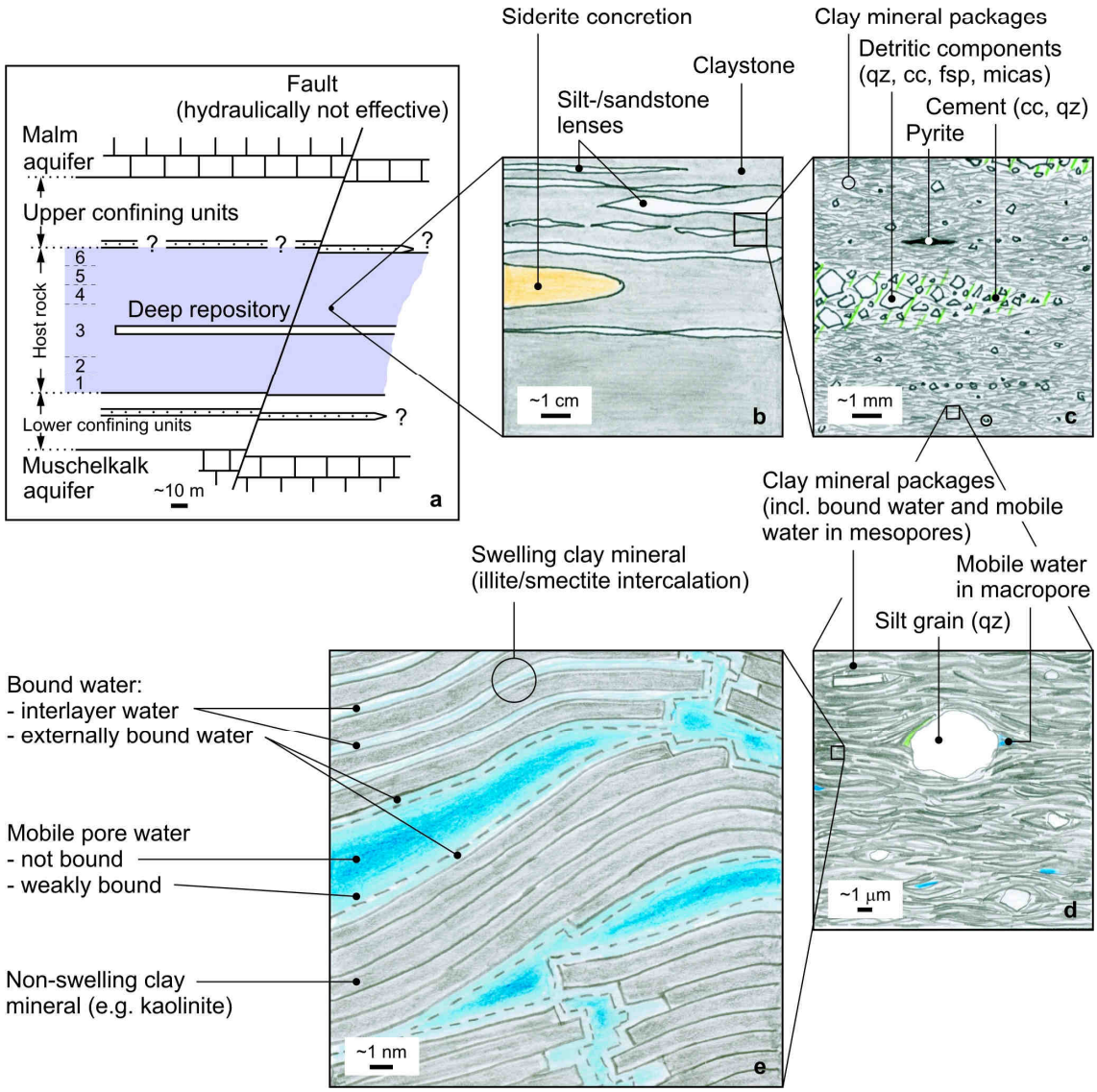

A.2.3.1 Types of clay minerals

Clay minerals have a layered crystalline structure (sheet structure; 'phyllosilicates'). Internally, each clay mineral is composed of at least one of the following two types of layers (Figure A.2-2; Grim 1968):

- Tetrahedral layer (T)
- Octahedral layer (O).

Predominately, it is the number and sequence of the tetrahedral and octahedral layers and the type of chemical bonding between those layers which define the clay mineral (Tables A.2-5 and A.2-6 and Figure A.2-2). The bond between the respective T- and O-Layers varies to certain degrees, depending on the type of clay mineral and the physico-chemical environment of the porewater.

Table A.2-5. Overview of the most important clay mineral groups and some of their representatives (after Jasmund and Lagaly 1992; from Lambert 1997)

Clay Mineral Group	**Example of clay mineral**	**Structure (ref. to text)** T = tetrahedral layer; O = octahedral layer
Kaolins	Kaolinite Halloysite; Dickite	2-Layer minerals [T – O] [T – O]
Smectites	Montmorillonite; Saponite; Beidellite; Nontronite	3-Layer minerals [T – O – T] [T – O – T] ↑ H_2O cations
Illites	Illite	
Vermiculites	Vermiculite	
Micas	Muscovite; Biotite	
Chlorites	Chlorite	4-Layer minerals [T – O – T] O [T – O – T]
Sepiolite-Palygorskites	Meerschaum Attapulgite	Fibrous clay minerals [T – O – T] [T – O – T] [T – O – T]

Clay particles are commonly characterised by tabular shapes with a very high ratio of diameter (D) [respectively length (L) and/or width (W)] in respect to thickness (T). The ratio is in the order of $D \cong L \cong W \approx 100 * T$ (Table A.2-6).

Table A.2-6. Physical characteristics of some of the most important clay minerals (after Yong and Warkentin 1975; Mitchell 1993)

Type of clay mineral	**Basic structure** (ref. to text)	**Diameter**	**Thickness**	**Specific surface** [m²/g]	**Cation exchange capability** [meq/100g]
		of clay particle [μm]			
Kaolinite	T - O	0.3 - 4	0.03 - 1	10 - 30	3 - 15
Illite	T - O - T	0.1 - 2	0.01 - 0.20	65 - 100	10 - 50
Montmorillonite	T - O - T	0.01 - 1	0.001 - 0.01	700 - 800	80 - 150

Clay particles have dimensions in the order of a micrometer [μm] or less. This feature, in combination with their sheet structure and the more or less limited bond between their respective T- and O-Layers leads to a very high specific surface of the particles.

Moreover, the surface of clay minerals carry residual negative charges, mainly as a result of the isomorphous substitution of Al^{3+} for Si^{4+} (within the T-Layer) and of Mg^{2+}, Fe^{2+}, Zn^{2+} or Li^{2+} for Al^{3+} (within the O-Layer). Processes which also, however to a minor degree, contribute to the charge deficit of clay mineral surfaces are the dissociation of hydroxyl ions (Wong and Wang 1997) and ph-dependent edge effects.

Electric surface charges in combination with a large specific surface provide the clay particles with a high adsorption potential. Exchangeable cations and water molecules (due to their dipole characteristics) are attracted to the particle surface.

The attraction force of the cations decreases with increasing distance from the clay particle surface. This causes the cations to form a disperse layer adjacent to the particle (Figure A.2-3). Hereby the cation concentration decreases with increasing distance from the particle surface until the concentration becomes equal to that in the 'normal water' in the void space (Wong and Wang 1997). The veil of ions surrounding the clay particle is about 100 Å thick.

Figure A.2-2. Crystal structure of clay minerals (after Trollope 1981).
(a) Top: Kaolinite
(b) Bottom: Montmorillonite

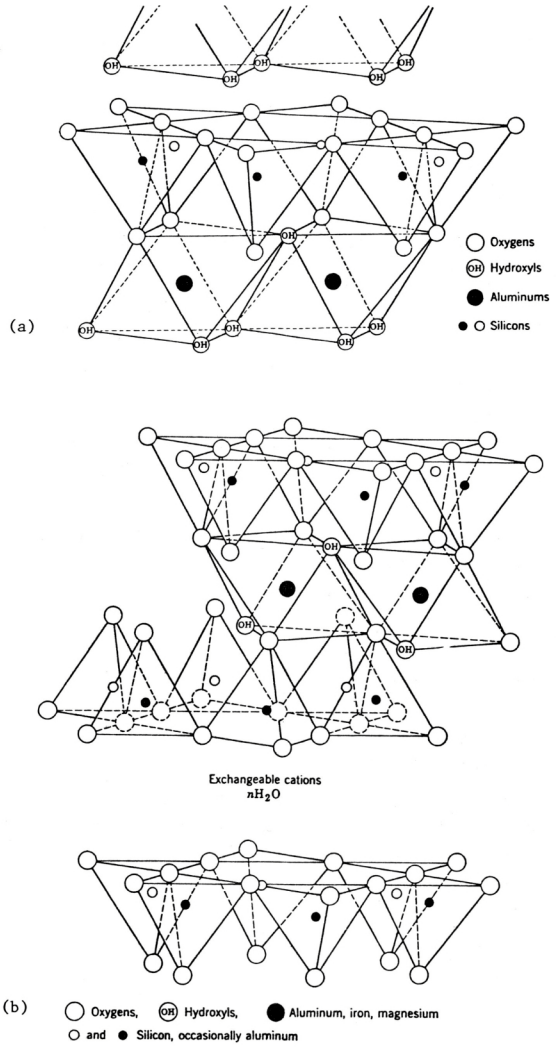

A. 2.3.2 Structure, water and porosity

Water is a most important constituent of clays and one of the controlling factors of its geomechanical and geochemical behaviour. Pores in clay rocks are generally rather small, with large contact areas between the solid surfaces and water. This typically leads to large resistance for flow of water through clay rocks or, correspondingly, to low permeabilities. At the same time, it entails large sorption capacities and thus potentially large retardation for the spreading of solutes. In fact, flow and transport properties of clay rocks are largely determined by the microstructure of the porous medium, that is, the spatial arrangement of the solids and the porewater.

Water can occur in the following forms (Nüesch 1991) (ref. to Figure A.2-4 and Section A.3.2):

1. Crystalline (or hydration OH^-) water:
   Water within the crystal structure of clay minerals ('intramatrix'). Up to about 4 layers of water molecules can be absorbed into the flaky crystal lattice.

2. Movement of water by osmosis (Mitchell 1993), either absorbed in between clay lamellae (2a) ('interlamellar) or adsorbed at the free lamella surface (2b). The build-up of more than about 4 diffuse double layers is thus possible.

3. Capillary water at the edges and contact points of the clay minerals.

4. Free water in the pores

Water Types 1 to 3 have an increased density with ρ greater than 1, whereas water Type 4 is non-densified with $\rho \cong 1$. In particular smectite can hold significant quantities of water both intermatrix and interlamellar. Velde (1992) schematically showed how the three types of bound water, i.e. crystalline water (1), absorbed bound water (2a) and adsorbed surface water (2b) (Figure A.2-5 left), are each associated with clay particle swelling, and how each type could be related to a specific weight loss during heating (Figure A.2-5 right).

Figure A.2-3. Electric double layer model after Gouy. Distribution and decrease of concentration of ions immediately next to a clay particle surface (after Mitchell 1976).

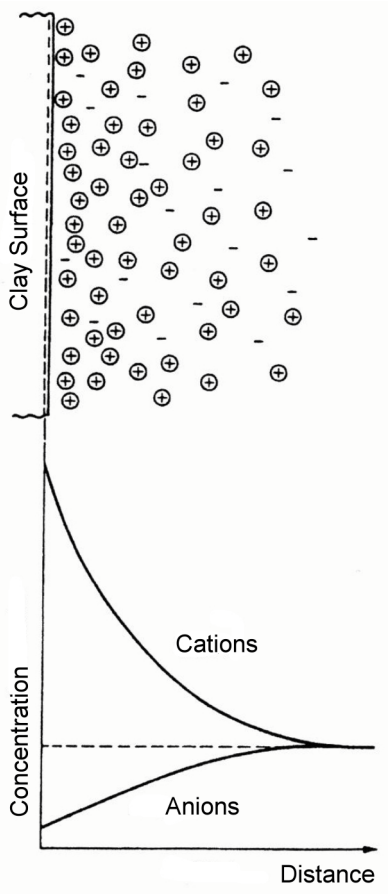

Figure A.2-4. Schematic presentation of the various types of water in clay

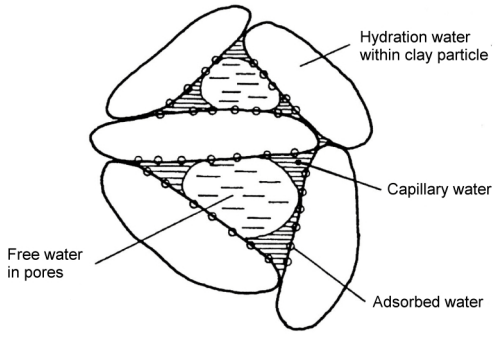

Figure A.2-6 illustrates the microstructure and the various states of the water of the Opalinus Clay on scales of millimetre to nanometre (Mazurek *et al.* 2008). On those scales the rock is made up of clay mineral platelets, quartz grains and other minerals, building complex structures of solid matter with high surface areas. Similar conceptualisations were developed for the Callovo-Oxfordian, as shown in Figure A.2-7.

Figure A.2-5. Schematic illustration of the types of water (left) and their relation to specific weight loss during heating (after Velde 1992)
(1) Crystalline water (OH) – (2a) Absorbed bound water – (2b) Adsorbed surface water – (4) Free water. - Note: Capillary water (3) not indicated in sketch

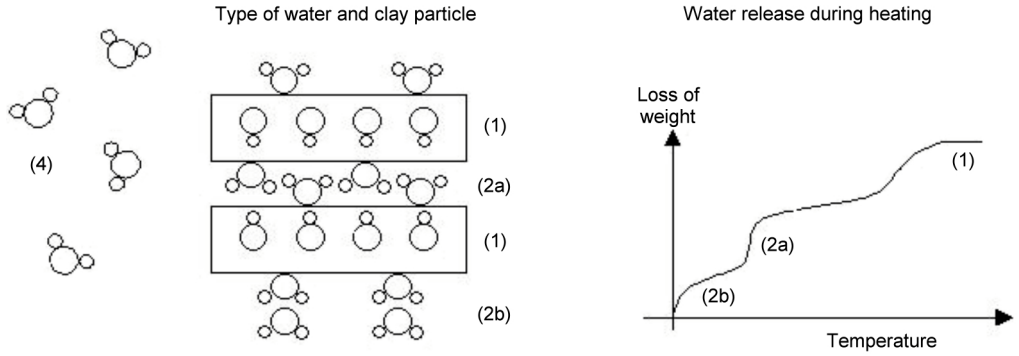

Figure A.2-6. Microstructure and porewater in Opalinus Clay on scales of mm (thin-section), µm (SEM) and nm (schematic representation after Mazurek *et al.* 2008)

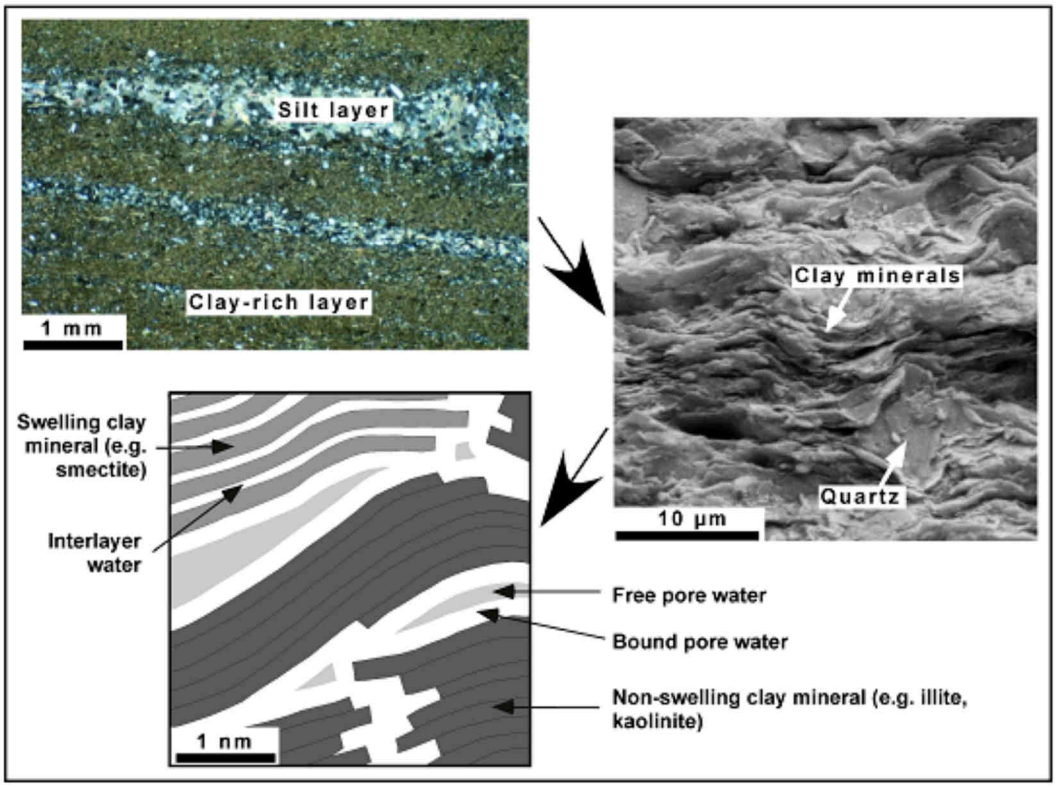

The total matrix porosity of a clay may be considered as the sum of the porosity associated with each of the size classes: micropores (<2 nm), mesopores (2-50 nm) and macropores (>50 nm). In the micropores of a saturated clay the water is described as internal and external layer water ("bound water"), whereas weakly bound and free porewater are found in the meso- and macropores (e.g.

Horseman *et al.* 1996). The accessibility of the different size classes to solutes and gases is different. This has an important implication on porosity determination, because different methods for porosity determination explore different fractions of the total pore space. A variety of methods has been used to describe the porosity of clay formations, including pycnometer porosity, water loss porosity, mercury injection porosity, diffusion porosity, geochemical porosity and flow porosity (e.g. Pearson *et al.* 2003).

Figure A.2-7. Schematic sketch of microstructure of the Callovo-Oxfordian formation on the scale 10 – 1000 nm
(Andra 2005a)

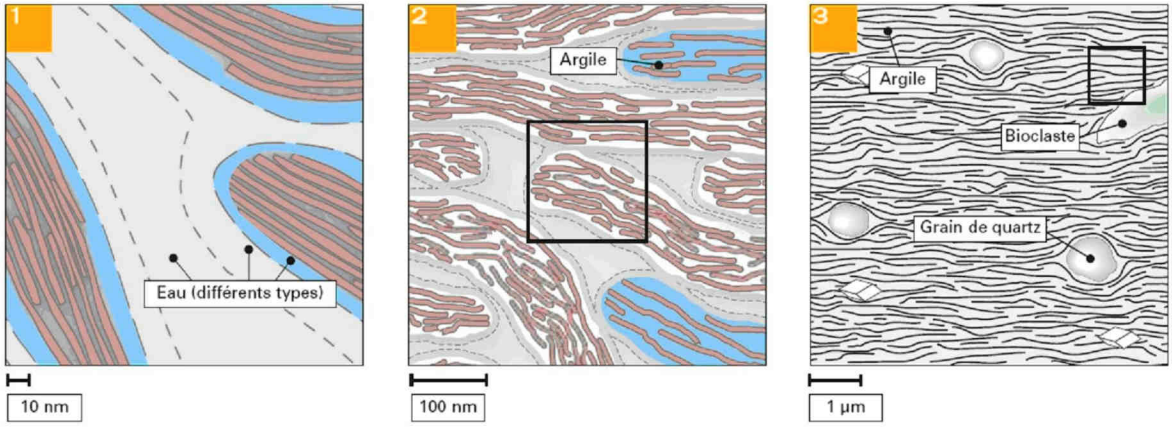

A comparison of the different porosities provides valuable insight regarding the micro-structural characteristics of clay rocks, serving as an indicator for the pore size distribution and the mobility of the porewater. Consequently, it seems important for clays to adopt complementary methods for porosity determination and, obviously, to specify the measuring method whenever porosity determinations are made (Marschall *et al.* 2008b).

A.2.4 Aspects of geological history – The deposition / burial / erosion cycle

A.2.4.1 General

The current state of any argillaceous formation, considered as host rock for deep disposal, is predominately a result of its specific geological history. Amongst the most important parameters which characterise the state conditions are the natural water content and the *in situ* stress state (ref. to Section A.2.5).

Typically, the geological history can be characterised by a sequence of events as follows (Figure A.2-8):

1. Flocculation and aggregation of clay particles.
   Flocculation of the clay particles typically occurred in sea water and, still in the state of suspension, these particles accumulated in form of larger aggregates (Stage A of Figure A.2-8). As is typical for sea water environments, the aggregates were in form of an edge-to-face texture (‘card-house’ texture; ref. to Figure A.2-8, top and Figure A.2-9, left).

Figure A.2-8. Development of the texture of a sedimentary deposited clay in course of the three stages of formation (flocculation) in sea water (Stage A), sedimentation (Stage B) and burial (Stage C) (after O'Brien and Slatt 1990)

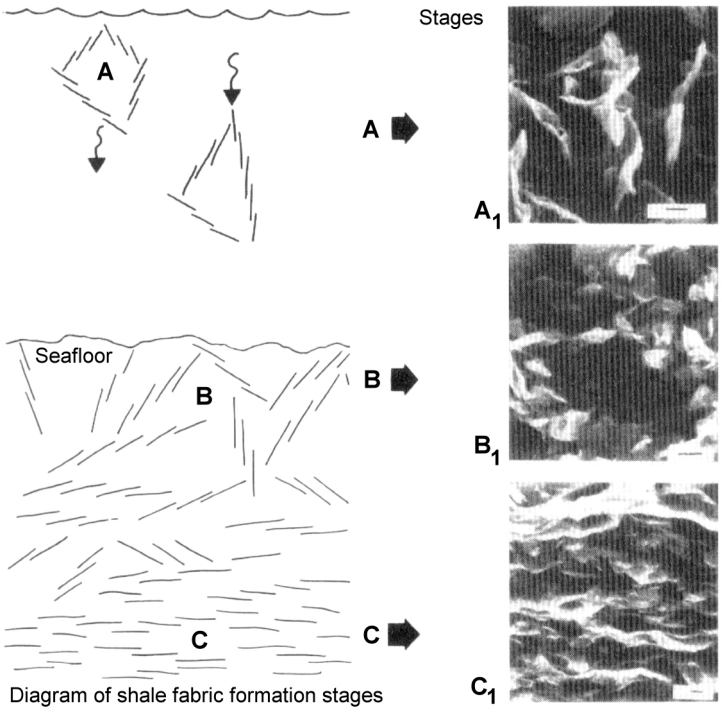

2. Sedimentation of the clay aggregates at the (sea-) floor, eventually in combination with other fine-grained clastic particles (silt), and subsequent burial.
   After sinking to the seafloor (Stage B), the aggregates became gradually buried by continuous deposition of other aggregates (Stage C of Figure A.2-8).

3. Compaction due to steadily increased effective overburden pressure.
   The compaction process is associated with a number of major physical and structural changes, in particular:

   - drainage of free porewater (with the seafloor as the principal drainage surface) in line with a decrease of the porosity;

   - development of excess porewater pressures (if drainage remains incomplete); and

   - rotation of the clay particles into a sub-horizontal, flaky structure, similar to that indicated in Figure A.2-8 (right).

   The above effects are most pronounced for overburden depths of up to about 500 m ("burial stage"; Müller 1967). At greater overburden depths (>500m; "deep-burial stage") the significance of the mechanical compaction is less well developed and chemical processes such as cementation, re-crystallisation and growth of new minerals become dominant (Wolf and Chilingarian 1992).

   After reaching maximal overburden, eventually combined with tectonic stressing, finally:

4. Uplift (not necessarily back to the surface) and reduction of the overburden pressure by vertical erosion.

   Typically, the texture of the clay minerals remain essentially unchanged, i.e. the clay particles are locked-in and preserved as in the stage of compaction (Figure A.2-9).

Figure A.2-9. Clay mineral fabric (schematic) of the Opalinus Clay (after Feeser 1986).
Left: At sedimentation in marine environment: "card-house" texture
Right: After compaction and / or tectonic events: Rhomboid texture

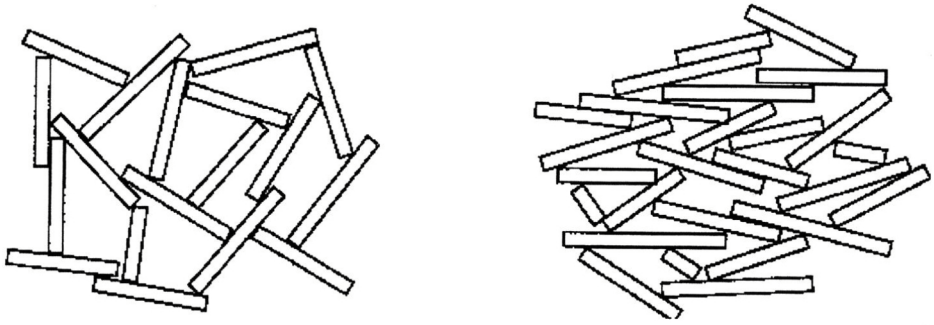

A.2.4.2 Examples of the burial history of some selected sites

The following three examples, depicted in Figures A.2-10 to A.2-12, show that, at specific sites, the above burial –compaction – uplift - erosion sequence is generally well recognisable, however with some major modifications.

Figure A.2-10. Burial history of the Boom Clay formation in the Mol region
(Mertens *et al.* 2004)

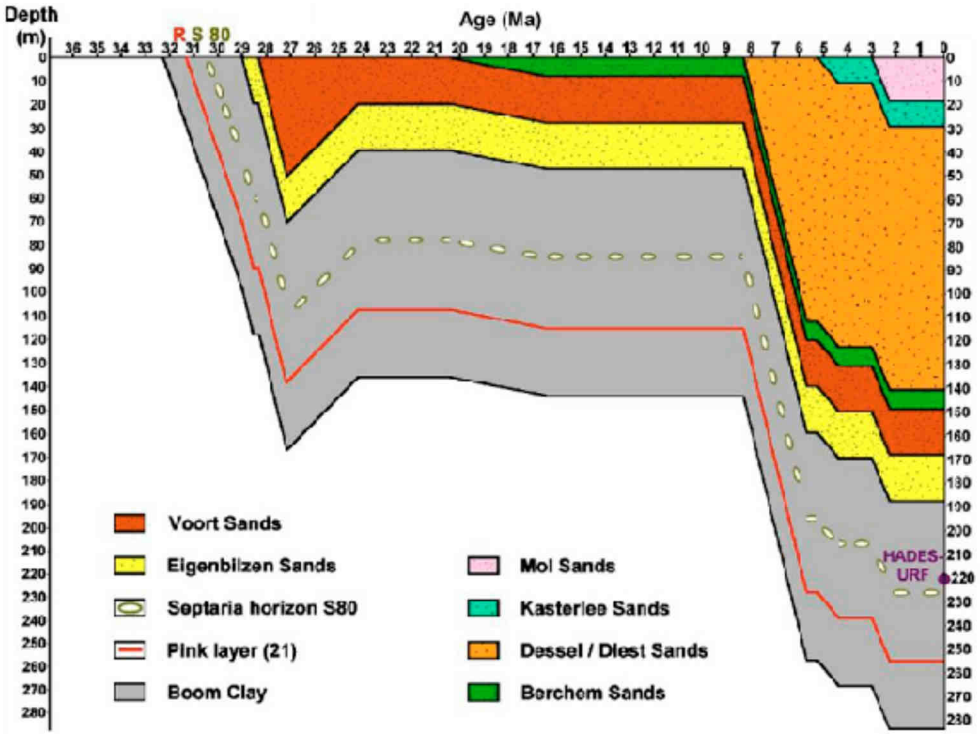

Figure A.2-10 shows the burial history of plastic Boom Clay at Mol, an uncemented fine-grained compacted mud with a well-developed particle alignment (bedding) and a high porosity. It can be seen that, apart from a minor uplift of about 40 m between 25 and 20 million years ago (at the end of the Oligocene period), uplift and erosion are virtually non-existent, The maximum burial depth of the Boom Clay (185 to 285 m at Mol) was reached some 2 Ma ago, what still is the present depth of the Boom Clay (Mertens *et al.* 2004). Dehandschutter (2004) has shown that even this apparently minor geologic uplift event at the end of the Oligocene period had major implications in the formation of the natural fracture pattern still evident today (ref. to Section A.4.1).

On the other hand, the geologic history of the Opalinus Clay in the Zürcher Weinland region in northern Switzerland (Figure A.2-11) is characterised by a well recognisable recent uplift and erosion phase. Amongst other factors, that phase is responsible for its current state as an indurated argillaceous media with substantially different mechanical properties to those of the Boom Clay (ref. also to Tables A.3-2 and A.3-3).

Figure A.2-11. Burial history of the sedimentary formations in the Zürcher Weinland region of northern Switzerland (out of Nagra 2002 b)

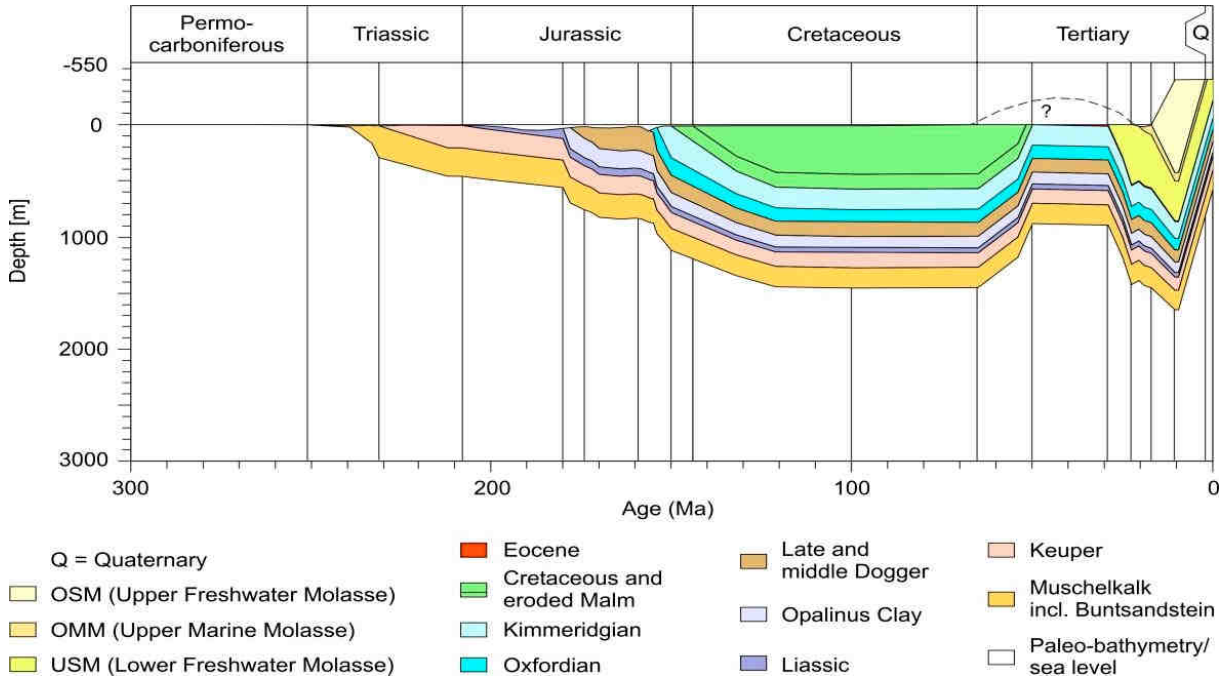

The Opalinus Clay was deposited in shallow sea waters during the Dogger – Aalenian epoch of the Jurassic period (Ziegler 1990). The Opalinus Clay reached a burial depth of about 1000 m during the Cretaceous, between about 65 and 120 million years ago. The region was affected by the rifting of the Rhine Graben (commencing about 40 million years ago) and by differential vertical movements that resulted in considerable uplift of the area during the mid-Tertiary, followed by down-warping and burial under late Tertiary sediments. This resulted in the Opalinus Clay reaching its greatest burial depth, at about 1700 m below the surface, in the Miocene stage of the Alpine orogeny, the last major tectonic event to affect the region. From about 10 million years ago, Alpine uplift and erosion brought the Opalinus Clay progressively up to its present burial depth of about 600 to 700 m in

the region of interest. The thermal gradient in the area is about 4.2°C/100 m. The present temperature of the Opalinus Clay at 650 m (at the Benken location) is 38°C. During its burial and compaction history it has experienced maximum temperatures of about 85°C.

The burial history of the Callovo-Oxfordian formation in the Meuse/Haute-Marne Region is shown in Figure A.2-12. The site is located at the eastern margin of the Paris Basin. The geologic history of that basin is generally well known (Guillocheau *et al.* 2000). The Callovo-Oxfordian formation was deposited in the late Dogger epoch of the Jurassic period. Geologically, it thus is slightly younger than the Opalinus Clay which was deposited in early Dogger.

Figure A.2-12. Burial history of the sedimentary formations in the Meuse/Haute-Marne region of the Paris Basin (from Andra 2000)

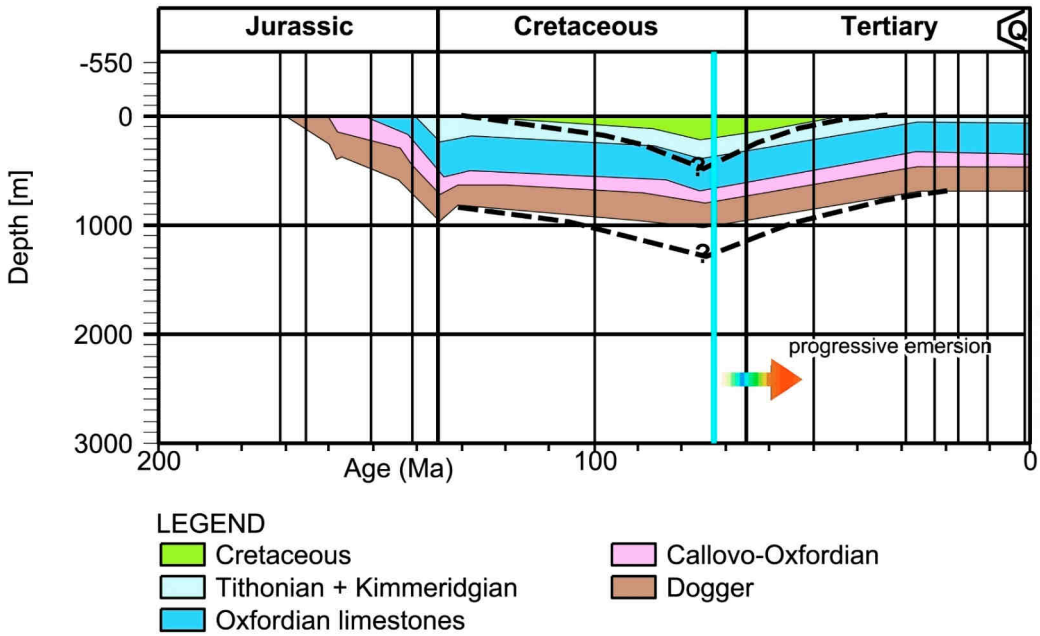

The earlier Dogger epoch of the Paris Basin is characterised by a complex distribution of reef platforms. The Callovo-Oxfordian stage then led to a progressive submersion of the basin, setting off a complete paleogeographic change. The bathymetric depth of the basin increased and sedimentation changed to mainly detrital, leading to a progressive filling up of the basin from North to South West.

The following Malm epoch is characterised by a return to carbonated shelves, with some detrital episodes during the Kimmeridgian time. The burial of the Callovo-Oxfordian formation steadily increased over the entire period. The epoch ended with a shallow depth marine environment (as evidenced by evaporites), or even emergence and erosion due to a major tectonic compression in the Middle Cimmerian phase. It seems that a 200m-thick upper part of the Jurassic sediments was eroded in this phase.

The subsequent Lower Cretaceous period was characterised by terrigenous sedimentation. The sedimentation rate was rather low leading to an about 200 m thick sequence in the central part of the basin of which some 20 m were lateron eroded during the Albian epoch. Throughout this period, the increase of the burial of the Callovo-Oxfordian formation was rather marginal; at the very best the Cretaceous deposits just compensated the burial loss of the Cimmerian erosion. In the Upper Cretaceous period a substantial sequence of chalk layer was deposited, the thickness of which is about 800 m in the central part of the Paris Basin. At the Meuse/Haute-Marne site, sedimentation ceased in the Campanian deformation phase. At this point in time, the burial of the Callovo-Oxfordian formation reached its maximum. In the whole basin, the onset of erosion coincides with the Cretaceous –Tertiary boundary. The erosion was induced by a thermally-induced uplift (tumescence), a precursor of the Oligocene rifting. The erosion process continues right until now, however at a steadily decreasing rate.

The Upper Cretaceous subsidence of the Paris Basin was associated with tilting and uplifting of the eastern margin. That mechanism led to a reduction of the deposit thickness on its margin, but it remains difficult to specify a reliable reduction ratio. For the first modelling of the evolution of the Paris Basin (Burrus 1997) that ratio was taken equal to 0.5 (i.e. a 500 m-thick Cretaceous sequence). The maximal burial depth of the Callovo-Oxfordian formation at the Meuse/Haute-Marne site would then have been close to 1000 m (dashed ?-lines in Figure A.2-12). However, sterane isomerisation reactions show that the organic matter maturity in the Callovo-Oxfordian formation can only be a result of heating at an average temperature of around 38 °C (Andra 2000). This finding is consistent with the homogenisation temperatures of the fluid inclusions in the Oxfordian limestones (but the latter must be considered as minimal values; no age data allowing to determine when these inclusions were trapped). Such a sterane transformation rate implies that the maximal burial depth of the Callovo-Oxfordian formation has been limited to 730 to 870 m.

A.2.5 State conditions

Figure A.2-13 provides a generalised picture of some of the main effects of burial and subsequent uplift and erosion on a stratum of mudstone (Skempton 1964; Fleming *et al.* 1970; see also Figure 2-3 of main part).

A.2.5.1 Water content, porosity and void ratio

At the time of deposition, shown as Point (a) in Figure A.2-13, a fine- to very fine-grained sediment consisting of silt and clay (= ‘mud’) may have a water content w in the range of 80 to 100%. As additional sediments accumulate on top, their weight must be borne by the mud layer. The increase in stress causes water to be expelled leading to a decrease in porosity and void ratio. Provided that the deposition of sediments is not interrupted and is not too rapid, the newly formed mudstone will follow the path defined by Points (a), (b) and (c). The fabric will alter in response to the increased effective stress and the platy clay minerals will become oriented towards right angles to the vertical compression direction. Using soil mechanics terminology, the mudstone at any point on this path is ‘normally consolidated’, since its porosity and water content are always commensurate with its depth of burial. A mudstone in this condition is considered to be in a state of hydraulic equilibrium with its surroundings.

If deposition is rapid, in particular if the rate of the effective vertical stress increase due to deposition exceeds the porewater expulsion rate, excess porewater pressure will develop. The porosity, void ratio and water content of the mudstone will each be higher than might be anticipated from its

current burial depth. The mudstone then is in a state of 'underconsolidation' (or 'undercompaction') and of hydraulic disequilibrium.

Figure A.2-13. Typical effects of a simple deposition – burial – erosion cycle on some principal state conditions of a mudstone
(after Horseman *et al.* 2005) - Top: Water content; Bottom: Stress state

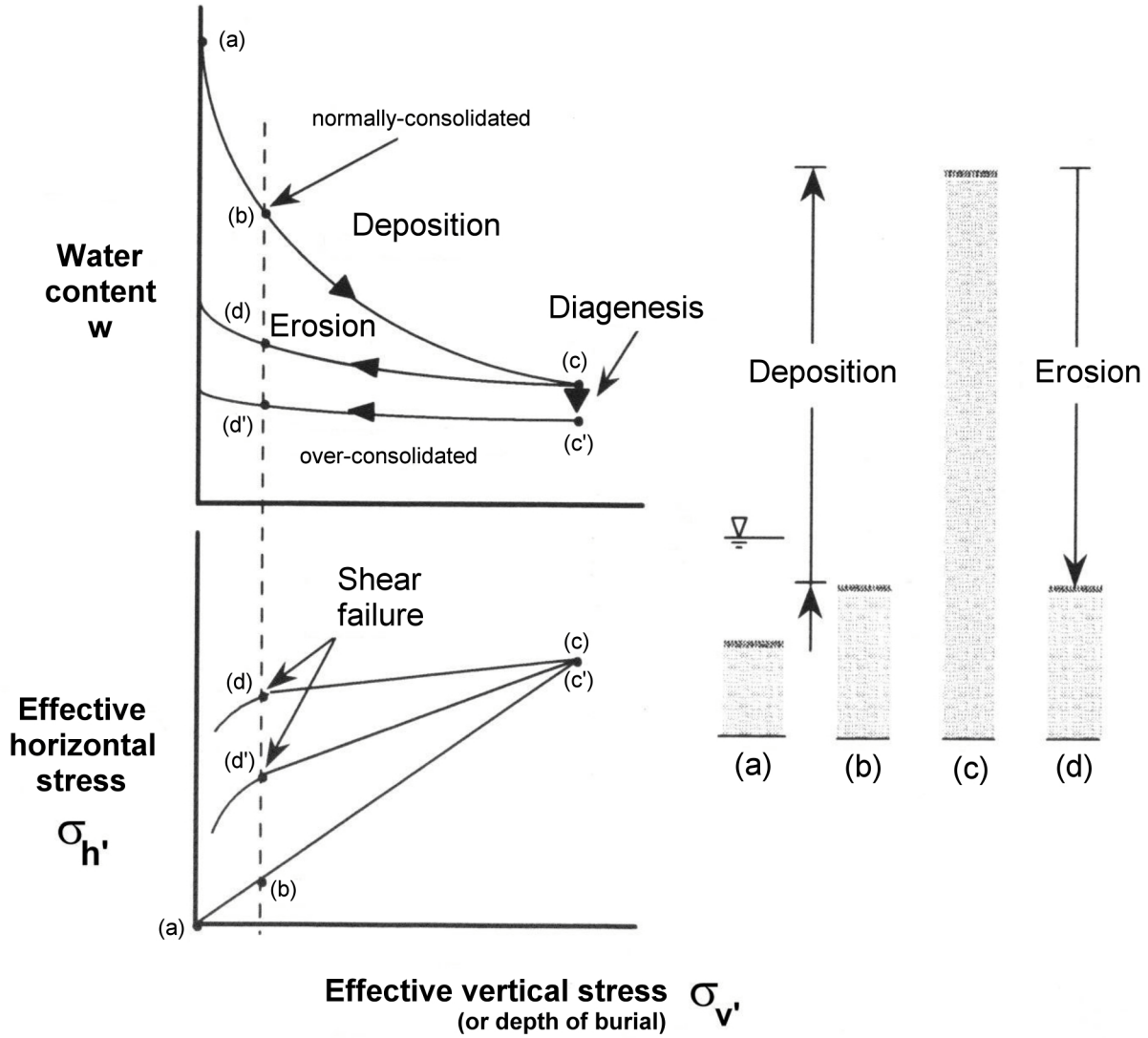

At Point (c) of Figure A.2-13, deposition ceases. If the depositional phase is immediately followed by a period of erosion, then the mudstone follows path (c) to (d). The material is subject to an effective stress that is less than the maximum burial stress and is said to be 'overconsolidated'. The reduction in effective stress is accompanied by an increase in water content (known as rebound), but this increase is far less than the decrease in water content during consolidation. Thus, whilst the material at Point (d) is under the same effective stress as the material at Point (a), the water content of the over-consolidated mudstone is considerably less. The particles are therefore in a much denser state of packing than in the normally consolidated mudstone.

If there is a considerable time-lapse between the end of the depositional phase and the start of the erosion, the mudstone may follow the path (c) to (c'), which is characterised by a loss of water under constant effective stress and by the development of diagenetic bonds. This period may be sufficiently long for minerals to recrystallise, for strong particle adhesion to develop, or for a cementing medium to be precipitated in the interparticle spaces. The more strongly developed the interparticle bonding, the smaller will be the increase in water content on unloading path (c') to (d').

A.2.5.2 In situ stress state in the deposition / erosion cycle

Figure A.2-13 also shows the relationship of the effective horizontal stress, σ_h', to the effective vertical stress, σ_v', during the deposition / erosion cycle. Generally, the horizontal stress response to the increasing overburden pressure is not elastic in nature, and is therefore characterised by an empirical parameter K_0 which, in soil mechanics, is known as the 'coefficient of earth pressure at rest':

$$\sigma_h' = K_0 * \sigma_v' \qquad \text{(A.2-1)}$$

The value of K_0 must lie within upper and lower bounds, to stay compatible with the long-term strength properties of the mudstone. In effect, if K_0 is excessively large or, alternatively, excessively small, the shear stress will exceed the strength, leading to non-reversible permanent deformation and to structural change of the mudstone material. During the depositional phase, $K_{0(NC)}$ for the normally consolidated mudstone is generally smaller than 1, typically in the range of about 0.4 to 0.75 (Mandl 2005).

Regional uplift in combination with vertical erosion (i.e. a reduction of the overburden thickness) leads to a decrease of σ_v' and, due to the suppression of the Poisson effect, also to a decrease of σ_h'. The decrease of the respective stresses σ_h' and σ_v' will be at an unequal rate; the stress reduction rate will be greatest in vertical direction and smallest in horizontal direction. The consequence is that K_0 is increased. Typical values of $K_{0(OC)}$ for an over-consolidated mudstone are commonly considered to be in the range 1 to 4, with the maximum value probably limited by the shear strength. The state of stress developed in a highly overconsolidated mudstone can therefore lead, at shallow depth, to spontaneous shear and surface-parallel extension fractures, dilatation and the formation of local reverse faults [Path (c) → (d), respectively (c') → (d') in Figure A.2-13, bottom].

The reduction in the total horizontal normal stress $\Delta\sigma_h$ is a linear function of the decreases in total overburden stress $\Delta\sigma_v$, in pore pressure Δp and in temperature ΔT. This functional relationship can be derived from the linear poro-thermo-elastic equations resulting in the following equation:

$$\Delta\sigma_h = \nu\,(1-\nu)\,\Delta\sigma_v + E\,(1-\nu)\,[\,a * \Delta p / (K * 3) + \alpha * \Delta T/3] \qquad \text{(A.2-2)}$$

where:
- E = Young's modulus
- ν = Poissson ratio
- a = $1 - K/K_s$
  - where:
  - K = compression modulus of the bulk material of the porous rock
  - K_s = compression modulus of the solid material of the porous rock
- α = thermal volumetric expansion of the unconstrained porous rock

As all three Δ–terms are negative (decreasing overburden stress σ_v, decreasing pore pressure u and decreasing temperature T), $\Delta\sigma_h$ will also be negative, indicating the development of tensile stresses.

$\Delta\sigma_h$ has, however, to be superimposed with the initial compressive horizontal stress $\sigma_h^{o'}$ which is acting within the layer at the onset of uplift. In fact, the amount of $\sigma_h^{o'}$ is the direct result of the overburden pressure and of K_0 of the subsidence phase as outlined before. Mandl (2005) concluded that, in normal geological and geotechnical circumstances, the resulting (superimposed) effective horizontal stress σ_h' will remain compressive throughout all uplift phases. At shallow depth σ_h' will produce horizontal effective compressive stresses of several MPa and will become the major principal stress, thus generating a $K_0 > 1$. However, exemptions of this trend may be possible in a number of scenarios. These include:

- Unusually stiff rock
- unusually soft rock
- rocks under very high geothermal gradients
- influence from the geometry of a sediment basin.

With regard to the *in situ* stress states of the specific sites considered for waste disposal in argillaceous formations, the FEPCAT review (Mazurek *et al.* 2003) revealed no clear evidence for a distinct *in situ* stress pattern in the sense of a $K_0 > 1$ (Table A.2-7). If there is any tendency recognisable than that of an about isotropic *in situ* stress state which might be adjusted by active tectonic stresses as is evidenced in Bure, Mont Terri and Zürcher Weinland.

A.2.6 Geological conditions of sites considered in current studies of radioactive waste disposal

The following compilation is based on the FEPCAT review (2003), which has been updated where necessary. In this regard mention should be made to Boisson (2005) who has compiled a comprehensive catalogue comprising the geological characteristics of a variety of argillaceous formations, studied in the context of radioactive waste disposal. It provides an overview of the available geoscientific data sources on argillaceous formations. For each formation, the presented parameters were grouped in categories, such as mineralogy, rock and porewater chemistry, petrophysical parameters, flow and transport parameters and geomechanical parameters.

A.2.6.1 Callovo-Oxfordian at Bure, France (see Figure 3-49)

In the eastern part of the Paris Basin, Andra is investigating a site near Bure (also called "Site Meuse-Haute Marne" or "Site de l'Est"), mainly targeting a flat-lying, ca. 130 m thick argillaceous formation of Callovo-Oxfordian age at 420 - 550 m below surface. The research activities are dedicated to study the feasibility of reversible, deep geological disposal of high-activity, long-lived radioactive wastes. So far, the URL consists of two shafts, an experimental drift at 445 m level and a set of technical and experimental drift at the main -490 m Level (Delay *et al.* 2007). French Law, which was passed in 2006, requests Andra to apply for a licence to construct a high-level and long-lived waste repository in the neighbourhood of Bure by 2015.

Table A.2-7. *In situ* stress state of sites considered in waste disposal studies
(actualised after Mazurek *et al.* 2003)

Formation / Site / Reference	Experimental Techniques employed	Main Results
Toarcian-Domerian at Tournemire	Hydraulic fracturing	Two campaigns have been performed but lead to difficulties in interpretation of the results.
Callovo-Oxfordian at Bure (Lebon 2009)	Convergence of vertical shaft	*In situ* stresses in Borehole EST361 at 504 m depth (which is at about the -490 m Level of the Bure URL): $\sigma_v = 12.7 \pm 0.2$ MPa $\sigma_H = 14.8 \pm 0.5$ MPa (oriented 155° ±10°) $\sigma_h = 12.4 \pm 0.5$ MPa (oriented 065° ±10°) σ_H is oriented in SSE – NNW direction (155° ±10°) in agreement with European far-field stresses
San Pedro Formation (Duero Basin): Compacted clays from lacustrine deposits	Tests (presumably hydraulic fracturing) performed in one only vertical exploratory drillhole	*In situ* stresses at depth z = 230 m: $\sigma_1 = \sigma_v = \rho\ g\ z \approx 5.9$ MPa $\sigma_2 = \sigma_H = 5.0$ MPa (in N-125°-E direction) $\sigma_3 = \sigma_h = 4.2$ MPa
Opalinus Clay at Mont Terri (Vietor *et al.* 2006)	Under- and overcoring, borehole slotting, hydraulic fracturing and backanalysis from convergence behaviour of URL	*In situ* stresses at URL level: $\sigma_1 \approx \sigma_v \approx 6.5$ MPa (sub-vertical) $\sigma_H \approx \sigma_2 \approx 4.3$ MPa (sub-horizontal, 140° direction) $\sigma_h \approx \sigma_3 \approx 2.2$ MPa (sub-horizontal, 050° direction) σ_H is oriented in SE – NW direction (140°) about in agreement with European far-field stresses.
Opalinus Clay in the Zürcher Weinland	Hydraulic fracturing and borehole breakout analysis	*In situ* stresses at depth z = 650 m: $\sigma_1 = \sigma_H \approx 1.5\ \sigma_h$ (≈ 22.6 MPa) $\sigma_2 = \sigma_3 = \sigma_h \approx \sigma_v\ (\rho\ g\ z) = 15.1$ MPa σ_H oriented in SSE – NNW direction (170° ±10°) in agreement with European far-field stresses.
Boom Clay at Mol	Piezometers, self-boring pressuremeter	*In situ* stresses at URL level: $\sigma_v(\rho\ g\ z)$ =4.6 MPa (theory), 3.4 MPa (measurement) $K_0 = \sigma_h / \sigma_v = 0.9 – 1.2$
Boda Clay Formation at Mecsek	Hydraulic fracturing, sleeve fracturing and overcoring.	Current experimental data suggest a quasi-isotropic compression stress field.
Mizunami Group at Tono Kamaishi mine (hard crystalline rock)	Various methods, amongst them measurements on cores and acoustic emission. Study on the applicability of the existing stress measuring methods.	Generally: *In situ* stress conditions differ quite considerably in soft rock from those in hard crystalline rock. In soft rock the *in situ* stress state is uninfluenced by a major geological fault (Tsukiyoshi fault). There is an indication that the measured vertical stress component corresponds with the overburden pressure at any depth.
Pierre Shale in south Dakota	Borehole methods (unspecified)	Essentially a lithostatic stress state with no deviatoric stresses.

A.2.6.2 Toarcian-Domerian at Tournemire, France

In 1989-1990, IRSN initiated *in situ* research in argillaceous formations. An underground research laboratory was built in two galleries excavated from a former railway tunnel near Tournemire (Aveyron - southern France). The tunnel is 100 years old and 1885 m long. It penetrates a flat lying, 250 m thick sequence of shaly and marly lithologies of Toarcian - Domerian age which is sandwiched between limestone aquifers above (Aalenian) and below (Carixian).

The Tournemire project aims at generic studies related to the disposal of radioactive waste. The main geological, stratigraphic, tectonic and hydrogeological characteristics of the site have been studied. The research programme deals mainly with the hydrogeological properties, in order to characterise fluid flow and solute transport through the argillaceous formation and to quantify the relevant processes in numeric models.

The site is not under consideration for a real radioactive waste repository, but provides support for generic studies for this purpose.

Investigations performed mainly by: IRSN, France. Key reference: Boisson (1998).

A.2.6.3 Spanish Reference Clay, Spain

The Spanish Reference Clay refers to one of the numerous argillaceous formations retained in Spain for future characterisation studies when so decided by the Spanish authorities.

Investigations performed mainly by: Enresa, Spain. Key reference: Enresa (1999).

A.2.6.4 Opalinus Clay at Mont Terri, Switzerland (see Figure 3-24)

The Mont Terri Underground Research Laboratory (URL) is a generic rock laboratory run by 12 international partner organisations. It is for research purposes only and any future disposal of radioactive waste in the laboratory is clearly excluded. The URL is located in north-western Switzerland (Canton Jura) and consists of a gallery system adjacent to a security tunnel of the A16 Motorway tunnel across the Mont Terri anticline in the Folded Jura Mountains. It is located in Opalinus Clay, a middle Jurassic marine shale formation. The formation is over-consolidated and ca. 270 m below surface at laboratory level. Research was started 1996 and is documented in synthesis reports (Nagra 2002b; Bossart and Thury 2008). In future, the main focus will be long-term experiments (Bossart and Thury 2007).

A.2.6.5 Opalinus Clay in the Zürcher Weinland, Switzerland

In 1994, the Opalinus Clay (a Middle Jurassic marine shale formation) was identified as the priority sedimentary host rock option for the disposal of spent fuel and vitrified high-level waste in Switzerland, and the Zürcher Weinland (north-east Switzerland) as the first-priority area for site-related investigations. Detailed characterisation of the host rock and the potential siting area followed after 1994. The key elements of this research programme were a 3D seismic campaign in the Zürcher Weinland covering an area of around 50 km^2, an exploratory borehole (Benken), experiments as part of the international research programme in the Mont Terri underground research laboratory (Canton Jura), comparative regional studies on the Opalinus Clay including deep boreholes in the near and far

vicinity of the siting area, and comparisons with clay formations that are under investigation in other countries in connection with geological disposal.

Investigations performed mainly by: Nagra. Key reference: Nagra (2002b).

A.2.6.6 Boom Clay at Mol, Belgium (see Figure 3-42)

The Oligocene Boom Clay under the nuclear site of Mol/Dessel in the north-east of Belgium is considered as the Belgian reference host formation for the methodological study of the disposal of long lived medium and high level radioactive waste in deep clay layers. The first characterisation works under the site were launched in 1975 by the Nuclear Energy Research Centre of Mol (SCK•CEN). Since that time three sampled deep drillings with extensive geophysical logging and two high resolution seismic campaigns have been carried out on site. Moreover, a large number of parameters of different natures have been determined in laboratory and/or *in situ*. An underground research laboratory at the depth of 220 m (HADES URF) was built and progressively extended for numerous *in situ* experiments. In the framework of the PRACLAY project (a large-scale demonstration test) the HADES URF has recently been extended. A second shaft and a connection gallery have been built.

Investigations performed mainly by: Ondraf/Niras and SCK/CEN, Belgium. Key reference: Ondraf/Niras (2002).

A.2.6.7 Ypresian Clays at Doel, Belgium

Ypresian Clays (Kortrijk and Tielt Formations) under the nuclear site of Doel along the River Schelde in North Belgium are considered, on governmental request, as alternative host rocks to the Boom Clay. Geologically, the Ypresian Clays are of Lower Eocene age and thus significantly older than the Boom Clay. Stratigraphically, they are equivalent with the London Clay. The characterisation works under the site were launched in 1995 by the drilling of fully cored deep boreholes with extensive geophysical logging. No underground research laboratory exists at Doel.

Investigations performed mainly by: Ondraf/Niras and SCK/CEN, Belgium. Key reference: Ondraf/Niras (2002).

A.2.6.8 Boda Clay Formation, Hungary

The Boda Clay Formation occurs in SW Hungary, west of the City of Pécs. The Permian, 250-260 Ma old formation is known to occur over an area larger than 150 km^2. A comprehensive characterisation programme was carried out here between 1993 and 1999. An underground research laboratory was run at a depth of 1030-1080 m below surface in tunnel excavated from an existing tunnel previously built for mining purposes. Work was discontinued after 1999, and the tunnel system has been flooded.

The formation originates from lacustrine sediments deposited under oxidising and alkaline conditions. The main lithology are albitic claystones. The formation was buried to 3.5 - 4.5 km below surface and so is highly indurated, It contains fractures and faults originating from a number of tectonic events. Solute transport is dominated by advection in brittle structures.

Investigations performed mainly by: Mecsek Ore Environment and Puram, Hungary. Key references: Kovacs (1999, 2003).

A.2.6.9 Mizunami Group at Tono, Japan

The Miocene sedimentary cover of the basement (mostly Cretaceous granitic rocks) of the Tono region has been investigated in connection with the uranium exploration activities and palaeontological and geoscientific studies. It is being characterised in the course of the drilling and mining activities for the planned underground research laboratory (in granitic basement) at the nearby locality of Mizunami. The thickness of the sedimentary cover is variable, between 0 and several hundreds of metres.

Miocene argillaceous sequences include the Toki Lignite-bearing Formation (non-marine; basal conglomerate, sandstone and mudstone interbedded with lignite-bearing facies, hosting uranium ore bodies; up to 170 m in thickness), the Akeyo Formation (marine; mudstone and tuffaceous sandstone interbedded with pumice tuff; up to 280 m in thickness), the Oidawara Formation (marine; basal conglomerate and massive siltstone and mudstone; up to 160 m in thickness). These sedimentary sequences are cut by the Tsukiyoshi fault with vertical reverse displacement about 30 m in the Tono mine.

Investigations performed mainly by: JNC and Mizunami Fossil Museum, Japan. Key reference: Yusa *et al.* (1993).

A.2.6.10 Ordovician argillaceous limestone at Tiverton, Ontario, Canada

A Deep Geologic Repository (DGR) for the long-term management of operational Low and Intermediate Level Radioactive Waste is being proposed by Ontario Power Generation (OPG) at the Bruce Nuclear site near Tiverton, Ontario, situated 225 km northwest of Toronto on the eastern shore of Lake Huron. Target formation is an 850 m thick sedimentary sequence of Cambrian to Devonian age near horizontally bedded, weakly deformed shales, carbonates and evaporates of the Michigan Basin. Within this sedimentary pile, the proposed DGR would be excavated within the low permeability argillaceous limestone Cobourg Formation at depth of 680 m, which is overlain by 200 m of upper Ordovician shale formations.

In 2007, an Environmental Assessment for the proposed DGR was underway in accordance with the Canadian Environmental Assessment Act.

Key reference: Intera Engineering Ltd. (2006).

A.2.6.11 Pierre Shale in South Dakota, USA

The Pierre Shale is a Cretaceous, smectite-rich unit occurring in large parts of the western USA and Canada, with thickness between 0 and ca. 2000 m and a high porosity of ca. 30 vol %. Most relevant work was done in central south Dakota (Pierre Shale cropping out on the surface).

Investigations performed mainly by: US Geological Survey. Key references: Neuzil (1993, 1995a).

A.2.6.12 Palfris Formation at Wellenberg, Switzerland

In Switzerland an underground repository is foreseen for the disposal of L/ILW. In 1993, following a comprehensive investigation programme including seven exploratory boreholes, a site at Wellenberg was selected. Wellenberg is located in Central Switzerland (Canton Nidwalden) in the Helvetic Alps, which lie along the northern margin of the Alps. The investigated potential host rock consists of the very low permeability Palfris Formation (dominating by volume, mainly argillaceous marls) and the Vitznau Marls of the Drusberg nappe, including Interhelvetic Mélange and Tertiary shales of the Axen nappe. The Palfris Formation is one of the major décollement horizons of the Helvetic Alps and, although normally only 200 m thick, at Wellenberg has been thickened by tectonic processes (folding, imbrication) to a large mass exceeding 1000 m. All these rocks were buried to *ca.* 10 km below surface some 20 Ma ago and so are highly indurated.

For any underground construction and investigation, a Cantonal mining license is required in addition to Federal permits. This gives the Canton the right to veto a project, even when already licensed by the Federal Government. In Nidwalden, this Cantonal license is subject to popular referendum. In 2002, an application for a concession for an exploratory drift to allow further geological investigation of the site was rejected by the people of Nidwalden and therefore the site was abandoned from further consideration.

Investigations performed mainly by: Nagra, Switzerland. Key reference: Nagra (1997).

APPENDIX 3

GEOMECHANICAL PROPERTIES OF ARGILLACEOUS FORMATIONS

Overview

This appendix provides, in addition to Section 2.3.2 of the main text, certain detailed information on the geomechanical properties of argillaceous formations essential for the understanding of self-sealing features and processes. It includes some general remarks on geo-engineering design, as expressed in the fundamental Eurocode 7 (2004; 2007), and an update on the necessary interaction between geo-scientists and geo-engineers in arriving at appropriate geo-engineering solutions (Section A.3.1). As an example of a comprehensive set of geomechanical parameters, the state and design parameters of the Opalinus Clay of the Mont Terri URL are presented in some detail (Section A.3.2). Beyond that, emphasis is laid on a review of the general strength properties and strength (failure) criteria (Sections A.3.3 and A.3.4) for gaining a better understanding of the fracturing process in argillaceous formations.

A.3.1 General remarks on geomechanics and geo-engineering

Geo-engineering, such as the design and construction of underground repositories, is based on a sound understanding of the mechanical behaviour of soils and rocks. That understanding is expressed in terms of idealised models, formulated within the disciplines of soil mechanics and rock mechanics (Figure A.3-1).

Figure A.3-1. The Triangle of Geomechanics
(Idealisation of geomaterial behaviour; after JEWG 2004)

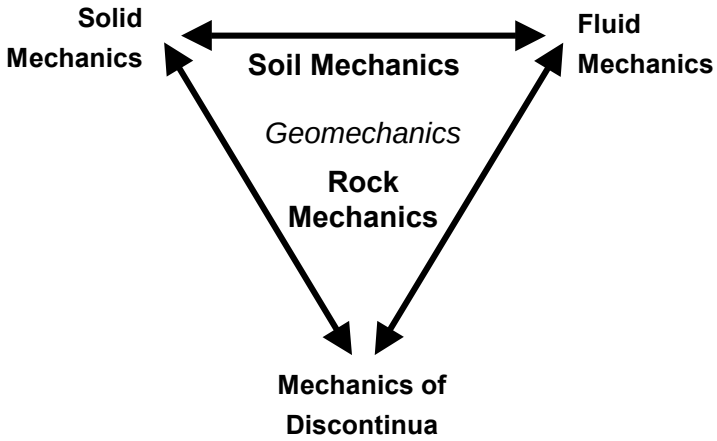

Due to the assemblage of solid particles and fluids and their intrinsic nature within a fractured system (ref. to Section A.2.3), the mechanical behaviour of geologic materials must incorporate principles of solid mechanics, fluid mechanics and the mechanics of discontinua. These three mechanical disciplines define the "Triangle of Geomechanics" (JEWG 2004) and the relative positions of soil mechanics and rock mechanics can be located within that triangle as shown in Figure A.3-1. Soil mechanics is the discipline that is characterised by the mechanical interaction

between solids and fluids, whilst rock mechanics has a strong adherence towards the mechanics of discontinua with major influences from solid and fluid mechanics.

Soil mechanics and rock mechanics, like solid mechanics, fluid mechanics and the mechanics of discontinua, are branches of 'Material Science'. Due to its major field of application, material science in general and soil and rock mechanics in particular, are commonly considered as engineering disciplines. Beyond geo-engineering, soil and rock mechanics are also indispensable in the mechanical understanding of geological processes such as sedimentation, faulting and jointing.

Geo-engineering in its broad sense is essentially a serial process which is directed towards the geo-engineering structure (reading Figure A.3-2 from left to right).

Figure A.3-2. The position of geomechanics (soil and rock mechanics) within the broader field of geo-engineering in context with the design and construction of an underground repository (modified after JEWG 2004)

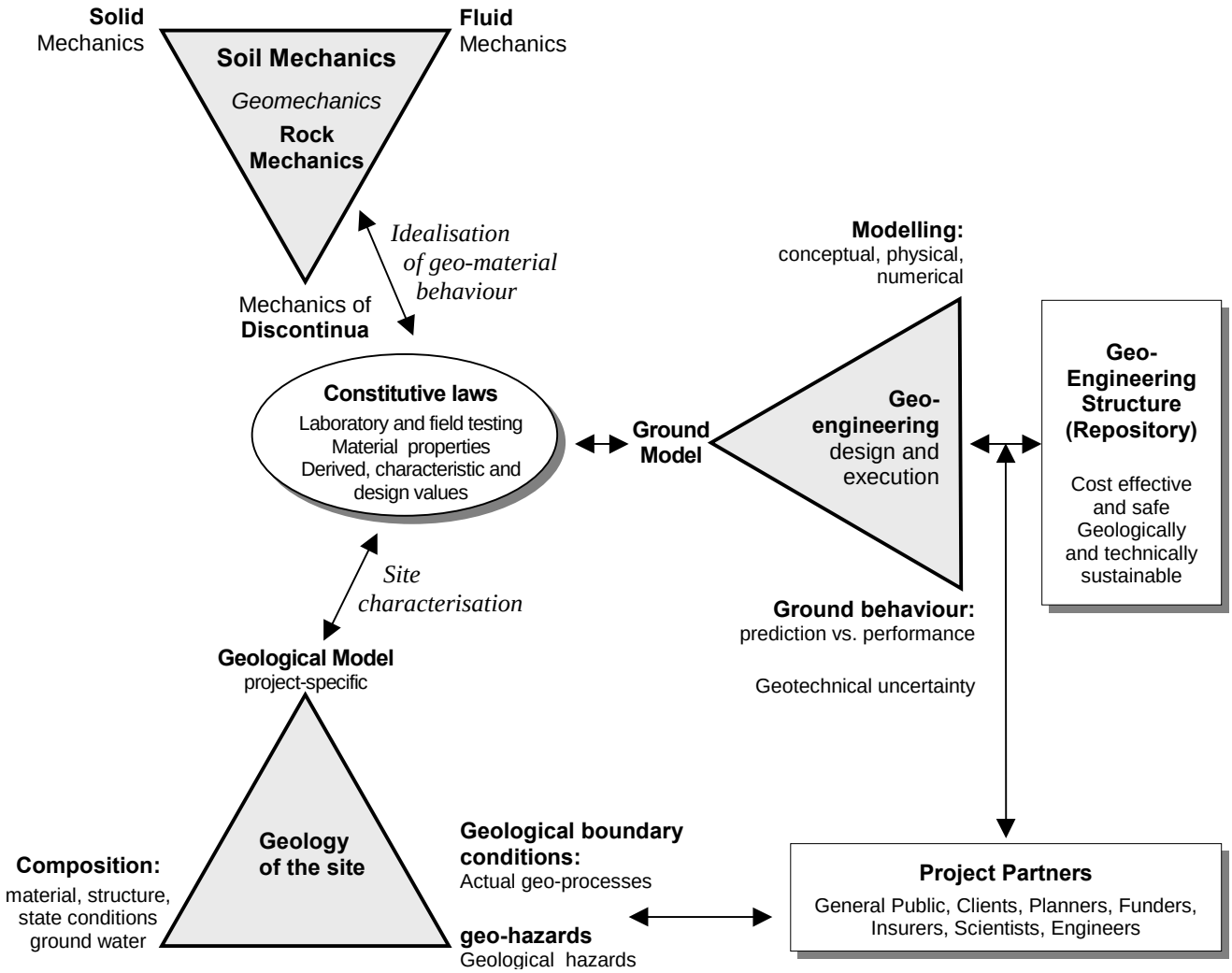

Effective geo-engineering requires feedback between and interaction across the various aspects involved (interaction arrows within Figures A.3-1 and A.3-2). This, in particular, applies to the 'central oval' of Figure A.3-2 which is characterised by the links between all major aspects involved. The development of the 'Ground Model' is central to this process and includes the embedment of engineering parameters and material properties into a site- and project-specific 'Geological Model'. The embedment requires the specification of constitutive laws appropriate for the soils and rocks in the model, the derivation of their mechanical properties in laboratory and/or field testing ('derived values' in the sense of EN 1997-2) and their interpretation in terms of 'characteristic' and 'design values' in the sense of EN 1997-1. The transfer from 'derived' to 'characteristic' and 'design' values is thereby based on the evaluation of the sampling and testing procedures, possible scale effects, regional experience and experience with the specific geo-material under consideration (Figure A.3-3). Specifications on laboratory and field tests of rocks can be found in the compilation of the Suggested Methods of the International Society for Rock Mechanics ISRM of the years 1974 - 2006 (Ulusay and Hudson 2007).

Figure A.3-3. Flow chart for the selection of geotechnical parameter values, modified after Eurocode EC 7 (EN 1997-1 and -2).

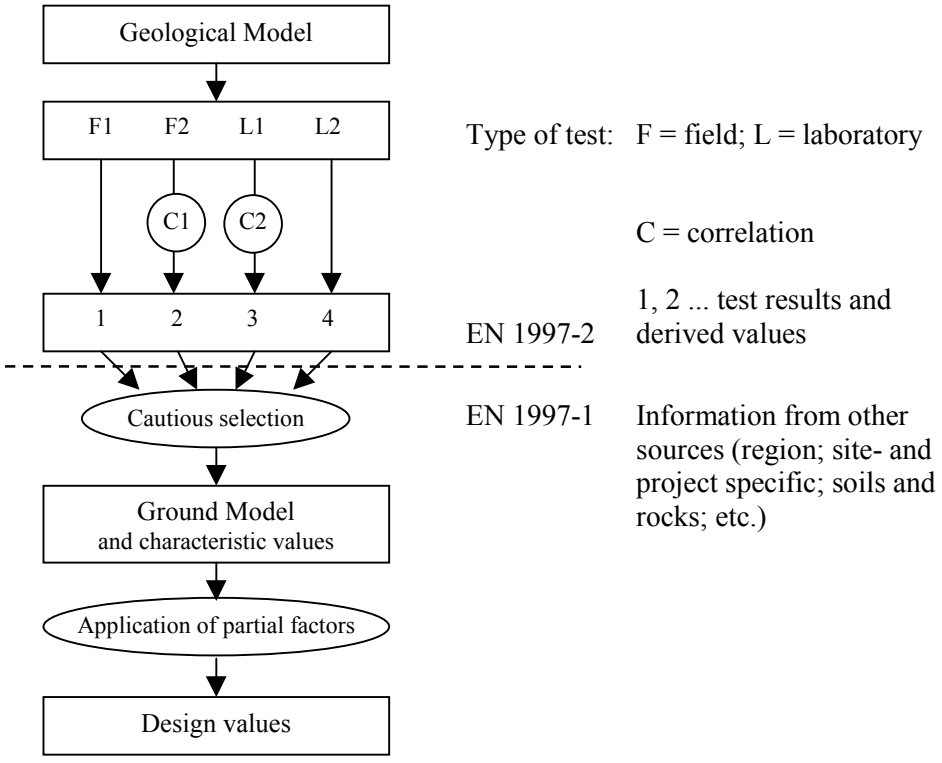

A.3.2 Examples of comprehensive sets of geomechanical parameter values

Given the large variety of argillaceous soils and rocks (ref. to Section A.2.1), it makes limited sense to compile and integrate information from various sites in order to arrive at a set of 'typical' geomechanical parameter values for argillaceous materials in general. This is evidenced in Table A.3-1 (extract from Horseman *et al.* 2005), which shows an extraordinary wide range of parameter values, to a degree that the listed values are factually useless.

Table A.3-1. Compilation of some geomechanical parameters values from 45 different types of argillaceous formations (extract from Horseman *et al.* 2005; table 3.1)

Geomechanical parameter	Clay	Mudrock	All
Unconfined compressive strength, q_u [MPa]	0.15 - 4	5 - 77.5	0.15 - 77.5
Modulus of elasticity E [GPa]	0.2 - 22.9	0.11 - 900	0.11 - 900
Poisson's ratio ν	0.25 - 0.42	0.13 - 0.5	0.13 - 0.5
Tensile strength T_0 [MPa]	2	0.5 - 6.75	0.5 - 6.75
Shear strength [MPa]	0.04 - 500	0.21 - 1450	0.04 - 1450
Friction angle ϕ [°]	8 - 64	35 - 59.9	8 - 64
Cohesion c [MPa]	4.5 - 20	3.1 - 6.3	3.1 - 20

Instead, appropriate project-specific data sets are required, if applicable, with a differentiation for the various lithologic soil and rock units prevailing at the site. The latter approach was taken, for example, by Bock (2001; 2009) in comprehensive reviews of the numerous laboratory and field test data of the Opalinus Clay of the Mont Terri URL and by Dehandschutter (2004) in a compilation of the geotechnical properties of the Boom Clay. The resulting parameter values are compiled in Tables A.3-2 and A.3-3 for the Opalinus Clay and in Table A.3-4 for the Boom Clay. Reference is also made to Table 2-3 of the main text.

Table A.3-2. State and index parameter values of the Opalinus Clay of the Mont Terri URL
(after Bock 2009 supplemented by Vietor *et al.* 2006)

State / Index Parameter	Section in Bock (2009)	Symbol	Value	Stand. Dev.	[Unit]
Bulk Density	3.1	ρ	= 2 430	± 30	[kg/m³]
Bulk Density (dry)	3.2	ρ_d	= 2 330	± 50	[kg/m³]
Grain Density	3.3	ρ_s	= 2 700	± 20	[kg/m³]
Water content	3.4	w	= 6.4	± 1.0	[%]
Porosity	3.5	n	= 13.7	± 2.5	[%]
P-wave velocity	3.6	$v_{p\ //\ ss}$	= 3 350	± 150	[m/s]
		$v_{p\ \perp\ ss}$	= 2 620	± 150	[m/s]
S-wave velocity		$v_{s\ //\ ss}$	= 1 920	± 100	[m/s]
		$v_{s\ \perp\ ss}$	= 1 510	± 50	[m/s]
Dynamic Young's modulus	3.6	$E_{dyn\ //\ ss}$	= 22		[GPa]
		$E_{dyn\ \perp\ ss}$	= 14		[GPa]
Dynamic Poisson's ratio		$\nu_{dyn\ //\ ss}$	= 0.26		[-]
		$\nu_{dyn\ \perp\ ss}$	= 0.25		[-]
Atterberg Limits	3.7	w_l	= 38	± 5	[%]
		w_p	= 23	± 2	[%]
		P.I.	= 15	± 3	[%]
Carbonate content	3.8	C_{RCO3}	= 11	± 4	[%]
$CaSO_4$ content	3.9	C_{CaSO4}	= 0.26	± 0.05	[%]
Fracture toughness	3.10	$K_{IC\ //\ ss}$	= 0.53	± 0.09	[MN/m$^{1.5}$]
		$K_{IC\ \perp\ ss}$	= 0.12	± 0.03	[MN/m$^{1.5}$]
Bridgman pinch-off	3.11	$p_{mco\ //\ ss}$	= 13	± 9	[MPa]
In situ stress state (at an overburden of 250 m)	Vietor *et al.* (2006)	$\sigma_1 \approx \sigma_v \approx$ 6.5 MPa, sub-vertically $\sigma_2 \approx \sigma_H \approx$ 4.3 MPa, sub-horizontally, oriented 140° $\sigma_3 \approx \sigma_h \approx$ 2.2 MPa, sub-horizontally, oriented 050°			

Table A.3-3. Design values of the Opalinus Clay of the Mont Terri URL
(under ambient conditions with an overburden of 250 m; Bock 2009)

Design Parameter		Section in Bock (2009)	Recommended design value			
♦ Deformation parameters of isotropic rock model						
Tangent modulus		4.1.1	$E_{t\text{-}50}$	=	3	[GPa]
Unloading, reloading, Young's			$E_u = E_r = E$	=	7	[GPa]
Poisson's ratio			ν	=	0.29	[-]
♦ Deformation parameters of transverse isotropic rock model						
Tangent modulus		4.1.1	$E_{t\text{-}50\ 1}$	=	3	[GPa]
			$E_{t\text{-}50\ 2\ and\ 3}$	=	4	[GPa]
Unloading, reloading and Young's modulus			E_1	=	4	[GPa]
			$E_2 = E_3$	=	10	[GPa]
Poisson's ratio			ν_{23}	=	0.35	[-]
			$\nu_{12} = \nu_{13}$	=	0.25	[-]
Shear modulus			$G_{12} = G_{13}$	=	3.5	[GPa]
Bedding plane stiffness		4.1.2	k_n	=	8	[GPa/m]
			k_s	=	10	[GPa/m]
Steady-state creep		4.1.3	$\Delta\varepsilon / \Delta t$	=	$500 * 10^{-12}$	[s^{-1}]
♦ Strength parameters						
Unconfined compressive strength		4.2.1	$q_{u\ \perp ss}$	=	15	[MPa]
			$q_{u\ //\ ss}$	=	11	[MPa]
Unconfined tensile strength			$T_{0\ \perp ss}$	=	0.6	[MPa]
			$T_{0\ //\ ss}$	=	1.2	[MPa]
Mohr Coulomb shear strength	material	4.2.2	$c'_{//\ ss}$	=	4.0	[MPa]
			$c'_{\perp ss}$	=	3.0	[MPa]
			$\phi'_{//\ ss}$	=	23	[°]
			$\phi'_{\perp ss}$	=	22	[°]
	bedding planes		$c'_{bedding}$	=	0.8	[MPa]
			$\phi'_{bedding}$	=	21	[°]
Hoek & Brown material parameters			$m_{//\ ss}$	=	5 – 10	[–] (s = 1)
			$m_{\perp ss}$	=	1 – 5	[-] (s = 1)
Dilatation of material		4.2.3	$\delta_{\perp ss}$	=	$-2\,000 * 10^{-6}$	[-]
			$\delta_{//\ ss}$	=	$-4\,000 * 10^{-6}$	[-]
Dilatation angle			i	=	0 ± 2	[°]
♦ Permeability parameters						
Hydraulic conductivity		4.3	$K_{isotropic}$	=	$2 * 10^{-13}$	[m/s]
			$K_{\perp ss}$	=	$0.7 * 10^{-13}$	[m/s]
			$K_{//\ ss}$	=	$2 * 10^{-13}$	[m/s]

♦ Hydro-mechanically coupled parameters					
Compression index	4.4.1	C_c	=	0.020	[-]
Swelling strain index	4.4.2	$S_{\varepsilon \perp ss}$	=	7	[%]
		$S_{\varepsilon // ss}$	=	1	[%]
Swelling pressure		$p_{s \perp ss}$	=	1.2	[MPa]
		$p_{s // ss}$	=	0.6	[MPa]
♦ Thermal parameters					
Linear thermal expansion coefficient	4.5.1	heating	$\alpha_{\perp ss}$ =	$2.0 * 10^{-5}$	[K^{-1}]
			$\alpha_{// ss}$ =	$1.5 * 10^{-5}$	[K^{-1}]
		cooling	$\alpha_{\perp ss}$ =	$2.5 * 10^{-5}$	[K^{-1}]
			$\alpha_{// ss}$ =	$1.0 * 10^{-5}$	[K^{-1}]
Specific heat capacity	4.5.2	c	=	1 050	[$J * kg^{-1} * K^{-1}$]
Thermal conductivity	4.5.3	$\lambda_{\perp ss}$	=	1.2	[$W * m^{-1} * K^{-1}$]
		$\lambda_{// ss}$	=	2.2	[$W * m^{-1} * K^{-1}$]

Table A.3-4. Compilation of the averaged geotechnical parameter values of the Boom Clay in surface outcrops and at the HADES URF (Dehandschutter 2004)

Boom Clay Geotechnical Parameter		**At the surface**	**At depth of URF in Mol**
Bulk density (saturated) [kg/m³]		1 900	2 000 – 2 100
Water content w [%]		25 – 30	22 – 27
Total porosity		0.35	0.33
Atterberg limits	Liquid Limit w_l [%]	70	70 – 83
	Plastic Limit w_p [%]	25	25 – 28
	Plasticity Index P.I. [%]	45	58
Cohesion c [kPa]		150 – 200	600 – 1 200
Angle of friction ϕ [°]		18	10
Modulus of Elasticity E [GPa]		0.11 – 0.20 (?)	0.20 – 0.40 (?)
Poisson's ratio ν [-]		0.4	0.4
Shear modulus G [GPa]		0.40	?
Undrained shear strength [kPa]		170 – 200	2 000
Tensile strength T [kPa]		100 (?)	300 (?)
OCR (overconsolidation ratio)		not defined (as σ_v=0)	1 – 2
p'_c [MPa]		0.85	6

Common characteristics of the formations are their low hydraulic conductivity and their mineralogical composition. Qualitatively, the mineralogy of the formations at all sites is very similar except that the clay mineral content of the Callovo-Oxfordian is lower and its lithological variability in the vertical dimension is more pronounced when compared to the other formations (cf. also Mazurek *et al.* 2008).

The key differences in rock characteristics are related to the different burial depths. The Boom Clay represents a normal-consolidated plastic clay with high porosity, low strength and insignificant mechanical anisotropy. The Callovo-Oxfordian and the Opalinus Clay were subjected to a deeper burial, which is reflected by a higher degree of consolidation and a more pronounced anisotropy of a number of geomechanical and transport parameters. This is particularly the case for the Opalinus Clay in the Zürcher Weinland with a maximum burial depth of 1600-1700 m, leading to a comparatively low porosity and marked signs of over-consolidation (e.g. distinct bedding, marked anisotropy in elastic properties and strength).

A.3.3 Strength properties and understanding of fracturing

For considerations on self-sealing in argillaceous media, the strength properties are of particular concern as they are closely linked to fracturing and failure and thus to permeability and self-sealing.

A.3.3.1 Terminology

Experience has shown that the terminology used in discussions of rock 'strength' and 'failure' can cause confusion. In this report, the terminology and meanings are used as outlined in Table A.3-5.

Table A.3-5. Terminology on strength, fractures and some associated terms

Term	Definition	Comment
(Peak) Strength	Maximum stress level which the material can sustain without failing	One of the principal material properties in engineering design
Failure	Loss of the material's capability to adequately support the forces applied to it or otherwise fulfil its engineering function	Failure might be by exceeding a stress condition ('brittle failure') or a strain condition ('ductile failure')
Post-failure	State of a material after failure	the failed material may still have some load-bearing capacity.
Failure criterion	Stress or strain relationship characterising the occurrence of failure in the material	The criterion is either theoretically or empirically derived
Brittle failure	Mode of failure with a subsequent (often sudden) loss of strength	Associated with "strain-softening" material behaviour
Ductile failure	Mode of failure with excessive deformation resulting in a loss of engineering function	Associated with "strain-hardening" material behaviour
Rupture	Stage in the development of a fracture where instability occurs	Synonymous with violent (brittle) failure.

Fracture	Planes of separations in a solid material	-
Crack	Partial fracture, with some parts still cohering	Usually of little extent
Fracturing	Process of the formation of fractures. It involves the breaking of cohesive bonds to form new surfaces.	The onset of fracturing is not necessarily synonymous with failure or with the attainment of peak strength
Tension fracture	Brittle fracture in a tensile stress field with minor principal effective stress $\sigma_3' < 0$	whether or not a tensile fracture progresses into a tensile failure depends on energy considerations
Extension fracture	Brittle fracture in a compressive stress field with major principal effective stress $\sigma_1' >> 0$	only occurring at relatively small σ_3' values ≥ 0
Shear failure	Mode of failure, characterised either by the development of a discrete shear plane or of abundant shear planes in the material	A discrete shear plane is often developing after the formation of numerous extension fractures
Discontinuity	Generic term for all types of fractures and failure planes which are mechanically relevant	The term includes geotechnical as well as geologic (refer to Section A.4.1) fracture and failure planes.

A.3.3.2 Brittle and ductile behaviour

Figure A.3-4 shows a number of standard tests on cylindrical rock samples indicating the types of fractures which may develop in axial-symmetric loading. The sample may be laterally unconfined (Types A and B) or supported by a uniform effective confining pressure $\sigma_3' > 0$ (Types C and D). Figure A.3-5 shows schematically the corresponding stress-strain curves recorded in the axial loading tests depicted in Figure A.3-4. The failure modes A, B and C in Figure A.3-4 with associated stress-strain responses (A, B and C in Figure A.3-5) commonly exhibit the existence of a peak stress and post-peak strain softening. Such behaviour is commonly termed 'brittle' (Jaeger and Cook 1976).

Figure A.3-4. Types of failure and fractures in cylindrical rock sample in axial-symmetric loading (after Mandl 2005)
A. Tension failure – B. Extension fracture – C. Shear failure - D. Multi-shear failure

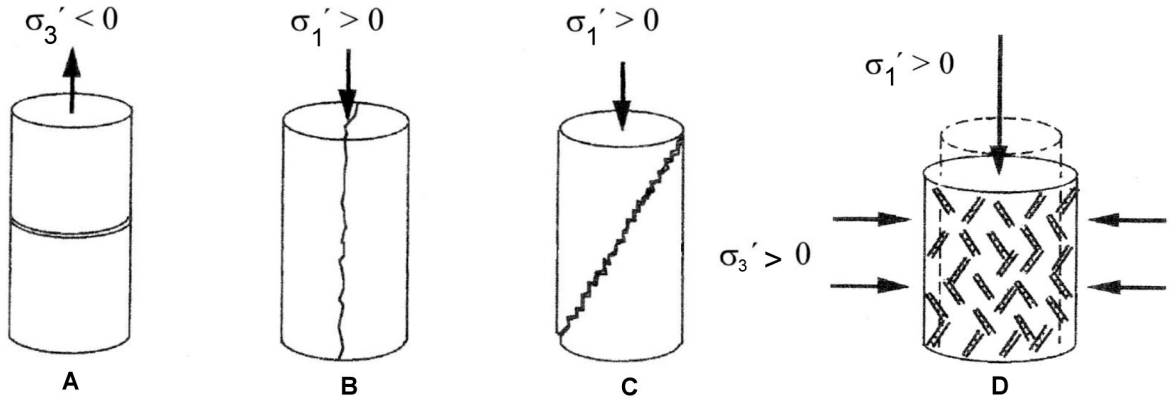

Figure A.3-5. Typical stress-strain response of tests shown in Figure A.3-4

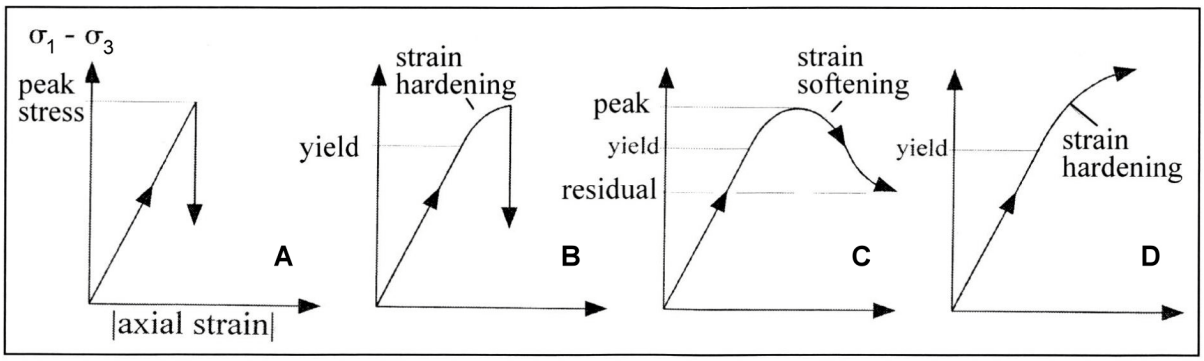

Mandl (2005) pointed out that there is a further characteristic of a brittle material of equal importance to the peak stress and post-peak strain-softening characteristics. This characteristic is the rate independence of the pre- and post-peak deformation and fracturing processes. It is evident that any inelastic deformation and fracturing of a brittle material observed at the macroscale must somehow be reflected by deformation and fracturing processes that operate at the microscale. Amongst typical rate-insensitive processes at the microscale are the breakage of intergranular bonds, the abrasion, breakage or crushing of grains, frictional intergranular sliding, reorientation of grains, the growth of microcracks, and the associated volume dilation. Brittle behaviour can therefore be defined as follows (Mandl 2005, p. 8):

> "A macroscopic deformation process is 'brittle' in a general sense if it is rate-independent and demonstrates strain-softening in the post-peak region".

In this definition, it is of little relevance whether the post-peak softening occurs as a sudden rupturing and complete loss of strength or as a more gradual reduction of the material strength to a residual level.

The schematised stress-strain curves of Figure A.3-5 B and D comprise certain sections which, beyond an ill-defined stress level ('yield point') indicates that the sample can withstand a further increase in load whilst deforming at a higher rate than in the linear-elastic region. This behaviour is generally known as 'strain-hardening' and associated with the term 'ductile'. Ductility refers to a rate-sensitive deformation process associated with 'viscous' flow, creep and stress relaxation phenomena (Mandl 2005). At the micro scale, ductile deformations result from diffusive transport processes inside the grains, along grain boundaries, or through the porewater, pressure solutions and intra-crystalline plasticity.

The distinction between rate-insensitive ('brittle') and rate-sensitive ('ductile') behaviour strictly pertains to the deformation process itself and not to the state or environmental conditions under which the deformation takes place. A sample of argillaceous material, for instance, which deforms in a brittle manner in triaxial testing at room temperature, can be made to deform in a ductile mode by increasing the confining pressure and/or the temperature. Thus one and the same material can deform either way, in a brittle or in a ductile mode, depending on the actual testing conditions ('brittle – ductile transition'; Table A.3-6). Argillaceous materials are particularly sensitive to testing conditions and in their deformational behaviour often subject to brittle-ductile transitions.

Table A.3-6. Factors affecting the brittle vs. ductile behaviour of argillaceous media

Influencing factor	Trend towards	
	.... brittle behaviour ...	... ductile behaviour ...
Confining pressure p_c	... if p_c low	... if p_c high
Temperature T	... if T low	... if T high
Pore pressure u	... if u high	... if u low
Water content w	... if w low	... if w high
Degree of induration D	... if D high	... if D low
Strain rate dε/dt	factor negligible	factor important

A.3.3.3 Fracture and failure in argillaceous rock

Reference is made to the four simple test configurations, as shown in Figure A.3-4, with the view to discuss the resulting fractures in some more detail.

Tension fracture and failure (A in Figure A.3-4)

Tension fractures form and open *perpendicular* to the direction of the *minor* principal effective stress σ_3' (with $\sigma_3' < 0$) when the magnitude of σ_3' approaches a critical tension value:

$$\sigma_3' \rightarrow -T_0 \qquad \text{(A.3-1)}$$

The fracture plane is a *brittle tension fracture* and the critical value T_0 the tensile strength of the material at zero confining pressure.

As simple as the concept of direct tensile testing appears to be, the experimental determination of the uniaxial tensile strength in the so-called '*direct* tensile test' is far from trivial as it requires cumbersome sample preparation and a sophisticated testing set-up[26]. Moreover, it produces test data with considerable scatter.

For a long time the direct tensile test has raised fundamental questions on the mechanics of fracturing in brittle materials. In considering fracturing as the breaking of interatomic bonds of a material across a continuous fracture plane, the theory of interatomic forces suggest that the interatomic cohesive strength σ_m should be about ⅓ of the Young's modulus E (Fairhurst 1972):

Interatomic bond theory:

$$\sigma_m \approx E / 3 \qquad \text{(A.3-2)}$$

That theoretical σ_m value, however, is orders of magnitude larger than actually observed in macroscale tensile testing. For the Opalinus Clay of Mont Terri, for instance, Table A.3-3 reveals the following values:

[26] This is significantly in contrast to the *indirect* ('Brazilian') tensile test

Macroscale: Example Opalinus Clay Mont Terri:

$$T_0 \approx E / 3\,000 \qquad \text{(A.3-3)}$$

where: T_0 = 2MPa and E = 6 GPa

The hypothesis of Griffith (1921) is an attempt to explain the obvious discrepancy. It postulates the existence of numerous sub-microscopic cracks which are ubiquitously distributed throughout an otherwise homogeneous, isotropic elastic material *('Griffith cracks')*. Based on that assumption Griffith advanced the hypothesis that the applied effective tensile stress σ_3' produces intense local stress concentrations at the tips of the cracks. Thus locally acting stresses might be high enough to initiate an extension of the crack even at moderate average stress levels. Whether or not crack extension will progress and may finally lead to a complete separation (i.e. failure) of the test sample is a function of the energies involved in that process[27]. Though not widely used in practical geo-engineering problems, the Griffith's energy instability concept has formed the basis of the relatively new science of fracture mechanics.

The set-up of Test A shown in Figure A.3-4 is that of a uniaxial tensile test. Some ideas of the effective confining pressure σ_2' and σ_1' that would still allow tensile fractures to develop may be obtained from an extension of the Griffith theory to compressive stress states (Griffith 1924). According to that theory, the limiting confining pressure for the formation of tensile fractures is 3 T_0. Applying a tensile load to a specimen under a higher confining pressure would produce shear failure without the tensile stress reaching the tensile strength. Thus the conditions for tensile fracturing are:

$$\sigma_3' = -T_0 \qquad \text{(under the condition of } \sigma_2' = \sigma_1' < 3\,T_0\text{)} \qquad \text{(A.3-4)}$$

Note that the first condition ($\sigma_3' = -T_0$) is purely empirical whereas the second one ($\sigma_2' = \sigma_1' < 3\,T_0$) is purely theoretical as it was derived for an ideal fracture shape.

Extension fracture (B in Figure A.3-4)

Extension fractures form *parallel* and open perpendicular to the direction of the *major* principal effective stress σ_1' (with $\sigma_1' > 0$) when the magnitude of σ_1' approaches a critical compression value:

$$\sigma_1' \rightarrow q_u \qquad \text{(A.3-5)}$$

The fracture plane is a *brittle extension fracture* and the critical value q_u the compressive strength of the material at zero confining pressure. Extension fractures have identical morphologies (surface roughness; plumose structures; Bankwitz *et al.* 2000) as tensile fractures.

Extension fractures are basically understood as being initiated at the microscale by compression-induced local tension stresses inside a specimen. Figure A.3-6 illustrates four such mechanisms A to D as follows (out of Mandl 2005):

[27] The following three energy terms are identifiable: (1) potential energy of the applied tensile load; (2) strain energy of the loaded sample and (3) surface energy of the crack surfaces

Figure A.3-6. Schematised brittle micro-mechanisms capable of generating localised tensile stresses for the formation of extension fractures
(from Mandl 2005)
(Reprinted with kind permission of Springer Science and Business Media and the author)

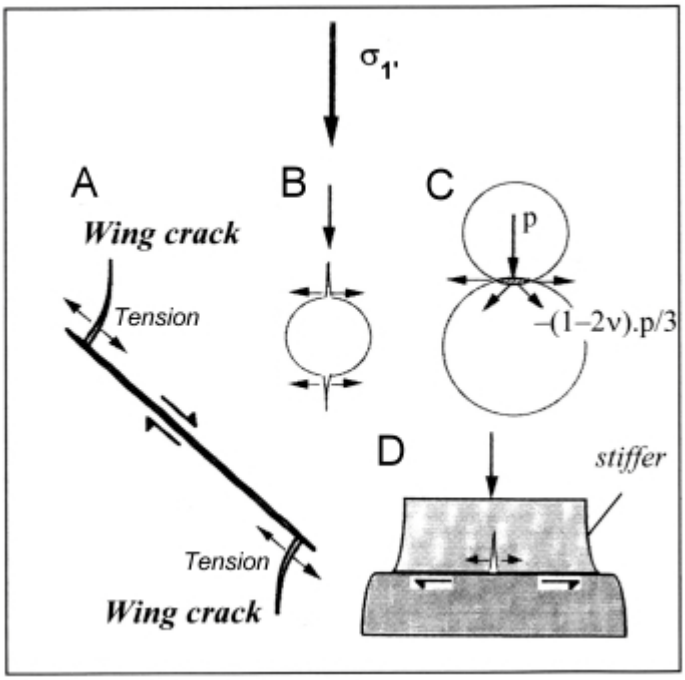

Mechanism A: 'Wing crack' model

This is the mechanism which is favoured by most theoreticians. It derives from the modified Griffith theory (1924) for compression which was subsequently enhanced by Brace and Bombolakis (1963) and Hoek and Bieniawski (1965). The model considers a crack which is inclined with respect to the remote major effective compressive stress σ_1'. Contrary to what might be expected, the shear crack will not propagate in its own plane when σ_1' is raised, but will develop 'wing cracks' at the receding sites near the crack tips. At these locations, the crack wall-parallel tensile stress attains its highest value and can produce tensile fractures when the remote σ_1' is sufficiently raised. The wing cracks grow in a stable manner requiring progressively higher σ_1' and tend to align themselves parallel to the direction of the remote compressive stress σ_1'.

Mechanism B: Void model

The presence of a spherical or elliptical hole in an elastic continuum under remote uniaxial compressive stress σ_1' will cause wall-parallel (tangential) tension at the points of the cavity wall which are aligned in direction of σ_1' (B in Figure A.3-6; refer also to the Kirsch solution and the EDZ development in Section A.4.2.3). Again, tensile cracks will start growing in a stable manner when the remote σ_1' is progressively raised.

Mechanism C: Grain contact model

If two elastic spheres (as a model of e. g. rounded mineral grains) are pressed together, contact pressures will develop which will be highest at the centre of the contact area (solution of Hertz 1881). The stress distribution within the spheres is such that there is a shear stress component in outward direction from the centre axis (C in Figure A.3-6) thus generating tensile stresses perpendicular to the axis.

Mechanism D: Elastic mismatch model

Case D of Figure A.3-6 depicts a stiffer body which is in contact with a weaker body along a common interface. Most sensitive to mechanism D are interface planes which are oriented normal to the remotely acting compressive stress σ_1'. In loading, the weaker body has the tendency to extend further in the lateral direction than the stiffer body but bonds or contact friction will prevent slippage along the plane. This will induce shear stresses in the interface and will put the stiffer layer under tension which, at increasing loads, will eventually produce a tensile fracture progressing from the interface into the body of the stiffer layer.

The tensile fractures of all cases, A to D, have in common that they grow in a stable manner under a progressively increasing compressive load, and align, in a statistical sense, along the direction of the compressive stress σ_1'. At some stress level, some fractures may become interlinked, which will localise the progress of fracturing and produce, finally, macroscopic extension fractures (see below).

Theoretical and experimental results show that the propagation of tensile microfractures and, consequently, the formation of macroscopic extension fractures parallel to the imposing compressive stress σ_1' are completely suppressed by confining pressures $p_c = \sigma_3$' if they amount to more than a few percent of σ_1'.

Amongst the geological and geotechnical features which are commonly considered to be typical extension fractures are spalling of borehole and tunnel walls and surface-parallel exfoliation fractures.

Shear failure (C in Figure A.3-4)

Even taking into account that, in brittle regimes, extension fractures are pervasive, they do not yet constitute a viable failure mechanism. In this regard Figure A.3-7 depicts three potential alternatives. Possibly the most common failure mode is Mode (2) in Figure A.3-7, i.e. linkage of extensional fractures with shear cracks to form a macroscopic composite failure plane (ref. also to Figure A.3-8). In fact, the formation of such a plane is a highly complex process and various micro-mechanical models have been suggested. One of the insights is provided by the studies of Lockner and Madden (1991). They considered the growth of horizontal, vertical and diagonal (45°) cracks in a biaxially stressed (σ_1', σ_2') plate, and found that under low effective confining pressure σ_2', the crack growth is predominately parallel to the direction of the effective major principal stress σ_1', but at higher confining pressures σ_2', the domination is on the growth of diagonally inclined cracks. The complexity with which composite shear/extensional failure planes may develop in argillaceous rocks was impressively evidenced in one of the EDZ self-sealing experiments carried out in the Mont Terri URL (Figure A.3-9).

Figure A.3-7. Alternative failure mechanisms of extension-fractured samples in uniaxial compression (from Bock 1980b)
(1) Kinking - (2) Linkage with shear cracks with development of composite shear failure plane(s) - (3) Coalition of extension cracks with the formation of local wedges and subsequent disintegration (crumbling) of the material

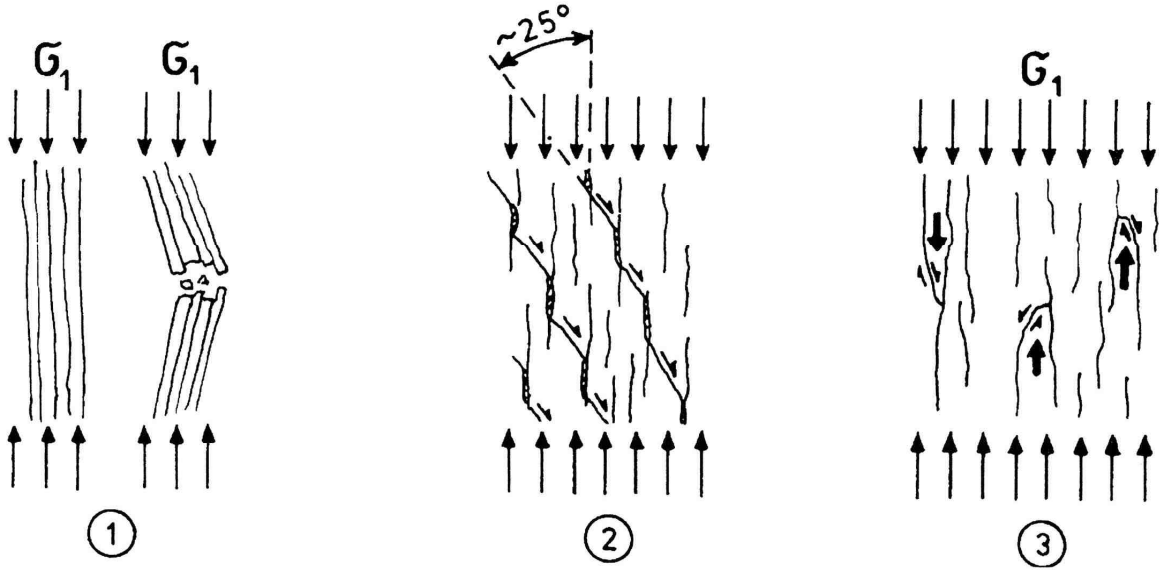

Figure A.3-8. Coalescence of extensional cracks (Boom Clay sample)
(from Dehandschutter 2004)

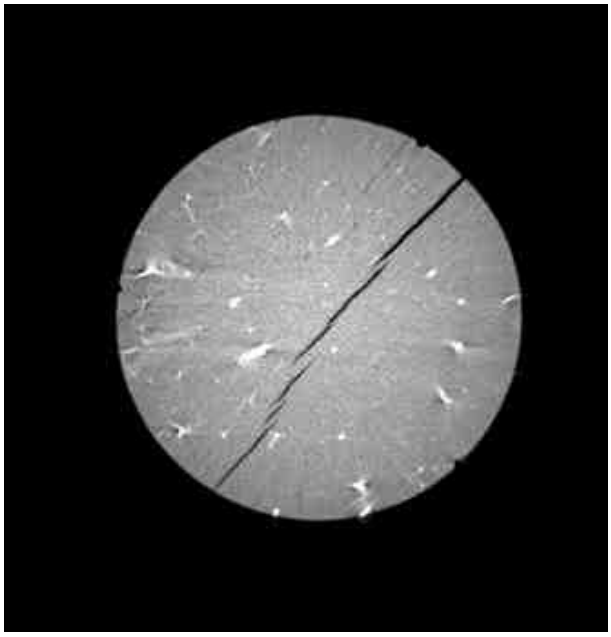

Figure A.3-9. Example of an off-balance fracture growth pattern in a hydraulic fracturing experiment at Mont Terri URL (from Daneshy *et al.* 2004)

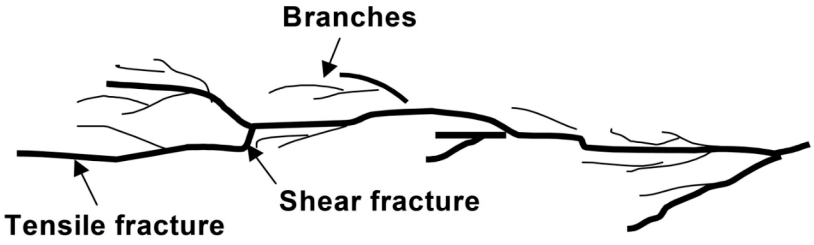

In the following some experimental and numerical evidence is compiled to elucidate the above failure mechanism in some more detail.

Experimental Evidence (Hallbauer et al. 1973)

In rock testing, the stress-strain curve (and also the lateral strain ε_{lat} vs. axial strain ε_{ax} curve) can be subdivided in several characteristic regions as outlined in the classical paper of Hallbauer *et al.* (1973). In that study an argillaceous quartzite sample was tested in triaxial compression (Figures A.3-10 and A.3-11). The respective regions can be described as follows:

Region I is marked by the closure of those pre-existing cracks which are oriented normal or inclined to the direction of the major principal stress σ_1'. This is manifested in a slightly convex upward path of the stress-strain curve.

Region II is characterised by an approximately linear elastic behaviour.

Region III is characterised by crack growth and sliding along pre-existing crack interfaces and the occurrence of first local extensional micro-fractures, predominately in the central portion of the specimen. Volume change turns from contractant to dilatant behaviour ('damage' or 'dilatancy threshold' σ_{dam}; Zhang and Rothfuchs 2008).

Figure A.3-10. Idealised complete axial stress σ_{ax} – axial strain ε_{ax} curve (top) and axial strain ε_{ax} – lateral strain ε_{lat} curves (bottom) (out of Hallbauer *et al.* 1973)

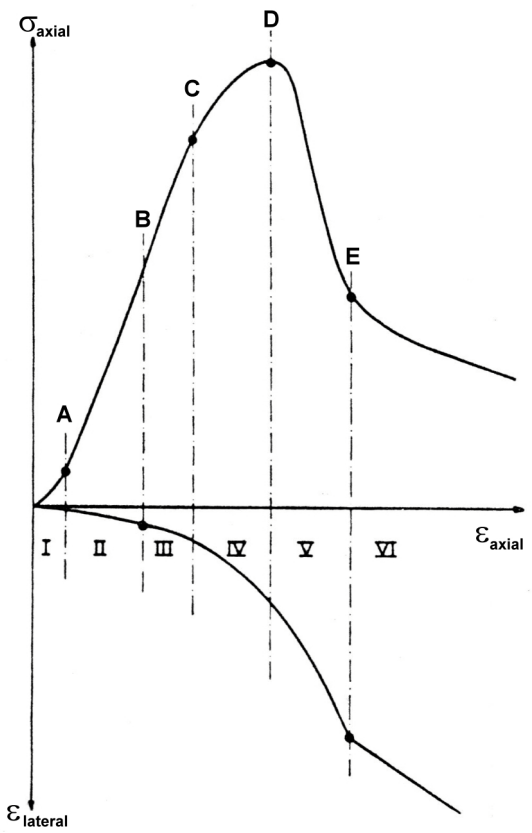

Region IV shows a drastic increase in the micro-crack density right up to the peak strength of the specimen. As in Region III, the micro-cracks are predominately extensional and oriented in axial direction. On reaching the peak strength, a macroscopic failure plane develops in the central portion of the specimen by step-wise joining of the extensional micro-cracks. The plane progresses from the centre towards one or both ends of the specimen. In addition to this, relatively large cracks appear near mid-height and approximately parallel to the free sides of the sample, leading to the formation of some rock chips ('spalling'). Immediately prior to the peak strength σ_F at about $\sigma_P \approx 0.9\ \sigma_F$ there might be a 'percolation threshold' σ_P at which the permeability increases drastically up to several orders of magnitude (Zhang and Rothfuchs 2008).

Region V is characterised by the formation of distinct macroscopic failure plane(s) ('shear localisation'). After the preceding phases of micro-fracturing and fracture coalescence, damage concentrates into a complex shear zone, angled typically at 20 – 30° to the axial load direction. The angle tends to increase with increased confining pressure.

Region VI is characterised by continuous sliding along the macroscopic failure plane associated with increasing deterioration and crushing of the rock fragments in the Mode (3) of Figure A.3-7. The final result is a loose mass of broken material.

Figure A.3-11. Axial sections through the specimens stopped at various stages of the compression test of Figure A.3-10 to show micro-crack and shear band development
(after Hallbauer *et al.* 1973). Note: σ_{max} = peak strength of the sample

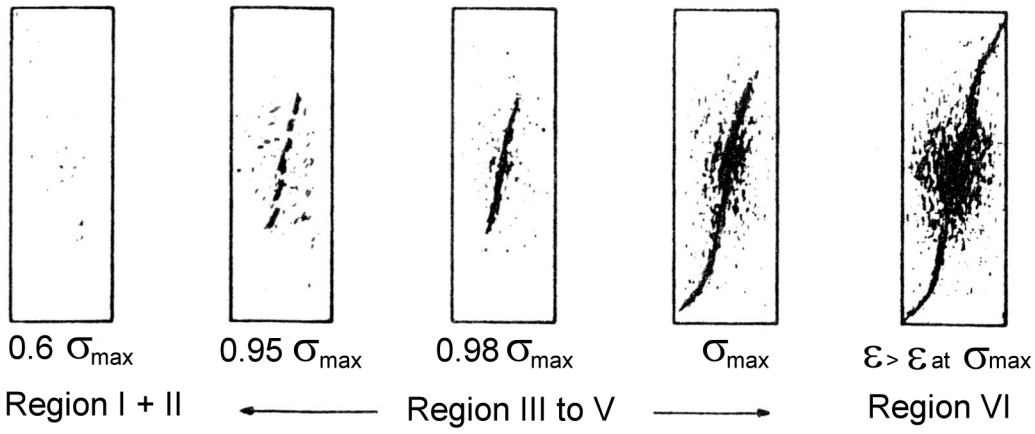

Experience has shown that for argillaceous rocks the damage threshold σ_{dam} in unconfined compression testing is of the following order of magnitude (Blümling 2005):

$\sigma_{dam} \approx 0.8$ to $0.9 * \sigma_{peak}$ (Opalinus Clay)

$\sigma_{dam} \approx 0.9 * \sigma_{peak} - 13$ MPa (Callovo-Oxfordian – carbonate rich)

$\sigma_{dam} \approx 0.6 * \sigma_{peak} - 2$ MPa (Callovo-Oxfordian – clay rich)

In a recent experimental study, based on triaxial tests with ultrasonic velocity measurements of Opalinus Clay, Popp and Salzer (2007) distinguished between a lower "initial damage boundary" (≈ 0.5 to $0.6 * \sigma_{peak}$) and a higher "dilatancy boundary" (≈ 0.8 to $0.9 * \sigma_{peak}$).

The development of discrete shear planes, as described above and shown in Regions IV and V of Figure A.3-11, is termed "shear-banding" and subject to intensive ongoing research. A more recent experimental study is shown in Figure A.3-12.

Numerical Evidence: Shear-banding and PFC Modelling

Research on the shear-banding problem is particularly intense in numerical modelling. For instance, within the frame of the SELFRAC project (Bernier *et al.* 2004), an important progress has been achieved in terms of the fracturing process modelling. The strain localisation analysis, studied for more than 20 years for mono-phase materials, was extended to a coupled hydromechanical analysis. The CLoE model, implemented within the finite element code LAGAMINE, has been calibrated for Boom Clay and Opalinus Clay on the basis of laboratory test results. Numerical simulations showed that such a theoretical framework is capable of fully describing the hydromechanical behaviour of the material, including the occurrence of localised deformation and related local drainage phenomena.

Figure A.3-12. Number of tensile and shear cracks developing in course of a complete unconfined compression test (top) and their locations within the tested sample (bottom)
(schematised after Diederichs 2003)

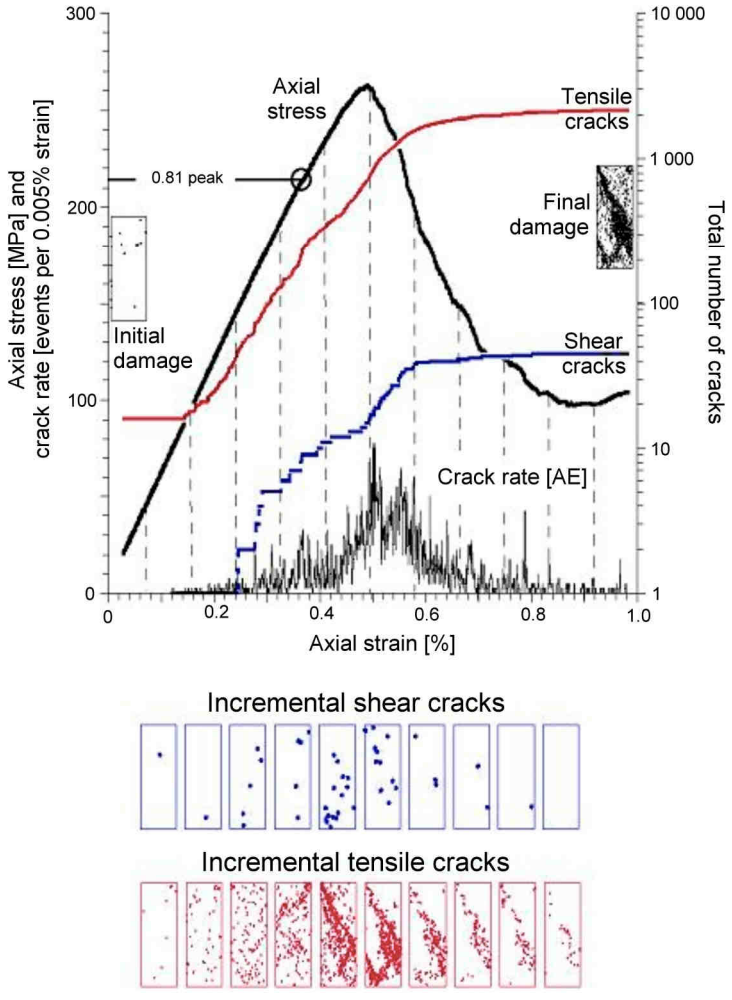

Another numerical study, in which shear banding could be reproduced, is the investigation on the micro-mechanical behaviour of the Opalinus Clay (Bock *et al.* 2006). The numerical model, established as part of the studies, was based on the Particle Flow Code (PFC) developed by Itasca Corp. The pertinent composition and structure of the Opalinus Clay, as established in the local engineering geology of Switzerland, were introduced into the model such as elongated clay platelets, various layers of densified water around the platelets, free water in the pores and the specific anisotropic texture of the platelets due to compaction. The model was numerically subjected to a series of loading stages.

Figure A.3-13. Numerical study on the micro-mechanical behaviour of the Opalinus Clay
(from Bock *et al.* 2006, p. 205): Normalised stress-strain curve (top) and stages of crack development in the sample (bottom).
(I). Cracks developing within the respective stress-strain intervals A to F
(II). Accumulated cracks. Note the tendency for shear band development.
(Reprinted with kind permission from Springer Science and Business Media)

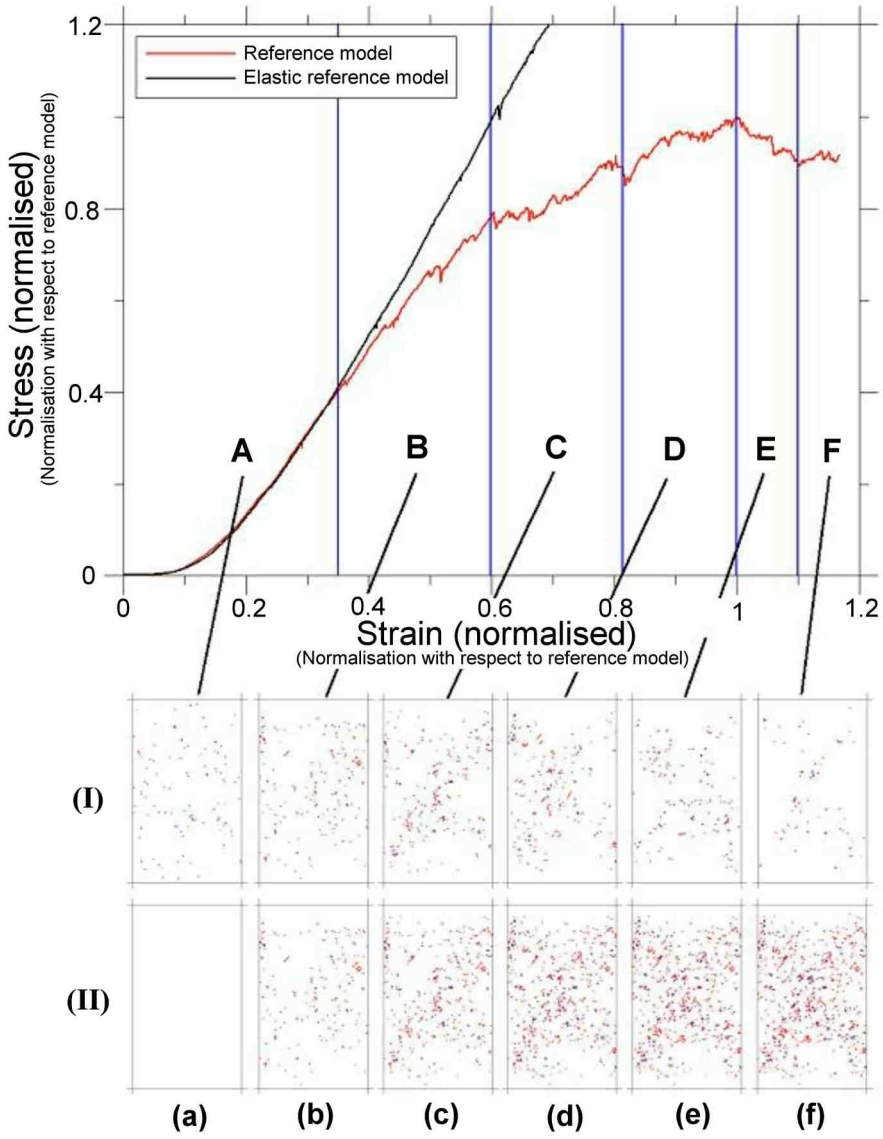

The model reproduced a number of interesting features, in particular (Figure A.3-13):

- at the micro scale, the deformation of the sample is distinctively inhomogeneous;
- when the axial stress reaches a level of about 40% of the peak strength, there is an onset of micro-mechanical damaging which incorporates both shear and tension cracks (Figure A. 3-13 bottom; Stages b and c). Initially, the damage occurs throughout the sample area. Close to the peak strength, cracking is progressively clustering along distinct shear bands (Figure A.3-13, Stages d to f); and
- there is, simultaneously, a breakage of bonds as well as the formation of new contacts during the course of loading. In the pre-failure range the number of newly formed bonds exceeds that of the broken ones whereas in the post-failure range it is the reverse.

Multi-shear failure (D in Figure A.3-4)

In ductile deformation regimes (Table A.3-6) a network of shear fractures is developing, accompanied by plastic deformation and strain hardening (D in Figure A.3-4). In this case, failure is commonly defined as the excess of a certain deformation threshold value at which the material looses its engineering function. In the test, failure is typically manifested by excessive sample bulging which, in fact, is an artefact of the test due to the friction between sample and load platens of the testing machine.

Shear fractures are pervasively distributed throughout the sample. Micro-mechanically, a distinction can be made between 'cataclastic flow' and 'dislocation glide':

- *'Cataclastic flow'* is a "semi-brittle" process (Mandl 2005; p. 8), where deformation occurs through the disaggregation of grains into successively smaller pieces (the process of 'cataclasis'). Whilst in shear localisation, this deformation concentrates into discrete shear bands it is, in cataclastic flow, pervasively distributed throughout the sample.
- *'Dislocation glide'* is a ductile process in which the dominant micro-mechanical process involves internal distortion of crystalline grains as a result of slippage along crystallographic planes. Dislocation motions maintain perfect crystalline structures which, macroscopically, yields isovolumetric conditions.

In both cases, two sets of failure planes are developing macroscopically ('conjugate failure planes'), and the acute angle between the two sets is bisected by the direction of the major principal effective stress σ_1'. The volume change, associated with the formation of the conjugate failure planes, is (slightly) negative (i. e. volume increase) for the 'cataclastic flow' type and zero, if not slightly positive (i. e. volume decrease = contractant), for the 'dislocation glide' deformation type.

A.3.4 Strength criteria[28]

"A strength criterion is a relation between stress components which will permit the strengths developed under various stress combinations to be predicted" (Brady and Brown 1985: 105). The general engineering form of the peak strength criterion therefore is:

$$\sigma_1 = f(\sigma_2, \sigma_3). \qquad \text{(A.3-6)}$$

For a general theoretical formulation of some of the most important strength criteria[29] in terms of stress space, octahedral normal (volume) stress σ_{oct} and shear (deviatoric) stress τ_{oct}, refer to Jaeger and Cook (1976) and Chen and Mizuno (1990).

Table A.3-7 provides an overview of the strength criteria which have been applied to various types of fractures and failures in argillaceous media delineated in Section A.3.3.3. From inspection of Table A.3-7 it immediately becomes evident that there does not exist a single criterion which is applicable to all possible loading and stress scenarios in the different types of argillaceous media.

Table A.3-7 Strength hypotheses applicable to failures and fractures in argillaceous media
(as outlined in Section A.3.3.3)

Type		Failure Hypothesis		Section
A (tensile)		Maximum normal stress theory: $\sigma_3' = -T_0$ Griffith's (1921) energy criterion for the propagation of fractures		A.3.4.1
B (extensional)	Wing crack	Griffith (1924) for fractures in compression	in combination with maximum normal stress theory	A.3.4.2
	Void model	Kirsch solution		
	Grain contact	Hertz solution		
	Mismatch	numerical modelling		
C (discrete shear)		Mohr-Coulomb criterion		3.4.3 a
		Hoek and Brown criterion		3.4.3 b
D (multi-shear)		Critical State concept and Cam-Clay model		3.4.4

A.3.4.1 Maximum normal stress criterion

In geologic repository design of argillaceous media, the maximum normal stress theory is applicable e.g. for hydraulic and pneumatic (gas) fracturing and possibly for spalling of some parts of the excavated underground opening and of boreholes under the action of porewater pressures. The Griffith energy criterion provides a theoretical frame for the progression and extent of the fractures.

[28] Depending on the scope, various terms are in use, such as 'strength criterion', 'peak or residual strength criterion', 'failure criterion' or even 'fracture criterion'. For this refer to the terminology of Table A.3-7.

[29] Amongst the generalised strength criteria are those of Tresca (1868), von Mises (1913), Mohr-Coulomb (1900), Drucker and Prager (1952) and Lade and Duncan (1975).

A.3.4.2 Extensional fracturing criteria

In geologic repository design of argillaceous media, the various theories for the generation of extensional fractures are of importance in association with the shear failure theories (see below). As shown before, extensional fractures as such do not constitute a viable failure mechanism. However, they are important as they are pervasive throughout the stressed area under consideration, thus changing its material characteristics and structure, and stimulating the occurrence of composite extensional/shear failures.

A.3.4.3 Shear failure criteria

In geologic repository design of argillaceous media, there are various theories applicable for discrete shear failures. The most commonly used criteria are those of Mohr-Coulomb, Hoek and Brown and the Cam-Clay model within the Critical State concept. The former two are commented as follows, whilst the Cam-Clay model is discussed in A.3.4.4.

Shear strength criterion after Mohr-Coulomb

In geomechanics this is one of the most common strength criterion:

$$\tau = c + \sigma_n \tan \phi \qquad \text{(A.3-7)}$$

where: c = cohesion
ϕ = angle of friction

The Mohr-Coulomb criterion can be considered as a linear approximation of the limiting conditions of all possible stress states at which the strength of the material is exceeded. The limiting conditions can be graphically represented in the Mohr- (τ-σ) diagram (Figure A.3-14, left), or alternatively in the principal stress (σ_1-σ_3) diagram (Figure A.3-14, right).

Figure A.3-14. Alternative graphical representation of the Mohr-Coulomb peak strength criterion: (a) Left: Mohr diagram (b) Right: Principal stress diagram

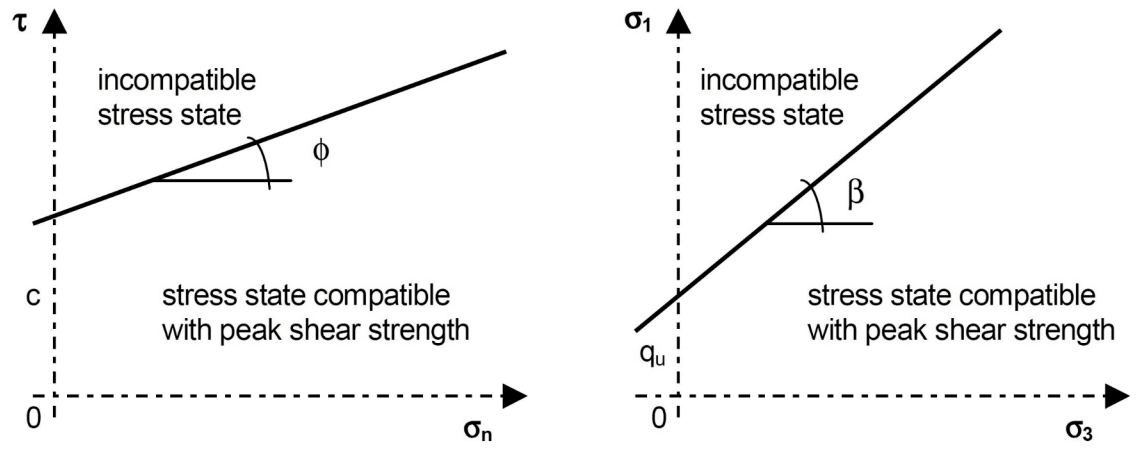

The limiting conditions of the two diagrams can be related by the following transformation equations (Brady & Brown 1985: 105 ff):

$$\sin \phi = (\tan \beta - 1) / (\tan \beta + 1) \qquad \text{(A.3-8)}$$

$$c = q_u * (1 - \sin \phi) / (2 * \cos \phi) \qquad \text{(A.3-9)}$$

or

$$\tan \beta = (1 + \sin \phi) / (1 - \sin \phi) \qquad \text{(A.3-10)}$$

$$q_u = 2\, c * \cos \phi / (1 - \sin \phi) \qquad \text{(A.3-11)}$$

where: ϕ = angle of inclination of the strength line in the τ / σ diagram (= angle of friction)
c = intercept of the strength line with the τ-axis in the τ / σ diagram (= cohesion)
β = angle of inclination of the strength line in the σ_1 / σ_3 diagram
q_u = intercept of the strength line with the σ_1-axis in the σ_1 / σ_3 diagram (= unconfined compressive strength)

The arguments in favour of the Mohr-Coulomb criterion are its wide-spread use in geomechanics, its relative simplicity, its implementation in all pertinent geotechnical computer codes and its proven suitability for indurated argillaceous media.

The main argument against the Mohr-Coulomb criterion is that its linear approximation is often not a good enough fit of the experimental strength data. Moreover, it clearly fails to adequately characterise the strength and fracture patterns of the extensional and tensile regions. Against this background non-linear strength curves have been proposed, for instance by Hoek and Brown (see below). These arguments against the use of the Mohr-Coulomb criterion, however, are not anymore convincing as contemporary computer codes (e.g. FLAC, PLAXIS) can accommodate any non-linearity by defining step-wise linear failure boundaries and a 'tension cut-off'.

Strength criterion after Hoek-Brown

The Hoek and Brown (1980) strength criterion was originally developed to provide an input for the design of underground excavations in rocks. In its original form it reads:

$$\sigma_1' / q_u = \sigma_3' / q_u + [m * \sigma_1'/\sigma_3' + s]^{1/2} \qquad \text{(A.3-12)}$$

$$T_0 = q_u / 2\, [m - (m^2 + 4\, s)^{1/2}] \qquad \text{(A.3-13)}$$

where: q_u = unconfined compressive strength of the intact rock
T_0 = unconfined tensile strength of the rock mass
m and s = material constants (s = 1 for intact rock)

Analysis of published strength data suggests that the factor m increases with rock type in the following general way (Brady and Brown 1985):

m = 7 "for carbonate rocks with well developed crystal cleavage (dolomite, limestone, marble)"

$m = 10$ "for lithified argillaceous rocks (mudstone, siltstone, shale, slate)"

$m = 15$ "for arenaceous rocks with strong crystals and poorly developed crystal cleavage (sandstone, quartzite)"

.....

$m = 25$ "for coarse-grained polymineralic igneous and metamorphic rocks (amphibolite, gabbro, gneiss, granite, norite, quartz-diorite)".

Table A.3.8 provides the actual Hoek & Brown strength parameters of the Callovo-Oxfordian argillite of the Bure URL.

Table A.3-8. Hoek & Brown strength parameters for Callovo-Oxfordian argillites
(Andra 2005d)

Callovo-Oxfordian argillite		**S**	**m**	**q_u [MPa]**
Upper carbonated layers	Lower values	0.374	1.5	33.5
	Mean values	0.734	2.0	33.5
Lower layers	Lower values	0.128	2.0	33.5
	Mean values	0.430	2.5	33.5

In subsequent years, the Hoek and Brown criterion was modified several times (Hoek and Marinos 2007). Significantly, it became empirically linked to geological observations and classification systems such as the Rock Mass Rating, RMR (Bieniawski 1973) and the Geological Strength Index, GSI (Hoek 1994). The "generalised Hoek and Brown criterion" reads as follows (Hoek *et al.* 2002):

$$\sigma_1' = \sigma_3' + q_u \, [m_b * \sigma_3'/q_u + s_m]^{\,a} \qquad \text{(A.3-14)}$$

where the factor m_b extrapolates the intact rock constant m_i to the rock mass by:

$$m_b = m_i * \exp [(GSI - 100) / (28 - 14D)] \qquad \text{(A.3-15)}$$

where: GSI = Geological Strength Index (Hoek 1994)
D = rock mass disturbance factor (undisturbed $0 \le D \le 1$ disturbed)
s_m and a = rock mass characteristics constants as defined as follows:

$$s_m = \exp [(GSI - 100) / (9 - 3D)] \qquad \text{(A.3-16 a)}$$

$$a = \tfrac{1}{2} + {}^{1}/_{6} \, [\exp (-GSI / 15) - \exp (-20 / -3)] \qquad \text{(A.3-16 b)}$$

Considering the comments made earlier on the Mohr-Coulomb strength criterion, there is, in our opinion, no immediate merit in selecting the Hoek-Brown criterion for the excavation design in argillaceous rock repositories. A possible exemption is the preliminary design of underground openings. Such a design, however, has to be verified at a later stage by in-depth studies requiring appropriate design parameters which are derived from laboratory and field tests (ref. to Figure A.3-3). It has to be kept in mind that the Hoek and Brown criterion is entirely empirically derived.

Furthermore, it does not seem to be sensitive enough to characterise the structural and geotechnical diversity of argillaceous rocks to a degree that is required in PA.

A.3.4.4 Critical State concept and Cam-Clay model

In geologic repository design of argillaceous media, the limiting conditions of pervasive multiple-shear failure types may be characterised by the Cam-Clay model within the Critical State concept originally developed for granular soil (Roscoe and Burland 1968). For the plastic Boom Clay at Mol, Barnichon (2002) employed this concept for the interpretation of the mechanical response of the Boom Clay to the excavation of a 65 m long test drift gallery.

In the Critical State concept the limiting stress conditions are defined within the three-dimensional p'- q' - v parametric space in which:

p' = mean effective normal stress σ_n
q' = mean effective shear (= deviatoric) stress τ (note: q' = q)
v = void ratio

All possible states are synoptically considered, e.g. normally-consolidated and over-consolidated materials. Consequently, within the p'- q' - v space the limiting conditions are characterised by a composite, partly curved plane (envelope) as indicated in Figure A.3-15 (left). The intercept of this envelope with the p'-q' plane is shown in Figure A.3-15 (right). Parts of the envelope are associated with dilatant failure behaviour, other parts with contractant failure behaviour. The 'Critical State Line' (CSL) is defined as the locus of the envelope at which no volume change occurs for very large shear deformations. The CSL therefore separates a dilatant ('dry') region ('Hvorslev surface') from a contractant ('wet') region ('Roscoe surface'). The two regions as well as the CSL itself may be analytically described by empirical functions (Schofield and Wroth 1968).

Figure A.3-15. The critical state model of soil mechanics (after Horseman *et al.* 2005)
Left: Composite surface of the limiting conditions in the p'-q'-v space with tension line (TL), normal consolidation line (NCL) and critical state line (CSL)
Right: Intercept of the limiting surface with the p'-q' plane, with intersections of the Hvorslev and Roscoe surfaces

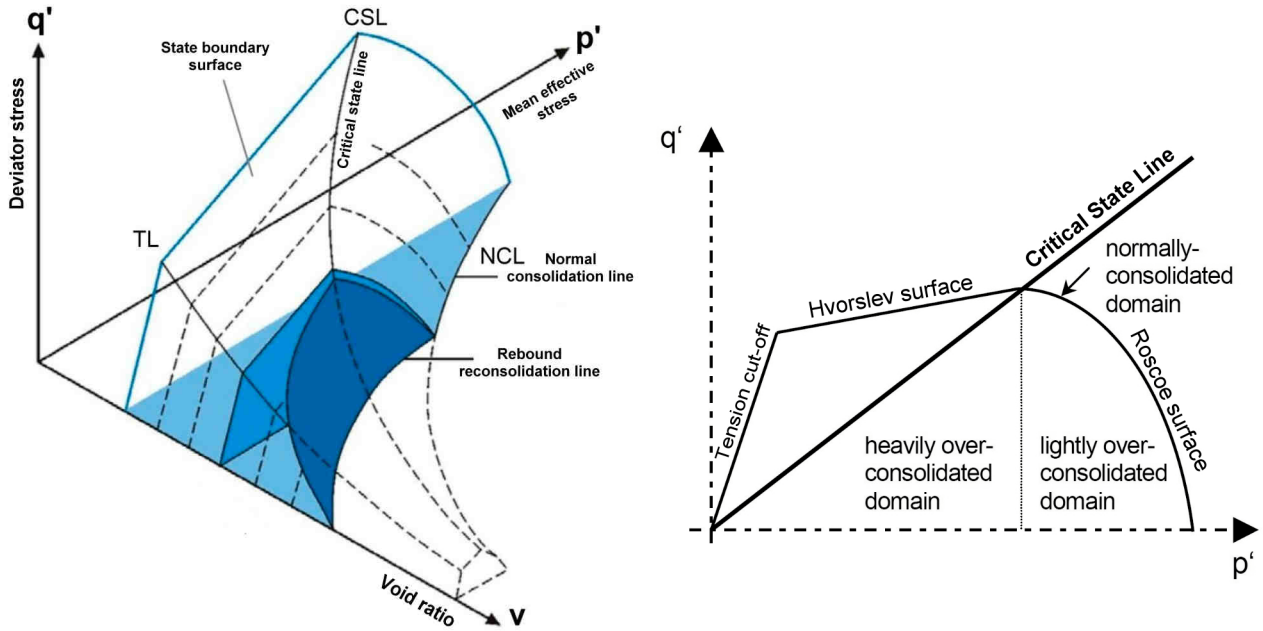

The Cam-Clay model thus aims to describe the full range of deformational responses experienced by soils in a quantitative manner. Numerous extensions and modifications have been suggested, such as the incorporation of non-linear elasticity and coupled elasto-visco plasticity (Figure A.3-16). Today, the Critical State concept is well-established in soil mechanics.

It has been suggested to apply the Critical State concept to some rocks such as sandstone and shale (for a review, ref. to Horseman *et al.* 2005). However, the general consensus is that this may be inappropriate for most rocks, especially in the Hvorslev region (Cuss 1999). This is primarily due to the complications introduced by lithification and general rock-forming processes. The state boundary surface might then be partially replaced by some alternative failure criteria, such as the replacement of the no-tension and Hvorslev regions by the Mohr-Coulomb or Hoek-Brown criteria.

Figure A.3-16. The Critical State concept with visualisation of some coupled hydro-mechanical effects (from Marschall 2006)

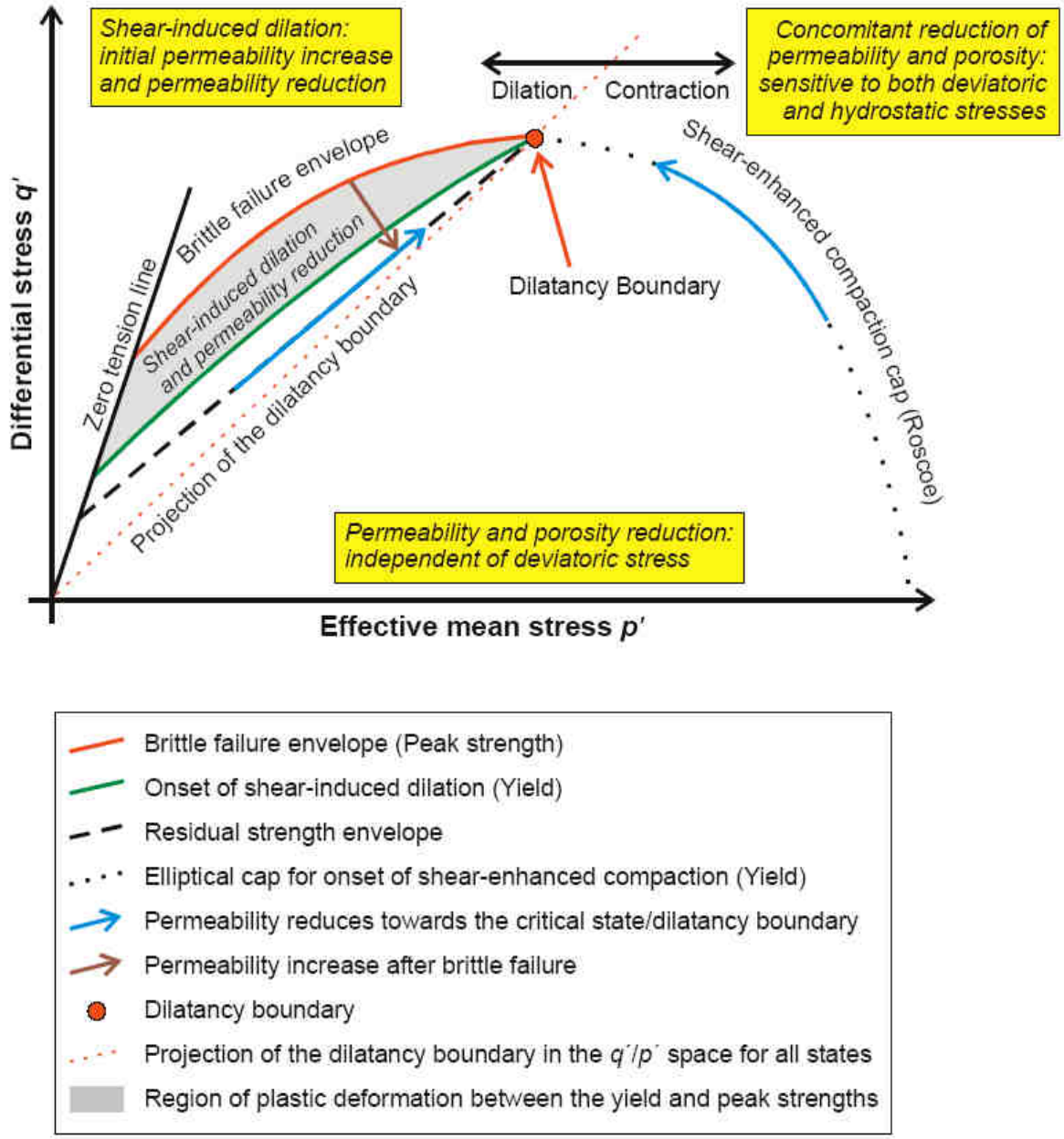

APPENDIX 4
NATURAL AND ARTIFICIALLY-INDUCED FRACTURES IN ARGILLACEOUS FORMATIONS

Overview

This appendix provides, in addition to Section 2.3.3 of the main text, some detailed information on fractures in argillaceous formations It includes natural fractures (Section A.4.1) and artificially-induced fractures (Section 4.2). Geological and geomechanical knowledge on these fractures is one of the prerequisites for the understanding self-sealing features and processes.

Detailed fracture mapping of the Boom Clay in large open pits provided the base for understanding the occurrence and genesis of natural fractures in argillaceous formations. The Boom Clay constitutes that formation which, from its geological history, can be considered as the most elementary one with regard to its fracture inventory. The collected evidence is supported by fracture observations in the moderately indurated Opalinus Clay and the Callovo-Oxfordian formations. Detailed mapping have also been carried out with regard to artificial EDZ fractures, generated by drilling or underground excavation works, in the URLs at Meuse/Haute-Marne, Mol and Mont Terri.

A.4.1 Natural fractures

Natural water-conducting features can be of sedimentary origin (lithologic heterogeneities, such as calcareous or sandy beds) or of tectono-mechanical origin (e.g. faults, joints). FEPCAT (2005) states that sedimentary heterogeneities are reasonably well understood and not critical to PA. The significance of tectono-mechanical features for self-sealing and PA, however, is beyond any reasonable doubt for both plastic clays as well as indurated formations. A thorough review of natural fractures is therefore indicated.

A.4.1.1 Types, terminology and classification

Mechanically and hydraulically relevant natural fractures[30] in argillaceous formations are macroscopically visible features such as bedding plane breaks, fissures, cracks, joints and faults. Table A.4-1 provides a summary on the characteristics and Figures A.4-1 and A.4-2 some field examples. Note that in Table A.4-1 the distinction between 'joints' and 'faults' hinges on the term *'visible'* which depends on the scale of observation.

[30] As a generic term for all mechanical breaks in rock masses, the International Society for Rock Mechanics, ISRM, prefers the term 'discontinuity' rather than 'fracture'.

Table A.4-1. Important macroscopic natural fracture types in argillaceous formations
(after Mandl 2005 and Ulusay and Hudson 2007)

Usual Extent	Geologic Term	Phenomenological characteristics
small ↓ large	Crack	Partial fracture, with some parts still cohering (as in Table A.3-5)
	Fissure	Open crack, arranged in an irregular, non-systematic manner
	Bedding plane	Latent break, susceptible to opening in unloading regimes (e.g. tunnel excavation); mechanically of particular importance when activated in shear
	Joint	Break in the continuity of a geologic body along which there has been *no visible* displacement. Most frequently arranged in a systematic manner (set of joints; conjugate and/or orthogonal joint system).
	Fault	Shear fracture or fracture zone along which there has been *a visible* displacement, from a few centimetres to a few kilometres in scale.

Figure A.4-1. Examples of natural fractures in argillaceous formations:
a. Fissures in Liassic mudstone (Horseman *et al.* 2005)
b. Shrinkage cracks in desiccated clay crust (Horseman *et al.* 2005)
c. Orthogonal joints in Boom Clay (Dehandschutter *et al.* 2005a)
d. Orthogonal joint system in Kimmeridgian mudstones (Horseman *et al.* 2005)

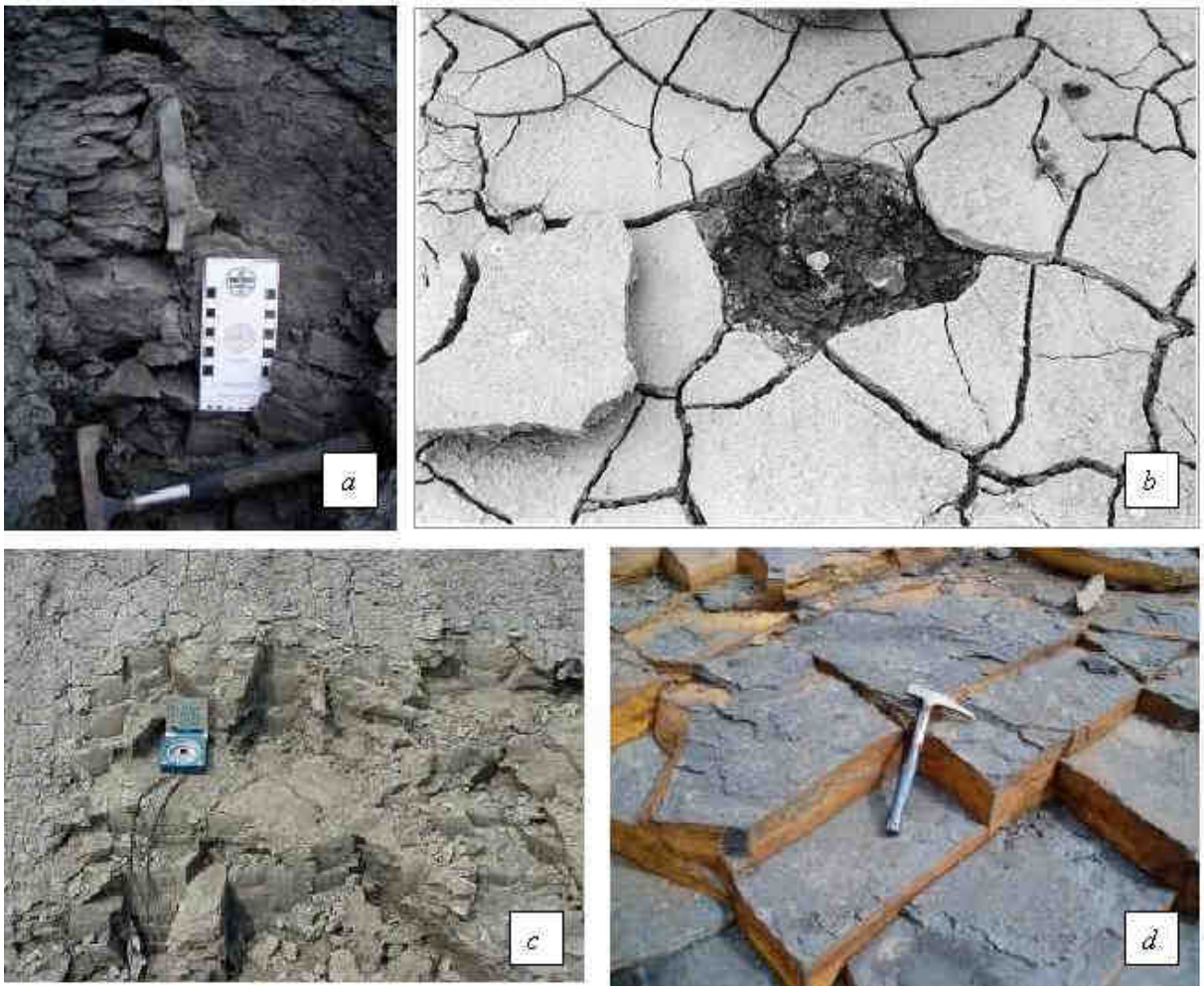

A.4.1.2 Natural fractures in plastic clay: Boom Clay

A.4.1.2.1 General

Of particular importance for the self-sealing topic are joints and faults. "Joints are probably the most ubiquitous and, at the same time most confusing features of crustal rocks. They vary greatly in appearance, dimensions, and arrangement, and occur in quite different tectonic environments" (Mandl 2005, p. 1). Faults are important because of their substantial dimension which they can have in regard to persistence (extent) and thickness ('fault zone'). Changes of the material properties within and near the fault zone are quite common and of concern to self-sealing (see Figure A.4-2).

Due its comparatively simple geologic history in its deposition – burial – erosion evolution (ref. Section A.2.4 and Figure A.2-10), the Boom Clay is of principal importance in identifying that particular fracture inventory which can be considered to be the most elementary one in argillaceous formations. Relevant studies have been carried out by Dehandschutter (Dehandschutter 2004; Dehandschutter *et al.* 2005a; 2005b) both at the surface in large clay open pits and underground in the HADES URF.

Figure A.4-2. Normal fault in the Boom Clay at Kruibeke, Belgium, with a throw of some 50 cm
Note core sampling holes in the hanging wall (bottom right) and footwall (top left) of the fault plane for investigation on the structural and mechanical changes adjacent to the fault plane
(from Dehandschutter *et al.* 2005b)

A.4.1.2.2 Observations in surface outcrops

In surface outcrops three types of systematic natural fractures were identified as follows:

1. "Meso-planes" (m-scale): Discrete shear planes: Normal faults

Figure A.4-2 shows a fault which, in fact, is one in a series of several sub-parallel normal faults observed. Fault spacing is about 10 m and the throw of a normal fault about 1m. The persistence of the faults could be traced over about 4-6 m vertically and at least 80 m horizontally. The individual faults themselves are composed of a series of sub-parallel undulating and segmented slip surfaces expressed as striated slickensides composing an up to 60 cm thick shear zone. The fault planes have a preferred orientation, striking about N125°E (i. e. NW-SE) and dipping of between 40° and 65° (Figure A.4-4).

2. "Micro-planes" (cm-scale): Multiple shear joints

These are pervasive planes which were observed in all investigated clay pits. Like the meso-planes, they are slickensided, however, their persistence is much smaller (order of magnitude 3 to 6 cm) than that of the meso-planes. Their surface is generally smooth (shiny and polished) and striated, with slickenlines oriented parallel, sometimes conically. Although the striae on the planes indicate a certain amount of shear displacement, its magnitude could not be determined macroscopically. Based on microscopic observations, the magnitude is supposed to be in the order of μm and the type of shear displacement is predominately normal slip (hanging wall down). The orientation of the micro-planes seems random at first sight, however, a detailed statistical analysis revealed a certain pattern with a dominant strike between N110°E and N130°E and a dip angle of around 50° to 60°.

3. "Sub-vertical joints" (dm- to m-scale): Mixed-mode extensional fractures

These joints are pervasive planes which were observed in all clay pits investigated and beyond. They occur as two regular sets of about mutually perpendicular planes, becoming particularly pronounced after weathering (similar to Figure A.4-1d). The joint spacing ranges from 1 m in clay-rich layers to several metres in silt-rich layers. They are sub-vertically inclined and very persistent in trend with a main strike of the first set of N130°E and the second set of N030°E (Figure A.4-3).

Figure A.4-3. Pole plot of the orthogonal joint system measured in the Kruibeke clay pit
(equal area, lower hemisphere projection; out of Dehandschutter 2004)

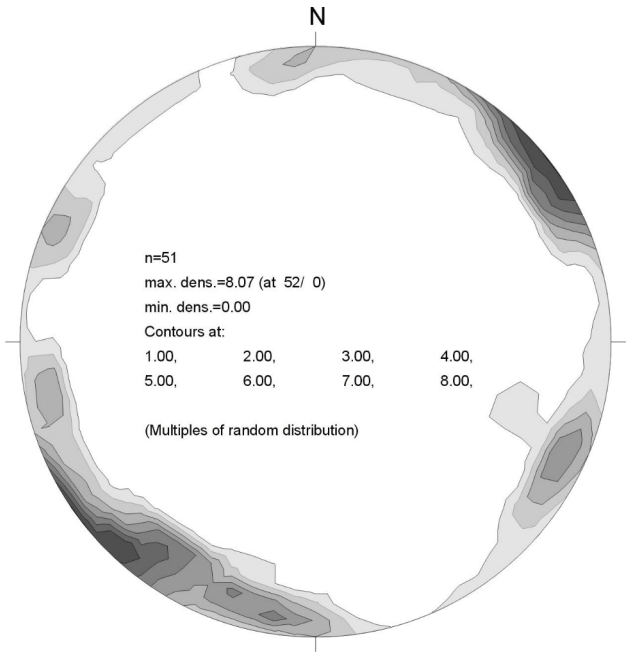

Structural studies (Dehandschutter 2004; Dehandschutter *et al.* 2005a) showed that, kinematically, all three natural fracture types (normal faults, multiple-shear joints and mixed-mode joints) fit into one and the same geologic deformational regime (Figure A.4-4). Based on further detailed studies (Dehandschutter *et al.* 2005b), involving fracture dynamics and microfabrics, he

suggested that the three fracture types have a common origin in terms of driving force and deformation evolution. They were generated in a gravity-dominated stress field with $\sigma_v' > \sigma_H' > \sigma_h'$ in which the difference between the effective horizontal stresses σ_H' and σ_h' might have been quite marginal. He postulated that the driving mechanism for $\sigma_H' \neq \sigma_h'$, and thus for the regularity of the fracture pattern orientation in the Boom Clay was a gentle trend of gravity sliding of the strata into NNE direction, i.e. towards the North Sea basin. That sliding took place in the late Oligocene period and was triggered by an episodic uplift of a mere 40 m of the south-western part of the 'London-Brabant Massif' (Figure A.2-10; Dehandschutter at al. 2005a).

Figure A.4-4. Outcrop map of the Boom Clay in Belgium and synoptic kinematic diagrams of the three fracture types observed

Meso-planes (bottom right), micro-planes (left) and sub-vertical joints (top right), all indicating an extensional stress regime in NNE-SSW direction
(Dehandschutter 2004)

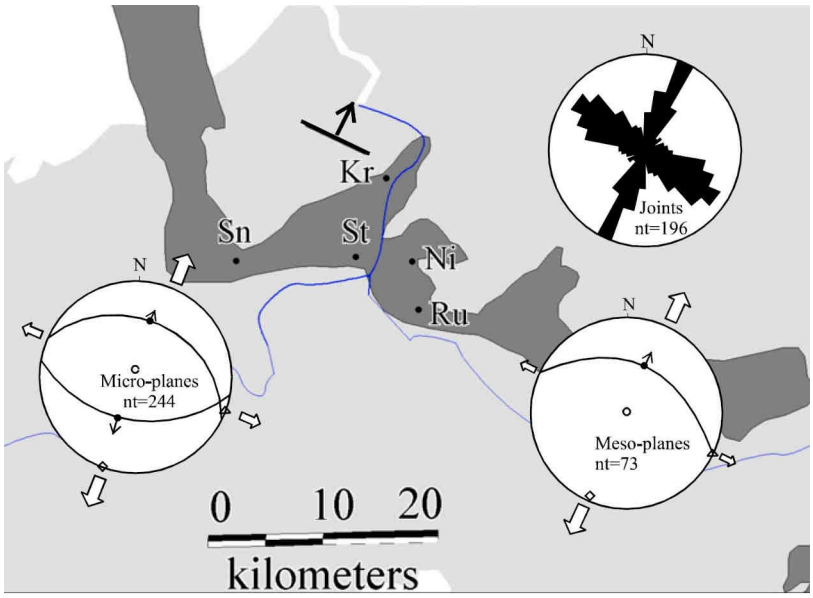

Mechanically, the coexistence of ductile fractures (meso- and micro-shear planes) and brittle fractures (orthogonal mixed-mode extensional joints) was interpreted in terms of the Critical State concept as follows (Figure A.4-5; ref. also to Section A.3.4.4; Dehandschutter 2004; Dehandschutter *et al.* 2005a): At the onset of uplift, the Boom Clay leaves the compaction K_0 stress path (1), and ductile (plastic) deformation forms contractional shear bands (slickensides), causing pore pressure increase, reducing, along with erosive overburden reduction, the mean effective stress p' (2). At a certain stage during uplift (and related ductile shear and pore-pressure increase) the dilatancy-boundary is reached and brittle failure occurs in the form of jointing (3). At the onset of brittle failure the mean effective stress has to come below a limit, approximately at around 0.5 MPa for Boom Clay (3). This implies that at depths greater than around 70 meters (order of magnitude), no vertical joints will develop in Boom Clay. After brittle failure, the stress drops to the residual strength or critical state of the material, after which deformation stops (4).

Figure A.4-5. Stress path in the p'-q diagram of the Boom Clay buried to a depth of 100 m
P.S. = Peak strength; R.S = Residual strength; CSL = Critical State line; B.F. = brittle failure (Hvorslev surface)
(from Dehandschutter 2004)

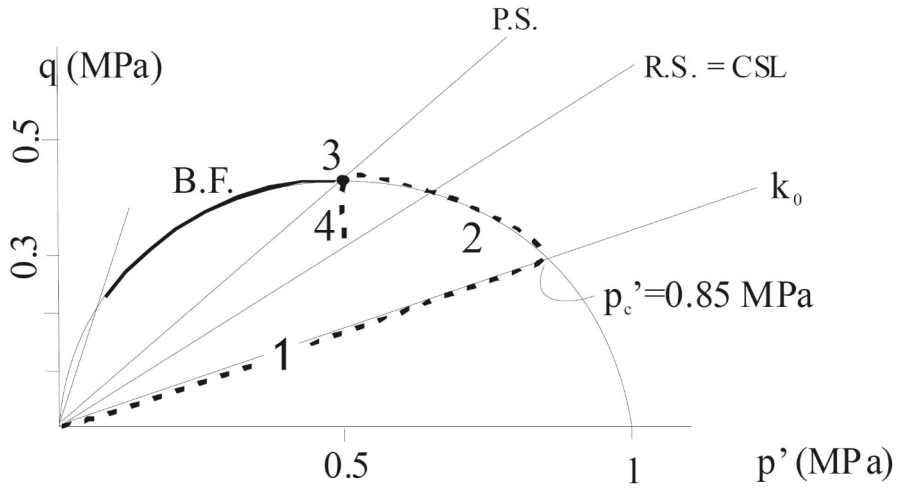

A 4.1.2.3 Observations in the HADES URF

The natural fractures and joints, described in Section 4.1.2.2, could only be observed in surface outcrops. They have not been observed underground in the HADES URF at 223 m depth below the surface, neither during the excavation of the Connecting Gallery, nor during subsequent core drilling in various directions (Dehandschutter 2004). Here solely artificial excavation-induced fractures have been observed (see Section A.4.2).

Geologically, the absence of sub-vertical joints at depth is somehow surprising as, in other geological settings, they are commonly prevailing also at greater depth. This finding warrants further discussion, particularly against the background that the mixed-extensional-mode joints would have acted, or may still do so, as preferential conduits for fluid migration (ref. to Section 4.1.4.2).

A.4.1.3 Natural fractures in indurated formations

A.4.1.3.1 Surface outcrops

Studies on the Opalinus Clay were carried out by Mazurek *et al.* (1996) in clay pits of northern Switzerland (e.g. Siblingen, Erzingen, Schinznach) and for argillaceous formations in general by Arnould (2006). Characteristic are sub-vertical extensional joints. Surface water infiltrate along these joints into the rock as is evidenced by oxidation seams. Identical to the Dehandschutter's (2004) observations in the Boom Clay, the occurrence of these joints is limited to the uppermost strata of the Opalinus Clay (order of decametres). They could not be observed at greater depths neither in boreholes nor in the Mont Terri URL.

Faults were rarely observed in the investigated outcrops. Figure A.4-6 shows the structural map of the biggest fault observed which could be traced over a distance of some tens of metres in the clay pit of Siblingen.

Figure A.4-6 Structural map of a fault in Opalinus Clay
(Clay pit of Siblingen; from Nagra 2002b)

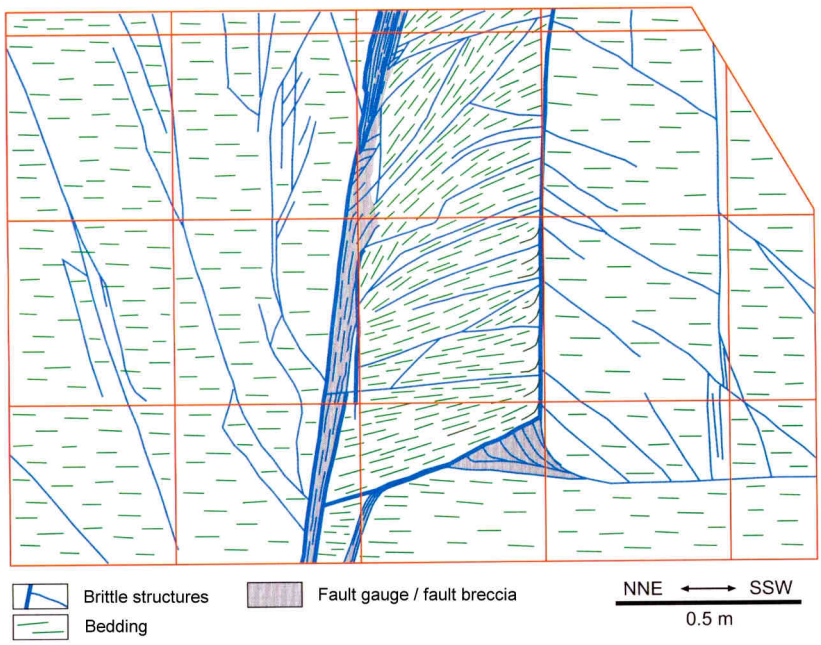

A.4.1.3.2 Sub-surface

Opalinus Clay in the Mont Terri URL

In the Mont Terri URL, Switzerland, natural fractures of various kinds have been observed in the Opalinus Clay (Table A.4-2; review by Yong *et al.* 2004). It was, however, found that, even close to and within tectonically disturbed zones, there was no increase whatsoever in permeability (Marschall *et al.* 2003; Tevissen and Soler 2003 in Nagra, 2002b). That finding is in line with earlier observations in old (partly > 100 years) railway tunnels intersecting the Opalinus Clay formation where significant transmissivities were absent once the overburden becomes greater than 200 m (Gautschi 2001; see Section 3.3.2 of main text). The overburden of the Mont Terri URL varies between 230 and 320 m. Irrespectively of this, natural fractures, even when completely sealed, remain of some interest as they might be reactivated in course of the repository construction or constitute nuclei for new fractures in the EDZ.

The different types of discontinuity features are associated with different extent, orientation, connectivity and hydraulic properties. Table A.4-3 lists the types and classifies, in accordance with Lanyon (2008), their hydraulic significance.

Table A.4-2. Natural fracture types observed in the Mont Terri URL
(extended after Yong *et al.* 2004)

Fracture Type		Features
Veins	Extension	- rare - predominately sub-parallel to bedding - filled with fibrous minerals (calcite or gypsum with pyrite, sphalerite and celestite as accessory vein infills) - crystal growth is normal to vein wall - mostly uneven fracture wall
	Shear	- oblique crystalline growth
Kink folds		- straight links - very sharp hinges - occurs only in sandy facies - fault planes trend through hinges as axial planes
Bedding plane breaks		- Dipping ~45° (mean) (range from 32 to 50°) to SE - Latent break, mechanically of particular importance when activated in shear
Tectonic joints		absent
Fault planes		- discrete planes (reverse, thrust and strike-slip; Figure A.4-9). When reactivated in the EDZ, they act as normal fault. - may contain fibre (calcite) lineations, movement striae on slickensided surfaces, fault gouge (cohesionless wallrock flour)
Fault zones		- primarily thin zones with the exception of one major zone, "Main Fault" (Figures 2-4 and A.4-7 to -8) - metres to tens of metres in extent

Fault planes (minor, discrete, individual elements) are, besides bedding, the most frequent structural features encountered in the Mont Terri URL (Figure A.4-9). The planes have extents in the order of metres to tens of metres, and the fault plane walls are often slickensided and polished. Most faults in the URL are closed, and when they are filled, the infilling is tightly compacted and of marginal thickness (in the order of tens of millimetres). The dip angle of the faults ranges from sub-horizontal to sub-vertical with a maximum of 35-50°, which is sub-parallel to bedding.

The arrows in Figure A.4-9 indicate the sense and direction of the shear displacements which have occurred in connection with a reactivation of the faults in the EDZ in course of the excavation work. The reactivated shear movements are in the sense of a normal fault system. This has become apparent by offsets of the hanging- and foot-walls in the galleries. The original tectonic movement of the faults, shown in Figure A.4-9, was thrusting as revealed by slickensides analysis.

Fault zones were also found but most of them were thin, isolated zones, measuring 0.15 - 0.65 m in thickness and of some 50 m in extent. Only one major tectonic fault zone of an intermediate scale was identified ("Main Fault", identified as a thrust fault; Figure 2-4 in main part; Figures A.4-7 and A.4-8), and it was found to extend continuously through all three tunnels. This 1 - 3 m thick zone is oriented along bedding, however at a slightly steeper dip angle. Internally, it consists of a number of large fault planes (with a frequency greater than 20/m) forming tectonised elements such as fault breccia, displaying loss of cohesion and completely disturbed bedding or drag folds (Figure A.4-7). Most of these fault planes contain movement striae and some are sealed with shear fibres. All these features indicate a general movement mechanism to be one of overthrusting with little lateral movement.

Table A.4-3. Types of discontinuity features derived from tunnel mapping in the Mont Terri URL (after Nussbaum and Bossart 2008, and Lanyon 2008)

Feature type	Logged in core	Extent	Open/closed	Hydraulically significant
SSE dipping faults	Yes	Extensive >10m	May be reactivated in EDZ, closed in rock mass	Potentially significant within EDZ
S-SW dipping faults	Yes	<5m Seem to be bounded by SSE dipping faults	May be reactivated in EDZ, closed in rock mass	Potentially significant within EDZ
N-NNE trending faults (corres-ponding to Bresse-Rhine system).	Yes	< 5m	May be reactivated in EDZ, closed in rock mass	Potentially significant within EDZ
Bedding planes	?	Extensive	May fail in slip in EDZ, closed in rock mass	Potentially significant within EDZ
Stress induced fractures (extensional)	Yes	0.5-1m	Open	Open but may be limited in connectivity
Desiccation cracks	No (logged in BHGA18, A26)	0.5-1.5m	Open at tunnel wall	Probably only open very local to tunnel wall and likely to close on resaturation
Siderite layers	Not recorded	0.2-1m	Weakly cemented but not open	May be more locally permeable than host rock but of no significance compared to fractures.

Figure A.4-7. Structural map of the Main Fault in the Mont Terri URL (from Nagra 2002b)

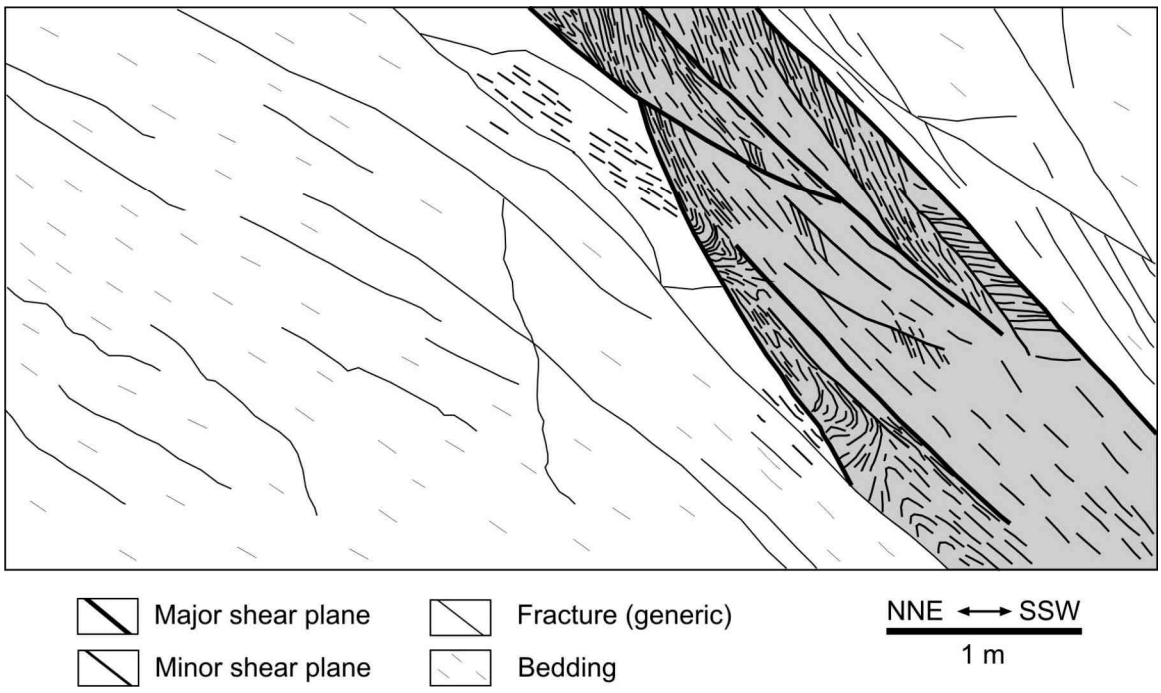

Thin section analyses of the Main Fault have indicated a "finely-braided, connected network" of open fractures, where it is apparent that fractures have developed along recently reactivated shear veins (Figure A.4-8). Veins are generally rare, and when present they are filled with calcite, dolomite and celestite.

Figure A.4-8. Detail of the fracture network of the Main Fault in the Mont Terri URL
(Thury and Bossart 1999)

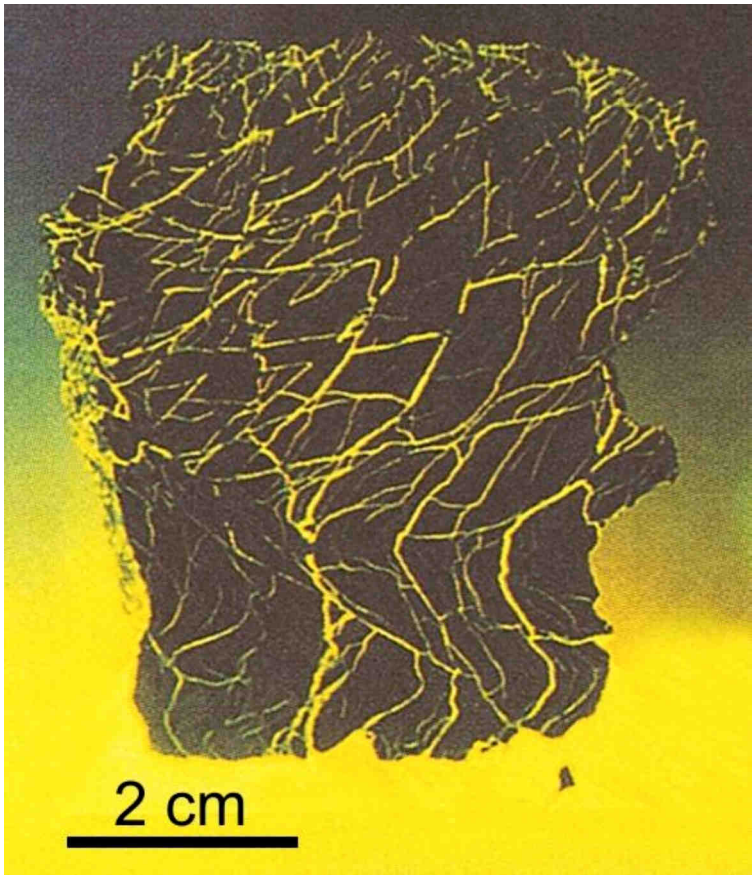

Figure A.4-9. Tectonic fault planes observed in the EZ-B Niche of the Mont Terri URL
Top: Side view onto two types of SSE-dipping faults
Bottom: Top view onto bedding parallel fault plane
(after Nussbaum *et al.* 2005)

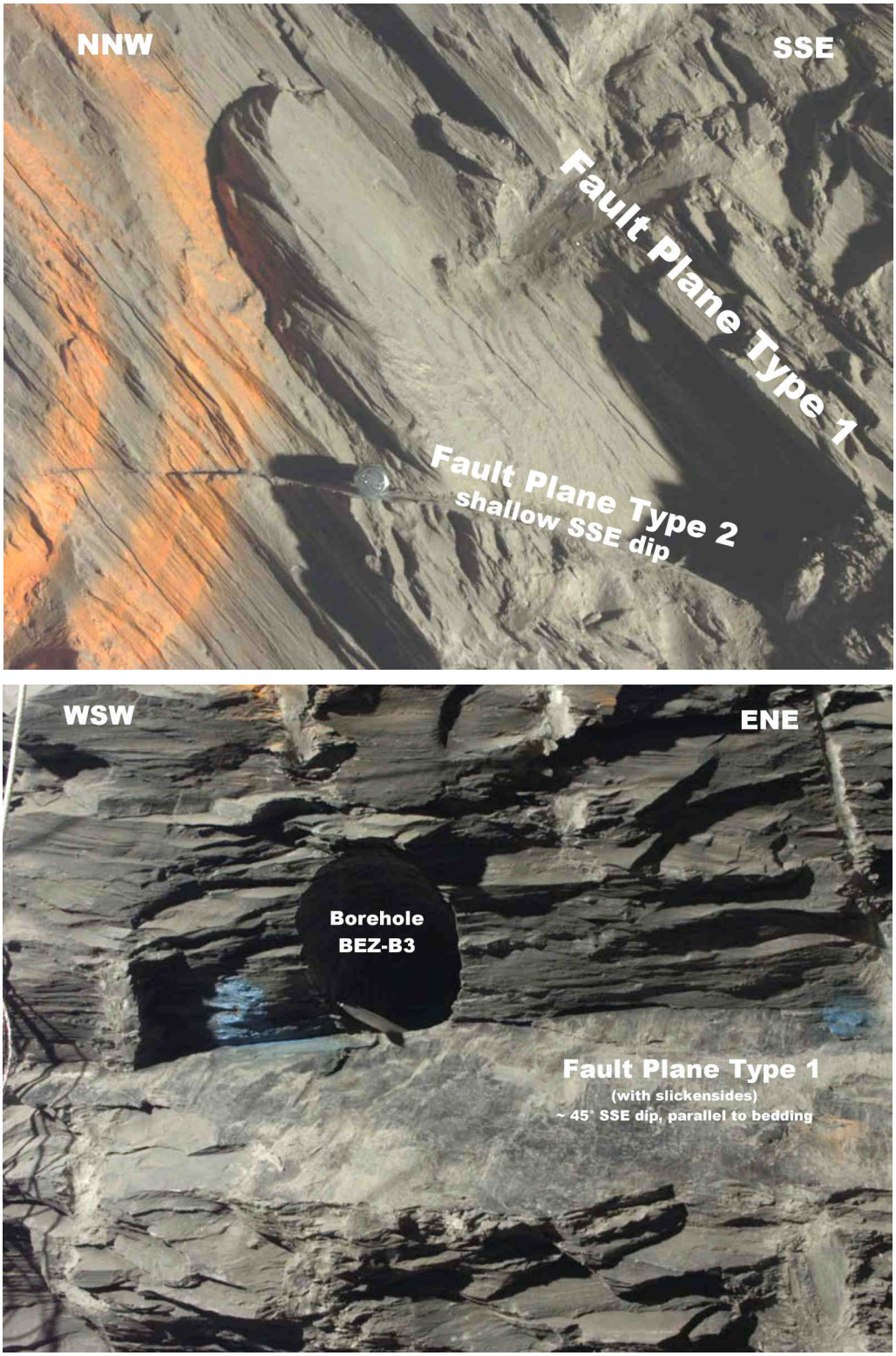

Callovo-Oxfordian formation at Bure URL

Following regional geological reconnaissance operations during the years 1994-2000, the focus of investigations shifted more to the local conditions of the URL site at Bure, particularly on potential minor faults having a maximum 5 m vertical throw. The exploratory borehole programme conducted in 2004 on EST210, EST211 and EST361 revealed that there was no fracturing of this kind in the Callovo-Oxfordian layer or in the underlying carbonate formation of the Bathonian (Distinguin *et al.* 2003 and 2004). That finding was also confirmed by observations in the shafts and drifts of the URL (Delay *et al.* 2007). Moreover, 3-D seismic data, reprocessed to a resolution approaching 3 metres, shows no evidence of minor faults in the Callovo-Oxfordian layer or in its overlying formations that could influence the geometry of the layers (Cuilhé and Bruneton 2003).

The following structures were observed in borehole cores (ANDRA 2006b):

Micro-faults

Two micro-faults were observed at a depth of around 451 metres (EST211). Not exceeding one metre in length, they are probably related to compaction and have no influence on the geometry of the layers.

Joints

Natural joints are sometimes difficult to distinguish from mechanical fractures induced by core extraction. Their natural origin is generally confirmed by a fine calcite deposit, or, more rarely, a clay film. Although the inclined boreholes cross the Callovo-Oxfordian at great length (particularly EST211 and EST361) and are ideally oriented for intersecting these types of structures (perpendicular to the direction of the dominant fractures), only a very small quantity of joints were observed.

Tensile cracks

Such cracks are generally filled with calcite. The thickness is commonly between 1 and 2 mm, except in borehole EST210, where a 10 mm-thick filling was found. Their extent is rather limited and ends when they intersect with stylolites. All tensile cracks are completely sealed. In the EST 211 and EST 361 boreholes, and again in the main and auxiliary shafts (434-440 metres), six subvertical cracks N19°-37°E show that a harder zone exists (between 445.5 and 450 metres) within the same lithostratigraphic level. A single structure with siliceous filling, apparently parallel to stratification, has been identified (EST209).

Stylolites

Stylolites are generally between 1 and 2 mm thick, or more exceptionally 6 mm, with an argillaceous or occasionally carbonaceous filling. Traces of calcite and pyrite are sometimes found. Most are parallel to the stratification, but others have varying orientations, organised in networks that are sometimes sub-vertical**.**

Veins

Celestite veins were observed in boreholes and shafts at different depths. They are particularly well developed in a 4 m-thick horizon that is located between 453 m and 457 m where the top of the silty argillite ("Argiles de la Woëvre" substage) is in contact with the base of the "Terrain à chailles" substage silty marls. The filling, often polyphase, is made up of whitish celestite. The normal

displacement of the fault walls is likely to have formed at the same time, or slightly after, as the cracks were filled. This is suggested by the sigmoidal form of the celestite fibres. These structures have been interpreted as diagenetic. *In situ* flow tests have highlighted the fact that the present day permeability of these structures is as low as that of sound argillites.

A.4.1.4 Conceptualisation

A.4.1.4.1 Faults

The formation of the faults observed in both the Boom Clay and the Opalinus Clay can be understood in line with the classical theory of Anderson (1951). The internal architecture of the faults fit well into the system proposed by Caine *et al.* (1996) (Figure A.4-10). The Main Fault at Mont Terri (Figures A.4-7 to A.4-8), for instance, represents a 'localised deformation zone' (bottom right in Figure A.4-10), whereas the fault in the clay pit of Siblingen (Figure A.4-6) is more of the type 'composite deformation zone' (top right).

There is no evidence whatsoever of any actual water transmissivity along the faults. In context with some *'what – if'* scenarios, Nagra (2002a and b) nevertheless considered cases where an enhanced transmissivity was assumed for faults.

Figure A.4-10. Types of internal structures of geological faults (after Caine *et al.* 1996)

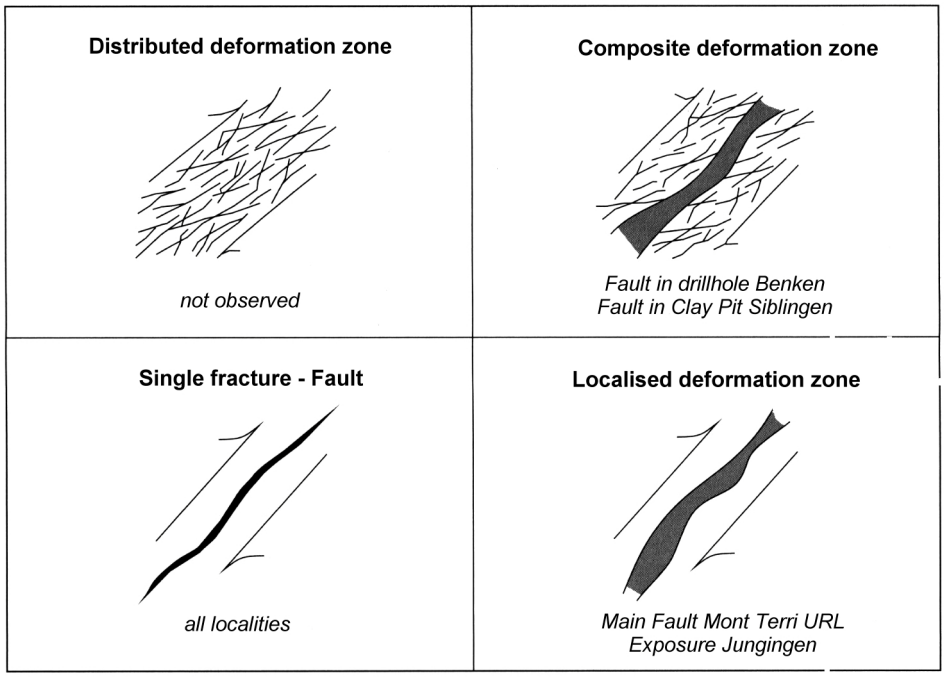

A.4.1.4.2 Orthogonal Joint System

Figures A.4-1.c – d, A.4-3 and A.4-4 give evidence of a sub-vertical joint system occurring in clay pit surface outcrops. The system is characterised by two fairly regular sets of about mutually

perpendicular joint planes. That configuration is very common in almost all types of geologic materials, particularly in flat-lying sedimentary rocks, and is generally known as 'orthogonal' or 'fundamental joint system' (Nickelsen and Hough 1967; Hodgson 1961; see also Figure A.4-11).

Figure A.4-11. The Orthogonal Joint System in horizontally bedded sedimentary rocks as shown in block diagrams (a and b) and as traces on top of a single bedding plane (c and d) (from Bock 1980a).

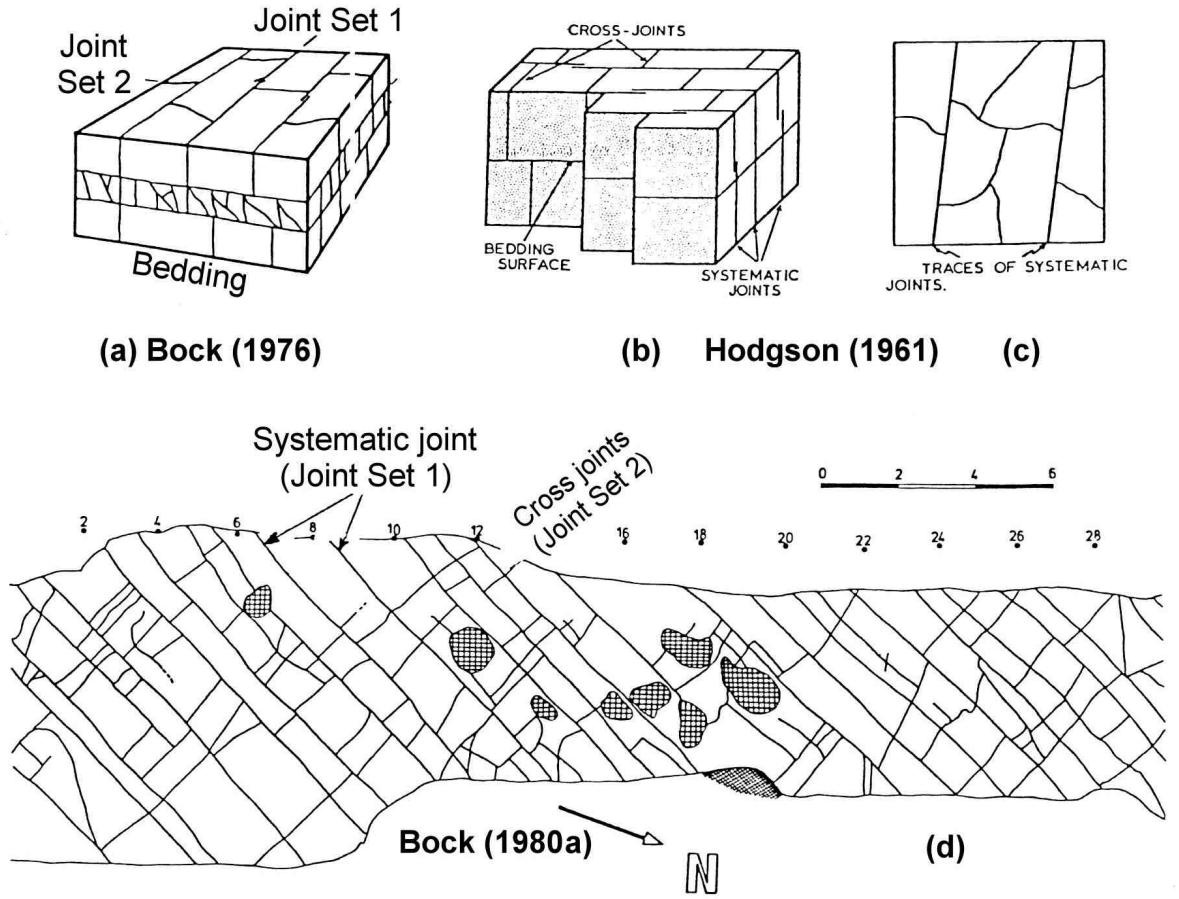

The orthogonal joint system is oriented about normal to bedding, irrespectively of any tilting or folding of the bedding planes. Mechanical models of the genesis of the orthogonal joint system were developed e.g. by Bock (1980a) and Price and Cosgrove (1990). Common to the above models are the following general conditions:

(1) existence of a gravity-dominated stress field with $\sigma_v' > \sigma_H' > \sigma_h'$;

(2) existence of a (marginal) difference in the magnitudes of σ_H' and σ_h';

(3) sediment basin dynamics as triggering mechanism for $\sigma_H' > \sigma_h'$; and

(4) formation of the joints in the uplift phase.

Points (1) to (4) fully coincide with Dehandschutter's (2004) findings on the stress conditions which must have prevailed at the time of the joint formation in the Boom Clay. From the occurrence of natural vertical joints in surface pits and their absence at depth in the HADES URF, Dehandschutter *et al.* (2005b) inferred that the orthogonal joint system of the Boom Clay was formed during uplift and close to the topographic surface where the mechanical conditions (low confining pressure, extensional deformation) allowed the formation of such a system. At deeper levels they could have been sealed or (partially) healed during subsequent subsidence-related increase in confining pressure.

Mandl (2005) considered the mechanics of the orthogonal joint formation in context with the subsidence and uplifting of sedimentary basins in some detail. In the subsidence mode he was unable to delineate a plausible mechanism for the joints under consideration. In the uplifting mode and when selecting common rock material parameters and even taking into account the combined effects of the declines in overburden, porewater pressure and temperature, he found that the decrease in the minor effective horizontal stress σ_h' is generally too low to establish tensile stresses sufficient for the joint formation (ref. also to Section A.2.5.2). However, he noted (Mandl 2005: 108) that '*very weak* (e.g. clayey) rocks' might constitute an exception. Considering geotechnical parameters typical for that case he found that the horizontal effective stress σ_h' might well become tensile, thus making the formation of mixed-mode or extensional fractures plausible. Similarly, the stress regime derived for the Boom Clay during uplift indicates that the moderate extension in the slightly overconsolidated sediments caused by the tilting of the Boom Formation due to basement faulting and differential uplift in the London-Brabant massif could have led to the specific conditions for orthogonal joint formation in the Boom Clay (Dehandschutter *et al.* 2005a and 2005b).

A.4.2 Artificially-induced fractures in underground openings

Artificial fractures are induced into the host formation by intentional human actions such as exploration drilling and repository construction. For a high-level nuclear waste repository, the damaged zone caused by sub-surface excavation is of particular concern for PA as it might affect the radio-nuclide migration. The damaged zone is initiated during the repository construction. Its behaviour is a dynamic problem, depending on changing conditions that vary from open-drift period, to initial closure period and to the entire heating-cooling cycle of the decaying waste (Section 2.2). Other factors concern the even longer-term issues of chemical reactions and biological activities.

A.4.2.1 Types, terminology and classification

For artificially-induced fractures the geomechanical terminology and classification is applicable (ref. to Table A.3-5). Terms and fracture phenomena which are especially related to exploration drilling and underground construction are compiled in Table A.4-4. For the physical causes of the various fracture types refer to Section A.3.3.3.

A.4.2.2 Fractures around underground openings, EDZ and EdZ

Any excavation of an underground opening (borehole, tunnel, gallery, shaft, etc.) causes a redistribution of the geologic stress field in the vicinity of the new opening. The degree of redistribution is quite significant. It depends on numerous factors such as structure of the host rock, size, shape and orientation of the excavation, geological stress field ('primary stress state') and even on the manner in which the excavation was technically carried out (drilling & blasting; roadheader;

TBM - tunnel boring machine). Based on closed-form theoretical solutions and numerical models, there exists comprehensive knowledge about the state of the redistributed stresses (also termed 'secondary stress state'). That state is characterised by a generally increased deviatoric stress level ('stress concentration') at and near the excavation. Away from the excavation the degree of stress redistribution gradually eases, until, at an ill-defined outer boundary, it becomes 'negligible' (a term commonly used in Applied Mechanics), where it converges towards the primary stress state.

Table A.4-4. Terminology of artificially-induced fractures (in addition to Table A.3-5)

Term	Definition	Comment
General fracture terms: as in Table A.3-5		
Desiccation fracture	Fractures developing due to moisture extraction and associate material shrinkage	In argillaceous materials commonly restricted to shallow depth
Spalling	Breaking-off of plate-like pieces from a free underground rock surface (e.g. in tunnel)	Violent spalling => rock burst At topographic surface = Slabbing
Buckling (or 'kinking')	Instability in the form of sudden deflection of a series of slender rock columns	Well-bedded rock particularly amenable to this type of instability

Fractures will appear once the stress concentration around the new opening exceeds the strength of the host rock material. Again from theory including physical and numerical modelling in geotechnical and mining engineering, comprehensive knowledge is readily available on the types of fractures which may develop, their location in relation to the underground opening and extent to which they will progress towards the far-field. With regard to argillaceous formations this knowledge has been significantly advanced recently by observations and experiments in the URLs of Meuse/Haute-Marne, Mol and Mont Terri.

Within the SELFRAC project (Bernier *et al.* 2004) it was proposed to distinguish between an Excavation Damaged Zone (EDZ) and an Excavation disturbed Zone (EdZ) as follows (Figure A.4-12; see also Section 2.1 of main part):

The **Excavation disturbed Zone** (**EdZ**) is defined as a zone with hydro-mechanical and geochemical modifications, *without major changes* in flow and transport properties. Within the EdZ there are no negative effects on the long-term safety.

The **Excavation Damaged Zone** (**EDZ**) is defined as a zone with hydro-mechanical and geochemical modifications inducing *significant changes* in flow and transport properties. These changes can, for example, include one or more orders of magnitude increase in flow permeability.

Bernier *et al.* (2004) stated that the above definitions should be further detailed for each type of rock and each site. In particular, the terms 'significant' and 'major' should be quantified and the time effect should be discussed for each particular site. For the Belgian reference case (Boom Clay of the HADES URF at Mol), for instance, an increase of the hydraulic conductivity 'by less than a factor ten is not significant or major' (Bastiaens *et al.* 2007: 601).

Figure A.4-12. To the definition of EDZ and EdZ
(modified from Blümling 2005)

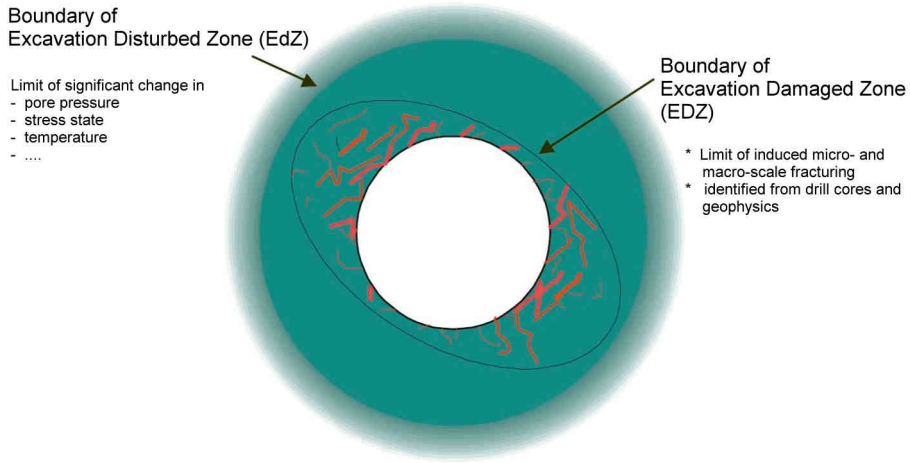

Note that the above EDZ and EdZ definitions were made from a hydro-mechanical perspective *('changes in flow and transport properties')*, thus reflecting the overriding importance of the radio-nuclide migration issue in PA. This is in contrast to geo-engineering tunnel design and construction, where the prime concern is the influence of fracturing on the secondary stress and displacement fields around the underground opening. In geomechanics, the term *'Critical Radius'* is well established which separates an inner 'plastic (= fractured) zone', adjacent to the excavation, from an outer 'elastic (= non-fractured) zone' towards the far-field. Both, the inner 'plastic' and the outer 'elastic zones' are characterised by significant stress redistribution, but it is only the inner 'plastic' zone which is affected by structural changes.

A.4.2.3 Brief review of the theory of stress-induced EDZ fractures in homogeneous isotropic media

In order to understand the occurrence and to appropriately classify the pattern of stress-induced EDZ fractures it is necessary to review some of the classical stress redistribution solutions around underground openings (e.g. Kiersch solution; review in Hoek and Brown 1980). Figure A.4-13 is based on the simple case of a circular hole in an elastic homogeneous plate[31] which is biaxially stressed by σ_v and σ_h (thus σ_h' / σ_v' = K_0; see A.2.5.2). Figure A.4-13 (left) shows the stress concentrations which are occurring right at the boundary of the circular opening and Figure A.4-13 (right) the distribution of tangential stresses σ_θ in the rock adjacent to the excavation boundary.

[31] A circular hole might represent a borehole or a TBM-tunnel. Beyond that, such idealised geometry provides insights into some principal features of almost any underground opening irrespectively of its shape.

Figure A.4-13. Variation in ratio of tangential stress σ_θ to vertical applied effective stress σ_v' for a circular tunnel (r = a) (after Hoek and Brown 1980)

Left: Variation of the boundary stresses $\sigma_{\theta\,(r=a)}$ with variation in the ratio K_0 of applied stresses. Considered are boundary points $\theta = 0°$ (roof) [180° (invert)] and $\theta = 90°$ [respectively 270°] (sidewalls)

Right: Variation with ratio of radial distance r to tunnel radius a along horizontal axis ($\theta = 90°$) for $K_0 = 0$

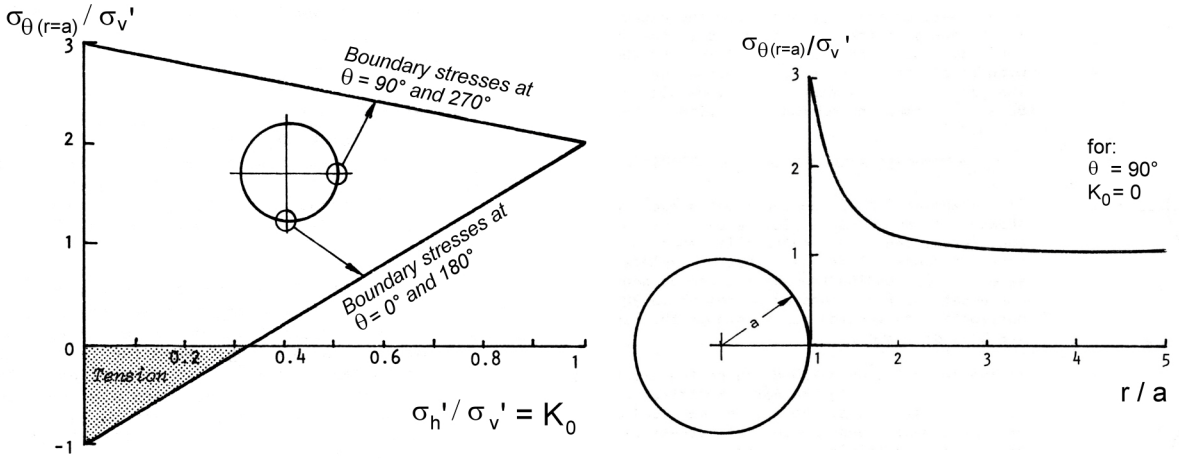

It is useful to denote, from Figure A.4-13 (left), the following distinct cases:

Case 1: $K_0 = 0$; uniaxial stress state with σ_h'$= 0$; σ_v'>0:

- At the sidewalls, the boundary stresses σ_θ are concentrated by a factor of +3
- In the roof and invert, the boundary stresses σ_θ are concentrated by a factor –1 (i.e. tensile)

Case 2: $K_0 = 1$; isotropic stress state σ_h' $= \sigma_v$':

- At all points, the boundary stresses σ_θ are concentrated by a factor of +2

Case 3: $K_0 \sim 0.3$ to 0.4 (where the K_0-axis of Figure A.4-13 (left) is intercepted by the line of the invert/roof):

- At the sidewalls, the boundary stresses σ_θ are concentrated by a factor of ~ 2.6
- In the roof and invert, the boundary stresses σ_θ are about 0.

In Case 1, extensional fractures (Type B of Figure A.3-4) may be expected in the highly stressed sidewalls as a precursor for composite extensional/shear ('mixed-mode') fractures (Type C of Figure A.3-4 or Type (2) of Figure A.3-7). The depth (as measured from the excavation surface) to

which extension fracturing will occur depends on the material properties and the secondary stress level. That depth might progressively increase in course of further stress redistributions associated with plastic deformation and fracturing processes in the EDZ. From theory, hardly anything can be said on the spacing of the extensional fractures to be expected. In the roof (and also in the invert, here, however often obscured by floor debris), tensile fractures might occur (Type A of Figure A.3-4). These fractures might progress, particularly in the roof and under the action of gravity forces, into macro-scale failures of sizeable rock blocks or wedges.

In Case 2, there should be a uniform fracture pattern in all segments of the excavation. In indurated clay formations there will be a tendency for the development of extensional fractures (Type B of Figure A.3-4) and associated failures; in plastically behaving formations multi-shear fractures (Type D of Figure A.3-4). In plastic clays and, if the excavated surface is left unsupported, the latter case might develop into what, in underground construction, is classified as a 'squeezing rock'.

In Case 3, there will be no tensile fractures anymore. Most likely is the occurrence of extensional fractures as in Case 1, but this depends also on the degree of induration.

From Figure A.4-13 (right) it can be seen that the stress concentrating effect of the hole dies away fairly rapidly and that, at r ~ 3a (a = radius of hole), the stress concentration becomes negligible. It must be recognised that this configuration is for elastic rock only without any fracturing and thus a development of an EDZ. If fractures occur, the zone, which is subject to stress concentrations, may spread well beyond the r ~ 3a boundary into the undisturbed rock.

The above picture is substantially modified when pre-existing natural discontinuities are considered together with excavation-induced fractures. Particularly relevant for argillaceous media are bedding planes, as they provide a high degree of deformational and strength anisotropy. This becomes apparent when considering fracture pattern actually observed in the URLs.

So far, only a 2-D state (plain strain) was considered. For the delineation of 3-D states of stress, deformation and/or fracturing, numeral modelling techniques are required. Such 3-D states are characteristic at the tunnel excavation face, in complex geometries (e. g. shaft / gallery intersection) or where the orientation of geological structures (e. g. bedding planes) is misaligned with the 2-D plane considered.

A.4.2.4 EDZ fracture pattern observed in argillaceous formations

A.4.2.4.1 Plastic clay: Boom Clay in the HADES URF at Mol

In 2001/2, the HADES URF at Mol was extended with a gallery (the *Connecting Gallery*). It was the first gallery ever to be constructed in a plastic clay at a depth of the order of some 200 m below surface using industrial techniques. During excavation, a detailed survey was carried out in which all faults and joints which became visible in the freshly excavated clay were mapped and recorded (Bastiaens *et al.* 2003; Mertens *et al.* 2004; Dehandschutter 2004). The survey resulted in a detailed database describing fracture type and orientation over the entire length of the gallery.

Figure A.4-14 provides impressions of the observed fractures, Figures A.4-15 and A.4-16 schematise the observed fractures with regard to the excavation of the gallery.

Figure A.4-14. Impressions of excavation-induced fractures in Boom Clay at Mol URF

a + b View from road-header onto tunnel face with conjugate inclined shear fractures
c View onto sidewall with inclined shear fracture
d Assembly of shear fracture (shadowed) and extension fractures (plumose structure)
e Shear fracture with polished striated surface (also: road-header excavation marks)
f Mixed-mode fractures in the corner between tunnel face and sidewall

The following observations were made and conclusions drawn:

- numerous fractures were observed. Dominantly they occur in the excavation face as conjugate shear fractures, in the corner between face and sidewall as mixed-mode fractures and, locally, in the roof as extension fractures (sketch of Figure A.4-15);

- the fractures are arranged in a consistent pattern which clearly relates to the gallery excavation (Figures A.4-16 to -17). The distance between successive fracture planes usually was a few decimetres. The pattern consisted of two conjugated fracture planes. Dips were about 60° at mid-height of the gallery; at the fracture tip, dips could be as low as 30°; and

- the shape of the fractures can be explained by the stress redistribution ahead of the excavation face. Furthermore, the presence of bedding planes may have influenced fracture orientation. Modelling and observations showed that fractures originated about 6-8 m ahead of the excavation face (which is about 4 to 5 times the radius of the shield). Examination of clay cores from the sidewall (Figure A.4-16, bottom) indicated a radial extent of the fractures of maximally 1 m from the sidewall into the rock (~1.5 times the shield radius). The extent determined on vertical cores was somewhat lower than on horizontal or inclined cores.

Figure A.4-15. Sketch of fractures observed in the excavation face of the Connecting Gallery
(Ring 17; from Dehandschutter 2004)

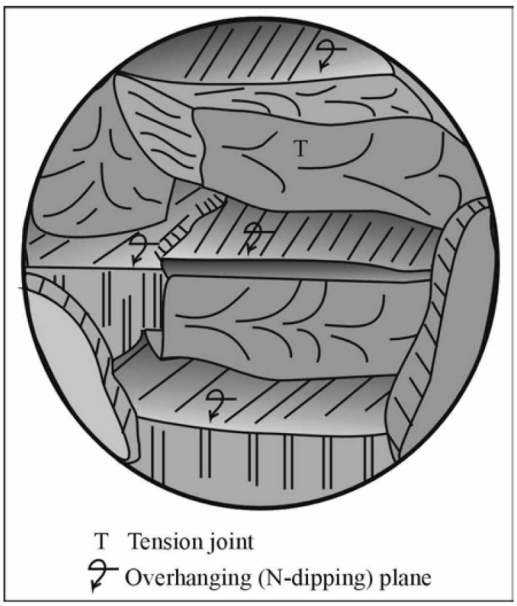

One fine example of the mode of EDZ fracturing in plastic clay was disclosed when the excavation face of the connecting gallery struck a horizontal borehole. As shown in Figure A.4-18 conjugate slip planes were detected laterally of the borehole which resemble slip lines as predicted in Bray's (1967) elasto-plastic theory.

Figure A.4-16. Vertical cross-section of the Connecting Gallery indicating observed fractures around the excavation face (from Bernier *et al.* 2004)
Radial extent is up to 1 m and the fractures originate about 6 m ahead of the excavation face
Bottom: Drillcore recovered from the sidewall (detail)

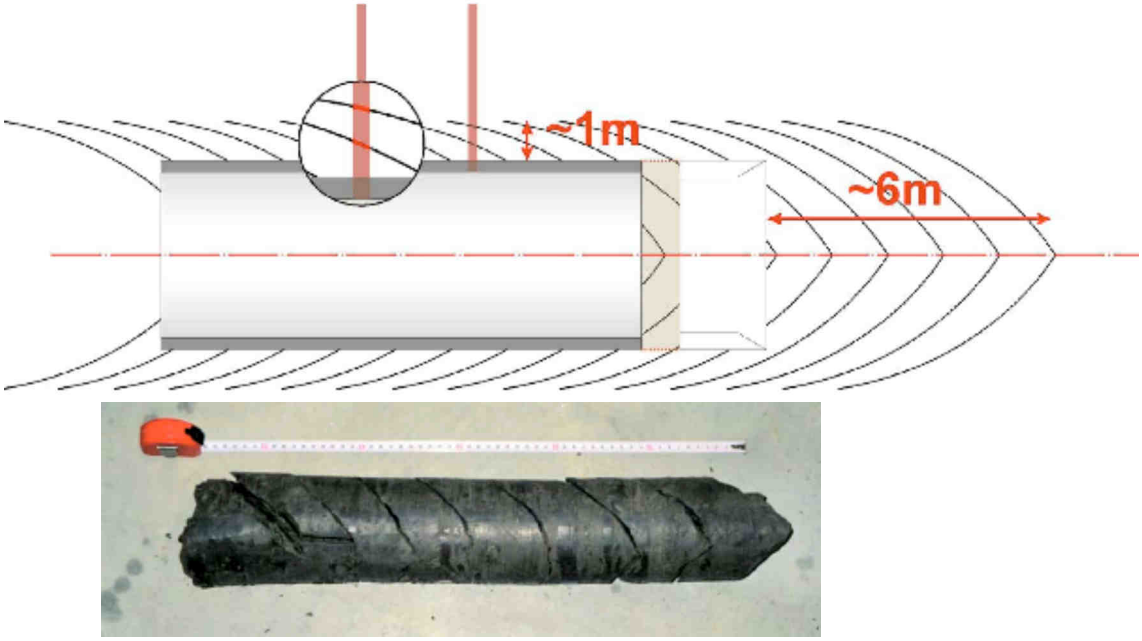

Figure A.4-17. Plan view (left) and sectional view (right) of observed fractures around the excavation shield of the Connecting Gallery. Top: Contoured hemisphere projection of poles of all measured fault planes (from Dehandschutter 2004).

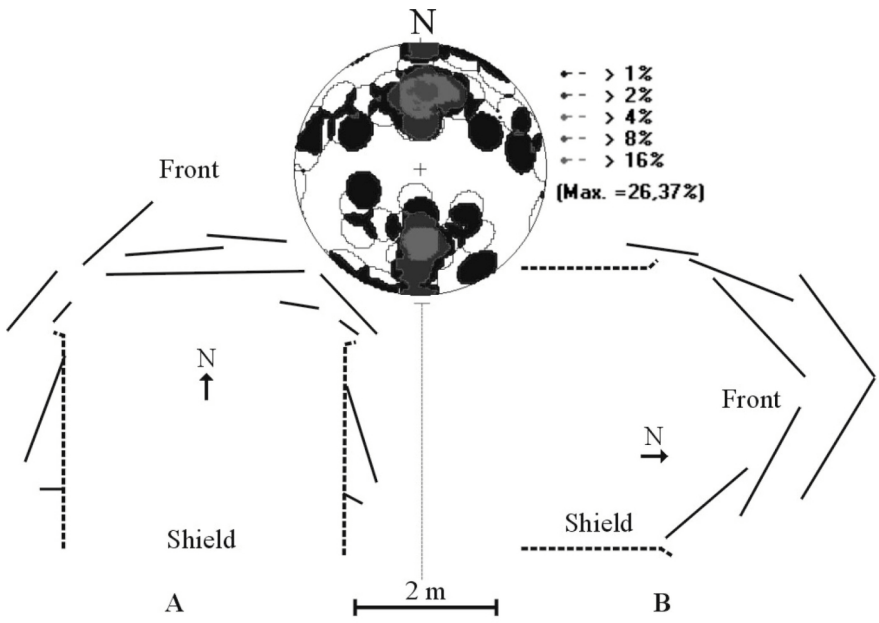

Figure A.4-18. Shear fractures around a ~100 mm diameter borehole in the excavation face of the Connecting Gallery of the Mol URF (from Dehandschutter 2004)

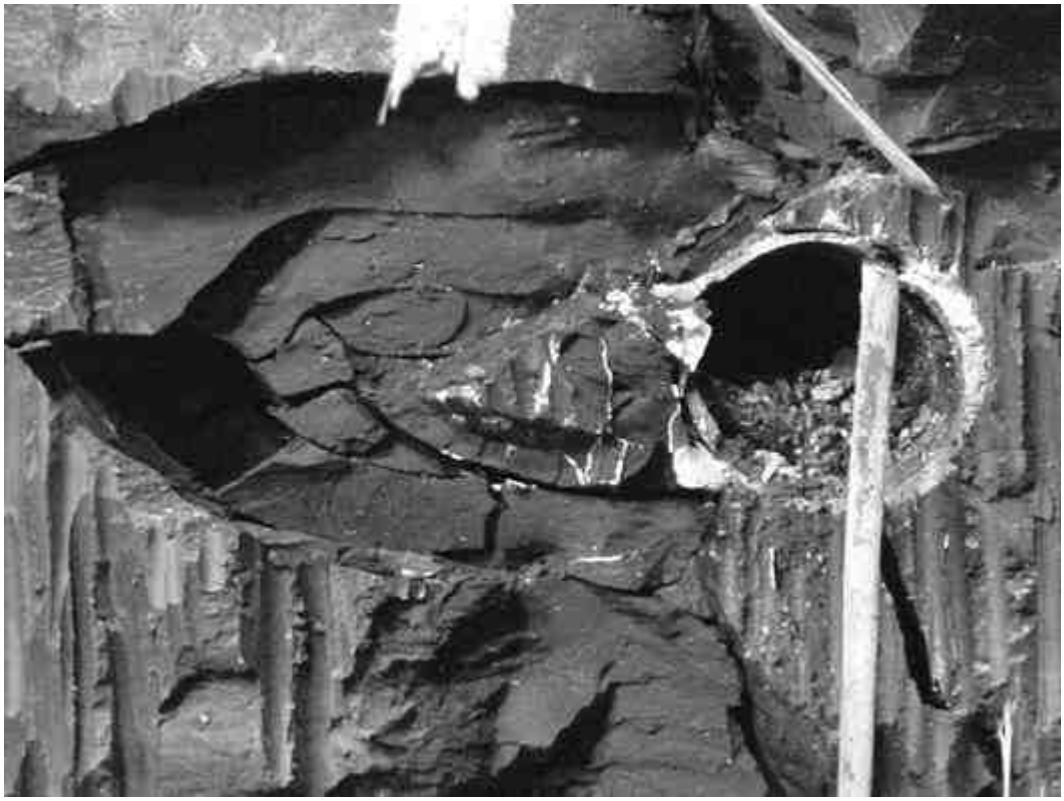

Overall, fracturing was found to be quite intense over most parts of the excavation zone. Most, if not all of the observed fractures are genuine new fractures, however, it could not be fully excluded that some of the observed fractures are natural pre-existing faults ('meso-planes'; Section A.4.1.2) which have been reactivated or simply acted as weakness zones delimiting collapsed blocks.

A.4.2.4.2 Moderately indurated formation: Opalinus Clay at Mont Terri URL

Abundant observations on EDZ fractures were made in boreholes, niches, tunnels and galleries. They can be roughly classified into two categories: (1) Extensional brittle fractures in the sidewall and (2) anisotropy- and stress-induced breakouts near the roof (and suppressed by gravity also near the invert).

Extensional brittle fractures

The EDZ at Mont Terri is most likely initiated by micro-scale extensional cracks (see A.3.3.3) induced by the tangential compression in the sidewalls of the underground excavation (see A.4.2.3). Figure A.4-19 shows extensional fracturing, often with plumose fracture surfaces, which can become quite intense, particularly at gallery intersections and niches off-sets.

Figure A.4-19. Intense extensional EDZ fracturing in the sidewall of the Mont Terri URL
Photo: B. Niederberger

Figure A.4-20. Coalescence of extension and shear fractures to form a network of composite fracture planes observed in the sidewall of the Reconnaissance Gallery of the Mont Terri URL
(modified from Thury and Bossart 1999; from Yong *et al.* 2004)

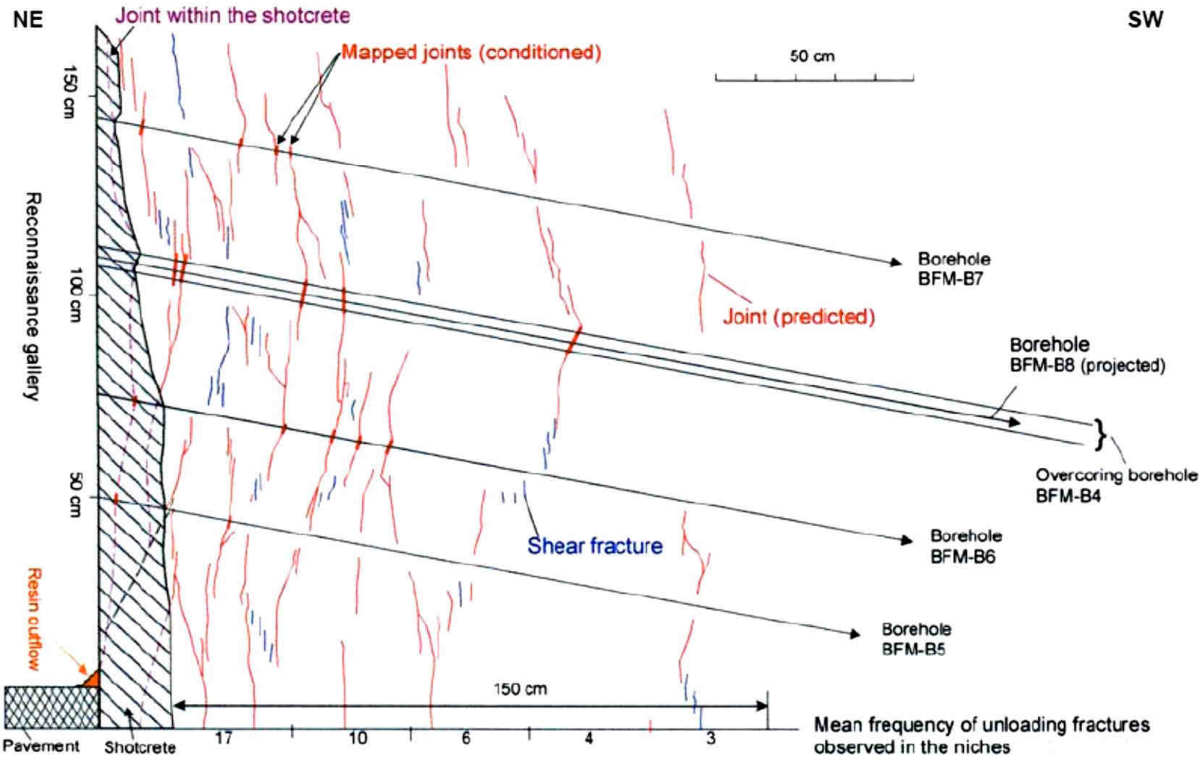

Some detailed study on the spacing of the extensional fractures and their coalescence mechanism with shear fractures to form composite fracture planes were carried out Thury and Bossart (1999) (Figure A.4-20).

Generally, the extensional fractures are oriented parallel to the tunnel wall, irrespective of the bedding trend. The combination of bedding planes intersecting with narrowly spaced subvertical extension fractures can lead to the formation of "pencil-shaped" rock fragments as noted by Nussbaum and Bossart (2006) during mapping the HG-A microtunnel 11 months after its excavation,.

Anisotropy- and stress-controlled borehole breakouts

The controlling anisotropy factor at Mont Terri is bedding. Figure A.4-21 shows instability of some roof strata in a buckling mode (Failure mode 1 in Figure A.3-7).

Figure A.4-21. Buckling of strata in a borehole (left) and geologically-induced overbreak in a gallery of the Mont Terri URL (right; with mechanism indicated; hatched = bedding planes). Photos: Comet, Zurich (modified after Blümling *et al.* 2007)

Delayed breakouts

A follow-up mapping of the HG-A microtunnel some 11 months after the excavation was carried out Nussbaum and Bossart (2006). The microtunnel is oriented parallel to the strike of the bedding planes. The mapping led to substantial refinements of the description of the EDZ fracture network. Newly formed breakouts have detached some wedge-shape pieces from the microtunnel walls thus enabling an extended tunnel section to be observed. The mapping showed that the development of breakouts reflects a long-term process.

Breakouts could be identified at two distinct locations of the circumference of the ~1m ∅ microtunnel (Figure A.4-22) as follows:

(1) In one of the upper sidewalls of the tunnel (Figure A.4-22, right).
These breakouts initiated at a point where the bedding planes and SSE-dipping fault planes are tangentially oriented to the microtunnel, leading to an overprofile at this location (in the sense of Figure A.4-21).

(2) At about mid-height of the opposing sidewall (Figure A.4-22, left).
Stress-induced breakouts result from the presence of extensional fractures behind the tunnel wall (in the sense of Figures A.4-19 to -20).

In a more recent mapping Nussbaum and Bossart (2006) supported a model in which particular emphasis is placed on the bedding planes which, with a certain time delay, are activated in slip.

Figure A.4-22. Delayed breakouts in the HG-A micro-tunnel at Mont Terri, some 11 months after excavation (after Nussbaum and Bossart 2006)

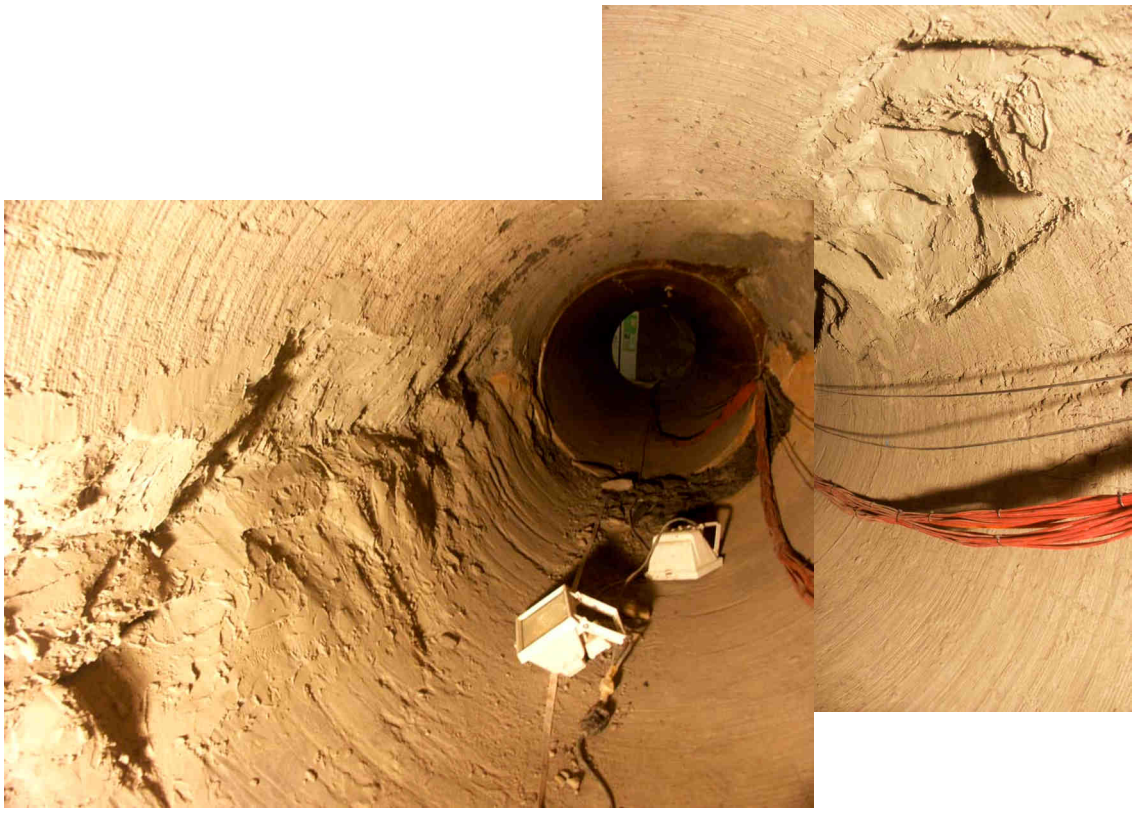

Conceptual model for EDZ around emplacement tunnels in the Opalinus Clay

Discrete fracture network models of the EDZ around emplacement tunnels in a hypothetical repository at depth in the Opalinus Clay have been developed by Lanyon *et al.* (2005). The models were based on studies performed in support of the application for 'siting feasibility' for a HLW repository in the Zürcher Weinland (Nagra 2002b). The observations of the Mont Terri URL, as

shown above, were pivotal for these studies, irrespectively of some geotechnical differences between the two sites (e. g. different *in situ* stress regimes; different inclination of bedding, i.e. sub-horizontal in the Zürcher Weinland versus ~45° inclined at Mont Terri). Figure A.4-23 shows results of a FLAC model of deformation around an emplacement tunnel.

Figure A.4-23. FLAC model prediction of deformation around a repository tunnel in the Opalinus Clay of the Zürcher Weinland (Nagra, 2002b).
(a) Displacements (red; 30x exaggerated)
(b) Max. incremental shear deformation indicating shape and extent of the EDZ

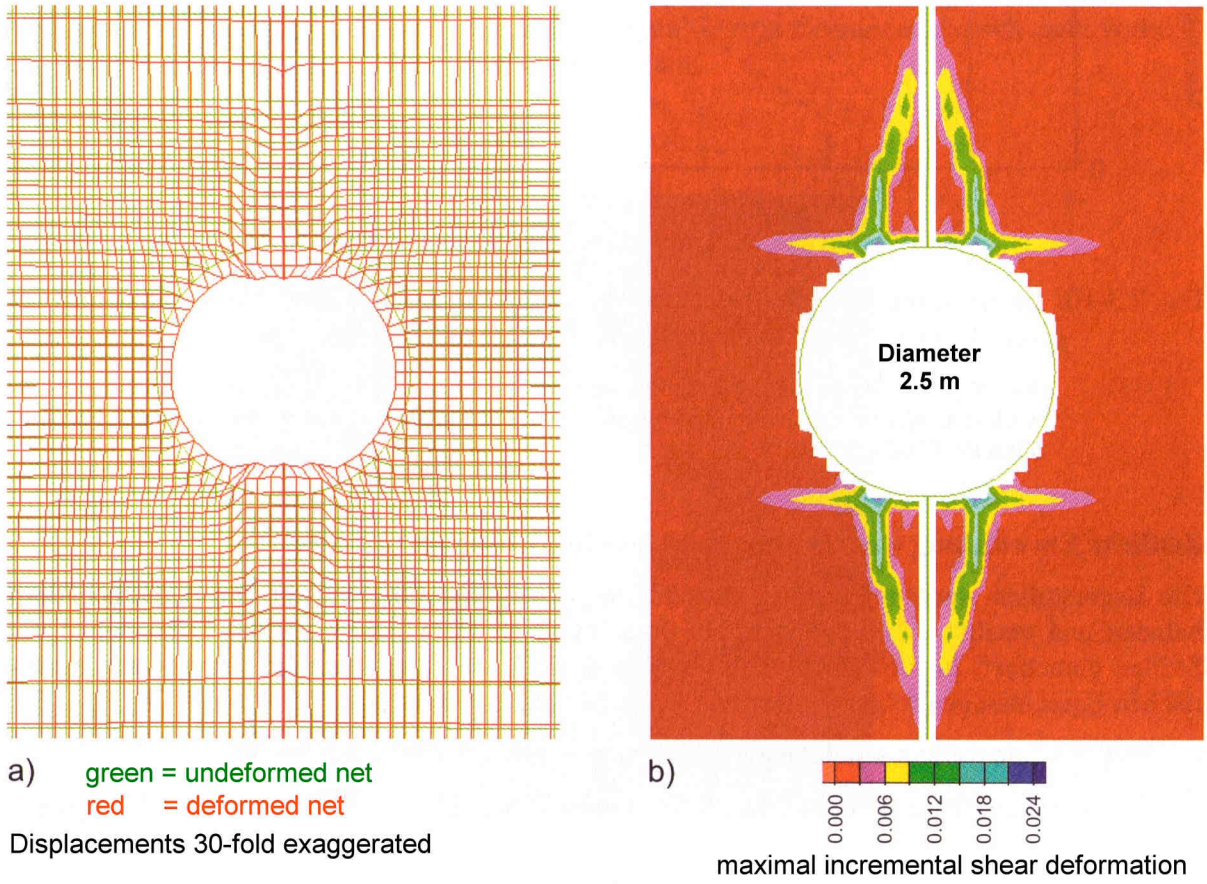

The pattern of deformation is similar to that observed by Økland and Cook (1998) in hollow cylinder laboratory tests of North Sea shales. Økland and Cook identified 'buckling' failure modes in the shales when boreholes were drilled sub-parallel to bedding. Figure A.4-24 shows a detail from the FLAC models overlain by the fracture pattern from Økland and Cook.

Figure A.4-24. Detail of FLAC model prediction of volumetric deformation around a repository tunnel, overlain by fracture pattern from Økland and Cook (1998)
(from Nagra 2002b)

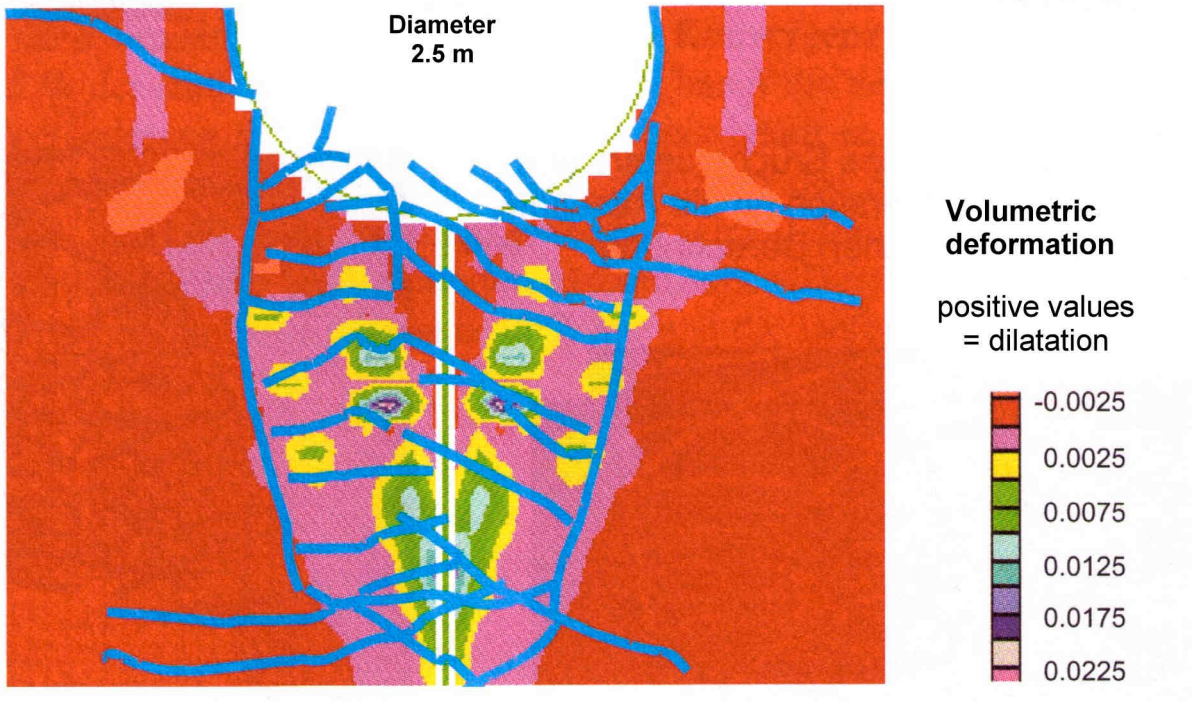

A.4.2.4.3 Slightly indurated formation: Callovo-Oxfordian argillites (COX) in the Bure URL

In most argillaceous parts of the COX formation, a thickness of the 'deconfining' zone of maximally 0.5 m was observed in the immediate vicinity of the experimental drifts and galleries of the -490 m Level (Delay *et al.* 2007). That zone consists mostly of sheared 'oblique chevron' fractures which appeared at the face and walls of the excavation and developed at a maximum distance of 2.5 m off the face. They have a striking similarity with the fracture pattern observed in the plastic Boom Clay at Mol (Figure A.4-25).

Figure A.4-25. 'Oblique chevron' fractures at the tunnel excavation face (top) and in drill cores (bottom). Comparison between behaviour in plastic clay (left; HADES URF; see also Figure A.4-16) and in slightly indurated clayey rocks (right; Bure URL) (from Wileveau and Bernier 2007)

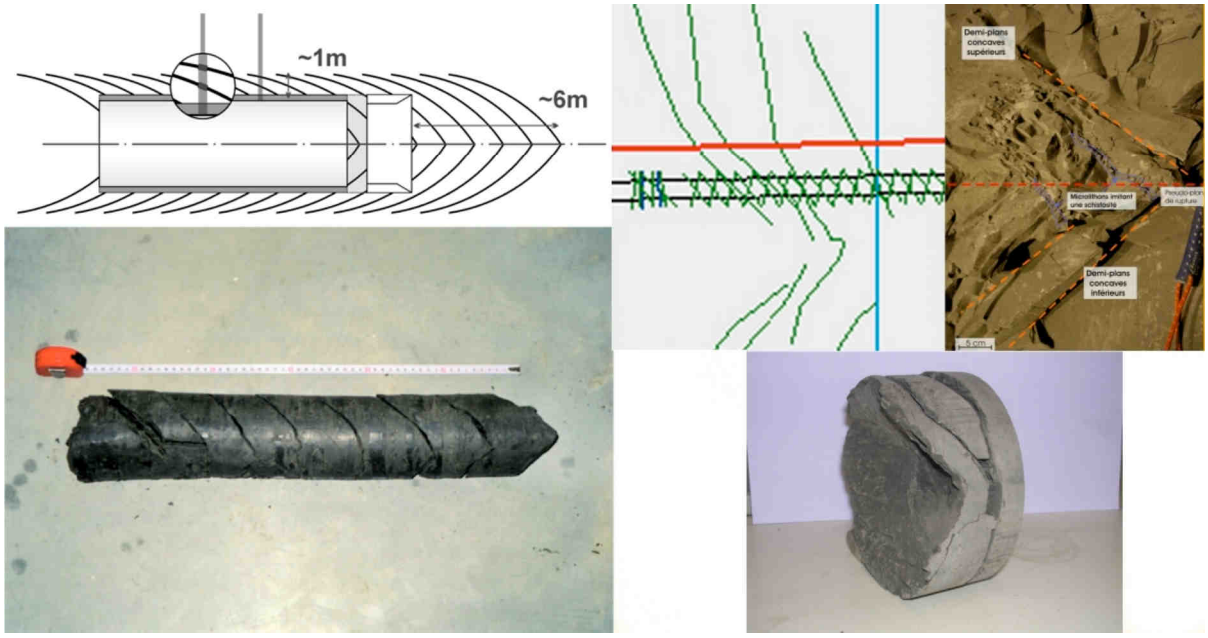

The occurrence of sheared fractures and their geometry appears to depend on the excavation conditions and techniques, such as speed and continuity of the excavation work, installation of the ground support, the support of the drift face and the direction of the drift with respect to the *in situ* stress field (Figure A.4-26).

Figure A.4-26. Conceptual model of the EDZ fractures around a drift at 490 m depth in the Callovo-Oxfordian formation at Bure (from Andra 2005d)

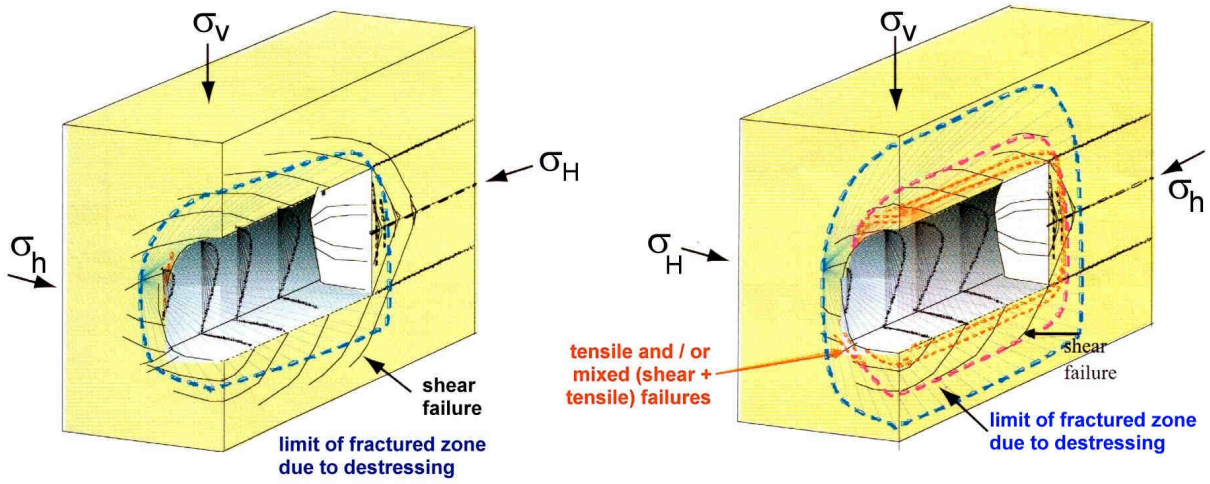

The characterisation of the damaged and disturbed zones was carried out by means of several methods: structural analysis of core samples, micro-seismic borehole logging, seismic refraction, surface wave measurements and of permeability to gas and water measurements (Figure A.4-27).

Figure A.4-27. EDZ around a drift at the -490 Level of the Bure URL as determined by fracture mapping, *in situ* gas testing and seismic measurement (Andra 2005d)

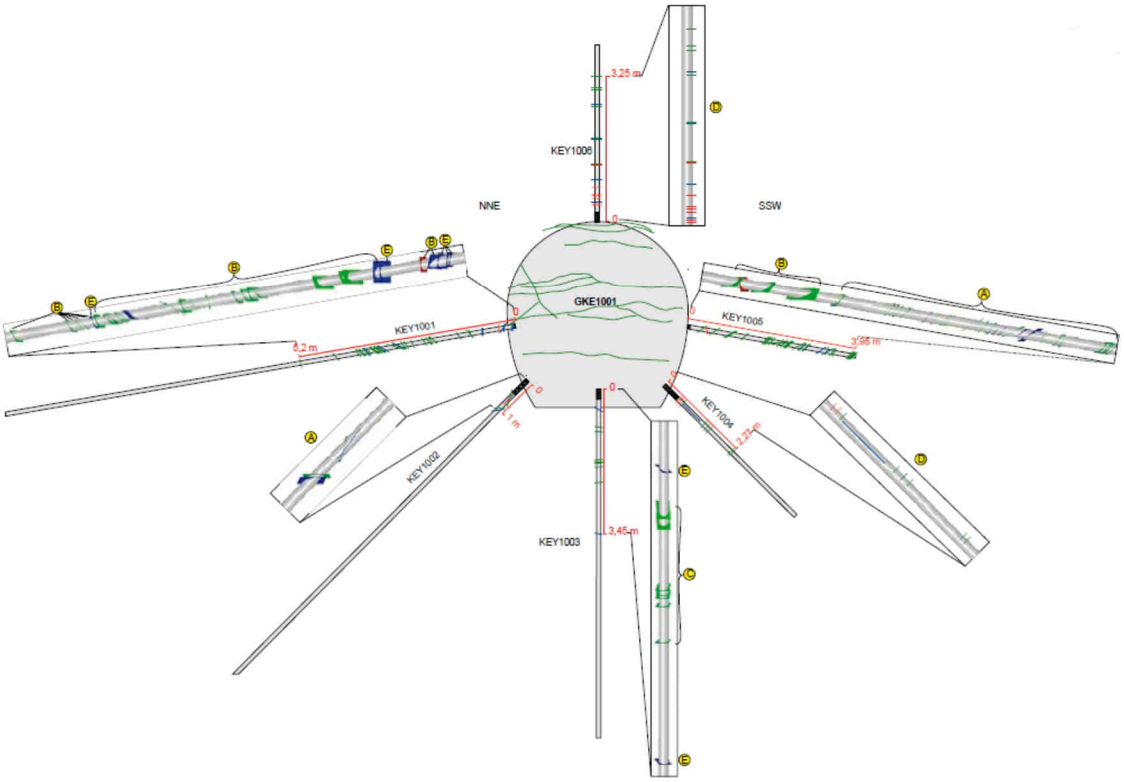

Only the sections of fractures closest to the gallery have a hydraulic conductivity higher than that of the undisturbed COX formation. In the GMR Drift, momentarily being that structure most isolated from other underground openings, the extension of the high permeability zone is about 0.5 m horizontally (in the sidewalls) and 1 m vertically (in the floor).

A Performance Assessment (PA) model of the permeability values of the various zones are given in Figure A.4-28.

Figure A.4-28. PA model of the hydraulic conductivity K of the various zones in and around a gallery of the Bure URL (after Plas and Aranyossy 2005)

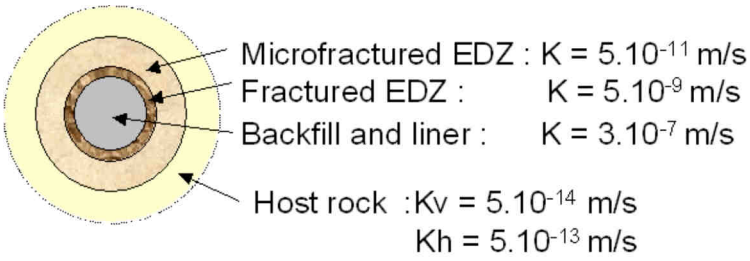

A.4.2.5 Opening and closure of EDZ fractures by tunnel climate variation

Changes in the underground opening's ventilation system might lead to de-saturation / resaturation processes within the EDZ rock and, as a possible consequence, also to changes in the aperture of the EDZ fractures and their transmissivity. The Ventilation Experiment (VE) of the Mont Terri URL (Mayor *et al.* 2007; Mayor and Velasco 2008) is a relevant demonstration test in this regard, as it was performed at relatively large scale along a 10 m-long section of a non-lined microtunnel, ∅ = 1.3 m. Also the duration of the VE Experiment is comparatively long with two de-/resaturation phases lasting about 25 months in total.

The microtunnel was excavated by raise boring technique in 1999, and oriented perpendicular to the bedding strike direction of the shaly facies of the Opalinus Clay (mean value of the bedding dip ≈ 25° in the test section). In 2002, 3.4 years after the microtunnel excavation, the selected VE test section was instrumented and sealed-off by means of two double wooden doors. Since then, two de-saturation phases, called VE-I and VE-II, have been performed. The first one (VE-I) had a duration of about 8 months and was terminated in January 2004. After a resaturation period of about 17 months, the second phase (VE-II) was implemented, lasting for approximately 17 months until December 2006.

The following main conclusions can be drawn from the VE Experiment:

- due to drift ventilation, the desaturation of clayey rocks of low hydraulic conductivity ($K < 10^{-12}$ m/s) is very small. In both desaturation periods, the clayey rock around the 1.3 m diameter microtunnel remained practically fully saturated, except in a small ring of thickness about 30 cm, despite suction developed up to a distance of approximately 2.0 – 2.5 m into the rock;

- the geochemical changes in the clayey rock near-field, around a microtunnel excavated more than eight years ago and after two extreme artificial ventilation periods, have a negligible effect upon the hydromechanical behaviour of this clayey rock (see also Sections 3.2 and 4.5 of main text);

- following the desaturation (= ventilation) phases only very small shrinkage fractures were detected. The average width of these fractures was about 0.9 mm which reduced to about 0.1 mm in subsequent resaturation, and

- the extent of the EDZ stays practically constant along relatively long and extreme desaturation periods. Macroscopic fractures (> 30μm) appear to be concentrated in the first 40 cm.

APPENDIX 5

CONCEPTS OF MASS TRANSPORT IN ARGILLACEOUS FORMATIONS

Overview

This appendix provides, in addition to Section 2.3.4 of the main text, some detailed information on those concepts of mass transport (fluid flow and movement of solutes) which are important for the understanding of self-sealing features and processes in argillaceous formations. It includes reviews of the concept of porosity (Section A.5.2) and of single flow through unfractured porous media and fractured media (Sections A.5.3 and A.5.4). After reference is made to theoretical definitions, experimental results upon the main argillaceous formations are considered for radioactive waste confinement, with special emphasis on Callovo-Oxfordian (COX) argillite (Bure, France), derived through both laboratory and *in situ* research. The self-sealing ability of COX argillite is clearly shown.

A.5.1 Introduction

The theoretical framework developed to quantify fluid flow and the movement of solutes in geological media is based largely on the properties of a porous medium (Horseman *et al.* 2005). The underlying assumptions are that:

a. the medium has a rigid or only slightly deformable solid framework,

b. the pores are of sufficient size so that interfacial effects do not exercise a dominant control on mass transport,

c. the pore fluid displays Newtonian rheological behaviour with a fixed viscosity equal to that of the bulk fluid, and

d. the main constraint on the movement of the fluid is viscous drag in the tortuous pore channels of the medium.

When looking at the wide variety of naturally occurring argillaceous formations (ref. to Section A.2), it becomes apparent that a number of these assumptions are not generally valid. Many clays have a very deformable matrix (Figures A.2-1, A.2-8 and A.2-9) so that small variations in pore pressure can lead to substantial changes in pore volume. This is the object of the *poro-mechanics* approach (Coussy 2004). Most clays interact strongly with permeating aqueous solutions (e.g. Dormieux *et al.* 2006a; Karnland *et al.* 2006; Cariou *et al.* 2007). The associated chemical interactions can cause changes to both the interparticle spacing and the fabric of a clay. Furthermore, the typical interparticle spaces in an argillaceous rock can be so small that interfacial effects gain a dominant influence on mass transport within the clay matrix (Dormieux *et al.* 2006a; ref. also to Section 4.1.4). The viscosity of the water present in a claystone may also be higher than that of bulk

water, and the possibility that the porewater may exhibit non-Newtonian behaviour cannot be excluded.

Despite these obvious difficulties, porous media theory is almost universally applied to the problem of groundwater transport in clays, and often provides an acceptable mathematical description. Indeed, in practice, this approach is generally sufficient to account for the main phenomena occurring during fluid transport, and more refined notions are introduced only if necessary (Cariou *et al.* 2007). This has not proven to be the case presently in investigating the self-sealing of argillaceous formations. The review of certain key terms, as presented in the following Sections A.5.2 to A.5.4, should be considered against this background.

A.5.2 Porosity

A.5.2.1 Assumptions and definitions

A porous medium is assumed to be constituted of a solid matrix and of empty spaces (i.e. pores). The pores may be interconnected or not. The porosity n of such porous medium may be defined as:

$$n = (V_p / V) * 100 [\%] = [1 - (V_s / V)] * 100 [\%] \quad \text{(Eq. A.5-1)}$$

or

$$n = (1 – \rho_d / \rho_s) * 100 [\%] \quad \text{(Eq. A.5-2)}$$

where: n = porosity [dimensionless]
V_p = volume of pores (or voids) [m^3]
V = volume of the bulk sample [m^3]
V_s = volume of solids (or grains) [m^3]
Note: $V = (V_p + V_s)$
ρ_d = density of dry bulk material [kg/m^3]
ρ_s = density of solids (or grains) [kg/m^3].

Within this definition, two notions of porosity may be referred to: (1) the Eulerian porosity n refers to the non-deformed material state ($V = V_o$ is the initial volume in Eq. A.5-1), whereas (2): the Lagrangian porosity φ is defined with reference to the deformed state ($V = V(t)$ is the sample material current volume in Eq. A.5-1).

Percolation of a fluid phase throughout a porous medium requires a minimum amount of interconnected pores. At the field scale, logging techniques are available, such as nuclear magnetic resonance logging, which preserve the material hydration level. In the laboratory, when applying the usual experimental means such as mercury intrusion porosimetry (MIP), the accessible pore volume is only a part of the interconnected pore volume, and the true total pore volume V_p is not very easily accessible (Yven *et al.* 2007; ref. also to Section A.2.3.2). Additional measuring techniques may be used: Gas-adsorption techniques provide access to a wider pore range (Yven *et al.* 2007), and 2-D imaging techniques (optical microscopy, scanning electron microscopy, autoradiography, etc.; Yven *et al.* 2007) provide insights into the pore texture and arrangement. Transport properties are not only influenced by the medium's porosity n (or φ when the sample deformation is considered), but also by its interconnected pore network tortuosity and pore size distribution (Dormieux *et al.* 2006b).

If it is assumed that the solid matrix is deformable, and time-dependent deformation is not considered, then all of the above equations and statements remain valid for any constant load level Moreover, as a first approximation, these may be used in a step-by-step approach whenever the solid matrix is actually subjected to deformations. Indeed, the issue is that a porous medium such as argillaceous rock is made up of a multi-modal pore structure and the specification of a "porosity" may not be sufficient to adequately describe the hydro-mechanical behaviour of the medium when subjected to mechanical load. Thus, the connectedness of the porosity could change by incremental load applications if the pore system is close to its percolation threshold. Similarly, time-dependent deformation (creep) could give rise to sudden changes in pore connectivity. Consequently, permeability may not develop continuously, even though the porosity evolution exhibits a continuous behaviour. Therefore, using the above-mentioned equations "in a step-by-step approach" may not be correct in a strict sense.

A further assumption is that fluid transport through a porous medium may be represented by fluid mechanics equations, which implies that a representative elementary volume of a fluid (respectively a fluid particle) may be defined so that, at the relevant scale, the fluid properties may be considered homogeneous and constant.

A.5.2.2 Case of argillaceous formations

Table A.5-1 compiles the porosity values which are encountered in the Boom Clay at Mol, the Opalinus Clay at Mont Terri and the Callovo-Oxfordian (COX) formation at Bure.

Table A.5-1. Porosity values of some argillaceous URL sites
(ref. also to Tables A.3-2 and A.3-4)

Formation (Location)	Porosity n [%]	Reference
Boom Clay (Mol, HADES URF)	36.3	Bernier *et al.* (2004)
Opalinus Clay (Mont Terri URL)	13.7 ± 2.5	Bock (2009)
Callovo-Oxfordian (Bure URL)	14 (carbonated levels) to 19.5 (argillaceous levels)	Yven *et al.* (2007)

In a synthesis of previous studies, Yven *et al.* (2007) have performed a thorough evaluation of COX argillite pore network, using MIP, nitrogen gas-adsorption curves and 2-D imaging techniques for both boreholes and laboratory samples. As seen in Table A.5-1, porosity values depend upon the argillite location and mineralogy (either mainly carbonated or mainly argillaceous). Three pore scales are identified and quantified as follows: Micropores, smaller than 2nm, represent less than 2% of the total accessible porosity; mesopores, ranging from 2 to 50nm, amount to 60 to 80%, and macropores, larger than 50nm, represent 20 to 40% of the total accessible pores.

A.5.3 Single-phase flow through porous media: Darcy's law and notion of permeability – limits and validity

A.5.3.1 Review of some fundamental equations

When considering the 3-D case of an incompressible Newtonian viscous fluid flowing at a sufficiently low velocity through a homogeneous and isotropic medium, generalised Darcy's law writes, for any fluid particle:

$$\mathbf{v} = -(k / \mu)(\nabla p - \rho g \nabla \mathbf{z}) \qquad \text{(Eq. A.5-3)}$$

where:
- $\mathbf{v}$ = convective (or filtration, or Darcy's, or superficial) flow velocity vector [m/s]
- k = intrinsic (or specific) permeability to the solid matrix [m²]
- μ = dynamic viscosity of the percolating fluid [Pa * s]
- p = hydrostatic pressure [Pa or N/m^2]
- ρ = fluid density [kg/m^3]
- g = gravitational acceleration [equal to 9.81m * s^{-2}]
- $\mathbf{z}$ = ascending vertical unit vector [m]

The intrinsic permeability k has the dimension of a surface [m^2]. It depends solely upon the porous solid phase. Eq. A.5-3 may be simplified by neglecting the gravitational term $\rho g \nabla \mathbf{z}$, provided that it is significantly lower than the hydrostatic pressure gradient ∇p. Permeability describes phenomena which are related between the porous medium conductivity and the filtration (or flow) of a Newtonian viscous fluid. For anisotropic porous media, a second order permeability tensor has been proposed in (Eq. A.5-3). Its symmetry is discussed in various studies, such as in Bear (1988) and Dullien (1992).

Under permanent conditions for an incompressible Newtonian viscous fluid and assuming a uniform flow field through a homogeneous and isotropic porous medium, Darcy's law simplifies to (Dana, 1999):

$$Q = (k A / \mu)(\Delta p / L) \qquad \text{(Eq. A.5-4)}$$

or, alternately, to:

$$k = (Q \mu / A)(L / \Delta p) \qquad \text{(Eq. A.5-5)}$$

where:
- Q = flow rate of the fluid volume [m^3/s]
- μ = dynamic viscosity of the percolating fluid [Pa * s]
- A = cross-sectional area of the flow path [m^2]
- L = length of the flow path [m]
- Δp = pressure difference between upstream and downstream medium sides (i.e. entrance and exit) [Pa or N/m^2]

Complementarily, the hydraulic conductivity K [m/s] is defined as:

$$K = Q L / (\Delta h A) \qquad \text{(Eq. A.5-6)}$$

where: Δh = hydraulic head increment (= $\Delta p / \mu$) [m]

The dimensionless hydraulic gradient i is defined as:

$$i = \Delta h / L \qquad \text{(Eq. A.5-7)}$$

The parameters K and k are interrelated as follows:

$$K = k * \rho * g / \mu \qquad \text{(Eq. A.5-8)}$$

For water at an ambient temperature of 20° C (i.e. $\mu = 10^{-3}$ Pa $*$ s), it is:

$$K \approx 10^{7} * k \qquad \text{(Eq. A.5-9)}$$

A. 5.3.2 Experimental methodologies

Several methods exist to measure porous material permeability k under loading. Which of these methods to employ depends mainly on the order of magnitude of k (Skoczylas and Fleureau 2003). The methods usually consist in applying an axial one-dimensional steady state or transient fluid flow, corresponding to a given pressure difference, through a circular cylindrical sample placed in a conventional triaxial test rig. Whatever the method, particular attention has to be paid to calibrate pressure and flow rate measurements and to control micro-seepage, flow geometry, etc.

For $k \geq 10^{-19}$ m^2, steady state flow permeability tests are usually a good choice, as Darcy's law (ref. to Eq. A.5-5) can be applied directly to derive k from the imposed flow rate and pressure conditions (Meziani and Skoczylas 1999; Loosveldt *et al.* 2002).

For $k < 10^{-19}$ m^2, steady state flow test duration becomes extremely long (from several weeks to several months for one measurement). Hence, transient techniques are preferred, such as pulse test or harmonic method. The pulse test, as described by Brace *et al.* (1968), consists in placing a circular cylindrical specimen between two fluid reservoirs at the same initial static pressure level p_1. A small pressure increase is then applied upstream and the fluid (liquid or gas) is let to flow while measuring the evolution of the differential pressure between upstream and downstream circuits, (p_1-p_2) versus time t (ref. Figure A.5-1). Simplified analytical methods (Skoczylas and Henry 1995; Hsieh *et al.* 1981; Neuzil *et al.* 1981) describe the differential pressure evolution by way of an exponential approach:

$$(p_1 - p_2)(t) = \Delta p_1 \exp(-c\, k\, t) \qquad \text{(Eq. A.5-10)}$$

where: c = constant, depending on the experimental set-up
k = permeability.

Adequately interpreted, $(p_1-p_2)(t)$ measurements provide, within some few hours, reliable results for very low k values (even below $10^{-20} m^2$). Tests can be conducted either under gas or liquid flow. Pulse tests can have an accuracy better than 5%, as shown by Skoczylas and Fleureau (2003) using an experimental rig for water flow experiments, which is much better than with steady state flow tests. The transient pulse testing technique requires the measurement of only upstream and downstream side pressures p_1 and p_2 with time t, and in this manner it is quite quick and simple to set and operate. As the initial permanent flow regime is only scarcely disturbed, boundary effects are limited. The pressure micro-pulse Δp_1, applied on the sample upstream side at time t = 0, is quite small and represents about 5% of the amount of the static pressure p_1. There is general agreement that such small perturbation is insufficient to notably modify the saturation rate by an expulsion of water (Dana

1999). This technique has been successfully applied to granite (Skoczylas and Henry 1995), sandstones (Dana 1999) and COX argillite (Davy *et al.* 2007). Nevertheless, whenever possible (i.e. predominately time permitting), quasi-stationary permeability tests are preferable to transient tests. This is because storage effects and flow effects cannot be measured separately with transient tests. Another point is that transient tests cannot unambiguously identify the occurrence of non-linear flow behaviour. Moreover, testing with gas introduces not only problems associated with highly compressible fluids, but also the capillary aspect (finite entry pressures of the material; etc.).

An alternative to the pulse test is the harmonic method as developed by Jouanna and Fras (1979), which consists of creating a sinusoidal pressure wave in the upstream reservoir. Following transmission through the specimen, the amplitude and phase of the downstream wave are analysed and k and other poro-mechanical properties are derived. It appears that the harmonic testing technique is more delicate to implement than the pulse test.

Figure A.5-1. Sketch of the experimental device used for the pulse test technique, enabling the determination of very low permeabilities (k values $<10^{-19}$ m²)
(from Davy *et al.* 2007)

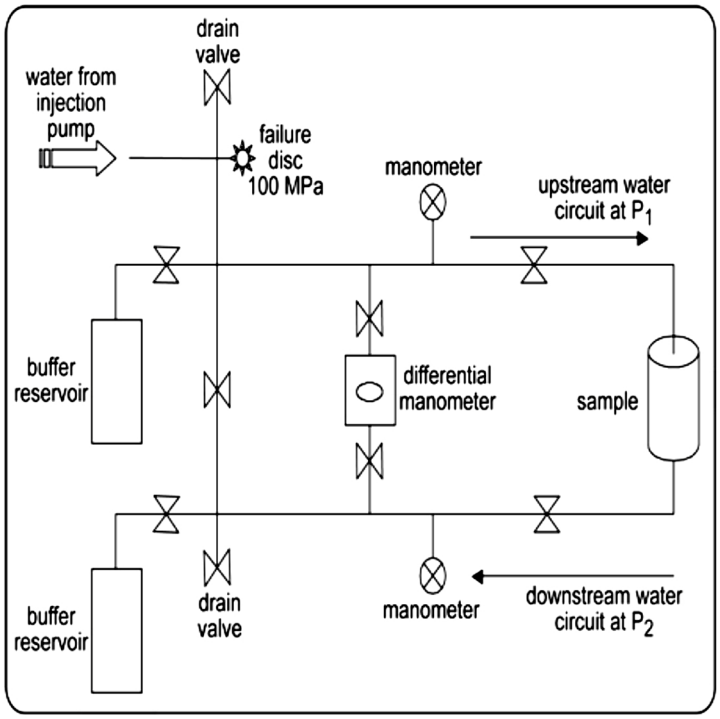

A.5.3.3 Case of argillaceous formations

Tables 2-7 and A.5-2 specify the permeability values (and via Eq. A.5-9 implicitly also those of the hydraulic conductivity) encountered in the undisturbed formations of the Boom Clay at Mol, the Opalinus Clay at Mont Terri and the Callovo-Oxfordian argillites (COX) at Bure.

For intact COX argillites (i.e. those without any noticeable micro- or macro-cracking), water permeability along the bedding planes ranges from $10^{-19}m^2$ down to $10^{-21}m^2$ with increasing confining pressure (Zhang and Rothfuchs 2004). This is less than an order of magnitude lower than the permeability measured perpendicular to bedding. Gas permeability of the initially dry intact rock ranges from $10^{-17}m^2$ down to $10^{-19}m^2$, possibly due to the presence of micro-cracks generated during drying. Initially dry intact rock exhibits a greater anisotropy than fully saturated rock. As shown by Montes *et al.* (2004), the saturation level strongly influences the microstructure of the argillite, particularly the frequency of micro cracks and pores. Similarly, Chiarelli *et al.* (2003) provide an average value of $10^{-20}m^2$ for COX argillite intrinsic water permeability, evaluated at the laboratory scale using initially quasi-saturated intact samples (i.e. samples without cracks). A French benchmark study (GDR FORPRO 2003) has also provided water permeability measurements for intact fully saturated COX argillites, with results ranging from 10^{-20} to $10^{-21}m^2$, which is in accordance with the former.

Table A.5-2. Intrinsic permeability values of some argillaceous URL sites
(see also Table 2-7)

Formation (Location)	Permeability k [m^2]	Reference
Boom Clay (Mol, HADES URF)	k_{water} 200 - 400 $*$ 10^{-21}	Bernier *et al.* (2004)
Opalinus Clay (Mont Terri URL)	$k_{\perp ss\ water}$ $7 * 10^{-21}$ $k_{// ss\ water}$ $20 * 10^{-21}$	Bock (2009)
Callovo-Oxfordian (Bure URL)	k_{water} 10^{-19} to 10^{-21}	Andra (2005a) Delay *et al.* (2006)

A.5.3.4 Limits to Darcy's law application

Darcy's law provides a linear relationship between the convective fluid velocity **v** and the hydraulic charge gradient ∇p. Whenever the fluid velocity becomes sufficiently high, an inertial pressure loss is generated by the acceleration and deceleration of the fluid occurs as it flows through the tortuous paths of the porous medium. This phenomenon, termed the **Forchheimer's effect**, manifests itself as a non-linearity in the dependency of the flow rate upon the pressure drop. Incorporating this effect into Darcy's law results in the Forchheimer's equation (Gostick *et al.* 2006):

$$-\nabla p = (\mu/k)\,\mathbf{v} + \beta\,\rho\,|\mathbf{v}|\,\mathbf{v} \qquad \text{(Eq. A.5-11)}$$

where: ρ = fluid density [kg/m^3]
β = inertial coefficient [m^{-1}], also referred to as Forchheimer or non-Darcy coefficient.

It is generally acknowledged that Darcy's law is valid for flows characterised by a Reynolds number Re ranging from 1 to 10 (ref. e.g. to Bear 1988). By definition, the Reynolds number Re measures the ratio between the inertial forces and the viscosity forces within the fluid. For a porous medium (ref. to De Marsily 1986a), Re may be defined in analogy with the classical fluid mechanics circular cylindrical pipe as follows:

$$Re = \rho V l / \mu \qquad \text{(Eq. A.5-12)}$$

where: ρ = fluid density [kg/m^3]
V = average velocity of fluid [m/s]
l = characteristic length of the porous network [m]
μ = dynamic viscosity of the fluid [Pa * s]

The term l may be approximated as ($\sqrt{k}$) (De Marsily 1986a). A Reynolds number Re between 1 and 10 corresponds to a low filtration velocity flow regime of a laminar type, for which viscosity forces may not be neglected when compared with inertial forces. Outside of this flow regime, for Re<1 or Re>10, Darcy's law is generally corrected by adding non-linear velocity terms (see Bear 1988; Dana 1999). In particular, Forchheimer's formula (Eq. A.5-11) provides a correction for Re <1000 with a non-linear term also dependent upon the medium porosity. Admittedly there exists a minimal hydraulic gradient below which no noticeable fluid flow occurs: this is potentially interpretable as a consequence of a counter-current formation, which oppose the fluid flow. To our knowledge, no research study has been performed to date upon argillaceous rock transport properties, accounting for Re <1 or >10. Indeed, porosity being so small in an argillaceous host rock, Re <1 or >10 are very possibly not obtainable and/or realistic scenarios.

Another particular phenomenon worth mentioning is the **Klinkenberg effect**, which may be encountered under gas flow. Indeed, contrary to laminar liquid flow, low pressure gas flow throughout a porous medium occurs at higher velocities than predicted. Fluid mechanics shows that any gas flowing through a capillary tube of diameter comparable to the mean free path of gas molecules has a higher velocity than that predicted by the Poiseuille's equation which describes the laminar flow regime. The contact between the gas molecules and the capillary tube wall is not perfect, i.e. the gas molecules may *slide* upon the tube wall. Therefore, wherever the gas molecule mean free path is comparable to the solid medium pore network size, sliding at the pore surface will add a contribution to the laminar flow predicted by Poiseuille's Law.

A.5.4 Single-phase flow through *fractured* porous media: notion of fracture

A.5.4.1 Review of some fundamental equations

Fluid transport through fractured media may be tackled as intact media with the notion of permeability (see Section A.5.3), with the advantage that values for intact as well as for fractured porous media may be directly compared. Nevertheless, hydro-geologists and geologists usually work with the notion of **fracture transmissivity** (De Marsily 1986a).

For an isotropic horizontal fluid flow, for instance inside a water-bearing bed, the transmissivity T is defined as (De Marsily 1986a):

$$T = K * e \qquad \text{(Eq. A.5-13)}$$

where: T = fracture transmissivity [m^2/s]
K = hydraulic conductivity [m/s]
e = fluid flow thickness [m]

The fluid flow thickness e is the smallest dimension perpendicularly to the flow axis. For a single macro-cracked material under a fluid flow parallel to its fracture planes, e is equivalent to the

fracture aperture a_h. Yet, in general, the flow network may consist of several discontinuities or a discontinuity network. In the case of granitic rock, and very possibly quite specifically for this type of rock, Pusch (1995) developed a rock structure model for discontinuities, with a hierarchy of seven orders based on their geometry (Table A.5-3), which aids in the characterisation of the fracture transmissivity versus the hydraulic conductivity.

Considering Equation A.5-8, the transmissivity T can also be denoted as:

$$T = e * k * \rho * g / \mu \qquad \text{(Eq.A.5-14)}$$

If a laminar fluid flow is assumed between two parallel walls of a fracture plane at a distance a_h from one another, Poiseuille's solution also provides (De Marsily 1986a) $k = (a_h^2/12)$, so that finally:

$$T = \rho * g * a_h^3 / (12\,\mu) \qquad \text{(Eq. A.5-15)}$$

where: ρ = density of porewater [g/m^3]
g = gravitational acceleration [N/kg] or [m/s^2]
a_h = aperture of fracture [m]
μ = dynamic viscosity of the fluid [Pa * s]

Similarly to permeability k, transmissivity T may be anisotropic and therefore defined as a second order symmetrical tensor (De Marsily 1986a).

Table A.5-3. Hierarchy rock structure model for discontinuities in granite
(from Pusch 1995)

Geometry of Discontinuity				Hydraulic Characteristics	
Order	**Length [m]**	**Spacing [m]**	**Width [m]**	**Transmissivity [m²/s]**	**Hydraulic conductivity [m/s]**
1st	$> 10^6$	$> 10^3$	$> 10^2$	$10^{-5} – 10^{-2}$	$10^{-7} – 10^{-5}$
2nd	$10^3 – 10^4$	$10^2 – 10^3$	$10^1 – 10^2$	$10^{-7} – 10^{-4}$	$10^{-8} – 10^{-6}$
3rd	$10^2 – 10^3$	$10^1 – 10^2$	$10^0 – 10^1$	$10^{-9} – 10^{-6}$	$10^{-9} – 10^{-7}$
4th	$10^1 – 10^2$	$10^0 – 10^1$	-	-	$10^{-11} – 10^{-9}$
5th	$10^0 – 10^1$	$10^{-1} – 10^0$	-	-	$10^{-12} – 10^{-10}$
6th	$10^{-1} – 10^0$	$10^{-2} – 10^{-1}$	-	-	$10^{-13} – 10^{-11}$
7th	$< 10^{-1}$	$< 10^{-2}$	-	-	$< 10^{-13}$

Some extensions of Eq. A.5-15 were developed to account for the surface roughness of the fracture walls (Bear 1993). Bandis *et al.* (1983) coupled the transmissivity equation with the normal stress σ_n which is acting normal to the fracture plane. For COX argillite, Davy *et al.* (2007) coupled k with the hydrostatic pressure p_c applied to a circular cylindrical macro-cracked sample (i.e. $p_c = \sigma_1 = \sigma_2 = \sigma_3 < 0$).

A.5.4.2 Case of argillaceous formations

For COX argillites, Davy *et al.* (2007) have performed laboratory experiments on initially macro-cracked samples subjected to hydrostatic pressure aimed at reproducing *in situ* lithostatic pressures. The initial macro crack in the diametric plane of the sample is obtained by means of a Brazilian splitting test. This provides some variability in the initial fracture opening geometry, similar to that encountered *in situ*. The experimental set-up allows the accurate measurement of the crack closure (denoted cc) during the mechanical loading provided by a triaxial cell (see Figure 3-20 of main text). Whenever the hydrostatic pressure is fixed at a given value, both crack closure cc and the permeability k are measured. Permanent regime gas permeability measurements were performed, showing a clear non-linear dependency of both crack closure cc and gas permeability k_{gas} to hydrostatic pressure p_c. All experimental data relating the gas permeability k_{gas} to the crack closure cc may be described, independent of the sample, by a single relationship (ref. Figure A.5-2). After the first loading cycle, during which it is believed some crack asperities are irreversibly crushed, gas permeability also demonstrates a bi-univocal relationship with hydrostatic loading, independent of the sample.

The second test phase is of particular relevance to the self-sealing topic. After the injection of gas (inert 99% pure Argon) through macro-cracked argillite, water pulse injection experiments (transient technique as described in Section A.5.3) were performed for days (and months!) to evaluate the evolution of the water permeability over time, and to collect evidence of any potential COX argillite sealing. First and as expected, water permeability decreases with increased hydrostatic pressures p_c (e.g. Stages 0→1, 2→3, etc. in Figure A.5-3). However, at stages during which the hydrostatic pressure was held constant (e.g. Stages 1→2, 3→4, etc.), there was a tendency to a negative crack closure, i.e. an apparent crack opening. This is mainly attributed to swelling of the interfacial fracture zone surfaces due to wetting through test-related water injection.

Figure A.5-2. Dependency between normalised permeability k/k_0 and macro crack closure variation ($cc-cc_0$) in gas injection tests of three samples
(from Davy *et al.* 2007)

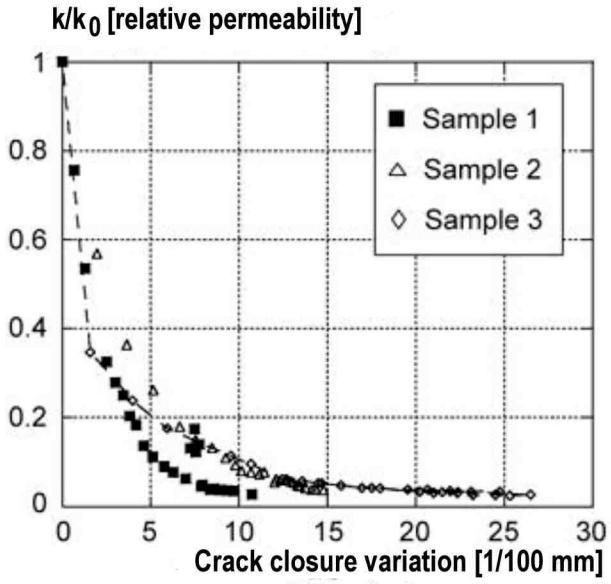

Figure A.5-3. Water permeability experiment of a macro-cracked COX argillite specimen (Sample 5). Swelling is recorded as apparent crack opening at stages when the hydrostatic pressure p_c is held constant. Numbers: Successive stages of the test.

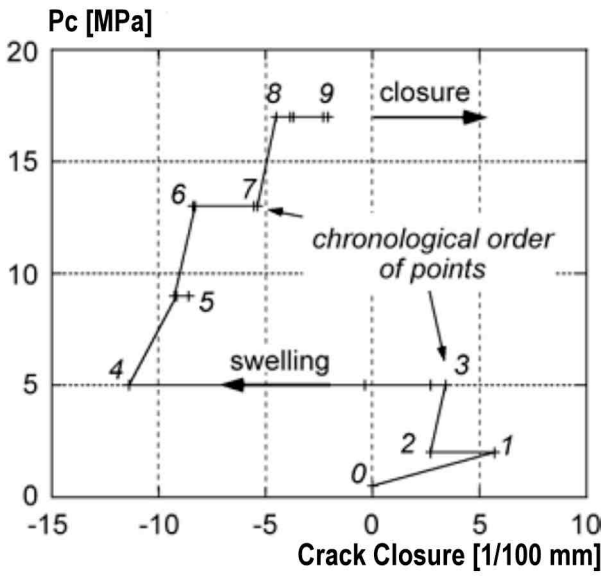

With regard to the overall evolution of the water permeability, the macro-cracked sample loses several orders of magnitude with increasing hydrostatic load, and the initial values are never recovered during subsequent load cycles (Figure A.5-4). Most interestingly, this phenomenon is not fully reversible: after losing several orders of magnitude during initial loading, the water permeability k never fully recovers during unloading, even following an increased duration of water injection. After some two to ten days of maintaining constant water injection flow, a water permeability of the order of 10^{-20} to 10^{-21} m^2 is attained, which corresponds with the water permeability of intact COX argillites (see Figure A.5-5 and Table A.5-2).

In brief, there is, at the laboratory scale, clear evidence of the sealing of COX argillites, which we find as being due to two factors:

- Increased hydrostatic loading up to an order of the expected *in situ* lithostatic pressure levels (of up to 17 MPa); and
- swelling of the fracture wall rock material.

Compared with the effects of the hydrostatic loading, swelling is particularly effective in the sealing process and might be attributed to the presence of non-negligible amounts of smectite-type clay particles within the argillaceous rock (Yven *et al.* 2007). An additional factor may be clogging of clay particles within the fracture lips, yet this contribution appears to be very limited. Indeed, sealing occurs even in the absence of an actual fluid flow, due to suction generated during the course of resaturation.

Figure A.5-4. Evolution of the water permeability k in course of a hydrostatic load test of a macro-cracked COX argillite specimen
(Sample 2; numbering = successive test stages). The initial permeability is never recovered after the first loading phase

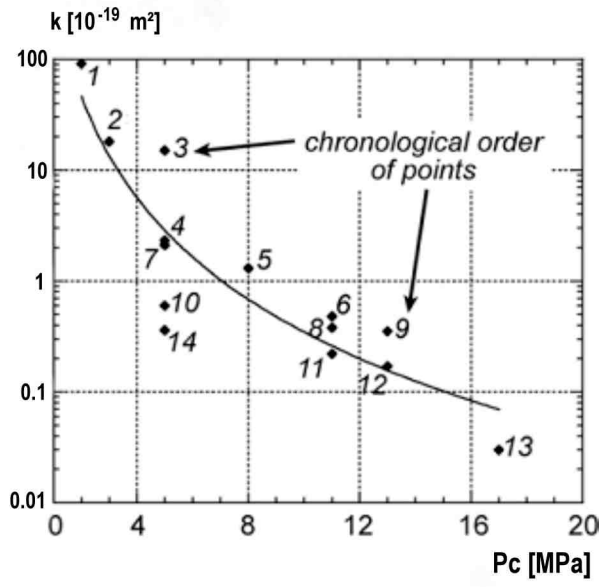

Figure A.5-5. Evolution of the water permeability k in dependency of the duration of the water injection test of a macro-cracked COX argillite specimen
(Sample 5; out of Davy *et al.* 2007)

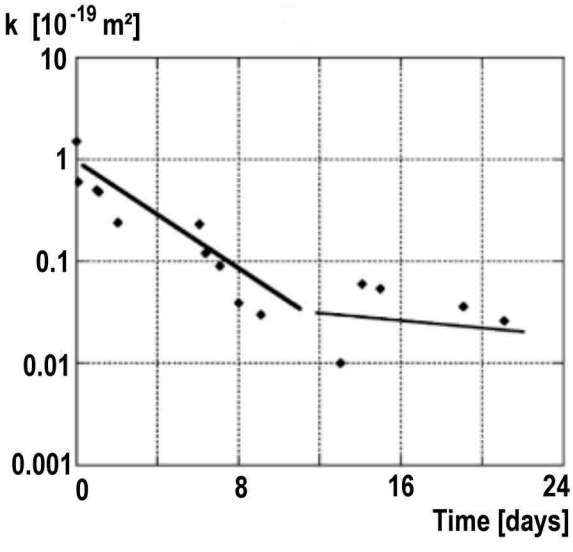

For the Opalinus Clay of the Mont Terri URL, the transmissivity and hydraulic aperture to air and water have been calculated for short borehole intervals in the EDZ of the EZ-A site. Additional work on the self-sealing of EDZ fractures due to water flow has been performed within the EH- and EZ-A Experiments. The results are shown in Figure A.5-6. Although not a normalised transmissivity plot, this figure shows the ratio between saturation dependent gas/water permeability. One comment arising from Figure A.5-6 is that gas permeability tests and water permeability tests are difficult to compare with each other, unless the *in situ* water saturation is well known. Yet, notwithstanding this, it can be depicted that the Mont Terri *in situ* results compare well with the laboratory experiments involving macro-cracked COX argillites performed by Davy *et al.* (2007).

Figure A.5-6. Normalised transmissivity reduction from EH and EZA *in situ* experiments at Mont Terri (Opalinus Clay) in course of resaturation, compared with laboratory test results of macro-cracked COX argillites subjected to long-lasting water flow
(Davy *et al.* 2007)

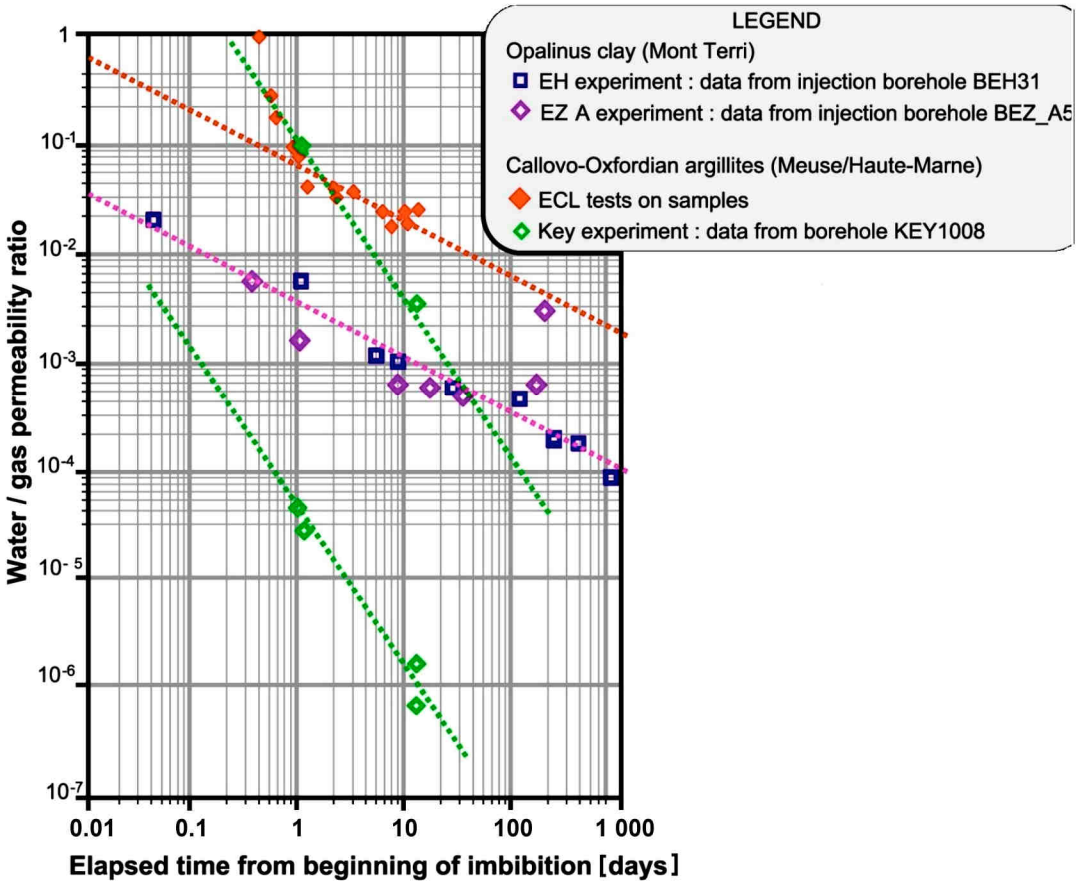

Moreover, Figure A.5-6 shows that water permeability decreases with imbibition time, i.e. the time over which the macro-cracked argillite sample becomes increasingly water-saturated. Although effective gas permeability very possibly also decreases as saturation increases (and imbibition time), overall, Figure A.5-6 clearly testifies a decrease of the water to gas permeability ratio of varied argillite samples, which can only be attributed to the increased difficulty for both water and gas to flow through the argillite. The exact saturation state is not specified in Figure A.5-6. Borehole

drilling were carried out at regular intervals to measure water content profiles in two galleries of the Bure URL at the -490 m Level. Desaturation takes place in the fractured zone. The degree of saturation is around 40% at the wall and 85-90% at the limit between fractured and perturbed zones. These values are acquired within less than three months. The profile is very stable, and it is the same in both galleries and also similar to the profile measured in Ventilation Test drift at Mont Terri. Figure A.5-6 is based on gas permeability tests in the fractured zone concerning initially widely open fractures, and then desatured fractures. In this case their results can be compared with those of the water permeability tests.

Self-sealing of both Mont Terri Opalinus Clay and COX argillite is therefore clearly evidenced and occurs within some ten days of resaturation time. The permeability (or transmissivity) is decreased by one to three orders of magnitude.

APPENDIX 6

MINERALOGICAL AND GEOCHEMICAL ASPECTS

Tracking and characterising past fluid flow through argillaceous formations

Overview

This appendix provides, in addition to Section 2.3.5 of the main text, some detailed information on mineral precipitation which are important for the understanding of self-sealing features and processes in argillaceous formations. Fractures or faults filled with minerals that are younger than the host rock are commonly termed veins. Their presence can mostly be considered as a physical trace of past fluid flow. Veins record events in which the self-sealing capacity of the considered rock was overpassed, at least transiently. Thus, the relative abundance of veins in a sedimentary unit is directly related to its self-sealing capacity over geological time, from sedimentation time to present. The involved fluids can be internally (fluid flow is parallel to bedding) and/or externally (fluid flow is perpendicular to bedding) sourced, the latter situation implying open-system behaviour. The study of vein materials gives a unique opportunity to characterise the involved fluids (temperature, geochemistry), their flow path, source and age, and to understand the mechanisms (in general related to major geodynamic events) that allowed their circulation. This is relevant for the evaluation of the long-term hydraulic behaviour of clay formations in the past, and it helps to understand future system behaviour.

This appendix is organised into three sections, the first (Section A.6.1) being a general introduction about veins in clay-rich rocks, the second (Section A.6.2) presenting a few case studies, and the third (Section A.6.3) being an overview of some of the techniques most frequently used for the characterisation of past fluid flow.

A.6.1 Introduction

Argillaceous media have low permeability and their mechanical characteristics (swelling, ductility) favour self-sealing of fractures. However, under specific circumstances, significant fluid flow is possible in clay-rich rocks, at least for short time periods (e.g. Sibson, 2001; Cox, 2005; Cox *et al.* 2001). Evidence includes the presence of veins and mineralogical, chemical, and isotopic disturbances associated with tectonic structures in clay-rich rocks. Examples are, among others, calcite (±celestite, barite, sulfides) veins cross cutting Opalinus Clay in the Swiss Jura (e.g. Pearson *et al.* 2003; Waber and Schürch 2000), the Effingen Beds (calcareous marls) at Oftringen in Switzerland (de Haller *et al.* 2009), and the Boda Clay Formation (see Figure 3-58), and stratiform copper deposits in black shales (the Kupferschiefer in Germany and Poland and the Zairian-Zambian copper belt; Cathles and Adams, 2005; Selley *et al.* 2005; Hitzman *et al.* 2005).

Table A.6-1 provides an overview of clay content, porosity and vein frequency for selected units, and the mineralogical composition is shown graphically in Figure A.6-1. Despite the limited number of examples considered, the following points can be made:

- Veins become more frequent with decreasing porosity of the formation. For a formation with a given clay content, porosity is a proxy of the compaction (maximum burial depth) that the formation has experienced (refer also to Figures 2-3 and 4-1 of main text). With increasing degrees of induration rocks are less ductile, and fracturing becomes progressively more prominent, thereby opening fluid pathways that may (or may not) be sealed by vein materials. Soft and slightly indurated formations, such as the Boom Clay at Mol or the Callovo-Oxfordian at Bure are, at the URL level, essentially devoid of natural fractures and therefore of veins. Moderately indurated formations, such as Opalinus Clay in northern Switzerland, do contain minor amounts of vein materials. Veins become more frequent at porosities below 10% (e.g. Effingen Beds), and in the Palfris Formation at Wellenberg (Switzerland) vein materials account for several % of the rock volume.

- Vein mineralogy is dominated by calcite, with frequent but quantitatively minor admixtures of sulfides (pyrite, sphalerite) and/or sulfates (celestite, barite), and, more rarely, quartz.

- Veins may be reactivated by later deformation and thereby lose their sealing effect, at least transiently.

- The provenance of the fluids from which vein minerals were precipitated is not always well characterised in argillaceous rocks. Local sources, e.g. from pressure solution along stylolites, have been put forward for some units (e.g. Mazurek 1999 for the Palfris Formation). On the other hand, the provenance of celestite veins in Opalinus Clay at Mont Terri is not currently clarified but could be from the underlying Triassic evaporites. In a recent study (de Haller *et al.* 2009), it has been shown that calcite ±celestite-pyrite in veins cutting the Effingen Beds at Oftringen were likely formed from infiltrating Burdigalian sea water.

- In lithologically heterogeneous units consisting of interbedded limestone and more clay-rich beds, such as the Palfris Formation at Wellenberg or the Effingen Beds at Oftringen, veins occur more frequently in the limestone beds.

Table A.6-1. Overview of vein occurrence in various clay-rich units
The list is sorted by descending porosity

Formation and site	Lithology	Clay content, mean and range [wt.%)]	Mean water-accessible porosity [%]	Occurrence of veins
Boom Clay at Mol	Shale - sandy shale	60 (30 - 70)	37	Not observed.
Callovo-Oxfordian at Bure	Shale - marl	45 (25 - 60)	18	Very rare and volumetrically negligible amounts of calcite and celestite.
Opalinus Clay at Benken, Mont Terri and Mont Russelin	Shale	60 (23 - 93)	12 (Benken) 18 (Mont Terri)	Vein infills are infrequent, even in highly tectonised zones, and consist of calcite ± celestite, pyrite and sphalerite. Most brittle structures have no vein infills.
Effingen Beds at Oftringen	Limy marl - limestone	22 (4 - 37)	8	Frequently observed calcite (± celestite, pyrite) veins, mainly in carbonate-rich beds.
Toarcian-Domerian at Tournemire	Shale - marl	38 (25 - 50)	7	Frequent calcite (± pyrite, barite) veins of Eocene age.
Boda Claystone formation in the Pécs area	Sandy shale – shaly sandstone	40 (10 - 55)	2	Veins are frequent and dominated by calcite.
Palfris Formation at Wellenberg	Shaly marl - limy marl - limestone	29 (17 - 44)	1-2	Calcite (± ankerite, pyrite) veins are ubiquitous, in particular in limestone beds and in ductile shear zones. Younger brittle shear zones are almost uncemented.

Note: Clay contents from Boisson (2005) and Waber *et al.* (2009) for the Effingen Beds.
Porosities from Mazurek *et al.* (2009), Boisson (2005) for the Boda and Palfris Formations and Waber *et al.* (2009) for the Effingen Beds.

Figure A.6-1. Mineralogical composition of various formations considered in the framework of radioactive waste disposal (adapted from Nagra 2002b)
Data for the Boda Clay formation from Kovács (1999), data for the Effingen Beds from Waber *et al.* (2009). Rock nomenclature follows the German scheme of Füchtbauer (1988).

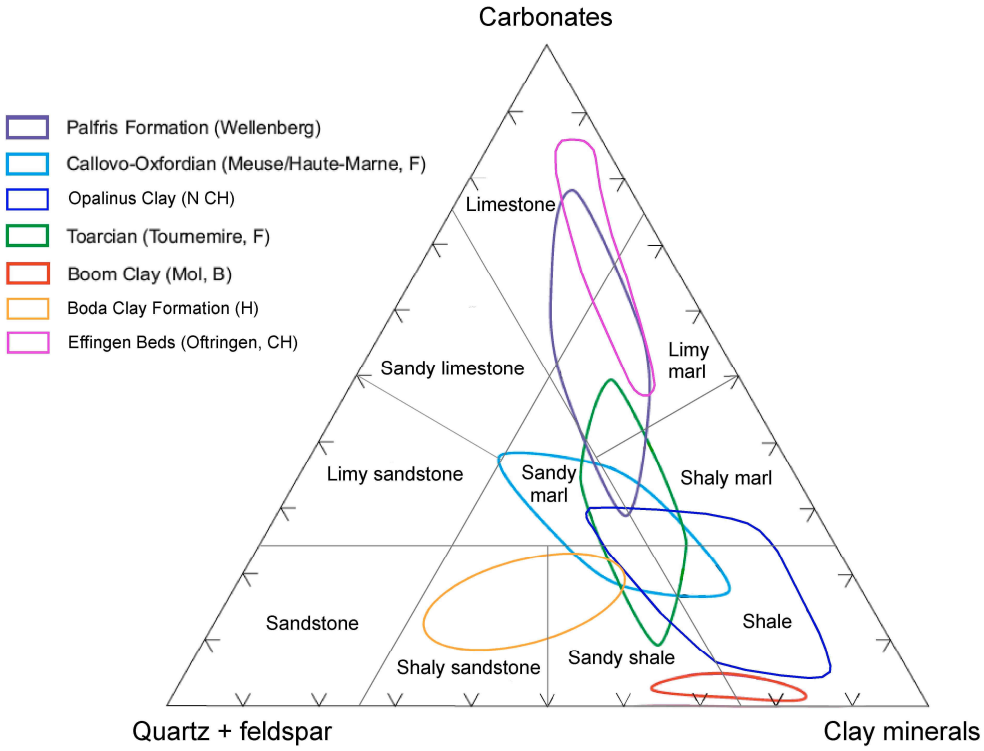

A.6.2 Case studies

A.6.2.1 Case Study I: Toarcian-Domerian at Tournemire (Aveyron, France)

The URL at Tournemire, operated by IRSN, is located in the Causses Basin of southern France (ref. to Section A.2.6.2). Due to deep burial (Barbarand *et al.* 2001; Peyaud *et al.* 2006) and intense diagenetic cementation, the shales and marls of the Toarcian-Domerian are well consolidated, relatively massive rocks. The high degree of induration is the probable reason for the presence of abundant fractures, some of which are filled with calcite. Some of these fractures are weakly water conducting in the underground laboratory (ref. to Figure 2-5).

The genesis and geochemistry of fracture infills in the Toarcian-Domerian shale at Tournemire was studied in detail by Boisson *et al.* (1998). Vein minerals frequently fill and seal tectonic structures (fractures and faults) of Tertiary age, and an example is shown in Figure A.6-2. Let us note that sealing by vein minerals is incomplete (i.e. there are structures without vein infills), and that several veins were reactivated by later tectonic movements and still may discharge small amounts of water into the tunnel. Mineralogically, the veins are dominated by calcite, with accessory pyrite and barite. At least three structural types of veins can be distinguished. One shows a rhythmic banding, interpreted as the result of recurrent stages of fracture activation and subsequent sealing. The chemical

compositions and $\delta^{13}C$ values of fracture and matrix calcite are generally very similar, suggesting a local origin for the fluid from which the vein calcite precipitated. However, locally there are indications for the ingress of external fluids, highlighted by distinct $^{87}Sr/^{86}Sr$ in vein calcite, and by $\delta^{13}C$ of calcite. In some intervals, $\delta^{13}C$ of vein calcite is ca. 2 ‰ higher when compared to matrix calcite, and in other intervals, negative deviations are observed (Figure A.6-3). Interestingly, the fractures with anomalous $\delta^{13}C$ are normal faults (i.e. created in a tensile regime), in contrast to the bulk of the fractures that are thrust faults and so were created in a compressive regime. The anomalies in $\delta^{13}C$ have been interpreted as being due to fluids that migrated downwards into the shale from the overlying Aalenian limestone along fractures generated in a tensile stress regime. Uncertainties remain regarding the source of the fluids and the timing of the flow event(s).

In a spatially more focussed study, Peyaud *et al.* (2006) analysed geochemical profiles across a fault that was penetrated by two boreholes. This fault is essentially sealed today by calcite and accessory pyrite and barite. Despite a somewhat limited data base, Peyaud *et al.* (2006) conclude that a zone about 1 m thick on each side of the fault has some minor geochemical anomalies, in particular in the O and C stable isotope composition of the carbonate cement. This anomaly is interpreted as being due to the downward passage of waters containing a meteoric component. The calcite veins filling the main fracture planes also precipitated from this water. The source of the water is interpreted as being the Aalenian aquifer, located 40 m above the sampling site. It needs to be noted that 1) the evidence is inconclusive due to the limited number of analyses that were produced to characterise the profile, and 2) the study refers to one single fault, so it is not clear yet how these findings can be generalised.

Figure A.6-2. 360° borehole-wall image of a fracture-sealing vein in the Toarcian shale at Tournemire
(developed view of the wall of Borehole ID 180; height 19 cm)
(from Boisson *et al.* 1998, figure IV-29, p. 231)

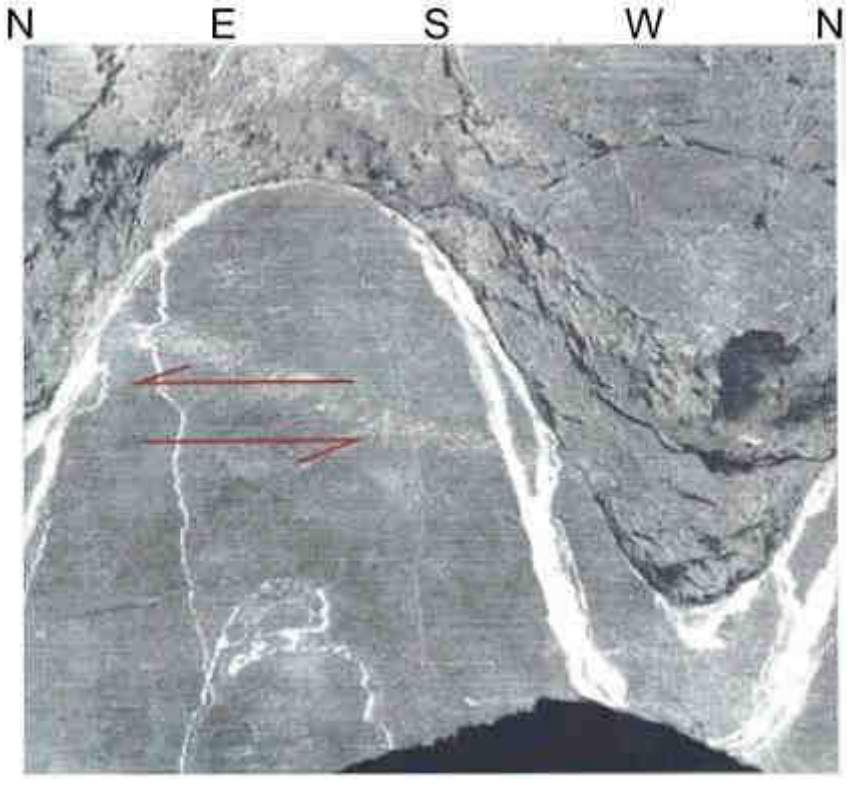

Figure A.6-3. Isotopic composition of carbon in vein and matrix calcite of the Toarcian shale and overlying Aalenian limestone at Tournemire
(adapted from Boisson 1998).

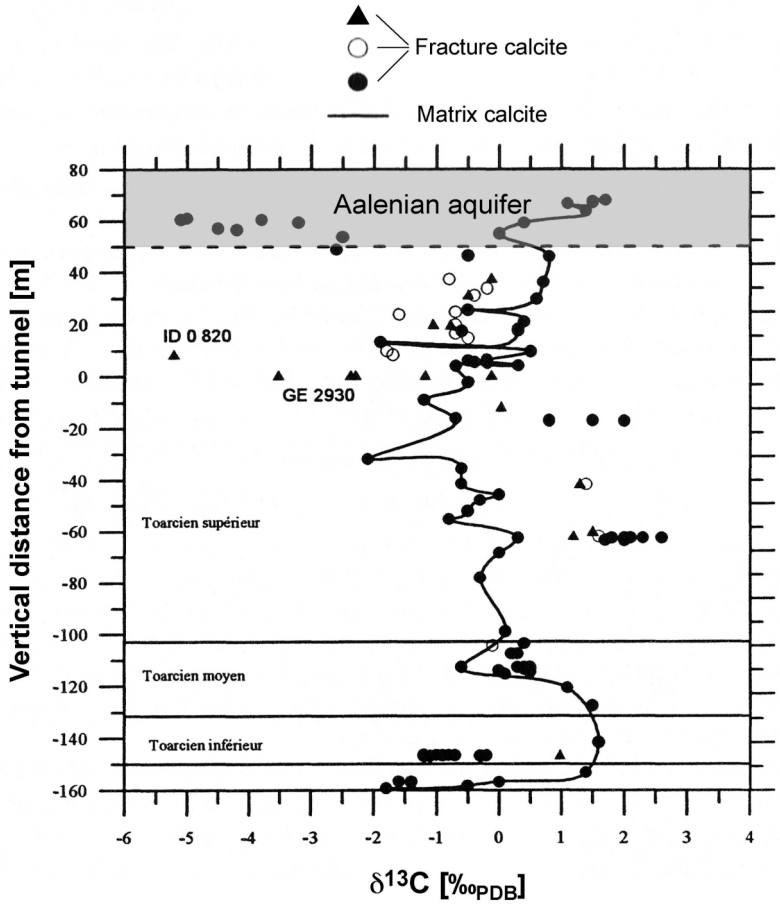

A.6.2.2 Case Study II: Opalinus Clay at Mont Terri and at Mont Russelin (Jura, Switzerland)

Mont Terri and Mont Russelin are the most external anticlines in the Folded Jura of northwestern Switzerland (Pearson *et al.* 2003; Marschall *et al.* 2004). Opalinus Clay occurs in the cores of both anticlines and is accessed underground from a reconnaissance gallery excavated for a motorway tunnel (Mont Terri; see Section A.2.6.4), and from the safety tunnel running parallel to the motorway tunnel (Mont Russelin). In the Mont Terri URL, it is only weakly deformed, and only one major structure, the approx. 1 m thick Main Fault, is observed (see also Figure 2-4 of main text and Section A.4.1.3.2). At Mont Russelin, the degree of deformation linked to the folding of the anticline is much higher than in Mont Terri. There are several thrust faults and long sections of the tunnel run through highly faulted rock. Imbrication of Opalinus Clay and underlying Liassic rocks is another element adding to geometric complexity. Despite the deformation, there are no water inflows or moisture zones in the Opalinus Clay sections at both locations.

The Main Fault at Mont Terri is illustrated in Figures A.4-7 to -8 of Section A.4.1.3. The approx. 1 m thick structure is interpreted by Freivogel and Huggenberger (2003) as a blind thrust ending within Opalinus Clay. It contains several discrete horizons of movement delineated by fault breccia or gouge. While the rock material from the fault is crumbly and unstable in tunnel outcrop, there are no moisture zones, and hydraulic testing in boreholes penetrating the fault indicates that the current hydraulic conductivity of the fault is within the range of that for undeformed Opalinus Clay

(Marschall *et al.* 2004). Vein materials in the fault are extremely scarce, and only some mm-thin calcite infills can be found. The scarcity of veins suggests that during and after the main deformation event, fluid flow through the fault was very limited. The vein infills were explained as local products of pressure solution.

Another set of fractures at Mont Terri includes flat-lying structures of limited thickness and probably with much less shear movement compared to the Main Fault. According to Nussbaum *et al.* (2005a), these structures were also created during thrusting and folding of the Mont Terri anticline and contain frequent infills of calcite and celestite and are up to 2 cm thick (Figure A.6-4).

Figure A.6-4. Core slab showing a fracture at Mont Terri completely sealed by celestite and calcite. This flat-lying vein can be identified over several metres.

At Mont Russelin, vein infills are more frequent, consisting of calcite and accessory pyrite and celestite. As all information is based on a limited number of boreholes, and outcrops are not available at all, it is difficult to better constrain the geometric and genetic attributes of the veins.

In summary, fracture infills at Mont Terri and at Mont Russelin consist of calcite, celestite and pyrite. It is remarkable how infrequent they are, despite substantial deformation during the thrusting and folding of the anticlines. The scarcity of veins is taken as evidence for a high self-sealing capacity of Opalinus Clay throughout its evolution. One unresolved question is the provenance of the fluid that deposited the vein-filling celestite. A potential source of sulfate could be the underlying Triassic evaporites, leached and transported by fluids during deformation. This hypothesis is currently the topic of a dedicated study (SF project of the Mont Terri Consortium).

A.6.2.3 Case Study III: Effingen Beds at Oftringen (near Olten, Switzerland)

The Oftringen borehole (Waber *et al.* 2009) is located in the Swiss Molasse Basin near the town of Olten. It intersects, from top to bottom, Quaternary sediments, Tertiary Lower Freshwater Molasse (USM), and Jurassic rocks from Malm to Dogger. The Effingen Beds (Malm) are a sequence of interbedded calcareous marls and limestones, characterised by numerous veins filled by calcite ± celestite and minor pyrite. Vein frequencies reach up to eight per metre and are shown in Figure A.6-5.

Figure A.6-5. Density of veining along the Oftringen borehole
Each value is the average of 6-7 m long core segments (vertical bars). From de Haller *et al.* (2009).

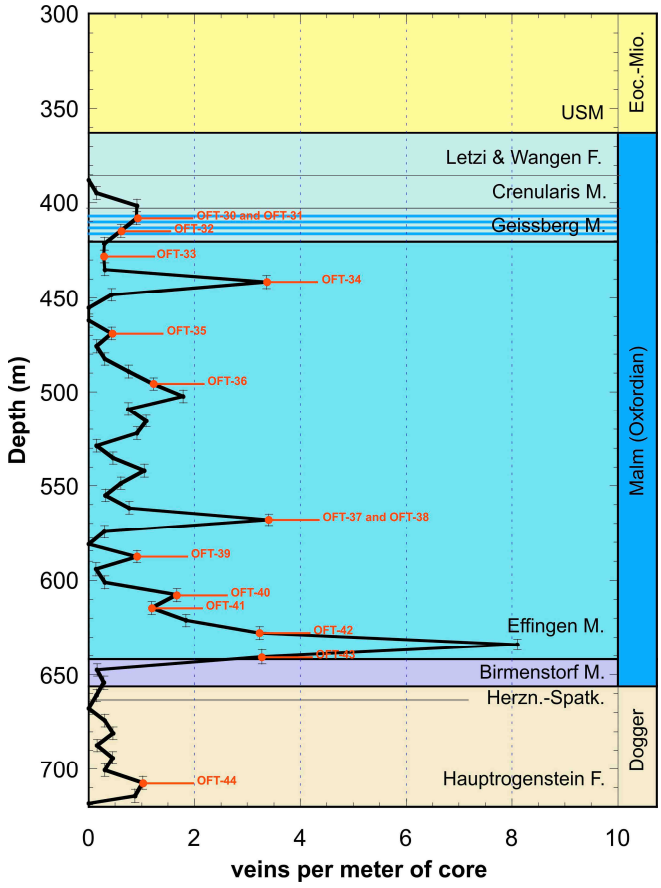

The carbon and oxygen isotopic compositions of the whole-rock carbonate correspond to well-defined depth profiles (see Figure A.6-6 for $\delta^{18}O$). The oxygen values are compatible with carbonate precipitation from sea water at tropical temperatures (20 to 30 °C) and are similar to what is found in other carbonate rocks of the same age of eastern Switzerland (Marquer and Burkhard 1992). The $\delta^{18}O$ of vein calcite, also shown in Figure A.6-6, yields distinctly lower values, indicating precipitation at higher temperature than the host-rock carbonate or fluids with a meteoric component. Similarly, the $\delta^{13}C$ values indicate disequilibrium between host-rock calcite and vein calcite.

Figure A.6-6. $\delta^{18}O$ isotope composition of whole-rock carbonate and vein calcite versus depth along borehole

Errors (1σ) are less than the symbol size. From de Haller *et al.* (2009).

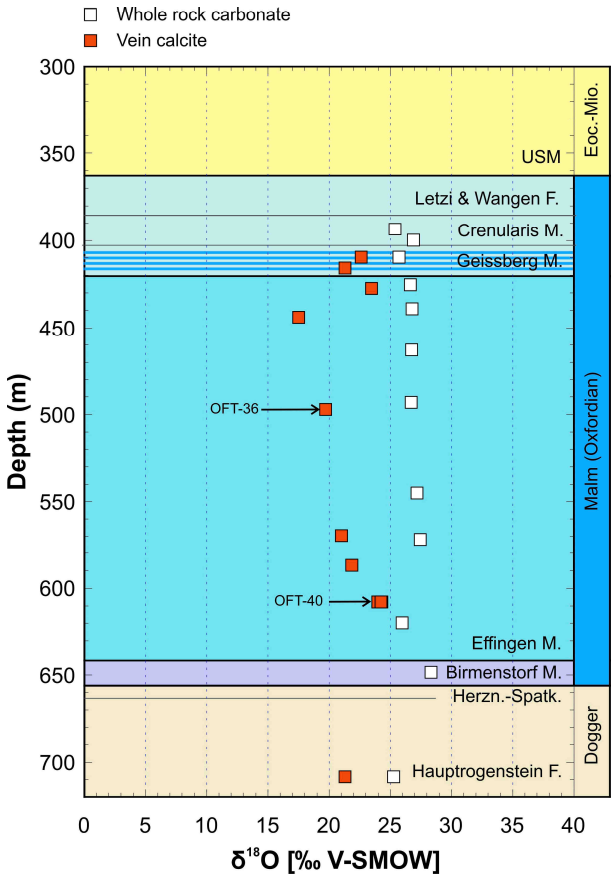

The $^{87}Sr/^{86}Sr$ ratios of whole-rock carbonate follow a regular depth profile (Figure A.6-7). In the Effingen Beds, only samples with the lowest $^{87}Sr/^{86}Sr$ ratio coincide with the Oxfordian (Malm) sea water value. Similarly, the $^{87}Sr/^{86}Sr$ ratio of the underlying Hauptrogenstein limestone falls within the range of Dogger sea water. All the other samples are enriched in radiogenic Sr compared to contemporary sea water. While a discussion of the mechanisms that led to the elevated $^{87}Sr/^{86}Sr$ in whole-rock carbonate are out of scope for this report, it is remarkable that, apart from two early diagenetic structures (OFT-36 and OFT-40), the $^{87}Sr/^{86}Sr$ ratios of younger vein calcite and celestite show systematically higher values compared to the adjacent whole-rock carbonate. In the Geissberg Member, the unit directly overlying the Effingen Beds, values are reached that are known only for Neogene sea water. Similarly, the $\delta^{18}O$ and $\delta^{34}S$ of vein celestite suggests the sulfate source was of Miocene age, since no other source can fit with the observed bacterial reduction trend. It is concluded that veins in the studied units have an external source and probably are of Miocene age, i.e. indicate descending waters at that time. Let us note that, today, the Effingen Member is a low-permeability unit with hydraulic conductivities of $1 * 10^{-11}$ m/s or less (Fisch *et al.* 2008).

Figure A.6-7. $^{87}Sr/^{86}Sr$ of whole-rock carbonate, vein calcite, and vein celestite versus depth along borehole

The range of seawater $^{87}Sr/^{86}Sr$ ratio at the time of deposition of each lithostratigraphic unit is shown as green boxes. The sea water $^{87}Sr/^{86}Sr$ ratio variation through geological time intervals is shown in the upper part of the figure. Unless visible, error bars (2σ) are less than the symbol size. From de Haller *et al.* (2009).

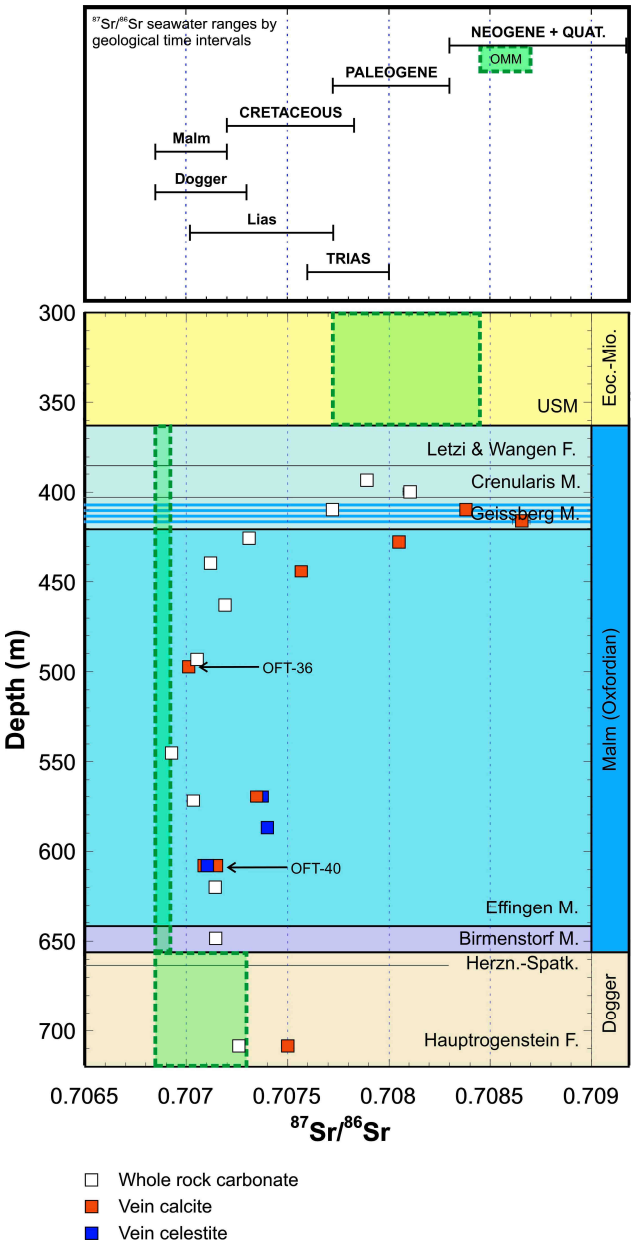

A.6.2.4 Case Study IV: Kupferschiefer (Germany and Poland)

Huge sedimentary rock-hosted stratiform copper deposits (±Zn, Pb, U, Co, Au, Ag) are represented by the Kupferschiefer belt (Poland and Germany) and the Zairian and Zambian Copper belt (whose combined reserves and past production are about 190 million tons Cu). The deposits occur where thick, coarse-grained, continental, oxidised detrital sequences (red beds; "Weissliegendes" in Figure A.6-8) are capped by organic carbon- and pyrite-rich shales (about 1 m thick for the Kupferschiefer, but 20-25 m thick for the Zambian Copper Belt; Cathles and Adams 2005; Hitzman *et al.* 2005; Selley *et al.* 2005). Ore deposits formed where overpressured oxidised metal-rich brines were forced up from the red beds aquifers through the black shales and reacted with these (pyrite and carbonate replacement by base metal sulfides). In the Lubin basin (Poland), about 20% of the ore occurs in veinlets concordant and perpendicular to the bedding of the black shale (Cathles and Adams 2005). In the Kupferschiefer, alteration minerals consist of base metals sulfides (no pyrite) and hematite that replaced earlier diagenetic pyrite. The same occur in the Zambian Copper belt, accompanied by a complex association of early Ca-Mg-SO_4 alteration (anhydrite and dolomite) followed by a K alteration (K-feldspar and muscovite-illite). Because of their high content of diagenetic pyrite and organic carbon and locally carbonate, black shales are chemically more reactive than other shales, and this is favourable for base-metal sulfide mineralisations. The mineralisations record intense fracturing of thin shale beds, possibly triggered by overpressured fluids in an extensional tectonic regime.

Figure A.6-8. Typical distribution of Cu, Pb, Zn, and Fe sulfides in the Kupferschiefer stratigraphic column (from Mayer and Piestrzynski 1985)

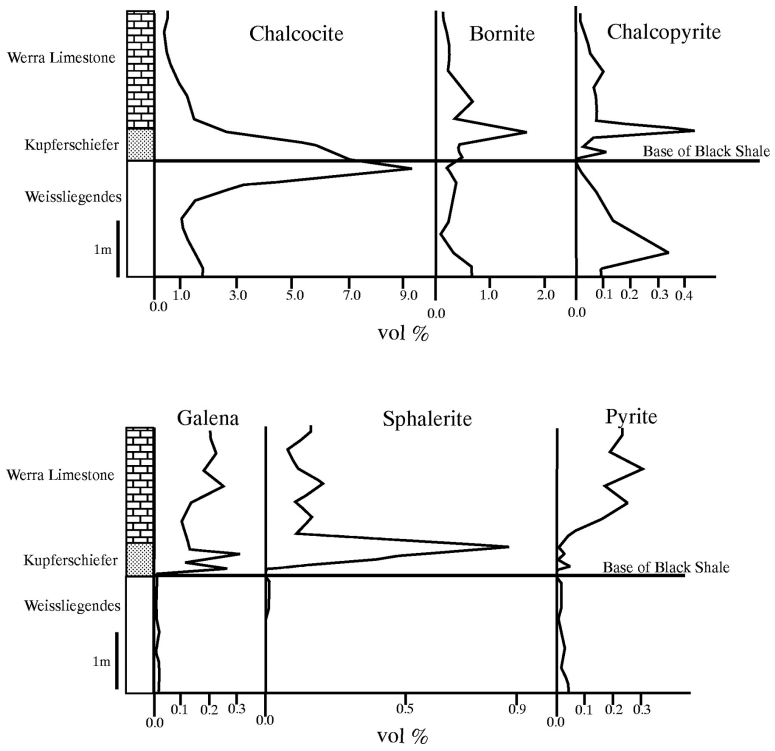

A.6.3 Methods commonly used for tracking and characterising past fluid flows

A.6.3.1 Introduction

Many techniques are used in various geological contexts for the tracking of past and present fluid flows, and for the characterisation of some of their physico-chemical properties and pathways. These tools and techniques rely on the fact that, unlike stagnant pore fluids, fluids flowing along permeable channels are generally in thermodynamic (and commonly isotopic) disequilibrium with their host rock, especially when passing boundaries separating different geological units, or through thermal gradients (many geochemical characteristics are temperature-dependent). This disequilibrium state may lead to processes like mineral dissolution or precipitation, mineral transformation, and isotopic exchanges between the fluid and the solids. The induced modifications of the rock (mineralogy, chemistry, isotopic composition, texture...) are traces of these fluids and can be studied today. The magnitude of the geochemical and mineralogical imprint of past fluid flows depends on the minerals, elements or isotopes that are considered, the amount and lifetime of flow and fluid mixing (if any) that occurred, the relative amounts and chemical reactivity (kinetics) of the rock minerals, the respective chemical buffering capacities and the degree of initial disequilibrium between the fluid and the rock. Importantly, it has to be noted that the absence of a mineralogical and geochemical perturbation in a rock does not prove that fluid did not pass through it. Indeed, if flowing fluids have already equilibrated with the rock (in terms of chemistry, temperature and pressure), there is no more fluid-rock interaction and therefore no mineralogical or isotopic imprint of that flow. It means that the fluid-induced perturbation recorded in rocks is space-dependent and tends to decrease with increasing distance from lithologic boundaries (geochemical gradient) or thermal anomalies (thermal gradient). Consequently, the rock material that is best suited for the study of past fluid flows is located where the highest geochemical and/or thermal gradients have occurred.

In the following, we present an overview of some of the techniques used for tracking and characterising past fluid flows, with particular emphasis on those aspects applicable to fluid circulation in clay-rich rocks. Only common situations and minerals are discussed. Similarly, only tools and techniques that are broadly used and of well demonstrated reliability are presented. These are commonly employed and continuously developed in diverse fields including, among others, ore geology, oil industry, geothermal energy, and nuclear waste management.

A.6.3.2 Starting information

The application of the methods and tools used for tracking and characterising past fluid flows requires that at least basic geological background information on the studied area already exists. Of importance is the availability of good knowledge of the geological setting, the tectonic structures and, if present, of the distribution and nature of specific features like alteration halos, veins, and other infills occurring within the studied area. A good understanding of the tectonic framework is highly desired, as tectonic structures are potentially major fluid channels.

A.6.3.3 Mineralogy

A.6.3.3.1 Generalities

Good mineralogical information is the basis for the characterisation (physico-chemical properties, sources) of past fluid flows. In addition to instrumental analyses, information about textural relationships obtained by microscopic studies is essential for the definition of the chronology of mineral deposition/dissolution and of possible links with tectonic events (paragenetic sequence). Mineralogical studies are needed on wall-rock, open space fillings and fault structures.

Hydrothermal alteration involves the modification of the mineralogical and chemical composition of a rock due to its interaction with a fluid (e.g. Reed, 1997). It depends on six factors: temperature, pressure, initial (unaltered) rock composition, initial (unreacted) fluid(s) composition(s) (including external and porewater fluids), fluid-to-rock ratio (total mass of fluid that reacted with a defined mass of rock, which also depends on the rock porosity and permeability), and the duration of the fluid flow (kinetics of the geochemical buffers). The characterisation and possible zonation in the mineralogy of altered wall rock can be obtained through whole-rock XRD analyses (semi-quantitative data are normally sufficient) along profiles perpendicular to potential fluid channels.

One of the main post-depositional mineralogical modifications of clay-rich rocks is the transformation of smectite and chlorite into illite, which occurs due to burial diagenesis (e.g. Rousset and Clauer 2003; Hutcheon *et al.* 1994) or due to fluid flow (e.g. Schaltegger *et al.* 1995; Clauer *et al.* 1997). However, because clay-rich rocks have very low permeability, fluid-rock interaction is dominated by diffusion and so is generally slow. Furthermore, because fluid flows through shales are generally transient (see Sibson 2001; Cox 2005; Cox *et al.* 2001) and short-lived, the degree and size of observable alteration may be in the range of millimetres, if not less. Because of their high content of diagenetic pyrite and organic carbon, and locally carbonate, black shales are chemically more reactive than other shales, and they may host epigenetic base metal sulfide mineralisations like the Kupferschiefer (Poland and Germany; see Section A.6.2.4) and the Zairian and Zambian Copper Belt.

The study of vein minerals allows the definition of the paragenetic sequence (chronology of the mineral deposition) based on textural evidence. As for alteration minerals, information about the mineralogical zoning (vertical and lateral) can be useful in understanding the whole system (e.g. Guilbert and Park 1996). Since minerals that fill veins commonly precipitated simultaneously with wallrock alteration, both are frequently part of the same geochemical system. Common vein minerals in shales include calcite (and other carbonates), celestite, barite, quartz, and pyrite (e.g. Pearson *et al.* 2003; Waber and Schürch 2000; Rousset *et al.* 2005; Nagra 1997).

A.6.3.3.2 Implications

Any change of the rock mineralogy which is found to be geometrically related to a potentially permeable structure (fault, stratigraphic horizon) may indicate past fluid flow. All the minerals that are found filling open spaces (e.g. veins) were precipitated from fluids that potentially may have been sourced outside the shale unit. However, local sources are also possible. As an example, the good spatial correlation of stylolites and calcite veins in the Palfris Formation at Wellenberg (Switzerland) suggests only local transport, driven by pressure solution along the stylolites and precipitation in veins that represent pressure shadows.

A.6.3.4 Geochemistry

Geochemical and mineralogical studies are ideally performed on the same samples. Profiles of the chemical whole-rock composition across potential fluid channels (faults, veins, permeable horizons) help in characterising the magnitude and nature of the chemical exchanges during past fluid flow, if present (see MacLean 1990; Leitch and Lentz 1994; Reed 1997). Ideally, such profiles are placed within homogeneous rock units so that the chemical effect of the fluid circulation is not mixed with chemical variations related to lithology (e.g. Peyaud *et al.* 2006).

Ca^{++}, Mg^{++}, Sr^{++}, Ba^{++}, Fe^{++}, K^{+}, Na^{+}, H^{+}, CO_3^{--} and S are frequently exchanged during fluid-rock interaction and are therefore potentially good indicators of past fluid circulation. In contrast, halogens (Cl^{-}, Br^{-}, I^{-}) are not incorporated into low-solubility minerals and are therefore essentially conservative (e.g. Pearson *et al.* 2003). In some cases, trace-element concentrations in the finest clay fraction (<0.4 or <0.2 μm) have been successfully used to detect past fluid circulation in clay-rich rocks (e.g. REE in Clauer *et al.* 1997; Pb, Sr and Ba in, Rousset *et al.* 2005).

A.6.3.5 Isotope geochemistry

Isotope geochemistry is widely used for tracking past fluid flow. Emphasis is given here to some stable (S, C, O, and H) and radiogenic (Sr, K-Ar) isotope systems. General overviews of stable and radiogenic isotopes applied to hydrothermal systems are found in Campbell and Larson (1998) and Richards and Noble (1998). Other review literature includes Faure (1986), Ohmoto and Goldhaber (1997), Seal *et al.* (2000), Seal (2006), and Taylor (1997).

A.6.3.5.1 Sulfur isotopes of sulfate and sulfide and oxygen isotopes of sulfate minerals

Generalities

The sulfur isotopic ratio ($^{34}S/^{32}S$) is expressed in the delta notation ($\delta^{34}S$) as permil (‰) deviation from the CDT standard (Troilite of the Cañon Diablo meteorite; Ault and Jensen 1963). The oxygen isotopic ratio ($^{18}O/^{16}O$) is expressed as permil $\delta^{18}O$ relative to SMOW (Standard Mean Ocean Water; Craig 1961). Oxidised sulfur species (HSO_4^{-}, SO_4^{--}) tend to concentrate heavy sulfur (^{34}S) compared to reduced species (H_2S, HS^{-}).

In the context of sedimentary basins (without volcanic activity), sulfur can be sourced from essentially four reservoirs: 1) sea water, 2) evaporite (anhydrite and gypsum), 3) diagenetic pyrite, 4) sulfides of the crystalline basement. Sulfate minerals have the same (sulfur) or nearly the same (oxygen) isotopic composition as the aqueous sulfate from which they precipitated. For this reason, isotope ratios of evaporites match the sea-water sulfate composition and its variation through geological times (typically between 15 and 22 ‰ during the Mesozoic; Claypool *et al.* 1980). In contrast, the sulfur isotopic composition of sulfide minerals does not match the isotopic composition of the aqueous H_2S from which they formed due to significant isotopic fractionation, especially at low temperatures (Figure A.6-9). Once precipitated, sulfate and sulfide minerals are closed to isotopic exchange with the fluid, except through dissolution. Oxidation of pyrite generates aqueous sulfate with a $\delta^{34}S$ identical to that of the original sulfide, and a $\delta^{18}O$ value in equilibrium with the water and its dissolved oxygen (e.g. Claypool *et al.* 1980; Seal *et al.* 2000). Similarly, dissolution of sulfate minerals would produce aqueous sulfate with the same isotopic composition (O and S).

The sulfur and oxygen isotopic composition of sulfide and sulfate minerals depends on the source(s) of their components and on the precipitation processes. Both sulfur and oxygen isotopic systems are temperature-dependent, the former being further sensitive to the redox and pH conditions (Figure A.6-9). Fractionation factors depend on equilibrium and kinetically controlled processes.

The SO_4-H_2S isotopic system is almost inert over geologically relevant time scales below 200°C at near neutral pH. This explains, for example, why oxygen of sea-water sulfate is not at isotopic equilibrium with seawater (Claypool *et al.* 1980). At temperatures below 100°C, thermochemical redox reactions and isotopic equilibrium are precluded, and the sulfur system is controlled by bacterial activity, which is a fast process at low temperatures. Sulfate reducing bacteria are found in anoxic environments and can survive over a wide range of temperatures (0 to 110°C), at pH from 5 to 9.5, and at almost any salinity (e.g. Seal *et al.* 2000; and references therein).

Figure A.6-9. Equilibrium isotopic fractionation factors between sulfur compounds and $H_2S_{(g,\ aq.)}$ (from Ohmoto and Goldhaber 1997)
(Reproduced with permission of John Wiley & Sons, Inc.)

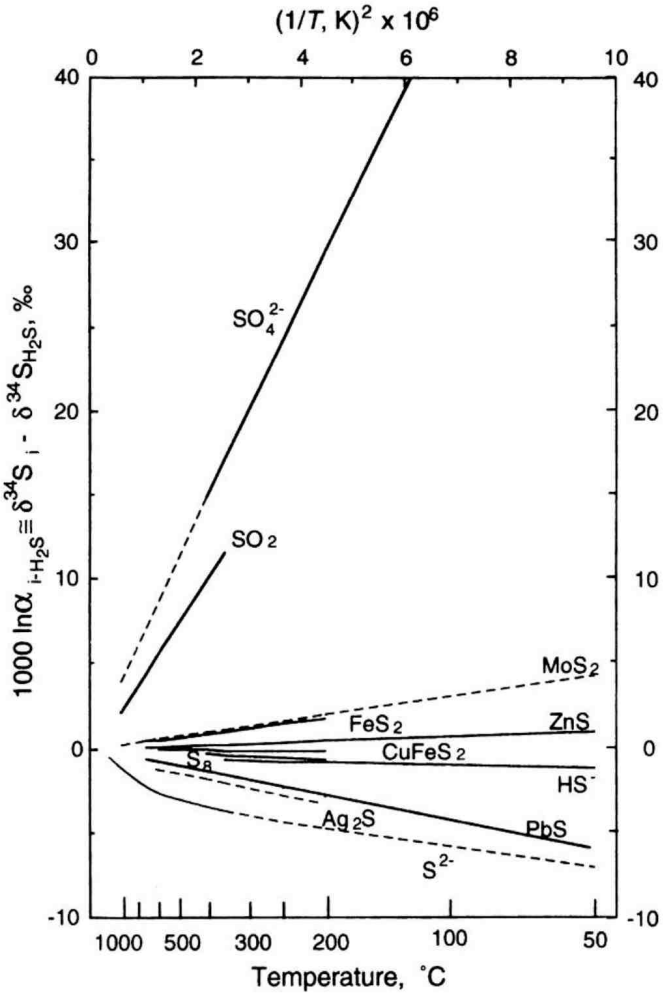

Implications

The use of sulfur and oxygen isotopes of sulfate minerals as tracers relies on the following observations:

- The isotopic composition (O and S) of sulfate minerals records the isotopic composition of the aqueous sulfate from which they formed and so defines the source. It follows that evaporite sulfates (gypsum, anhydrite) record the isotopic composition of sea-water sulfate and its isotopic variations trough geologic times.

- $\delta^{18}O$ and $\delta^{34}S$ of dissolved sulfate can be enriched through bacterial sulfate reduction.

- Diagenetic pyrite forms through bacterial sea-water sulfate reduction and has heterogeneous $\delta^{34}S$ values, ranging from extremely negative to positive.

- Aqueous sulfate generated through sulfide mineral oxidation has the same sulfur isotopic composition of the sulfide and an oxygen composition at equilibrium with the water and its dissolved O_2.

- Aqueous sulfate isotopes (O and S) do not thermochemically equilibrate with aqueous H_2S or sulfide minerals and water at temperatures < 200°C. In such conditions, the only mechanism able to alter the S and O isotopes composition of aqueous sulfate is bacterial sulfate reduction and, possibly, reduction by light hydrocarbon gases (e.g. Krouse *et al.* 1988).

A.6.3.5.2 Carbon and oxygen isotopes of carbonates

Generalities

Stable carbon isotopes are ^{13}C and ^{12}C, and the isotopic composition is expressed as $\delta^{13}C$ relative to the $^{13}C/^{12}C$ of the PDB standard (Belemnite from the Peedee Formation). The oxygen isotopic ratio ($^{18}O/^{16}O$) is expressed as permil $\delta^{18}O$ relative to the SMOW (Standard Mean Ocean Water; Craig, 1961) or PDB standard.

Carbon isotopes undergo fractionation during phase transitions (gaseous - aqueous - solid) and during redox processes (e.g. Mook *et al.* 1974). The $\delta^{13}C$ value is comparatively high in the carbonate system (carbonate minerals, CO_2, HCO_3^- and CO_3^{-2}) and low in the reduced organic compounds (CH_4, hydrocarbons; e.g. Ohmoto and Goldhaber 1997). The carbon isotopic fractionation factors between carbonate minerals and HCO_3^- is <3‰ at 25°C, decreasing at higher temperatures (idem; Romanek *et al.* 1992). The isotopic equilibration time between oxidised and reduced carbon species is extremely long, and the carbon isotopic system can be considered to be totally inert at temperatures below 300°C (no isotopic exchange between coexisting reduced and oxidised species). Modern marine limestones have $\delta^{13}C$ at 0 ±2‰ V-PDB, mostly at equilibrium with sea-water HCO_3^-, while organic matter in the ocean is at -25 ±5‰ V-PDB, in agreement with fractionation due to photosynthesis.

Decomposition of organic matter by aerobic, iron- and manganese-reducing, or sulfate-reducing bacteria would produce aqueous carbonate species showing the same carbon isotopic composition as the precursor sedimentary organic matter; that is, around -25‰ V-PDB. This explains why diagenetic

calcite cements frequently show negative values, typically between -5 and -15‰ V-PDB (mixture of carbon from organic matter and from dissolution of marine carbonate), compared to normal marine limestone near 0‰ V-PDB.

The oxygen isotopic composition of aqueous carbonate species is normally at equilibrium with the water, and its fractionation factor depends on the temperature (O'Neil *et al.* 1969; Kim and O'Neil 1997; Zhou and Zheng 2003; Horita and Clayton 2007). Therefore, the oxygen isotopic composition of carbonate minerals depends on the temperature and isotopic composition of the fluid from which these precipitated. The $\delta^{18}O$ of present day mean oceanic water is at 0 ‰ (V-SMOW) and is thought to have remained nearly constant through geologic times (e.g. Taylor 1997; and references therein). The isotopic composition of meteoric water follows a general trend toward negative $\delta^{18}O$ and $\delta^{2}H$ depending on climatic and altitude parameters.

Implications

The carbon isotopic composition of vein carbonates can be useful in tracing the source of the carbon (organic matter oxidation versus marine carbonate dissolution) while the oxygen isotopic composition can help in constraining the temperature of precipitation, provided the isotopic composition of the coexisting water can be estimated. However, the carbon isotopic composition of carbonate minerals is also dependent on redox and bacterial processes. These potential perturbations should be considered when interpreting data. Irrespective of the underlying processes, differences in the carbon and oxygen isotopic compositions of fracture infills and adjacent wallrocks can, in many cases, be interpreted as indicators of externally derived fluids.

A.6.3.5.3 Hydrogen and oxygen isotopes

Generalities

The O and H isotope composition of water at the time of mineral precipitation can be calculated from the O and H isotopic composition of many OH and H_2O-bearing minerals (anhydrite, gypsum, clay minerals, mica, etc.), provided their precipitation temperature is known (e.g. Taylor 1997). This last parameter is commonly difficult to establish with any degree of certainty. The O isotope composition of water can also be calculated from that of calcite or other carbonates.

Oxygen isotopes have been used for tracking past fluid flow in clay-rich rocks. Because authigenic and epigenetic clays are likely to be finer grained than detrital clay (<2 μm), the oxygen isotopic composition of the <0.2 μm fraction is likely to be more strongly affected by post-depositional fluid-rock interaction. An isotopic perturbation of the fine clay fraction from faults has been documented (e.g. Clauer *et al.* 1997), but no such study on the fine clay fraction is known for hydrogen isotopic composition.

Implications

Analysing O and H isotopes in different grain-size clay fractions may provide information on post-depositional fluid-rock interaction. This may be the case in the matrix (e.g. diagenetic growth of new clay minerals) and/or record specific flow events along faults.

A.6.3.5.4 Strontium isotopes

Generalities

The Sr isotopic composition of rocks and minerals is commonly expressed as the ratio $^{87}Sr/^{86}Sr$. The systematics of this isotopic system are related to the Rb-Sr system, where radioactive ^{87}Rb decays into ^{87}Sr (e.g. Faure 1986). Strontium isotopes are widely used as a tracer of the fluid source because they are not fractionated by physico-chemical or biological processes. Minerals that contain little or no Rb (and therefore K, because Rb substitutes K) compared to Sr (as major component: celestite and barite; or as substitution for Ca in carbonates and other minerals) have isotopic compositions that reflect the isotopic composition of the fluid at the time of their precipitation. Biogenic aragonite typically contains thousands of ppm Sr, which is then released to porewater during diagenetic transformation into calcite (tens of ppm Sr). For Rb-bearing minerals, the Sr isotopic composition at the time of mineral precipitation needs to be corrected for the radiogenic ^{87}Sr produced since then. This is commonly difficult because the age of the mineral has to be known. In general, old and/or Rb-rich rocks, or rocks derived from them, have high Sr isotopic ratios compared to young and/or Rb-poor rocks. The Sr isotopic composition of the carbonate fraction of a rock is conserved through time unless re-crystallisation in contact with an aqueous source of Sr with a different isotopic ratio has occurred.

Measurements on calcitic and aragonitic fossils show that the sea-water Sr isotopic composition has fluctuated during geological times. From the Mesozoic to the present, the sea-water Sr isotopic composition is sufficiently well constrained to serve as an indirect dating tool, although not very precise (McArthur *et al.* 2001; Veizer *et al.* 1999).

Implications

Sr-bearing minerals (sulfate, carbonate) are commonly used to fingerprint the source of the fluid from which they precipitated. For example, differences in $^{87}Sr/^{86}Sr$ between fracture infill materials and adjacent wallrock point to an external source of the mineralising fluid that has passed through the fracture.

A.6.3.5.5 Potassium-argon isotopic system

Generalities

K-Ar ages of clay minerals in shale are influenced 1) by the age(s) of the detrital minerals (typical ages are older than that of deposition of the sediment) and 2) by the age of authigenic clay minerals grown during diagenesis. If the latter can be separated (which is difficult in many cases), they may provide geologically meaningful dates. The former yield mixed ages reflecting the source material of the sediment. Specific techniques have been developed to investigate rock-water interactions in clay-rich rocks based on the observation that the finest (< 0.2 μm) clay portion tends to be of predominantly authigenic origin, thus recording events related to diagenesis and/or interaction with later fluids (e.g. Clauer *et al.* 1992; Rousset and Clauer 2003; Clauer and Chaudhuri 2001). In most cases, the K-Ar dates obtained on various clay fractions (typically from <0.2 μm to 2 μm) reflect mixed ages of the detrital and authigenic clay minerals, and these ages are geologically not meaningful (e.g. Clauer and Chaudhuri 2001; Środoń *et al.* 2002; Rousset and Clauer 2003; Lerman and Clauer

2005). Nevertheless, they can still be useful as fingerprints of water-rock interaction because, if fluid flow has occurred in specific places and led to an enhanced crystallisation of authigenic/epigenetic illite, the K-Ar age would be distinctly younger than that of the adjacent unaffected matrix (Clauer *et al.* 1997; Rousset *et al.* 2005). In the absence of post-depositional mineral growth, such a rejuvenation would not be observed. Combination of the K-Ar data with Rb-Sr, $\delta^{18}O$, and REE data of clay minerals and whole-rocks can further help in constraining the mineral-growth processes and, eventually, in characterising the fluid source(s) (Clauer *et al.* 1997; Clauer *et al.* 2003). In the case of the Kupferschiefer, Bechtel *et al.* (1999) showed that detrital and authigenic illite have different crystallographic structures (polytypes) that correlate with apparent K/Ar ages of different clay size fractions (see also Nawrocki 2000; and Bechtel *et al.* 2000).

Implications

Fluid-rock interaction can be evidenced by a rejuvenation of the K-Ar age of the finest clay fraction (<0.2μm) of shale and fault gouge, which is potentially of authigenic/epigenetic origin. In specific cases, combination with the illite polytype determination may assist in obtaining the real age of the authigenic and detrital illites. Also, comparative studies of clays from fault infills (gouge) and undeformed wallrock may help in tracing fluid-flow events through the faults.

A.6.3.6 Solubility of some common minerals in sedimentary basins

The solubility of minerals can give valuable information about the precipitation mechanisms, fluid sources, and physicochemical conditions that prevailed during deposition-dissolution. Any interpretation of the origin of vein minerals should consider thermodynamic properties. General references on sulfate, carbonate, silica, and sulfide minerals solubilities include, among others, Rimstidt (1997) and Seward and Barnes (1997).

A.6.3.7 Fluid inclusions

The microthermometric study of fluid inclusions trapped in transparent minerals gives direct information about the precipitation temperature and the nature of the fluids (Roedder 1984; Shepherd *et al.* 1985). These include salinity (in NaCl wt.% equivalent), in certain cases the type of salts (NaCl, $CaCl_2$, $MgCl_2$, KCl), and the recognition of CO_2 (if present). Homogenisation temperatures are generally not reliable for sulfates (gypsum, anhydrite, celestite) due to fluid inclusion leaking (these are fragile minerals), but good results can be obtained for carbonate and quartz. Detection of CO_2 and CH_4, and determination of minute minerals can be performed by Raman microspectroscopy on the fluid inclusions.

In fine-grained sediments, fluid inclusions can typically only be observed in fracture mineralisations but not in the rock matrix. Frequently, the small size of the inclusions precludes the relevant measurements. Overall, fluid conclusions may provide valuable information about the physico-chemical conditions at the time of mineral precipitation, and they may yield information on the fluid source.

APPENDIX 7

REFERENCES

Alheid, H.-J.; Kontar, K. and Trick, Th. (2004). Engineered Barrier Emplacement (EB) Experiment in Opalinus Clay: Hydrogeological characterisation of the EDZ. – Mont Terri Project Techn. Note, **2004-56**: 104 p., Geotechnical Inst. Ltd., Switzerland.

Anderson, E.M. (1951). The dynamics of faulting and dyke formation with application to Britain. – 2nd Ed. 206 p., Edinburgh (Oliver & Boyd).

Andra (2000). Thermicité du Callovo-Oxfordien du site de l'Est. Détermination d'un paléoenfouissement maximum. Etude complémentaire. - Rapport Andra n° D.RP.OCRE.00-03.

Andra (2005a). Dossier 2005 Argile – Synthesis, Evaluation of the feasibility of a geological repository in an argillaceous formation - Meuse/Haute-Marne site, Andra editor rapport series, December 2005.

Andra (2005b). Premiers resultats – Experimentation KEY. Laboratoire de recherches souterrain de Meuse / Haute-Marne. – Andra Rep. D.RP.ADPE.05.0910, 200 p., Nov. 2005.

Andra (2005c). Dossier 2005 Argile - Tome phenomenological evolution of a geological repository. - Andra editor rapport series, pp. 122-126, December 2005.

Andra (2005d). Dossier 2005 Argile – Référentiel du site de Meuse/Haute-Marne Tome 2: Caractérisation comportementale du milieu géologique sous perturbation - Andra editeurr rapport series, Décembre 2005.

Andra (2006a). Experimentation KEY – Rapport de fin d'operation (RO) - Laboratoire de recherches souterrain de Meuse / Haute-Marne. – Andra Rep. D.RP.ADPE.06.0137, 146 p., Feb. 2006.

Andra (2006b). Projet HAVL-Argile: Fracturing and faulting in the Callovo-Oxfordian argillites of Meuse/Haute-Marne. – State of knowledge on characteristics and self-sealing processes. – Unpubl. manuscript, 33 p.

Aranyossy, J.F. (2005). Key processes related to the initiation and the evolution of the Excavation Disturbed (Damaged Zone (EDZ). - 17 p., Presentation Workshop, 19th Oct. 2005, Cardiff

Armand, G.; Blümling, P.; Frank, E.; Frieg, B.; Mayor, J.-C. and Volckaert, G. (2008). EDZ (including self-sealing) experiments. – In : Bossart, P. and Thury, M. (Eds.): Mont Terri Rock Laboratory, project programme 1996–2007 and results. – Rep. No. **2008-1**, Chapter 11: 131-144, Wabern (Swiss Geol. Survey).

Armand, G.; Lebon, P.; Cruchaudet, M.; Rebours, H.; Morel, J. and Wileveau, Y. (2007). Characterisation of the Excavation-Damaged-Zone in the Meuse Haute Marne Underground Research Laboratory. - Internat. Meeting Clays in natural & engineered barriers for radioactive waste confinement, 17-18 Sept. 2007, Lille, Paper O/010A/3.

Arnould, M. (2006). Discontinuity networks in mudstones: a geological approach - Implications for radioactive wastes isolation in deep geological formations in Belgium, France, Switzerland. - Bull Eng Geol Environ., **65**: 413–422.

Ault, W.V. and Jensen, M.L. (1963). Summary of sulfur isotope standards. - In: Jensen, M.L. (ed.): Biogeo-chemistry of sulfur isotopes. – Nat. Sci. Foundation Sympos.Proceed., Yale Univ., p. 16-29.

Badertscher, N.; Girardin, C. and Nussbaum, Ch. (2008). RA experiment: Study of self sealing zones identified in BEZ-A33/34 and BEZ-A38 drillcores. - Mont Terri Project Techn. Note, **2007-25**: 17 p., Geotechnical Inst. Ltd., Switzerland.

Bandis, S.C.; Lumsden, A.C. and Barton, N.R. (1983). Fundamentals of rock joint deformation. – Int. J. Rock Mech. Min. Sci. & Geomech. Abstr., **20**: 249-268.

Bankwitz, P.; Bahat, D. and Bankwitz, E. (2000). Joints in granite – State of knowledge 80 years after Hans Cloos (in German). – Z. geol. Wiss., **28**: 87-110.

Barbarand, J.; Lucazeau, F.; Pagel, M. and Séranne, M. (2001). Burial and exhumation history of the south-eastern Massif Central (France) constrained by apatite fission-track thermochronology. – Tectonophysics, **335**: 275 - 290.

Barnichon, J.D. (2002). Contribution of the bounding surface plasticity to the simulation of gallery excavation in plastic clays. – Eng. Geol., **64**: 217-321.

Bastiaens, W.; Bernier, F.; Buyens, M.; Demarche, M.; Li, X.L.; Linotte, J.M. and Verstricht, J. (2003). The connecting gallery – the extension of the HADES underground research facility at Mol, Belgium. - EURIDICE Rep., **03-294**, EIG EURIDICE, Mol.

Bastiaens, W.; Bernier, F. and Li, X.L. (2007). SELFRAC: Experiments and conclusions on fracturing, self-healing and self-sealing processes in clays. - Phys. & Chem. of the Earth, **32:** 600-615.

Bear, J. (1988). Dynamics of fluids in porous media. – 784 p., New York (Dover Publication Inc.).

Bear, J. (1993). Modelling flow and contaminant transport in fractured rocks. - In: Bear J.; Tsang, C.F. and de Marsily, G. (Eds): Flow and contaminant transport in fractured rock – San Diego (Academic Press), pp. 1-38.

Bechtel, A.; Elliott, W.C.; Wampler, J.M. and Oszczepalski, S. (1999). Clay mineralogy, crystallinity, and K-Ar ages of illites within the Polish Zechstein Basin: Implications for the age of Kupferschiefer mineralization. - Economic Geology, **94**: 261-272.

Bechtel, A.; Elliott, W.C.; Wampler, J.M. and Oszczepalski, S. (2000). Clay mineralogy, crystallinity, and K-Ar ages of illites within the Polish Zechstein Basin: Implications for the age of Kupferschiefer mineralization - A reply. Economic Geology, **95**: 243-244.

Bernier, F.; Li, X.L.; Bastiaens, W.; Ortiz, L.; van Geet, M.; Wouters, L.; Frieg, B.; Blümling, P.; Desrues, J.; Viaggiani, G.; Coll, C.; Chanchole, S.; De Greef, V.; Hamza, R.; Malinsky, L.; Vervoort, A.; Vanbrabant, Y.; Debecker, B.; Verstraelen, J.; Govaerts, A.; Wevers, M.; Labiouse, V.; Escoffier, S.; Mathier, J.-F.; Gastaldo, L. and Bühler, Ch. (2004). SELFRAC – Fractures and self-healing within the excavation disturbed zone in clays. – Final Report, 64 p., 5th EURATOM Framework Progr., Brussels (EU-Commission)

Bieniawski, Z.T. (1973). Engineering classification of jointed rock masses. –Transact. S. Afr. Inst. Civil Eng., **15**: 335-344.

Billaux, D. (1990). Hydrogéologie des milieux fracturés. Géométrie, connectivité, et comportement hydraulique. - Ph.D. Thesis, Ecole des Mines de Paris, BRGM document No. 186.

Billaux, D.; Dedecker, F. and Cundall, P. (2004). A novel approach to studying rock damage: the three dimensional Adaptive Continuum / Discontinuum Code. – In: Schubert, W. (Ed.): Proc. EUROCK 2004 & 53rd Geomechanics Colloquium, pp. 723-728, Essen (VGE).

Billaux, D. and Guérin, F. (1993). Connectivity and the Continuum Approximation in Fracture Flow Modelling. - Proc. 4th Annual Int. Conf. on High Level Radioactive Waste Management, Las Vegas, New York, **2**: 1118-1122.

Blatt, H.; Middleton, G. and Murray, R. (1980). Origin of sedimentary rocks. – 2nd ed., 766 pp., Englewood Cliffs (Prentice-Hall).

Blümling, P. (2005a). Comments on the BGS Draft report: Potential of self-healing of fractures in plastic clays and argillaceous rocks under repository conditions. – Unpubl. note, 12 p.

Blümling, P. (2005b). Key processes related to the initiation and evolution of the EDZ. - 44 p., NF-PRO Workshop, 19th Oct. 2005, Cardiff.

Blümling, P. (2009). Comments on self-sealing draft report of March 2009.

Blümling, P.; Bernier, F.; Lebon, P. and Martin, C.D. (2007). The excavation damaged zone in clay formations time-dependent behaviour and influence on performance assessment. – Phys. & Chem. of the Earth, **32:** 588-599.

Bock, H. (1976). Geometric properties of joint planes and their influence on the strength of geological bodies (in German).- Habil-Thesis, 201 p., Bochum (Ruhr University).

Bock, H. (1980a). The Fundamental Joint System (in German). - Z. deutsch. Geol. Ges., **131**: 627-650.

Bock, H. (1980b). The importance of material science in respect to the mechanical interpretation of geological fractures (in German). –N. Jb. Geol. Paläont., **160**: 380 – 405, Stuttgart (Schweizerbart).

Bock, H. (2001). RA Experiment: Data report on rock mechanics. - Mont Terri Project Techn. Rep., **TR 2000-02**: 1-52, Swiss Nat. Hydrol. Geol. Surv.

Bock, H. (2009). RA Experiment. Updated Review of the Rock Mechanics Properties of the Opalinus Clay of the Mont Terri URL based on Laboratory and Field Testing. - Mont Terri Project Techn. Rep., **TR 2008-04**: 1-66, Swiss Nat. Hydrol. Geol. Surv.

Bock, H.; Blümling, P. and Konietzky, H. (2006). Study of the micro-mechanical behaviour of the Opalinus Clay: an example of co-operation across the ground engineering disciplines. – Bull. Eng. Geol. Environm., **65**: 195-207.

Bock, H. and Konietzky, H. (1997). The Plate Load Test in theory and praxis – a critical review (in German). – Presentation 47th Geomech. Colloquium, Salzburg, 7 p.

Boisson J.-Y. (2005). Catalogue of characteristics of argillaceous rocks. Introductory brochure + specific databases in a CD-ROM (Excel versions) per formation. - OECD/NEA/RWMC/IGSC (Working Group on measurement & Physical understanding of Groundwater flow through argillaceous media), NEA Report n° 4436, 72 p., Paris (OECD / NEA).

Boisson, J.-Y.; Cabrera, J. and De Windt, L. (1998). Étude des écoulements dans un massif argileux, laboratoire souterrain de Tournemire. - CEC Nuclear Sci. & Techn. Series, Luxembourg, EUR 18338.

Bossart, P.; Meier, P.M.; Moeri, A.; Trick, Th. and Mayor, J.-C. (2002). Geological and hydraulic characterisation of the excavated disturbed zone in the Opalinus Clay of the Mont Terri Rock Laboratory. – Eng. Geol., **66**: 19-38.

Bossart, P.; Trick, Th.; Meier, P.M. and Mayor J.-C. (2004). Structural and hydrogeological characterisation of the excavation-disturbed zone in the Opalinus Clay (Mont Terri Project, Switzerland). – Appl. Clay Science. Special Issue: Clays in natural and engineered barriers for radioactive waste confinement: ANDRA meeting, Reims, 2002, Paper 26/1–4: 429–448.

Bossart, P. and Thury, M. (2007). Research in the Mont Terri rock laboratory: Quo vadis?. – Phys. & Chem. of the Earth, **32:** 19-31.

Bossart, P. and Thury, M. (Eds.) (2008): Mont Terri Rock Laboratory, project programme 1996–2007 and results. – Rep. No. **2008-1**, Wabern (Swiss Geol. Survey).

Bowden, F.P. and Tabor, D. (1964). The friction and lubrication of solids. – Part 2, Oxford (Clarendon Press).

Brace, W.F. and Bombolakis, E.G. (1963). A note on brittle crack growth in compression. – J. Geophys. Res., **68**: 3709-3713.

Brace, W.F.; Walsh, J.B. and Frangos, W.T. (1968). Permeability of granite under high pressure. - J. of Geophys. Res., **73**: 2225-2235.

Brady, B.H.G. and Brown, E.T. (1985). Rock mechanics for underground mining. – 527 p., London (Allen & Unwin).

Bray, J.W. (1967). A study of jointed and fractured rock – Part II: Theory of limiting equilibrium. – Rock Mech. & Eng. Geol., **5**: 197-216.

Bühler, Ch. (2005). Selfrac (SE) Experiment: Long term dilatometer experiment. - Mont Terri Project Techn. Note, **2003-17**: 66 p., Swiss Nat. Hydrol. Geol. Surv.

Burrus, J. (1997). Contribution à l'étude du fonctionnement des systèmes pétroliers: apport d'une modélisation bi-dimensionnelle. Mémoire de thèse de doctorat de l'Ecole des Mines de Paris. - Rapport IFP n° 44153.

Buzzi, O.; Hans, J.; Boulon, M.; Deleruyelle, F. and Besnus, F. (2007). Hydromechanical study of rock-mortar interfaces. - Phys. & Chem. of the Earth, **32:** 820-831.

Caine, J.S.; Evans, J.P. and Foster C.B. (1996). Fault zone architecture and permeability structure. – Geology, **24**: 1025-1028.

Campbell, A.R. and Larson, P.B. (1998). Introduction to Stable Isotope Applications in Hydrothermal Systems: Soc. of Economic Geologists Rev., **10**: 173-193.

Cannière de, P.; Put, M.J. and Neerdael, B. (1994). Hydraulic characterization of the Boom Clay formation from the HADES underground laboratory in Mol: Evolution and Assessment of the Piezometric techniques. – Proceed. Internat. Workshop on Hydraulic and Hydrochamical Characterisation of Argillaceous Rocks, Nottingham, UK, 7-9 June, pp. 159-166.

Cariou, S.; Davy, C.; Skoczylas, F.; Dormieux, L.; Lebon, P. and Barnichon, J.-D. (2007). Bentonite sealing efficiency: gas transport and swelling properties - Experimental and modelling approaches. – Poster to the 3rd Int. Meeting on Clays in Natural and Engineered Barriers for Radioactive Waste Confinement, Lille (France), 17-20 Sept. 2007.

Cathles, L.M. and Adams, J.J. (2005). Fluid flow and petroleum and mineral resources in the upper (<20 km) continental crust. - In: Hedenquist, J.W.; Thompson, J.F.H.; Goldfarb, R.J. and Richards, J. (eds.): Economic Geology 100th Anniv. Volume, p. 77-110.

Charpentier, D.; Cathelineau, M.; Mosser-Ruck, R. and Bruno, G. (2001). Évolution minéralogique des argiles en zone sous-saturée oxydée: example des parois du tunnel de Tournemire (Aveyron, France).- C. R. Acad. Sci., **332**: 601-607.

Charpentier, D.; Tessier, D. and Cathelineau, M. (2003). Shale microstructure evolution due to tunnel excavation after 100 years and impact of tectonic paleo-fracturing. Case of Tournemire, France. – Eng. Geol., **66**: 1-15.

Chen, W.F. and Mizuno, E. (1990). Nonlinear analysis in soil mechanics – Theory and implementation. - Development in Geotech. Eng., Vol. 53. – 661 pp., Amsterdam (Elsevier).

Clauer, N. (2005). EDZ characterization and short-term evolution. – 17 p., NF-PRO Workshop, 19th Oct. 2005, Cardiff.

Clauer, N. and Chaudhuri, S. (2001). Extracting K-Ar ages from shales: the analytical evidence. - Clay Minerals, **36**: 227-235.

Clauer, N.; Savin, S.M. and Chaudhuri, S. (1992). Isotopic compositions of clay minerals as indicators of the timing and conditions of sedimentation and burial diagenesis. - In: Clauer, N. and Chaudhuri, S. (eds.): Isotopic signatures and sedimentary records. - p. 239-286, Berlin Heidelberg (Springer)

Clauer, N.; Weber, F.; Gauthier-Lafaye, F.; Toulkeridis, T. and Sizun, J.-P. (1997). Mineralogical, geochemical (REE), and isotopic (K-Ar, Rb-Sr, $\delta^{18}O$) evolution of the clay minerals from faulted, carbonate-rich, passive paleomargin of southeastern Massif Central, France. – J. Sedimentary Res., **67**: 923-934.

Clauer, N.; Zwingmann, H. and Gorokhov, I.M. (2003). Postdepositional evolution of platform claystones based on a simulation of thermally induced diffusion of radiogenic ^{40}Ar from diagenetic illite. - J. Sedimentary Res., **73**: 58-63.

Claypool, G.E.; Holser, W.T.; Kaplan, I.R.; Sakai, H. and Zak, I. (1980). The age curves of sulfur and oxygen isotopes in marine sulfate and their mutual interpretation. - Chemical Geol., **28**: 199-260.

Coussy, O. (2004). Poromechanics. – 312 p., New York (J. Wiley & Sons).

Cox, S.F. (2005). Coupling between deformation, fluid pressures, and fluid flow in ore-producing hydrothermal systems at depth in the crust. - In: Hedenquist, J.W.; Thompson, J.F.H.; Goldfarb, R.J. and Richards, J. (eds.): Economic Geology 100th Anniv. Volume, p. 39-75.

Cox, S.F.; Knackstedt, M.A. and Braun, J. (2001). Principles of structural control on permeability and fluid flow in hydrothermal systems. – Soc. of Economic Geologists Rev., **14**: 1-24.

Craig, H. (1961). Isotopic variations in meteoric waters. - Science, **133**: 1702-1703.

Cuilhé L. and Bruneton A. (2003). Site Meuse/Haute-Marne. Sismique 3D après retraitement 2002. Rapport d'interprétation géologique et structurale. - Rapport Andra n° C.RP.0BEI.03.002.A

Cuss, R.J. (1999). An experimental investigation of the mechanical behaviour of sandstones with reference to borehole stability. – PhD Thesis, Univ. Manchester.

Dana, E. (1999). Contribution à la caractérisation des écoulements biphasiques dans les matériaux poreux. Etude expérimentale sur trois grès. - PhD thesis, 138 p., Université Lille I.

Daneshy, A.; Blümling, P.; Marschall, P. and Zuidema, P. (2004). Interpretation of field experiments and observation of fracturing process. – Int. Sympos. on Formation Damage Control, Lafayette, 18-20 Feb. 2004, Soc. Petrol. Eng., SPE 86486, 8 p.

Davy, C.A.; Skoczylas, F.; Barnichon, J.-D. and Lebon, P. (2007). Permeability of macro-cracked argillite under confinement: Gas and water testing. - Phys. & Chem. of the Earth, **32:** 667-680.

Dedecker, F.; Cundall, P.; Billaux, D. and Groeger, T. (2007). Evaluation of damage-induced permeability using a three-dimensional Adaptative Continuuum/Discontinuum Code (AC/DC). – Int. Meeting "Using natural and engineered clay-based barriers for the containment of radioactive waste", Tours 14-18 March, 2005, pp. 681-690.

Degueldre, C.; Scholtis, A. and Thomas, B. (1998). Opalinus clay groundwaters and colloids. A sampling exercise at Mt. Terri (June/July 1997). Analytical results. - Mont Terri Project, Technical Note **TN 97-20A**, Swiss Nat. Hydrol. Geol. Surv.

Dehandschutter, B. (2004). Faulting and jointing in clay – A geological and geotechnical approach. – 156 p., Final Rep., Leuven (Katholieke Univ.).

Dehandschutter, B.; Vandycke, S.; Sintubin, M.; Vandenberghe, N. and Wouters, L. (2005a). Brittle fractures and ductile shear bands in argillaceous sediments: inferences from Oligocene Boom Clay (Belgium). – J. Structural Geol., **27:** 1095-1112.

Dehandschutter, B.; Gaviglio, P.; Sizun, J.P.; Sintubin, M.; Vandycke, S.; Vandenberghe, N. and Wouters, L. (2005b). Volumetric matrix strain related to intraformational faulting in argillaceous sediments. – J. Geol. Soc. London, **162:** 801-813.

Delay, J.; Forbes, P.L. and Roman, J. (2007). The Meuse/Haute-Marne Underground Research Laboratory: Seven years of scientific investigations. - Internat. Meeting Clays in natural & engineered barriers for radioactive waste confinement, 17-18 Sept. 2007, Lille, Paper O/01/1.

Delay, J.; Trouiller, A. and Lavanchy, J-M. (2006). Propriétés hydrodynamiques du Callovo-Oxfordien dans l'Est du basin de Paris: comparaison des resultants obtenus selon différentes approaches. - C.R. Geosciences, **338**: 892-907.

Delay, J.; Vinsot, A.; Krieguer, J.-M.; Rebours, H. and Armand, G. (2007). Making of the underground scientific experimental programme at the Meuse/Haute-Marne underground research laboratory, North Eastern France. – Phys. & Chem. of the Earth, **32:** 2-18.

Dewhurst, D.N.; Yang, Y. and Aplin, A.C. (1999). Permeability and fluid flow in natural mudstones. – In: Aplin, A.C.; Fleet, A.J. and Macquaker, J.H.S. (Eds.): Mud and mudstones. Physical and fluid flow properties. – Geol. Soc. London, Spec. Publ., **158**: 23-43.

Diederichs, M.S. (2003). Rock fracture and collapse under low confinement conditions. - Rock Mech. Rock Eng., **36:** 339-381.

Distinguin, M.; Robin, P.; Rebours, H.; De Wonck S. and Drouiller, Y. (2003). Laboratoire de recherche souterrain de Meuse/Haute-Marne. Expérimentation FRF up1 CCE. Rapport Andra n° D.CC.ADPE.03.0626.A.

Distinguin, M.; Rebours, H.; Andre, G.; Robin, P. and Wileveau, Y. (2004). Synthèse FRF UP1. Forages de reconnaissance de la formation. Laboratoire de recherche souterrain de Meuse/Haute-Marne. Rapport Andra n° D.RP.ADPE.04.0797.

Dormieux, L.; Lemarchand, E. and Sanahuja, J. (2006a). Comportement macroscopique des matériaux poreux à microstructure en feuillets. - C.R. Mecanique, **334**: 304-310.

Dormieux, L.; Kondo, D. and Ulm, F.-J. (2006b). Microporomechanics. – 328 p., London (J. Wiley & Sons Ltd).

Drucker, D.C. and Prager, W. (1952). Soil mechanics and plastic analysis of limit design. – Quart. Appl. Math., **10**: 157-165.

Dullien, F.A.L. (1992). Porous media, fluid transport and pore structure. - 2nd ed., 416 p., San Diego (Academic Press).

Enachescu, C.; Blümling, P.; Castelao, A. and Steffen, P. (2002). Mont Terri GP-A and GS Experiments Synthesis Report. – Nagra Internal Rep., **02-51**: 1-65.

Eurocode 7. Geotechnical design –
EN 1997-1. Part 1: General rules (2004)
EN 1997-2. Part 2: Ground investigation and testing (2007)

Fairhurst, Ch. (1972). Fundamental considerations relating to the strength of rock. – Veröff. Inst. Bodenmech. Felsmech. Uni Karlsruhe, Vol. **55**: 1-56.

Faure, G. (1986). Principles of isotope geology. - 2nd ed., 589 p., New York (Whiley),

Feeser, V. (1986). Geomechanical concept of the development of the fabric and stress history of glacially deformed clays (in German). – PhD-Thesis, 127 p., Techn. Univ. Braunschweig.

Fisch, H.R.; Rösli, U.; Reinhardt, S.; Yeatman, B.; Senger, R. and Dale, T. (2008). Oftringen borehole - hydraulic packer testing. - Nagra Arbeitsbericht NAB 08-15, Wettingen, Switzerland. (Nagra)

Fleming, R.W.; Spencer, G.S. and Banks, D.C. (1970). Empirical study of the behaviour of clay shale slopes. – U.S. Army Engineering Nuclear Cratering Group, NGC Tech. Rep., **15(1)**: 93 p.; **15(2)**: 304 p.

Fouché, O.; Wright, H.; Le Cléac'h, J.-M. and Pellenard, P. (2004). Fabric control on strain and rupture of heterogeneous shale samples by using a non-conventional mechanical test. – Appl. Clay Sci., **26**: 367-387.

Freivogel, M. and Huggenberger, P. (2003). Modellierung bilanzierter Profile im Gebiet Mont Terri – La Croix (Kanton Jura). In: Heitzmann, P. and Tripet, J. P. (eds.): Mont Terri Project - Geology, paleohydrogeology and stress field of the Mont Terri region. - Federal Office for Water and Geology, Rep. **4**: 7 - 44, Bern, Switzerland.

Fröhlich, H. (2004). Self healing of clay at elevated temperatures. – NF-PRO, Deliv. 4.4.4, Final Rep., 29 p.

Füchtbauer, H. (1988). Sedimente und Sedimentgesteine. –1141 p., Stuttgart (E. Schweizerbart)

Gautschi, A. (2001). Hydrogeology of a fractured shale (Opalinus Clay): Implications for deep geological disposal of radioactive wastes. – Hydrogeology J., **9**: 97-107.

GDR-FORPRO (French research laboratories group). Action 2000.II, Benchmark "Perméabilité".- Final Rep. (in French), 200 p., J.M. Fleureau Ed..

Goodman, R.E. (1974). The mechanical properties of joints. – Proceed. 3rd Congr. Int. Soc. Rock Mech., Denver, Vol. 1, Part A: 127-140, Washington (Nat. Acad. Sciences).

Gostick, J.T.; Fowler, M.W.; Pritzker, M.D.; Ioannidis, M.A. and Behra L.M. (2006). In-Plane and through-plane gas permeability of carbon fiber electrode backing layers. - J. Power Sources, **162**: 228-238.

Griffith, A. A. (1921). The phenomena of rupture and flow in solids. – Philos. Trans. Roy. Soc. London, **A 221**: 163-198.

Griffith, A.A. (1924). Theory of rupture. – Proceed. 1st Int. Congr. Appl. Mech., pp. 55-63, Delft (J. Waltman).

Grim, R. E. (1968). Clay mineralogy. – 596 p, New York (Mc Graw-Hill).

Guilbert, J.M. and Park, C.F. (1996). The geology of ore deposits. – 5th edition, 985 p., W.H. Freeman & Co, USA.

Guillocheau, F.; Robin, C.; Allemand, P.; Bourquin, S.; Brault, N.; Dromart, G.; Friedenberg, R.; Garcia, J.-P.; Gaulier, J.-M.; Gaumet, F.; Grosdoy, B.; Hanot, F.; le Strat, P.; Mettraux, M.; Nalpas, T.; Prijac, C.; Rigollet, C.; Serrano, O. and Granjean, G. (2000). - Meso-Cenozoic geodynamic evolution of the Paris Basin: 3D stratigraphic constraints. - Geodynamica Acta, **13**: 189-246.

Gutierreza, M.; Øinob, L.E. and Nygardc, R. (2000). Stress-dependent permeability of a de-mineralised fracture in shale. – Marine & Petr. Geol., **17**: 895-907.

Hallbauer, D.K.; Wagner, H. and Cook, N.G.W. (1973). Some observations concerning the microscopic and mechanical behaviour of quartzite specimens in stiff, triaxial compression tests. – Int. J. Rock Mech. Min. Sci., **10**: 713-726.

Haller de, A.; Tarantola, A.; Mazurek, M. and Spangenberg, J. (2009). Vein fillings and past fluid flow. - In: Waber, H.N. (ed.): Borehole Oftringen: Mineralogy, porosimetry, geochemistry, pore water chemistry. - Nagra Arbeitsbericht **NAB 08-18**, Wettingen, Switzerland (Nagra) (in prep.)

Heitz, D.; Trick, Th. and Bühler, Ch. (2003). Selfrac (SE) Experiment: Long term plate load experiment. - Mont Terri Proj., Techn. Note, **2003-51**: 106 p., Swiss Nat. Hydrol. Geol. Surv.

Hekel, U. (1994). Hydrogeologische Erkundung am Beispiel des Opalinustons (Unteres Aalenium). – Tübinger geowiss. Arbeiten, **C18**, Univ. Tübingen

Hertz, H. (1881). Über die Berührungfester elastischer Körper. – J. reine angew. Mathem., Vol. 92.

Hitzman, M.; Kirkham, R.; Broughton, D.; Thorson, J. and Selley, D. (2005). The sediment-hosted stratiform copper ore system. - In: Hedenquist, J.W.; Thompson, J.F.H.; Goldfarb, R.J. and Richards, J. (eds.): Economic Geology 100th Anniv. Volume, pp. 609-642.

Hodgson, R.A. (1961). Regional study of jointing in Comb Ridge-Navajo Mountain area, Arizona and Utah. – Bull Amer. Ass. Petrol. Geol., **45**: 1-38.

Hoek, E. (1994). Strength of rock and rock masses. – ISRM News Journal, **2(2)**: 4-16.

Hoek, E. and Bieniawski, Z. T. (1965). Brittle fracture propagation in rock under compression. – Int. J. Rock Mech. Min. Sci., **1**: 137-155.

Hoek, E. and Brown, E.T. (1980). Empirical strength criterion for rock masses. – J. Geotech. Eng. Div. ASCE, **106**: 1013-1035.

Hoek, E. and Marinos, P. (2007). A brief history of the development of the Hoek-Brown failure criterion. – Soils & Rocks, São Paulo, **30**: 85-92.

Hoek, E.; Marinos. P. and Benissi, M. (1998). Applicability of the Geological Strength Index (GSI) classification for very weak and sheared rock masses. The case of the Athens Schist Formation. – Bull. Eng. Geol. Env., **57**: 151-160.

Holland, M.; Urai, J.L.; van der Zee, W.; Stanjek, H. and Konstanty, J. (2006). - Fault gouge evolution in highly overconsolidated claystones. – J. Structural Geol., 28: 323-332.

Horita, J. and Clayton, R.N. (2007). Comment on the studies of oxygen isotope fractionation between calcium carbonates and water at low temperatures by Zhou and Zheng (2003; 2005). - Geochim. Cosmochim. Acta, **71**: 3131-3135.

Horseman, S.T.; Higgo, J.J.W.; Alexander, J. and Harrington, J.F. (1996). Water, gas and solute movement through argillaceous media. Nuclear Energy Agency Rep. CC-96/1, Paris, OECD.

Horseman, S. T.; Cuss, R. J. and Reeves, H. J. (2004). Clay Club initiative: Self-healing of fractures in clay-rich host rocks. - In: Proceed. "Clay Club" Workshop, Braunschweig, 9-11 Dec. 2003, OECD NEA Publ. No. **5303**: 117-134.

Horseman, S.T.; Cuss, R. J.; Reeves, H. J. and Noy, D. (2005). Potential for self-healing of fractures in plastic clays and argillaceous rocks under repository conditions". - Draft report NEA-CC-3 Version 1.0; 351 p., Nottingham (BGS).

Horseman, S.T.; Harrington, J.F.; Birchall, D.J.; Noy, D.J. and Cuss, R.J. (2006). Hydrogeologic analyses and synthesis (HA Experiment): Consolidation and rebound properties of Opalinus clay: A long-term, fully-drained test. – Mont Terro Project, **TN 2003-03**: 1-60.

Hsieh, P.A.; Tracy, J.V.; Neuzil, C.E.; Bredehoeft, J.D. and Silliman, S.E. (1981). A transient laboratory method for determining the hydraulic properties of tight rocks – I – Theory. - Int. J. Rock Mech. Min. Sci. & Geomech. Abstr., **18**: 245-252.

Hutcheon, I.; de Caritat, P. and Abercrombie, H.J. (1994). Clay minerals - Equilibrium models and temperature indicators. - In Lentz, D.R. (ed.): Alteration and alteration processes associated with ore-forming systems. – Geol. Assoc. of Canada, Short Course Notes, **11**: 43-68.

Intera Engineering Ltd. (2006). Geoscientific Site Characterisation Plan Deep Geologic Repository Bruce Nuclear site – Final Report. OPG Report No. 002160REP-03902-00002-R00.

ISO 14688 Geotechnical investigation and testing – Identification and classification of soil.
Part 1 (2002). Identification and description, 12 p.
Part 2 (2004). Principles for a classification, 13 p.

ISO 14689 Geotechnical investigation and testing – Identification and classification of rock.
Part 1 (2003). Identification and description, 16 p.

Itasca (2004). Evaluation par modélisations particulaires de la géométrie et des propriétés hydrauliques des zones fracturées et endommagées lors du creusement d'une galerie dans des argilites (seconde phase) Rapport final. - Rapport Andra No. C.RP.0ITA.04.011.B

Jacobi, O. (1981). Praxis der Gebirgsbeherrschung. – 2nd ed., 576 p., Essen (Glückauf).

Jaeger, J. C. and Cook, N. G. W. (1976). Fundamentals of rock mechanics. – 2nd ed., 585 p., London (Chapman & Hall).

Jasmund, K. and Lagaly, G. (Ed.) (1992). Tonminerale und Tone. Strukturen, Eigenschaften, Anwendung und Einsatz in Industrie und Umwelt. - Darmstadt (Steinkopf).

JEWG (2004). Professional tasks, responsibilities and co-operation in ground engineering. – Report of the Joint European Working Group to the Presidents of the IAEG, ISRM and ISSMGE, pp. 1-20.

Jolley, S.J.; Dijk, H.; Lamens, J.H.; Fisher, Q.J.; Manzocchi, T.; Eikmans, H. and Huang, Y. (2007). Faulting and fault sealing in production simulation models: Brent Province, northern North Sea. – Petroleum Geoscience, **13**: 321-340.

Johnson, D.L.; Koplik, J. and Schwartz, L.M. (1986). New pore size parameter characterizing transport. - Porous Media. Phys. Rev. Lett. **57**: 2564-2567.

Jouanna, P. and Fras, G. (1979). Introduction à la reconnaissance, dans l'espace des fréquences, de milieux fissurés par essais d'eau transitoires. Notion de signatures spectrales et application au cas d'horizons fissurés reconnus par pompage harmonique: unicité des solutions. - C.R. Acad. Sci. Paris - Série II, **t313**: 989-994.

Karnland, O.; Olsson, S. and Nilsson, U. (2006). Mineralogy and sealing properties of various bentonites and smectite-rich clay minerals. – Techn. Rep. TR-06-30, SKB, Sweden.

Kempfert, H.-G. and Raithel, M. (2007). Bodenmechanik und Grundbau. Vol. 1: Bodenmechanik. – 371 p., Berlin (Bauwerk).

Kim, M.H.M.; Inoue, J. and Horii, H. (2004). Flow analysis of jointed rock masses based on excavation-induced transmissivity change of rough joints. – Int. J. Rock Mech. Min. Sci., **41**: 959-971.

Kim, S.T. and O'Neil, J.R. (1997). Equilibrium and non-equilibrium oxygen isotope effects in synthetic carbonates. - Geochimica et Cosmochimica Acta, **61**: 3461-3475.

Koroleva, M.; Mazurek, M. and Alt-Epping, P. (in prep.): Natural tracer profiles in the Mont Terri anticline. Mont Terri Technical Note.

Kovács, L. (ed.) (1999). Short-term qualification program of the Boda Claystone Formation. – Final Rep., Vol. 9 (overview report), Pécs - Paks, Hungary (Mecsekerc Environmental & PURAM).

Kovács, L. (2003). Digest on the results of the short-term characterisation programme of the Boda Claystone Formation. – Report, Pécs - Paks, Hungary (Mecsekerc Environmental & PURAM).

Krouse, H.R.; Viau, C.A:, Eliuk, L.S.; Ueda, A. and Halas, S. (1988). Chemical and isotopic evidence of thermochemical sulfate reduction by light hydrocarbon gases in deep carbonate reservoirs. - Nature, **333**: 415-419.

Lade, P.V. and Duncan, J. M. (1975). Elastoplastic stress-strain theory for cohesionless soil. – J. Geotech. Eng. Div. ASCE, **IOI**: 1037-1053.

Lanyon, G.W. (2008). HG-A (gas path through host rock and along seals) experiment: Discrete fracture network models of Excavation Damage Zone at the HG-A site. - Mont Terri Project Techn. Note TN 2007-07, 67 p.

Lanyon, G.W. (2005). iConnect Club / Year 3 – Nagra supported studies on the understanding flow in fractured rock. - Nagra Working Report NAB05-13, Switzerland.

Lanyon, G.W. (2006). iConnect Club / Year 4 – Nagra supported studies on the understanding flow in fractured rock. - Nagra Working Report NAB06-22, Switzerland.

Lanyon, G. W.; Marschall, P: and Blümling, P. (2005). Modelling of groundwater flow along the excavation damage zone of a tunnel in the Opalinus Clay. - Clays in Natural & Engineered Barriers for Radioactive Waste Confinement. 2nd Int. Meeting, Tours, March 14-18, 2005.

Lavanchy, J.M.; Croisé, J.; Schwarz, R.; Armand, G. and Cruchaudet, M. (2007). Clay formation at the Meuse/Haute-Marne URL: Evaluation of the impact of resin filled slots on flow paths characteristics within the EDZ. – Abstracts of Internat. Meeting Clays in natural & engineered barriers for radioactive waste confinement, 17-18 Sept. 2007, Lille, Paper O/011A/1: 169-170.

Lebon, P. (2005). Outcomes and recommendations for a path forward on Self-Healing Report. – Unpubl. notes, 3 +1 pp.

Lebon, P. (2009). Personal e-mail communication with H. Bock of 11 August.

Leitch, C.H.B. and Lentz, D.R. (1994). The Gresens approach to mass balance constraints of alteration systems: methods, pitfalls, examples. In Lentz, D.R. (ed.): Alteration and alteration processes associated with ore-forming systems. – Geol. Assoc. of Canada Short Course Notes, **11**: 161-192.

Lerman, A. and Clauer, N. (2005). Losses of radiogenic ^{40}Ar in the fine-clay size fractions of sediments. - Clays and Clay Minerals, **53**: 234-249.

Leussink, H.; Visweswaraiya, T.G. and Brendlin, H. (1964). Beitrag zur Kenntnis der bodenphysikalischen Eigenschaften von Mischböden. – Veröff. Inst. Bodenmech. Grundbau TH Karlsruhe, **15**: 1-75.

Li, X.L.; Bernier, F. and Wouters, L. (2005). Remarks concerning "Potential for self-healing of fractures in plastic clays and argillaceous rocks under repository conditions". Draft report NEA-CC-3 Version 1.0 – Unpubl. note, 2 p.

Lockner, D.A. and Madden, T.R. (1991). A multiple-crack model of brittle fracture, II Time-dependent simulations. – J. Geophys. Res., **96**: 19643 –54.

Loosveldt, H.; Lafhaj, Z. and Skoczylas, F. (2002). Experimental study of gas and liquid permeability of a mortar. - Cement & Concrete Res., **32**: 1357-1363.

Low, P.F. (1987). Structural components of the swelling pressure of clay. – Lanmuir, **3**: 18-25.

Lundegard, P.D. and Samuels, N.D. (1980). Field classification of fine-grained sedimentary rocks. – J. Sediment. Petrology, **50**: 781-786.

Lux, K.-H.; Düsterloh, U. and Czaikowski, O. (2007). Final report laboratory tests on indurated clay, Deliverable 4.4.13. – Rep. NF-PRO, EDZ long term evolution (WP 4.4), 64 p., Clausthal (Univ. of Technology).

MacLean, W.H. (1990). Mass change calculations in altered rock series. - Mineralium Deposita, **25**: 44-49.

McArthur, J.M.; Howarth, R.J. and Bailey, T.R. (2001). Strontium isotope stratigraphy: LOWESS Version 3: Best fit to the marine Sr-isotope curve 0-509 Ma and accompanying look-up table for deriving numerical age. – J. Geology, **109**: 155-170.

Mäder, U.K. and Mazurek, M. (1998). Oxidation phenomena and processes in Opalinus Clay: evidence from the excavation-disturbed zones in Hauenstein and Mt. Terri tunnels, and Siblingen open clay pit. – In: McKinley, I.G. and McChombie, Ch. (Eds.): Scientific basis for nuclear waste management XXI. – Materials Res. Soc. Sympos. Proceed., **506**: 731-739.

Makurat, A. and Gutierreza, M. (1997). Fracture flow and fracture cross-flow experiments. – Proceed. SPE Annual Tech. Conf. and Exhibition, Denver, CO, **SPE 36732:** 511-519.

Mandl, G. (2005).Rock Joints, The mechanical genesis. - 221 p., Berlin (Springer).

Marle, C.M. (1981). Multiphase flow in porous media. – 272 p., Paris (Ed. Technip).

Marquer, D. and Burkhard, M. (1992). Fluid circulation, progressive deformation and mass-transfer processes in the upper crust: the example of basement-cover relationships in the External Crystalline Massifs, Switzerland. - J. Struct. Geol., **14**: 1047-1057.

Marschall, P. (2005). EDZ long-term evolution (self sealing and gas transfer). – 40 p., NF-PRO Workshop, 20th Oct. 2005, Cardiff.

Marschall, P. (2006). NF-PRO, Topic 3: Water solute and gas transport in the EDZ for different disposal systems: Indurated clay. – 16 p., NF-PRO Workshop, 15th Nov. 2006, Cardiff.

Marschall, P.; Blümling, P. and Mazurek, M. (2003). Geoscientific basis for making the safety case for a SF/HLW/ILW repository in Opalinus Clay in NE Switzerland (Project *Entsorgungsnachweis*) – III: Repository-induced effects: EDZ, repository gas release, self-sealing. – OECD/NEA AMIGO Workshop, June 3-5, 2003, Yverdon-les-Bains, PPT presentation, 27 p.

Marschall, P.; Croisé, J.; Schlickenrieder, L.; Boisson, J. Y.; Vogel, P. and Yamamoto, S. (2004). Synthesis of hydrogeological investigations at the Mont Terri site (Phases 1 to 5). In: Heitzmann, P. (ed.) Mont Terri project – Hydrogeological synthesis, osmotic flow. Federal Office for Water and Geology, Rep. **6**: 7 - 94, Bern, Switzerland.

Marschall, P.; Distinguin, M.; Shao, H.; Bossart, P.; Enachescu, C. and Trick, T. (2006). Creation and Evolution of Damage Zones Around a Microtunnel in a Claystone Formation of the Swiss Jura Mountains. - Paper presented at the 2006 SPE Int. Sympos. & Exhib. on Formation Damage Control, Lafayette, L.A., 15–17 Feb. 2006. SPE-98537-PP.

Marschall, P.; Blümling, P. and Mazurek, M. (2008a). Geoscientific basis for making the safety case for a SF/HLW/ILW repository in Opalinus Clay in NE Switzerland (Project *Entsorgungsnachweis*) – III: Repository-induced effects: EDZ, repository gas release, self-sealing. - NEA Rep., **4309**: 1-9.

Marschall, P.; Cuss, R.; Wieczorek, K. and Popp, T. (2008b). NF-PRO, Deliverable 4.4.1, State of the Art on Gas Transport in the Tunnel Nearfield / EDZ, Interim Report, 66 p.

Marschall, P.; Trick, T.; Lanyon, G.W.; Delay, J. and Shao, H. (2008c). Hydro-mechanical evolution of damaged zones around a microtunnel in a claystone formation of the Swiss Jura Mountains. – ARMA (Amer. Rock Mech. Assoc.), **08-193**, 10 pp.

Marsily, G. de (1986a). Hydrogéologie quantitative. – 215 p., Paris (Masson Ed.).

Marsily, G. de (1986b). Quantitative hydrogeology. – New York (Academic Press).

Martin, C.D.; Lanyon, G.W.; Blümling, P. and J.-C. Mayor, J.-C. (2002). The Excavation Disturbed Zone around a Test Tunnel in the Opalinus Clay. - Proc. 5th North Americ. Rock Mech. Sympos. & 17th Tunnelling Assoc. of Canada Conf., NARMS/TAC 2002, Univ. of Toronto Press, Vol. **2**: 1581-1588.

Martin, C.D. and Lanyon, G.W. (2002). EDZ in clay shale: Mont Terri Rock Laboratory. - Mont Terri Project Techn. Rep., **TR 2001-01**, Swiss Nat. Hydrol. Geol. Surv.

Martin, C.D. and Lanyon, G.W. (2003). Measurement of *in situ* stress in weak rocks at Mont Terri Rock Laboratory, Switzerland. – Int. J. Rock Mech. Min. Sci., **40**: 1077-1088.

Martino, J.B.; Dixon, D.A.; Kozak, E.T.; Gascoyne, M.; Vignal, B.; Sugita, Y.; Fujita, T. and Masumoto, K. (2007). The tunnel sealing experiment: An international study of full-scale seals. - Phys. & Chem. of the Earth, **32:** 93-107.

Mayer, W. and Piestrzynski, A. (1985). Ore minerals from Lower Zechstein sediments at the Rudna mine, fore-Sudetic monocline, SW Poland. - Prace Mineralogiczne, **75**: 2–72.

Mayor, J-C.; Velasco, M. and García-Siñeriz, J.-L. (2007). Ventilation experiment in the Mont Terri underground laboratory. - Phys. & Chem. of the Earth, **32:** 616-628.

Mayor, J-C. and Velasco, M. (2008). NF-PRO, Deliverable 4.3.18, The Ventilation Experiment Phase II. – Interim Rep., 31 p.

Mazurek, M. (1999). Evolution of gas and aqueous fluid in low-permeability argillaceous rocks during uplift and exhumation of the Central Swiss Alps. – Appl. Geochemistry, **15**: 211-234.

Mazurek, M.; Alexander, W.R. and MacKenzie, A.B. (1996). Contaminant retardation in fractured shales: Matrix diffusion and redox front entrapment. – J. Contaminant Hydrol., **21**: 71-84.

Mazurek, M.; Pearson, F.J.; Volckaert, G. and Bock, H. (2003). Features, events and processes. Evaluation catalogue for argillaceous media. – OECD, NEA 4437, ISM 92-64-02148-5.

Mazurek, M. and Mäder, U. (2005). Comments to: BGS Self sealing draft report, Chapter 10: Geochemical changes. – Unpubl. note, 4 p.

Mazurek, M.; Gautschi, A.; Marschall, P.; Vigneron, G.; Lebon, P. and Delay, J. (2008). Transferability of geoscientific information from various sources (study sites, underground rock laboratories, natural analogues) to support safety cases for radioactive waste repositories in argillaceous formations. – Phys. & Chem. of the Earth, **33:** 95 – 105.

Mazurek, M.; Alt-Epping, P.; Bath, A.; Gimmi, T. and Waber, H. N. (2009). Natural tracer profiles across argillaceous formations: The CLAYTRAC project. - OECD/NEA report 6253, Paris, France.

Meier, P.M.; Trick, Th.; Blümling, P. and Volckaert, G. (2002). Self-healing of fractures within the EDZ at the Mont Terri Rock Laboratory: results after one year of experimental work. – In: Hoteit, N.; Su, K.; Tijani, M. and Shao, J.-F. (Eds.): Hydromechanical and thermohydromechanical behaviour of deep argillaceous rocks. – Intern. Workshop, Paris, 11-12 Oct. 2000, p. 267-274, Lisse (Swets & Zeitlinger).

Mertens, J.; Vandenberghe, N.; Wouters, L. and Sintubin, M. (2003). The origin and development of joints in the Boom Clay Formation (Rupelian) in Belgium. In: Van Rensbergen, P.; Hillis, P.R.; Maltman, A.J. and Morley, C.K. (Eds.): Subsurface Sediment Mobilization. - Geol. Soc. London, Spec. Publ., **217**: 311-323.

Mertens, J.; Wouters, L. and Marcke, Ph. van (2004). Burial history of two potential clay host formations in Belgium. – In: Proceed. "Clay Club" Workshop, Braunschweig, 9-11 Dec. 2003, OECD NEA Publ. No. **5303**: 183-186.

Meziani, H. and Skoczylas, F. (1999). An experimental study of the mechanical behaviour of a mortar and of its permeability under deviatoric loading. - Materials & Structures, **32**: 403-409.

Min, K.R.; Rutqvist, J.; Tsang, C.F. and Jing, L. (2004). Stress-dependent permeability of fractured rock masses: a numerical study. - Int. J. Rock Mech. Min. Sci., **41**: 1191-1210.

Mitchell, J. K. (1993). Fundamentals of soil behavior. – 2nd Ed., 422 p., New York (Wiley).

Montes, H.G.; Duplay, J.; Martinez, L.; Escoffier, S. and Rousset, D. (2004).Structural modifications of Callovo-Oxfordian argillite under hydration/dehydration conditions. – Appl. Clay Sci., **25**: 187-194.

Mook, W.G.; Bommerson, J.C. and Staverman, W.H. (1974). Carbon isotope fractionation between dissolved bicarbonate and gaseous carbon dioxide. - Earth & Planetary Sci. Letters, **22**: 169-176.

Müller, G. (1967). Diagenesis in argillaceous sediments. – In: Larsen, G. and Chilingarian, G. V. (Eds.): Diagenesis in sediments. - Developments in Sedimentology, **8:** 1-551, Amsterdam (Elsevier)

Nagra (1997). Geosynthese Wellenberg 1996: Ergebnisse der Untersuchungsphasen 1 und 2. – Nagra Techn. Ber. **NTB 96-01**, Wettingen (Nagra)

Nagra (2002a). Project Opalinus Clay – Safety Report. – Nagra Techn. Ber. **NTB 02-05**: 1-360, Wettingen (Nagra).

Nagra (2002b). Projekt Opalinuston – Synthese der geowissenschaftlichen Untersuchungsergebnisse. – Nagra Techn. Ber. **NTB 02-03**: 1-659, Wettingen (Nagra).

Nagra (2009). Vorschlag geologischer Standortgebiete für das SMA- und das HAA-Lager: Darstellung der hydraulischen Durchlässigkeit versus Tongehalt in Sedimentgesteinen aus Tiefbohrungen in der Nordschweiz und am Wellenberg im Hinblick auf die Beurteilung der SGT-Kriterien 'Hydraulische Barrierenwirkung' und 'Freisetzungspfade'. - Nagra Arbeitsber. **NAB 09-28**: Wettigen (Nagra) (in print).

Nawrocki, J. (2000). Clay mineralogy, crystalinity, and K-Ar ages of illites within the Polish Zechstein Basin: Implications for the Age of Kupferschiefer Mineralization – A Discussion. - Economic Geology, **95**: 241-242.

NEA (2007). Linkage of geoscientific arguments and evidence in supporting the Safety Case. – Proceed.2nd AMIGO workshop, Toronto, 20 - 22 Sept. 2005. Rep. **6119**: 1-179, Paris (OECD/NEA).

Neuzil, C.E. (1993). Low fluid pressure within the Pierre Shale: A transient response to erosion. – Water Resources Res., **29:** 2007-2020.

Neuzil, C.E. (1995). Abnormal pressures as hydrodynamic phenomena. – Amer. J. Sci., **295:** 742-786.

Neuzil, C.E.; Cooley, C.; Silliman, S.E.; Bredehoeft, J.D. and Hsieh, P.A. (1981). A transient laboratory method for determining the hydraulic properties of tight rocks – II – Applications. - Int. J. Rock Mech. Min. Sci. & Geomech. Abstr., **18**: 253-258.

Nickelsen, R.P. and Hough, N.S. (1967). Jointing in the Appalachian Plateau of Pennsylvania. – Geol. Soc. Amer. Bull., **78**: 609-630.

Nüesch, R. (1991). The mechanical behaviour of the Opalinus Clay (in German). – Mitt. geol. Inst. ETH and Univ. Zürich, N.F., **293:** 1-244.

Nussbaum, C.; Armand, G.; Meier, O.; Badertscher, N. and Bossart, P. (2005a). EZ-A (EDZ cut-off) experiment: Identification of water conducting features and conceptual model of the water flowpaths at the EH section. - Mont Terri Project Techn. Note, **TN 2005-54**rev., 88 p., Swiss Nat. Hydrol. Geol. Surv.

Nussbaum, C.; Bossart, P.; Burrus, F.; Badertscher, N.; Meier, O. and Nold, A. (2005b). Excavation of Gallery 04: General documentation, deformation measurements and geological surveys. - Mont Terri Project Techn. Note, **TN 2005-05**, Swiss Nat. Hydrol. Geol. Surv.

Nussbaum, C. and Bossart, P. (2006). HG-A experiment: Mapping of new breakouts developed in the HG-A microtunnel about 11 months after the excavation. - Mont Terri Project Techn. Note, **TN 2006-31**, 17 p., Swiss Nat. Hydrol. Geol. Surv.

Nussbaum, C. and Bossart, P. (2008). Geology. - In : Bossart, P. and Thury, M. (Eds.): Mont Terri Rock Laboratory, project programme 1996–2007 and results. – Rep. No. **2008-1**, Chapter 2: 25-37, Wabern (Swiss Geol. Surv.).

O'Brien, N. R. and Slatt, R. M. (1990). Argillaceous rock atlas. – 141 p., New York (Springer).

Økland, D. and Cook, J.M. (1998). Bedding-related borehole instability in high-angle wells. – Eurock '98, Trondheim, Norway, 8-10 July 1998, Proc. SPE/ISRM 47285.

Ohmoto, H. and Goldhaber, M.B. (1997). Sulfur and carbon isotop. – In: Barnes, H.L. (ed.): Geochemistry of hydrothermal ore deposits. – 3rd edition, p. 517-611, New York (Wiley & Sons)

Olsen, H.W. (1962). Hydraulic flow through saturated clays. – Clays and Clay Minerals, **9**: 131-161.

Ondraf/Niras (2002). SAFIR 2: Safety assessment and feasibility report 2, NIROND Report 2001-06-E.

O'Neil, J.R.; Clayton, R.N. and Mayeda, T.K. (1969). Oxygen isotope fractionation in divalent metal carbonates. – J. Chemistry & Physics, **51**: 5547-5558.

Oyama, T. and Chigira, M. (1999). Weathering rate of mudstone and tuff on old unlined tunnel walls. Eng. Geol., **55**: 15-27.

Pearson, F.J. (1999). What is the porosity of a mudrock? - *In:* Aplin, A. C., Fleet, A.J. and Macquaker, J.H.S. (eds.): Muds and mudstones: Physical and fluid flow properties. - Geol. Soc. London, Spec. Publ., **158**: 9 - 21.

Pearson, F.J.; Arcos, D.; Bath, A.; Boisson, J.-Y.; Fernández, A.M.; Gäbler, H.E.; Gaucher, E.; Gautschi, A.; Griffault, L.; Hernan, P. and Waber, H.N. (2003). Geochemistry of water in the Opalinus Clay formation at the Mont Terri Rock Laboratory – Synthesis Report. Bern, Switzerland, Ber. Bundesamtes Geol. & Wasser – Serie Geologie, Nr. 30.

Peyaud, J. B.; Pagel, M.; Cabrera, J. and Pitsch, H. (2006). Mineralogical, chemical and isotopic perturbations induced in shale by fluid circulation in a fault at the Tournemire experimental site (Aveyron, France). – J. of Geochem. Exploration, **90**: 9-23.

Plas, F. and Aranyossy, J.F. (2005). Integration of EDZ issues in an overall system performance assessment. – Presentation to NF-Pro Workshop, Cardiff, 19 Oct. 2005.

Popp, T. and Salzer, K. (2007). HE-D Experiment: Influence of bedding planes (IfG), Final Report. - Mont Terri Project Techn. Rep., **TR 2007-04**: 69 p., Swiss Nat. Hydrol. Geol. Surv.

Potter, P.E.; Maynard, J.B. and Pryor, W.A. (1980). Sedimentology of shale. – 366 pp., New York (Springer).

Price, N.J. and Cosgrove, J.W. (1990). Analysis of geological structures. – Cambridge (Univ. Press).

Pusch, R. (1995). Rock mechanics on a geological base. – Developments in Geotechnical Engineering, **77**: 498 pp., Amsterdam (Elsevier).

Reed, M.H. (1997). Hydrothermal alteration and its relationship to ore fluid composition. – In: Barnes, H.L. (ed.): Geochemistry of hydrothermal ore deposits. – 3rd ed., p. 303-365, New York (Wiley & Sons)

Richards, J. P. and Noble, S. R. (1998; 2005 reprint). Application of radiogenic isotope systems to the timing and origin of hydrothermal processes. - Soc. of Economic Geol. Reviews, **10**: 195-233.

Rimstidt, J.D. (1997). Gangue mineral transport and deposition. – In: Barnes, H.L. (ed.): Geochemistry of hydrothermal ore deposits. – 3rd ed., p. 487-515, New York (Wiley & Sons)

Rodwell, W. R.; Harris A.W. and Horseman S.T. (1999). Gas migration and two-phase flow through engineered and geological barriers for a deep repository for radioactive waste. A Joint EC/NEA Status Report, European Commission, 1999, EUR 19122 EN.

Roedder, E. (1984). Fluid inclusions. – Mineral. Soc. of America, Reviews in Mineralogy, **12**: 1-646.

Romanek, C.S.; Grossman, E.L. and Morse, J.W. (1992). Carbon isotopic fractionation in synthetic aragonite and calcite: effects of temperature and precipitation rate. - Geochim. Cosmochim. Acta, **56**: 419-430.

Roscoe, K.H. and Burland, J.B. (1968). On the generalised stress-strain behaviour of 'wet' clay. – In: Heyman, J. and Leckie, F.A. (Eds.): Engineering Plasticity, pp. 535-609, Cambridge (Univ. Press).

Rousset, D. and Clauer, N. (2003). Discrete clay diagenesis in a very low-permeable sequence constrained by isotopic (K-Ar and Rb-Sr) study. - Contributions to Mineralogy & Petrography, **145**: 182-198.

Rousset, D.; Lancelot, J.; Verdoux, P.; Clauer, N. and Leclerc, S. (2005). Influence of local fluid flow on properties of low permeability Cretaceous siltstones (South-Eastern France): Implications for a nuclear waste deep repository. - J. of Geochem. Exploration, **87**: 1-18.

Salzer, K.; Konietzky, H. and Günther, R.-M. (1998). A new creep law to describe the transient and secondary creep phase. – Proceed. NUMEG 98, Wien (Springer).

Schaltegger, U.; Zwingmann, H.; Clauer, N.; Larqué, P. and Stille, P. (1995). K-Ar dating of a Mesozoic hydrothermal activity in Carboniferous to Triassic clay minerals of northern Switzerland. – Schweiz. Mineralog. & Petrogr. Mitt., **75**: 163-176.

Schofield, A.N. and Wroth, C.P. (1968). Critical state soil mechanics. – 310 p., London (Mc Graw-Hill).

Seal, II, R.R.; Alpers, C.N. and Rye, R.O. (2000). Stable isotope systematics of sulfate minerals. – In: Alpers, C.N.; Jambor, J.L. and Nordstrom, D.K. (eds.): Sulfate minerals: crystallography, geochemistry, and environmental significance. – Rev. in Mineral. & Geochem., **40**: 541-602

Seal, II, R.R. (2006). Sulfur isotope geochemistry of sulfide minerals. – Rev. in Mineral. & Geochem., **61**: 633-677.

Selley, D.; Broughton, D.; Scott, R.; Hitzman, M.; Bull, S.; Large, R.; McGoldrick, P.; Croaker, M.; Pollington, N. and Barra, F. (2005). A new look at the geology of the Zambian Copperbelt. - In: Hedenquist, J.W.; Thompson, J.F.H.; Goldfarb, R.J. and Richards, J. (eds.): Economic Geology 100th Anniv. Volume, p. 965-1000.

Seward, T.M. and Barnes, H.L. (1997). Metal transport by hydrothermal ore fluids. – In: Barnes, H.L. (ed.): Geochemistry of hydrothermal ore deposits. – 3rd ed., p. 435-486, New York (Wiley & Sons)

Shao, H.; Schuster, K.; Sönnke, J. and Bräuer, V. (2007). *In situ* gas test for the characterisation of Excavated Disturbed Zone at the Meuse/Haute-Marne URL.- Internat. Meeting Clays in natural & engineered barriers for radioactive waste confinement, 17-18 Sept. 2007, Lille, Paper O/011/3.

Shepherd, T.; Rankin, A.H. and Alderton, D.H.M. (1985). A practical guide to fluid inclusion studies. - 239 p., Glasgow (Blackie & Son Ltd.)

Sibson, R.H. (2001). Seismogenic framework for hydrothermal transport and ore deposition. - Soc. of Economic Geol. Reviews, **14**: 25-50.

Skempton, A.W. (1964). Long-term stability of clay slopes (4th Rankine Lecture). – Géotechnique, **14**: 77-101.

Skoczylas, F. and Fleureau, J.M. (2003). GDR FORPRO-Benchmark "Perméabilité" sur mortier et argilite. Synthèse des résultats. – Proceed. Nat. Sympos. GDR-FORPRO, 22-24 Sept., p. 200.

Skoczylas, F. and Henry, J.P. (1995). A study of the intrinsic permeability of granite to gas. - Int. J. Rock Mech. Min. Sci. & Geomech. Abstr., **32**: 171-179.

Środoń, J.; Clauer, N. and Eberl, D.D.D. (2002). Interpretation of K-Ar dates of illitic clays from sedimentary rocks aided by modeling. - American Mineralogist, **87**: 1528-1535.

Szücs, I.; Csicsák, J.; Óvári, Á.; Kovács, L. and Nagy, Z. (2005). Confinement performance of Boda Claystone formation, Hungary. - In: Proceed. "Clay Club" Workshop, Braunschweig, 9-11 Dec. 2003, OECD NEA Publ. No. **5303**: 209-224.

Taylor, H.P. (1997). Oxygen and hydrogen isotopes in hydrothermal mineral deposits. - In: Barnes, H.L. (ed.): Geochemistry of hydrothermal ore deposits. – 3rd ed., p. 229-302, New York (Wiley & Sons)

Trollope, D. H. (1981). Introduction – In: H. Bock (Ed.): An introduction to rock mechanics, 342 p., Townsville / Australia (James Cook Univ.).

Tsang, Ch.-F. and Bernier, F. (2005). Definitions of excavation disturbed zone and excavation damaged zone. – In: Davies, C. and Bernier, F. (eds.): Impact of the excavation disturbed or damaged zone (EDZ) on the performance of radioactive waste geological repositories, **EUR 21028 EN**: 5-8, Brussels (European Commission)

Ulusay, R. and Hudson, J. A. (2007). The complte ISRM Suggested Methods for rock characerization, testing and monitoring: 1974 – 2006. – 628 p., Ankara (ISRM Turkish National Group), ISBN 978-975-93675-4-1.

Valfouskaya, A.; Adler, P.M.; Thovert, J.-F. and Fleury, M. (2005). Nuclear-magnetic-resonance diffusion simulations in porous media . - J. Appl. Phys., **97**: 083510.

Veizer, J.; Ala, D.; Azmy, K.; Bruckschen, P.; Buhl, D.; Bruhn, F.; Carden, G.A.F.; Diener, A.; Ebneth, S.; Godderis, Y.; Jasper, T.; Korte, C.; Pawellek, F.; Podlaha, O.G. and Strauss, H. (1999). $^{87}Sr/^{86}Sr$, $\delta^{13}C$ and $\delta^{18}O$ evolution of Phanerozoic seawater. - Chemical Geology, **161**: 59-88.

Velde, B. (1992). Introduction to clay minerals. – 198 p., London (Chapman & Hall).

Vietor, T.; Blümling, P. and Armand, G. (2006). Failure mechanisms of the Opalinus Clay around underground excavations. – EUROCK, Sympos. on multiphysics coupling and long-term behaviour in rock mechanics. - In: Van Cotthem A. (ed): EUROCK 2006: Multiphysics coupling and long-term behaviour in rock mechanics. Proceedings Internat. Sympos. of the ISRM, 9-12 May, Liège, Belgium. p. 479-484, Leiden (Taylor & Francis / Balkema).

Voegelin, A. and Kretzschmar, R. (2001). Stability and mobility of colloids in Opalinus clay. - Nagra Internal Report, Switzerland.

Waber, H.N. and Schürch, R. (2000). WS-A experiment: fracture mineralogy and geochemistry as constraints on porewater composition. - Mont Terri Project, Technical Note, **TN 99-83**: 1-27.

Waber, H.N. (ed.) (2009). Borehole Oftringen: Mineralogy, Porosimetry, Geochemistry, Pore Water Chemistry, NAB 08-18.

Waber, H.N. *et al.* (in prep.). EWS Borehole Oftringen: Pore water in the Effinger-Member and surrounding rock formations. - Nagra Arbeitsber., Wettingen, Switzerland.

Wallner, M.; Lux, K.-H.; Minkley, W. and Hardy, H.R. (2007). The mechanical behavior of salt – Understanding of THMC Processes in salt. – Proceed. Saltmech6, Hannover, Germany, 22-25 May, 2007, 453 p., London (Taylor & Francis).

Wileveau, Y. and Bernier, F. (2007). Similarities in hydro-mechanical response of Callovo-Oxfordian Clay nad Boom Clay during gallery excavation. - Internat. Meeting Clays in natural & engineered barriers for radioactive waste confinement, 17-18 Sept. 2007, Lille, Paper O/010A/1.

Wileveau, Y. and Rothfuchs, T. (2007). THM behaviour of host rock (HE-D) Experiment: Study of thermal effects on Opalinus Clay. - Mont Terri Project Techn. Rep., **TR 2006-01**: 1-111, Swiss Nat. Hydrol. Geol. Surv.

Wolf, K.H. and Chilingarian, G.V. (1992). Diagenesis, III. – 674 p., Amsterdam (Elsevier).

Wolter, K.E. (2003). Rock mechanical analyses (RA) experiment: Petrophysical analyses of drill cores from the Opalinus Clay formation of the Mont Terri Rock Laboratory. - Mont Terri Project Techn. Note, **TN 2002-46**: 1-15, Swiss Nat. Hydrol. Geol. Surv.

Wong, P.Z. and Pengra D.B. (1995). Pore size, permeability and electrokinetic phenomena. – In: Pinnavaia, T.J. and Thorpe, M.F. (Eds.): Access in Nanoporous Materials. – pp. 295-317, New York (Plenum Press).

Wong, R.C.K. and Wang, E.C. (1997). Three-dimensional anisotropic swelling model for clay shale - A fabric approach. – Int. J. Rock Mech. Min. Sci. & Geomech. Abstracts, **34**: 187-198.

Yong, R.N. and Warkentin, B.P. (1975). Soil properties and behaviour. – Developments in Geotech. Eng., **5:** 1-449, Amsterdam (Elsevier).

Yong, S.; Evans, K.F.; Fidelibus, C. and Loew, S. (2004). Fracture generation (EZ-B Experiment): A review of the Mont Terri project literature. - Mont Terri Project Techn. Note, **TN 2004-40**: 1-52, Swiss Nat. Hydrol. Geol. Surv.

Yusa, Y.; Ishimaru, K.; Ota, K. and Umeda, K. (1993). Geological and geochemical indicators of paleohydrogeology in Tono uranium deposits, Japan. – In: Paleohydrogeological methods and their applications. Proceed. OECD/NEA Workshop, 9-10 November 1992, 117-146, Paris (OECD/NEA).

Yven B.; Sammartino S.; Géraud Y.; Homand F. and Villiéras F. (2007). Mineralogy, texture and porosity of Callovo-Oxfordian argillites of the Meuse/Haute-Marne region (Eastern Paris Basin). - Mém. Soc. géol. France, n.s., **178**: 73-90.

Zee v.d. W. and Urai, J. (2005). Processes of normal fault evolution in a siliciclastic sequence: a case study from Miri, Sarawak, Malaysia. – J. Structural Geol., **27**: 2281-2300.

Zhang, C.-L. and Rothfuchs, T. (2004). Experimental study of the hydro-mechanical behaviour of the Callovo-Oxfordian argillite. – Appl. Clay Sci., **26**: 325-336.

Zhang, C.-L.; Rothfuchs, T.; Moog, H.; Dittrich, J. and Müller, J. (2004). Experiments and modelling of thermo-hydro-mechanical and geochemical behaviour of the Callovo-Oxfordian argillite and the Opalinus Clay. – GRS Report, **GRS-202**, ISBN 3-931995-69-0.

Zhang, C.-L.; Rothfuchs, T.; Jockwer, N.; Wieczorek, K.; Dittrich, J.; Müller, J.; Hartwig, L. and Komischke, M. (2007a). HE-D Experiment: Thermal effects on the Opalinus Clay – A joint heating experiment of ANDRA and GRS at the Mont Terri URL. - Mont Terri Project Techn. Rep., **TR 2007-02**: 1-199, Swiss Nat. Hydrol. Geol. Surv.

Zhang, C.-L.; Rothfuchs, T.; Su, K. and Hoteit, N. (2007b). Experimental study of the thermo-hydro-mechanical behaviour of indurated clays. - Phys. & Chem. of the Earth, **32**: 957-965.

Zhang C.-L and Rothfuchs T. (2007). Moisture effects on argillaceous rocks. - Proc. 2nd Internat. Conf. of Mechanics of Unsaturated Soils. – In: Schanz, T. (Ed.): Proceedings in Physics, **112**: 319-326, Berlin / Heidelberg (Springer).

Zhang, C.-L.; Rothfuchs, T.; Dittrich, J. and Müller, J. (2008). Investigations on self-sealing of indurated clay. – GRS Report, **GRS-230**: 1-67, ISBN 978-3-939355-04-5.

Zhang, C.-L. and Rothfuchs, T. (2008). Damage and sealing of clay rocks detected by measurements of gas permeability. - Phys. & Chem. of the Earth, **33**: 363 – 373.

Zhang C –L.; Wieczorek, K. and Xie M.-L. (2009). Swelling experiments on mudrocks. – Internat. Sympos. on Unsaturated Soil Mechanics and Deep Geological Nuclear Waste Disposal (UNSAT-WATE 2009), 24-28 August 2009, Shanghai, China.

Zhou, G.-T. and Zheng, Y.-F. (2003). An experimental study of oxygen isotope fractionation between inorganically precipitated aragonite and water at low temperatures. - Geochim. Cosmochim. Acta, **67**: 387-399.

Ziegler, P.A. (1990). Geological atlas of Western and Central Europe. – 2nd ed., Shell International, Amsterdam (Elsevier).

APPENDIX 8

INDEX

A.8.1 Subject and location index

A.8.2 Author index

Legend: Straight numbers = in text; *numbers in italics = in List of References (Chapter A.7)*

OECD PUBLICATIONS, 2 rue André-Pascal, 75775 PARIS CEDEX 16
Printed in France.